UNIVERSIDADE D
COIMBRA

Fabian Cabrera Exeni

One-Dimensional Modelling of the Space Behaviour of Linearly Elastic Tapered Thin-Walled Bars with Open Cross-Section – Some Contributions

Tese no âmbito do Doutoramento em Engenharia Civil na Especialidade de Estruturas orientada pelos Professores Doutores Anísio Alberto Martinho de Andrade e Paulo Manuel Mendes Pinheiro da Providência e Costa e apresentada ao Departamento de Engenharia Civil da Faculdade de Ciências e Tecnologia da Universidade de Coimbra.

Agosto de 2019

UNIVERSIDADE D
COIMBRA

Fabian Cabrera Exeni

ONE-DIMENSIONAL MODELLING OF THE SPACE BEHAVIOUR OF LINEARLY ELASTIC TAPERED THIN-WALLED BARS WITH OPEN CROSS-SECTION – SOME CONTRIBUTIONS

Tese no âmbito do Doutoramento em Engenharia Civil na Especialidade de Estruturas orientada pelos Professores Doutores Anísio Alberto Martinho de Andrade e Paulo Manuel Mendes Pinheiro da Providência e Costa e apresentada ao Departamento de Engenharia Civil da Faculdade de Ciências e Tecnologia da Universidade de Coimbra.

Agosto de 2019

I want to learn more and more to see as beautiful what is necessary in things; then I shall be one of those who makes things beautiful. ***Amor fati***: let that be my love henceforth! I do not want to wage war against what is ugly. I do not want to accuse; I do not even want to accuse those who accuse. Looking away shall be my only negation. And all in all and on the whole: someday I wish to be only a Yes-sayer.

FRIEDRICH NIETZSCHE, *THE GAY SCIENCE*

ABSTRACT

The main body of the thesis is divided into two largely self-contained parts. The first one is devoted to the development of a continuous one-dimensional linear model for the stretching, bending and twisting of tapered thin-walled bars with open cross-sections under general quasi-static loading conditions. These bars are treated as two-dimensional Kirchhoff-Love shells, exhibiting both membrane and flexural behaviours. To achieve the necessary dimensional reduction, the classical assumptions of Vlasov and Kirchhoff-Love are regarded systematically as internal constraints, that is, a priori restrictions, of a constitutive nature, on the possible deformations of the bars (alternatively, they may also be viewed as holonomic-scleronomic constraints). Moreover, the internal forces are decomposed additively into active and reactive parts and this is shown to lead to a dual one-dimensional description of kinematics and statics. Two examples illustrate the application of the developed one-dimensional model, shed light on its physical aspects and demonstrate the shortcomings of piecewise prismatic models, regardless of the number of prismatic segments used (indeed, even in the limit when the length of these segments tends to zero).

The main original contributions in this first part of the thesis may be summarized as follows:

(i) The second fundamental form of the middle surface of a bar and the change of curvature tensor are established in general form.

(ii) The displacement field of a whole bar (not just of its middle surface) is completely characterized, thus including the so-called through-the-thickness (or secondary) warping deformation.

(iii) In the characterization of the internal forces in the bar, the shell bending and twisting moments and the transverse shear forces are taken into account, in addition to the membrane forces.

(iv) The Saint-Venant contribution to the strain energy and the corresponding component of the total torque are derived consistently.

(v) A set of fundamental inequalities concerning the cross-sectional properties is established.

The second part of the thesis is restricted to the important special case of depth-tapered singly symmetric I-section bars and deals with one-dimensional models of the Hencky bar-chain type, whose nature is intrinsically discrete. Indeed, a Hencky bar-chain model consists of a finite number of rigid units linked by elastic springs (or, more generally, by rheological elements) – it can be thought of not only as an idealization of a (continuous) member, but also as an actual mechanical structure in its own right, the inherent simplicity and transparency of which make its qualitative behaviour more easily grasped. Two types of problem are addressed in successive chapters: (i) the linear mechanical behaviour in three-dimensional space under general quasi-static loading conditions and (ii) the linearized flexural-torsional buckling behaviour under bending (in the plane of symmetry, which is also the plane of greatest flexural rigidity) and compression, including the so-called Wagner effect associated with the asymmetry of the flanges. Particular attention is paid to the calibration of the spring stiffnesses and to the appropriate definition of boundary conditions. It is shown that the bar-chain models are consistent with (but not subordinate to or in any away dependent on) previously developed Vlasov-type continuum models, in the sense that the local truncation errors tend to zero as the length of the rigid units approaches zero. Several illustrative examples, including prismatic and flangeless members (i.e., members with narrow rectangular cross-sections), are solved in order to verify the discrete Hencky bar-chain models and to assess their convergence rates.

RESUMO

Contributos para a Modelação Unidimensional do Comportamento Tridimensional de Barras Não Prismáticas com Secção de Parede Fina Aberta

A tese encontra-se dividida em duas partes em larga medida independentes. A primeira é dedicada ao desenvolvimento de um modelo linear unidimensional contínuo para a flexão e torção de barras com secção aberta de paredes finas, continuamente variável, submetidas a carregamentos quase-estáticos genéricos. Estas barras são tratadas como cascas de Kirchhoff-Love (bidimensionais), considerando tanto o comportamento de membrana como o de flexão. Para levar a cabo a necessário redução dimensional, as hipóteses clássicas de Vlasov e Kirchhoff-Love são tratadas sistematicamente como constrangimentos internos, isto é, restrições de natureza constitutiva às possíveis deformações de uma barra (alternativamente, aquelas hipóteses podem também ser vistas como constrangimentos holonómicos-escleronómicos). Assim, as forças internas são decompostas em parcelas activa e reactiva, o que conduz a uma descrição dual (unidimensional) da cinemática e da estática. São apresentados dois exemplos que ilustram a aplicação do modelo unidimensional desenvolvido, esclarecem os seus aspectos físicos e atestam as limitações dos modelos seccionalmente prismáticos (ou "em escada"), independentemente do número de segmentos prismáticos utilizados (de facto, estas limitações mantêm-se mesmo no processo de passagem ao limite quando o comprimento dos segmentos tende para zero).

Os principais contributos originais nesta primeira parte da tese podem ser resumidos da seguinte forma:

(i) Obtêm-se expressões gerais para a segunda forma fundamental da superfície média de uma barra e para o tensor de mudança de curvatura

(ii) Generaliza-se a definição do campo de deslocamentos da superfície média para todo a barra, incluindo assim a caracterização do empenamento na espessura das paredes (também designado por empenamento secundário).

(iii) Na caracterização dos esforços internos, são tidos em consideração não apenas os esforços de membrana, mas também os momentos flectores e torsor e as forças de corte transversais "de casca".

(iv) A contribuição de Saint-Venant para a energia de deformação e a componente correspondente do momento torsor total são obtidas de forma consistente.

(v) Estabelece-se um conjunto de desigualdades fundamentais relativas às propriedades mecânicas das secções transversais.

A segunda parte da tese, cujo âmbito se restringe ao importante caso particular de barras com secção em I monossimétricas e altura variável, trata de modelos unidimensionais do tipo Hencky, cuja natureza é intrinsecamente discreta. De facto, um modelo de Hencky consiste num número finito de unidades rígidas ligadas por molas elásticas (ou, mais geralmente, por elementos reológicos) e pode ser encarado não apenas como uma idealização de um elemento estrutural contínuo, mas também como uma estrutura real por direito próprio. A sua simplicidade e transparência faz com que o seu comportamento, de um ponto de vista qualitativo, seja mais facilmente apreendido. São abordados dois tipos de problema em capítulos sucessivos: (i) o comportamento linear no espaço tridimensional, sob acções quase-estáticas genéricas e (ii) a encurvadura por flexão-torção (linearizada) de vigas e colunas-viga solicitadas à flexão no seu plano de simetria (que é também o plano de maior rigidez à flexão), incluindo o chamado efeito Wagner associado à assimetria dos banzos. É dada uma especial atenção à calibração das rigidezes das molas e à definição apropriada das condições de fronteira. Mostra-se que os modelos de Hencky, se bem que desenvolvidos de forma totalmente independente, são consistentes com os modelos contínuos do tipo Vlasov previamente desenvolvidos, na medida em que os erros de truncatura locais tendem para zero à medida que o comprimento das unidades rígidas também se aproxima de zero. Apresentam-se vários exemplos ilustrativos, que incluem elementos prismáticos e elementos de secção rectangular fina, de forma a verificar os modelos discretos de Hencky e avaliar as suas taxas de convergência.

KEYWORDS

Tapered thin-walled bars with open cross-sections

Constrained Kirchhoff-Love shell

One-dimensional models

Discrete Hencky bar-chain models

Non-uniform torsion

Flexural-torsional buckling

PALAVRAS-CHAVE

Barras não prismáticas com secção de parede fina aberta

Casca de Kirchhoff-Love com constrangimentos internos

Modelos unidimensionais

Modelos discretos de Hencky

Torção não uniforme

Encurvadura por flexão-torção

ACKNOWLEDGMENTS

I would like to express my sincere gratitude to Prof. Anísio Alberto Martinho de Andrade and Prof. Paulo Manuel Mendes Pinheiro da Providência e Costa, for introducing and letting me take part in this important field of research, and for their valuable guidance and encouragement throughout the course of the work.

I am very grateful to University of Coimbra and the Department of Civil Engineering for providing the academic training and the opportunity to meet remarkable colleagues and wonderful people around the world. I feel lucky to had this academic experience, that open more challenges in my professional carrier.

It is very difficult to express the feelings a person has in his Ph.D. journey, begin through the comfort zone to the growth zone, passing over many stages as the lack of self-confidence, deal with challenges and problems. But at the end, we find purpose, set new goals and conquer objectives, for that, special thanks go to my family, colleagues and friends, for their constant support along this dissertation.

The financial support of the PRECIoSA – Programme of Exchange & Cooperation for International Studies between Europe and South America, during the academic years 2013–2016 is gratefully acknowledged.

TABLE OF CONTENTS

LIST OF FIGURES

Chapter 2

Chapter 3

Chapter 4

LIST OF TABLES

Chapter 2

Chapter 4

LIST OF SYMBOLS

Sets and maps

$\in$	is an element of, belongs to
$\forall$	universal quantifier
$\cap$	intersection
$\{x_1,\ldots,x_n\}$	set of elements of a finite sequence
$\{x \in X \mid P(x)\}$	set of elements of X having the property P
$X \times Y$	Cartesian product of the sets X and Y
$\mathbb{R}$	field of real numbers
$\mathbb{R}^+$	set of positive real numbers
$\mathbb{R}^2$	two-dimensional field of real numbers
$[a,b]$	set of all real numbers $x \in \mathbb{R}$ satisfying $a \le x \le b$
$f : X \to Y$	map, or function, from X into Y, i.e., $x \in X \mapsto f(x) \in Y$
$f(x)$	value of the map f at x

Linear algebra and geometry

$\cdot$	inner product on three-dimensional Euclidean vector space
:	double product or double contraction of two tensors
$\times$	cross product on three-dimensional Euclidean vector space
$\| \ \|$	norm on three-dimensional Euclidean vector space
$\otimes$	tensor product
$\oplus$	union of tensor fields
δ^i_j	Kronecker delta, equals to one if $i = j$ and equals to zero if $i \neq j$

$[\ ]^{linear}$	denotes the linearized change in the expression, associated with any displacement field defined on it
$\text{span}\{\ \}$	a set of linear combinations of the elements that span a space
$\det[\ ]$	determinant of a square matrix
$\{\ \}^T$	transpose of a column vector
$[\ ]^T$	transpose of a matrix

Differential calculus (reference shape and differential geometry of surfaces)

$C^{\mathrm{p}}[\mathrm{a},\mathrm{b}]$	a real-valued function defined on an interval $[\mathrm{a},\mathrm{b}]$ with $\mathrm{a}<\mathrm{b}$, is p-times continuously differentiable on that interval
$\frac{df}{d\,\mathrm{a}}$	derivative of f with respect to the variable a
$D_\alpha f$	partial derivative of f with respect to the α^{th} variable, with $\alpha=1,2$ corresponding to the Gaussian coordinates θ^1 and θ^2 respectively
$D_\alpha^2 f$	second-order partial derivative of f, i.e., $D_\alpha^2 f = D_\alpha\left(D_\alpha f\right)$
$D_\alpha D_\beta f$	second-order partial derivative of f with $\alpha,\beta=1,2$ corresponding to the Gaussian coordinates θ^1 and θ^2 respectively
δ	variation

Finite differences and total derivatives

$\Delta_\chi D_\pm(\square)_k$ first order differences forwards, i.e., $\Delta_\chi D_+(\square)_k = (\square)_{k+1} - (\square)_k$, first order differences backwards, i.e., $\Delta_\chi D_-(\square)_k = (\square)_k - (\square)_{k-1}$

$\Delta_\chi D_o(\square)_k$ first order differences central, i.e., $\Delta_\chi D_o(\square)_k = \dfrac{(\square)_{k+1} - (\square)_{k-1}}{2}$

$\left(\Delta_\chi\right)^2 D^3_\pm(\square)_k$ third order differences forwards, i.e., $\left(\Delta_\chi\right)^2 D^3_+(\square)_k = \Delta_\chi D^2_o(\square)_{k+1} - \Delta_\chi D^2_o(\square)_k$, third order differences backwards, i.e., $\left(\Delta_\chi\right)^2 D^3_-(\square)_k = \Delta_\chi D^2_o(\square)_k - \Delta_\chi D^2_o(\square)_{k-1}$

$\left(\Delta_\chi\right)^2 D^2_o(\square)_k$ second order differences central, i.e., $\left(\Delta_\chi\right)^2 D^2_o(\square)_k = \Delta_\chi D_+(\square)_k - \Delta_\chi D_+(\square)_{k-1}$

Δ_χ reference of the segment length

$f'(x_o)$, $f''(x_o)$, $f'''(x_o)$, $f^{IV}(x_o)$ the total derivatives up to fourth-order of a function $f(x)$ at x_o respectively

Reference shape and differential geometry of surfaces

$\mathcal{A}^*$ cross-sectional area evaluated with the reduced wall thickness t^*

$\mathcal{A}_{x_1}$ intersection of $\mathcal{B}$ and the plane orthogonal to $\boldsymbol{e}_1$ at position x_1

$\mathcal{A}_0, \mathcal{A}_L$ end cross-sections areas

$\mathcal{A}_{\alpha\beta}$ metric coefficients (first fundamental form) of the middle surface $\mathcal{S}$

$\boldsymbol{A}_1, \boldsymbol{A}_2$ covariant basis at $(\theta^1, \theta^2) \in \bar{\Omega}$ associated with the position vector $\bar{\boldsymbol{X}}$

$\boldsymbol{A}_3$ unit vector orthogonal to $\boldsymbol{A}_1(\theta^1, \theta^2)$ and $\boldsymbol{A}_2(\theta^1, \theta^2)$

$a_{\alpha\beta}$ metric coefficients (first fundamental form) of the middle surface S

$a^{\alpha\beta}$ contravariant metric coefficients of the middle surface S

a determinant of the matrix $[a_{\alpha\beta}]$ of metric coefficients

$\boldsymbol{a}_1, \boldsymbol{a}_2$ covariant basis at $(\theta^1, \theta^2) \in \bar{\Omega}$ associated with the position vector $\bar{\boldsymbol{x}}$

$\boldsymbol{a}_3$ unit vector orthogonal to $\boldsymbol{a}_1(\theta^1, \theta^2)$ and $\boldsymbol{a}_2(\theta^1, \theta^2)$

$\boldsymbol{a}^1, \boldsymbol{a}^2, \boldsymbol{a}^3$ contravariant basis, that has the property of $\boldsymbol{a}^i(\theta^1, \theta^2) \cdot \boldsymbol{a}_j(\theta^1, \theta^2) = \delta^i_j$, with $\boldsymbol{a}^3(\theta^1, \theta^2) = \boldsymbol{a}_3(\theta^1, \theta^2)$

$[a_{\alpha\beta}]$ matrix of the Riemann metric in the coordinate system (θ^1, θ^2), i.e., the matrix of metric coefficients

$B_{\alpha\beta}$ covariant components of the curvature tensor of the middle surface s

$\mathcal{B}$ reference body shape of a tapered thin-walled bar with open cross-sections, in its unloaded state (or material configuration)

$b_{\alpha\beta}$ covariant components of the curvature tensor of the middle surface S

$\mathcal{b}$ reference body shape of a tapered thin-walled bar with open cross-sections, in its loaded state (or spatial configuration)

b^B bottom flange width

b^T top flange width

b_f when $b^B = b^T = b_f$

$C^{\alpha}_{\Sigma}, C^{\beta}_{\mathit{\Lambda}}$ coefficients use in the linear transformation law between the covariant basis $(\alpha, \beta = 1, 2)$ and the orthonormal basis $(\Sigma, \mathit{\Lambda} = \mathrm{I}, \mathrm{II})$

F parametrisation of the middle surface S, i.e., $F : \bar{\Omega} \to \bar{\mathcal{X}}$

h cross-section depth (in I- and C-section bars, is measured between flange middle lines), i.e., $h(0) = h_o$ and $h(L) = h_L$. To maintain Andrade's notation, we used $h = b$.

I^*_2, I^*_3, I^*_{23} cross-sectional second moments of area evaluated with the reduced wall thickness t^*

$I^*_{2\omega}, I^*_{3\omega}, I^*_{\omega}$ cross-sectional second sectorial moments evaluated with the reduced wall thickness t^*

$S^*_{\psi}, I^*_{\psi}, I^*_{2\psi}, I^*_{3\psi}, I^*_{\omega\psi}$ geometrical properties concerning the taper function ψ and thus peculiar to tapered bars of open cross-section, evaluated with the reduced wall thickness t^*

g_1, g_2 are real-valued functions on $[0, L]$

$\boldsymbol{E}_1, \boldsymbol{E}_2, \boldsymbol{E}_3$	orthonormal basis, defined in the spatial frame of reference
$\boldsymbol{e}_1, \boldsymbol{e}_2, \boldsymbol{e}_3$	orthonormal basis, defined in the material frame of reference
J^*	geometrical property concerning the torsion of the cross-section evaluated with the reduced wall thickness t^*, i.e., the generalization of the torsion constant of the tapered bar
$\mathcal{J}$	longitudinal edge of a bar with irregular middle surface
L	Length of the bar, measured in the direction $\boldsymbol{e}_1$
$\mathcal{L}_{x_1}$	intersection of S and the plane orthogonal to $\boldsymbol{e}_1$ at position x_1, i.e., $\mathcal{L}_{x_1} = \mathcal{L}_{\theta^1}$
$\mathcal{L}_0, \mathcal{L}_L$	end cross-sections middle lines
$\boldsymbol{O}_{\mathrm{I}}, \boldsymbol{O}_{\mathrm{II}}$	orthonormal ordered basis for $T_{F(\theta^1,\theta^2)}s$
$\boldsymbol{o}_{\mathrm{I}}, \boldsymbol{o}_{\mathrm{II}}$	orthonormal ordered basis for $T_{F(\theta^1,\theta^2)}S$
S_2^*, S_3^*	cross-sectional first moments of area evaluated with the reduced wall thickness t^*
S_ω^*	cross-sectional first sectorial moment evaluated with the reduced wall thickness t^*
S	middle surface of $\mathcal{B}$, identified with the middle surface of the bar in its material configuration
s	middle surface of $\mathcal{b}$, identified with the middle surface of the bar in its spatial configuration
t	wall thickness, measured along the perpendicular line of the tangent plane $T_{F(\theta^1,\theta^2)}S$ of S at the point $F(\theta^1, \theta^2)$
t^*	reduced wall thickness, i.e., $t^* = t/\sqrt{a^3}$
t_B	bottom flange thickness
t_T	top flange thickness
t_f	when $t_T = t_B$, we used $t_T = t_B = t_f$

t_W web thickness. To maintain Andrade's notation, we used $t_W = t_w$

$T_{F(\theta^1,\theta^2)}S$ tangent plane to S at the point $F(\theta^1,\theta^2)$

$\boldsymbol{\mathcal{X}}$ position vector of a spatial point, located at the reference body shape $\mathcal{B}$, that Cartesian coordinates are defined by X_i with $i=1,2,3$.

$\bar{\boldsymbol{\mathcal{X}}}$ position vector of a spatial point, located at the middle surface s, that Cartesian coordinates are defined by $\bar{X}_i$ with $i=1,2,3$.

$\boldsymbol{\chi}$ position vector of a material point, located at the reference body shape $\mathcal{B}$, that Cartesian coordinates are defined by χ_i with $i=1,2,3$

$\bar{\boldsymbol{\chi}}$ position vector of a material point, located at the middle surface S, that Cartesian coordinates are defined by $\bar{\chi}_i$ with $i=1,2,3$

z^B χ_3-coordinate of the bottom flange middle plane, i.e., $z^B = z^T + h$

z^T χ_3-coordinate of the top flange middle plane

α taper ratio (that for prismatic bars it is equal to $\alpha = 1$)

γ slope factor of the web with respect to the planes spanned by $\boldsymbol{e}_1$-$\boldsymbol{e}_2$

γ_B^f, γ_T^f slopes factor of the flanges with respect to the planes spanned by $\boldsymbol{e}_1$-$\boldsymbol{e}_3$

φ_B, φ_T inclinations of the flanges with respect to the planes spanned by $\boldsymbol{e}_1$-$\boldsymbol{e}_2$

φ_B^f, φ_T^f inclinations of the flanges with respect to the planes spanned by $\boldsymbol{e}_1$-$\boldsymbol{e}_3$

$\kappa_{\omega 0}$ non-dimensional ratio, i.e., $\kappa_{\omega 0} = (\pi / L)\sqrt{\left(\tilde{E}I_\omega^*(0)\right) / \left(\tilde{G}J^*(0)\right)}$

κ_{J0} non-dimensional ratio, i.e., $\kappa_{J0} = \left(h_0 t_w^3\right) / \left(3J^*(0)\right)$

μ non-dimensional ratio, i.e., $\mu = \left(M_{L,1} L\right) / \left(\tilde{G}J^*(0)\right)$

$\bar{\Omega}$ domain of the parametrisation F, i.e., $F : \bar{\Omega} \to \bar{\boldsymbol{\mathcal{X}}}$

θ^1, θ^2 Gaussian coordinates of S associated with the parametrisation F

θ^3 transverse variable, i.e., $-t(\theta^1,\theta^2) \le 2\theta^3 \le t(\theta^1,\theta^2)$

$\boldsymbol{\vartheta}$ arbitrary second-order tensor, with covariant components $\vartheta_{\alpha\beta}$

Kinematics ─ continuous one-dimensional model

q the coordinate of a point of $F \in \mathcal{L}_{x_1}$, defined by the distance from the origin parallel to the direction of the vector $\boldsymbol{a}_2$ in F

r the coordinate of a point of $F \in \mathcal{L}_{x_1}$, defined by the distance from the origin perpendicular to the direction of the vector $\boldsymbol{a}_2$ in F

$\bar{\boldsymbol{U}}$ admissible displacement field of the middle surface S

$\boldsymbol{U}$ admissible displacement field of any material point $\mathcal{X} \in \mathcal{B}$

$\boldsymbol{W}$ translation vector, i.e., $\boldsymbol{W}(\theta^1) = W_i(\theta^1)\,\boldsymbol{e}_i$

W_1, W_2, W_3, Φ_1 generalised displacements

$\boldsymbol{\Phi}$ infinitesimal rotation vector, i.e., $\boldsymbol{\Phi}(\theta^1) = \Phi_i(\theta^1)\,\boldsymbol{e}_i$

ζ out-of-plane warping displacement

$\Gamma^{\sigma}_{\alpha\beta}$ Christoffel symbols of the second kind

$\varepsilon, \kappa_1, \kappa_2, \kappa_3, \Gamma$ generalised strains

$\boldsymbol{\gamma}$ linearized membrane strain tensor field

$\gamma_{\alpha\beta}$ covariant component fields of $\boldsymbol{\gamma}$

$\gamma_{\Lambda\cdot\Sigma}$ components of $\boldsymbol{\gamma}$ with respect to the orthonormal ordered basis $\{\boldsymbol{o}_{\mathrm{I}}, \boldsymbol{o}_{\mathrm{II}}\}$

$\boldsymbol{\rho}$ linearized change of curvature tensor

$\rho_{\alpha\beta}$ covariant component fields of $\boldsymbol{\rho}$

$\rho_{\Lambda\cdot\Sigma}$ components of $\boldsymbol{\rho}$ with respect to the orthonormal ordered basis $\{\boldsymbol{o}_{\mathrm{I}}, \boldsymbol{o}_{\mathrm{II}}\}$

ψ taper function, that has the geometrically components relative to the non-standard stiffness terms peculiar to the tapered geometry

ω warping function; sectorial coordinate

Kinematics ─ discrete one-dimensional model

$\mathbf{q}^F$ generalized coordinates at the fundamental equilibrium configuration

q_i generalized coordinates. In column vector notation $\{\mathrm{q}\}$

W_{xk}, W_{yk}, W_{zk} discrete displacements, correspond to the *x*-, *y*- and *z*- directions respectively

$W_{yk}^{dAk}, W_{zk}^{dAk}$ discrete displacements, correspond to the *y*- and *z*- directions of the differential area dA_k

$w_{xk}^{sc}, w_{yk}^{sc}, w_{zk}^{sc}$ discrete displacements, associated to a second longitudinal axis χ-, corresponding to the shear centre axis

$w_k^{II(\theta z)}$ second-order axial shortening given by the out-of-plane bending

θ_k^{II-y} second-order curvature in the loading plane *xz*

θ_k^z first-order minor axis curvature

ϕ_k discrete twist rotations

Φ_{yk}, Φ_{zk} discrete bending rotations

Ψ_k cross-section planes in the buckled configuration

ψ_k cross-section planes in the undeformed configuration

Constitutive equations and energy functional

μ constrained elasticity tensors due to the extensional (i.e., $\mu = \varepsilon$) and flexural (i.e., $\mu = \theta$) rigidity respectively

E_{I} Young modulus relative to the direction $\boldsymbol{o}_{\mathrm{I}}$

$\tilde{E}$ modified elastic modulus

$\{e\}$ column vector of generalised strains, i.e., $\{e\} = \{\varepsilon\ \kappa_1\ \kappa_2\ \kappa_3\ \Gamma\}^T$

$G_{\Lambda\cdot\Sigma}$ shear modulus relative to the ordered pairs $\{\boldsymbol{o}_\Lambda, \boldsymbol{o}_\Sigma\}$, with $\Lambda\cdot\Sigma = \{\mathrm{I}\cdot\mathrm{II},\ \mathrm{II}\cdot\mathrm{I}\}$

$\tilde{G}$ modified shear modulus

$[K]$ stiffness matrix, such that $\{\sigma^{(A)}\} = [K]\{e\}$

$[\,k\,]$ diagonal matrix of the stiffness matrix, i.e., $[\,k\,] = [Q][K][Q]^T$

$[L]$ matrix linear operator, such that $\{e\} = [L]\{\mathrm{w}\}$

$[L]^\dagger$ adjoint operator of $[L]$, i.e., $\int_0^L \{\sigma^{(A)}\}^T \{[L]\{\mathrm{w}\}\}\, d\theta^1 = \int_0^L \{\mathrm{w}\}^T \{[L]^\dagger \{\sigma^{(A)}\}\}\, d\theta^1$

P operator on a tensor space, i.e., $\mathsf{P}_\mu \mathsf{C}_\mu = \mathsf{C}_\mu$ and $\mathsf{P}_\mu^\perp \mathsf{C}_\mu^\perp = \mathsf{C}_\mu^\perp$

$\boldsymbol{P}_\Sigma$ projection tensor field, regarded as linear map onto its respective space, with $\Sigma = \{\mathrm{I},\ \mathrm{I}\cdot\mathrm{II},\ \mathrm{II}\cdot\mathrm{I}\}$

$[Q]$ orthogonal matrix, such that $[\,k\,][Q] = [Q][K]$

$\{\mathrm{q}\}$ column vector of bar loads, i.e., $\{\mathrm{q}\} = \{q_1 \quad -m_3' + q_2 \quad m_2' + q_3 \quad b' + m_1\}^T$

S_μ unconstrained elasticity tensors due to the extensional (i.e., $\mu = \varepsilon$) and flexural (i.e., $\mu = \theta$) rigidity respectively

$\mathcal{U}$ strain energy

$\mathcal{W}_e$ work of the external loads

$(\widehat{W}_i, \widehat{\Phi}_1)$ arbitrary displacements fields in the domain D

$\{\mathrm{w}\}$ column vector of generalised displacements, i.e., $\{\mathrm{w}\} = \{W_1 \ W_2 \ W_3 \ \Phi_1\}^T$

C^i tensor fields, with $i = 1,2,3$

C_μ constraint spaces of the mechanical shell due to its membrane state (i.e., $\mu = \varepsilon$), and its flexure state (i.e., $\mu = \theta$) respectively

$\mathsf{C}_\mu^\perp$ orthogonal complement of space C_μ, with $\mu = \{\varepsilon, \theta\}$

D domain where the generalised displacements (i.e., W_i, Φ_1) are defined

$\tilde{\mu}$ ratio of the modified shear and elastic modulus, i.e., $\tilde{\mu} = \tilde{G} / \tilde{E}$

$\nu_{\Lambda\cdot\Sigma}$ Poisson ratio relative to the ordered pairs $\{\boldsymbol{o}_\Lambda, \boldsymbol{o}_\Sigma\}$, with $\Lambda\cdot\Sigma = \{\mathrm{I}\cdot\mathrm{II},\ \mathrm{II}\cdot\mathrm{I}\}$

Π total potential energy

$\left\{\sigma^{(A)}\right\}$ column vector of active stress resultants, i.e., $\left\{\sigma^{(A)}\right\} = \left\{N \; M_1^{(A)} \; M_2 \; M_3 \; B\right\}^T$

$\left\{\sigma^{(R)}\right\}$ column vector of reactive stress resultants, i.e., $\left\{\sigma^{(R)}\right\} = \left\{V_2 \; V_3 \; M_1^{(R)}\right\}^T$

Energy functional ─ discrete one-dimensional model

A_k^* cross-sectional area evaluated with the bar-chain model

A_k cross-sectional area

$\tilde{\mathbf{G}}$ non-dimensional (global) geometrical matrix of the discrete mechanical system

$\mathbf{H}$ Hessian operator, i.e., $\mathbf{H} = \nabla \otimes \nabla$

I_{yk}^*, I_{zk}^* cross-sectional second moments of area evaluated with the bar-chain model

$I_{z\omega k}^*, I_{\omega k}^*$ cross-sectional second sectorial moments evaluated with the bar-chain model

$I_{\psi k}^*, I_{z\psi k}^*, I_{\omega\psi k}^*$ geometrical properties concerning the taper function ψ and thus peculiar to tapered bars of open cross-section, evaluated with the bar-chain model

J_k^* geometrical property concerning the torsion of the cross-section evaluated with the bar-chain model

$[K]$ constitutive (block) matrix (whose submatrices are defined as $[K_{\psi\zeta}] \in \mathbb{R}^{n^\psi \times n^\zeta}$ with $\psi, \zeta = x, y, z, \phi$), such that $[K]\{q\} = \{f\}$ $\mathcal{U}$ stored elastic energy in the bar-chain model

$\tilde{\mathbf{K}}$ non-dimensional (global) stiffness matrix of the discrete mechanical system

r_{ok} polar radius of gyration. For prismatic bar-chains $r_{ok} = r_o$

S_{yk}^* cross-sectional first moment of area evaluated with the bar-chain model

S_{yk} cross-sectional first moment of area

$\mathbf{S}_{ij}$ the coefficients of a symmetric matrix $\mathbf{S}$, given by the Hessian operator applied to the total potential energy, i.e., $\mathbf{S}_{ij} = \mathbf{e}_i \circ \mathbf{H}(\Pi)\mathbf{e}_j$

$\mathcal{U}$ stored elastic energy in the bar-chain model

$\mathcal{W}_e^{II}$ work of the applied loading, taking second-order effects

$\mathcal{W}_c^{II}$ work due to the curvature of the buckled bar-chain

$\mathcal{W}_{P\theta z}^{II}$ work of the axial compressive load under bending, taking second-order effects

$\mathcal{W}_{P\phi}^{II}$ work of the axial compressive load under twisting, taking second-order effects

$\mathcal{W}_P^{II}$ work of the axial compressive load, i.e., $\mathcal{W}_P^{II} = \mathcal{W}_{P\theta z}^{II} + \mathcal{W}_{P\phi}^{II}$

β_{yk} geometric property of the monosymmetric cross-section, related to the asymmetry of the flanges. For prismatic bar-chains $\beta_{yk} = \beta_y$

ε_o non-dimensional eccentricity, i.e., $\varepsilon_o = \dfrac{z_Q}{\alpha L}\sqrt{\dfrac{EI_z(0)}{GJ(0)}}$ or $\varepsilon_o = \dfrac{z_q}{L}\sqrt{\dfrac{EI_z}{GJ}}$

λ non-dimensional load parameter

λ_{cr} critical non-dimensional load parameter

$\tilde{\Pi}$ non-dimensional total potential energy, i.e., $\tilde{\Pi}(q_i;\lambda) = \dfrac{1}{2}\mathbf{q}^T\tilde{\mathbf{S}}\mathbf{q}$

$\Upsilon_T^c, \Upsilon_B^c$ non-dimensional variable, that defined the position of the centroidal axis

$\Upsilon_T^{sc}, \Upsilon_B^{sc}$ non-dimensional variable, that defined the position of the shear centre

Shell forces, loads and cross-sectional stress resultants

B bimoment

B_0, B_L applied concentrated bimoments at the end sections

b applied distributed bimoment load per unit length of the line segment $\{O+\theta^1\boldsymbol{e}_1, 0 \le \theta^1 \le L\}$, evaluated with the warping function ω

M_1 torque about the line $\{O+\theta^1\boldsymbol{e}_1, 0 \le \theta^1 \le L\}$

$M_1^{(A)}$ active part of the torque M_1

$M_1^{(R)}$ reactive part of the torque M_1

M_2 bending moment relative to the axis through $O+\theta^1\boldsymbol{e}_1$ and spanned by $\boldsymbol{e}_2$

M_3 bending moment relative to the axis through $O+\theta^1\boldsymbol{e}_1$ and spanned by $\boldsymbol{e}_3$

M_f bending moment relative to each flange

$\boldsymbol{M}_0, \boldsymbol{M}_L$ applied concentrated moments at the end sections, i.e., $\boldsymbol{M}_0 = M_{0.i}\,\boldsymbol{e}_i$ and $\boldsymbol{M}_L = M_{L.i}\,\boldsymbol{e}_i$ respectively

$\mathbf{m}$ applied distributed moment per unit length of the line segment $\{O+\theta^1\boldsymbol{e}_1, 0 \le \theta^1 \le L\}$, i.e., $\mathbf{m} = m_i\boldsymbol{e}_i$

$\boldsymbol{m}$ shell moment tensor field

$\boldsymbol{m}^{(A)}$ active part of $\boldsymbol{m}$

$\boldsymbol{m}^{(R)}$ reactive part of $\boldsymbol{m}$

$m_{\Lambda\cdot\Sigma}^{(A)}$ active components of $\boldsymbol{m}$ with respect to the orthonormal ordered basis $\{\boldsymbol{o}_{\mathrm{I}}, \boldsymbol{o}_{\mathrm{II}}\}$, with $\Lambda\cdot\Sigma = \{\mathrm{I}\cdot\mathrm{II},\ \mathrm{II}\cdot\mathrm{I},\ \mathrm{I}\cdot\mathrm{I}\}$

$m_{\Lambda\cdot\Sigma}^{(R)}$ reactive components of $\boldsymbol{m}$ with respect to the orthonormal ordered basis $\{\boldsymbol{o}_{\mathrm{I}}, \boldsymbol{o}_{\mathrm{II}}\}$, with $\Lambda = \Sigma = \mathrm{II}$

N normal force

$\boldsymbol{n}$ membrane force tensor field

$\boldsymbol{n}^{(A)}$ active part of $\boldsymbol{n}$

$\boldsymbol{n}^{(R)}$ reactive part of $\boldsymbol{n}$

$n_{\Lambda\cdot\Sigma}^{(A)}$ active components of $\boldsymbol{n}$ with respect to the orthonormal ordered basis $\{\boldsymbol{o}_{\mathrm{I}}, \boldsymbol{o}_{\mathrm{II}}\}$, with $\Lambda = \Sigma = \mathrm{I}$

$n_{\Lambda\cdot\Sigma}^{(R)}$ reactive components of $\boldsymbol{n}$ with respect to the orthonormal ordered basis $\{\boldsymbol{o}_{\mathrm{I}}, \boldsymbol{o}_{\mathrm{II}}\}$, with $\Lambda\cdot\Sigma = \{\mathrm{I}\cdot\mathrm{II},\ \mathrm{II}\cdot\mathrm{I},\ \mathrm{II}\cdot\mathrm{II}\}$

$Q_{\Sigma}^{(R)}$ transverse shear force, with $\Sigma = \{\mathrm{I},\ \mathrm{II}\}$

$\boldsymbol{Q}_0, \boldsymbol{Q}_L$ applied concentrated forces at the end sections, i.e., $\boldsymbol{Q}_0 = Q_{0.i}\,\boldsymbol{e}_i$ and $\boldsymbol{Q}_L = Q_{L.i}\,\boldsymbol{e}_i$ respectively

$\boldsymbol{q}$ applied distributed force per unit length of the line segment $\left\{O + \theta^1 \boldsymbol{e}_1, 0 \le \theta^1 \le L\right\}$, i.e., $\boldsymbol{q} = q_i \boldsymbol{e}_i$

V_2 shear force parallel to $\boldsymbol{e}_2$

V_3 shear force parallel to $\boldsymbol{e}_3$

V_f shear force relative to each flange

Forces, loads and cross-sectional stress resultants ─ discrete one-dimensional model

B_k bimoment

b_k applied discrete bimoment load per unit length, described by self-equilibrated quasi-tangential moments

$\{\mathrm{f}\}$ known loading coefficients, grouped into a column vector

M_{zk}, M_{yk} bending moments about the *z* and *y* –direction respectively

M_{yk}^F bending moment in the fundamental equilibrium state

$M_{i.\mathrm{x}}, M_{i.\mathrm{y}}, M_{i.\mathrm{z}}$ applied concentrated moments at the end sections, i.e., $i = 0$ and $i = L$ respectively

$m_{\mathrm{x}k}$, $m_{\mathrm{y}k}$, m_{zk} applied discrete moment per unit length

N_k axial force

P point load at the *x* –direction

Q point load at the *z* –direction

$Q_{i.\mathrm{x}}, Q_{i.\mathrm{y}}, Q_{i.\mathrm{z}}$ applied concentrated forces at the end sections, i.e., $i = 0$ and $i = L$ respectively

$q_{\mathrm{x}k}$, $q_{\mathrm{y}k}$, q_{zk} applied discrete forces per unit length

T_k twist moment given by the superposition of two torsional effects, i.e., $T_k = T_k^{\omega} + T_k^{\phi}$

T_k^{ω} warping torsion

T_k^{ϕ} torsion due to the torsional spring

$T_k^{P\phi}$ second-order twist moment, given by the effect of the compressive load under twisting

T_k^{d} second-order disturbing torque, given by the out-of-balance forces due to the twist of the flanges

V_{zk}, V_{yk} shear force about the *z* and *y* –direction respectively

General springs characterization

A area of the cross-section

ξ type of spring, i.e., axial $\xi = \varepsilon$, flexural $\xi = \theta n$ or torsional $\xi = \phi$

C_k^{ξ} spring constant ξ at position k with $k = 1, 2, ..., \mathrm{n}-1$. For prismatic bar-chains $C_k^{\xi} = C^{\xi}$

E Young's modulus

G shear modulus

I_n second moment of area with respect to $\boldsymbol{n}$

J torsional constant

L length of the bar, measured along the *x*-axis

ℓ projection of L on χ

n number of segments with equal lengths, i.e., $\Delta = L / \mathrm{n}$

$\boldsymbol{n}$ vector in three dimensional space, where the flexural spring θn is defined

S^{ξ} cross-sectional stiffness of the prismatic continuum bar, i.e., $S^{\varepsilon} = EA$, $S^{\theta n} = EI_n$ and $S^{\phi} = GJ$

S_k^{ξ} discrete non-prismatic stiffness, defined as $S_k^{\xi} = S^{\xi}(k\Delta_{\chi})$ with $k = 1, 2, ..., \mathrm{n}-1$, where the non-prismatic stiffness functions $S^{\xi}(\chi)$ are equal to $S^{\varepsilon}(\chi) = EA(\chi)$, $S^{\theta n}(\chi) = EI_n(\chi)$ and $S^{\phi}(\chi) = GJ(\chi)$

U_k^{ξ} stored elastic energy at spring ξ with $k = 1, 2, ..., \mathrm{n}-1$

U^{ξ} stored elastic energy of a generic bar-chain, i.e., $U^{\xi} = \sum_{k=1}^{\mathrm{n}-1} U_k^{\xi}$

$w_k^{\chi}, w_k^{\perp\chi}, \phi_k$ the displacements $w_k^{\chi}, w_k^{\perp\chi}$ and twist rotation ϕ_k are defined in the direction-χ, where $w_k^{\perp\chi}$ refers to the displacement of the right most end of the segment, while w_k^{χ}, ϕ_k refer to any point on the χ axis in the segment, i.e., its longitudinal displacement and rotation respectively.

Γ_k^{ξ} scale factor, i.e., $\Gamma_k^{\xi}(\mathrm{n}) C_k^{\xi}(\mathrm{n}) = S_k^{\xi}$ with $k = 1, 2, ..., \mathrm{n}-1$. For prismatic bar-chains $\Gamma_k^{\xi} = \Gamma^{\xi}$ so $\Gamma^{\xi}(\mathrm{n}) C^{\xi}(\mathrm{n}) = S^{\xi}$

Δ_{χ} reference of the segment length, i.e., $\Delta_{\chi}(\mathrm{n})\,\mathrm{n} = \ell$, where ℓ is the projection of L on χ

Δ reference of the segment length, i.e., $\Delta(\mathrm{n})\,\mathrm{n} = L$

θ_k^{ξ} spring deformation ξ (i.e., θ_k^{ε}, $\theta_k^{\theta n} \equiv \theta_k^{n}$ and θ_k^{ϕ}) at position k with $k = 1, 2, ..., \mathrm{n}-1$

θ_i^{μ} the subscript μ is defined by the following spring deformations: bending $\mu = \{Tz, Bz, (h/2)y, (\mathrm{c})y\}$, torsional warping $\mu = \{T\omega, B\omega\}$, pure axial deformation $\mu = \{T\varepsilon, B\varepsilon, (h/2)\varepsilon, (\mathrm{c})\varepsilon\}$, axial due to bending $\mu = \{T\varepsilon y, B\varepsilon y, (h/2)\varepsilon y\}$ and torsional deformation $\mu = \{\phi\}$, with the labels *T*: top, *B*: bottom, *h*/2: web mid-height and c : centroid of the cross-section

Λ_k^{ξ} constant, such that $C_k^{\xi}(\mathrm{n})/\mathrm{n} = \Lambda_k^{\xi}$ with $k = 1, 2, ..., \mathrm{n}-1$. For prismatic bar-chains $C^{\xi}(\mathrm{n})/\mathrm{n} = \Lambda^{\xi}$

χ direction-χ (not necessarily parallel to the *x*-axis)

Abbreviations

e.g.	for example
eq.	equation
et al.	and others
etc.	and other similar things
i.e.	that is
p.	page
pp.	pages
resp.	respectively
vide supra	see above
§	section

Chapter 1

GENERAL INTRODUCTION

> Basic research leads to new knowledge. It provides scientific capital. It creates the fund from which the practical applications of knowledge must be drawn. New products and new process do not appear full-grown. They are founded on new principles and new conceptions, which in turn are painstakingly developed by research in the purest realms of science.
>
> VANNEVAR BUSH, *SCIENCE, THE ENDLESS FRONTIER*

> Many of the scientific treatises of today are formulated in a half-mystical language, as though to impress the reader with the uncomfortable feeling that he is in the permanent presence of a superman. The present book is conceived in a humble spirit and is written for humble people.
>
> CORNELIUS LANCZOS, *THE VARIATIONAL PRINCIPLES OF MECHANICS*

1.1 MOTIVATION AND MAIN OBJECTIVES

Open section thin-walled bars[1] are highly efficient structural members to resist bending actions, a feature that explains their attractiveness. In particular, tapered (i.e., non-prismatic, with a smoothly varying cross-section) thin-walled beams are ideally suited to withstand variable bending moments, provided that the cross-section variation matches the moment envelope as closely as possible. In fact, they allow designers an increased freedom in combining efficiency, economy and aesthetics – the three ideals of structural art, according to Billington (1985) [pp. 3-26]. However, the competitiveness

[1] Thin-walled bars are distinguished by the fact that their characteristic dimensions are all of different orders of magnitudes — the wall thickness is small compared with the diameter of the cross-section, which, in turn, is much smaller than the length of the bar (e.g., Vlasov 1961).

of tapered structural members is negatively affected by the fact that their space (i.e., three-dimensional) behaviour is still poorly understood and by the lack of consistent and efficient methods for their analysis and design. Due to their geometrical characteristics, tapered thin-walled bars are natural candidates to one-dimensional modelling (i.e., involving a single independent space variable) and, indeed, it is not feasible to treat them as a three-dimensional continuum, at least in routine applications – the computational cost and post-processing difficulties would make this prohibitive. However, the piecewise prismatic (or stepped) approach, in which the tapered thin-walled bar is replaced by a sequence of prismatic segments (whose number is increased until convergence is achieved), has been shown to be generally incorrect when the member is subjected to torsion with restrained warping (e.g., Andrade and Camotim 2005 or Boissonnade and Maquoi 2005).

The development of special purpose one-dimensional models for tapered thin-walled bars is therefore of great practical, as well as theoretic, importance. A recent step in this direction was taken by Andrade (2013), who developed a continuum linear one-dimensional linear model for the stretching, bending and twisting of tapered thin-walled bars with arbitrary open cross-sections under general quasi-static loading conditions. But this Vlasov-type model, which can be described as a constrained membrane shell, is not fully consistent. From a theoretical point of view, its main shortcoming is the inability to derive rationally the Saint-Venant contribution to the strain energy (and, subsequently, the corresponding component of the total torque). In fact, this contribution is an ad hoc addition to that model, whose sole justification, ultimately, is the fact that it seems to work (i.e., to yield accurate predictions). One objective of the present thesis is thus to remove this shortcoming and, in so doing, to obtain a fully consistent model. Moreover, the applicability of this fully consistent model should not be restricted to bars whose shape allows them to resist biaxial bending by membrane action of their walls (as in Andrade 2013) but ought to include also members with narrow rectangular cross-section.

Even if the underlying ideas are fairly simple, a general continuum model such as the one perfected here involves, and must necessarily involve, a considerable amount of detail and complexity. An overall view of its physical aspects may therefore be difficult to attain. Discrete models consisting of a finite number of rigid units linked by

elastic springs (or, more generally, by rheological elements) – often associated with the name of Hencky in the structural engineering literature –, which have seen a wealth of recent applications in the fields of micro and non-local mechanics, seem to hold a great deal of potential to remedy this undesirable situation. Indeed, their inherent conceptual simplicity and transparency make the qualitative behavioural features of this class of models more easily intuited and grasped.[2] This line of thought leads directly to the second main objective of this thesis: to develop Hencky bar-chain (one-dimensional) models to describe the mechanical behaviour in three-dimensional space of depth-tapered singly symmetric I-section bars, which is possibly the most significant special case in design practice. Such a development is to be carried out in a manner that is independent of any pre-existing continuum model. Within this framework, two types of problem are addressed: (i) the linear mechanical behaviour in three-dimensional space under general quasi-static loading conditions and (ii) the linearized flexural-torsional buckling behaviour under bending (in the plane of symmetry, which is also the plane of greatest flexural rigidity) and compression, including the so-called Wagner effect.

A final objective is to investigate the connections that tie together discrete and continuum models as alternative (though independent) descriptions of the same physical phenomena, namely their mutual consistency. It is perhaps worth recalling here briefly the concept of consistency. In general, the solution to the continuum model will not satisfy exactly the equations of the discrete model – the discrepancy is called the local truncation error. The two models, continuum and discrete, are said to be (mutually) consistent if the local truncation error tends to zero as the length of the rigid units in the discrete model approaches zero (e.g., LeVeque 2007 [pp. 17-19]).

[2] From a mathematical point of view, the formalism of differential geometry that features so prominently in the development of continuum models for tapered thin-walled bars is avoided in Hencky's discrete approach. Moreover, Hencky models offer the added advantage of being naturally formulated in terms of difference (algebraic) equations, easily synthesized into matrix form, rather than differential equations.

1.2 SCOPE AND OUTLINE OF THE THESIS

The main body of the thesis can be divided into two largely independent parts.

The first part, consisting of chapter 2, is devoted to the development of a continuum one-dimensional linear model for the stretching, bending and twisting of tapered thin-walled bars with arbitrary open cross-sections under general quasi-static loading conditions. As in Andrade (2013) [p. 3], the induced-constraint approach is adopted. However, a more encompassing parent theory – the linearly elastic Kirchhoff-Love shell model, with both membrane and flexural behaviours – is now taken as the starting point (in Andrade 2013, the parent theory was a membrane shell model, and this is the root cause of subsequent inconsistencies). The classical assumptions of Vlasov and Kirchhoff-Love are treated systematically as internal constraints, that is, a priori restrictions, of a constitutive nature, on the possible deformations of the bars (Podio-Guidugli 1989). The Vlasov assumptions are crucial to achieve the necessary dimensional reduction (from two independent space variables to a single one) and to characterize the displacement field of the middle surface of a given bar and the associated membrane strain tensor. The Kirchhoff-Love assumption is used to extend the characterization of the displacement field from the middle surface to the whole bar (thus including the so-called through-the-thickness or secondary warping) and to define the change of curvature tensor. The shell forces are decomposed additively into active and reactive parts, with the constitutive dependence of the active shell forces on the strain measures reflecting the maximal material symmetry compatible with the assumed internal constraints. A consistent derivation of the Saint-Venant contribution to the strain energy and of the corresponding component of the total torque is thus achieved, while still obtaining a dual one-dimensional description of kinematics and statics. It should also be noted that all shell forces (bending and twisting moments, transverse shear forces and membrane forces) are taken into account in the definition of the cross-sectional stress resultants. The model of Vlasov for prismatic bars, in the slightly more general form expounded by Gjelsvik (1981), is found as a special case. Two examples concerning the torsional and coupled flexural-torsional behaviours of web-tapered I-section and C-section cantilevers, already tackled by Andrade (2013), illustrate the application of the developed one-dimensional model. They serve a twofold purpose: (i) to shed light on

the physical aspects of the model, particularly those that are peculiar to tapered bars, and (ii) to demonstrate and explain the shortcomings of piecewise prismatic (stepped) models, regardless of the number of prismatic segments used – indeed, the results of shell finite element analyses corroborate the one-dimensional tapered bar model and falsify the stepped approach.

The second part of the thesis, comprising chapters 3 and 4, deals with one-dimensional models of the Hencky bar-chain type. Its scope is limited to the important special case of depth-tapered singly symmetric I-section bars. Two types of problem are addressed: (i) the linear mechanical behaviour in three-dimensional space under general quasi-static loading conditions (chapter 3) and (ii) the linearized flexural-torsional buckling behaviour under bending (in the plane of symmetry, which is also the plane of greatest flexural rigidity) and compression, including the so-called Wagner effect (chapter 4). Since Hencky models consist of a finite number of rigid units linked by elastic springs, the assignment of specific stiffnesses to the connecting springs is a fundamental step in their construction. In recent works, this problem, which is called here the "calibration problem," is evaded through a comparison between the physical Hencky bar-chain model and the finite difference discretization of a pre-existing continuum model (e.g., Challamel et al. 2015, Ruocco et al. 2016, 2017, Wang et al. 2017 and Zhang et al. 2013, 2016, 2017). This has the undesirable consequence of making the Henky approach dependent on some underlying continuum model and, therefore, deficient as a modelling tool. In this thesis, an attempt is made to set up a general framework for solving, in a direct and independent manner, the calibration problem. Then, it becomes meaningful to investigate the connections that tie together discrete and continuum models as alternative (but independent, except that they stem from a common set of material and kinematic hypotheses) descriptions of the same physical phenomena. This leads to a proof of their mutual consistency and to the realization that the discrete may be used to illuminate the continuum. Several illustrative examples, including prismatic and flangeless members (i.e., members with narrow rectangular cross-sections), are solved in order to verify the discrete Hencky bar-chain models and to assess their convergence rates.

Finally, chapter 5 summarizes the main results and conclusions of the thesis. It also contains recommendations for future research in the fields of tapered thin-walled bars and discrete elastic systems.

* * *

Each chapter is divided into a number of sections and subsections, including an introduction with the pertinent literature review and its own list of references. Equations, figures and tables are numbered consecutively within each section; footnotes are numbered consecutively within each chapter.

REFERENCES

Andrade, A. (2013). “One-dimensional models for the spacial behaviour of tapered thin-walled bars with open cross sections: static, dynamic and buckling analyses.” *Ph.D. thesis, Universidade de Coimbra*.

Andrade, A., and Camotim, D. (2005). “Lateral-torsional buckling of singly symmetric tapered beams: theory and applications.” *Journal of Engineering Mechanics, ASCE*, 131(6), 586–597.

Billington, D. P. (1985). *The tower and the bridge: the new art of structural engineering*. Princeton University Press.

Boissonnade, N., and Maquoi, R. (2005). “A geometrically and materially non-linear 3-D beam finite element for the analysis of tapered steel members.” *International Journal of Steel Structures*, 5(5), 413–419.

Challamel, N., Camotim, D., Wang, C. M., and Zhang, Z. (2015). “On lateral-torsional buckling of discrete elastic systems: A nonlocal approach.” *European Journal of Mechanics A/Solids*, 49, 106–113.

Gjelsvik, A. (1981). *The theory of thin walled bars*. Wiley.

LeVeque, R.J. (2007). *Finite difference methods for ordinary and partial differential equations – Steady-state and time-dependent problems*. Society for Industrial and Applied Mathematics (SIAM).

Podio-Guidugli P. (1989). "An exact derivation of the thin plate equation." *Journal of Elasticity*, 22(2-3), 121-133.

Ruocco, E., Wang, C. M., Zhang, H., and Challamel, N. (2017). "An approximate model for optimizing Bernoulli columns against buckling." *Engineering Structures*, 141, 316–327.

Ruocco, E., Zhang, H., and Wang, C. M. (2016). "Hencky bar-chain model for buckling analysis of non-uniform columns." *Engineering Structures*, 73–84.

Vlasov, V. Z. (1961). *Thin-walled elastic beams*, [English translation of the 2nd Russian edition of 1959]. Jerusalem: Israel Program for Scientific Translation.

Wang, C. M., Zhang, H., Challamel, N., and Duan, W. H. (2017). "On boundary conditions for buckling and vibration of nonlocal beams." *European Journal of Mechanics A/Solids*, 61, 73–81.

Zhang, Z., Challamel, N., and Wang, C. (2013). "Eringen's small length scale coefficient for buckling of nonlocal Timoshenko beam based on microstructured beam model." *Journal of Applied Physics*, 114(11).

Zhang, H., Wang, C. M., and Challamel, N. (2016). "Buckling and vibration of Hencky bar-chain with internal elastic springs." *International Journal of Mechanical Sciences*, 119, 383–395.

Zhang, H., Wang, C. M., and Challamel, N. (2017). "Small length scale coefficient for Eringen's and lattice-based continualized nonlocal circular arches in buckling and vibration." *Composite Structures*, 165, 148–159.

Part I.

CONTINUOUS ONE-DIMENSIONAL MODEL

Chapter 2

A Linear One-Dimensional Model for the Stretching, Bending and Twisting of Tapered Thin-Walled Bars with Open Cross-Sections

The Static Case

I have gained enormous respect for mathematics,
whose more subtle parts I considered until now,
in my ignorance, as pure luxury.
Albert Einstein, *Letter to Sommerfeld in 1912*

In those sciences where mathematical demonstrations are
applied to natural phenomena. The principles, once established,
become the foundation of the entire superstructure.
Galileo Galilei, *Dialogues Concerning Two New Sciences*

Some who defend deductivist style claim that deduction is the heuristic pattern,
that the logic of discovery is deduction. Others realize that this is not true,
but draw from this realization the conclusion that discovery is a completely non-rational affair,
thus they will claim that although discovery does not proceed deductively,
if we want our presentation of discoveries to proceed rationally,
it must proceed in the deductivist style.
Imre Lakatos, *Proofs and Refutations: The Logic of Mathematical Discovery*

2.1 INTRODUCTION

Open section thin-walled bars are structural members, that have been used in diverse fields of engineering, owing to their high strength capacity with a minimum of material. As a 3D body, their characteristic dimensions have different orders of magnitudes, i.e., its thickness is smaller with respect to the dimensions of the cross-section, that, in turn, are small with respect to the length of the bar. This fact allows to simulate their mechanical behaviour by one-dimensional models, i.e., the variables in the equations depend only on the longitudinal coordinate, relative to the length of the bar. Among its mechanical properties that makes them unique structures, is the way that bending actions develop torsional effects (so-called the warping torsion), which causes the major difficulties in its description by any approach adopted.

The first attempts to derive one-dimensional models for the warping behaviour of tapered thin-walled bars with open cross-sections were restricted to I-section beams, e.g., Lee (1956) & Lee and Szabo (1967). The problem was tackled by regarding each plated component as an Euler-Bernoulli member, an ingenious approach pioneered by Timoshenko in 1905 (Mansfield and Young 1973) and further developed by Weber (1926) and Bleich and Bleich (1936), see Figures 2.1.1-2.1.2.

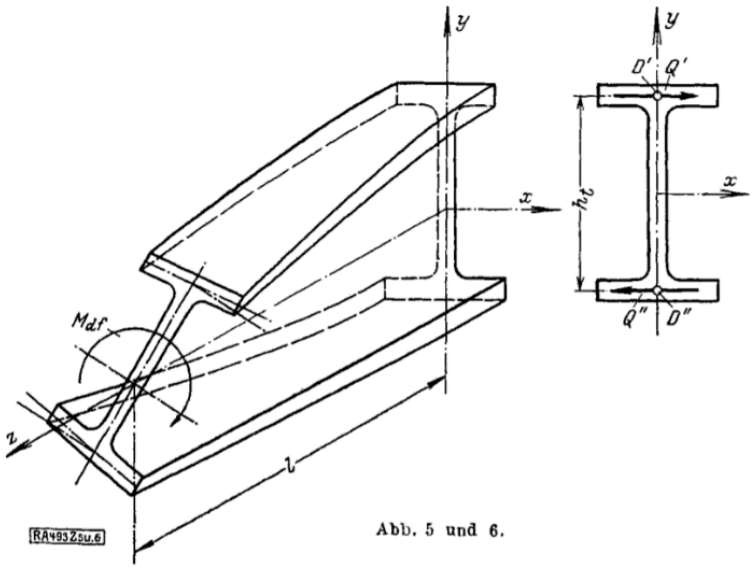

Figure 2.1.1: Torsional warping for prismatic I-beams by Weber (1926)

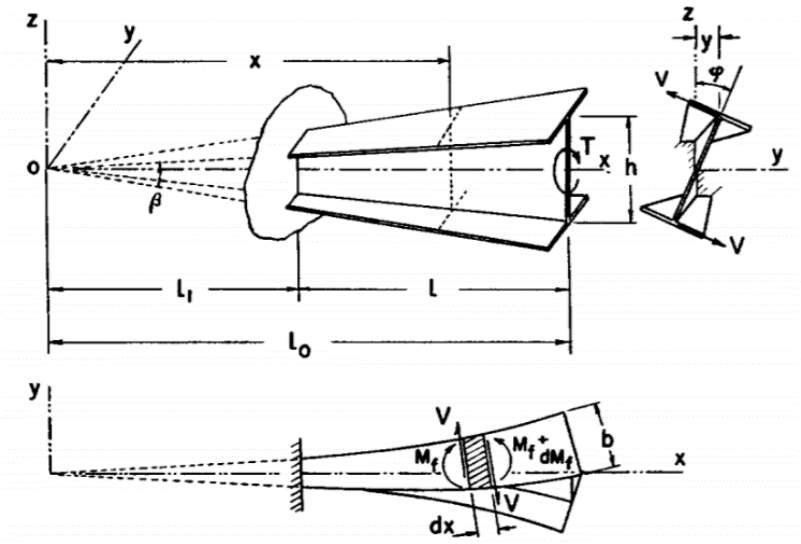

Figure 2.1.2: Torsional warping for tapered I-beams by Lee (1956)

The same approach was used later by Kitipornchai and Trahair (1972, 1975), who also dealt with the problem of elastic lateral-torsional buckling. Bažant (1965) and Wilde (1968) developed the one-dimensional models for the general case, i.e., the stretching, bending and twisting of tapered bars of arbitrary open cross-sections under a general static loading. Bažant applies the theory of prismatic thin-walled beams (Vlasov 1961) and assumes that the tapered member is locally equivalent to the behaviour of prismatic sections, see Figure 2.1.3.

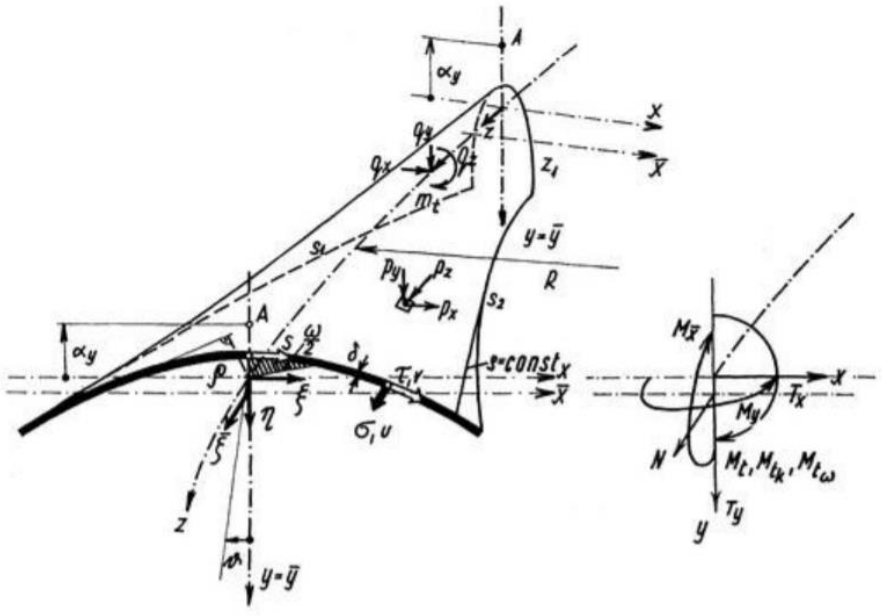

Figure 2.1.3: Arbitrary open cross-section under a general static loading (Bažant 1965)

In contrast, Wilde adopts a more remarkable approach, he incorporates the classical assumptions of Vlasov[1] as kinematical constraints of the middle surface, modelled as a membrane shell. In this way, he employs two powerful analytical tools: (i) the curvilinear coordinates and (ii) the Green-Lagrange strain tensor, e.g., Green and Zerna (1968) [eq. 2.1.22]. In spite of that, Wilde assumes an isotropic elastic material, therefore, he cannot find the constitutive nature of the internal constraints.

Later on, Wekezer (1984, 1985) by using the above approach, developed a finite element formulation, which agrees, in essence, with the one derived by Ronagh et al. (2000a; b) from a geometrically non-linear model. Despite having other dissertations with similar procedures, e.g., Yang and Yau (1987), Chan (1990) & Rajasekaran (1994), it is not until the original work of Andrade (2013), that a consistent induced-constraint approach for the derivation of one-dimensional models was developed.[2] Where, the thin-walled beams are basically consider as internally constrained membrane shells, that extend the tapered case in such a way as to retain an intrinsic geometrical meaning, i.e., the idea that mechanical laws should be independent of the choice of the coordinate system. I kept Andrade's approach, preserving the notation for the membrane shell distortion, i.e., stretching effect, but adding the change of curvature, that in general, are functions of the displacement field associated to the middle surface, modelled as a *two-dimensional internally constrained shell*. Hence a third constraint assumption had to be incorporated, corresponding to the Kirchhoff-Love hypotheses developed originally for the plate bending theory, e.g., Ventsel and Krauthammer (2001) [p. 294].

Thus, besides the outcomes of Andrade's approach, the following results are obtained: (i) the establish of the second fundamental form of the middle surface, (ii) the alternative definition of the internal constraints as holonomic-scleronomic constraints, (iii) the complete characterization of the displacement field of the middle surface, i.e., the displacement of any point inside the thickness, (iv) the warping deformation through-the-thickness, (v) the contribution of the shear moduli into the constitutive equations, (vi) the

[1] Vlasov based his theory for prismatic thin-walled beams of open-cross sections, under the following geometrical hypothesis: (i) the bar cross-sections are rigid (undeformable) in their own planes and (ii) the shearing deformation of the middle surface is negligible.

[2] Dennis and Jones (2017) called them, the Andrade's equations.

energy components associated with the warping thickness,[3] (vii) the effect of the bending and twisting moments, as well as the transverse shear forces over the thickness and (viii) the fundamental inequalities concerning the cross-sectional properties of the bar. Accordingly, by using the theorem of Podio-Guidugli and Vianello (1992), the shell actions are decomposed additively into active and reactive parts respectively, with the constitutive dependence of the active forces on the membrane strains and the active moments on the change of curvatures, reflecting the maximal symmetry compatible with the assumed internal constraints. So, the cross-sectional stress resultants are likewise split into active and reactive categories, leading to a dual one-dimensional description of kinematics and statics, avoiding any reference to centroidal or shear centre lines.

At the final section, I applied the one-dimensional equations to solve two illustrative examples, concerning the torsional and coupled flexural-torsional behaviours of web-tapered I-section and C-section cantilevers. The illustrative examples were taken from Andrade (2013) [pp. 80-114], whose further reading is recommended, in order to compare the subtle outcomes of the continuous one-dimensional model developed, which final results are found to be consistent with the Timoshenko's approach, regarding each plated component as an Euler-Bernoulli member in bending with axial forces.

2.2 THE REFERENCE SHAPE OF THE BAR

I do not define time, space, place and motion,

as being well known to all.

ISAAC NEWTON, *MATHEMATICAL PRINCIPLES OF NATURAL PHILOSOPHY*

In this section, I cover the description of the reference shape of the bar, i.e., its body shape $\mathcal{B}$ and corresponding middle surface S in its undeformed configuration, so that a consistent parametrization of the middle surface is made. Above notation will help us to mathematically described the kinematic of the two-dimensional shell, between its material and spatial configuration, and establish the main equations for the one-dimensional models.

[3] One of these components is associated with the Saint-Venant torsion, so that a generalization of the torsion constant of the cross-section is gotten.

2.2.1 General description

In its undeformed state, a tapered thin-walled bar with open cross-section fills a region $\mathcal{B}$ of the Euclidean three-space, that defines the reference body shape of the bar in its material configuration, that middle surface is denoted by $\mathcal{S}$, which defined the middle surface of the bar, see Figure 2.2.1. It is assumed that $\mathcal{S}$ is generated by the translation, along a straight line segment of length L, of a smoothly varying planar open curve $\mathcal{L}_{x_1}$. Thus a Cartesian frame of reference with corresponding orthonormal basis $\{\boldsymbol{e}_1, \boldsymbol{e}_2, \boldsymbol{e}_3\}$ is defined, so that $\boldsymbol{e}_1$ should be parallel to the straight line segment used to generate $\mathcal{S}$. Hence, I assumed that the length L is much larger with respect to the length of any curve of the family $\mathcal{L}_{x_1}$, which in turn, are much larger than its thickness.

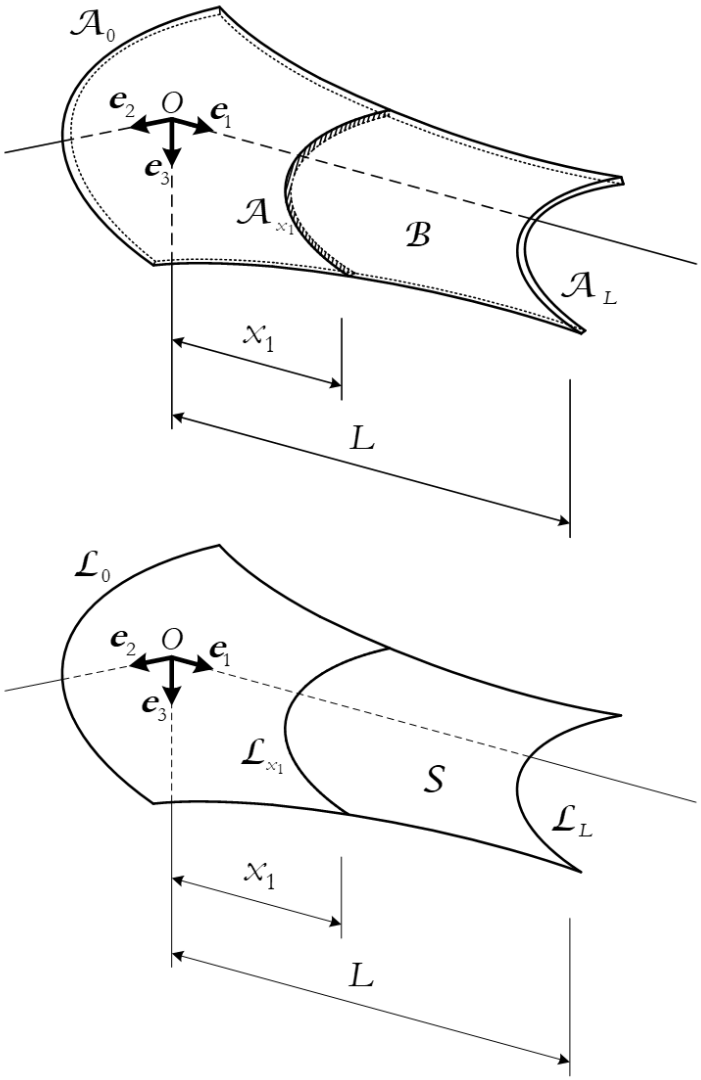

Figure 2.2.1: Reference body shape $\mathcal{B}$ of a tapered thin-walled bar with open cross-sections and its middle surface $\mathcal{S}$, adapted from Andrade (2013) [p. 24]

The intersection of S and the plane orthogonal to $\boldsymbol{e}_1$ at a distance x_1 from O is denoted by $\mathcal{L}_{x_1}$ and is identified with a cross-section middle line ($0 \le x_1 \le L$). The corresponding cross-section, $\mathcal{A}_{x_1}$, is obtained by cutting $\mathcal{B}$ perpendicular to S through $\mathcal{L}_{x_1}$.

2.2.2 The parametrisation of S

The reference shape S of the middle surface of the bar is unambiguously described by a parametrisation F with the following features:

(i) Its domain $\bar{\Omega}$ is a subset of $\mathbb{R}^2$ of the form

$$\bar{\Omega} = \left\{ (\theta^1, \theta^2) \in \mathbb{R}^2 \,\middle|\, 0 \le \theta^1 \le L \text{ and } g_1(\theta^1) \le \theta^2 \le g_2(\theta^1) \right\} \tag{2.2.1}$$

where g_1 and g_2 are real-valued functions on $[0, L]$ satisfying the conditions $g_1(\theta^1) < g_2(\theta^1)$ and $0 \in \left[g_1(\theta^1), g_2(\theta^1) \right]$ for every $\theta^1 \in [0, L]$.

(ii) For fixed $\theta^1 \in [0, L]$, the partial function $\theta^2 \mapsto F(\theta^1, \theta^2)$, defined on the interval $\left[g_1(\theta^1), g_2(\theta^1) \right]$, is an arc-length parametrisation of $\mathcal{L}_{\theta^1}$, see Figure 2.2.2.

Therefore, for each material point $\bar{x}$ on the middle surface S, there exists a unique ordered pair $(\theta^1, \theta^2) \in \bar{\Omega}$ and vice versa, i.e., $F(\theta^1, \theta^2)$ is an injective parametrisation, where the real numbers θ^1 and θ^2 are called the Gaussian coordinates of S in the parametrisation F (Neutsch 1996) [p. 29].

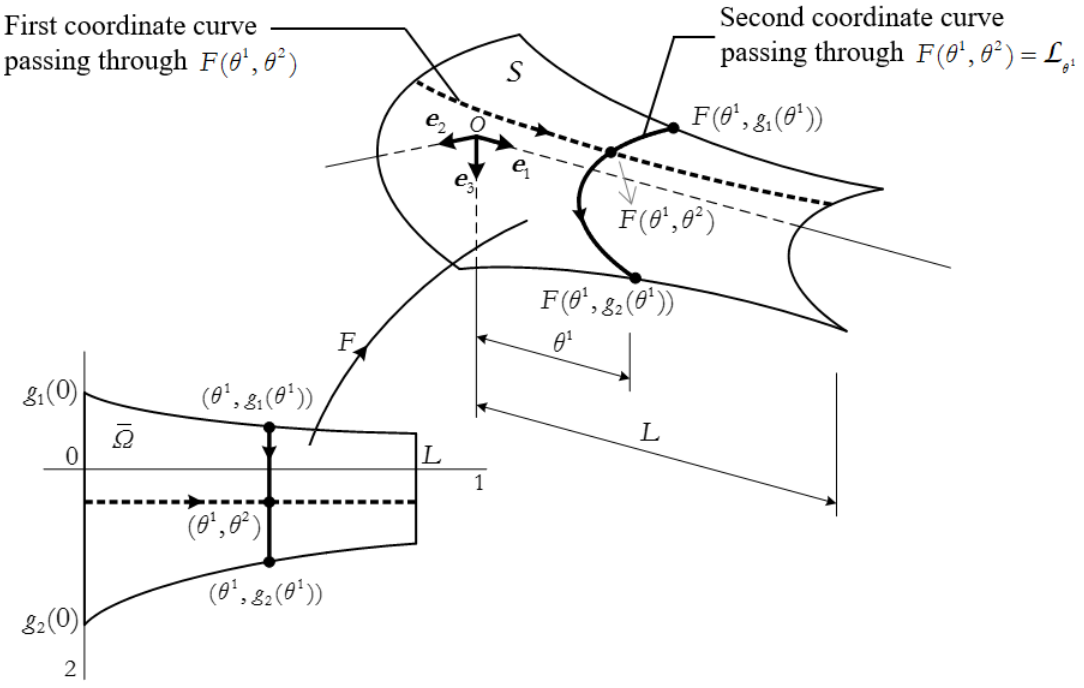

Figure 2.2.2: Parametrisation of S, adapted from Andrade (2013) [p. 26]

The first Gaussian coordinate θ^1 identifies the cross-section middle line to which the point belongs, while θ^2 locates the point on that middle line. The Cartesian coordinates of the position vector $\bar{\boldsymbol{x}}(\theta^1, \theta^2) \in S$, regarded as functions of the Gaussian coordinates, are denoted with an over-bar:

$$\bar{x}_i = \bar{x}_i(\theta^1, \theta^2) \ . \tag{2.2.2}$$

In particular, $\bar{x}_1 = \theta^1$. Above parametrisation, is not sufficiently general to include complex cross-section shapes, e.g., I-section bars. Nevertheless, it allows us to develop the equations in their simplest possible terms, so that irregular middle surface can be defined by the union of several simple regions, each defined by a smooth parametrisation.

2.2.3 The tangent planes to S and the covariant base vectors

For each $(\theta^1, \theta^2) \in \bar{\Omega}$, the vectors:

$$\boldsymbol{a}_\alpha(\theta^1, \theta^2) = D_\alpha \, F(\theta^1, \theta^2) \tag{2.2.3}$$

span the tangent plane to S at the position $\bar{\boldsymbol{x}}(\theta^1, \theta^2)$, denoted by $T_{F(\theta^1, \theta^2)}S$. In view of our choice of parametrisation, $\boldsymbol{a}_2(\theta^1, \theta^2)$ is a unit vector tangent to $\mathcal{L}_{\theta^1}$ at $F(\theta^1, \theta^2)$. In terms of the ordered basis $\boldsymbol{e}_i$, the covariant base vectors are given by [4]

$$\boldsymbol{a}_\alpha(\theta^1, \theta^2) = D_\alpha \, \bar{x}_i(\theta^1, \theta^2) \, \boldsymbol{e}_i \ . \tag{2.2.4}$$

For our specific choice of parametrisation, I have $\bar{x}_1(\theta^1, \theta^2) = \theta^1, \forall (\theta^1, \theta^2) \in \bar{\Omega}$. Hence the preceding equation specialises into

$$\boldsymbol{a}_1(\theta^1, \theta^2) = \boldsymbol{e}_1 + D_1 \, \bar{x}_2(\theta^1, \theta^2) \, \boldsymbol{e}_2 + D_1 \, \bar{x}_3(\theta^1, \theta^2) \, \boldsymbol{e}_3 \tag{2.2.5}$$

$$\boldsymbol{a}_2(\theta^1, \theta^2) = D_2 \, \bar{x}_2(\theta^1, \theta^2) \, \boldsymbol{e}_2 + D_2 \, \bar{x}_3(\theta^1, \theta^2) \, \boldsymbol{e}_3 \ . \tag{2.2.6}$$

To each position vector $\bar{\boldsymbol{x}}(\theta^1, \theta^2)$, it is possible assign a unit vector $\boldsymbol{a}_3(\theta^1, \theta^2)$ orthogonal to $T_{F(\theta^1, \theta^2)}S$ (see Figure 2.2.3) by setting

$$\boldsymbol{a}_3(\theta^1, \theta^2) = \frac{\boldsymbol{a}_2(\theta^1, \theta^2) \times \boldsymbol{a}_1(\theta^1, \theta^2)}{\left\| \boldsymbol{a}_2(\theta^1, \theta^2) \times \boldsymbol{a}_1(\theta^1, \theta^2) \right\|} \ . \tag{2.2.7}$$

The vectors $\{\boldsymbol{a}_1, \boldsymbol{a}_2, \boldsymbol{a}_3\}$ defined the covariant base vectors of $T_{F(\theta^1, \theta^2)}S$.

[4] The covariant basis is a generalization of the affine coordinate basis to curvilinear coordinate systems. It is called the local coordinate basis since it varies from one point to another (Grinfeld 2016) [p. 55].

2.2.4 Description of the reference body shape $\mathcal{B}$

The description through-the-thickness of the reference body shape $\mathcal{B}$ is done by mapping a continuous function $(\theta^1,\theta^2)\in\bar{\Omega}\mapsto t(\theta^1,\theta^2)\in\mathbb{R}^+$, that defines the wall thickness $t(\theta^1,\theta^2)$ at each position vector $\bar{\boldsymbol{x}}(\theta^1,\theta^2)\in S$, measured along the direction of its normal vector $\boldsymbol{a}_3(\theta^1,\theta^2)$, i.e., along the perpendicular line of the tangent plane $T_{F(\theta^1,\theta^2)}S$ of S at the point $F(\theta^1,\theta^2)$. Hence, for any material particle in the position vector $\boldsymbol{x}\in\mathcal{B}$, corresponds a unique ordered triplet $(\theta^1,\theta^2,\theta^3)\in\bar{\Omega}\times\left[-\frac{t}{2},\frac{t}{2}\right]$ such that

$$\boldsymbol{x}(\theta^1,\theta^2,\theta^3)=\bar{\boldsymbol{x}}(\theta^1,\theta^2)+\theta^3\,\boldsymbol{a}_3(\theta^1,\theta^2)\ , \tag{2.2.8}$$

where the curvilinear coordinate $\theta^3\in\left[-\frac{t}{2},\frac{t}{2}\right]$ is called the transverse variable (Ciarlet 2000) [p. 145]. Above equation is valid except for negligible inaccuracies closely the end cross-sections $\mathcal{A}_0$ and $\mathcal{A}_L$.

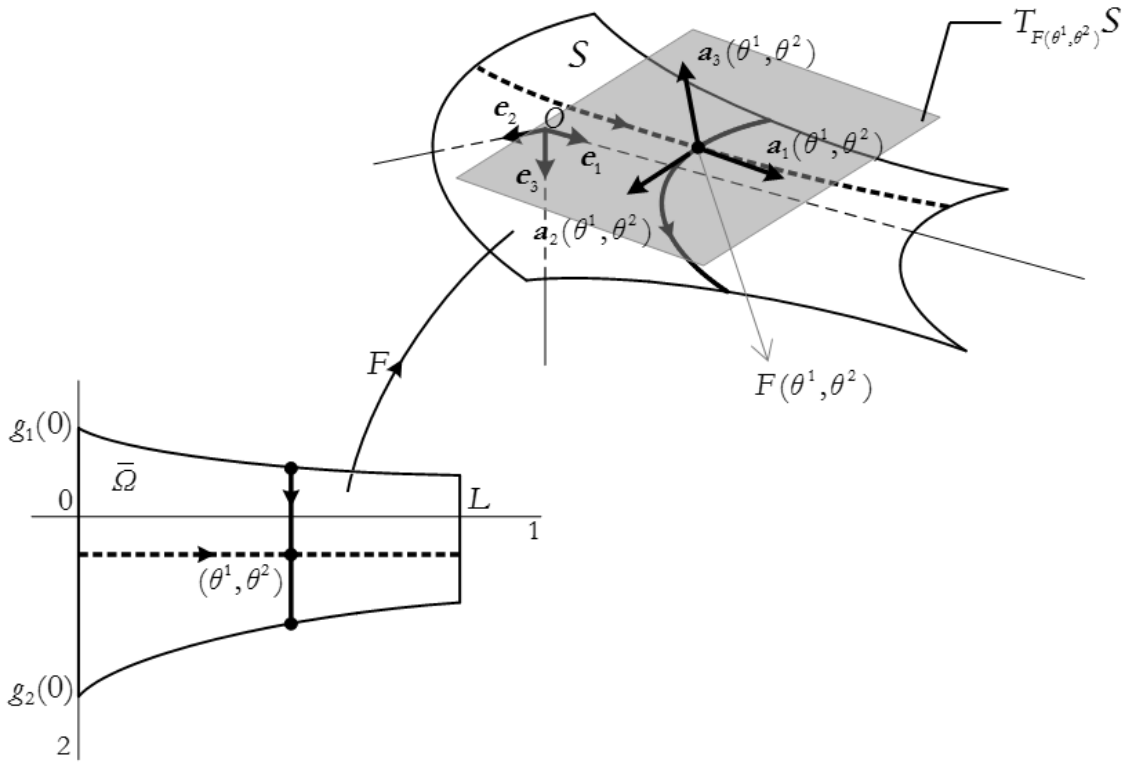

Figure 2.2.3: The tangent plane $T_{F(\theta^1,\theta^2)}S$ and the normal vector $\boldsymbol{a}_3(\theta^1,\theta^2)$ at position $F(\theta^1,\theta^2)=\bar{\boldsymbol{x}}(\theta^1,\theta^2)$, adapted from Andrade (2013) [p. 27]

2.2.5 The first fundamental form of S

The first fundamental form of S is defined by the metric coefficients $a_{\alpha\beta}$, defined by the pairwise dot products of the covariant basis vectors, e.g., Ciarlet (2000) [p. 69],

$$a_{\alpha\beta}(\theta^1,\theta^2) = \boldsymbol{a}_\alpha(\theta^1,\theta^2)\cdot\boldsymbol{a}_\beta(\theta^1,\theta^2)\ . \tag{2.2.9}$$

Specifically, in view of equations (2.2.5)-(2.2.6)

$$a_{11}(\theta^1,\theta^2) = \boldsymbol{a}_1\cdot\boldsymbol{a}_1 = 1+\left(D_1\bar{x}_2\right)^2+\left(D_1\bar{x}_3\right)^2 \tag{2.2.10}$$

$$a_{12}(\theta^1,\theta^2) = a_{21}(\theta^1,\theta^2) = \boldsymbol{a}_1\cdot\boldsymbol{a}_2 = D_1\bar{x}_2\ D_2\bar{x}_2 + D_1\bar{x}_3\ D_2\bar{x}_3 \tag{2.2.11}$$

$$a_{22}(\theta^1,\theta^2) = \boldsymbol{a}_2\cdot\boldsymbol{a}_2 = \left(D_2\bar{x}_2\right)^2+\left(D_2\bar{x}_3\right)^2 = 1\ . \tag{2.2.12}$$

Above coefficients represents the entries of a symmetric and positive definite matrix $\left[a_{\alpha\beta}(\theta^1,\theta^2)\right]$, called matrix of the Riemann metric in the coordinate system (θ^1,θ^2) (Rossmann 2003) [p. 67]. Thus, if the real-values (θ^1,θ^2) map the determinant

$$a(\theta^1,\theta^2) = \det\left[a_{\alpha\beta}(\theta^1,\theta^2)\right]\ , \tag{2.2.13}$$

i.e., $(\theta^1,\theta^2)\in\mathbb{R}^2 \mapsto a(\theta^1,\theta^2)\in\mathbb{R}$, it must satisfy $a(\theta^1,\theta^2)>0\ \ \forall\ (\theta^1,\theta^2)\in\bar{\Omega}$, where

$$a(\theta^1,\theta^2) = 1+\left(D_1\bar{x}_2(\theta^1,\theta^2)\,D_2\bar{x}_3(\theta^1,\theta^2) - D_2\bar{x}_2(\theta^1,\theta^2)\,D_1\bar{x}_3(\theta^1,\theta^2)\right)^2\ . \tag{2.2.14}$$

The first fundamental form of S, carries the complete information about any measure on the middle surface, e.g., length of curves, areas of regions etc. without referring back to the embedded space. Hence, the area element over S is given by

$$dS(\bar{\boldsymbol{x}}) = \sqrt{a(\theta^1,\theta^2)}\ d\theta^1 d\theta^2\ , \tag{2.2.15}$$

e.g., Ciarlet (2000) [p. 71]. Moreover, it proved to be

$$\sqrt{a(\theta^1,\theta^2)} = \left\|\boldsymbol{a}_2(\theta^1,\theta^2)\times\boldsymbol{a}_1(\theta^1,\theta^2)\right\|\ , \tag{2.2.16}$$

i.e., the area element over the position vector $\bar{\boldsymbol{x}}(\theta^1,\theta^2)\in S$ is locally defined by the area of the parallelogram constitutes by the vectors $\boldsymbol{a}_1$ and $\boldsymbol{a}_2$.

2.2.6 The contravariant base vectors

The contravariant basis $\boldsymbol{a}^i(\theta^1,\theta^2)$ for the reference shape $\mathcal{B}$ is defined as

$$\boldsymbol{a}^\alpha(\theta^1,\theta^2)=a^{\alpha\beta}(\theta^1,\theta^2)\boldsymbol{a}_\beta(\theta^1,\theta^2)\ , \tag{2.2.17}$$

with $\boldsymbol{a}^3(\theta^1,\theta^2)=\boldsymbol{a}_3(\theta^1,\theta^2)$, that has the property to be mutually orthonormal with the covariant basis, i.e.,

$$\boldsymbol{a}^i(\theta^1,\theta^2)\cdot\boldsymbol{a}_j(\theta^1,\theta^2)=\delta^i_j\ . \tag{2.2.18}$$

Replacing expression (2.2.17) into (2.2.18) and by definition of the metric coefficients (2.2.9), it is reduced to

$$a^{ik}(\theta^1,\theta^2)a_{kj}(\theta^1,\theta^2)=\delta^i_j\text{, with }a^{i3}=a^{3i}=a_{i3}=a_{3i}=\delta^i_3\ . \tag{2.2.19}$$

Hence, the nonzero contravariant coefficients are

$$a^{11}(\theta^1,\theta^2)=\frac{1}{a(\theta^1,\theta^2)}\ ,\qquad a^{22}(\theta^1,\theta^2)=\frac{a_{11}(\theta^1,\theta^2)}{a(\theta^1,\theta^2)} \tag{2.2.20}$$

$$a^{12}(\theta^1,\theta^2)=a^{21}(\theta^1,\theta^2)=-\frac{a_{12}(\theta^1,\theta^2)}{a(\theta^1,\theta^2)}\ ,\qquad a^{33}(\theta^1,\theta^2)=1\ , \tag{2.2.21}$$

that defined the contravariant metric tensor a^{ij} of the reference body shape $\mathcal{B}$.

2.2.7 The second fundamental form of S

The second fundamental form of S is defined by the covariant components of the curvature tensor $b_{\alpha\beta}$, is given by

$$b_{\alpha\beta}(\theta^1,\theta^2)=\boldsymbol{a}_3(\theta^1,\theta^2)\cdot D_\alpha\boldsymbol{a}_\beta(\theta^1,\theta^2)\ , \tag{2.2.22}$$

e.g., Green and Zerna (1968) [eq. 1.13.32], Danielson (1997) [eq. 8.48], Ciarlet (2000) [p. 76], Ciarlet and Larsonneur (2002) [eq. 3.1]. Whence, by using the covariant base vectors (2.2.5)-(2.2.6), I get

$$b_{11}(\theta^1,\theta^2)=\boldsymbol{a}_3(\theta^1,\theta^2)\cdot D_1\boldsymbol{a}_1(\theta^1,\theta^2)=\frac{1}{\sqrt{a}}\left[D_1^2\,\bar{x}_2D_2\bar{x}_3-D_1^2\,\bar{x}_3D_2\bar{x}_2\right] \tag{2.2.23}$$

$$b_{12}(\theta^1,\theta^2)=b_{21}(\theta^1,\theta^2)=\boldsymbol{a}_3\cdot D_1\boldsymbol{a}_2(\theta^1,\theta^2)=\frac{1}{\sqrt{a}}\left[D_1D_2\bar{x}_2D_2\bar{x}_3-D_1D_2\bar{x}_3D_2\bar{x}_2\right] \tag{2.2.24}$$

$$b_{22}(\theta^1,\theta^2)=\boldsymbol{a}_3(\theta^1,\theta^2)\cdot D_2\boldsymbol{a}_2(\theta^1,\theta^2)=\frac{1}{\sqrt{a}}\left[D_2^2\,\bar{x}_2D_2\bar{x}_3-D_2^2\,\bar{x}_3D_2\bar{x}_2\right]\ . \tag{2.2.25}$$

The coefficients $b_{\alpha\beta}$ are the projections of the second-order partial derivative of $\bar{\boldsymbol{x}}(\theta^1,\theta^2)$ onto the normal line to $T_{F(\theta^1,\theta^2)}S$ at the point $(\theta^1,\theta^2)\in\bar{\Omega}$, i.e., represent the quadratic form of $T_{F(\theta^1,\theta^2)}S$ at position $\bar{\boldsymbol{x}}(\theta^1,\theta^2)$ (Abate and Tovena 2012) [p. 189].

2.2.8 The definition of the orthonormal basis for $T_{F(\theta^1,\theta^2)}S$

The covariant and contravariant bases are local reference systems; which basis vectors are not necessarily orthogonal. Thus, to simplify the equations, the following unit vectors are defined

$$\boldsymbol{o}_{\mathrm{I}}(\theta^1,\theta^2)=\frac{1}{\sqrt{a}}\left(\boldsymbol{a}_1-a_{12}\,\boldsymbol{a}_2\right)\ , \qquad \boldsymbol{o}_{\mathrm{II}}(\theta^1,\theta^2)=\boldsymbol{a}_2\ , \tag{2.2.26}$$

e.g., Wekezer (1984) [eq. 20], with the unit vector $\boldsymbol{a}_3(\theta^1,\theta^2)$, they form an orthonormal basis for $T_{F(\theta^1,\theta^2)}S$, that has the same orientation as the covariant basis, i.e.,

$$\boldsymbol{o}_{\mathrm{II}}(\theta^1,\theta^2)\times\boldsymbol{o}_{\mathrm{I}}(\theta^1,\theta^2)=\boldsymbol{a}_3(\theta^1,\theta^2)\ . \tag{2.2.27}$$

Moreover, by doing the inner product between these two bases, I get

$$\boldsymbol{o}_{\Sigma}(\theta^1,\theta^2)=C_{\Sigma}^{\ \alpha}(\theta^1,\theta^2)\,\boldsymbol{a}_{\alpha}(\theta^1,\theta^2)\ , \tag{2.2.28}$$

with

$$C_{\mathrm{I}}^{\ 1}(\theta^1,\theta^2)=\frac{1}{\sqrt{a(\theta^1,\theta^2)}}\ , \qquad C_{\mathrm{I}}^{\ 2}(\theta^1,\theta^2)=-\frac{a_{12}(\theta^1,\theta^2)}{\sqrt{a(\theta^1,\theta^2)}}\ , \tag{2.2.29}$$

$$C_{\mathrm{II}}^{\ 1}(\theta^1,\theta^2)=0\ , \qquad C_{\mathrm{II}}^{\ 2}(\theta^1,\theta^2)=1\ . \tag{2.2.30}$$

I am keeping Andrade's notation convention (Andrade 2013) [eq. 2.2.26]. Thus, to distinguish the orthonormal basis to the other bases, e.g., covariant or contravariant, I employ upper-case Greek letters and Roman numerals for the down indices. Einstein summation convention applies as usual, to twice-repeated upper-case indices. As with vectors, the covariant components of a second-order tensor $\vartheta_{\alpha\beta}(\theta^1,\theta^2)$, are related to the orthonormal basis components $\vartheta_{\Sigma\Lambda}(\theta^1,\theta^2)$ via

$$\vartheta_{\Sigma\Lambda}(\theta^1,\theta^2)=C_{\Sigma}^{\ \alpha}(\theta^1,\theta^2)C_{\Lambda}^{\ \beta}(\theta^1,\theta^2)\,\vartheta_{\alpha\beta}(\theta^1,\theta^2)\ , \tag{2.2.31}$$

e.g., Jeevanjee (2016) [pp. 57-59]. Notice how well the Einstein summation convention and the upper-case Greek letters work together in the contraction of the covariant indices.

2.3 KINEMATICS

The term kinematics refers to the description of motion and deformation (of the structural member) independent of the action that causes it. In the case of tapered thin-walled bar with open cross-sections, it is described as a constraint shell, whose middle surface S is subjected to the following internal constraints (i.e., Andrade 2013) [p. 32] :

(V1) *Each cross-section middle line* $\mathcal{L}_{\theta^1}$ *does not deform in its own plane.*[5]

(V2) *On the middle surface of the bar, the linearized shear strain* $\gamma_{\mathrm{I}\cdot\mathrm{II}} = \gamma_{\mathrm{II}\cdot\mathrm{I}}$ *with respect to the orthonormal basis field* $\{\boldsymbol{o}_{\mathrm{I}}(\theta^1,\theta^2), \boldsymbol{o}_{\mathrm{II}}(\theta^1,\theta^2)\}$ *vanishes.*

These internal constraints are an extension to the tapered case of the original hypotheses of the classical theory of Vlasov (1961) [p. 7]. The constraint (V1) in particular, precludes any consideration of local-distortional phenomena. Its reasonableness depends, among other factors, on the wall thickness, the geometry of the middle line, the loading and support conditions and the possible existence of stiffeners or diaphragms. Furthermore, a third constraint (V3) is added, corresponding with the classical assumption of Kirchhoff-Love hypothesis for the theory of flexible shells[6] :

(V3) *Any material vector initially normal to* S *remains normal to the middle surface during the deformation process, preserving its original length.*

The internal constraints (V1)-(V3) can be defined alternatively as holonomic-scleronomic constraints, equivalent to the motion of a rigid body,[7] see equations (2.3.15)-(2.3.18), e.g., Ray and Shamanna (2006) [eq. 1], Pars (1964) [eq. 1.6.1], Greenwood (1977) [eq. 1.26].

---

[5] In fact, this constraint is required to hold only to within the first order in the linear model considered in this chapter – the implication is that it is actually the projection of the cross-section middle line on its original plane that remains undeformed.

[6] Kirchhoff formulated his famous hypothesis on the laws of plate deformation that extend Bernoulli's assumption for bending of a prismatic beam. Since Kirchhoff's hypothesis was extended by Love to shell theory, it is often called the Kirchhoff-Love hypothesis (Lebedev 2010) [p. 249].

[7] The distance between any two given points of a rigid body remains constant in time regardless of external forces exerted on it (Tarasov 2010) [§ 3]. So, I can use the properties of a rigid body, if all the particles (of the shell) maintain the same distance (resp. rotations) relative to each other in relation to specific projections (resp. directions) during motion, e.g., (V1) represents a rigid cross-section middle line on its projection to its original plane, (V2) is equivalent to a rigid-shear membrane and (V3) is the motion of rigid lines, with normal directions to the middle surface.

The next step is to examine which displacement field of the middle surface, i.e., the displacement of the material points whose reference positions are $\bar{\boldsymbol{x}}(\theta^1,\theta^2)\in S$, satisfy the restriction (V1). Hence, the family of infinitesimal displacements of an arbitrary cross-section middle line $\mathcal{L}_{\theta^1}$, that is, the restriction to $\{\theta^1\}\times[g_1(\theta^1),g_2(\theta^1)]$, admits the representation

$$\boldsymbol{W}(\theta^1)+\boldsymbol{\Phi}(\theta^1)\times\left(\bar{x}_2(\theta^1,\theta^2)\,\boldsymbol{e}_2+\bar{x}_3(\theta^1,\theta^2)\,\boldsymbol{e}_3\right)\,, \tag{2.3.1}$$

e.g., Gurtin (1981) [p. 69], Goldstein et al. (2014) [p. 171] or Pandrea and Stănescu (2016) [eq. 2.5]. Where the vectors $\boldsymbol{W}(\theta^1)=W_i(\theta^1)\,\boldsymbol{e}_i$ and $\boldsymbol{\Phi}(\theta^1)=\Phi_i(\theta^1)\,\boldsymbol{e}_i$ are the translation and the infinitesimal rotation vector respectively. In this model, I must to incorporate an extra term, corresponding to the out-of-plane warping displacement, that is normal to the plane of the rotated middle line, i.e., along the direction $\boldsymbol{e}_1+\boldsymbol{\Phi}(\theta^1)\times\boldsymbol{e}_1$ (Simo and Vu-Quoc 1991) [eq. 7], that upon retaining only first-order terms, reduces to $\zeta(\theta^1,\theta^2)\,\boldsymbol{e}_1$ (Atanackovic 1997) [eq. 1.1.13]. Hence, the displacement field $\bar{\boldsymbol{U}}:\bar{\Omega}\to\mathbb{R}^3$ of $\bar{\boldsymbol{x}}(\theta^1,\theta^2)\in S$ is written by

$$\bar{\boldsymbol{U}}(\theta^1,\theta^2)=\boldsymbol{W}(\theta^1)+\boldsymbol{\Phi}(\theta^1)\times\left(\bar{x}_2(\theta^1,\theta^2)\,\boldsymbol{e}_2+\bar{x}_3(\theta^1,\theta^2)\,\boldsymbol{e}_3\right)+\zeta(\theta^1,\theta^2)\,\boldsymbol{e}_1\,. \tag{2.3.2}$$

In terms of the Cartesian components, i.e., $\bar{U}_i(\theta^1,\theta^2)=\bar{\boldsymbol{U}}.\,\boldsymbol{e}_i$,

$$\bar{U}_1(\theta^1,\theta^2)=W_1(\theta^1)+\bar{x}_3(\theta^1,\theta^2)\Phi_2(\theta^1)-\bar{x}_2(\theta^1,\theta^2)\Phi_3(\theta^1)+\zeta(\theta^1,\theta^2) \tag{2.3.3}$$

$$\bar{U}_2(\theta^1,\theta^2)=W_2(\theta^1)-\bar{x}_3(\theta^1,\theta^2)\,\Phi_1(\theta^1) \tag{2.3.4}$$

$$\bar{U}_3(\theta^1,\theta^2)=W_3(\theta^1)+\bar{x}_2(\theta^1,\theta^2)\,\Phi_1(\theta^1)\,. \tag{2.3.5}$$

In the equation (2.3.3) for the displacement component along $\boldsymbol{e}_1$, the sum $W_1(\theta^1)+\zeta(\theta^1,\theta^2)$ is well-defined, but the individual terms $W_1(\theta^1)$ and $\zeta(\theta^1,\theta^2)$ are not, therefore, for definiteness, the following condition is appended (Andrade 2013) [eq. 2.3.7]

$$\zeta(\theta^1,0)=0,\ \forall\theta^1\in[0,L]\,. \tag{2.3.6}$$

The transition between the undeformed middle surface $\bar{\boldsymbol{x}}\in S$ (resp. $\boldsymbol{x}\in\mathcal{B}$ with Cartesian basis $\boldsymbol{e}_i$) and its deformed configuration $\bar{\boldsymbol{\chi}}\in s$ (resp. $\boldsymbol{\chi}\in\mathcal{b}$ with Cartesian basis $\boldsymbol{E}_i$), results in the displacement field (2.3.2). Hence

$$\bar{\boldsymbol{\chi}}(\theta^1,\theta^2)=\bar{\boldsymbol{U}}(\theta^1,\theta^2)+\bar{\boldsymbol{x}}(\theta^1,\theta^2)\,. \tag{2.3.7}$$

For convenience, the spatial basis $\boldsymbol{E}_i$ is chosen to be identical with the material configuration, see Figure 2.3.1.

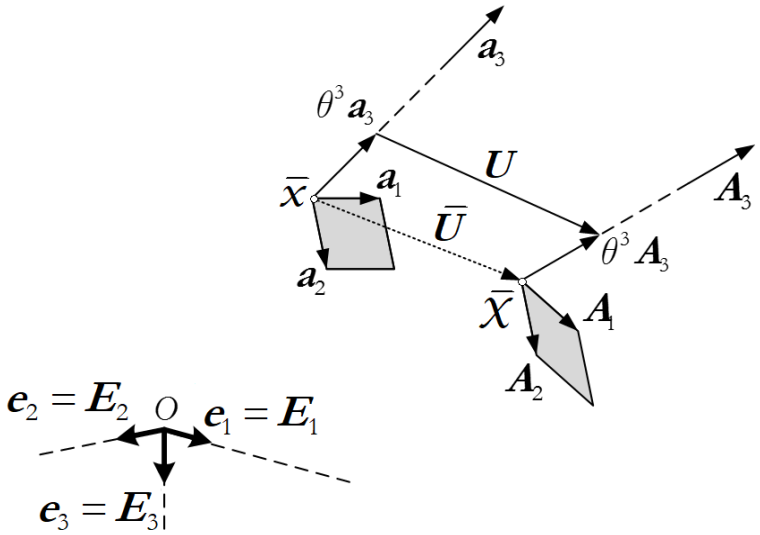

Figure 2.3.1: General motion of the deformable shell

Moreover, the vectors and tensor components at the spatial configuration are described by upper-case letters of their corresponding material counterpart, e.g., the Cartesian components of the spatial position vector $\bar{\boldsymbol{X}}(\theta^1,\theta^2)\in \mathcal{S}$, is written as

$$\bar{X}_i = \bar{X}_i(\theta^1,\theta^2)\ . \tag{2.3.8}$$

Analogous to equation (2.2.9), the first fundamental form of the deform middle surface $\mathcal{S}$ is describe by the spatial metric, defined by the covariant components $\mathcal{A}_{\alpha\beta}$, equal to

$$\mathcal{A}_{\alpha\beta}(\theta^1,\theta^2) = \boldsymbol{A}_\alpha(\theta^1,\theta^2)\cdot\boldsymbol{A}_\beta(\theta^1,\theta^2)\ , \tag{2.3.9}$$

where the spatial covariant vectors $\left\{\boldsymbol{A}_1(\theta^1,\theta^2),\boldsymbol{A}_2(\theta^1,\theta^2),\boldsymbol{A}_3(\theta^1,\theta^2)\right\}$ are given by

$$\boldsymbol{A}_\alpha(\theta^1,\theta^2) = D_\alpha\,\bar{X}_i(\theta^1,\theta^2)\,\boldsymbol{E}_i\ , \tag{2.3.10}$$

with the orthonormal vector $\boldsymbol{A}_3(\theta^1,\theta^2)$ be unambiguously gotten via

$$\boldsymbol{A}_3(\theta^1,\theta^2) = \frac{\boldsymbol{A}_2(\theta^1,\theta^2)\times\boldsymbol{A}_1(\theta^1,\theta^2)}{\left\|\boldsymbol{A}_2(\theta^1,\theta^2)\times\boldsymbol{A}_1(\theta^1,\theta^2)\right\|}\ , \tag{2.3.11}$$

and the orthonormal basis for $T_{F(\theta^1,\theta^2)}\mathcal{S}$ defined as

$$\boldsymbol{O}_{\mathrm{II}}(\theta^1,\theta^2) = \boldsymbol{A}_2\ , \qquad \boldsymbol{O}_{\mathrm{I}}(\theta^1,\theta^2) = \boldsymbol{A}_3(\theta^1,\theta^2)\times\boldsymbol{O}_{\mathrm{II}}(\theta^1,\theta^2)\ . \tag{2.3.12}$$

In the same way, the second fundamental form of $\mathcal{S}$ is defined by the spatial curvature tensor, with covariant components $B_{\alpha\beta}$, see equation (2.2.22), defined as

$$B_{\alpha\beta}(\theta^1,\theta^2) = \boldsymbol{A}_3(\theta^1,\theta^2)\cdot D_\alpha\boldsymbol{A}_\beta(\theta^1,\theta^2)\ . \tag{2.3.13}$$

The motion of the continuum shell, is characterize as the transition between the undeformed to the deformed configuration (see Figure 2.3.1), resulting in the displacement field of any material point $\mathcal{X} \in \mathcal{B}$ uniquely defined by the mapping $\boldsymbol{U} : \bar{\Omega} \times \left[-\frac{t}{2}, \frac{t}{2}\right] \to \mathbb{R}^3$. It is natural to likewise invoke the kinematic constraint (V3) so that

$$\boldsymbol{U}(\theta^1, \theta^2, \theta^3) = \bar{\boldsymbol{U}}(\theta^1, \theta^2) + \theta^3 \left[\boldsymbol{A}_3(\theta^1, \theta^2) - \boldsymbol{a}_3(\theta^1, \theta^2) \right]^{linear} , \tag{2.3.14}$$

i.e., the linearized change of the orthonormal vectors at the position $F(\theta^1, \theta^2)$, allow us to complete the kinematic description $(\theta^1, \theta^2, \theta^3) \in \bar{\Omega} \times \left[-\frac{t}{2}, \frac{t}{2}\right] \mapsto \boldsymbol{U}(\theta^1, \theta^2, \theta^3) \in \mathbb{R}^3$. Therefore, the internal constraints (V1)-(V3) can be defined alternatively as the following holonomic-scleronomic constraints:

(V1) *Rigid cross-section middle line on its projection to its original plane*

$$\left\| \left(\boldsymbol{e}_2 \otimes \boldsymbol{e}_2 + \boldsymbol{e}_3 \otimes \boldsymbol{e}_3 \right) \left(\bar{\boldsymbol{X}}(\theta^1, \theta^2 + \Delta\theta^2) - \bar{\boldsymbol{X}}(\theta^1, \theta^2) \right) \right\| = \left\| \bar{\boldsymbol{x}}(\theta^1, \theta^2 + \Delta\theta^2) - \bar{\boldsymbol{x}}(\theta^1, \theta^2) \right\| . \tag{2.3.15}$$

(V2) *Rigid shear membrane*

$$\boldsymbol{O}_{\mathrm{I}}(\theta^1, \theta^2) \cdot \boldsymbol{O}_{\mathrm{II}}(\theta^1, \theta^2) = 0 . \tag{2.3.16}$$

(V3) *Rigid normal lines with respect to the middle surface*

$$\left\| \boldsymbol{A}_3(\theta^1, \theta^2) \right\| = 1 , \tag{2.3.17}$$

$$\left(\boldsymbol{O}_{\mathrm{I}}(\theta^1, \theta^2) \otimes \boldsymbol{O}_{\mathrm{II}}(\theta^1, \theta^2) + \boldsymbol{O}_{\mathrm{II}}(\theta^1, \theta^2) \otimes \boldsymbol{O}_{\mathrm{I}}(\theta^1, \theta^2) \right) \boldsymbol{A}_3(\theta^1, \theta^2) = \boldsymbol{0} . \tag{2.3.18}$$

To summarize, equations (2.3.7)-(2.3.14) aim to clarify the procedure to measure the deformation of the constraint shell associated to the admissible displacement field, quantified by the (linearized) change of the metric tensor, i.e., equations (2.2.9) & (2.3.9) , and the change of the curvature tensor associated with equations (2.2.22) & (2.3.13).

2.3.1 Membrane strain tensor

Let $\boldsymbol{\gamma}$ denote the linearized membrane strain tensor field (or linearized change of metric tensor field) defined by

$$\gamma_{\alpha\beta}(\theta^1, \theta^2) = \frac{1}{2} \left[A_{\alpha\beta}(\theta^1, \theta^2) - a_{\alpha\beta}(\theta^1, \theta^2) \right]^{linear} , \tag{2.3.19}$$

e.g., Green and Zerna (1968) [eq. 2.1.22], Ciarlet (2000) [p. 91].

Keeping only the linear terms, I get

$$\gamma_{\alpha\beta}(\theta^1,\theta^2)=\frac{1}{2}\left(\boldsymbol{a}_\alpha(\theta^1,\theta^2)\cdot D_\beta\bar{\boldsymbol{U}}(\theta^1,\theta^2)+\boldsymbol{a}_\beta(\theta^1,\theta^2)\cdot D_\alpha\bar{\boldsymbol{U}}(\theta^1,\theta^2)\right)\ . \tag{2.3.20}$$

Replacing equation (2.2.4) and (2.3.2) into the membrane strain tensor, yield to

$$\begin{aligned}\gamma_{11}(\theta^1,\theta^2)=&D_1\bar{U}_1(\theta^1,\theta^2)+D_1\bar{x}_2(\theta^1,\theta^2)\left(W_2'(\theta^1)-\bar{x}_3(\theta^1,\theta^2)\Phi_1'(\theta^1)\right)\\&+D_1\bar{x}_3(\theta^1,\theta^2)\left(W_3'(\theta^1)+\bar{x}_2(\theta^1,\theta^2)\Phi_1'(\theta^1)\right)\end{aligned} \tag{2.3.21}$$

$$\begin{aligned}\gamma_{12}(\theta^1,\theta^2)=\gamma_{21}(\theta^1,\theta^2)=\frac{1}{2}\Big[&D_2\bar{U}_1(\theta^1,\theta^2)+D_2\bar{x}_2(\theta^1,\theta^2)\left(W_2'(\theta^1)-\bar{x}_3(\theta^1,\theta^2)\Phi_1'(\theta^1)\right)\\&+D_2\bar{x}_3(\theta^1,\theta^2)\left(W_3'(\theta^1)+\bar{x}_2(\theta^1,\theta^2)\Phi_1'(\theta^1)\right)\Big]\end{aligned} \tag{2.3.22}$$

$$\gamma_{22}(\theta^1,\theta^2)=0\ . \tag{2.3.23}$$

The constraint (V2) requires that $\gamma_{\mathrm{I\cdot II}}(\theta^1,\theta^2)=\gamma_{\mathrm{II\cdot I}}(\theta^1,\theta^2)=0$. So that, by using the transformation law (2.2.31), it is found that such requirement is equivalent to satisfy $\gamma_{12}(\theta^1,\theta^2)=\gamma_{21}(\theta^1,\theta^2)=0,\ \forall(\theta^1,\theta^2)\in\bar{\Omega}$. Therefore, equation (2.3.22) is equal to

$$\begin{aligned}D_2\bar{U}_1(\theta^1,\theta^2)=&-D_2\bar{x}_2(\theta^1,\theta^2)\left(W_2'(\theta^1)-\bar{x}_3(\theta^1,\theta^2)\Phi_1'(\theta^1)\right)\\&-D_2\bar{x}_3(\theta^1,\theta^2)\left(W_3'(\theta^1)+\bar{x}_2(\theta^1,\theta^2)\Phi_1'(\theta^1)\right)\ ,\end{aligned} \tag{2.3.24}$$

after integration with respect to the second coordinate θ^2

$$\begin{aligned}\bar{U}_1(\theta^1,\theta^2)=&\bar{U}_1(\theta^1,0)+\bar{x}_2(\theta^1,0)W_2'(\theta^1)+\bar{x}_3(\theta^1,0)W_3'(\theta^1)\\&-\bar{x}_2(\theta^1,\theta^2)W_2'(\theta^1)-\bar{x}_3(\theta^1,\theta^2)W_3'(\theta^1)-\omega(\theta^1,\theta^2)\Phi_1'(\theta^1)\end{aligned} \tag{2.3.25}$$

with

$$\omega(\theta^1,\theta^2)=\int_0^{\theta^2}r(\theta^1,s)ds=\int_0^{\theta^2}\left(\bar{x}_2(\theta^1,s)D_2\bar{x}_3(\theta^1,s)-\bar{x}_3(\theta^1,s)D_2\bar{x}_2(\theta^1,s)\right)ds\ , \tag{2.3.26}$$

where $\omega(\theta^1,\theta^2)$ represents the sectorial coordinate,[8] defined geometrically as twice the area inside the arc-length of the curve $\mathcal{L}_{\theta^1}$ and the radial vectors between the sectorial origin $F(\theta^1,0)$ and the generic position $F(\theta^1,\theta^2)$ at $O+\theta^1\boldsymbol{e}_1$, i.e., $\theta^1\in[0,L]$ is fixed, see Figure 2.3.2. By definition, see equation (2.3.6)

$$\omega(\theta^1,0)=0\ ,\ \forall\theta^1\in[0,L]\ . \tag{2.3.27}$$

[8] The law of sectorial areas due to Vlasov (1961) [p. 16] for the longitudinal displacement $\bar{U}_1(\theta^1,\theta^2)$, remains valid. Moreover, the field $\omega:\bar{\Omega}\to\mathbb{R}$ is continuous on $\bar{\Omega}(\theta^1,\theta^2)$ with continuous partial derivative $D_1\omega(\theta^1,\theta^2)$.

Moreover, the comparison of equation (2.3.3) in relation to (2.3.25), provides

$$W_1(\theta^1) = \bar{U}_1(\theta^1, 0) + \bar{x}_2(\theta^1, 0) W_2'(\theta^1) + \bar{x}_3(\theta^1, 0) W_3'(\theta^1) \tag{2.3.28}$$

$$\Phi_2(\theta^1) = -W_3'(\theta^1) \tag{2.3.29}$$

$$\Phi_3(\theta^1) = W_2'(\theta^1) \tag{2.3.30}$$

$$\zeta(\theta^1, \theta^2) = -\omega(\theta^1, \theta^2) \Phi_1'(\theta^1) \ . \tag{2.3.31}$$

Therefore, the first component of the displacement field is written as

$$\bar{U}_1(\theta^1, \theta^2) = W_1(\theta^1) - \bar{x}_2(\theta^1, \theta^2) W_2'(\theta^1) - \bar{x}_3(\theta^1, \theta^2) W_3'(\theta^1) - \omega(\theta^1, \theta^2) \Phi_1'(\theta^1) \ . \tag{2.3.32}$$

The family of displacements $\bar{\boldsymbol{U}} : \bar{\Omega} \to \mathbb{R}^3$ that satisfies the internal constraint (V1), i.e., equation (2.3.2) with equations (2.3.28)-(2.3.31), have the form

$$\bar{\boldsymbol{U}}(\theta^1, \theta^2) = \boldsymbol{W}(\theta^1) + \boldsymbol{\Phi}(\theta^1) \times \left(\bar{x}_2(\theta^1, \theta^2) \boldsymbol{e}_2 + \bar{x}_3(\theta^1, \theta^2) \boldsymbol{e}_3 \right) - \omega(\theta^1, \theta^2) \Phi_1'(\theta^1) \boldsymbol{e}_1 \tag{2.3.33}$$

$$\boldsymbol{W}(\theta^1) = W_i(\theta^1) \boldsymbol{e}_i \tag{2.3.34}$$

$$\boldsymbol{\Phi}(\theta^1) = \Phi_1(\theta^1) \boldsymbol{e}_1 - W_3'(\theta^1) \boldsymbol{e}_2 + W_2'(\theta^1) \boldsymbol{e}_3 \ , \tag{2.3.35}$$

with (i) $W_1(\theta^1)$ continuously differentiable on $\theta^1 \in [0, L]$ and (ii) $W_2(\theta^1)$, $W_3(\theta^1)$ and $\Phi_1(\theta^1)$ twice continuously differentiable on the same interval, see equations (2.3.39)-(2.3.43). In the same way, the admissible displacement field $\boldsymbol{U} : \bar{\Omega} \times \left[-\frac{t}{2}, \frac{t}{2} \right] \to \mathbb{R}^3$ of any material point $\boldsymbol{\chi} \in \mathcal{B}$, i.e., equation (2.3.14), after routine calculations, yields to

$$\boldsymbol{U}(\theta^1, \theta^2, \theta^3) = \boldsymbol{W}(\theta^1) + \boldsymbol{\Phi}(\theta^1) \times \left[\left(\bar{x}_2 + \frac{\theta^3 D_2 \bar{x}_3}{\sqrt{a(\theta^1, \theta^2)}} \right) \boldsymbol{e}_2 + \left(\bar{x}_3 - \frac{\theta^3 D_2 \bar{x}_2}{\sqrt{a(\theta^1, \theta^2)}} \right) \boldsymbol{e}_3 \right]$$

$$- \left(\omega(\theta^1, \theta^2) - \frac{\theta^3 q(\theta^1, \theta^2)}{\sqrt{a(\theta^1, \theta^2)}} \right) \Phi_1'(\theta^1) \boldsymbol{e}_1 \ . \tag{2.3.36}$$

The variable $q(\theta^1, \theta^2)$, see Figure 2.3.2, is the projection of the position vector $\bar{\boldsymbol{x}}(\theta^1, \theta^2) \in S$ over the direction $\boldsymbol{a}_2(\theta^1, \theta^2)$ at $O + \theta^1 \boldsymbol{e}_1$, i.e.,

$$q(\theta^1, \theta^2) = \bar{\boldsymbol{x}}(\theta^1, \theta^2) \cdot \boldsymbol{a}_2(\theta^1, \theta^2) = \bar{x}_2 D_2 \bar{x}_2 + \bar{x}_3 D_2 \bar{x}_3 \ . \tag{2.3.37}$$

Equation (2.3.36) can be interpreted as an infinitesimal rigid displacement of the material point $\boldsymbol{\chi} \in \mathcal{B}$ with the addition of the out-of-plane warping displacement due to the middle surface and the influence of the thickness warping, they are often called them, the contour warping and the secondary warping respectively (Attard and Lawther 1989).

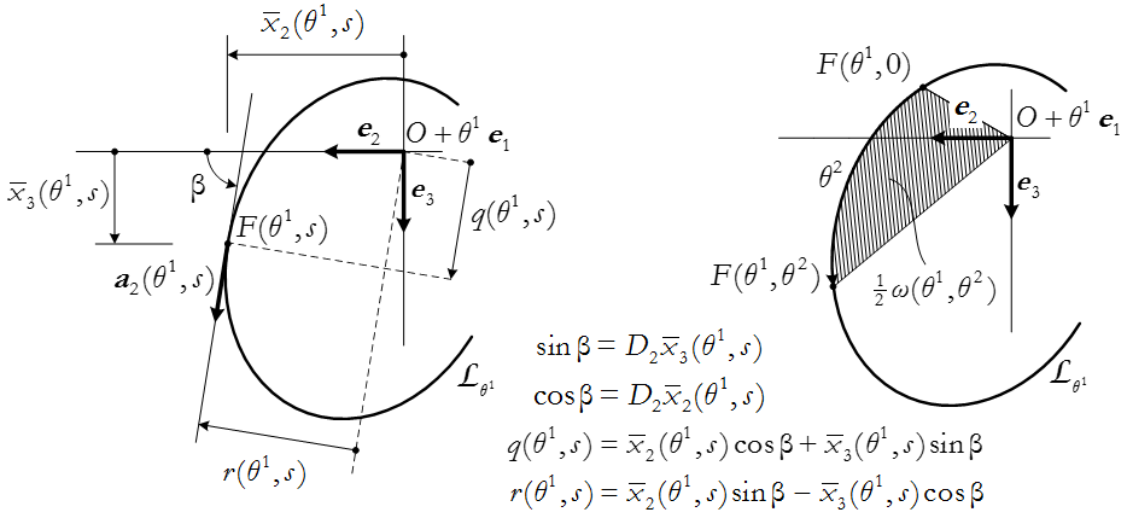

Figure 2.3.2: Geometrical interpretation of $q(\theta^1,\theta^2)$ and $\omega(\theta^1,\theta^2)$, adapted from Andrade (2013) [p. 35]

Summarizing, with respect to the orthonormal basis field $(\theta^1,\theta^2)\in\bar{\Omega}\mapsto\{\boldsymbol{o}_{\mathrm{I}},\boldsymbol{o}_{\mathrm{II}}\}$, there is but one non-vanishing linearized membrane strain component corresponding to

$$\gamma_{\mathrm{I\cdot I}}=\frac{1}{a}\left(\varepsilon+\bar{x}_2\,\kappa_3+\bar{x}_3\,\kappa_2+\omega\,\Gamma+\psi\,\kappa_1\right)\,, \tag{2.3.38}$$

where the generalised strains are defined by

$$\varepsilon(\theta^1)=W_1'(\theta^1) \tag{2.3.39}$$

$$\kappa_1(\theta^1)=\Phi_1'(\theta^1) \tag{2.3.40}$$

$$\kappa_2(\theta^1)=-W_3''(\theta^1) \tag{2.3.41}$$

$$\kappa_3(\theta^1)=-W_2''(\theta^1) \tag{2.3.42}$$

$$\Gamma(\theta^1)=-\Phi_1''(\theta^1)\,. \tag{2.3.43}$$

This is why the set of components of the translation vector $W_i(\theta^1)$ and the twist rotation $\Phi_1(\theta^1)$ are collectively named the generalised displacements, defined as the mappings $W_i,\Phi_1:[0,L]\to\mathbb{R}$. Finally, the variable

$$\psi(\theta^1,\theta^2)=\bar{x}_2(\theta^1,\theta^2)\,D_1\bar{x}_3(\theta^1,\theta^2)-\bar{x}_3(\theta^1,\theta^2)\,D_1\bar{x}_2(\theta^1,\theta^2)-D_1\omega(\theta^1,\theta^2)\,, \tag{2.3.44}$$

defined the taper function $(\theta^1,\theta^2)\in\bar{\Omega}\mapsto\psi(\theta^1,\theta^2)\in\mathbb{R}$, having the geometrically components relative to the non-standard stiffness terms peculiar to the tapered geometry, that the piecewise prismatic approach is not able to modelled.

Furthermore, since the taper function $\psi : \bar{\Omega} \to \mathbb{R}$ has a continuous real-value,[9] i.e., $\gamma_{\mathrm{I}\cdot\mathrm{I}} : \bar{\Omega} \to \mathbb{R}$, can be thought as the superposition of five basic strain modes, namely

$$\frac{1}{a}\ , \qquad \frac{\bar{x}_2}{a}\ , \qquad \frac{\bar{x}_3}{a}\ , \qquad \frac{\omega}{a}\ , \qquad \frac{\psi}{a}\ , \tag{2.3.45}$$

whose amplitudes are modulated by the generalised strains (Andrade 2013) [eq. 2.3.34].

2.3.2 Change of curvature tensor

The (linearized) change of curvature tensor $\boldsymbol{\rho}(\theta^1, \theta^2)$, associated with the admissible displacement field $\bar{\boldsymbol{U}} : \bar{\Omega} \to \mathbb{R}^3$, be defined by the covariant components $\rho_{\alpha\beta}$, given by

$$\rho_{\alpha\beta}(\theta^1, \theta^2) = \Big[B_{\alpha\beta}(\theta^1, \theta^2) - b_{\alpha\beta}(\theta^1, \theta^2) \Big]^{linear}\ , \tag{2.3.46}$$

e.g., Stumpf (1981) [eq. 2.1] or Ciarlet (2000) [p. 93]. Keeping only the linear part

$$\rho_{\alpha\beta}(\theta^1, \theta^2) = \Big[D_\alpha D_\beta \bar{\boldsymbol{U}}(\theta^1, \theta^2) - \Gamma^\sigma_{\alpha\beta} D_\sigma \bar{\boldsymbol{U}}(\theta^1, \theta^2) \Big] \cdot \boldsymbol{a}_3(\theta^1, \theta^2)\ , \tag{2.3.47}$$

i.e., Ciarlet et al. (2008). The Christoffel symbols of the second kind are defined as

$$\Gamma^\sigma_{\alpha\beta} = \boldsymbol{a}^\sigma(\theta^1, \theta^2) \cdot D_\alpha \boldsymbol{a}_\beta(\theta^1, \theta^2) = -\boldsymbol{a}_\beta(\theta^1, \theta^2) \cdot D_\alpha \boldsymbol{a}^\sigma(\theta^1, \theta^2) = \Gamma^\sigma_{\beta\alpha}\ , \tag{2.3.48}$$

e.g., Joshi (2005) [p. 282]. Replacing equations (2.2.7), (2.2.17) and (2.3.33) into (2.3.47) and neglecting the factor $\left(D_1\bar{x}_3\, D_2\bar{x}_2 - D_1\bar{x}_2\, D_2\bar{x}_3 \right)/\sqrt{a}$, that is considered very smaller than unity, I get

$$\rho_{11}(\theta^1, \theta^2) = \frac{1}{\sqrt{a}} \left(-2a_{12}\boldsymbol{\kappa}_1 + D_2\bar{x}_2\boldsymbol{\kappa}_2 - D_2\bar{x}_3\boldsymbol{\kappa}_3 + qI\Gamma \right) \tag{2.3.49}$$

$$\rho_{12}(\theta^1, \theta^2) = \rho_{21}(\theta^1, \theta^2) = -\frac{1}{\sqrt{a}}\boldsymbol{\kappa}_1\ , \qquad \rho_{22} = 0\ . \tag{2.3.50}$$

So that, by using the transformation law (2.2.31), I get the non-vanishing components with respect to the orthonormal basis field $\left\{ \boldsymbol{o}_{\mathrm{I}}(\theta^1, \theta^2), \boldsymbol{o}_{\mathrm{II}}(\theta^1, \theta^2) \right\}$, i.e.,

$$\rho_{\mathrm{I}\cdot\mathrm{I}}(\theta^1, \theta^2) = \frac{1}{a^{3/2}} \left(D_2\bar{x}_2\, \boldsymbol{\kappa}_2 - D_2\bar{x}_3\, \boldsymbol{\kappa}_3 + qI\Gamma \right) \tag{2.3.51}$$

$$\rho_{\mathrm{I}\cdot\mathrm{II}}(\theta^1, \theta^2) = \rho_{\mathrm{II}\cdot\mathrm{I}}(\theta^1, \theta^2) = \frac{\boldsymbol{\kappa}_1}{a}\ . \tag{2.3.52}$$

The sign change of equation (2.3.52) is done to be consistent with the sign convention of Figure 2.4.1, i.e., a positive $\rho_{\mathrm{I}\cdot\mathrm{II}}$ represent a twist moment in the positive direction of $\boldsymbol{o}_{\mathrm{I}}$.

[9] *Vide supra*, note 8 p. 27.

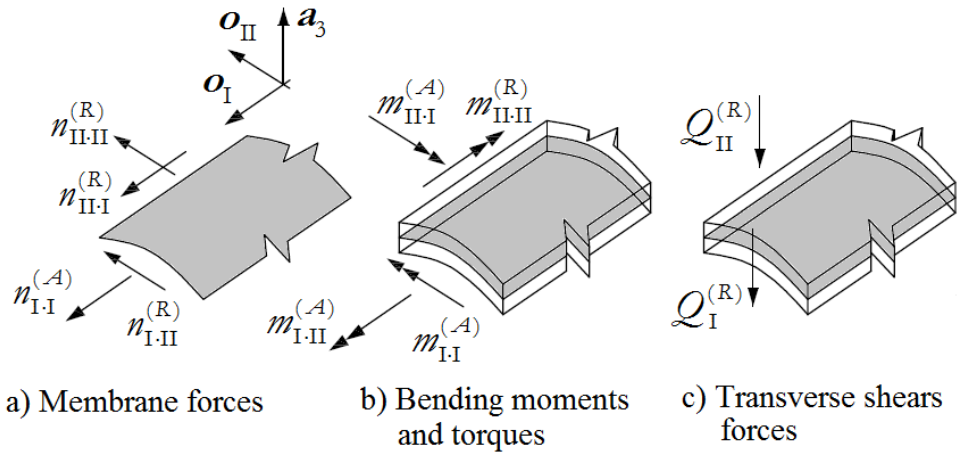

Figure 2.4.1: Shell forces, active and reactive

Furthermore, the fields $\left(\rho_{\text{I}\cdot\text{I}}, \rho_{\text{I}\cdot\text{II}} \equiv \rho_{\text{II}\cdot\text{I}}\right): \bar{\Omega} \to (\mathbb{R}, \mathbb{R})$, also can be thought as the superposition of basic curvatures modes, namely

$$\left(\frac{D_2\bar{x}_2}{a^{3/2}} \quad -\frac{D_2\bar{x}_3}{a^{3/2}} \quad \frac{q}{a^{3/2}}\right), \qquad \frac{1}{a}, \tag{2.3.53}$$

whose values are modulated by the corresponding generalised strains (2.3.40)-(2.3.43).

2.4 Membrane Forces and Shell Moments, Active and Reactive. Constitutive Equation

As we saw in the previous section, the internal constraints restrict the value at $(\theta^1, \theta^2) \in \bar{\Omega}$ of the membrane strain tensor $\boldsymbol{\gamma}$ and the change of curvature tensor $\boldsymbol{\rho}$ to lie in one or in a linear combination between the following tensor fields

$$\mathscr{C}^1(\theta^1, \theta^2) = \text{span}\left\{\boldsymbol{o}_{\text{I}}(\theta^1, \theta^2) \otimes \boldsymbol{o}_{\text{I}}(\theta^1, \theta^2)\right\} \tag{2.4.1}$$

$$\mathscr{C}^2(\theta^1, \theta^2) = \text{span}\left\{\boldsymbol{o}_{\text{II}}(\theta^1, \theta^2) \otimes \boldsymbol{o}_{\text{II}}(\theta^1, \theta^2)\right\} \tag{2.4.2}$$

$$\mathscr{C}^3(\theta^1, \theta^2) = \text{span}\left\{\boldsymbol{o}_{\text{I}}(\theta^1, \theta^2) \otimes \boldsymbol{o}_{\text{II}}(\theta^1, \theta^2) + \boldsymbol{o}_{\text{II}}(\theta^1, \theta^2) \otimes \boldsymbol{o}_{\text{I}}(\theta^1, \theta^2)\right\} . \tag{2.4.3}$$

In this way, the non-vanishing components of $\boldsymbol{\gamma}$ and $\boldsymbol{\rho}$ with respect to the orthonormal basis $\left\{\boldsymbol{o}_{\text{I}}(\theta^1, \theta^2), \boldsymbol{o}_{\text{II}}(\theta^1, \theta^2)\right\}$ are within the corresponding tensor spaces

$$\boldsymbol{\gamma} \in \mathscr{C}_\varepsilon(\theta^1, \theta^2) \text{ with } \mathscr{C}_\varepsilon(\theta^1, \theta^2) := \mathscr{C}^1(\theta^1, \theta^2) , \tag{2.4.4}$$

$$\boldsymbol{\rho} \in \mathscr{C}_\theta(\theta^1, \theta^2) \text{ with } \mathscr{C}_\theta(\theta^1, \theta^2) := \mathscr{C}^1(\theta^1, \theta^2) \oplus \mathscr{C}^3(\theta^1, \theta^2) . \tag{2.4.5}$$

The spaces $\mathscr{C}_\varepsilon(\theta^1,\theta^2)$ and $\mathscr{C}_\theta(\theta^1,\theta^2)$ define the constraint spaces of the mechanical shell due to its membrane state and its flexure state respectively. Therefore, the orthogonal complements of spaces (2.4.4)-(2.4.5) are respectively

$$\mathscr{C}_\varepsilon^\perp(\theta^1,\theta^2) := \mathscr{C}^2(\theta^1,\theta^2) \oplus \mathscr{C}^3(\theta^1,\theta^2) \tag{2.4.6}$$

$$\mathscr{C}_\theta^\perp(\theta^1,\theta^2) := \mathscr{C}^2(\theta^1,\theta^2) \ . \tag{2.4.7}$$

It follows that the values at $(\theta^1,\theta^2)\in\bar{\Omega}$ of the membrane force tensor field $\boldsymbol{n}(\theta^1,\theta^2)$ and the shell moment tensor field $\boldsymbol{m}(\theta^1,\theta^2)$ can be split into active $(\mathcal{A})$ and reactive (R) components, denoted by $\boldsymbol{n}^{(\mathcal{A})}(\theta^1,\theta^2)$, $\boldsymbol{n}^{(\mathrm{R})}(\theta^1,\theta^2)$ and $\boldsymbol{m}^{(\mathcal{A})}(\theta^1,\theta^2)$, $\boldsymbol{m}^{(\mathrm{R})}(\theta^1,\theta^2)$ respectively, so that, the active components are elements of the constraint spaces, while the reactive ones belong to the corresponding orthogonal complements, i.e.,

$$\boldsymbol{n}^{(\mathcal{A})} \in \mathscr{C}_\varepsilon \qquad\qquad \boldsymbol{n}^{(\mathrm{R})} \in \mathscr{C}_\varepsilon^\perp \tag{2.4.8}$$

$$\boldsymbol{m}^{(\mathcal{A})} \in \mathscr{C}_\theta \qquad\qquad \boldsymbol{m}^{(\mathrm{R})} \in \mathscr{C}_\theta^\perp \ . \tag{2.4.9}$$

Hence, the decomposition of the membrane force tensor and the shell moment tensor, between active and reactive components, see Figure 2.4.1, is uniquely defined by[10]

$$\boldsymbol{n}(\theta^1,\theta^2) = \boldsymbol{n}^{(\mathcal{A})}(\theta^1,\theta^2) + \boldsymbol{n}^{(\mathrm{R})}(\theta^1,\theta^2) \tag{2.4.10}$$

$$\boldsymbol{m}(\theta^1,\theta^2) = \boldsymbol{m}^{(\mathcal{A})}(\theta^1,\theta^2) + \boldsymbol{m}^{(\mathrm{R})}(\theta^1,\theta^2) \ . \tag{2.4.11}$$

[10] In fact, from (2.4.10)-(2.4.11) I can suppose that there are different combinations of elements, so that $\boldsymbol{n} = \boldsymbol{n}^{(\mathcal{A})} + \boldsymbol{n}^{(\mathrm{R})} = \boldsymbol{n}^{(\mathcal{A}*)} + \boldsymbol{n}^{(\mathrm{R}*)}$ with $\left\{\boldsymbol{n}^{(\mathcal{A})}, \boldsymbol{n}^{(\mathcal{A}*)}\right\} \in \mathscr{C}_\varepsilon$ and $\left\{\boldsymbol{n}^{(\mathrm{R})}, \boldsymbol{n}^{(\mathrm{R}*)}\right\} \in \mathscr{C}_\varepsilon^\perp$. In the same manner, $\boldsymbol{m} = \boldsymbol{m}^{(\mathcal{A})} + \boldsymbol{m}^{(\mathrm{R})} = \boldsymbol{m}^{(\mathcal{A}*)} + \boldsymbol{m}^{(\mathrm{R}*)}$ with $\left\{\boldsymbol{m}^{(\mathcal{A})}, \boldsymbol{m}^{(\mathcal{A}*)}\right\} \in \mathscr{C}_\theta$ and $\left\{\boldsymbol{m}^{(\mathrm{R})}, \boldsymbol{m}^{(\mathrm{R}*)}\right\} \in \mathscr{C}_\theta^\perp$, i.e.,

$$\left(\boldsymbol{n}^{(\mathcal{A})} - \boldsymbol{n}^{(\mathcal{A}*)}\right) \in \mathscr{C}_\varepsilon = \left(\boldsymbol{n}^{(\mathrm{R}*)} - \boldsymbol{n}^{(\mathrm{R})}\right) \in \mathscr{C}_\varepsilon^\perp$$

$$\left(\boldsymbol{m}^{(\mathcal{A})} - \boldsymbol{m}^{(\mathcal{A}*)}\right) \in \mathscr{C}_\theta = \left(\boldsymbol{m}^{(\mathrm{R}*)} - \boldsymbol{m}^{(\mathrm{R})}\right) \in \mathscr{C}_\theta^\perp \ ,$$

since $\mathscr{C}_\varepsilon \cap \mathscr{C}_\varepsilon^\perp = \{0\}$ and $\mathscr{C}_\theta \cap \mathscr{C}_\theta^\perp = \{0\}$, above decomposition is uniquely defined by

$$\boldsymbol{n}^{(\mathcal{A})} = \boldsymbol{n}^{(\mathcal{A}*)} \ , \qquad \boldsymbol{n}^{(\mathrm{R})} = \boldsymbol{n}^{(*\mathrm{R})} \ , \qquad \boldsymbol{m}^{(\mathcal{A})} = \boldsymbol{m}^{(\mathcal{A}*)} \ , \qquad \boldsymbol{m}^{(\mathrm{R})} = \boldsymbol{m}^{(*\mathrm{R})} \ .$$

I can go further and defined the operators $\mathbb{P}_\varepsilon$, $\mathbb{P}_\varepsilon^\perp$, $\mathbb{P}_\theta$ and $\mathbb{P}_\theta^\perp$, written as mapping projections of the corresponding spaces,[11] so that above equations can be rewritten as

$$\boldsymbol{n}(\theta^1,\theta^2)=\left(\mathbb{P}_\varepsilon+\mathbb{P}_\varepsilon^\perp\right)\boldsymbol{n}(\theta^1,\theta^2)=\mathbb{P}_\varepsilon\boldsymbol{n}(\theta^1,\theta^2)+\mathbb{P}_\varepsilon^\perp\boldsymbol{n}(\theta^1,\theta^2) \tag{2.4.12}$$

$$\boldsymbol{m}(\theta^1,\theta^2)=\left(\mathbb{P}_\theta+\mathbb{P}_\theta^\perp\right)\boldsymbol{m}(\theta^1,\theta^2)=\mathbb{P}_\theta\boldsymbol{m}(\theta^1,\theta^2)+\mathbb{P}_\theta^\perp\boldsymbol{m}(\theta^1,\theta^2)\ . \tag{2.4.13}$$

That means, the reactive contributions are orthogonal to their respective constraint spaces, whose roles are to maintain the kinematic constraints itself, that contribute nothing to the deformations in any admissible motion (Podio-Guidugli 1989). In the constitutive theory of linear elasticity, the membrane force tensor field $\boldsymbol{n}(\theta^1,\theta^2)$ and the shell moment tensor field $\boldsymbol{m}(\theta^1,\theta^2)$ are related to their corresponding linearized deformation tensor through linearly elastic constitutive equations of the form

$$\boldsymbol{n}(\theta^1,\theta^2)=\mathbb{S}_\varepsilon(\theta^1,\theta^2)\colon\boldsymbol{\gamma}(\theta^1,\theta^2) \tag{2.4.14}$$

$$\boldsymbol{m}(\theta^1,\theta^2)=\mathbb{S}_\theta(\theta^1,\theta^2)\colon\boldsymbol{\rho}(\theta^1,\theta^2)\ . \tag{2.4.15}$$

In above equations, $\mathbb{S}_\varepsilon(\theta^1,\theta^2)$ and $\mathbb{S}_\theta(\theta^1,\theta^2)$ are the unconstrained elasticity tensors due to the extensional and flexural rigidity respectively. When the internal constraints are imposed, e.g., Pipkin (1976), they need a careful reformulation in order to be compatible with the constrained spaces $\mathscr{C}_\varepsilon(\theta^1,\theta^2)$ and $\mathscr{C}_\theta(\theta^1,\theta^2)$, where the non-vanishing deformations are defined. The classical way to solve the problem is by applying the respective projection operator $\mathbb{P}_\varepsilon$ and $\mathbb{P}_\theta$ at both sites of the corresponding equation,[12] thus I get the maximal symmetry compatible with the imposed constraints, that in our model characterizes an orthotropic shell with orthotropic directions $\boldsymbol{o}_{\mathrm{I}}(\theta^1,\theta^2)$ and $\boldsymbol{o}_{\mathrm{II}}(\theta^1,\theta^2)$ at $\bar{\boldsymbol{x}}(\theta^1,\theta^2)$, e.g., Reddy (2006) [pp. 425-428]. Hence

$$\boldsymbol{n}^{(\mathcal{A})}(\theta^1,\theta^2)=\mathbb{C}_\varepsilon(\theta^1,\theta^2)\colon\boldsymbol{\gamma}(\theta^1,\theta^2) \tag{2.4.16}$$

$$\boldsymbol{m}^{(\mathcal{A})}(\theta^1,\theta^2)=\mathbb{C}_\theta(\theta^1,\theta^2)\colon\boldsymbol{\rho}(\theta^1,\theta^2)\ . \tag{2.4.17}$$

[11] An operator $\mathbb{P}$ on a tensor space is a projection if satisfy the idempotent property $\mathbb{P}^2\equiv\mathbb{P}$ (Renteln 2014) [p. 4], e.g., $\mathbb{P}_\varepsilon\,\mathscr{C}_\varepsilon=\mathscr{C}_\varepsilon$ (resp. $\mathbb{P}_\varepsilon^\perp\,\mathscr{C}_\varepsilon^\perp=\mathscr{C}_\varepsilon^\perp$) for all elements in $\mathscr{C}_\varepsilon$ (resp. $\mathscr{C}_\varepsilon^\perp$).

[12] See equations (2.4.12)-(2.4.13).

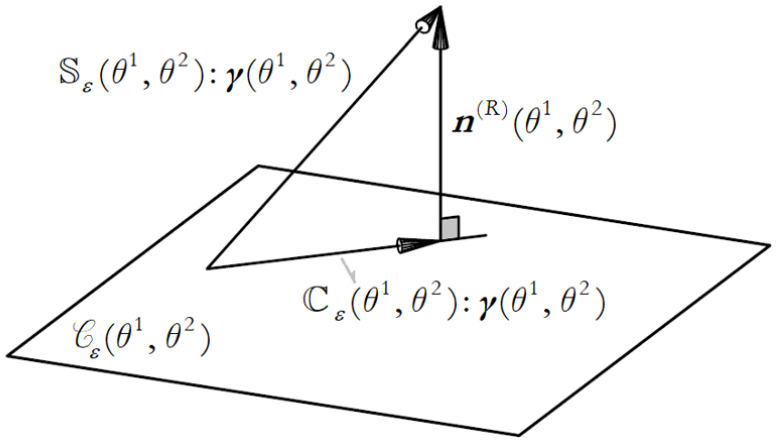

a) Constraint space $\mathscr{C}_\varepsilon$

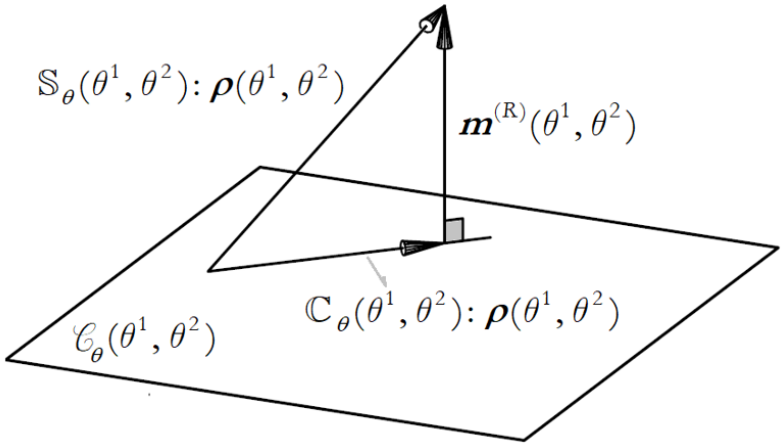

b) Constraint space $\mathscr{C}_\theta$

Figure 2.4.2: A geometrical interpretation of the constraint spaces $\mathscr{C}_\varepsilon$ and $\mathscr{C}_\theta$

The elasticity tensors $\mathbb{C}_\varepsilon(\theta^1,\theta^2)$ and $\mathbb{C}_\theta(\theta^1,\theta^2)$ in the respective constrained case are the restrictions to the constrained spaces $\mathscr{C}_\varepsilon(\theta^1,\theta^2)$ and $\mathscr{C}_\theta(\theta^1,\theta^2)$ of the corresponding unconstrained elasticity tensors $\mathbb{S}_\varepsilon$ and $\mathbb{S}_\theta$, see Figure 2.4.2. They are gotten by using a straightforward application of the theorem of Podio-Guidugli and Vianello (1992) [eq. 2.10], followed by composition with the orthogonal projections, i.e.,

$$\mathbb{C}_\varepsilon = \mathbb{P}_\varepsilon\,\mathbb{S}_\varepsilon\big|_{\mathscr{C}_\varepsilon}\ , \qquad \mathbb{C}_\theta = \mathbb{P}_\theta\,\mathbb{S}_\theta\big|_{\mathscr{C}_\theta}\ , \tag{2.4.18}$$

equal to

$$\mathbb{C}_\varepsilon(\theta^1,\theta^2) = \frac{E_{\mathrm{I}}\ t(\theta^1,\theta^2)}{1-\nu_{\mathrm{I\text{-}II}}\,\nu_{\mathrm{II\text{-}I}}}\,\boldsymbol{P}_{\mathrm{I}}(\theta^1,\theta^2)\otimes\boldsymbol{P}_{\mathrm{I}}(\theta^1,\theta^2)\ , \tag{2.4.19}$$

i.e., Andrade (2013) [eq. 2.4.8] and

$$\mathbb{C}_{\theta}(\theta^1,\theta^2)=\frac{E_{\mathrm{I}}\,t^3(\theta^1,\theta^2)}{12\left(1-\nu_{\mathrm{I\cdot II}}\,\nu_{\mathrm{II\cdot I}}\right)}\boldsymbol{P}_{\mathrm{I}}(\theta^1,\theta^2)\otimes\boldsymbol{P}_{\mathrm{I}}(\theta^1,\theta^2)+\frac{G_{\mathrm{I\cdot II}}\,t^3(\theta^1,\theta^2)}{6}\boldsymbol{P}_{\mathrm{I\cdot II}}(\theta^1,\theta^2)\otimes\boldsymbol{P}_{\mathrm{I\cdot II}}(\theta^1,\theta^2)$$

$$+\frac{G_{\mathrm{II\cdot I}}\,t^3(\theta^1,\theta^2)}{6}\boldsymbol{P}_{\mathrm{II\cdot I}}(\theta^1,\theta^2)\otimes\boldsymbol{P}_{\mathrm{II\cdot I}}(\theta^1,\theta^2)\ . \tag{2.4.20}$$

The elastic coefficient E_{I} is the Young modulus relative to the direction $\boldsymbol{o}_{\mathrm{I}}(\theta^1,\theta^2)$ and $\nu_{\mathrm{I\cdot II}}$, $\nu_{\mathrm{II\cdot I}}$, $G_{\mathrm{I\cdot II}}$ and $G_{\mathrm{II\cdot I}}$ are the Poisson ratios and shear moduli relative to the ordered pairs $\left\{\boldsymbol{o}_{\mathrm{I}}(\theta^1,\theta^2),\boldsymbol{o}_{\mathrm{II}}(\theta^1,\theta^2)\right\}$ and $\left\{\boldsymbol{o}_{\mathrm{II}}(\theta^1,\theta^2),\boldsymbol{o}_{\mathrm{I}}(\theta^1,\theta^2)\right\}$ of mutually orthogonal directions, with

$$\boldsymbol{P}_{\mathrm{I}}(\theta^1,\theta^2)=\boldsymbol{o}_{\mathrm{I}}(\theta^1,\theta^2)\otimes\boldsymbol{o}_{\mathrm{I}}(\theta^1,\theta^2) \tag{2.4.21}$$

$$\boldsymbol{P}_{\mathrm{I\cdot II}}(\theta^1,\theta^2)=\boldsymbol{o}_{\mathrm{I}}(\theta^1,\theta^2)\otimes\boldsymbol{o}_{\mathrm{II}}(\theta^1,\theta^2) \tag{2.4.22}$$

$$\boldsymbol{P}_{\mathrm{II\cdot I}}(\theta^1,\theta^2)=\boldsymbol{o}_{\mathrm{II}}(\theta^1,\theta^2)\otimes\boldsymbol{o}_{\mathrm{I}}(\theta^1,\theta^2)\ , \tag{2.4.23}$$

that are the projection tensor fields, regarded as linear maps onto their respective spaces. From equation (2.4.16) it follows that the active membrane force field, is given by

$$\boldsymbol{n}^{(\mathcal{A})}(\theta^1,\theta^2)=n_{\mathrm{I\cdot I}}^{(\mathcal{A})}(\theta^1,\theta^2)\,\boldsymbol{P}_{\mathrm{I}}(\theta^1,\theta^2)=\tilde{E}\,t(\theta^1,\theta^2)\,\gamma_{\mathrm{I\cdot I}}(\theta^1,\theta^2)\,\boldsymbol{P}_{\mathrm{I}}(\theta^1,\theta^2)\ , \tag{2.4.24}$$

while from equation (2.4.17) the active shell moment tensor field, is equal to

$$\begin{aligned}\boldsymbol{m}^{(\mathcal{A})}(\theta^1,\theta^2)&=m_{\mathrm{I\cdot I}}^{(\mathcal{A})}(\theta^1,\theta^2)\,\boldsymbol{P}_{\mathrm{I}}(\theta^1,\theta^2)+m_{\mathrm{I\cdot II}}^{(\mathcal{A})}\boldsymbol{P}_{\mathrm{I\cdot II}}(\theta^1,\theta^2)+m_{\mathrm{II\cdot I}}^{(\mathcal{A})}\boldsymbol{P}_{\mathrm{II\cdot I}}(\theta^1,\theta^2)\\&=\frac{\tilde{E}t^3(\theta^1,\theta^2)\rho_{\mathrm{I\cdot I}}}{12}\boldsymbol{P}_{\mathrm{I}}(\theta^1,\theta^2)+\frac{G_{\mathrm{I\cdot II}}\,t^3(\theta^1,\theta^2)\rho_{\mathrm{I\cdot II}}}{6}\boldsymbol{P}_{\mathrm{I\cdot II}}(\theta^1,\theta^2)\\&\quad+\frac{G_{\mathrm{II\cdot I}}\,t^3(\theta^1,\theta^2)\rho_{\mathrm{II\cdot I}}}{6}\boldsymbol{P}_{\mathrm{II\cdot I}}(\theta^1,\theta^2)\ ,\end{aligned} \tag{2.4.25}$$

with the modified elastic modulus $\tilde{E}$, defined as[13]

$$\tilde{E}=\frac{E_{\mathrm{I}}}{1-\nu_{\mathrm{I\cdot II}}\,\nu_{\mathrm{II\cdot I}}}\ , \tag{2.4.26}$$

and the fields $\left(n_{\mathrm{I\cdot I}}^{(\mathcal{A})},m_{\mathrm{I\cdot I}}^{(\mathcal{A})},m_{\mathrm{I\cdot II}}^{(\mathcal{A})},m_{\mathrm{II\cdot I}}^{(\mathcal{A})}\right):\bar{\Omega}\to\mathbb{R}^4$ being clearly continuous.

[13]The assumption that the modified elastic modulus is independent of the point $\bar{x}\in S$ is not mandatory. Furthermore, including the modified shear moduli (2.5.5) to this consideration, it is possible express $\tilde{E}$ and $\tilde{G}$ as functions of the Gaussian coordinates θ^1, θ^2, i.e., $\tilde{E}\left(\theta^1,\theta^2\right)$ and $\tilde{G}\left(\theta^1,\theta^2\right)$ respectively.

2.5 TOTAL POTENTIAL ENERGY

Assuming that there are not dissipative actions, the total potential energy of the bar-load system is defined by the sum of the elastic energy stored in the constraint shell and the negative of the work associated to the applied loading for an admissible displacement.

2.5.1 Elastic energy

In view of our previous results, the admissible displacement field $\bar{\boldsymbol{U}}:\bar{\Omega}\to\mathbb{R}^3$ of $\bar{\boldsymbol{x}}(\theta^1,\theta^2)\in S$ in terms of the generalised displacements $\theta^1\in[0,L]\mapsto W_i(\theta^1),\Phi_1(\theta^1)\in\mathbb{R}$ is characterized by the admissible deformation tensors $\boldsymbol{\gamma}\in\mathscr{C}_\varepsilon(\theta^1,\theta^2)$ and $\boldsymbol{\rho}\in\mathscr{C}_\theta(\theta^1,\theta^2)$, that are said to be work conjugate[14] with respect to their corresponding active tensors, i.e., the membrane force field $\boldsymbol{n}^{(\mathcal{A})}(\theta^1,\theta^2)$ and the shell moment field $\boldsymbol{m}^{(\mathcal{A})}(\theta^1,\theta^2)$ respectively. So that the elastic energy given by the contribution of the membrane state and the bending shell effect is given by

$$\mathcal{U}=\frac{1}{2}\int_S\left(\boldsymbol{n}^{(\mathcal{A})}(\theta^1,\theta^2):\boldsymbol{\gamma}(\theta^1,\theta^2)+\boldsymbol{m}^{(\mathcal{A})}(\theta^1,\theta^2):\boldsymbol{\rho}(\theta^1,\theta^2)\right)dS(\bar{\boldsymbol{x}})\,, \tag{2.5.1}$$

since the membrane strain tensor has only one component, and the area element is given by equation (2.2.15), it reduces to

$$\mathcal{U}=\frac{1}{2}\int_{\bar{\Omega}}\left(n^{(\mathcal{A})}_{\mathrm{I}\cdot\mathrm{I}}(\theta^1,\theta^2)\,\gamma_{\mathrm{I}\cdot\mathrm{I}}(\theta^1,\theta^2)+\boldsymbol{m}^{(\mathcal{A})}(\theta^1,\theta^2):\boldsymbol{\rho}(\theta^1,\theta^2)\right)\sqrt{a(\theta^1,\theta^2)}\,d\theta^1d\theta^2\,. \tag{2.5.2}$$

Replacing the constitutive equations (2.4.24)-(2.4.25) relating the active components $n^{(\mathcal{A})}_{\mathrm{I}\cdot\mathrm{I}}$, $\boldsymbol{m}^{(\mathcal{A})}$ to $\gamma_{\mathrm{I}\cdot\mathrm{I}}$, $\boldsymbol{\rho}$ respectively, and inserting equations (2.3.39)-(2.3.43) concerning the generalised displacements $W_i(\theta^1)$ and $\Phi_1(\theta^1)$, by routine calculations I get

[14] I said that $\boldsymbol{n}^{(\mathcal{A})}:\boldsymbol{\gamma}$ and $\boldsymbol{m}^{(\mathcal{A})}:\boldsymbol{\rho}$ are work conjugates with respect to the area element over S in the sense that their products give work per unit area. Moreover it is easy to proof that the corresponding reactive component perform no work in any admissible deformation, i.e., $\boldsymbol{n}^{(\mathrm{R})}:\boldsymbol{\gamma}=0$ and $\boldsymbol{m}^{(\mathrm{R})}:\boldsymbol{\rho}=0$ since $\mathscr{C}_\varepsilon\cap\mathscr{C}_\varepsilon^\perp=\{0\}$ and $\mathscr{C}_\theta\cap\mathscr{C}_\theta^\perp=\{0\}$.

$$\mathcal{U} = \frac{\tilde{E}}{2}\int_{\bar{\Omega}} \Big\{ \Big(W_1'(\theta^1) - \bar{x}_2(\theta^1,\theta^2) W_2''(\theta^1) - \bar{x}_3(\theta^1,\theta^2) W_3''(\theta^1) - \omega(\theta^1,\theta^2)\Phi_1''(\theta^1) + \psi(\theta^1,\theta^2)\Phi_1'(\theta^1) \Big)^2 t^*(\theta^1,\theta^2) + \frac{1}{12}\Big(-D_2\bar{x}_2(\theta^1,\theta^2) W_3''(\theta^1) + D_2\bar{x}_3(\theta^1,\theta^2) W_2''(\theta^1) - q(\theta^1,\theta^2)\Phi_1''(\theta^1) \Big)^2 a^2(\theta^1,\theta^2)\Big(t^*(\theta^1,\theta^2)\Big)^3 \Big\} d\theta^1\, d\theta^2 + \frac{\tilde{G}}{6}\int_{\bar{\Omega}} \Big(a(\theta^1,\theta^2)\, t^*(\theta^1,\theta^2)\Big)^3 \Big(\Phi_1'(\theta^1)\Big)^2 d\theta^1\, d\theta^2 \ . \tag{2.5.3}$$

To enhance the algebra, an equivalent thickness $t^*(\theta^1,\theta^2)$ and a modified shear modulus $\tilde{G}$ are introduced, where

$$t^*(\theta^1,\theta^2) = \frac{t(\theta^1,\theta^2)}{\sqrt{a^3(\theta^1,\theta^2)}} = \frac{t(\theta^1,\theta^2)}{\Big[1+\big(D_1\bar{x}_2 D_2\bar{x}_3 - D_2\bar{x}_2 D_1\bar{x}_3\big)^2\Big]^{3/2}} \tag{2.5.4}$$

can be seen as a reduced wall thickness, due to $0 < t^*(\theta^1,\theta^2) \le t(\theta^1,\theta^2),\ \forall(\theta^1,\theta^2)\in\bar{\Omega}$, only getting the equality if $a(\theta^1,\theta^2)=1$. While the modified shear modulus is defined as the average of the shear moduli relative to the mutually orthogonal directions

$$\tilde{G} = \frac{G_{I\cdot II} + G_{II\cdot I}}{2}\ .^{15} \tag{2.5.5}$$

The two-dimensional domain $\bar{\Omega}(\theta^1,\theta^2)$ is being bounded by a region between the functions $g_1(\theta^1) \le \theta^2 \le g_2(\theta^1)$, that are assumed to be single-valued continuous maps on $\theta^1 \in [0, L]$, therefore the integral in equation (2.5.3) is written as

$$\mathcal{U} = \frac{\tilde{E}}{2}\int_0^L \Bigg[\int_{g_1(\theta^1)}^{g_2(\theta^1)} \Big\{ \Big(W_1'(\theta^1) - \bar{x}_2(\theta^1,\theta^2) W_2''(\theta^1) - \bar{x}_3(\theta^1,\theta^2) W_3''(\theta^1) - \omega(\theta^1,\theta^2)\Phi_1''(\theta^1) + \psi(\theta^1,\theta^2)\Phi_1'(\theta^1) \Big)^2 t^*(\theta^1,\theta^2) + \frac{1}{12}\Big(-D_2\bar{x}_2(\theta^1,\theta^2) W_3''(\theta^1) + D_2\bar{x}_3(\theta^1,\theta^2) W_2''(\theta^1) - q(\theta^1,\theta^2)\Phi_1''(\theta^1) \Big)^2 a^2(\theta^1,\theta^2)\Big(t^*(\theta^1,\theta^2)\Big)^3 \Big\} d\theta^2 \Bigg] d\theta^1 + \frac{\tilde{G}}{2}\int_0^L \Bigg[\frac{1}{3}\int_{g_1(\theta^1)}^{g_2(\theta^1)} \Big(a(\theta^1,\theta^2)\, t^*(\theta^1,\theta^2)\Big)^3 d\theta^2 \Bigg] \Big(\Phi_1'(\theta^1)\Big)^2 d\theta^1 \ . \tag{2.5.6}$$

[15] Due to the principle of reciprocity (Reddy 2006) [p. 30], $\tilde{G} = G_{I\cdot II} = G_{II\cdot I}$.

Introducing the following continuous real-valued maps on $\theta^1 \in [0, L]$

$$A^*(\theta^1) = \int_{g_1(\theta^1)}^{g_2(\theta^1)} t^*(\theta^1, \theta^2)\, d\theta^2 \tag{2.5.7}$$

$$S_2^*(\theta^1) = \int_{g_1(\theta^1)}^{g_2(\theta^1)} \overline{x}_3(\theta^1, \theta^2)\, t^*(\theta^1, \theta^2)\, d\theta^2 \tag{2.5.8}$$

$$S_3^*(\theta^1) = \int_{g_1(\theta^1)}^{g_2(\theta^1)} \overline{x}_2(\theta^1, \theta^2)\, t^*(\theta^1, \theta^2)\, d\theta^2 \tag{2.5.9}$$

$$S_\omega^*(\theta^1) = \int_{g_1(\theta^1)}^{g_2(\theta^1)} \omega(\theta^1, \theta^2)\, t^*(\theta^1, \theta^2)\, d\theta^2 \tag{2.5.10}$$

$$I_2^*(\theta^1) = \int_{g_1(\theta^1)}^{g_2(\theta^1)} \left(\overline{x}_3^{\,2}(\theta^1, \theta^2)\, t^*(\theta^1, \theta^2) + \frac{a^2(\theta^1, \theta^2)\left(D_2 \overline{x}_2(\theta^1, \theta^2)\right)^2}{12} \left(t^*(\theta^1, \theta^2)\right)^3 \right) d\theta^2 \tag{2.5.11}$$

$$I_3^*(\theta^1) = \int_{g_1(\theta^1)}^{g_2(\theta^1)} \left(\overline{x}_2^{\,2}(\theta^1, \theta^2)\, t^*(\theta^1, \theta^2) + \frac{a^2(\theta^1, \theta^2)\left(D_2 \overline{x}_3(\theta^1, \theta^2)\right)^2}{12} \left(t^*(\theta^1, \theta^2)\right)^3 \right) d\theta^2 \tag{2.5.12}$$

$$I_{23}^*(\theta^1) = \int_{g_1(\theta^1)}^{g_2(\theta^1)} \left(\overline{x}_2 \overline{x}_3 t^*(\theta^1, \theta^2) - \frac{a^2(\theta^1, \theta^2) D_2 \overline{x}_2 D_2 \overline{x}_3}{12} \left(t^*(\theta^1, \theta^2)\right)^3 \right) d\theta^2 \tag{2.5.13}$$

$$I_{2\omega}^*(\theta^1) = \int_{g_1(\theta^1)}^{g_2(\theta^1)} \left(\overline{x}_3\, \omega\, t^*(\theta^1, \theta^2) + \frac{a^2(\theta^1, \theta^2) q(\theta^1, \theta^2) D_2 \overline{x}_2}{12} \left(t^*(\theta^1, \theta^2)\right)^3 \right) d\theta^2 \tag{2.5.14}$$

$$I_{3\omega}^*(\theta^1) = \int_{g_1(\theta^1)}^{g_2(\theta^1)} \left(\overline{x}_2\, \omega\, t^*(\theta^1, \theta^2) - \frac{a^2(\theta^1, \theta^2) q(\theta^1, \theta^2) D_2 \overline{x}_3(\theta^1, \theta^2)}{12} \left(t^*(\theta^1, \theta^2)\right)^3 \right) d\theta^2 \tag{2.5.15}$$

$$I_\omega^*(\theta^1) = \int_{g_1(\theta^1)}^{g_2(\theta^1)} \left(\omega^2(\theta^1, \theta^2)\, t^*(\theta^1, \theta^2) + \frac{a^2(\theta^1, \theta^2) q^2(\theta^1, \theta^2)}{12} \left(t^*(\theta^1, \theta^2)\right)^3 \right) d\theta^2 \tag{2.5.16}$$

$$S_\psi^*(\theta^1) = \int_{g_1(\theta^1)}^{g_2(\theta^1)} \psi(\theta^1, \theta^2)\, t^*(\theta^1, \theta^2)\, d\theta^2 \tag{2.5.17}$$

$$I_\psi^*(\theta^1) = \int_{g_1(\theta^1)}^{g_2(\theta^1)} \psi^2(\theta^1, \theta^2)\, t^*(\theta^1, \theta^2)\, d\theta^2 \tag{2.5.18}$$

$$I_{2\psi}^*(\theta^1) = \int_{g_1(\theta^1)}^{g_2(\theta^1)} \overline{x}_3(\theta^1, \theta^2)\, \psi(\theta^1, \theta^2) t^*(\theta^1, \theta^2)\, d\theta^2 \tag{2.5.19}$$

$$I_{3\psi}^*(\theta^1) = \int_{g_1(\theta^1)}^{g_2(\theta^1)} \overline{x}_2(\theta^1, \theta^2)\, \psi(\theta^1, \theta^2) t^*(\theta^1, \theta^2) d\theta^2 \tag{2.5.20}$$

$$I^*_{\omega\psi}(\theta^1) = \int_{g_1(\theta^1)}^{g_2(\theta^1)} \omega(\theta^1,\theta^2)\,\psi(\theta^1,\theta^2)\,t^*(\theta^1,\theta^2)d\theta^2 \tag{2.5.21}$$

$$J^*(\theta^1) = \frac{1}{3}\int_{g_1(\theta^1)}^{g_2(\theta^1)} \left(a(\theta^1,\theta^2)\;t^*(\theta^1,\theta^2)\right)^3 d\theta^2 \;\;, \tag{2.5.22}$$

that defined the cross-sectional properties of the bar, i.e., the (i) area $A^*(\theta^1)$, (ii) first moment of area $S^*_2(\theta^1), S^*_3(\theta^1)$, (iii) first sectorial moment $S^*_\omega(\theta^1)$, (iv) cross-sectional second moments of area $I^*_2(\theta^1), I^*_3(\theta^1), I^*_{23}(\theta^1)$, (v) cross-sectional second sectorial moments $I^*_{2\omega}(\theta^1), I^*_{3\omega}(\theta^1), I^*_\omega(\theta^1)$, (vi) geometrical properties associated with cross-sectional tapering $S^*_\psi(\theta^1), I^*_\psi(\theta^1), I^*_{2\psi}(\theta^1), I^*_{3\psi}(\theta^1), I^*_{\omega\psi}(\theta^1)$, and the (vii) torsional property $J^*(\theta^1)$. Allow us to express the stored elastic energy $\mathcal{U}$ into the form

$$\begin{aligned}\mathcal{U} = \frac{\tilde{E}}{2}\int_0^L \Big[& A^*(\theta^1)\left(W_1'(\theta^1)\right)^2 - 2\,S^*_3(\theta^1)W_1'(\theta^1)W_2''(\theta^1) - 2\,S^*_2(\theta^1)W_1'(\theta^1)W_3''(\theta^1) \\ & -2\,S^*_\omega(\theta^1)W_1'(\theta^1)\Phi_1''(\theta^1) + 2\,S^*_\psi(\theta^1)W_1'(\theta^1)\Phi_1'(\theta^1) + I^*_3(\theta^1)\left(W_2''(\theta^1)\right)^2 \\ & +2\,I^*_{23}(\theta^1)W_2''(\theta^1)W_3''(\theta^1) + 2\,I^*_{3\omega}(\theta^1)W_2''(\theta^1)\,\Phi_1''(\theta^1) \\ & -2\,I^*_{3\psi}(\theta^1)W_2''(\theta^1)\Phi_1'(\theta^1) + I^*_2(\theta^1)\left(W_3''(\theta^1)\right)^2 + 2\,I^*_{2\omega}(\theta^1)W_3''(\theta^1)\,\Phi_1''(\theta^1) \\ & -2\,I^*_{2\psi}(\theta^1)W_3''(\theta^1)\Phi_1'(\theta^1) + I^*_\omega(\theta^1)\left(\Phi_1''(\theta^1)\right)^2 - 2\,I^*_{\omega\psi}(\theta^1)\Phi_1''(\theta^1)\Phi_1'(\theta^1) \\ & +I^*_\psi(\theta^1)\left(\Phi_1'(\theta^1)\right)^2\Big]d\theta^1 + \frac{\tilde{G}}{2}\int_0^L J^*(\theta^1)\left(\Phi_1'(\theta^1)\right)^2\,d\theta^1 \;\;. \end{aligned} \tag{2.5.23}$$

The last energy component is intrinsically associated with the Saint-Venant torsion where $J^*(\theta^1)$ is a generalization of the torsion constant of the cross-section along the principal coordinate direction. In addition, an approximate solution sufficiently accurate can be establish, e.g., Andrade (2013) [eq. 2.5.11-2.5.13 and eq. 2.5.15-2.5.17], if in equations (2.5.11)-(2.5.16) the contribution of the curvature component $\rho_{\text{I-I}}$ is neglected in comparison with the contribution of the membrane state, for the reason that the reduce wall thickness (which value is relative small) has a third power in comparison with the first order term of the membrane state.

2.5.2 Work of the external loads

The middle surface of the shell is subjected to a set of load surface and edge loads, that are referred to as shell loads (Gjelsvik 1981) [pp. 15-16]. This statically effect can be characterize with continuous maps $\boldsymbol{q}, \mathbf{m} : [0, \mathrm{L}] \to \mathbb{R}^3$ and $b : [0, L] \to \mathbb{R}$, i.e., representing the respective applied distributed force, moment and bimoment[16] per unit length of the line segment $\{O + \theta^1 \boldsymbol{e}_1, 0 \le \theta^1 \le L\}$, and the applied concentrated forces $\boldsymbol{Q}_0$, $\boldsymbol{Q}_L$; moments $\boldsymbol{M}_0$, $\boldsymbol{M}_L$ and bimoments B_0, B_L placed at the end points O and $O + L\boldsymbol{e}_1$ respectively. They defined the bar loads (Gjelsvik 1981) [pp. 25-27], such that the work done for the admissible displacement field $\bar{\boldsymbol{U}} : \bar{\Omega} \to \mathbb{R}^3$ of the middle surface, see equations (2.3.33)-(2.3.35), has the form[17]

$$\mathcal{W}_e = \int_0^L \left(\boldsymbol{q}(\theta^1) \cdot \boldsymbol{W}(\theta^1) + \mathbf{m}(\theta^1) \cdot \boldsymbol{\Phi}(\theta^1) - b(\theta^1) \Phi_1'(\theta^1) \right) d\theta^1 + \boldsymbol{Q}_0 \cdot \boldsymbol{W}(0)$$
$$+ \boldsymbol{Q}_L \cdot \boldsymbol{W}(L) + \boldsymbol{M}_0 \cdot \boldsymbol{\Phi}(0) + \boldsymbol{M}_L \cdot \boldsymbol{\Phi}(L) - B_0 \Phi_1'(0) - B_L \Phi_1'(L) \ . \qquad (2.5.24)$$

Written in function of the Cartesian components,

$$\boldsymbol{q}(\theta^1) = q_i(\theta^1) \boldsymbol{e}_i \ , \qquad \mathbf{m}(\theta^1) = m_i(\theta^1) \boldsymbol{e}_i \ , \qquad (2.5.25)$$

$$\boldsymbol{Q}_0 = Q_{0.i} \boldsymbol{e}_i \ , \qquad \boldsymbol{Q}_L = Q_{L.i} \boldsymbol{e}_i \ , \qquad (2.5.26)$$

$$\boldsymbol{M}_0 = M_{0.i} \boldsymbol{e}_i \ , \qquad \boldsymbol{M}_L = M_{L.i} \boldsymbol{e}_i \ , \qquad (2.5.27)$$

so that, equation (2.5.24) is written as

$$\mathcal{W}_e = \int_0^L \left(q_i(\theta^1) W_i(\theta^1) + m_1(\theta^1) \Phi_1(\theta^1) - m_2(\theta^1) W_3'(\theta^1) + m_3(\theta^1) W_2'(\theta^1) - b(\theta^1) \Phi_1'(\theta^1) \right) d\theta^1$$
$$+ Q_{0.i} W_i(0) + Q_{L.i} W_i(L) + M_{0.1} \Phi_1(0) - M_{0.2} W_3'(0) + M_{0.3} W_2'(0)$$
$$+ M_{L.1} \Phi_1(L) - M_{L.2} W_3'(L) + M_{L.3} W_2'(L) - B_0 \Phi_1'(0) - B_L \Phi_1'(L) \ . \qquad (2.5.28)$$

[16] The bimoment per unit length is called the warping load (Gjelsvik 1981) [p. 27], that has no point of application. They are related to the warping of the cross-sections, i.e., the shell loads acting along $\boldsymbol{e}_1$.

[17] At this stage, it cannot be a priori assumed that any set of loading can be replace by another load system statically equivalent. Any replacement of longitudinal shell loads by another loads statically equivalent to them, amounts to subjecting the bar to an additional self-balancing longitudinal loads, i.e., the warping has a local character. Likewise, this property applies to tapered and prismatic bars. In this sense, the work performed by the bar loads in equations (2.5.24), is required to hold for every admissible displacement field of the middle surface.

2.5.3 Total potential energy

Equations (2.5.23) and (2.5.28) need a crucial clarification. They are deduced by using the set $(W_i, \Phi_1) \in \mathcal{D}$, corresponding to the generalised displacements fields at the position of equilibrium. Therefore, the total potential energy defined for an arbitrary displacements $(\widehat{W}_i, \widehat{\Phi}_1)$ in the same domain, i.e., $(\widehat{W}_i, \widehat{\Phi}_1) \in \mathcal{D}$ (satisfying the boundary conditions of the problem) is defined as the sum of the elastic energy (2.5.23) and the negative of the work (2.5.28) but using the hat notation into the displacements, i.e.,

$$\Pi(\widehat{W}_i, \widehat{\Phi}_1) = \mathcal{U}(\widehat{W}_i, \widehat{\Phi}_1) - \mathcal{W}_e(\widehat{W}_i, \widehat{\Phi}_1) \ . \tag{2.5.29}$$

The function of functions $(\widehat{W}_i, \widehat{\Phi}_1) \in \mathcal{D} \mapsto \Pi(\widehat{W}_i, \widehat{\Phi}_1) \in \mathbb{R}$ represent a quadratic functional[18] of the generalised displacements fields $(\widehat{W}_i, \widehat{\Phi}_1) \in \mathcal{D}$ with real-valued maps on $[0, L]$.

2.6 THE BOUNDARY VALUE PROBLEM FOR THE GENERALISED DISPLACEMENTS

> Nothing whatsoever takes place in the universe in which some relation of maximum and minimum does not appear. Wherefore there is absolutely no doubt that every effect in the universe can be explained as satisfactorily from final causes, by the aid of the method of maxima and minima, as it can from the effective causes themselves.
>
> LEONHARD EULER, *INTRODUCTION TO DE CURVIS ELASTICIS*

The derivation of the equilibrium equations, i.e., the Euler-Lagrange equations associated to the functional (2.5.29) at the equilibrium state $(W_i, \Phi_1) \in \mathcal{D}$, including the characterization of the natural with their corresponding essential boundary conditions,[19] are possible to obtain from a principle that considers the entire admissible displacement of the bar between positions O and $L\boldsymbol{e}_1$, and small virtual variations.

[18] See equation (2.8.21).

[19] The essential boundary conditions also known as the Dirichlet boundary conditions, are related to the physical displacements (that is the translation, rotation and bimoment displacement, i.e., the derivative of the rotation Φ_1) of the bar, while natural boundary conditions or Neumann boundary conditions, are related to the actions upon the above displacements, i.e., the forces, moments and bimoments. Mathematically speaking, the essential boundary conditions are identified by examining *k*, the highest order derivative in the functional, then the essential boundary conditions on that variable are those that involve only derivatives of order less than *k*, whereas those involving derivatives of order *k* or higher, up to 2*k*-1, are natural boundary conditions, e.g., Axelsson and Barker (1984) [p. 80].

A principle of this nature is known as an integral principle (Goldstein et al. 2014) [p. 34], that in the case of structural analysis it is known as the principle of the stationary value of total potential energy, e.g., El Naschie (1990) [§ 6], or principle of minimum potential energy, e.g., Dow (1998) [p. 10] or Sadd (2009) [p. 124]. First, the following assumptions concerning the smoothness of the geometrical properties of the cross-section and the bar loads must be established: (i) the maps $\mathcal{A}^*$, S_ψ^*, I_ψ^* and J^*, as well as m_2, m_3 and b, are continuously differentiable on $[0,L]$, with (ii) S_2^*, S_3^*, S_ω^*, I_2^*, I_3^*, I_ω^*, I_{23}^*, $I_{2\omega}^*$, $I_{3\omega}^*$, $I_{2\psi}^*$, $I_{3\psi}^*$ and $I_{\omega\psi}^*$ being twice continuously differentiable on $[0,L]$. Furthermore, the functional $(\widehat{W}_i,\widehat{\Phi}_1)\in\mathcal{D}\mapsto \Pi(\widehat{W}_i,\widehat{\Phi}_1)\in\mathbb{R}$, that domain is defined by the ordered quadruplets $(\widehat{W}_i,\widehat{\Phi}_1)$ of real-valued maps on the interval $[0,L]$, must satisfy the smoothness requirements (i) $\widehat{W}_1\in C^3[0,L]$ and (ii) $\widehat{W}_2,\widehat{W}_3,\widehat{\Phi}_1\in C^4[0,L]$.[20] Hence, the following statement of the boundary value problem for the generalised displacements is announced:

Of all generalised displacements $(\widehat{W}_i,\widehat{\Phi}_1)\in\mathcal{D}$ *satisfying the essential boundary conditions (i.e., kinematical) only those that fulfil the equilibrium* $(W_i,\Phi_1)\in\mathcal{D}$, *make the total potential energy a local minimum,* i.e.,

$$\Pi(W_i,\Phi_1)=\inf_{(\widehat{W}_i,\widehat{\Phi}_1)\in\mathcal{D}}\Pi(\widehat{W}_i,\widehat{\Phi}_1)\ . \tag{2.6.1}$$

Let $\delta W_i,\delta\Phi_1:[0,L]\to\mathbb{R}$ denote the admissible variations[21] of $(W_i,\Phi_1)\in\mathcal{D}$. If I analyse the perturbation only in the direction Φ_1, i.e., $\delta W_i=0$ and $\delta\Phi_1\in\mathcal{D}$, I get

$$\Pi(W_i,\Phi_1+\delta\Phi_1)\geq\Pi(W_i,\Phi_1)\ . \tag{2.6.2}$$

Replacing the functions W_i, $\Phi_1+\delta\Phi_1$ into equation (2.5.29)

$$\Pi(W_i,\Phi_1)+\Theta_{0\Phi}+\int_0^L\left(-m_1\delta\Phi_1+\Theta_{1\Phi}(\delta\Phi_1)'+\Theta_{2\Phi}(\delta\Phi_1)''\right)d\theta^1+O(\delta^2)\geq\Pi(W_i,\Phi_1) \tag{2.6.3}$$

where the functions $\Theta_{k\Phi}$ with $k=0,1,2$ are equal to

$$\Theta_{0\Phi}=-M_{0.1}\,\delta\Phi_1(0)+B_0\,\delta\Phi_1'(0)-M_{L.1}\,\delta\Phi_1(L)+B_L\,\delta\Phi_1'(L) \tag{2.6.4}$$

[20] A real-valued function defined on an interval [a,b] with $a<b$, is said to be p-times continuously differentiable on that interval, i.e., $C^p[a,b]$ with $p\in\mathbb{N}$, if its derivatives of order $\leq p$ exist and are continuous on [a,b].

[21] This variations near the equilibrium, have the same degree of smoothness as the generalised displacements themselves and satisfy the homogeneous form of the essential boundary conditions – they are elements of a linear space (Andrade 2013) [p. 47].

$$\Theta_{1\Phi} = \tilde{E}S^*_{\psi}(\theta^1)W_1'(\theta^1) - \tilde{E}I^*_{3\psi}(\theta^1)W_2''(\theta^1) - \tilde{E}I^*_{2\psi}(\theta^1)W_3''(\theta^1) - \tilde{E}I^*_{\omega\psi}(\theta^1)\Phi_1''(\theta^1)$$
$$+\tilde{G}J^*(\theta^1)\Phi_1'(\theta^1) + \tilde{E}I^*_{\psi}(\theta^1)\Phi_1'(\theta^1) + b(\theta^1) \ , \qquad (2.6.5)$$

$$\Theta_{2\Phi} = -\tilde{E}S^*_{\omega}(\theta^1)W_1'(\theta^1) + \tilde{E}I^*_{3\omega}(\theta^1)W_2''(\theta^1) + \tilde{E}I^*_{2\omega}(\theta^1)W_3''(\theta^1)$$
$$+\tilde{E}I^*_{\omega}(\theta^1)\Phi_1''(\theta^1) - \tilde{E}I^*_{\omega\psi}(\theta^1)\Phi_1'(\theta^1) \ . \qquad (2.6.6)$$

Reducing common terms, and taking only first order variations, i.e., higher orders are neglected, equation (2.6.3) reduces to

$$\Theta_{0\Phi} + \int_0^L \left(-m_1\delta\Phi_1 + \Theta_{1\Phi}(\delta\Phi_1)' + \Theta_{2\Phi}(\delta\Phi_1)''\right)d\theta^1 \geq 0 \ , \qquad (2.6.7)$$

integrating by parts (in view of the smoothness of the corresponding maps) and incorporating the commutative property of the calculus of variations, e.g., Pignataro et al. (1991) [pp. 339-344], above equation yields to

$$\int_0^L \Big[\left(-\tilde{E}S^*_{\omega}W_1' + \tilde{E}I^*_{3\omega}W_2'' + \tilde{E}I^*_{2\omega}W_3'' + \tilde{E}I^*_{\omega}\Phi_1'' - \tilde{E}I^*_{\omega\psi}\Phi_1'\right)''(\theta^1)$$
$$-\left(\tilde{E}S^*_{\psi}W_1' - \tilde{E}I^*_{3\psi}W_2'' - \tilde{E}I^*_{2\psi}W_3'' - \tilde{E}I^*_{\omega\psi}\Phi_1'' + \left(\tilde{G}J^* + \tilde{E}I^*_{\psi}\right)\Phi'\right)'(\theta^1)$$
$$-m_1(\theta^1) - b'(\theta^1) \ \Big]\delta\Phi_1(\theta^1)\,d\theta^1$$
$$+\Big[\Big(-\tilde{E}S^*_{\omega}(\theta^1)W_1'(\theta^1) + \tilde{E}I^*_{3\omega}(\theta^1)W_2''(\theta^1) + \tilde{E}I^*_{2\omega}(\theta^1)W_3''(\theta^1) + \tilde{E}I^*_{\omega}(\theta^1)\Phi_1''(\theta^1)$$
$$-\tilde{E}I^*_{\omega\psi}(\theta^1)\Phi_1'(\theta^1)\Big)\delta\Phi_1'(\theta^1)\Big]_0^L + B_0\,\delta\Phi_1'(0) + B_L\,\delta\Phi_1'(L)$$
$$-\Big[\Big\{\Big(-\tilde{E}S^*_{\omega}W_1' + \tilde{E}I^*_{3\omega}W_2'' + \tilde{E}I^*_{2\omega}W_3'' + \tilde{E}I^*_{\omega}\Phi_1'' - \tilde{E}I^*_{\omega\psi}\Phi_1'\Big)'(\theta^1)$$
$$-\tilde{E}S^*_{\psi}(\theta^1)W_1'(\theta^1) + \tilde{E}I^*_{3\psi}(\theta^1)W_2''(\theta^1) + \tilde{E}I^*_{2\psi}(\theta^1)W_3''(\theta^1)$$
$$+\tilde{E}I^*_{\omega\psi}(\theta^1)\Phi_1''(\theta^1) - \left(\tilde{G}J^*(\theta^1) + \tilde{E}I^*_{\psi}(\theta^1)\right)\Phi_1'(\theta^1) - b(\theta^1)\Big\}\delta\Phi_1(\theta^1)\Big]_0^L$$
$$-M_{0.1}\,\delta\Phi_1(0) - M_{L.1}\,\delta\Phi_1(L) \geq 0 \ . \qquad (2.6.8)$$

Similarly, by doing the same procedure to the other directions,

$$\Pi(W_1 + \delta W_1, W_2, W_3, \Phi_1) \geq \Pi(W_i, \Phi_1) \qquad (2.6.9)$$

$$\Pi(W_1, W_2 + \delta W_2, W_3, \Phi_1) \geq \Pi(W_i, \Phi_1) \qquad (2.6.10)$$

$$\Pi(W_1, W_2, W_3 + \delta W_3, \Phi_1) \geq \Pi(W_i, \Phi_1) \ , \qquad (2.6.11)$$

I get respectively

$$-\int_0^L\Big[\Big(\tilde{E}A^*W_1'-\tilde{E}S_3^*W_2''-\tilde{E}S_2^*W_3''-\tilde{E}S_\omega^*\Phi_1''+\tilde{E}S_\psi^*\Phi_1'\Big)'(\theta^1)+q_1(\theta^1)\Big]\delta W_1(\theta^1)\,d\theta^1$$
$$+\Big[\Big(\tilde{E}A^*(\theta^1)W_1'(\theta^1)-\tilde{E}S_3^*(\theta^1)W_2''(\theta^1)-\tilde{E}S_2^*(\theta^1)W_3''(\theta^1)-\tilde{E}S_\omega^*(\theta^1)\Phi_1''(\theta^1)$$
$$+\tilde{E}S_\psi^*(\theta^1)\Phi_1'(\theta^1)\Big)\delta W_1(\theta^1)\Big]_0^L-Q_{0.1}\,\delta W_1(0)-Q_{L.1}\,\delta W_1(L)\geq 0\ , \qquad (2.6.12)$$

$$\int_0^L\Big[\Big(-\tilde{E}S_3^*W_1'+\tilde{E}I_3^*W_2''+\tilde{E}I_{23}^*W_3''+\tilde{E}I_{3\omega}^*\Phi_1''-\tilde{E}I_{3\psi}^*\Phi_1'\Big)''(\theta^1)-q_2(\theta^1)+m_3'(\theta^1)\Big]\delta W_2(\theta^1)\,d\theta^1$$
$$+\Big[\Big(-\tilde{E}S_3^*(\theta^1)W_1'(\theta^1)+\tilde{E}I_3^*(\theta^1)W_2''(\theta^1)+\tilde{E}I_{23}^*(\theta^1)W_3''(\theta^1)+\tilde{E}I_{3\omega}^*(\theta^1)\Phi_1''(\theta^1)$$
$$-\tilde{E}I_{3\psi}^*(\theta^1)\Phi_1'(\theta^1)\Big)\delta W_2'(\theta^1)\Big]_0^L-M_{0.3}\,\delta W_2'(0)-M_{L.3}\,\delta W_2'(L)$$
$$-\Big[\Big\{\Big(-\tilde{E}S_3^*W_1'+\tilde{E}I_3^*W_2''+\tilde{E}I_{23}^*W_3''+\tilde{E}I_{3\omega}^*\Phi_1''-\tilde{E}I_{3\psi}^*\Phi_1'\Big)'(\theta^1)+m_3(\theta^1)\Big\}\delta W_2(\theta^1)\Big]_0^L$$
$$-Q_{0.2}\,\delta W_2(0)-Q_{L.2}\,\delta W_2(L)\geq 0\ , \qquad (2.6.13)$$

$$\int_0^L\Big[\Big(-\tilde{E}S_2^*W_1'+\tilde{E}I_{23}^*W_2''+\tilde{E}I_2^*W_3''+\tilde{E}I_{2\omega}^*\Phi_1''-\tilde{E}I_{2\psi}^*\Phi_1'\Big)''(\theta^1)-q_3(\theta^1)-m_2'(\theta^1)\Big]\delta W_3(\theta^1)\,d\theta^1$$
$$+\Big[\Big(-\tilde{E}S_2^*(\theta^1)W_1'(\theta^1)+\tilde{E}I_{23}^*(\theta^1)W_2''(\theta^1)+\tilde{E}I_2^*(\theta^1)W_3''(\theta^1)+\tilde{E}I_{2\omega}^*(\theta^1)\Phi_1''(\theta^1)$$
$$-\tilde{E}I_{2\psi}^*(\theta^1)\Phi_1'(\theta^1)\Big)\delta W_3'(\theta^1)\Big]_0^L+M_{0.2}\,\delta W_3'(0)+M_{L.2}\,\delta W_3'(L)$$
$$-\Big[\Big\{\Big(-\tilde{E}S_2^*W_1'+\tilde{E}I_{23}^*W_2''+\tilde{E}I_2^*W_3''+\tilde{E}I_{2\omega}^*\Phi_1''-\tilde{E}I_{2\psi}^*\Phi_1'\Big)'(\theta^1)-m_2(\theta^1)\Big\}\delta W_3(\theta^1)\Big]_0^L$$
$$-Q_{0.3}\,\delta W_3(0)-Q_{L.3}\,\delta W_3(L)\geq 0\ . \qquad (2.6.14)$$

Therefore, the only non-trivial solutions to satisfy (2.6.1) is that functions inside the brackets of equations (2.6.8), (2.6.12)-(2.6.14) vanish at any position on the open interval $(0,L)$, leading to the strong form of the boundary value problem, announced as:

Find the real-valued maps $W_1(\theta^1)$, $W_2(\theta^1)$, $W_3(\theta^1)$ and $\Phi_1(\theta^1)$ defined on the interval $\theta^1\in[0,L]$, with (i) $W_1(\theta^1)\in C^3[0,L]$ and (ii) $W_2(\theta^1),W_3(\theta^1),\Phi_1(\theta^1)\in C^4[0,L]$, satisfying the four differential equations

$$\Big(\tilde{E}A^*W_1'-\tilde{E}S_3^*W_2''-\tilde{E}S_2^*W_3''-\tilde{E}S_\omega^*\Phi_1''+\tilde{E}S_\psi^*\Phi_1'\Big)'(\theta^1)+q_1(\theta^1)=0 \qquad (2.6.15)$$

$$\Big(\tilde{E}S_3^*W_1'-\tilde{E}I_3^*W_2''-\tilde{E}I_{23}^*W_3''-\tilde{E}I_{3\omega}^*\Phi_1''+\tilde{E}I_{3\psi}^*\Phi_1'\Big)''(\theta^1)+q_2(\theta^1)-m_3'(\theta^1)=0 \qquad (2.6.16)$$

$$\left(\tilde{E}S_2^* W_1' - \tilde{E}I_{23}^* W_2'' - \tilde{E}I_2^* W_3'' - \tilde{E}I_{2\omega}^* \Phi_1'' + \tilde{E}I_{2\psi}^* \Phi_1'\right)''(\theta^1) + q_3(\theta^1) + m_2'(\theta^1) = 0 \qquad (2.6.17)$$

$$\begin{aligned}&\left(\tilde{E}S_\omega^* W_1' - \tilde{E}I_{3\omega}^* W_2'' - \tilde{E}I_{2\omega}^* W_3'' - \tilde{E}I_\omega^* \Phi_1'' + \tilde{E}I_{\omega\psi}^* \Phi_1'\right)''(\theta^1)\\ &\quad + \left[\tilde{E}S_\psi^* W_1' - \tilde{E}I_{3\psi}^* W_2'' - \tilde{E}I_{2\psi}^* W_3'' - \tilde{E}I_{\omega\psi}^* \Phi_1'' + \left(\tilde{G}J^* + \tilde{E}I_\psi^*\right)\Phi_1'\right]'(\theta^1)\\ &\quad + b'(\theta^1) + m_1(\theta^1) = 0\ ,\end{aligned} \qquad (2.6.18)$$

on the open interval $(0, L)$, together with the appropriate selection of (either natural or essential) boundary conditions at $\theta^1 = 0$ and $\theta^1 = L$, see Table 2.6.1.[22] On a final note, if I take a directional derivative from the position of equilibrium $\Pi(W_i, \Phi_1)$ in the direction $(\delta W_i, \delta\Phi_1)$ with a first order approximation

$$\Pi(W_i + \delta W_i, \Phi_1 + \delta\Phi_1) - \Pi(W_i, \Phi_1) \approx \delta\Pi(W_i, \Phi_1)[\delta W_i, \delta\Phi_1]\ , \qquad (2.6.19)$$

and introducing a parameter $\mathrm{a} \in \mathbb{R}$ to scale the admissible variations, i.e., $\mathrm{a}\delta W_i$, $\mathrm{a}\,\delta\Phi_1$; the first-order Taylor series expansion around $\mathrm{a} = 0$ is given by

$$\Pi(W_i + \mathrm{a}\delta W_i, \Phi_1 + \mathrm{a}\,\delta\Phi_1) \approx \Pi(W_i, \Phi_1) + \mathrm{a}\frac{d}{d\,\mathrm{a}}\Pi(W_i + \mathrm{a}\,\delta W_i, \Phi_1 + \mathrm{a}\,\delta\Phi_1)\Big|_{\mathrm{a}=0}\ , \qquad (2.6.20)$$

e.g., Bonet and Wood (1997) [eq. 1.25], taken $\mathrm{a} = 1$ and compare it with equation (2.6.19), an equation for the directional derivative emerge

$$\delta\Pi(W_i, \Phi_1)[\delta W_i, \delta\Phi_1] = \frac{d}{d\,\mathrm{a}}\Pi(W_i + \mathrm{a}\,\delta W_i, \Phi_1 + \mathrm{a}\,\delta\Phi_1)\Big|_{\mathrm{a}=0}\ , \qquad (2.6.21)$$

e.g., Wang and Truesdell (1973) [eq. 3.37] or Kim (2014) [eq. 3.61]. By the principle of the stationary value of total potential energy, the directional derivative evaluated at the equilibrium state must be zero for every admissible variation δW_i, $\delta\Phi_1$, i.e.,

$$\delta\Pi(W_i, \Phi_1)[\delta W_i, \delta\Phi_1] = 0\ . \qquad (2.6.22)$$

Thus, alternatively the differential equations (2.6.15)-(2.6.18) and corresponding boundary conditions shown in Table 2.6.1 are deduced, e.g., Andrade (2013) [§ 2.6].

.

[22] Notice that for each natural boundary condition opposes an essential one, that when one of these is enforced, the other must be free, i.e., the corresponding natural and essential boundary conditions cannot be enforced simultaneously. Hence, there are seven boundary conditions at each end of the bar.

Natural boundary conditions	Essential boundary conditions
$\tilde{E}A^*(0)W_1'(0) - \tilde{E}S_3^*(0)W_2''(0) - \tilde{E}S_2^*(0)W_3''(0) - \tilde{E}S_\omega^*(0)\Phi_1''(0) + \tilde{E}S_\psi^*(0)\Phi_1'(0) = -Q_{0.1}$	$W_1(0)$ prescribed (i.e., $\delta W_1(0) = 0$)
$\tilde{E}A^*(L)W_1'(L) - \tilde{E}S_3^*(L)W_2''(L) - \tilde{E}S_2^*(L)W_3''(L) - \tilde{E}S_\omega^*(L)\Phi_1''(L) + \tilde{E}S_\psi^*(L)\Phi_1'(L) = Q_{L.1}$	$W_1(L)$ prescribed (i.e., $\delta W_1(L) = 0$)
$\left(\tilde{E}S_3^* W_1' - \tilde{E}I_3^* W_2'' - \tilde{E}I_{23}^* W_3'' - \tilde{E}I_{3\omega}^* \Phi_1'' + \tilde{E}I_{3\psi}^* \Phi_1'\right)'(0) - m_3(0) = -Q_{0.2}$	$W_2(0)$ prescribed (i.e., $\delta W_2(0) = 0$)
$\left(\tilde{E}S_3^* W_1' - \tilde{E}I_3^* W_2'' - \tilde{E}I_{23}^* W_3'' - \tilde{E}I_{3\omega}^* \Phi_1'' + \tilde{E}I_{3\psi}^* \Phi_1'\right)'(L) - m_3(L) = Q_{L.2}$	$W_2(L)$ prescribed (i.e., $\delta W_2(L) = 0$)
$\tilde{E}S_3^*(0)W_1'(0) - \tilde{E}I_3^*(0)W_2''(0) - \tilde{E}I_{23}^*(0)W_3''(0) - \tilde{E}I_{3\omega}^*(0)\Phi_1''(0) + \tilde{E}I_{3\psi}^*(0)\Phi_1'(0) = M_{0.3}$	$W_2'(0)$ prescribed (i.e., $\delta W_2'(0) = 0$)
$\tilde{E}S_3^*(L)W_1'(L) - \tilde{E}I_3^*(L)W_2''(L) - \tilde{E}I_{23}^*(L)W_3''(L) - \tilde{E}I_{3\omega}^*(L)\Phi_1''(L) + \tilde{E}I_{3\psi}^*(L)\Phi_1'(L) = -M_{L.3}$	$W_2'(L)$ prescribed (i.e., $\delta W_2'(L) = 0$)
$\left(\tilde{E}S_2^* W_1' - \tilde{E}I_{23}^* W_2'' - \tilde{E}I_2^* W_3'' - \tilde{E}I_{2\omega}^* \Phi_1'' + \tilde{E}I_{2\psi}^* \Phi_1'\right)'(0) + m_2(0) = -Q_{0.3}$	$W_3(0)$ prescribed (i.e., $\delta W_3(0) = 0$)
$\left(\tilde{E}S_2^* W_1' - \tilde{E}I_{23}^* W_2'' - \tilde{E}I_2^* W_3'' - \tilde{E}I_{2\omega}^* \Phi_1'' + \tilde{E}I_{2\psi}^* \Phi_1'\right)'(L) + m_2(L) = Q_{L.3}$	$W_3(L)$ prescribed (i.e., $\delta W_3(L) = 0$)

Table 2.6.1: Natural and essential boundary conditions, e.g., Andrade (2013) [p. 51]

Natural boundary conditions	Essential boundary conditions
$\tilde{E}S_2^*(0)W_1'(0)-\tilde{E}I_{23}^*(0)W_2''(0)-\tilde{E}I_2^*(0)W_3''(0)-\tilde{E}I_{2\omega}^*(0)\Phi_1''(0)+\tilde{E}I_{2\psi}^*(0)\Phi_1'(0)=-M_{0.2}$	$W_3'(0)$ prescribed (i.e., $\delta W_3'(0)=0$)
$\tilde{E}S_2^*(L)W_1'(L)-\tilde{E}I_{23}^*(L)W_2''(L)-\tilde{E}I_2^*(L)W_3''(L)-\tilde{E}I_{2\omega}^*(L)\Phi_1''(L)+\tilde{E}I_{2\psi}^*(L)\Phi_1'(L)=M_{L.2}$	$W_3'(L)$ prescribed (i.e., $\delta W_3'(L)=0$)
$\left(\tilde{E}S_\omega^* W_1'-\tilde{E}I_{3\omega}^* W_2''-\tilde{E}I_{2\omega}^* W_3''-\tilde{E}I_\omega^* \Phi_1''+\tilde{E}I_{\omega\psi}^* \Phi_1'\right)'(0)$ $+\tilde{E}S_\psi^*(0)W_1'(0)-\tilde{E}I_{3\psi}^*(0)W_2''(0)-\tilde{E}I_{2\psi}^*(0)W_3''(0)$ $-\tilde{E}I_{\omega\psi}^*(0)\Phi_1''(0)+\left(\tilde{G}J^*(0)+\tilde{E}I_\psi^*(0)\right)\Phi_1'(0)+b(0)=-M_{0.1}$	$\Phi_1(0)$ prescribed (i.e., $\delta\Phi_1(0)=0$)
$\left(\tilde{E}S_\omega^* W_1'-\tilde{E}I_{3\omega}^* W_2''-\tilde{E}I_{2\omega}^* W_3''-\tilde{E}I_\omega^* \Phi_1''+\tilde{E}I_{\omega\psi}^* \Phi_1'\right)'(L)$ $+\tilde{E}S_\psi^*(L)W_1'(L)-\tilde{E}I_{3\psi}^*(L)W_2''(L)-\tilde{E}I_{2\psi}^*(L)W_3''(L)$ $-\tilde{E}I_{\omega\psi}^*(L)\Phi_1''(L)+\left(\tilde{G}J^*(L)+\tilde{E}I_\psi^*(L)\right)\Phi_1'(L)+b(L)=M_{L.1}$	$\Phi_1(L)$ prescribed (i.e., $\delta\Phi_1(L)=0$)
$\tilde{E}S_\omega^*(0)W_1'(0)-\tilde{E}I_{3\omega}^*(0)W_2''(0)-\tilde{E}I_{2\omega}^*(0)W_3''(0)-\tilde{E}I_\omega^*(0)\Phi_1''(0)+\tilde{E}I_{\omega\psi}^*(0)\Phi_1'(0)=-B_0$	$\Phi_1'(0)$ prescribed (i.e., $\delta\Phi_1'(0)=0$)
$\tilde{E}S_\omega^*(L)W_1'(L)-\tilde{E}I_{3\omega}^*(L)W_2''(L)-\tilde{E}I_{2\omega}^*(L)W_3''(L)-\tilde{E}I_\omega^*(L)\Phi_1''(L)+\tilde{E}I_{\omega\psi}^*(L)\Phi_1'(L)=B_L$	$\Phi_1'(L)$ prescribed (i.e., $\delta\Phi_1'(L)=0$)

Table 2.6.1 (continued): Natural and essential boundary conditions, e.g., Andrade (2013) [p. 52]

2.7 CROSS-SECTIONAL STRESS RESULTANTS, ACTIVE AND REACTIVE. EQUILIBRIUM

The natural boundary conditions associated with the differential equations, concerning the equilibrium of the tapered bar, see Table 2.6.1, serve as the inciting cause of the following definitions for the cross-sectional stress resultants, i.e., the generalised stresses, see Figure 2.7.1.

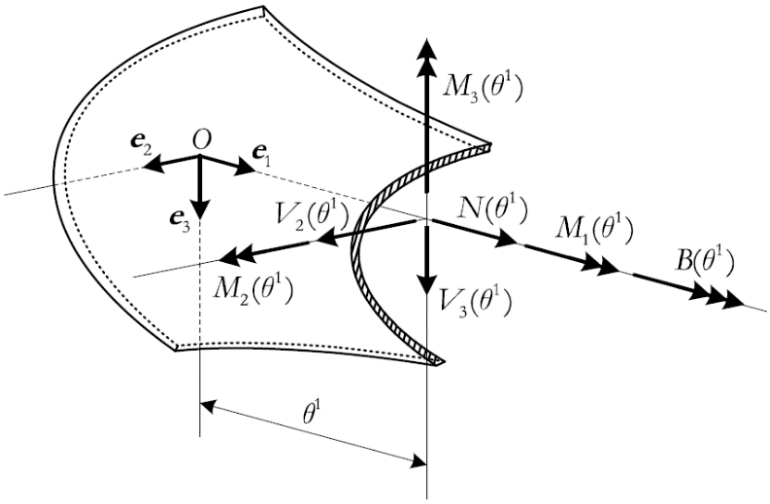

Figure 2.7.1: Cross-sectional stress resultants (Andrade 2013) [p. 53]

They are:

(i) Normal force

$$N(\theta^1) = \tilde{E}A^*(\theta^1)W_1'(\theta^1) - \tilde{E}S_3^*(\theta^1)W_2''(\theta^1) - \tilde{E}S_2^*(\theta^1)W_3''(\theta^1) - \tilde{E}S_\omega^*(\theta^1)\Phi_1''(\theta^1) + \tilde{E}S_\psi^*(\theta^1)\Phi_1'(\theta^1) \ . \tag{2.7.1}$$

(ii) Shear forces

$$V_2(\theta^1) = \left(\tilde{E}S_3^* W_1' - \tilde{E}I_3^* W_2'' - \tilde{E}I_{23}^* W_3'' - \tilde{E}I_{3\omega}^* \Phi_1'' + \tilde{E}I_{3\psi}^* \Phi_1'\right)'(\theta^1) - m_3(\theta^1) \tag{2.7.2}$$

$$V_3(\theta^1) = \left(\tilde{E}S_2^* W_1' - \tilde{E}I_{23}^* W_2'' - \tilde{E}I_2^* W_3'' - \tilde{E}I_{2\omega}^* \Phi_1'' + \tilde{E}I_{2\psi}^* \Phi_1'\right)'(\theta^1) + m_2(\theta^1) \ . \tag{2.7.3}$$

(iii) Bending moments (relative to the axes through $O + \theta^1 \boldsymbol{e}_1$ and spanned by $\boldsymbol{e}_2$ and $\boldsymbol{e}_3$)

$$M_2(\theta^1) = \tilde{E}S_2^*(\theta^1)W_1'(\theta^1) - \tilde{E}I_{23}^*(\theta^1)W_2''(\theta^1) - \tilde{E}I_2^*(\theta^1)W_3''(\theta^1) - \tilde{E}I_{2\omega}^*(\theta^1)\Phi_1''(\theta^1) + \tilde{E}I_{2\psi}^*(\theta^1)\Phi_1'(\theta^1) \tag{2.7.4}$$

$$M_3(\theta^1) = \tilde{E}S_3^*(\theta^1)W_1'(\theta^1) - \tilde{E}I_3^*(\theta^1)W_2''(\theta^1) - \tilde{E}I_{23}^*(\theta^1)W_3''(\theta^1)$$
$$-\tilde{E}I_{3\omega}^*(\theta^1)\Phi_1''(\theta^1) + \tilde{E}I_{3\psi}^*(\theta^1)\Phi_1'(\theta^1) \ . \qquad (2.7.5)$$

(iv) Torque (about the axis through O and spanned by $\boldsymbol{e}_1$)

$$M_1(\theta^1) = \left(\tilde{E}S_\omega^* W_1' - \tilde{E}I_{3\omega}^* W_2'' - \tilde{E}I_{2\omega}^* W_3'' - \tilde{E}I_\omega^* \Phi_1''\right)'(\theta^1)$$
$$+\tilde{E}S_\psi^*(\theta^1)W_1'(\theta^1) - \tilde{E}I_{3\psi}^*(\theta^1)W_2''(\theta^1) - \tilde{E}I_{2\psi}^*(\theta^1)W_3''(\theta^1)$$
$$+\left(\tilde{G}J^*(\theta^1) + \tilde{E}I_\psi^*(\theta^1) + \tilde{E}I_{\omega\psi}^{*\,\prime}\right)\Phi_1'(\theta^1) + b(\theta^1) \ . \qquad (2.7.6)$$

(v) Bimoment (in Figure 2.7.1, it is represented by a three-headed arrow, e.g., Gjelsvik (1981) [p. 25], without physical meaning)[23]

$$B(\theta^1) = \tilde{E}S_\omega^*(\theta^1)W_1'(\theta^1) - \tilde{E}I_{3\omega}^*(\theta^1)W_2''(\theta^1) - \tilde{E}I_{2\omega}^*(\theta^1)W_3''(\theta^1)$$
$$-\tilde{E}I_\omega^*(\theta^1)\Phi_1''(\theta^1) + \tilde{E}I_{\omega\psi}^*(\theta^1)\Phi_1'(\theta^1) \ . \qquad (2.7.7)$$

The real-valued maps $\theta^1 \mapsto N(\theta^1)$, $\theta^1 \mapsto V_2(\theta^1)$, $\theta^1 \mapsto V_3(\theta^1)$ and $\theta^1 \mapsto M_1(\theta^1)$ are continuously differentiable on $[0, L]$, while $\theta^1 \mapsto M_2(\theta^1)$, $\theta^1 \mapsto M_3(\theta^1)$ and $\theta^1 \mapsto B(\theta^1)$ are twice continuously differentiable on the same interval.[24]

[23] Consider the degrees-of-freedom for the end nodes of the beam element model shown in Figure 2.7.2.

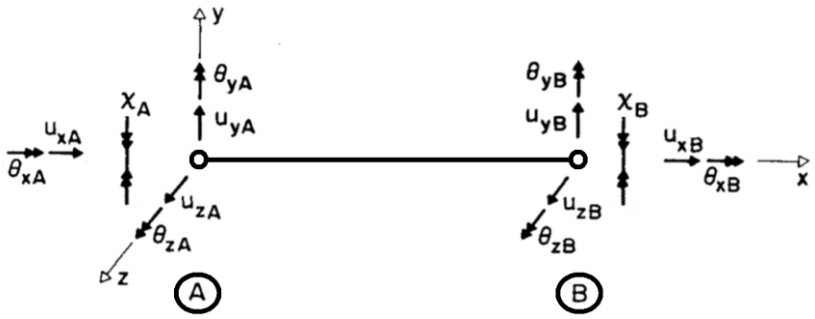

Figure 2.7.2: Degrees-of-freedom for beam element model (Yang and McGuire 1984)

An alternative graphical representation for the warping degree-of-freedom (i.e., the rate of twist) and its corresponding bimoment, is using self-equilibrating moment vectors, as shown in the previous figure.

[24] According to the smoothness assumptions stated at the beginning of §2.6.

Certainly, with above definitions, the natural boundary conditions are equivalent to the prescribing the stress resultants at the bar ends, with:

$$N(0) = -Q_{0.1} \qquad N(L) = Q_{L.1} \tag{2.7.8}$$

$$V_2(0) = -Q_{0.2} \qquad V_2(L) = Q_{L.2} \tag{2.7.9}$$

$$V_3(0) = -Q_{0.3} \qquad V_3(L) = Q_{L.3} \tag{2.7.10}$$

$$M_1(0) = -M_{0.1} \qquad M_1(L) = M_{L.1} \tag{2.7.11}$$

$$M_2(0) = -M_{0.2} \qquad M_2(L) = M_{L.2} \tag{2.7.12}$$

$$M_3(0) = M_{0.3} \qquad M_3(L) = -M_{L.3} \tag{2.7.13}$$

$$B(0) = -B_0 \qquad B(L) = B_L \ . \tag{2.7.14}$$

As in the case of the membrane forces and shell moments, the cross-sectional stress resultants (2.7.1)-(2.7.7) are split into active and reactive categories. The normal force, bending moments and bimoment are evidently active, as they can be obtained from the sole active membrane force $n_{\mathrm{I\cdot I}}^{(A)}$ (resp. shell moment $m_{\mathrm{I\cdot I}}^{(A)}$) through integration over the cross-section, i.e., interval $\left[g_1(\theta^1), g_2(\theta^1)\right]$,

$$N(\theta^1) = \int_{g_1(\theta^1)}^{g_2(\theta^1)} n_{\mathrm{I\cdot I}}^{(A)}(\theta^1,\theta^2)\, \boldsymbol{o}_{\mathrm{I}}(\theta^1,\theta^2)\cdot\boldsymbol{e}_1\, d\theta^2 \tag{2.7.15}$$

$$M_2(\theta^1) = \int_{g_1(\theta^1)}^{g_2(\theta^1)} \left(\bar{x}_3\, n_{\mathrm{I\cdot I}}^{(A)}(\theta^1,\theta^2) + \frac{\boldsymbol{o}_{\mathrm{II}}(\theta^1,\theta^2)\cdot\boldsymbol{e}_2}{\sqrt{a(\theta^1,\theta^2)}}\, m_{\mathrm{I\cdot I}}^{(A)}(\theta^1,\theta^2) \right) \boldsymbol{o}_{\mathrm{I}}(\theta^1,\theta^2)\cdot\boldsymbol{e}_1\, d\theta^2 \tag{2.7.16}$$

$$M_3(\theta^1) = \int_{g_1(\theta^1)}^{g_2(\theta^1)} \left(\bar{x}_2\, n_{\mathrm{I\cdot I}}^{(A)}(\theta^1,\theta^2) - \frac{\boldsymbol{o}_{\mathrm{II}}(\theta^1,\theta^2)\cdot\boldsymbol{e}_3}{\sqrt{a(\theta^1,\theta^2)}}\, m_{\mathrm{I\cdot I}}^{(A)}(\theta^1,\theta^2) \right) \boldsymbol{o}_{\mathrm{I}}(\theta^1,\theta^2)\cdot\boldsymbol{e}_1\, d\theta^2 \tag{2.7.17}$$

$$B(\theta^1) = \int_{g_1(\theta^1)}^{g_2(\theta^1)} \left(\omega\, n_{\mathrm{I\cdot I}}^{(A)}(\theta^1,\theta^2) + \frac{q(\theta^1,\theta^2)}{\sqrt{a(\theta^1,\theta^2)}}\, m_{\mathrm{I\cdot I}}^{(A)}(\theta^1,\theta^2) \right) \boldsymbol{o}_{\mathrm{I}}(\theta^1,\theta^2)\cdot\boldsymbol{e}_1\, d\theta^2 \ . \tag{2.7.18}$$

Meanwhile, the shear forces are clearly reactive, being related to the active cross-sectional stress, given by

$$V_2(\theta^1) = M_3'(\theta^1) - m_3(\theta^1) \tag{2.7.19}$$

$$V_3(\theta^1) = M_2'(\theta^1) + m_2(\theta^1) \ . \tag{2.7.20}$$

With respect the torque $M_1(\theta^1)$, it can be split into an active part $M_1^{(A)}(\theta^1)$ and a reactive part $M_1^{(R)}(\theta^1)$. Where the active part is equal to

$$\begin{aligned} M_1^{(A)}(\theta^1) &= \int_{g_1(\theta^1)}^{g_2(\theta^1)} \Big(\psi\, n_{\mathrm{I\cdot I}}^{(A)}(\theta^1,\theta^2) + \big(m_{\mathrm{I\cdot II}}^{(A)}(\theta^1,\theta^2) + m_{\mathrm{II\cdot I}}^{(A)}(\theta^1,\theta^2) \big) \boldsymbol{\kappa}_1(\theta^1) \Big) \boldsymbol{o}_{\mathrm{I}}(\theta^1,\theta^2)\cdot \boldsymbol{e}_1 \; d\theta^2 \\ &= \tilde{E} S_{\psi}^{*}(\theta^1) W_1'(\theta^1) - \tilde{E} I_{3\psi}^{*}(\theta^1) W_2''(\theta^1) - \tilde{E} I_{2\psi}^{*}(\theta^1) W_3''(\theta^1) \\ &\quad - \tilde{E} I_{\omega\psi}^{*}(\theta^1) \Phi_1''(\theta^1) + \big(\tilde{G} J^{*}(\theta^1) + \tilde{E} I_{\psi}^{*}(\theta^1) \big) \Phi_1'(\theta^1) \;, \end{aligned} \tag{2.7.21}$$

and the reactive part is simply

$$\begin{aligned} M_1^{(R)}(\theta^1) &= B'(\theta^1) + b(\theta^1) \\ &= \big(\tilde{E} S_{\omega}^{*} W_1' - \tilde{E} I_{3\omega}^{*} W_2'' - \tilde{E} I_{2\omega}^{*} W_3'' - \tilde{E} I_{\omega}^{*} \Phi_1'' + \tilde{E} I_{\omega\psi}^{*} \Phi' \big)'(\theta^1) + b(\theta^1) \;. \end{aligned} \tag{2.7.22}$$

With above distinction between active and reactive cross-sectional stress resultants, it is easy to proof, that the elastic energy (2.5.23), is equal to

$$\mathcal{U} = \frac{1}{2} \int_0^L \big(N\, \varepsilon(\theta^1) + M_1^{(A)}\, \boldsymbol{\kappa}_1(\theta^1) + M_2\, \boldsymbol{\kappa}_2(\theta^1) + M_3\, \boldsymbol{\kappa}_3(\theta^1) + B\, \Gamma(\theta^1) \big)\, d\theta^1 \;. \tag{2.7.23}$$

Physically, the active cross-sectional stress resultants are the only shell forces that distort the constraint shell, where ε, $\boldsymbol{\kappa}_1$, $\boldsymbol{\kappa}_2$, $\boldsymbol{\kappa}_3$ and Γ are the generalised strains introduced in (2.3.39)-(2.3.43), which are work conjugate to the active stress resultants. Furthermore, since the stored elastic energy (2.7.23) is independent to the reactive cross-sectional stress resultants, they act as a kind of nonworking reactions, only needed to maintain equilibrium due to the constraints (V1)-(V3).[25] With equations (2.7.1) and (2.7.4)-(2.7.6), the differential equations (2.6.15)-(2.6.18) are written into the classical local form of the equilibrium equations[26] on $(0, L)$

$$N'(\theta^1) + q_1(\theta^1) = 0 \tag{2.7.24}$$

$$M_3''(\theta^1) - m_3'(\theta^1) + q_2(\theta^1) = 0 \tag{2.7.25}$$

$$M_2''(\theta^1) + m_2'(\theta^1) + q_3(\theta^1) = 0 \tag{2.7.26}$$

$$M_1'(\theta^1) + m_1(\theta^1) = 0 \;. \tag{2.7.27}$$

[25] In fact, the reactive cross-sectional stress resultants, i.e., equations (2.7.19)-(2.7.20) and (2.7.22), are gotten by using equilibrium considerations.

[26] In equations (2.7.25)-(2.7.26), their second term on the left-hand, they are continuously differentiable moment per unit length distributions $\theta^1 \mapsto m_3(\theta^1)\boldsymbol{e}_3$ and $\theta^1 \mapsto m_2(\theta^1)\boldsymbol{e}_2$, of the line segment $\theta^1 \boldsymbol{e}_1$ with $0 \le \theta^1 \le L$. They are statically equivalent to a (i) distributed force per unit length $\theta^1 \mapsto -m_3'(\theta^1)\boldsymbol{e}_2$ and $\theta^1 \mapsto m_2'(\theta^1)\boldsymbol{e}_3$, of the same line segment plus (ii) concentrated forces $-m_3(0)\boldsymbol{e}_2$, $m_3(L)\boldsymbol{e}_2$ and $m_2(0)\boldsymbol{e}_3$, $-m_2(L)\boldsymbol{e}_3$ at the end points O and $O + L\boldsymbol{e}_1$ respectively.

Finally, last equation (2.7.27) can be written only in terms of active components as

$$B''(\theta^1) + M_1^{(A)\prime}(\theta^1) + b'(\theta^1) + m_1(\theta^1) = 0 \ . \tag{2.7.28}$$

Hence, the second-order derivative of the bimoment has units of torque per unit length.

2.8 FIELD EQUATIONS OF THE ONE-DIMENSIONAL MODEL A MATRIX APPROACH

The one-dimensional model rests on the base of four sets of dependent variables, that are all real-valued maps of the single real variable θ^1, defined on the interval $\theta^1 \in [0, L]$.

They are:

(i) The generalised displacements, written in the column vector

$$\{\mathrm{w}\} = \begin{Bmatrix} W_1 \\ W_2 \\ W_3 \\ \Phi_1 \end{Bmatrix} . \tag{2.8.1}$$

(ii) The generalised strains, represented by the column vector

$$\{e\} = \begin{Bmatrix} \varepsilon \\ \kappa_1 \\ \kappa_2 \\ \kappa_3 \\ \Gamma \end{Bmatrix} . \tag{2.8.2}$$

The generalised displacements $\{\mathrm{w}\}$ and the generalised strains $\{e\}$ are related by a compatibility equation via

$$\{e\} = [L]\{\mathrm{w}\} \tag{2.8.3}$$

with the operator $[L]$ defined as

$$[L] = \begin{bmatrix} D & \cdot & \cdot & \cdot \\ \cdot & \cdot & \cdot & D \\ \cdot & \cdot & -D^2 & \cdot \\ \cdot & -D^2 & \cdot & \cdot \\ \cdot & \cdot & \cdot & -D^2 \end{bmatrix} , \tag{2.8.4}$$

that represents the compact notation of equations (2.3.39)-(2.3.43).

(iii) The active cross-sectional stress resultants, which are work conjugate to the generalised strains, grouped in the column vector

$$\left\{\sigma^{(A)}\right\} = \begin{Bmatrix} N \\ M_1^{(A)} \\ M_2 \\ M_3 \\ B \end{Bmatrix} . \tag{2.8.5}$$

Furthermore, the active cross-sectional stress resultants $\left\{\sigma^{(A)}\right\}$ are given in terms of the generalised strains $\{e\}$, by the constitutive relation:

$$\left\{\sigma^{(A)}\right\} = [K]\{e\} \ , \tag{2.8.6}$$

see equations (2.7.1), (2.7.4)-(2.7.5), (2.7.7) and (2.7.21) where $[K]$ is the symmetric stiffness matrix, defined as

$$[K] = \begin{bmatrix} \tilde{E}A^* & \tilde{E}S_\psi^* & \tilde{E}S_2^* & \tilde{E}S_3^* & \tilde{E}S_\omega^* \\ \tilde{E}S_\psi^* & \left(\tilde{G}J^* + \tilde{E}I_\psi^*\right) & \tilde{E}I_{2\psi}^* & \tilde{E}I_{3\psi}^* & \tilde{E}I_{\omega\psi}^* \\ \tilde{E}S_2^* & \tilde{E}I_{2\psi}^* & \tilde{E}I_2^* & \tilde{E}I_{23}^* & \tilde{E}I_{2\omega}^* \\ \tilde{E}S_3^* & \tilde{E}I_{3\psi}^* & \tilde{E}I_{23}^* & \tilde{E}I_3^* & \tilde{E}I_{3\omega}^* \\ \tilde{E}S_\omega^* & \tilde{E}I_{\omega\psi}^* & \tilde{E}I_{2\omega}^* & \tilde{E}I_{3\omega}^* & \tilde{E}I_\omega^* \end{bmatrix} , \tag{2.8.7}$$

whose entries are known real-valued maps defined on $[0, L]$. Hence, the stored elastic energy (2.7.23) has the form

$$\mathcal{U} = \frac{1}{2}\int_0^L \left\{\sigma^{(A)}\right\}^T \{e\}\, d\theta^1 = \frac{1}{2}\int_0^L \{e\}^T [K]\{e\}\, d\theta^1 \ . \tag{2.8.8}$$

Since the matrix $[K]$ is symmetric, by using the spectral theorem, e.g., Strang and Borre (1997) [p. 233] or Miller and Takloo-Bighash (2006) [p. 459], exist an orthogonal matrix $[Q]$ and a real diagonal matrix $[\ k\ ]$ such that[27]

$$[K] = [Q]^T [\ k\ ][Q] \ . \tag{2.8.9}$$

[27] Suppose $[K]$ has five distinct eigenvalues λ_i $(i = 1,2,...,5.)$ and corresponding normalized eigenvectors $\{p_i\}$ $(i = 1,2,...,5.)$. Letting $[Q]^T = [\{p_1\}|...|\{p_5\}]$, i.e., $[Q]^T = [Q]^{-1}$, then $[\ k\ ] = [Q][K][Q]^T$ is a diagonal matrix with the eigenvalues λ_i are the diagonal.

Thus, the stored elastic energy (2.8.8) has the form

$$\mathcal{U}=\frac{1}{2}\int_0^L \{[\mathcal{Q}]\{e\}\}^T [\,k\,]\{[\mathcal{Q}]\{e\}\}\,d\theta^1 \ . \tag{2.8.10}$$

In order to have non-zero positive values of energy for any $(W_i,\Phi_1)\in\mathcal{D}$ and $W_i,\Phi_1\neq 0$, all the entries of $[\,k\,]$ must be positive, i.e., *the symmetric matrix* $[K]$ *must be positive-definite*. By using the Sylvester criterion,[28] it allows to establish four fundamental inequalities concerning the cross-sectional properties of the bar

$$A^*\left(\tilde{\mu}J^*+I_\psi^*\right)>\left(S_\psi^*\right)^2 \tag{2.8.11}$$

$$A^*I_2^*\left(\tilde{\mu}J^*+I_\psi^*\right)+2I_{2\psi}^*S_2^*S_\psi^*>\left(S_2^*\right)^2\left(\tilde{\mu}J^*+I_\psi^*\right)+\left(S_\psi^*\right)^2 I_2^*+\left(I_{2\psi}^*\right)^2 A^* \tag{2.8.12}$$

$$\det\begin{bmatrix} A^* & S_\psi^* & S_2^* & S_3^* \\ S_\psi^* & \left(\tilde{\mu}J^*+I_\psi^*\right) & I_{2\psi}^* & I_{3\psi}^* \\ S_2^* & I_{2\psi}^* & I_2^* & I_{23}^* \\ S_3^* & I_{3\psi}^* & I_{23}^* & I_3^* \end{bmatrix}>0 \tag{2.8.13}$$

$$\det\begin{bmatrix} A^* & S_\psi^* & S_2^* & S_3^* & S_\omega^* \\ S_\psi^* & \left(\tilde{\mu}J^*+I_\psi^*\right) & I_{2\psi}^* & I_{3\psi}^* & I_{\omega\psi}^* \\ S_2^* & I_{2\psi}^* & I_2^* & I_{23}^* & I_{2\omega}^* \\ S_3^* & I_{3\psi}^* & I_{23}^* & I_3^* & I_{3\omega}^* \\ S_\omega^* & I_{\omega\psi}^* & I_{2\omega}^* & I_{3\omega}^* & I_\omega^* \end{bmatrix}>0 \ , \tag{2.8.14}$$

where the non-dimensional variable $\tilde{\mu}$ is defined as the ratio between the modified shear and elastic modulus respectively

$$\tilde{\mu}=\frac{\tilde{G}}{\tilde{E}} \ . \tag{2.8.15}$$

Thus, for a general bar with open cross-section, above inequalities holds, and provides an existence and uniqueness theorem for the two-dimensional Kirchhoff-Love shell.

[28] A real symmetric $n\times n$ matrix $[A]$ is positive-definite, if and only if $\det[A_k]>0$ with $k=1,2,...,n$. where $[A_k]$ is the $k\times k$ matrix formed by the intersection of the first k rows and columns of $[A]$, e.g., Dahlquist and Björck (2003) [p. 163], Bažant and Cedolin (2003) [eq. 4.1.12].

(iv) The distributed bar loads compatible to the generalised displacements $\{\mathrm{w}\}$, collected in the column vector

$$\{\mathrm{q}\} = \begin{Bmatrix} q_1 \\ -m_3' + q_2 \\ m_2' + q_3 \\ b' + m_1 \end{Bmatrix} . \tag{2.8.16}$$

It must satisfy equation (2.5.28), i.e.,

$$\mathcal{W}_e = \int_0^L \{\mathrm{w}\}^T \{\mathrm{q}\}\, d\theta^1 + \text{Boundary terms} \ .^{29} \tag{2.8.17}$$

Since I fulfil the boundary terms, I can defined the adjoint operator $[L]^\dagger$ to the operator (2.8.4) e.g Wang and Truesdell (1973) [eq. 1.92] or Gantmakher (2000) [§ 8], with the following property

$$\int_0^L \left\{\sigma^{(A)}\right\}^T \left\{[L]\{\mathrm{w}\}\right\} d\theta^1 = \int_0^L \{\mathrm{w}\}^T \left\{[L]^\dagger \left\{\sigma^{(A)}\right\}\right\} d\theta^1 \ , \tag{2.8.18}$$

so that the adjoint operator is defined as

$$[L]^\dagger = \begin{bmatrix} -D & \cdot & \cdot & \cdot & \cdot \\ \cdot & \cdot & \cdot & -D^2 & \cdot \\ \cdot & \cdot & -D^2 & \cdot & \cdot \\ \cdot & -D & \cdot & \cdot & -D^2 \end{bmatrix} . \tag{2.8.19}$$

Hence, the transpose of the column vector $\{e\}$ inside the integral (2.8.8), is given by

$$\mathcal{U} = \frac{1}{2}\int_0^L \{e\}^T [K]\{e\}\, d\theta^1 = \frac{1}{2}\int_0^L \{\mathrm{w}\}^T [L]^\dagger [K][L]\{\mathrm{w}\}\, d\theta^1 \ . \tag{2.8.20}$$

Thus, the total potential energy has the following compact notation

$$\Pi(W_i, \Phi_1) = \int_0^L \left(\frac{1}{2}\{\mathrm{w}\}^T [L]^\dagger [K][L]\{\mathrm{w}\} - \{\mathrm{w}\}^T \{\mathrm{q}\} \right) d\theta^1 + \text{Boundary terms} . \tag{2.8.21}$$

If I take a directional derivative from the position of equilibrium, in the direction $\{\delta\mathrm{w}\}$ with a first order approximation, see expression (2.6.19),

$$\delta\Pi(W_i, \Phi_1)[\delta W_i, \delta\Phi_1] = \int_0^L \{\delta\mathrm{w}\}^T \left\{[L]^\dagger [K][L]\{\mathrm{w}\} - \{\mathrm{q}\}\right\} d\theta^1 \ ,^{30} \tag{2.8.22}$$

---

[29] Notice that in equation (2.5.28) the bar loads m_2, m_3 and b are associated with derivatives of generalised displacements while in equation (2.8.17) are their derivatives whose are associated with the generalised displacements. This equivalency is a direct consequence of equations (2.3.39)-(2.3.43).

[30] The boundary terms are being satisfied.

by the principle of stationarity of the total potential energy, i.e., $\delta\Pi(W_i, \Phi_1)[\delta W_i, \delta\Phi_1] = 0$, the non-trivial solution leads to the strong form of the boundary value problem

$$[L]^{\dagger}[K][L]\{\mathrm{w}\} = \{\mathrm{q}\} \ , \tag{2.8.23}$$

which are the governing equations (2.6.15)-(2.6.18) written in compact matrix form. Furthermore, by using the above equilibrium condition, the distributed bar loads $\{q\}$ are related to the active cross-sectional stress resultants $\{\sigma^{(A)}\}$ via

$$[L]^{\dagger}\{\sigma^{(A)}\} = \{\mathrm{q}\} \ . \tag{2.8.24}$$

All the previous matrices and column vectors already described, are summarised in Figure 2.8.1.[31] By last, the reactive cross-sectional stress resultants, written in the column vector

$$\{\sigma^{(R)}\} = \begin{Bmatrix} V_2 \\ V_3 \\ M_1^{(R)} \end{Bmatrix} \ . \tag{2.8.25}$$

The reactive cross-sectional stress resultants arise due to equilibrium considerations as

$$\{\sigma^{(R)}\} = \begin{Bmatrix} M_3' \\ M_2' \\ B' \end{Bmatrix} + \begin{Bmatrix} -m_3 \\ m_2 \\ b \end{Bmatrix} \ . \tag{2.8.26}$$

Hence, they can be thought as a superposition of the constraints and the external loading, e.g., Gjelsvik (1981) [eq. 1.60a-1.60c]. Finally, by taking the rows corresponding with the active cross-sectional stress resultants in the stiffness matrix (2.8.7) of the moments M_2, M_3 and the bimoment B, equation (2.8.26) is rewritten as

$$\{\sigma^{(R)}\} = \left(\begin{bmatrix} \tilde{E}S_3^* & \tilde{E}I_{3\psi}^* & \tilde{E}I_{23}^* & \tilde{E}I_3^* & \tilde{E}I_{3\omega}^* \\ \tilde{E}S_2^* & \tilde{E}I_{2\psi}^* & \tilde{E}I_2^* & \tilde{E}I_{23}^* & \tilde{E}I_{2\omega}^* \\ \tilde{E}S_\omega^* & \tilde{E}I_{\omega\psi}^* & \tilde{E}I_{2\omega}^* & \tilde{E}I_{3\omega}^* & \tilde{E}I_\omega^* \end{bmatrix} \begin{Bmatrix} W_1' \\ \Phi_1' \\ -W_3'' \\ -W_2'' \\ -\Phi_1'' \end{Bmatrix} \right)' + \begin{Bmatrix} -m_3 \\ m_2 \\ b \end{Bmatrix} \ . \tag{2.8.27}$$

[31] Diagrams such as this, originated in Enzo Tonti's work concerning the reasons for analogies between physical theories (e.g., Tonti 1975, 1976), are known as Tonti or classification diagrams.

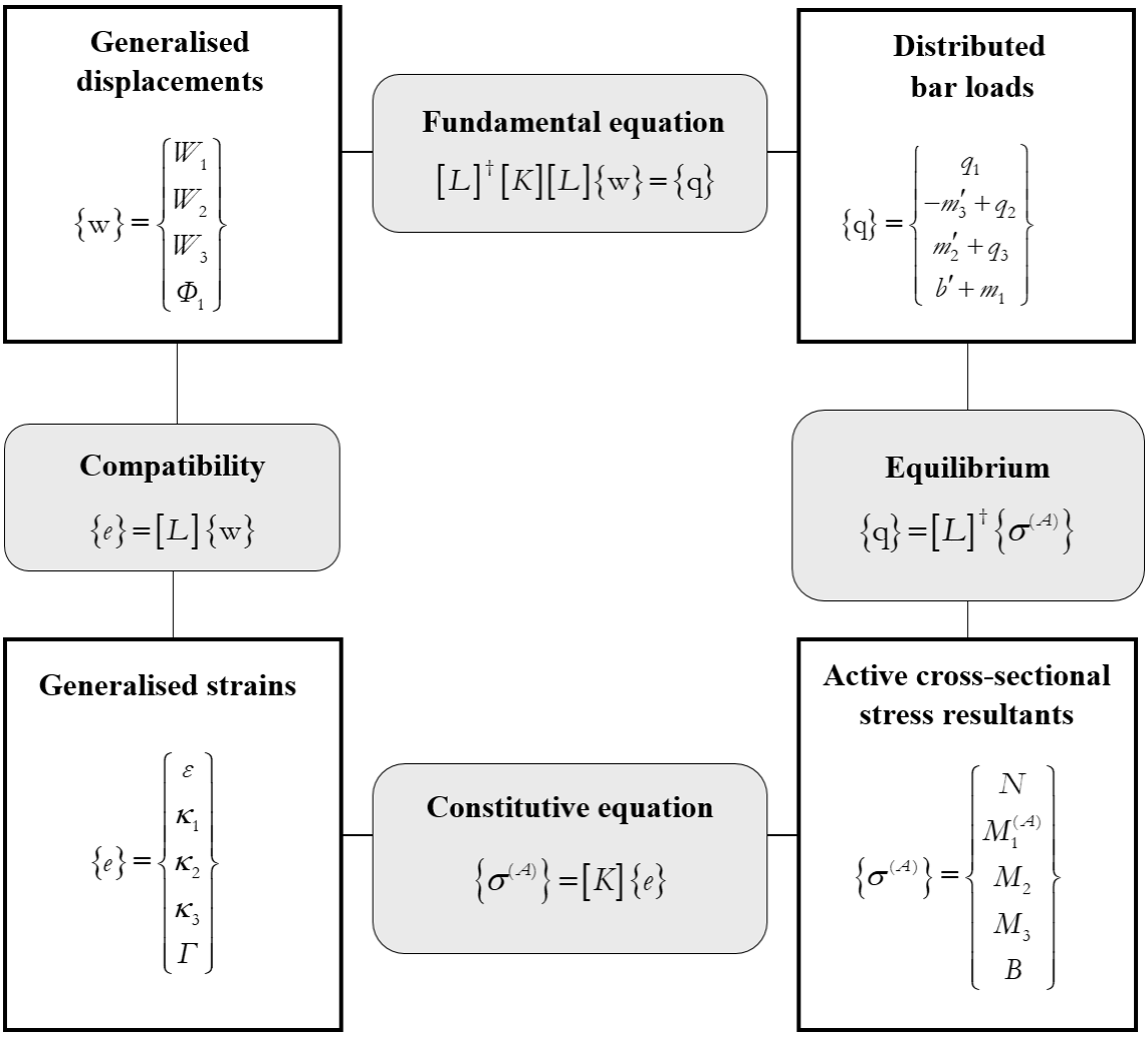

Figure 2.8.1: Framework for deriving the strong form of the boundary value problem (Andrade 2013) [p. 59]

2.9 BARS WITH IRREGULAR MIDDLE SURFACE

So far, I have only considered bars whose middle surface shape S is described by a single parametrisation F. This limiting framework is now extended to bars with irregular middle surfaces, made up of several surface elements, each defined via a single smooth enough parametrisation

$$F^{(\mathrm{k})}:\bar{\Omega}\to\mathbb{R}^3 \text{ with } \mathrm{k}=\{a,b,c,\ldots\}\ , \tag{2.9.1}$$

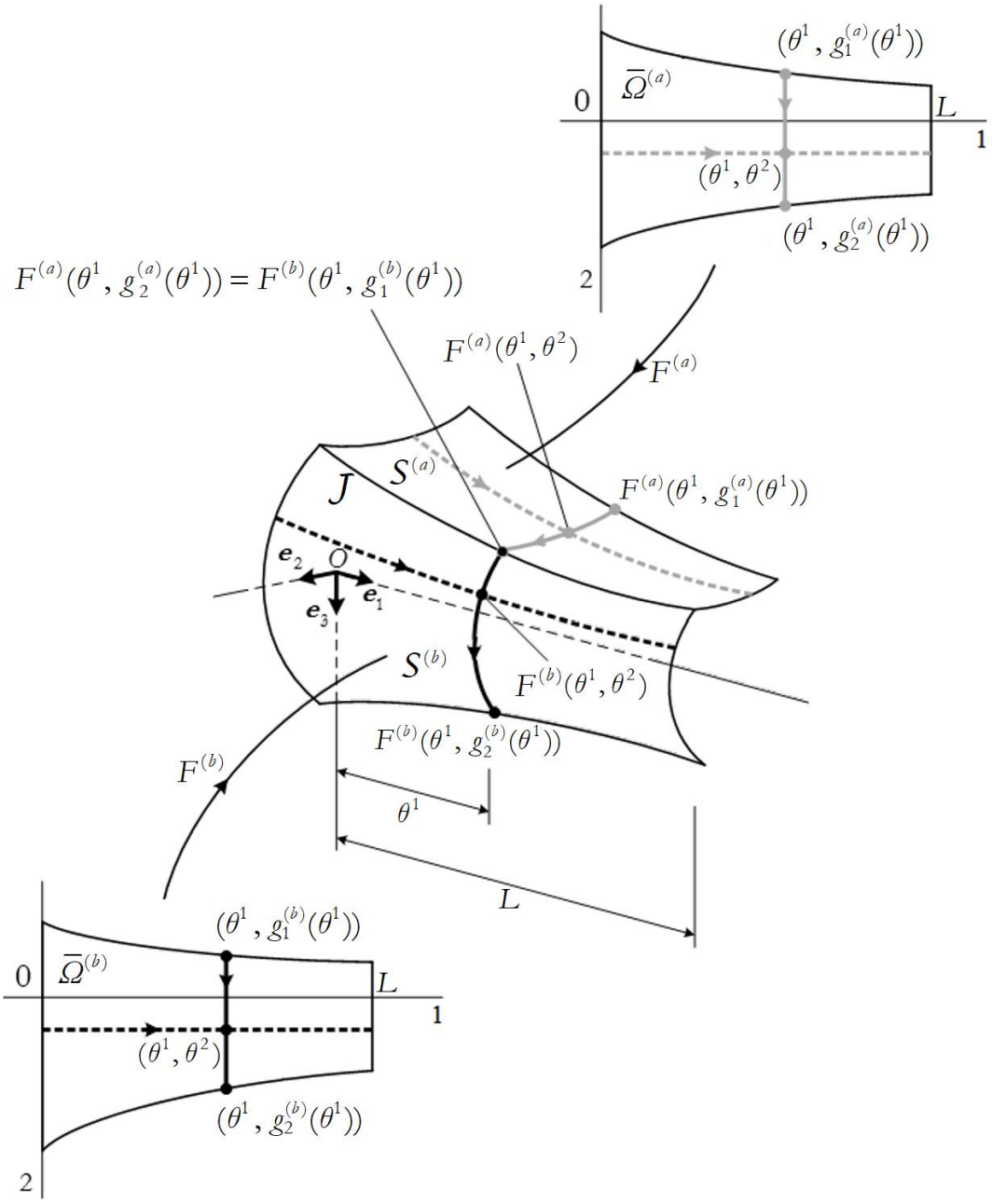

Figure 2.9.1: Irregular middle surface made up of two surface elements, $S^{(a)}$ and $S^{(b)}$, rigidly joined along the longitudinal edge $\mathcal{J}$, adapted from Andrade (2013) [p. 71]

and joined along longitudinal edges.[32] As an exemplary case, consider the bar shown in Figure 2.9.1, where its middle surface S is defined by two surface elements $S^{(a)}$ and $S^{(b)}$, rigidly joined along the edge $\mathcal{J}$

$$S = S^{(a)} \cup S^{(b)} , \qquad \mathcal{J} = S^{(a)} \cap S^{(b)} . \tag{2.9.2}$$

[32] As a general notational rule, the surface elements and all related quantities are indexed by a superscript k taking its values in the set $\mathrm{k} = \{a, b, c, \ldots\}$ and enclosed within parentheses.

Each surface element $S^{(\mathrm{k})}$ with $\mathrm{k}=\{a,b\}$ is described by the corresponding parametrisation $F^{(\mathrm{k})}$, with the features laid down in §2.2. In particular, the domain of $F^{(\mathrm{k})}$ is a subset in $\mathbb{R}^2$, of the form

$$\bar{\Omega}^{(\mathrm{k})}=\left\{(\theta^1,\theta^2)\in\mathbb{R}^2\,\middle|\,0\le\theta^1\le L \text{ and } g_1^{(\mathrm{k})}(\theta^1)\le\theta^2\le g_2^{(\mathrm{k})}(\theta^1)\right\} \text{ with } \mathrm{k}=\{a,b\}\ , \tag{2.9.3}$$

where $g_1^{(\mathrm{k})}$, $g_2^{(\mathrm{k})}$ are real-valued functions on $[0,L]$ and $g_1^{(\mathrm{k})}(\theta^1)<g_2^{(\mathrm{k})}(\theta^1)$ with $0\in\left[g_1^{(\mathrm{k})}(\theta^1),\,g_2^{(\mathrm{k})}(\theta^1)\right]$. Moreover, the continuous compatibility equation along the edge

$$F^{(a)}(\theta^1,g_2^{(a)}(\theta^1))=F^{(b)}(\theta^1,g_1^{(b)}(\theta^1))\quad\forall\,\theta^1\in[0,L]\ . \tag{2.9.4}$$

It follows, that the wall thickness on each surface element is given by

$$t^{(\mathrm{k})} \text{ with } \mathrm{k}=\{a,b\}\ . \tag{2.9.5}$$

All the quantities defined from F in §2.2.2-§2.2.7, can now be defined from each $F^{(\mathrm{k})}$ with $\mathrm{k}=\{a,b\}$.[33] The admissible middle surface displacement field

$$(\theta^1,\theta^2)\in\bar{\Omega}^{(\mathrm{k})}\mapsto\bar{\boldsymbol{U}}^{(\mathrm{k})}(\theta^1,\theta^2) \text{ with } \mathrm{k}=\{a,b\}\ , \tag{2.9.6}$$

satisfying the constraints (V1)-(V2),[34] is equal to

$$\bar{\boldsymbol{U}}^{(\mathrm{k})}(\theta^1,\theta^2)=\boldsymbol{W}+\boldsymbol{\Phi}\times\left(\bar{x}_2^{(\mathrm{k})}\,\boldsymbol{e}_2+\bar{x}_3^{(\mathrm{k})}\,\boldsymbol{e}_3\right)-\omega^{(\mathrm{k})}\,\Phi_1'\,\boldsymbol{e}_1 \text{ with } \mathrm{k}=\{a,b\}\ , \tag{2.9.7}$$

where the translation vector and the infinitesimal rotation vector are respectively

$$\boldsymbol{W}=W_i(\theta^1)\,\boldsymbol{e}_i\ ,\qquad\qquad \boldsymbol{\Phi}=\Phi_1(\theta^1)\,\boldsymbol{e}_1-W_3'(\theta^1)\,\boldsymbol{e}_2+W_2'(\theta^1)\,\boldsymbol{e}_3\ , \tag{2.9.8}$$

i.e., the functions W_i and Φ_1 are the generalised displacement fields defined in §2.3.1, with the warping functions given by

$$\omega^{(a)}(\theta^1,\theta^2)=\int_0^{\theta^2}\left(\bar{x}_2^{(a)}(\theta^1,s)\,D_2\bar{x}_3^{(a)}(\theta^1,s)-\bar{x}_3^{(a)}(\theta^1,s)\,D_2\bar{x}_2^{(a)}(\theta^1,s)\right)ds \tag{2.9.9}$$

$$\omega^{(b)}(\theta^1,\theta^2)=\int_{g_1^{(b)}(\theta^1)}^{\theta^2}\left(\bar{x}_2^{(b)}(\theta^1,s)\,D_2\bar{x}_3^{(b)}(\theta^1,s)-\bar{x}_3^{(b)}(\theta^1,s)\,D_2\bar{x}_2^{(b)}(\theta^1,s)\right)ds$$
$$+\omega^{(a)}(\theta^1,g_2^{(a)}(\theta^1))\ . \tag{2.9.10}$$

[33] It should be noted that the geometrical modelling of the reference shape of the bar, i.e., $\boldsymbol{\mathcal{X}}^{(\mathrm{k})}$ with $\mathrm{k}=\{a,b\}$, see equation (2.2.8), implies small inaccuracies at most junctions, that for practical reasons they are omitted.

[34] i.e., equations (2.3.26) and (2.3.33)-(2.3.35).

Observe that an admissible middle surface displacement field $\bar{\boldsymbol{U}}^{(\mathrm{k})}(\theta^1,\theta^2)$ should satisfy the compatibility condition at the edges, i.e.,

$$\bar{\boldsymbol{U}}^{(a)}(\theta^1, g_2^{(a)}(\theta^1)) = \bar{\boldsymbol{U}}^{(b)}(\theta^1, g_1^{(b)}(\theta^1)) \ , \tag{2.9.11}$$

which implies that

$$\omega^{(a)}(\theta^1, g_2^{(a)}(\theta^1)) = \omega^{(b)}(\theta^1, g_1^{(b)}(\theta^1)) \ .^{35} \tag{2.9.12}$$

To each $\bar{\boldsymbol{U}}^{(\mathrm{k})}$ with the above form, corresponds a linearized membrane strain tensor field whose single non-vanishing component with respect to the orthonormal ordered basis field $\{\boldsymbol{o}_{\mathrm{I}}^{(\mathrm{k})}, \boldsymbol{o}_{\mathrm{II}}^{(\mathrm{k})}\}$, $\mathrm{k} = \{a, b\}$ is

$$\gamma_{\mathrm{I}\cdot\mathrm{I}}^{(\mathrm{k})}(\theta^1,\theta^2) = \frac{1}{a^{(\mathrm{k})}}\left(W_1' - \bar{x}_2^{(\mathrm{k})} W_2'' - \bar{x}_3^{(\mathrm{k})} W_3'' - \omega^{(\mathrm{k})} \Phi_1'' + \psi^{(\mathrm{k})} \Phi_1'\right) \text{ with } \mathrm{k} = \{a, b\} \ , \tag{2.9.13}$$

where

$$\psi^{(\mathrm{k})}(\theta^1,\theta^2) = \bar{x}_2^{(\mathrm{k})} D_1 \bar{x}_3^{(\mathrm{k})} - \bar{x}_3^{(\mathrm{k})} D_1 \bar{x}_2^{(\mathrm{k})} - D_1\omega^{(\mathrm{k})} \ , \ \mathrm{k} = \{a, b\} \ . \tag{2.9.14}$$

Similarly, the non-vanishing components with respect to the (linearized) change of curvature tensor, yields to

$$\rho_{\mathrm{I}\cdot\mathrm{I}}^{(\mathrm{k})}(\theta^1,\theta^2) = \frac{1}{(a^{(\mathrm{k})})^{3/2}}\left(-D_2\bar{x}_2^{(\mathrm{k})} W_3'' + D_2\bar{x}_3^{(\mathrm{k})} W_2'' - q^{(\mathrm{k})}\Phi_1''\right) \tag{2.9.15}$$

$$\rho_{\mathrm{I}\cdot\mathrm{II}}^{(\mathrm{k})}(\theta^1,\theta^2) = \rho_{\mathrm{II}\cdot\mathrm{I}}^{(\mathrm{k})}(\theta^1,\theta^2) = \frac{\Phi_1'}{a^{(\mathrm{k})}} \ , \ \mathrm{k} = \{a, b\} \ . \tag{2.9.16}$$

The constitutive equations (2.4.24)-(2.4.25) remains valid and yields, for each surface element, the active membrane forces

$$n_{\mathrm{I}\cdot\mathrm{I}}^{(\mathcal{A})(\mathrm{k})} = \tilde{E}\, t^{(\mathrm{k})}\, \gamma_{\mathrm{I}\cdot\mathrm{I}}^{(\mathrm{k})}, \ \mathrm{k} = \{a, b\} \tag{2.9.17}$$

and the respectively active shell moment tensors

$$\boldsymbol{m}^{(\mathcal{A})(\mathrm{k})} = \frac{\tilde{E}\left(t^{(\mathrm{k})}\right)^3}{12}\rho_{\mathrm{I}\cdot\mathrm{I}}^{(\mathrm{k})}\,\boldsymbol{o}_{\mathrm{I}}\otimes\boldsymbol{o}_{\mathrm{I}} + \frac{G_{I\cdot II}\left(t^{(\mathrm{k})}\right)^3}{6}\rho_{\mathrm{I}\cdot\mathrm{II}}^{(\mathrm{k})}\,\boldsymbol{o}_{\mathrm{I}}\otimes\boldsymbol{o}_{\mathrm{II}} + \frac{G_{II\cdot I}\left(t^{(\mathrm{k})}\right)^3}{6}\rho_{\mathrm{II}\cdot\mathrm{I}}^{(\mathrm{k})}\,\boldsymbol{o}_{\mathrm{II}}\otimes\boldsymbol{o}_{\mathrm{I}} \tag{2.9.18}$$

with $\mathrm{k} = \{a, b\}$. The elastic store energy can now be obtained as expression (2.5.2), replacing the integral over $\bar{\Omega}$ with the sum of two integrals, over $\bar{\Omega}^{(a)}$ and $\bar{\Omega}^{(b)}$.

[35] For definiteness, I require that $\omega^{(a)}(\theta^1, 0) = 0$. For fixed θ^1, the piecing together of $\omega^{(a)}$ and $\omega^{(b)}$ represents a sectorial coordinate on the middle line $\mathcal{L}_{\theta^1}$, with origin at $F^{(a)}(\theta^1, 0)$ and pole at $O + \theta^1\,\boldsymbol{e}_1$.

This eventually leads to an expression that is formally identical to equation (2.5.23), once the integrals over $\left[g_1(\theta^1), g_2(\theta^1)\right]$ in the definitions (2.5.7)-(2.5.22) are replaced by the sum of two integrals over $\left[g_1^{(a)}(\theta^1), g_2^{(a)}(\theta^1)\right]$ and $\left[g_1^{(b)}(\theta^1), g_2^{(b)}(\theta^1)\right]$. For instance,

$$A^*(\theta^1) = \sum_{\mathrm{k}\in\{a,b\}} \int_{g_1^{(\mathrm{k})}}^{g_2^{(\mathrm{k})}} t^{*(\mathrm{k})}\, d\theta^2 \quad , \qquad I^*_{\omega\psi}(\theta^1) = \sum_{\mathrm{k}\in\{a,b\}} \int_{g_1^{(\mathrm{k})}}^{g_2^{(\mathrm{k})}} \omega^{(\mathrm{k})}\, \psi^{(\mathrm{k})}\, t^{*(\mathrm{k})}\, d\theta^2 \tag{2.9.19}$$

with

$$t^{*(\mathrm{k})} = \frac{t^{(\mathrm{k})}}{\sqrt{\left(a^{(\mathrm{k})}\right)^3}} \ , \ \mathrm{k} = \{a, b\} \ . \tag{2.9.20}$$

The remainder of the discussion in §2.5-§2.8 retains its validity without further amendments.

2.9.1 I-section bars with linearly varying web depth and/or flange width

> There exists a line of section such that, when the superfluous material has been removed, there will remain a solid of such figure that it will offer the same resistance at all points. Evidently one must, in passing from greater to less, encounter equality.
>
> GALILEO GALILEI, *DISCORSI E DIMOSTRAZIONI MATEMATICHE INTORNO A DUE NUOVE SCIENZE*

I-section bars with linearly varying changes in the cross-section dimensions, are very common in civil engineering steel structures because of the economies produced by reducing the cross-section in the low moment regions (Trahair 2014) [p. 299].[36] A possible fabrication procedure with little or no waste of material is by doing one longitudinal diagonal cut on the web of a conventional prismatic I-section bar, then, these halves are rotated and spliced to give the maximum depth at mid-span, e.g., Burke (1952), Fraser (1983) or Marques (2012) [p. 88], they can also be manufactured from hot-rolled beams (Trahair and Bradford 1998) [pp. 149-150].

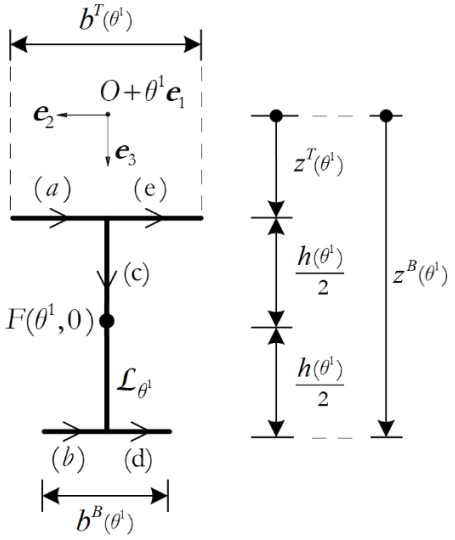

Figure 2.9.2: Tapered I-section bar – Parametrisation of the middle surface

In order to apply the criterion for bars with irregular middle surface developed in the above section, Figures 2.9.2-2.9.4 show the reference shape of a generic tapered I-section bar, with linearly varying web depth and/or flanges width, with constant thicknesses t_T, t_B and t_W respectively.

[36] In tapered I-section bars, the cross-section reductions are usually determined by in-plane bending criterions, that can reduce the lateral stiffness of the member so that a loss of stability due to flexural-torsional buckling may happen.

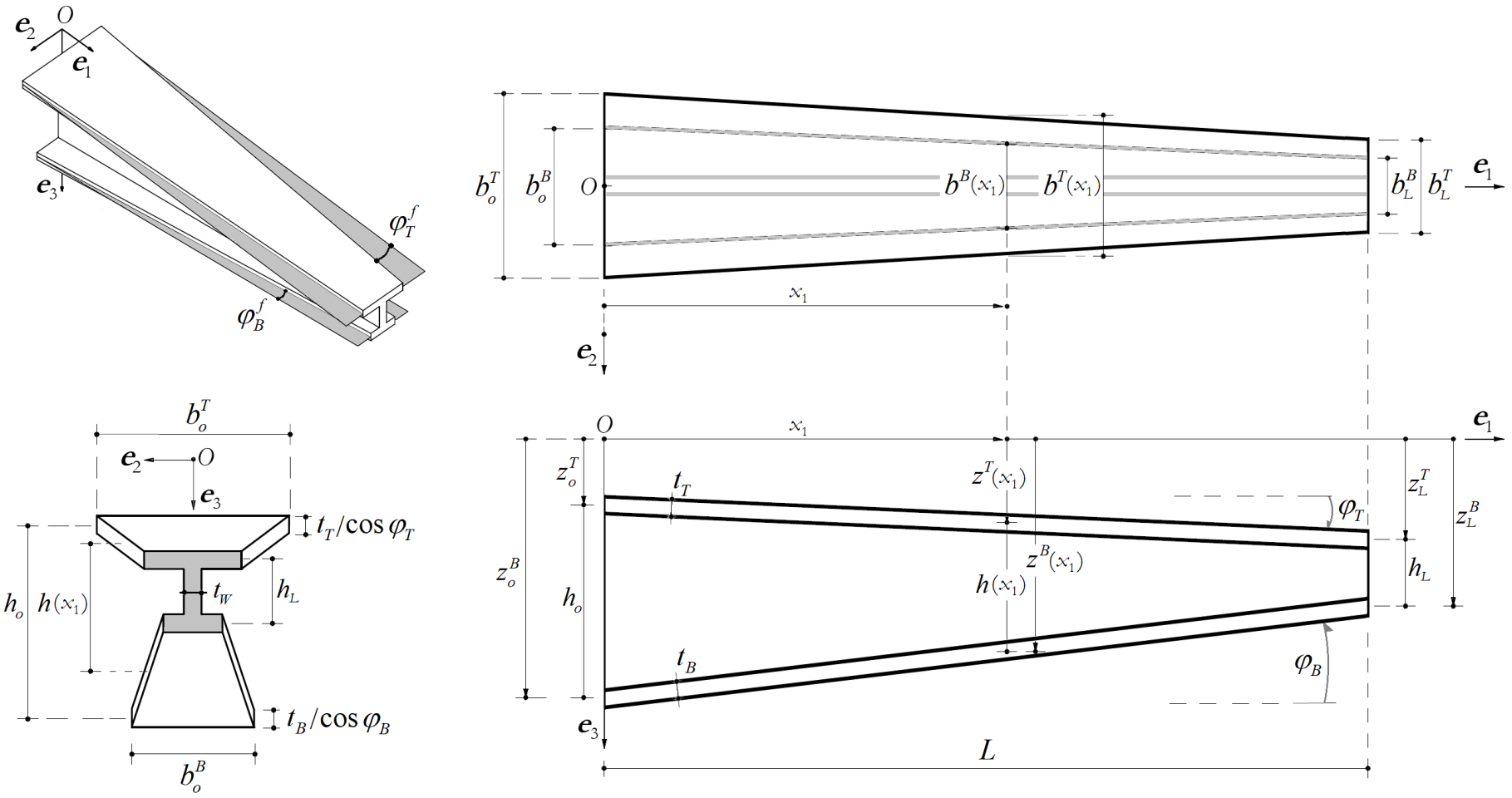

Figure 2.9.3: Reference shape – generic tapered I-section bar

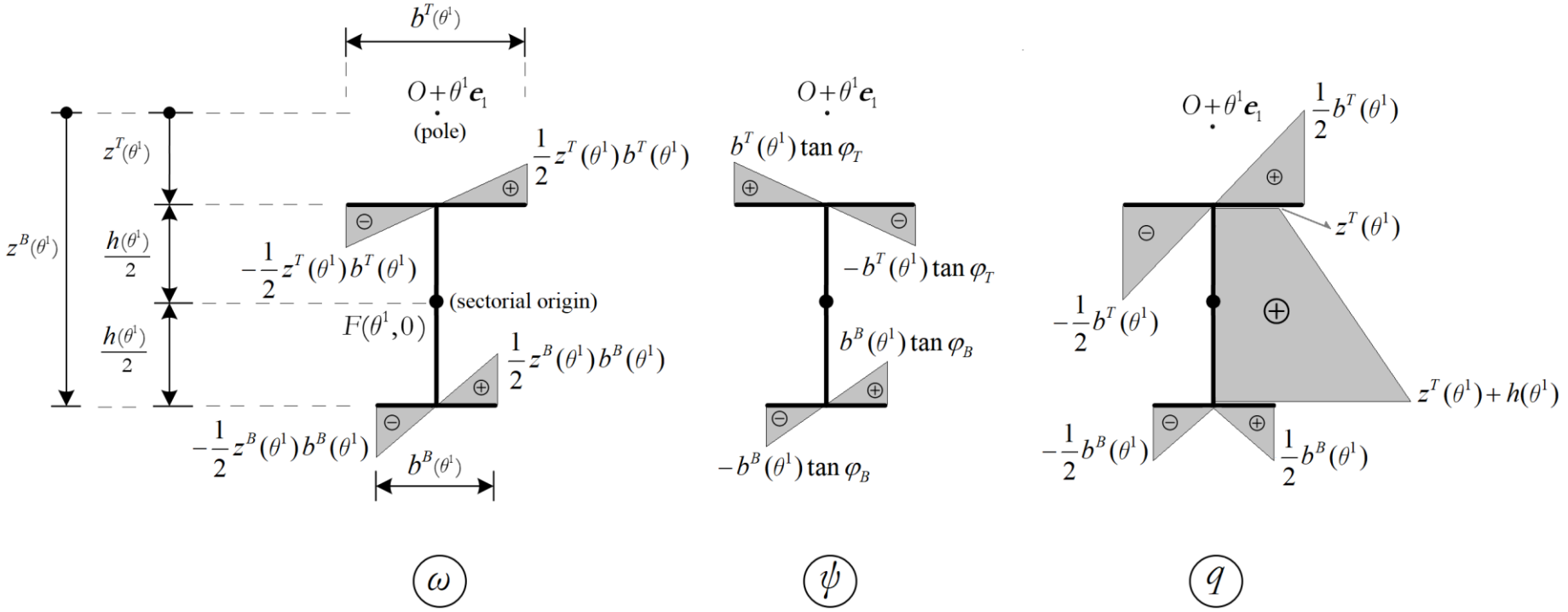

Figure 2.9.4: Tapered I-section bar – Schematic representations of the maps ω, ψ and q

The width of the flanges and the depth of the web are measured between flange middle lines, that can be express by using the respectively slope factor $\left\{\gamma_T^f, \gamma_B^f, \gamma\right\}$ given by

$$b^T(x_1) = b_o^T + \frac{\gamma_T^f L}{\cos\varphi_T}\left(\frac{x_1}{L}\right), \qquad \gamma_T^f = -2\tan\varphi_T^f \ , \tag{2.9.21}$$

$$b^B(x_1) = b_o^B + \frac{\gamma_B^f L}{\cos\varphi_B}\left(\frac{x_1}{L}\right), \qquad \gamma_B^f = -2\tan\varphi_B^f \ , \tag{2.9.22}$$

$$h(x_1) = h_o + \gamma L\left(\frac{x_1}{L}\right), \qquad \gamma = -\left(\tan\varphi_T + \tan\varphi_B\right) , \tag{2.9.23}$$

where the values at the end sections are defined as

$$b^T(0) = b_o^T \ , \qquad b^B(0) = b_o^B \ , \qquad h(0) = h_o \tag{2.9.24}$$

$$b^T(L) = b_L^T \ , \qquad b^B(L) = b_L^B \ , \qquad h(L) = h_L \tag{2.9.25}$$

and the x_3-coordinate of the corresponding top and bottom flange middle planes

$$z^T(x_1) = z_o^T + \frac{z_L^T - z_o^T}{L}x_1 \tag{2.9.26}$$

$$z^B(x_1) = z^T(x_1) + h(x_1) = (z_o^T + h_o) + \left[(z_L^T + h_L) - (z_o^T + h_o)\right]\left(\frac{x_1}{L}\right) , \tag{2.9.27}$$

where the slopes of the above flanges with respect to the projection on the plane $\boldsymbol{e}_1$-$\boldsymbol{e}_3$ are respectively

$$\varphi_T = \arctan\left(\frac{z_L^T - z_o^T}{L}\right) \tag{2.9.28}$$

$$\varphi_B = \arctan\left(\frac{z_o^B - z_L^B}{L}\right) \tag{2.9.29}$$

with $\varphi_T, \varphi_B \ll \pi/2$. The adopted parametrisation (see Table 2.9.1) of the reference shape of the middle surface $\mathcal{L}_{\theta^1}$, allow us to compute the maps ω, ψ and q, which schematic representations are shown in Figure 2.9.4.

	range of θ^2	$\bar{x}_2(\theta^1,\theta^2)$	$\bar{x}_3(\theta^1,\theta^2)$	$a(\theta^1,\theta^2)$	$t^*(\theta^1,\theta^2)$
$\bar{\Omega}^{(a)}$	$-\frac{h(\theta^1)}{2}-\frac{b^T(\theta^1)}{2}-\frac{b^B(\theta^1)}{2}<\theta^2<-\frac{h(\theta^1)}{2}-\frac{b^B(\theta^1)}{2}$	$-\left(\theta^2+\frac{h(\theta^1)}{2}+\frac{b^B(\theta^1)}{2}\right)$	$z^T(\theta^1)$	$1+\tan^2\varphi_T$	$t_T\cos^3\varphi_T$
$\bar{\Omega}^{(b)}$	$-\frac{h(\theta^1)}{2}-\frac{b^B(\theta^1)}{2}<\theta^2<-\frac{h(\theta^1)}{2}$	$-\left(\theta^2+\frac{h(\theta^1)}{2}\right)$	$z^B(\theta^1)$	$1+\tan^2\varphi_B$	$t_B\cos^3\varphi_B$
$\bar{\Omega}^{(c)}$	$-\frac{h(\theta^1)}{2}<\theta^2<\frac{h(\theta^1)}{2}$	0	$\theta^2+z^T(\theta^1)+\frac{h(\theta^1)}{2}$	1	t_w
$\bar{\Omega}^{(d)}$	$\frac{h(\theta^1)}{2}<\theta^2<\frac{h(\theta^1)}{2}+\frac{b^B(\theta^1)}{2}$	$-\left(\theta^2-\frac{h(\theta^1)}{2}\right)$	$z^B(\theta^1)$	$1+\tan^2\varphi_B$	$t_B\cos^3\varphi_B$
$\bar{\Omega}^{(e)}$	$\frac{h(\theta^1)}{2}+\frac{b^B(\theta^1)}{2}<\theta^2<\frac{h(\theta^1)}{2}+\frac{b^T(\theta^1)}{2}+\frac{b^B(\theta^1)}{2}$	$-\left(\theta^2-\frac{h(\theta^1)}{2}-\frac{b^B(\theta^1)}{2}\right)$	$z^T(\theta^1)$	$1+\tan^2\varphi_T$	$t_T\cos^3\varphi_T$

Table 2.9.1: Tapered I-section bar – Geometrical features

	$\omega(\theta^1,\theta^2)$	$\psi(\theta^1,\theta^2)$	$q(\theta^1,\theta^2)$
$\overline{\Omega}^{(a)}$	$z^T(\theta^1)\left(\theta^2+\frac{h(\theta^1)}{2}+\frac{b^B(\theta^1)}{2}\right)$	$-2\tan\varphi_T\left(\theta^2+\frac{h(\theta^1)}{2}+\frac{b^B(\theta^1)}{2}\right)$	$\theta^2+\frac{h(\theta^1)}{2}+\frac{b^B(\theta^1)}{2}$
$\overline{\Omega}^{(b)}$	$z^B(\theta^1)\left(\theta^2+\frac{h(\theta^1)}{2}\right)$	$2\tan\varphi_B\left(\theta^2+\frac{h(\theta^1)}{2}\right)$	$\theta^2+\frac{h(\theta^1)}{2}$
$\overline{\Omega}^{(c)}$	0	0	$\theta^2+z^T(\theta^1)+\frac{h(\theta^1)}{2}$
$\overline{\Omega}^{(d)}$	$z^B(\theta^1)\left(\theta^2-\frac{h(\theta^1)}{2}\right)$	$2\tan\varphi_B\left(\theta^2-\frac{h(\theta^1)}{2}\right)$	$\theta^2-\frac{h(\theta^1)}{2}$
$\overline{\Omega}^{(e)}$	$z^T(\theta^1)\left(\theta^2-\frac{h(\theta^1)}{2}-\frac{b^B(\theta^1)}{2}\right)$	$2\tan\varphi_T\left(\frac{h(\theta^1)}{2}+\frac{b^B(\theta^1)}{2}-\theta^2\right)$	$\theta^2-\frac{h(\theta^1)}{2}-\frac{b^B(\theta^1)}{2}$

Table 2.9.1 (continued): Tapered I-section bar – Geometrical features

Finally, by using the above geometrical features, the cross-sectional properties (2.5.7)-(2.5.22) are established

$$\mathcal{A}^*(\theta^1) = h(\theta^1)t_W + b^T(\theta^1)t_T\cos^3\varphi_T + b^B(\theta^1)t_B\cos^3\varphi_B \tag{2.9.30}$$

$$S_2^*(\theta^1) = \left(\frac{h(\theta^1)}{2} + z^T(\theta^1)\right)h(\theta^1)t_W + z^T(\theta^1)b^T(\theta^1)t_T\cos^3\varphi_T + z^B(\theta^1)b^B(\theta^1)t_B\cos^3\varphi_B \tag{2.9.31}$$

$$I_2^*(\theta^1) = \frac{h^3(\theta^1)t_W}{12} + \left(\frac{h(\theta^1)}{2} + z^T(\theta^1)\right)^2 h(\theta^1)t_W + \left(z^T(\theta^1)\right)^2 b^T(\theta^1)t_T\cos^3\varphi_T + \left(z^B(\theta^1)\right)^2 b^B(\theta^1)t_B\cos^3\varphi_B + \frac{b^T(\theta^1){t_T}^3\cos^5\varphi_T}{12} + \frac{b^B(\theta^1){t_B}^3\cos^5\varphi_B}{12} \tag{2.9.32}$$

$$I_3^*(\theta^1) = \frac{1}{12}\left(b^T(\theta^1)\right)^3 t_T\cos^3\varphi_T + \frac{1}{12}\left(b^B(\theta^1)\right)^3 t_B\cos^3\varphi_B + \frac{1}{12}h(\theta^1)\,{t_W}^3 \tag{2.9.33}$$

$$I_{3\omega}^*(\theta^1) = -\frac{1}{12}z^T(\theta^1)\left(b^T(\theta^1)\right)^3 t_T\cos^3\varphi_T - \frac{1}{12}z^B(\theta^1)\left(b^B(\theta^1)\right)^3 t_B\cos^3\varphi_B - \frac{{t_w}^3}{24}\left[\left(z^T(\theta^1)+h(\theta^1)\right)^2 - \left(z^T(\theta^1)\right)^2\right] \tag{2.9.34}$$

$$I_\omega^*(\theta^1) = \frac{1}{12}\left(z^T(\theta^1)\right)^2\left(b^T(\theta^1)\right)^3 t_T\cos^3\varphi_T + \frac{1}{12}\left(z^B(\theta^1)\right)^2\left(b^B(\theta^1)\right)^3 t_B\cos^3\varphi_B + \frac{\left(b^B(\theta^1)\,t_B\right)^3\cos^5\varphi_B}{144} + \frac{\left(b^T(\theta^1)\,t_T\right)^3\cos^5\varphi_T}{144} + \frac{{t_W}^3}{36}\left[\left(z^T(\theta^1)+h(\theta^1)\right)^3 - \left(z^T(\theta^1)\right)^3\right] \tag{2.9.35}$$

$$I_\psi^*(\theta^1) = \frac{1}{3}\left(b^T(\theta^1)\right)^3 t_T\tan^2\varphi_T\cos^3\varphi_T + \frac{1}{3}\left(b^B(\theta^1)\right)^3 t_B\tan^2\varphi_B\cos^3\varphi_B \tag{2.9.36}$$

$$I_{3\psi}^*(\theta^1) = \frac{1}{6}\left(b^T(\theta^1)\right)^3 t_T\tan\varphi_T\cos^3\varphi_T - \frac{1}{6}\left(b^B(\theta^1)\right)^3 t_B\tan\varphi_B\cos^3\varphi_B \tag{2.9.37}$$

$$I_{\omega\psi}^*(\theta^1) = -\frac{1}{6}z^T(\theta^1)\left(b^T(\theta^1)\right)^3 t_T\tan\varphi_T\cos^3\varphi_T + \frac{1}{6}z^B(\theta^1)\left(b^B(\theta^1)\right)^3 t_B\tan\varphi_B\cos^3\varphi_B \tag{2.9.38}$$

$$J^*(\theta^1) = \frac{1}{3}\left[h(\theta^1) t_W^3 + b^T(\theta^1)\left(t_T \cos\varphi_T\right)^3 + b^B(\theta^1)\left(t_B \cos\varphi_B\right)^3 \right] . \qquad (2.9.39)$$

Due to symmetry, the following cross-sectional properties are null

$$S_3^* = S_\omega^* = I_{23}^* = I_{2\omega}^* = S_\psi^* = I_{2\psi}^* = 0 \ . \qquad (2.9.40)$$

2.10 ILLUSTRATIVE EXAMPLES

In above sections, I developed a Vlasov-type linear one-dimensional model for the space behaviour (stretching, biaxial bending and twisting) of tapered thin-walled bars with open cross-sections, by incorporating the shell effect into Andrade's original equations (Andrade 2013). Now the application of the said model to a couple of illustrative examples are presented.[37] They are: (i) the torsional behaviour of doubly symmetric web-tapered I-section cantilevers and (ii) the coupled flexural-torsional behaviour of singly symmetric web-tapered C-section cantilevers. These examples serve a fourfold purpose: (i) to give a tangible meaning to the non-standard entities appearing in the one-dimensional bar model, (ii) to show that our Vlasov-type approach is entirely compatible with Timoshenko's, which consists of regarding each individual plated component as an Euler-Bernoulli member in bending with axial force (Timoshenko 1910), (Weber 1926), (Bleich and Bleich 1936), (iii) to underscore the differences between tapered and stepped (piecewise prismatic) models in dealing with restrained torsion-warping, regardless of the number of prismatic segments used in the stepped models (even in the limit when the length of these segments tends to zero), and (iv) to discuss the physical causes at the root of such discrepancies. The results of shell finite element analyses corroborate our one-dimensional model and falsify the stepped approach.

Illustrative example 1: Torsional behaviour of doubly symmetric web tapered I-section cantilevers

Consider the family of doubly symmetric web-tapered I-section cantilevers with linearly varying web and constant width flanges, with constant thicknesses t_f and t_w respectively, shown in Figure 2.10.1.

[37] The illustrative examples were taken from Andrade (2013) [pp. 80-114], whose further reading is recommended, in order to compare the subtle outcomes of the one-dimensional model developed.

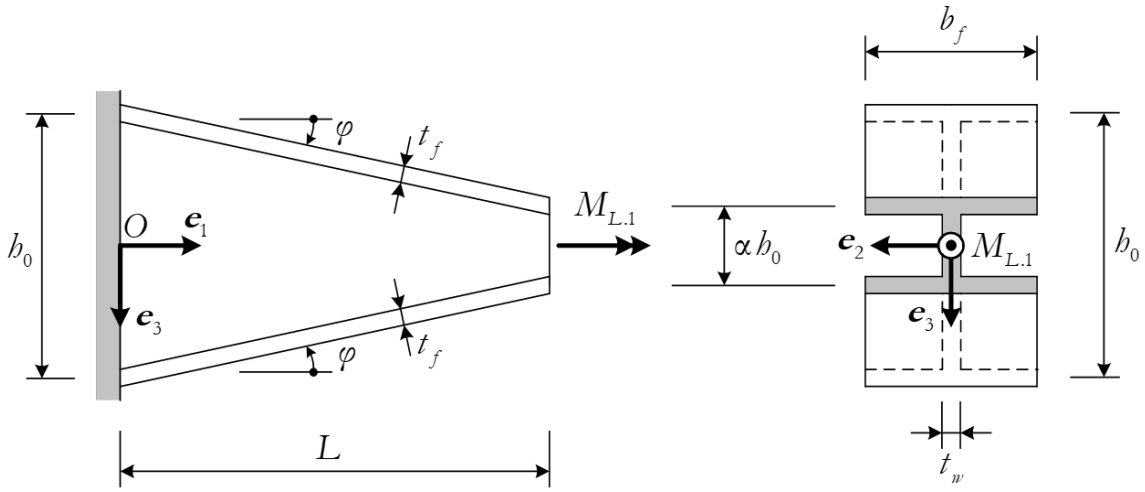

Figure 2.10.1: Illustrative example 1 – Reference shape, support conditions and applied torque, adapted from Andrade (2013) [p. 81]

The flanges have width b_f and exhibit symmetrical slopes $\pm\tan\varphi$ with respect to the plane projection $\boldsymbol{e}_1-\boldsymbol{e}_3$, while the web's depth h is measured between flange middle lines, according to

$$h(x_1)=\left(1-(1-\alpha)\frac{x_1}{L}\right)h_0\ ,\ (0<\alpha\leq 1)\ . \tag{2.10.1}$$

The non-dimensional variable α will be called simply the taper ratio (that for prismatic bars it is equal to $\alpha=1$). Moreover, it is related with the flanges slopes via

$$\tan\varphi=-\frac{h'}{2}=\frac{(1-\alpha)h_0}{2L}\ . \tag{2.10.2}$$

Considering the boundary conditions, the cantilever is clamped at its larger end and free at the smaller end, where a concentrated torque $M_{L.1}$ is applied. From the general results given in §2.9.1 (see Table 2.9.1) applied to the reference shape shown in Figure 2.10.1, I get the functions a, ω, ψ and q, with schematic graphs are shown in Figure 2.10.2. The graph of a is independent of the particular choice of parametrisation scheme; the same is true of the graphs of ω and ψ, as long as the sectorial origin remains the same. Concerning the symmetry and the reference shape in Figure 2.10.2, I get

$$S^*_{\psi}=I^*_{2\psi}=I^*_{3\psi}=S^*_{\omega}=I^*_{2\omega}=I^*_{3\omega}=0\ . \tag{2.10.3}$$

Hence, the torsional behaviour in function of the generalised displacements $W_i\ \ (i=1,2,3)$ and Φ_1 are entirely uncoupled.

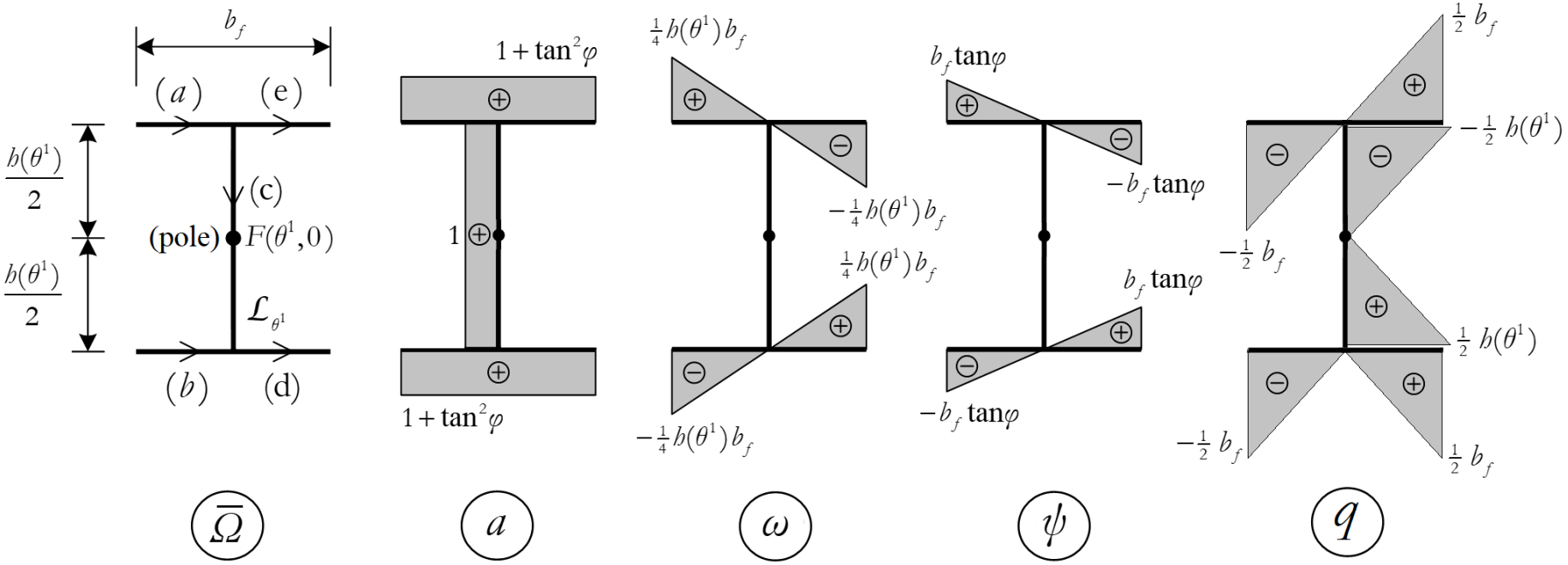

Figure 2.10.2: Illustrative example 1 – Parametrisation of the middle surface and schematic graphs of the functions a, ω, ψ and q

Thus, in view of the applied loading on the cantilever, it follows that W_i are all identically zero and the boundary value problem is reduced to:

Find $\Phi_1 : [0, L] \to \mathbb{R}$, with $\Phi_1 \in C^4[0, L]$, satisfying the ordinary differential equation

$$-\left(\tilde{E} I_{\omega}^{*} \Phi_1''\right)'' + \left[\left(\tilde{G} J^{*} + \tilde{E} I_{\psi}^{*} + \tilde{E} I_{\omega\psi}^{*}{}'\right) \Phi_1'\right]' = 0 \tag{2.10.4}$$

on the open interval $(0, L)$, together with the boundary conditions

$$\Phi_1(0) = 0 \tag{2.10.5}$$

$$\Phi_1'(0) = 0 \tag{2.10.6}$$

$$-\tilde{E} I_{\omega}^{*}(L) \Phi_1''(L) + \tilde{E} I_{\omega\psi}^{*}(L) \Phi_1'(L) = 0 \tag{2.10.7}$$

$$-\left(\tilde{E} I_{\omega}^{*} \Phi_1''\right)'(L) + \left(\tilde{G} J^{*}(L) + \tilde{E} I_{\psi}^{*}(L) + \tilde{E} I_{\omega\psi}^{*}{}'(L)\right) \Phi_1'(L) = M_{L.1}\,. \tag{2.10.8}$$

Where the above cross-sectional properties are

$$I_{\omega}^{*}(\theta^1) = \frac{1}{24} h^2(\theta^1) b_f^3 t_f \cos^3\varphi + \frac{1}{72} b_f^3 t_f^3 \cos^5\varphi + \frac{1}{144} h^3(\theta^1) t_w^3 \tag{2.10.9}$$

$$I_{\psi}^{*} = \frac{2}{3} b_f^3 t_f \tan^2\varphi \cos^3\varphi \tag{2.10.10}$$

$$I_{\omega\psi}^{*} = \frac{1}{6} h(\theta^1) b_f^3 t_f \tan\varphi \cos^3\varphi \tag{2.10.11}$$

$$J^{*}(\theta^1) = \frac{2}{3} b_f \left(t_f \cos\varphi\right)^3 + \frac{1}{3} h(\theta^1) t_w^3\,. \tag{2.10.12}$$

It should be noticed that in a good approximation

$$I_{\omega\psi}^{*}(\theta^1) \approx -I_{\omega}^{*}{}'(\theta^1)\,, \qquad I_{\psi}^{*} = -2\, I_{\omega\psi}^{*}{}'(\theta^1) \approx 2\, I_{\omega}^{*}{}''(\theta^1)\,.^{38} \tag{2.10.13}$$

In order to comprehend the influence and outcomes of our Vlasov-type linear one-dimensional model, I contrast in Figures 2.10.3-2.10.8 the warping-torsion behaviours of prismatic ($\alpha = 1$) and linearly depth-tapered ($0 < \alpha < 1$) doubly symmetric I-section bars (Cabrera et al. 2017). It is further worthy of notice the following facts:

[38] A word of caution, the validity of these identities is restricted to the particular bar geometry shown in Figure 2.10.1.

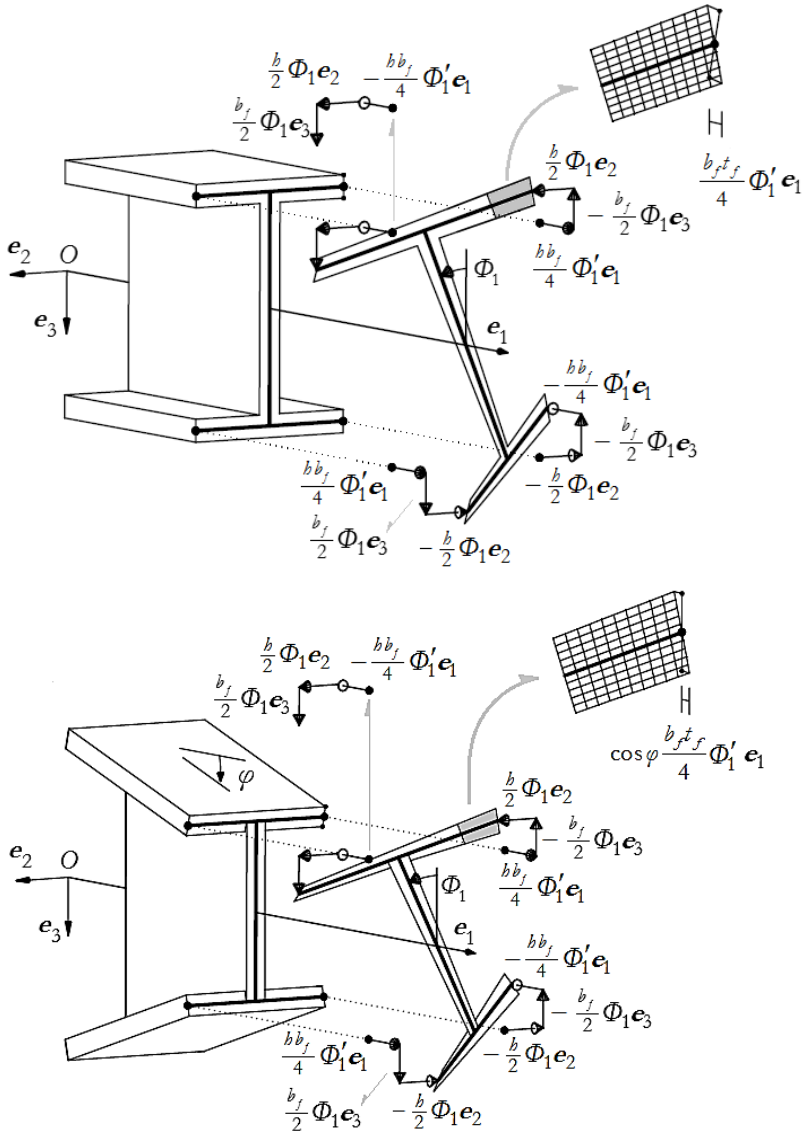

Figure 2.10.3: Contrasting the warping-torsion behaviours of prismatic and web-tapered doubly symmetric I-section bars – Displacement field of cross-section middle line and through the thickness

(i) Due to symmetry considerations, web-tapered and prismatic cases imply qualitatively similar displacement fields for the cross-section middle line at a distance θ^1 from the origin, see Figure 2.10.3: (i_1) the middle line rotates about the centroidal axis through an angle Φ_1 and (i_2) the flanges warp out of the plane by rotating $\pm\frac{h}{2}\Phi_1'$ about their major axes. However, in the web-tapered case, the displacements along $\boldsymbol{e}_3$ are obviously not orthogonal to the middle planes of the flanges, (i_3) concerning the displacement field through the thickness, the web-tapered case is more influence by the values of the scaling factor $1/\sqrt{a} = \cos\varphi$.

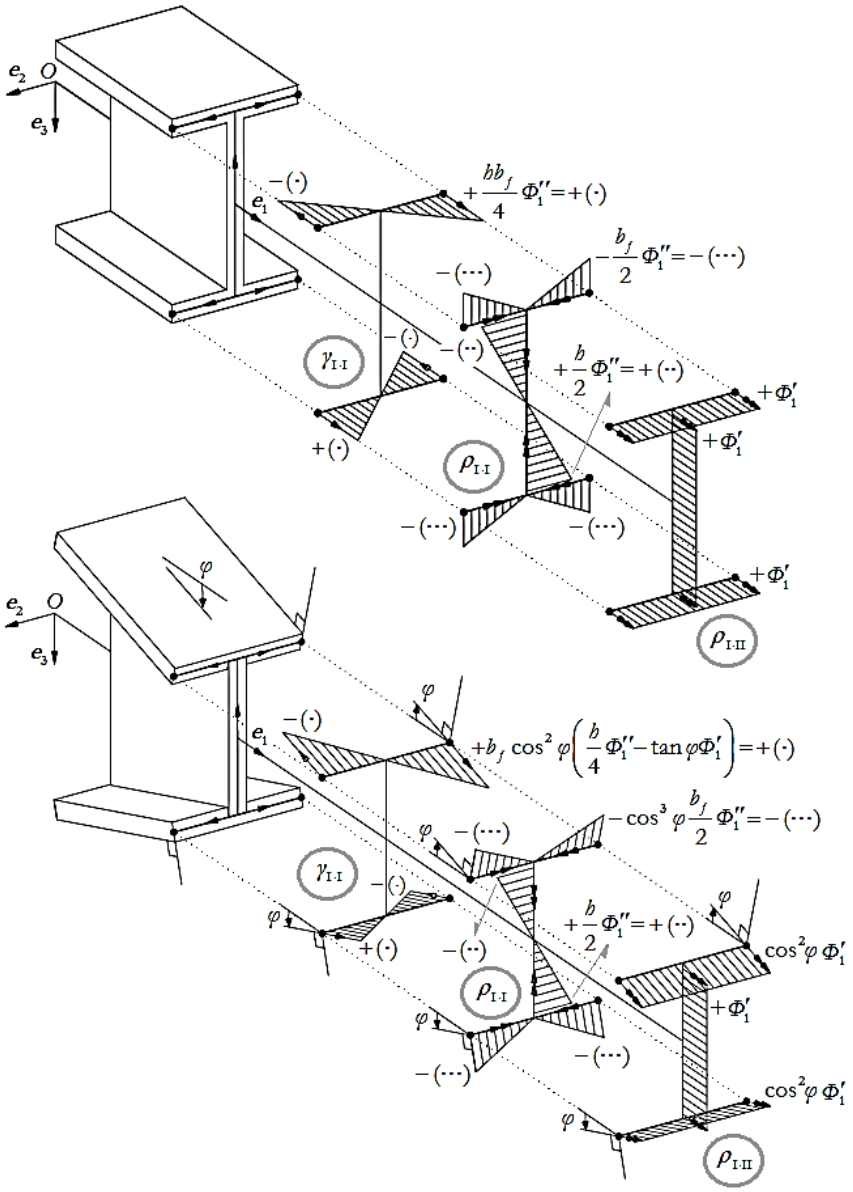

Figure 2.10.4: Contrasting the warping-torsion behaviours of prismatic and web-tapered doubly symmetric I-section bars – Membrane strains $\gamma_{\text{I·I}}$ and the change of curvatures $\rho_{\text{I·I}}$ - $\rho_{\text{I·II}}$

(ii) With the displacement fields already defined, it is possible to find the membrane strains $\gamma_{\text{I·I}}$ in the flanges by direct computation due to equation (2.9.13), see Figure 2.10.4. Comparing the prismatic and web-tapered case, it can be observed that the latter contains an additional term and a scaling factor ($\cos^2\varphi$), e.g., Cywinski and Kollbrunner (1971) [eq. 13]. This additional term is none other than $\psi\Phi_1'$ and the scaling factor is $1/a$. These remarks also apply to the (active) membrane forces $n_{\text{I·I}}$ in the flanges, as shown in Figure 2.10.5.

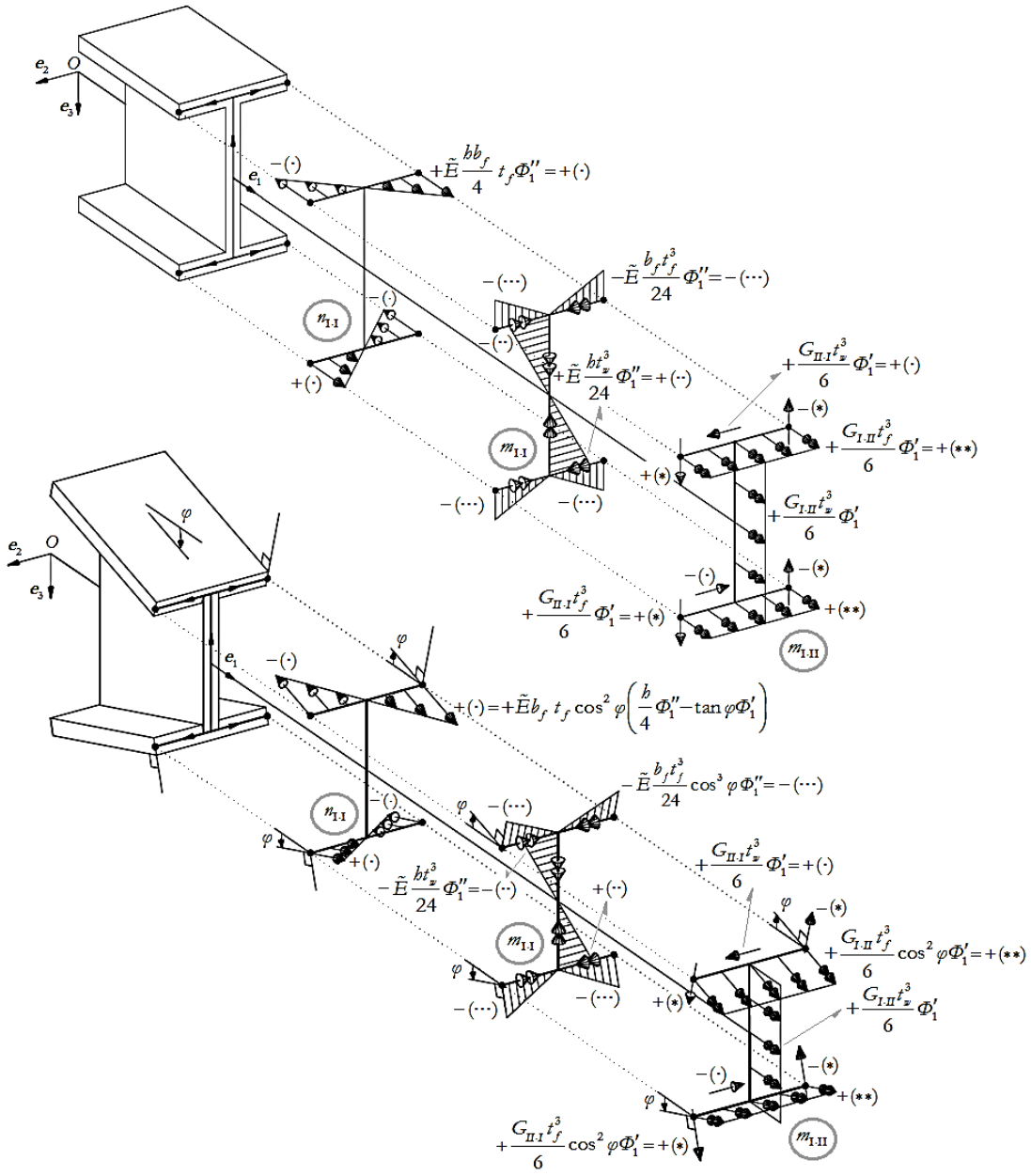

Figure 2.10.5: Contrasting the warping-torsion behaviours of prismatic and web-tapered doubly symmetric I-section bars – Membrane forces $n_{1\cdot I}$ and shell moments $m_{1\cdot I}$ - $m_{1\cdot II}$

(iii) The (linearized) change of curvatures $\rho_{1\cdot I}$ and $\rho_{1\cdot II} = \rho_{II\cdot I}$ also showed differences between the prismatic and tapered case, with the last one showing the scaling factors $\cos^3\varphi$ and $\cos^2\varphi$, i.e., the values $1/a^{3/2}$ and $1/a$ respectively, see Figure 2.10.4. This characterization also apply to the shell moments $m_{1\cdot I}$ and $m_{1\cdot II}$, see Figure 2.10.5, where the contribution of the shell moment $m_{II\cdot I}$ is represented at the ends of the cross-section by edge forces, e.g., Rand and Rovenski (2004) [eq. 5.64].

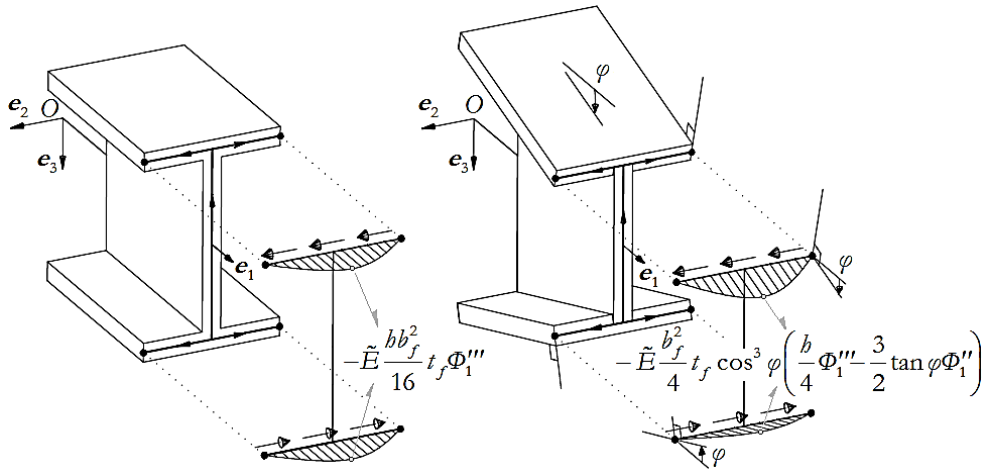

Figure 2.10.6: Contrasting the warping-torsion behaviours of prismatic and web-tapered doubly symmetric I-section bars – Membrane forces $n_{\text{I-II}}$ (reactive)

(iv) The membrane forces $n_{\text{I-II}}$ shown in Figure 2.10.6, which have a reactive character, may be found by considering the equilibrium of a "flange slice" acted by the previously obtained membrane forces $n_{\text{I-I}}$, as ordinarily done in standard textbooks on strength of materials.

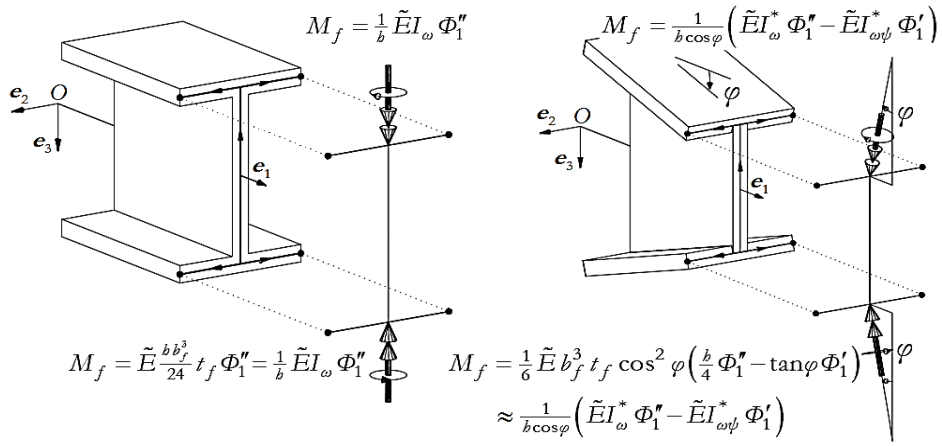

Figure 2.10.7: Contrasting the warping-torsion behaviours of prismatic and web-tapered doubly symmetric I-section bars – Bending moments M_f in the flanges

(v) The membrane forces $n_{\text{I-I}}$ (resp. $n_{\text{I-II}}$) are statically equivalent to a bending moment M_f (resp. shear force V_f) in each flange as it shown in Figures 2.10.7 and 2.10.8. In the web-tapered case, the warping stiffness $\tilde{E}I_\omega^*$, computed with the reduced flange thickness $t_f^*=t_f\cos^3\varphi$, and the stiffness $\tilde{E}I_{\omega\psi}^*$ associated with cross-sectional tapering arise naturally in this process:

$$M_f(\theta^1) = \frac{1}{6}\tilde{E} b_f^3 t_f \cos^2\varphi \left(\frac{h(\theta^1)}{4} \Phi_1''(\theta^1) - \tan\varphi \, \Phi_1'(\theta^1) \right)$$

$$\approx \frac{1}{h(\theta^1)\cos\varphi} \left(\tilde{E} I_\omega^*(\theta^1) \Phi_1''(\theta^1) - \tilde{E} I_{\omega\psi}^*(\theta^1) \Phi_1'(\theta^1) \right) \tag{2.10.14}$$

$$V_f(\theta^1) = -\frac{1}{12}\tilde{E} b_f^3 t_f \cos^3\varphi \left(\frac{h(\theta^1)}{2} \Phi_1'''(\theta^1) - 3\tan\varphi \, \Phi_1''(\theta^1) \right)$$

$$\approx \frac{1}{h(\theta^1)} \left(-\tilde{E} I_\omega^*(\theta^1) \Phi_1'''(\theta^1) + \frac{3}{2}\tilde{E} I_{\omega\psi}^*(\theta^1) \Phi_1''(\theta^1) \right) . \tag{2.10.15}$$

Observe that

$$M_f(\theta^1) = \tilde{E}\frac{b_f^3 t_f}{12}\cos^2\varphi \left(\frac{h}{2}\Phi_1 \right)''(\theta^1) , \tag{2.10.16}$$

$$V_f(\theta^1) = -\cos\varphi \, M_f'(\theta^1) . \tag{2.10.17}$$

Hence, each flange behaves as an Euler-Bernoulli beam undergoing deflections $\pm\frac{h}{2}\Phi_1$. When we are dealing with web-tapered bars, we must to distinguish between derivatives with respect to θ^1 and derivatives with respect to the arc length of the flange centroidal lines, whence the appearance of $\cos\varphi$ in equations (2.10.16)-(2.10.17). Clearly, a stepped model, regardless of the number of prismatic segments it comprises, cannot capture the second term on the right-hand side of $\frac{1}{2}\left(h\Phi_1\right)'' = \frac{1}{2}h\Phi_1'' + h'\Phi_1'$, nor can it capture the factor $\cos\varphi$.

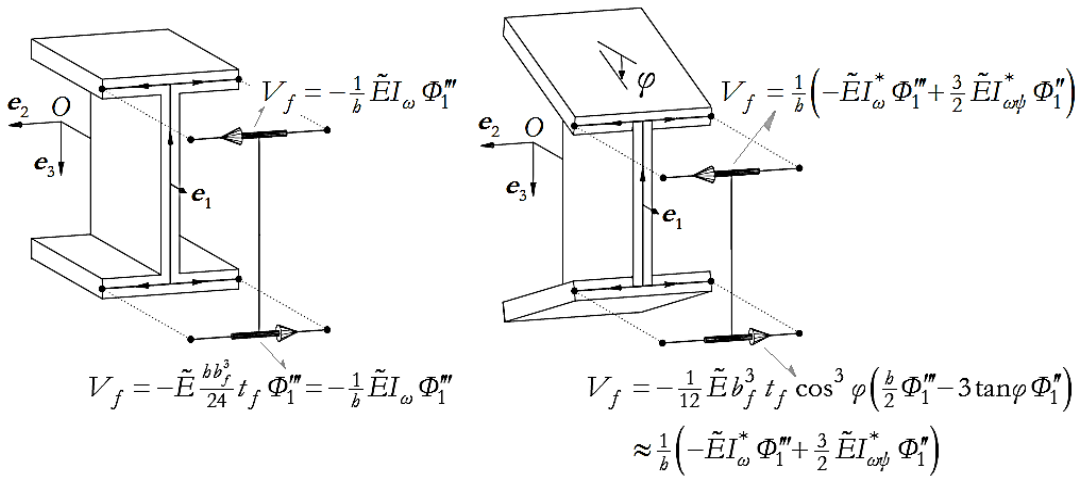

Figure 2.10.8: Contrasting the warping-torsion behaviours of prismatic and web-tapered doubly symmetric I-section bars – Shear forces V_f in the flanges

(vi) In web-tapered bars, the flange bending moments have an axial component, featuring $\tilde{E}I^*_{\omega\psi}$ and $\tilde{E}I^*_{\psi}$, which totals

$$-2\sin\varphi\, M_f(\theta^1)\boldsymbol{e}_1 = \frac{2\tan\varphi}{h(\theta^1)}\left(-\tilde{E}I^*_{\omega}(\theta^1)\Phi_1''(\theta^1)+\tilde{E}I^*_{\omega\psi}(\theta^1)\Phi_1'(\theta^1)\right)\boldsymbol{e}_1$$

$$=\frac{1}{2}\left(-\tilde{E}I^*_{\omega\psi}(\theta^1)\Phi_1''(\theta^1)+\tilde{E}I^*_{\psi}(\theta^1)\Phi'(\theta^1)_1\right)\boldsymbol{e}_1\ . \qquad (2.10.18)$$

In agreement with the general definition (2.7.6). Hence the total torque is

$$M_1(\theta^1) = -2\sin\varphi\, M_f(\theta^1)+V_f(\theta^1)h(\theta^1)+\tilde{G}J^*(\theta^1)\Phi_1'(\theta^1)$$

$$=-\tilde{E}I^*_{\omega}(\theta^1)\Phi_1'''(\theta^1)+\tilde{E}I^*_{\omega\psi}(\theta^1)\Phi_1''(\theta^1)+\left(\tilde{G}J^*(\theta^1)+\frac{1}{2}\tilde{E}I^*_{\psi}(\theta^1)\right)\Phi_1'(\theta^1)\ . \qquad (2.10.19)$$

Where the contribution of the flange bending moments to the torque is absent in prismatic bars and cannot be captured by the stepped approach. By last

$$\cos\varphi\, M_f(\theta^1)=\frac{1}{h(\theta^1)}\left(\tilde{E}I^*_{\omega}(\theta^1)\Phi_1''(\theta^1)-\tilde{E}I^*_{\omega\psi}(\theta^1)\Phi_1'(\theta^1)\right)=-\frac{B(\theta^1)}{h(\theta^1)}\ . \qquad (2.10.20)$$

(vii)The characterization between active and reactive parts of the torque (2.10.19) is rather subtle. By plugging equation (2.10.20) into (2.10.17), one gets

$$V_f(\theta^1)=\frac{1}{h(\theta^1)}\left(B'(\theta^1)+\frac{2\tan\varphi}{h(\theta^1)}B(\theta^1)\right)\ . \qquad (2.10.21)$$

Then, the active and reactive parts of the torque are respectively

$$M_1^{(A)}(\theta^1) = -2\sin\varphi\, M_f(\theta^1)+\frac{2\tan\varphi}{h(\theta^1)}B(\theta^1)+\tilde{G}J^*(\theta^1)\Phi_1'(\theta^1)$$

$$=-\tilde{E}I^*_{\omega\psi}(\theta^1)\Phi_1''(\theta^1)+\left(\tilde{G}J^*(\theta^1)+\tilde{E}I^*_{\psi}(\theta^1)\right)\Phi_1'(\theta^1) \qquad (2.10.22)$$

$$M_1^{(R)}(\theta^1)=B'(\theta^1)=\left(-\tilde{E}I^*_{\omega}(\theta^1)\Phi_1''(\theta^1)+\tilde{E}I^*_{\omega\psi}(\theta^1)\Phi_1'(\theta^1)\right)'\ , \qquad (2.10.23)$$

in accordance with equations (2.7.21)-(2.7.22).

After this brief digression, let us now return to the boundary value problem (2.10.4)-(2.10.8). By an appropriate approach, expressions (2.10.9)-(2.10.12) are rewritten as

$$I_{\omega}^{*}(\theta^1) \approx \frac{1}{24}\, h^2(\theta^1) b_f^3\, t_f \cos^3\varphi = \left(1-(1-\alpha)\frac{\theta^1}{L}\right)^2 I_{\omega}^{*}(0) \tag{2.10.24}$$

$$I_{\psi}^{*} = \frac{2}{3} b_f^3 \tan^2\varphi\, t_f \cos^3\varphi = \frac{4}{L^2}(1-\alpha)^2\, I_{\omega}^{*}(0) \tag{2.10.25}$$

$$I_{\omega\psi}^{*}(\theta^1) = \frac{1}{6} h(\theta^1) b_f^3 \tan\varphi\, t_f \cos^3\varphi = \frac{2}{L}(1-\alpha)\left(1-(1-\alpha)\frac{\theta^1}{L}\right) I_{\omega}^{*}(0) \tag{2.10.26}$$

$$J^{*}(\theta^1) = \frac{2}{3} b_f \left(t_f \cos\varphi\right)^3 + \frac{1}{3} h(\theta^1) t_w^3 = \left(1-\frac{h_0\, t_w^3}{3 J^{*}(0)}(1-\alpha)\frac{\theta^1}{L}\right) J^{*}(0)\ . \tag{2.10.27}$$

Hence, by using the following change of variable, i.e., $\theta^1 \in [0, L] \rightarrow s \in [0,1]$, defined as

$$s = \frac{\theta^1}{L}\ , \qquad\qquad \tilde{\Phi}(s) = \Phi_1(L\, s)\ , \tag{2.10.28}$$

and the introduction of the non-dimensional ratios

$$\kappa_{\omega 0} = \frac{\pi}{L}\sqrt{\frac{\tilde{E} I_{\omega}^{*}(0)}{\tilde{G} J^{*}(0)}} \tag{2.10.29}$$

$$\kappa_{J0} = \frac{h_0\, t_w^3}{3 J^{*}(0)} \tag{2.10.30}$$

$$\mu = \frac{M_{L,1}\, L}{\tilde{G} J^{*}(0)}\ . \tag{2.10.31}$$

Hence the boundary value problem is redefined into the following non-dimensional form

Illustrative example 1 (non-dimensional version)

Find $\tilde{\Phi}: [0,1] \rightarrow \mathbb{R}$, with $\tilde{\Phi} \in C^4[0,1]$, satisfying the ordinary differential equation

$$\begin{aligned} -\left(1-(1-\alpha)s\right)^2 \left(\frac{\kappa_{\omega 0}}{\pi}\right)^2 \tilde{\Phi}^{(4)}(s) + 4(1-\alpha)\left(1-(1-\alpha)s\right)\left(\frac{\kappa_{\omega 0}}{\pi}\right)^2 \tilde{\Phi}'''(s) \\ + \left(1-\kappa_{J0}(1-\alpha)s\right)\tilde{\Phi}''(s) - \kappa_{J0}(1-\alpha)\tilde{\Phi}'(s) = 0 \end{aligned} \tag{2.10.32}$$

on the open interval $(0,1)$, together with the boundary conditions

$$\tilde{\Phi}(0) = 0 \tag{2.10.33}$$

$$\tilde{\Phi}'(0) = 0 \tag{2.10.34}$$

$$\alpha\,\tilde{\Phi}''(1) - 2(1-\alpha)\,\tilde{\Phi}'(1) = 0 \tag{2.10.35}$$

$$-\alpha^2\left(\frac{\kappa_{\omega 0}}{\pi}\right)^2 \tilde{\Phi}'''(1) + 2\alpha(1-\alpha)\left(\frac{\kappa_{\omega 0}}{\pi}\right)^2 \tilde{\Phi}''(1) + \left[1 + 2(1-\alpha)^2\left(\frac{\kappa_{\omega 0}}{\pi}\right)^2 - \kappa_{J0}(1-\alpha)\right]\tilde{\Phi}'(1) = \mu \ . \tag{2.10.36}$$

It is important to remark, that $\{\alpha, \kappa_{\omega 0}, \kappa_{J0}, \mu\}$ constitutes a complete set of independent non-dimensional parameters describing the linear torsional behaviour of the family of cantilevers depicted in Figure 2.10.1. Furthermore, the parameter κ_{J0} is not required in the analysis of prismatic bars. In design practice, $\kappa_{\omega 0}$ ranges from 0.1 to 2.5, with low (resp. high) values of this parameter corresponding to long (resp. short) cantilevers and/or compact (resp. slender) cross-sections at the support (Kitipornchai and Trahair 1980). Concerning the value for κ_{J0}, that measures the relative contribution of the web to the Saint-Venant torsional rigidity of the clamped cross-section, it lies in the open interval $(0,1)$ – the limiting values $\kappa_{J0} = 0$ and $\kappa_{J0} = 1$, not addressed here, are associated with two extreme cases: webless and narrow rectangular beams, respectively. For the prismatic case ($\alpha = 1$), the solution to the non-dimensional version of the illustrative example 1 is equal to

$$\tilde{\Phi}(s) = \mu \frac{\tanh\left(\frac{\pi}{\kappa_{\omega 0}}\right)}{\frac{\pi}{\kappa_{\omega 0}}}\left(\frac{\sinh\left(\frac{\pi}{\kappa_{\omega 0}}(1-s)\right)}{\sinh\left(\frac{\pi}{\kappa_{\omega 0}}\right)} - 1 + \frac{\frac{\pi}{\kappa_{\omega 0}}s}{\tanh\left(\frac{\pi}{\kappa_{\omega 0}}\right)}\right), \ 0 \le s \le 1 \ , \tag{2.10.37}$$

e.g., Chen and Atsuta (1977) [p. 48]. In the tapered case ($0 < \alpha < 1$), no closed-form solution is available, therefore a mathematical software (Mathematica 2006) was used to obtain numerical solutions for selected values of the parameters $\kappa_{\omega 0}$ and α – since κ_{J0} is found to be relatively unimportant, I adopt the value $\kappa_{J0} = 0.1$,[39] for all the numerical solutions, plotted in Figure 2.10.9.

[39] For reference, members with $h_0 \cong 2b$ and $t_f \cong 2t_w$ have $\kappa_{J0} \cong 0.1$.

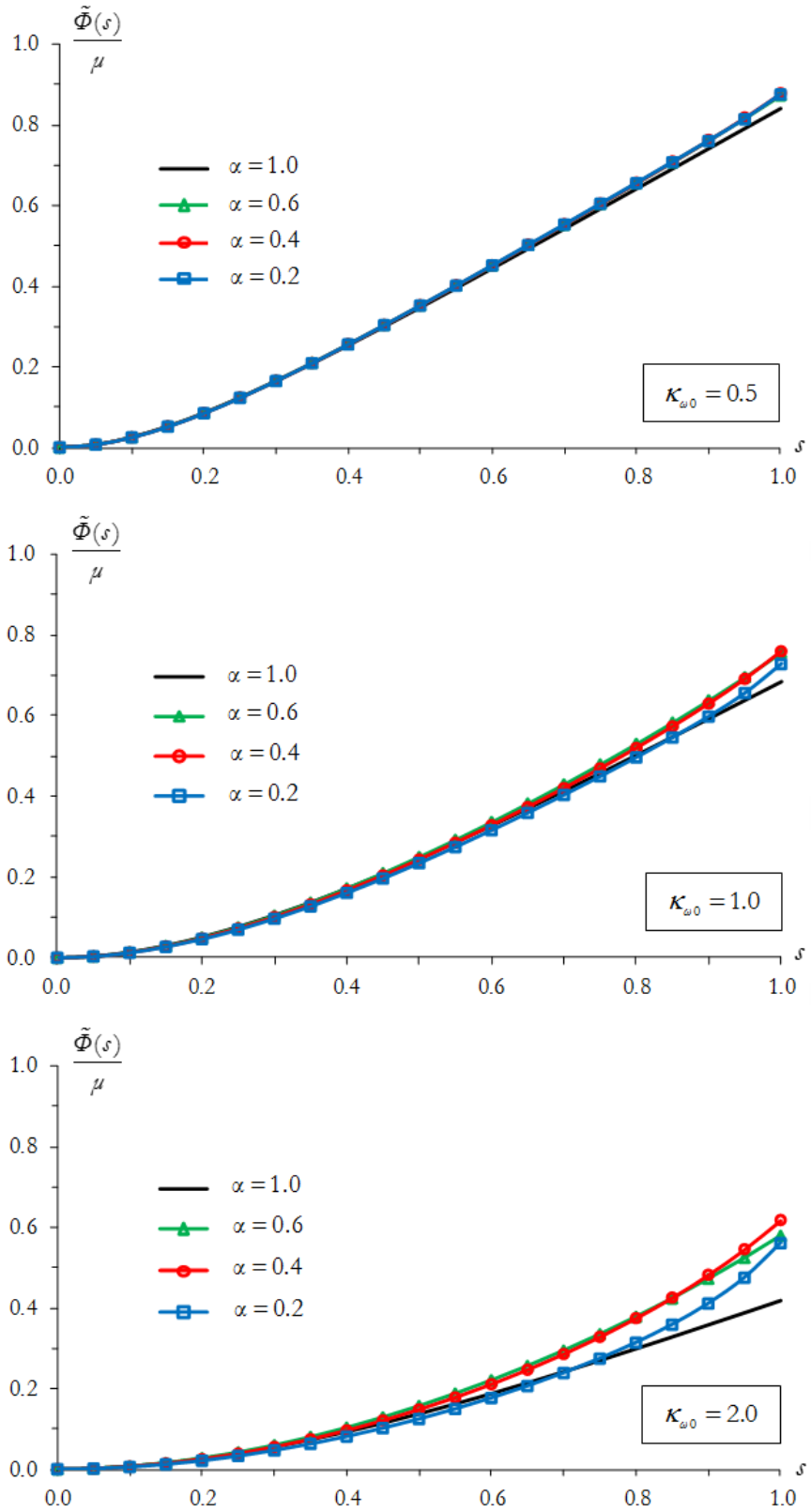

Figure 2.10.9: Illustrative example 1 ($\kappa_{J0} = 0.1$) – Solutions $\tilde{\Phi}$ to the non-dimensional version of the boundary value problem per unit non-dimensional torque μ, e.g., Andrade (2013) [p. 91]

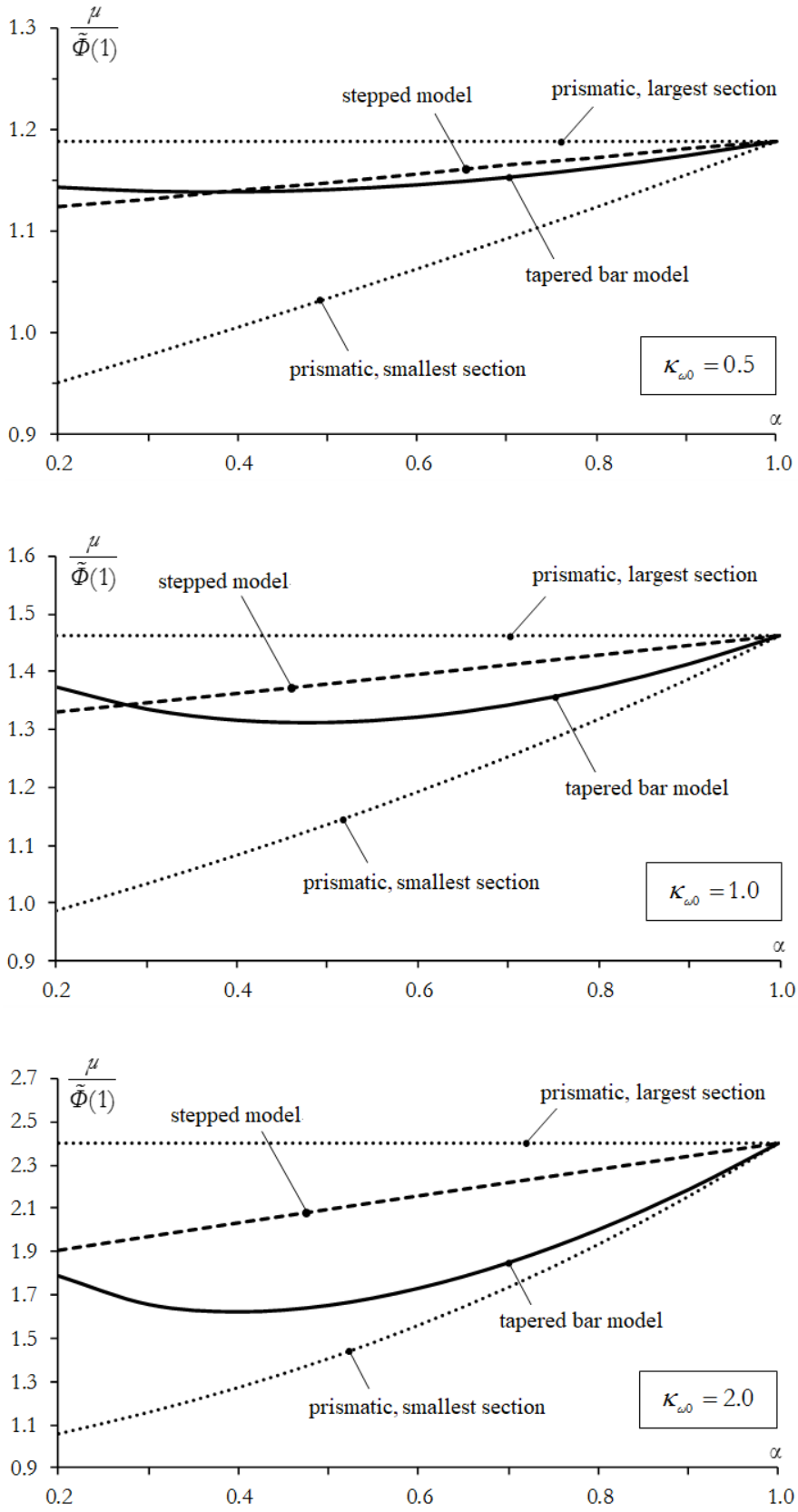

Figure 2.10.10: Illustrative example 1 ($\kappa_{J0} = 0.1$) – Non-dimensional torsional stiffness $\mu / \tilde{\Phi}(1)$ *versus* the taper ratio α, e.g., Andrade (2013) [p. 97]

The differences in warping-torsion behaviour between prismatic and web-tapered I-section cantilevers can be further illuminated by considering the non-dimensional torsional stiffness $\mu / \tilde{\Phi}(1)$, plotted *versus* the taper ratio α in Figure 2.10.10 (solid lines, labelled "tapered bar model"). Contrary to intuition (which is often misleading), $\mu / \tilde{\Phi}(1)$ is not a monotonic increasing function of α. Instead, it reaches a minimum for an intermediate value of α, dependent on $\kappa_{\omega 0}$. The difference between solid and dashed lines, (that is, between tapered and stepped models) becomes more pronounced as $\kappa_{\omega 0}$ increases, reflecting the growing importance of restrained warping to torsional stiffness.

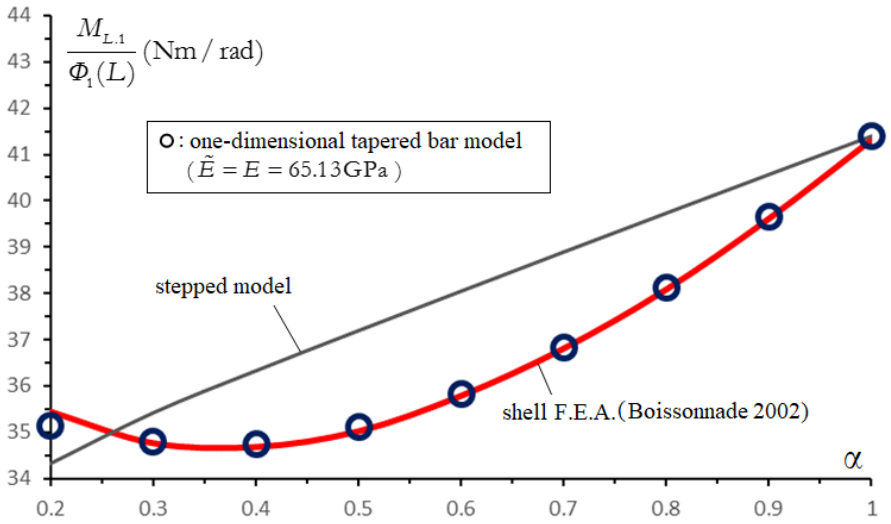

Figure 2.10.11: Illustrative example 1 – Comparison with shell finite element analyses

For reference purposes, Figure 2.10.10 also presents the non-dimensional torsional stiffness of prismatic cantilevers with the largest and the smallest cross-sectional dimensions, *i.e.*, with constant web depth h_0 and αh_0, respectively (dotted lines, labelled "prismatic, largest section" & "prismatic, smallest section"). As expected, the dotted lines form an envelope within which the solid lines lie for $\alpha < 1$ (dotted and solid lines obviously coincide for $\alpha = 1$). Boissonnade (2002) by using the shell finite element code FINELG, obtained the plot of torsional stiffness $M_{L,1} / \Phi_1(L)$ *versus* the taper ratio α shown in Figure 2.10.11, for a particular taper cantilever, with the following dimensions: $L = 762$ mm, $h_0 = 69.55$ mm, $t_w = 2.13$ mm, $b_f = 31.55$ mm and $t_f = 3.11$ mm, made of a linearly elastic isotropic material, characterised by the moduli $E = 65.13$ GPa and $G = 25.05$ GPa (hence the Poisson ratio is $\nu = 0.3$). There is an excellent qualitative agreement with the results delivered by the one-dimensional bar model (with $\tilde{E} = 65.13$ GPa and $\tilde{G} = 25.05$GPa). On the contrary, the stepped model is entirely off the mark.

Illustrative example 2: Flexural-torsional behaviour of singly symmetric web-tapered C-section cantilevers

Consider the family of singly symmetric web-tapered C-section cantilevers whose reference shape is shown in Figure 2.10.12. The flanges are uniform, with thickness t_f and width b_f (measured from their tip to the web middle line). While the web has constant thickness t_w and its depth h, measured between flange middle lines, that varies according to the non-dimensional parameter α, i.e., $0 < \alpha \leq 1$, called the taper ratio and the flanges exhibit symmetrical slopes in its projection $\boldsymbol{e}_1 - \boldsymbol{e}_2$, where

$$\tan\varphi = \frac{(1-\alpha)h_0}{2L} \ . \tag{2.10.38}$$

Similarly with the first example, the constrained material is characterised by the moduli $\tilde{E}$ and $\tilde{G}$. The cantilever is clamped at its larger end and free at the smaller end, where a point load $Q_{L.3}\boldsymbol{e}_3$ is applied at the position $O + L\boldsymbol{e}_1$.

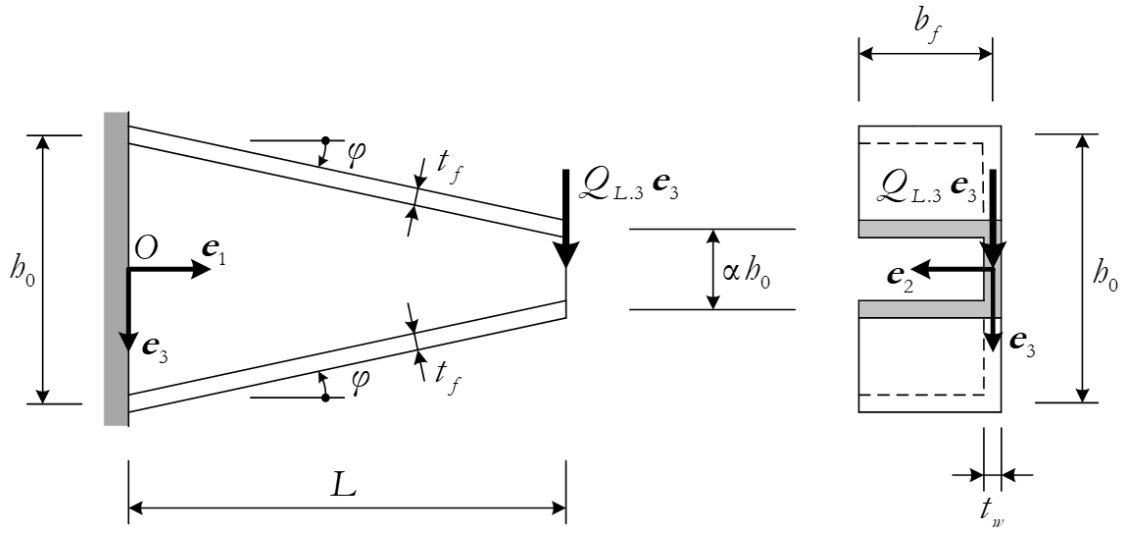

Figure 2.10.12: Illustrative example 1 – Comparison with shell finite element analyses (Andrade 2013) [p. 99]

The reference shape of the middle surface is made up of three surface elements, identified by the labels (a), (b) and (c). One possible scheme for its parametrisation is shown in Table 2.10.1 and Figure 2.10.13, together defined the geometrical features and schematic graphs of the functions a, ω, ψ and q respectively. I remark that the graph of a is independent of the particular choice of parametrisation scheme; the same is true of the graphs of ω, ψ and q as long as the sectorial origin remains the same.

With the geometrical features defined in Table 2.10.1, the cross-sectional properties of the singly symmetric web-tapered C-section are equal to

$$A^*(\theta^1) = h(\theta^1)\, t_w + 2\, b_f\, t_f \cos^3\varphi \tag{2.10.39}$$

$$S_3^* = b_f^2\, t_f \cos^3\varphi \tag{2.10.40}$$

$$I_{2\psi}^*(\theta^1) = -h(\theta^1)\; b_f^2\, t_f \tan\varphi \cos^3\varphi \tag{2.10.41}$$

$$I_{2\omega}^*(\theta^1) = -\frac{1}{4} h^2(\theta^1)\; b_f^2\, t_f \cos^3\varphi + \frac{1}{12} b_f^2 t_f^3\; \cos^5\varphi \tag{2.10.42}$$

$$I_3^*(\theta^1) = \frac{h(\theta^1)\; t_w^3}{12} + \frac{2}{3} b_f^3\, t_f \cos^3\varphi \tag{2.10.43}$$

$$I_2^*(\theta^1) = \frac{h^3(\theta^1)\; t_w}{12} + \frac{1}{2} h^2(\theta^1)\; b_f\, t_f \cos^3\varphi + \frac{1}{6} b_f\, t_f^3 \cos^5\varphi \tag{2.10.44}$$

$$I_\psi^* = \frac{8}{3} b_f^3\, t_f \tan^2\varphi \cos^3\varphi \tag{2.10.45}$$

$$I_\omega^*(\theta^1) = \frac{1}{6} h^2(\theta^1) b_f^3\, t_f \cos^3\varphi + \frac{1}{18} b_f^3 t_f^3\; \cos^5\varphi + \frac{1}{144} h^3(\theta^1) t_w^3 \tag{2.10.46}$$

$$I_{\omega\psi}^*(\theta^1) = \frac{2}{3} h(\theta^1) b_f^3 t_f \tan\varphi \cos^3\varphi \tag{2.10.47}$$

$$J^*(\theta^1) = \frac{1}{3} h(\theta^1) t_w^3 + \frac{2}{3} b_f \left(t_f \cos\varphi\right)^3 \; . \tag{2.10.48}$$

Due to symmetry

$$S_2^* = S_\omega^* = S_\psi^* = I_{23}^* = I_{3\psi}^* = I_{3\omega}^* = 0 \; . \tag{2.10.49}$$

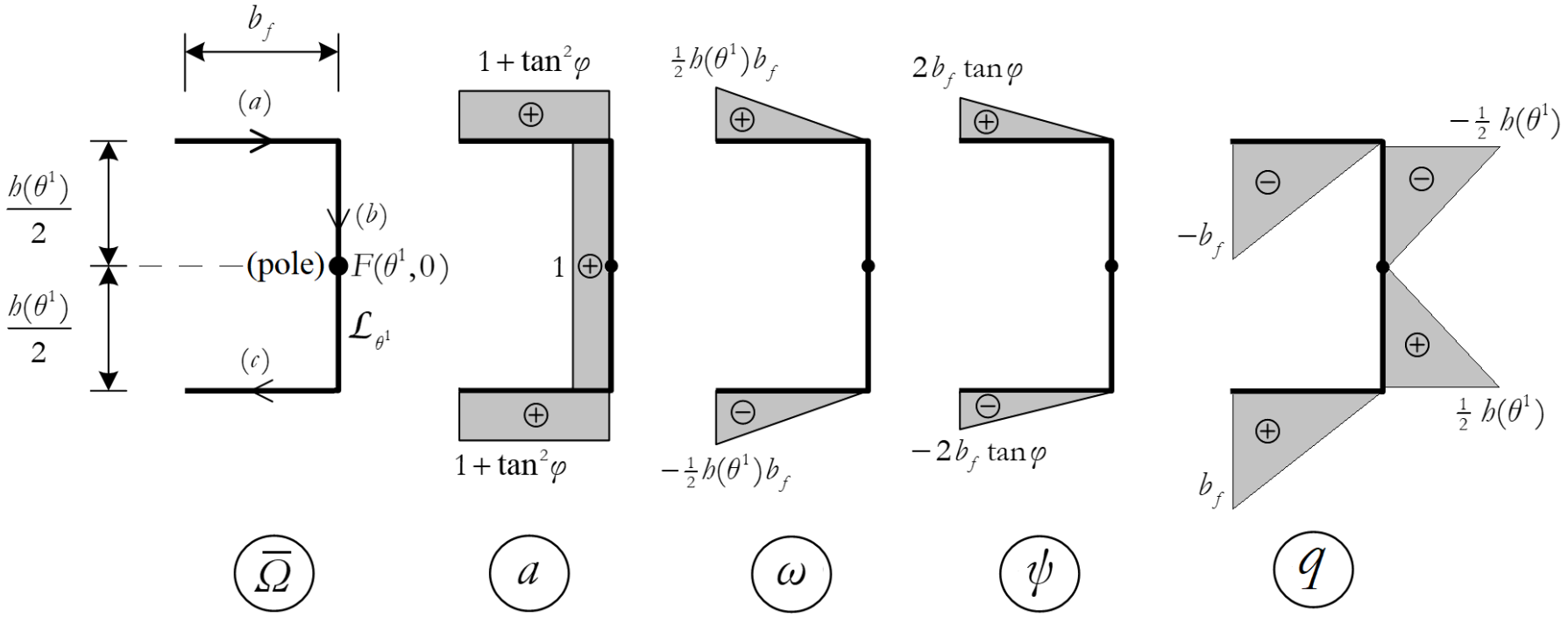

Figure 2.10.13: Illustrative example 2 – Parametrisation of the middle surface and schematic graphs of the functions a, ω, ψ and q

	range of θ^2	$\overline{x}_2(\theta^1,\theta^2)$	$\overline{x}_3(\theta^1,\theta^2)$	$a(\theta^1,\theta^2)$	$t^*(\theta^1,\theta^2)$	$\omega(\theta^1,\theta^2)$	$\psi(\theta^1,\theta^2)$	$q(\theta^1,\theta^2)$
$\overline{\Omega}^{(a)}$	$-\frac{h(\theta^1)}{2}-b_f<\theta^2<-\frac{h(\theta^1)}{2}$	$-\left(\theta^2+\frac{h(\theta^1)}{2}\right)$	$-\frac{h(\theta^1)}{2}$	$1+\tan^2\varphi$	$t_f\cos^3\varphi$	$-\frac{h(\theta^1)}{2}\left(\theta^2+\frac{h(\theta^1)}{2}\right)$	$-2\tan\varphi\left(\theta^2+\frac{h(\theta^2)}{2}\right)$	$\theta^2+\frac{h(\theta^2)}{2}$
$\overline{\Omega}^{(b)}$	$-\frac{h(\theta^1)}{2}<\theta^2<\frac{h(\theta^1)}{2}$	0	θ^2	1	t_w	0	0	θ^2
$\overline{\Omega}^{(c)}$	$\frac{h(\theta^1)}{2}<\theta^2<\frac{h(\theta^1)}{2}+b_f$	$\theta^2-\frac{h(\theta^1)}{2}$	$\frac{h(\theta^1)}{2}$	$1+\tan^2\varphi$	$t_f\cos^3\varphi$	$-\frac{h(\theta^1)}{2}\left(\theta^2-\frac{h(\theta^1)}{2}\right)$	$2\tan\varphi\left(\frac{h(\theta^2)}{2}-\theta^2\right)$	$\theta^2-\frac{h(\theta^2)}{2}$

Table 2.10.1: Illustrative example 2 – Geometrical features

Observe that

$$I^*_{2\psi}(\theta^1) = -I^{*\prime}_{2\omega}(\theta^1) \tag{2.10.50}$$

$$I^*_{\omega\psi}(\theta^1) \approx -I^{*\prime}_{\omega}(\theta^1) \tag{2.10.51}$$

$$I^*_{\psi} \approx 2\, I^{*\prime\prime}_{\omega}(\theta^1) \approx -2\, I^{*\prime}_{\omega\psi}(\theta^1) \tag{2.10.52}$$

Due to the symmetry condition (2.10.49), W_1 and W_2 are entirely uncoupled in relation to the generalized displacements W_3 and Φ_1, therefore from the skew-symmetry of the loading, W_1 and W_2 are identically zero. Hence the problem of finding W_3 and Φ_1, can be establish as follows:

Illustrative example 2

Find $W_3, \Phi_1 : [0, L] \to \mathbb{R}$, with $W_3, \Phi_1 \in C^4[0, L]$ satisfying the system of ordinary differential equations

$$\left(-\tilde{E}I^*_2\, W_3'' - \tilde{E}I^*_{2\omega}\, \Phi_1'' + \tilde{E}I^*_{2\psi}\, \Phi_1'\right)'' = 0 \tag{2.10.53}$$

$$-\left(\tilde{E}I^*_{\omega}\, \Phi_1''\right)'' + \left[-\tilde{E}I^*_{2\omega}\, W_3''' + \left(\tilde{G}J^* + \frac{1}{2}\tilde{E}I^*_{\psi}\right)\Phi_1'\right]' = 0 \tag{2.10.54}$$

on the open interval $(0, L)$, together with the boundary conditions

$$W_3(0) = 0 \tag{2.10.55}$$

$$W_3'(0) = 0 \tag{2.10.56}$$

$$\left(-\tilde{E}I^*_2\, W_3'' - \tilde{E}I^*_{2\omega}\, \Phi_1'' + \tilde{E}I^*_{2\psi}\, \Phi_1'\right)'(L) = Q_{L.3} \tag{2.10.57}$$

$$-\tilde{E}I^*_2(L) W_3''(L) - \tilde{E}I^*_{2\omega}(L)\Phi_1''(L) + \tilde{E}I^*_{2\psi}(L)\Phi_1'(L) = 0 \tag{2.10.58}$$

$$\Phi_1(0) = 0 \tag{2.10.59}$$

$$\Phi_1'(0) = 0 \tag{2.10.60}$$

$$\tilde{E}I^*_{2\omega}(L) W_3''(L) + \left(\tilde{E}I^*_{\omega}\, \Phi_1'\right)'(L) = 0 \tag{2.10.61}$$

$$-\left(\tilde{E}I^*_{\omega}\, \Phi_1''\right)'(L) - \tilde{E}I^*_{2\omega}(L) W_3'''(L) + \left(\tilde{G}J^*(L) + \frac{1}{2}\,\tilde{E}I^*_{\psi}(L)\right)\Phi_1'(L) = 0\ . \tag{2.10.62}$$

Before solving the differential equations, I compare the flexural-torsional behaviours of prismatic ($\alpha = 1$) and linearly depth-tapered ($0 < \alpha < 1$) bars:

(i) Figure 2.10.14 shows the displacement field of the cross-section middle line and through the thickness, where due to the constraint (V1), the displacements along $\boldsymbol{e}_2$ and $\boldsymbol{e}_3$ of the cross-section middle line at a distance θ^1 from the origin, for prismatic and web-tapered bars alike, are gotten by the superposition of (i_1) an infinitesimal rotation $\Phi_1(\theta^1)$ about the (reference) axis defined by the origin O and the Cartesian base vector $\boldsymbol{e}_1$, and (i_2) a translation $W_3(\theta^1)\boldsymbol{e}_3$. While the constraint (V2) provides the displacements along $\boldsymbol{e}_1$, which stem from (i_3) an infinitesimal rotation $-W_3'(\theta^1)$ about the (reference) axis defined by the point $O+\theta^1\boldsymbol{e}_1$ and the Cartesian base vector $\boldsymbol{e}_2$, and (i_4) torsion-warping of the cross-section middle line. By last, the constrained (V3), for prismatic and web-tapered bars, allow us to establish (i_5) the displacement distribution through the thickness along $\boldsymbol{e}_1$.

(ii) By the routine equations, one obtains the membrane strains $\gamma_{\text{I·I}}$ shown in Figure 2.10.15. Similarly with our first illustrative example, the strain-displacement relation in the web-tapered case exhibits the term $\psi\ \Phi_1'$ and the scaling factor $1/a$, which are absent in the prismatic case. The same is true of the (active) membrane forces $n_{\text{I·I}}$ as shown in Figure 2.10.16.

(iii) The (linearized) change of curvature ($\rho_{\text{I·I}}$, $\rho_{\text{I·II}} = \rho_{\text{II·I}}$) shown in Figure 2.10.15, as in the previous comment, exhibits the same scaling factors $1/a^{3/2}$, $1/a$, which does not appear in the prismatic case, corresponding with the ratios $\cos^3\varphi$, $\cos^2\varphi$ respectively. These remarks also apply to the (active) shell moments ($m_{\text{I·I}}$, $m_{\text{I·II}}$), where the effect of the (active) moment $m_{\text{II·I}}$ is added by an equivalent pair of forces as shown in Figure 2.10.16.

(iv) Figure 2.10.17 shows a force system statically equivalent to the membrane forces $n_{\text{I·I}}$ in the web and flanges. It comprises a web bending moment

$$M_w(\theta^1) = \tilde{E}\frac{h^3(\theta^1)t_w}{12}W_3''(\theta^1)\ , \tag{2.10.63}$$

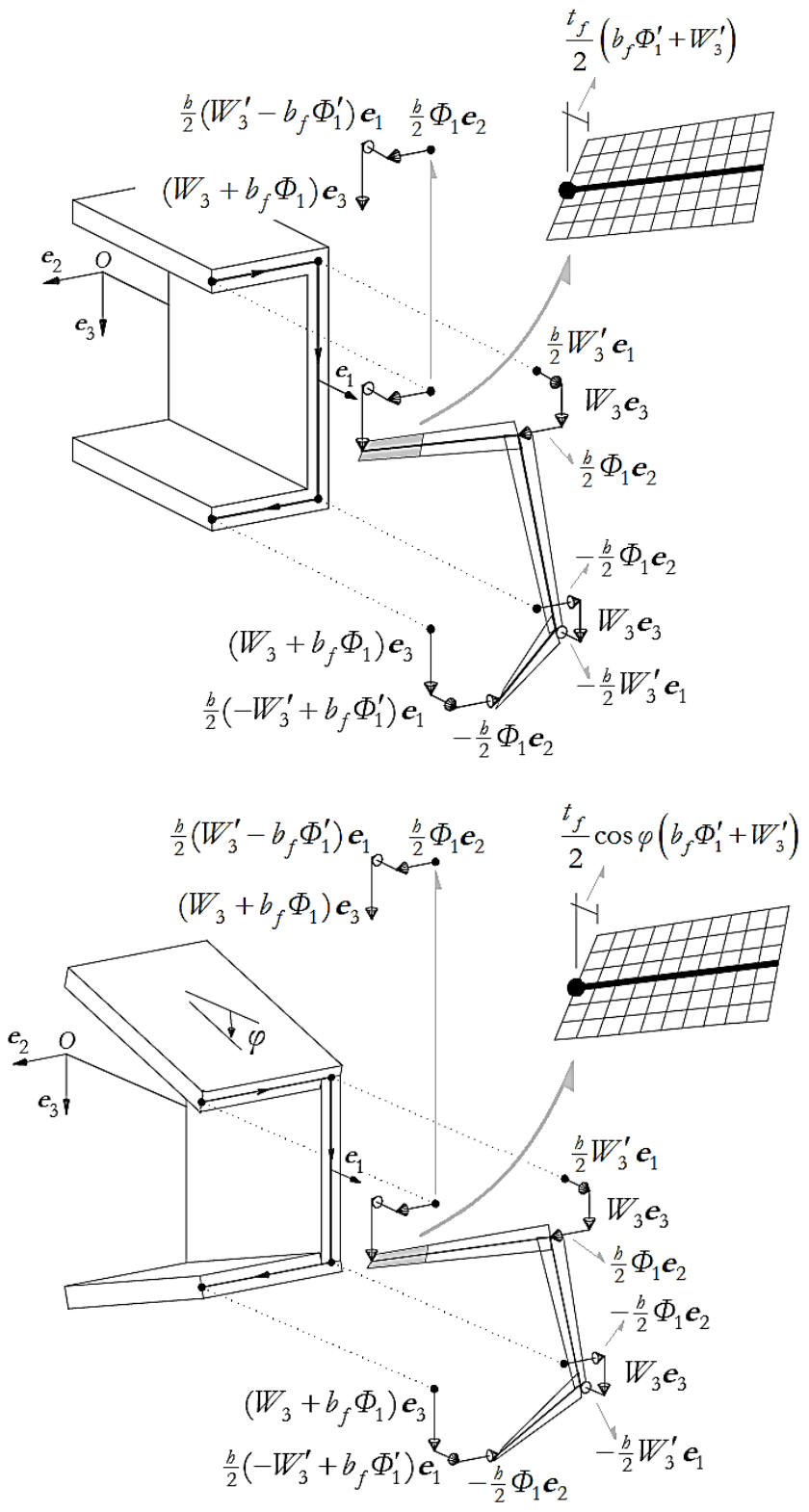

Figure 2.10.14: Contrasting the flexural-torsional behaviours of prismatic and web-tapered singly symmetric C-section bars – Displacement field of the cross-section middle line and through the thickness.

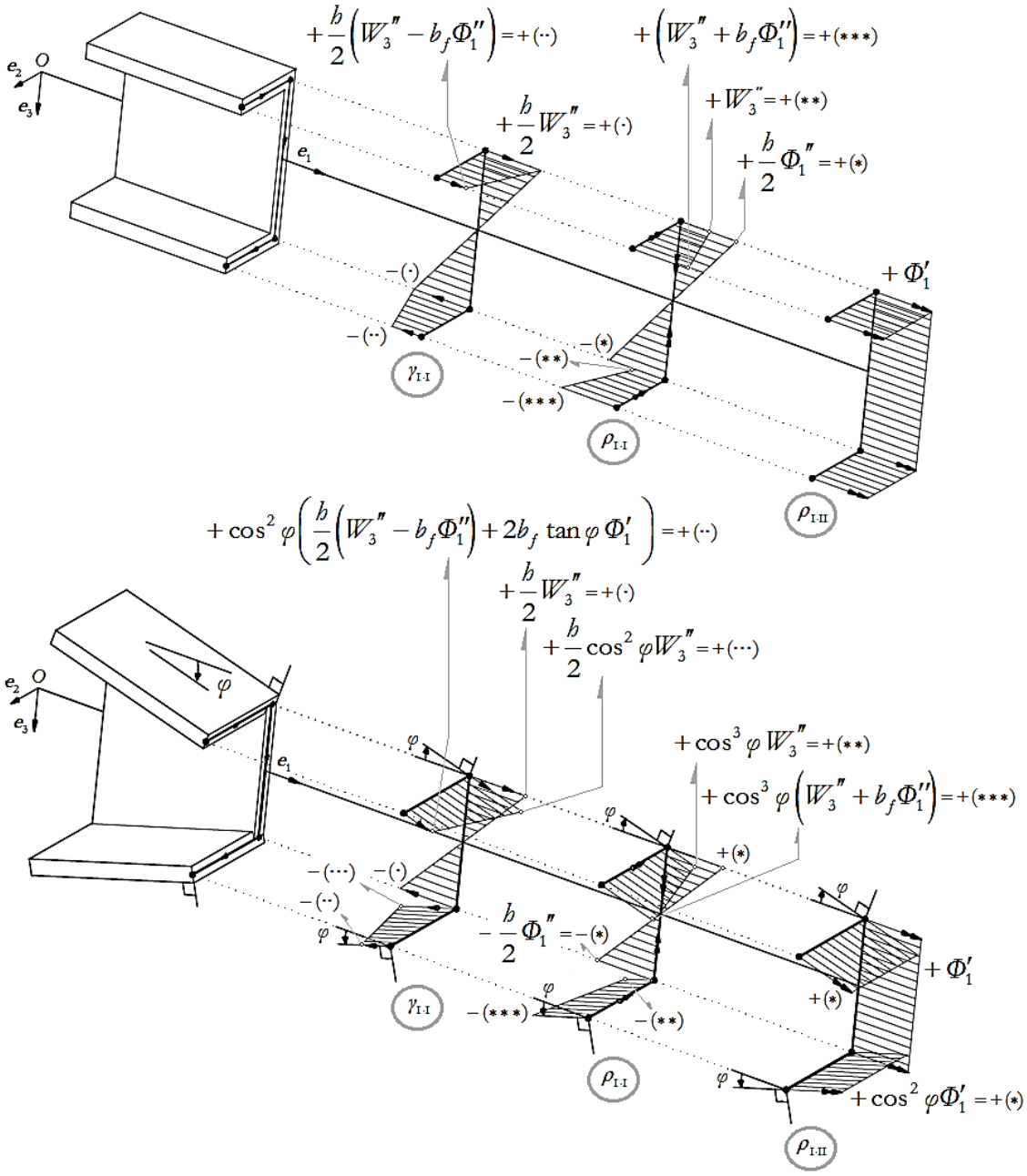

Figure 2.10.15: Contrasting the flexural-torsional behaviours of prismatic and web-tapered singly symmetric C-section bars – Membrane strains and change of curvatures

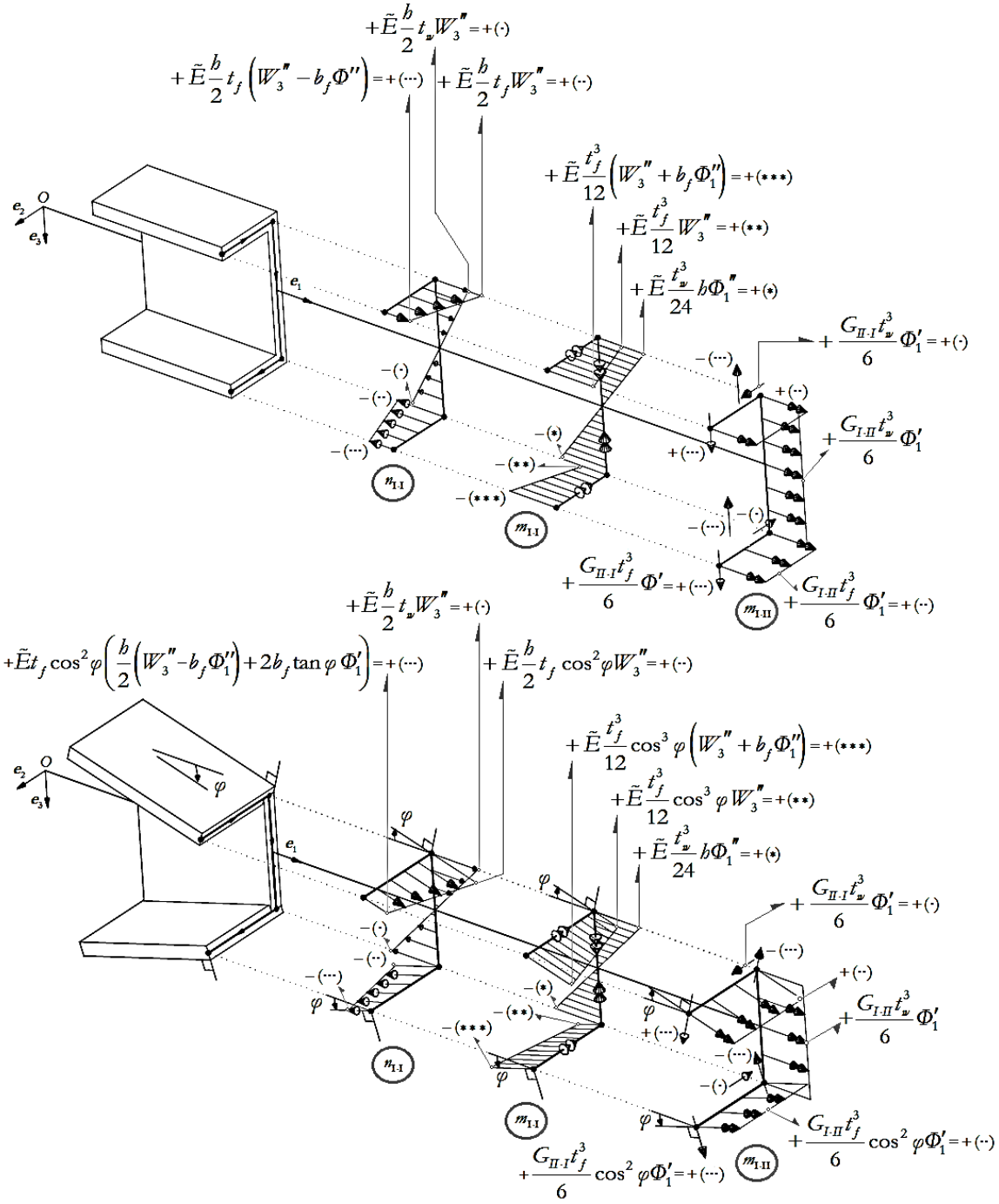

Figure 2.10.16: Contrasting the flexural-torsional behaviours of prismatic and web-tapered singly symmetric C-section bars – Membrane forces $n_{I\cdot I}$ and shell moments $m_{I\cdot I}$ - $m_{I\cdot II}$

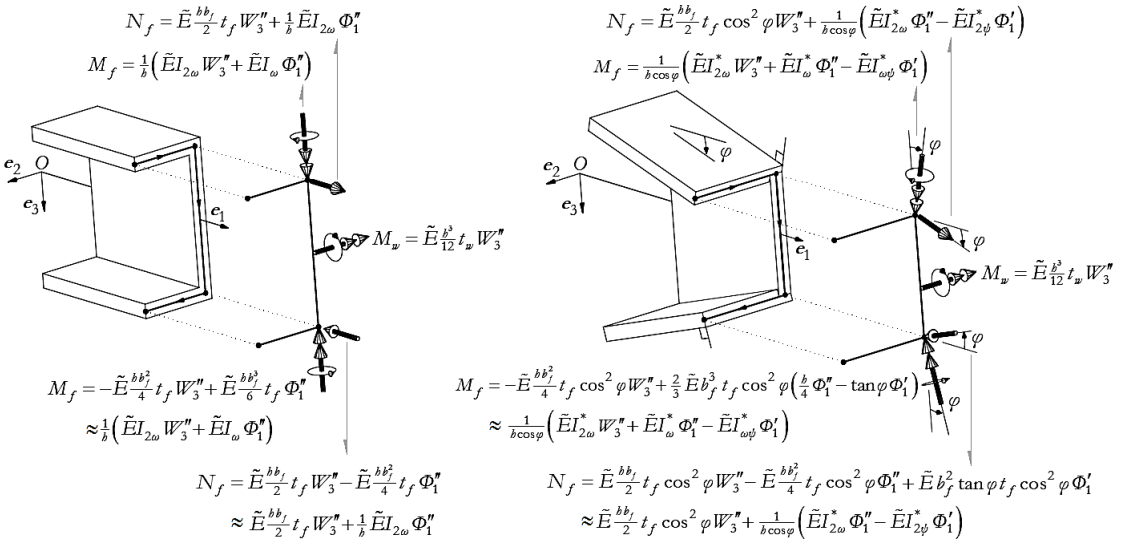

Figure 2.10.17: Contrasting the flexural-torsional behaviours of prismatic and web-tapered singly symmetric C-section bars – Force system statically equivalent to the membrane forces $n_{1\cdot 1}$ in the web and flanges

and, in each flange, a bending moment-normal force pair

$$M_f(\theta^1) = -\tilde{E}\frac{h(\theta^1)}{4}b_f^2 t_f \cos^2\varphi\, W_3''(\theta^1) + \frac{2}{3}\tilde{E}b_f^3 t_f \cos^2\varphi\left(\frac{h(\theta^1)}{4}\Phi_1''(\theta^1) - \tan\varphi\,\Phi_1'(\theta^1)\right)$$

$$\approx \frac{1}{h(\theta^1)\cos\varphi}\left[\tilde{E}I_{2\omega}^*(\theta^1)W_3''(\theta^1) + \left(\tilde{E}I_{\omega}^*(\theta^1)\Phi_1'(\theta^1)\right)'\right] \qquad (2.10.64)$$

$$N_f(\theta^1) = \tilde{E}\frac{h(\theta^1)}{2}b_f t_f \cos^2\varphi\, W_3''(\theta^1) - \tilde{E}b_f^2 t_f \cos^2\varphi\left(\frac{h(\theta^1)}{4}\Phi_1''(\theta^1) - \tan\varphi\,\Phi_1'(\theta^1)\right)$$

$$\approx \tilde{E}\frac{h(\theta^1)}{2}b_f t_f \cos^2\varphi\, W_3''(\theta^1) + \frac{1}{h(\theta^1)\cos\varphi}\left(\tilde{E}I_{2\omega}^*(\theta^1)\Phi_1'(\theta^1)\right)', \qquad (2.10.65)$$

with N_f acting along the junctions between the web and flanges. Notice that

$$M_w(\theta^1) + \cos\varphi\, N_f(\theta^1)h(\theta^1) = \tilde{E}I_2^*(\theta^1)W_3''(\theta^1) + \left(\tilde{E}I_{2\omega}^*(\theta^1)\Phi_1'(\theta^1)\right)' = -M_2(\theta^1) \qquad (2.10.66)$$

$$M_f(\theta^1) = \tilde{E}\frac{b_f^3 t_f}{12}\cos^2\varphi\left(\frac{h(\theta^1)}{2}\Phi_1(\theta^1)\right)'' - \frac{b_f}{2}N_f(\theta^1)\,. \qquad (2.10.67)$$

(v) The shear forces developed in the web and flanges can now be found by equilibrium considerations. Certainly, from Figure 2.10.18

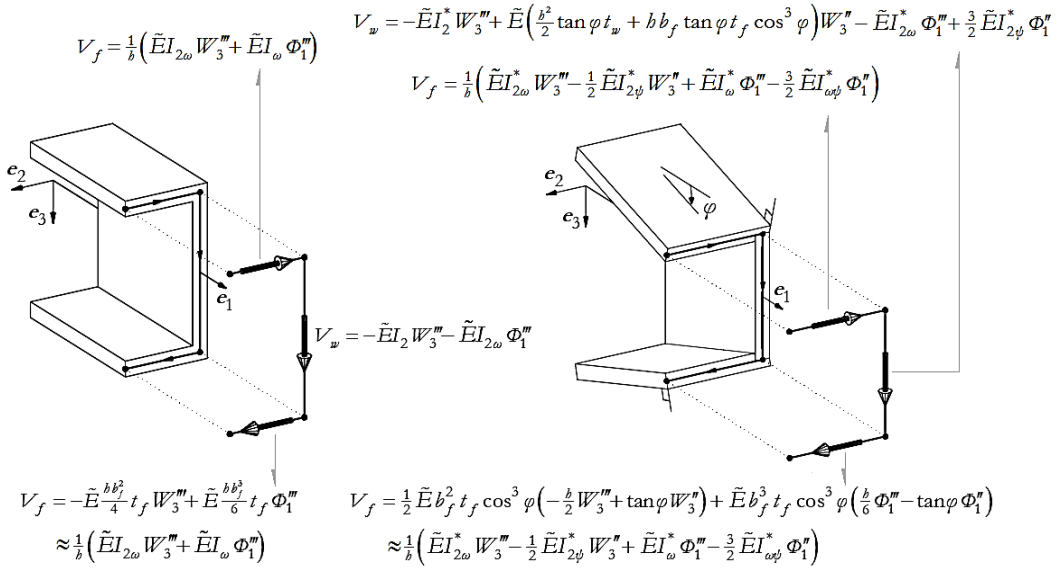

Figure 2.10.18: Contrasting the flexural-torsional behaviours of prismatic and web-tapered singly symmetric C-section bars – Shear forces in the flanges and web

I got,

$$V_w(\theta^1) + 2\sin\varphi\, N_f(\theta^1) = V_3(\theta^1) = M_2'(\theta^1) \tag{2.10.68}$$

$$V_f(\theta^1) = \cos\varphi\, M_f'(\theta^1) \tag{2.10.69}$$

where

$$V_w(\theta^1) = -\tilde{E}I_2^*(\theta^1)W_3'''(\theta^1) + \tilde{E}\left(\frac{h^2(\theta^1)}{2}\tan\varphi\, t_w + h(\theta^1)\, b_f \tan\varphi\, t_f \cos^3\varphi\right)W_3''(\theta^1)$$
$$-\tilde{E}I_{2\omega}^*(\theta^1)\Phi_1'''(\theta^1) + \frac{3}{2}\tilde{E}I_{2\psi}^*(\theta^1)\Phi_1''(\theta^1)\ , \tag{2.10.70}$$

and

$$V_f(\theta^1) = \frac{1}{2}\tilde{E}\, b_f^2\, t_f \cos^3\varphi\left(-\frac{h(\theta^1)}{2}W_3'''(\theta^1) + \tan\varphi\, W_3''(\theta^1)\right)$$
$$+\tilde{E}\, b_f^3\, t_f \cos^3\varphi\left(\frac{h(\theta^1)}{6}\Phi_1'''(\theta^1) - \tan\varphi\, \Phi_1''(\theta^1)\right)$$
$$\approx \frac{1}{h(\theta^1)}\left(\tilde{E}I_{2\omega}^*(\theta^1)W_3'''(\theta^1) - \frac{1}{2}\tilde{E}I_{2\psi}^*(\theta^1)W_3''(\theta^1)\right.$$
$$\left.+\tilde{E}I_{\omega}^*(\theta^1)\Phi_1'''(\theta^1) - \frac{3}{2}\tilde{E}I_{\omega\psi}^*(\theta^1)\Phi_1''(\theta^1)\right)\ . \tag{2.10.71}$$

(vi) In web-tapered bars, the flange bending moments have an axial component that totals

$$-2\sin\varphi\, M_f(\theta^1)\boldsymbol{e}_1 = -\frac{2\tan\varphi}{h(\theta^1)}\left(\tilde{E}I^*_{2\omega}(\theta^1)W_3'''(\theta^1)+\tilde{E}I^*_{\omega}(\theta^1)\Phi_1''(\theta^1)-\tilde{E}I^*_{\omega\psi}(\theta^1)\Phi_1'(\theta^1)\right)\boldsymbol{e}_1$$

$$=\frac{1}{2}\left(-\tilde{E}I^*_{2\psi}(\theta^1)W_3'''(\theta^1)-\tilde{E}I^*_{\omega\psi}(\theta^1)\Phi_1''(\theta^1)+\tilde{E}I^*_{\psi}(\theta^1)\Phi_1'(\theta^1)\right)\boldsymbol{e}_1\ . \quad (2.10.72)$$

In complete agreement with the general definition (2.7.6), the total torque thus amounts to

$$M_1(\theta^1) = -2\sin\varphi\, M_f(\theta^1) - V_f(\theta^1)h(\theta^1) + \tilde{G}J^*(\theta^1)\Phi_1'(\theta^1)$$

$$=-\tilde{E}I^*_{2\omega}(\theta^1)W_3'''(\theta^1)-\left(\tilde{E}I^*_{\omega}(\theta^1)\Phi_1''(\theta^1)\right)'+\left(\tilde{G}J^*(\theta^1)+\frac{1}{2}\tilde{E}I^*_{\psi}(\theta^1)\right)\Phi_1'(\theta^1)\ . \quad (2.10.73)$$

In Timoshenko approach, the contribution of the flange bending moments to the torque is neglected. Finally, notice that

$$\cos\varphi\, M_f(\theta^1) = \frac{1}{h(\theta^1)}\left[\tilde{E}I^*_{2\omega}(\theta^1)W_3'''(\theta^1)+\left(\tilde{E}I^*_{\omega}(\theta^1)\Phi_1'(\theta^1)\right)'\right] = -\frac{B(\theta^1)}{h(\theta^1)}\ , \quad (2.10.74)$$

similarly, as in the first illustrative example.

(vii) To split the torque (2.10.73) into its active and reactive component, I start by plugging (2.10.74) into (2.10.69), thus obtaining

$$V_f(\theta^1) = -\frac{1}{h(\theta^1)}\left(B'(\theta^1)+\frac{2\tan\varphi}{h(\theta^1)}B(\theta^1)\right)\ . \quad (2.10.75)$$

The active and reactive parts of the torque are then given by

$$M_1^{(A)}(\theta^1) = -2\sin\varphi\, M_f(\theta^1)+\frac{2\tan\varphi}{h(\theta^1)}B(\theta^1)+\tilde{G}J^*(\theta^1)\Phi_1'(\theta^1)$$

$$=-\tilde{E}I^*_{2\psi}(\theta^1)W_3'''(\theta^1)-\tilde{E}I^*_{\omega\psi}(\theta^1)\Phi_1''(\theta^1)+\left(\tilde{G}J^*(\theta^1)+\tilde{E}I^*_{\psi}(\theta^1)\right)\Phi_1'(\theta^1)\ . \quad (2.10.76)$$

$$M_1^{(R)}(\theta^1) = B'(\theta^1) = \left(-\tilde{E}I^*_{2\omega}(\theta^1)W_3'''(\theta^1)-\tilde{E}I^*_{\omega}(\theta^1)\Phi_1''(\theta^1)+\tilde{E}I^*_{\omega\psi}(\theta^1)\Phi_1'(\theta^1)\right)'\ , \quad (2.10.77)$$

in accordance with the general definitions (2.7.21)-(2.7.22).

Integrating one time the differential equations (2.10.53)-(2.10.54) with the boundary conditions (2.10.57)-(2.10.58) and (2.10.62), one obtains

$$W_3''(\theta^1) = -\frac{1}{\tilde{E}I_2^*(\theta^1)}\left[\left(\tilde{E}I_{2\omega}^*(\theta^1)\Phi_1'(\theta^1)\right)' + \mathcal{Q}_{L.3}(\theta^1 - L)\right] \tag{2.10.78}$$

$$-\tilde{E}I_{2\omega}^*(\theta^1)W_3''(\theta^1) - \left(\tilde{E}I_{\omega}^*(\theta^1)\Phi_1''(\theta^1)\right)' + \left(\tilde{G}J^*(\theta^1) + \frac{1}{2}\tilde{E}I_{\psi}^*(\theta^1)\right)\Phi_1'(\theta^1) = 0 \tag{2.10.79}$$

In fact, these two equations are merely the specialisation of the definitions (2.7.4) and (2.7.6). In particular, equation (2.10.78) puts us in a position to eliminate W_3 and formulate the illustrative example in terms of the single dependent variable Φ_1.

Illustrative example 2 (reduced version)

Find $\Phi_1 : [0, L] \to \mathbb{R}$ with $\Phi_1 \in C^4[0, L]$, satisfying, on the open interval $(0, L)$, the ordinary differential equation

$$\tilde{E}I_{2\omega}^*(\theta^1)\left\{\frac{1}{\tilde{E}I_2^*(\theta^1)}\left[\left(\tilde{E}I_{2\omega}^*(\theta^1)\Phi_1'(\theta^1)\right)' + M_2(\theta^1)\right]\right\}'$$

$$-\left(\tilde{E}I_{\omega}^*(\theta^1)\Phi_1''(\theta^1)\right)' + \left(\tilde{G}J^*(\theta^1) + \frac{1}{2}\tilde{E}I_{\psi}^*(\theta^1)\right)\Phi_1'(\theta^1) = 0\ , \tag{2.10.80}$$

where $M_2(\theta^1) = \mathcal{Q}_{L.3}(\theta^1 - L)$, together with the boundary conditions

$$\Phi_1(0) = 0 \tag{2.10.81}$$

$$\Phi_1'(0) = 0 \tag{2.10.82}$$

$$-\frac{\tilde{E}I_{2\omega}^*(L)}{\tilde{E}I_2^*(L)}\left(\tilde{E}I_{2\omega}^*\,\Phi_1'\right)'(L) + \left(\tilde{E}I_{\omega}^*\,\Phi_1'\right)'(L) = 0 \tag{2.10.83}$$

Once Φ_1 is known, W_3 can be obtained by solving the *initial* value problem formed by (2.10.78) and (2.10.55)-(2.10.56).

In the prismatic case ($\alpha = 1$), the solution to the above equation, is

$$\Phi_1 = \frac{Q_{L.3}\, d}{\tilde{G}J} \; \frac{\tanh\left(\sqrt{\frac{\tilde{G}J\, L^2}{\tilde{E}I_{\omega_S}}}\right)}{\sqrt{\frac{\tilde{G}J}{\tilde{E}I_{\omega_S}}}} \left[\frac{\sinh\left(\sqrt{\frac{\tilde{G}J}{\tilde{E}I_{\omega_S}}}\,(L-\theta^1)\right)}{\sinh\left(\sqrt{\frac{\tilde{G}J\, L^2}{\tilde{E}I_{\omega_S}}}\right)} - 1 + \frac{\sqrt{\frac{\tilde{G}J}{\tilde{E}I_{\omega_S}}}\,\theta^1}{\tanh\left(\sqrt{\frac{\tilde{G}J\, L^2}{\tilde{E}I_{\omega_S}}}\right)} \right] \tag{2.10.84}$$

$$W_3 = \frac{Q_{L.3}\, L}{2\tilde{E}I_2}\left(1 - \frac{\theta^1}{3L}\right)(\theta^1)^2 + d\,\Phi_1 \;, \quad 0 \le \theta^1 \le L \;, \tag{2.10.85}$$

e.g., Chen and Atsuta (1977) [p. 48], where

$$d = \frac{3 b_f^2\, t_f}{h_0\, t_w + 6 b_f\, t_f} \tag{2.10.86}$$

$$J = \frac{1}{3}\left(2 t_f^3\, b_f + t_w^3\, h_0\right) \tag{2.10.87}$$

$$I_{\omega_S} = \frac{h_0^2\, b_f^3\, t_f}{12} \, \frac{2 h_0\, t_w + 3 b_f\, t_f}{h_0\, t_w + 6 b_f\, t_f} \;. \tag{2.10.88}$$

Expression (2.10.86) is the distance from the web middle line to the shear centre and the cross-sectional property (2.10.88) is the sectorial moment of inertia for the sectorial coordinate ω_S with pole at the shear centre and origin at the corresponding sectorial centroid (midpoint of the web middle line), e.g., Vlasov (1961) [p. 61]. In the tapered case ($0 < \alpha < 1$), no closed-form solution is available. I adopted the geometry: $L = 4500\,\text{mm}$, $h_0 = 500\,\text{mm}$, $t_w = 12\,\text{mm}$, $b_f = 150\,\text{mm}$, $t_f = 18\,\text{mm}$ with $\tilde{E} = 210\,\text{GPa}$ and $\tilde{G} = 80.77\,\text{GPa}$. By using the mathematical software Mathematica (2006) to obtain numerical solutions for selected values of the web taper ratio α, varying from 0.4 to 1.0 . The results are plotted in Figures 2.10.19-2.10.20 (solid lines), where the results by adopting a stepped approach are also presented (dashed lines). The tapered bar model yields decreasing values of $\Phi_1(\theta^1) / Q_{L.3}$ with decreasing α, in particular, the stiffness $Q_{L.3} / \Phi_1(L)$ is a strictly decreasing function of α, see Figure 2.10.20, and falls outside the dotted-line envelope corresponding to prismatic cantilevers with the largest and the smallest cross-sectional dimensions, i.e., with web depth h_0 and αh_0, respectively.

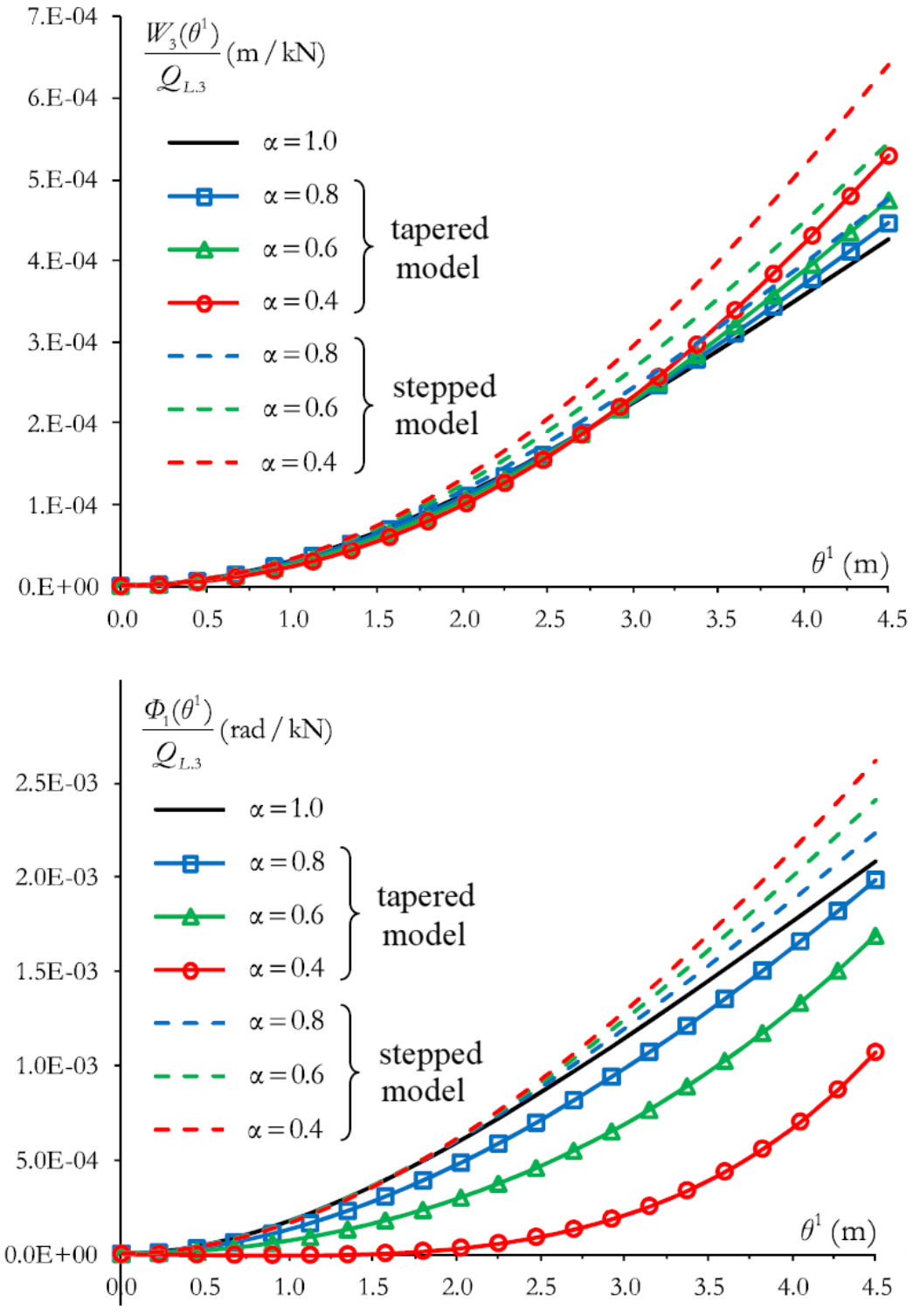

Figure 2.10.19: Illustrative example 2 – Vertical deflections W_3 and twists Φ_1 per unit load $Q_{L.3}$, e.g., Andrade (2013) [p. 112]

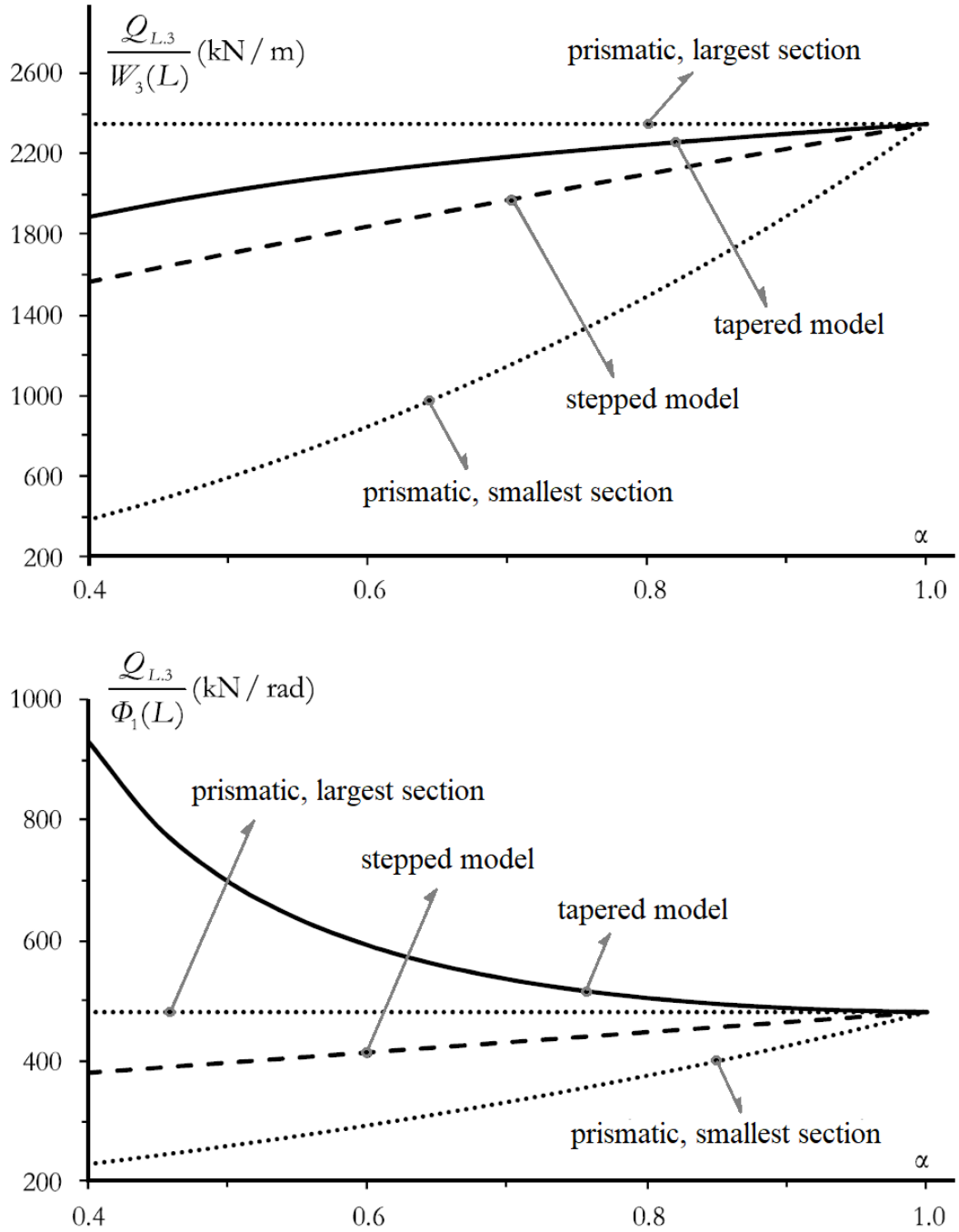

Figure 2.10.20: Illustrative example 2 – Stiffnesses $Q_{L.3}/W_3(L)$ and $Q_{L.3}/\Phi_1(L)$ *versus* the taper ratio α, e.g., Andrade (2013) [p. 113]

Hence the depth taper thus acts as an internal warping restraint over much of the span, the effectiveness of which increases as the flanges become more steeply inclined. The stepped model is notoriously incapable of capturing this internal warping restraint. Indeed, near the clamped end, the twist provided by the stepped model are practically independent of α and coincident with the prismatic solution ($\alpha = 1.0$).

REFERENCES

Abate, M., and Tovena, F. (2012). *Curves and surfaces*. Springer Science & Business Media.

Andrade, A. (2013). "One-dimensional models for the spacial behaviour of tapered thin-walled bars with open cross sections: static, dynamic and buckling analyses." *Ph.D. thesis, Universidade de Coimbra*.

Atanackovic, T. M. (1997). *Stability theory of elastic rods*. World Scientific.

Attard, M. M., and Lawther, R. (1989). "Effect of secondary warping on lateral buckling." *Engineering Structures*, 11(2), 112–118.

Axelsson, O., and Barker, V. A. (1984). *Finite element solution of boundary value problems: theory and computation*. Academic Press.

Bažant, Z. (1965). "Non-uniform torsion of thin-walled bars of variable section." *IABSE Zurich*, (25), 17–39.

Bažant, Z., and Cedolin, L. (2003). *Stability of structures: elastic, inelastic, fracture and damage theories*. Dover publications.

Bleich, F., and Bleich, H. (1936). "Bending, torsion and buckling of bars composed of thin walls." *IABSE Congress Report*, 871–894.

Boissonnade, N. (2002). "Mise au point d'un élément fini de type poutre à section variable et autres applications à la construction métallique [Development of a tapered beam finite element and other applications to steel construction]." *Ph.D. Thesis, Université Blaise Pascal, Clermont-Ferrand, France.*

Bonet, J., and Wood, R. D. (1997). *Nonlinear continuum mechanics for finite element analysis*. Cambridge university press.

Burke, W. F. (1952). *Method of manufacturing tapered beams*. Patent 2,617,179.

Cabrera, F., Andrade, A., Providência, P., and Camotim, D. (2017). "On the space behaviour of tapered thin-walled bars with open cross-sections." *Congress on Numerical Methods in Engineering, Valencia-Spain*, (606–626).

Chan, S. L. (1990). "Buckling analysis of structures composed of tapered members." *Journal of Structural Engineering*, American Society of Civil Engineers, 116(7), 1893–1906.

Chen, W. F., and Atsuta, T. (1977). *Theory of beam-columns, volume 2: space behaviour and design*. McGraw-Hill.

Ciarlet, P. G. (2000). "Mathematical Elasticity, Vol III, Theory of Shells." North-Holland.

Ciarlet, P. G., Gratie, L., Mardare, C., and Shen, M. (2008). "Saint Venant compatibility equations on a surface application to intrinsic shell theory." *Mathematical Models and Methods in Applied Sciences*, World Scientific, 18(02), 165–194.

Ciarlet, P. G., and Larsonneur, F. (2002). "On the recovery of a surface with prescribed first and second fundamental forms." *Journal de mathématiques pures et appliquées*, 81(2), 167–185.

Cywinski, Z., and Kollbrunner, C. F. (1971). "Drillknicken dünnwandiger I-stäbe mit veränderlichen, doppelt-symmetrischen querschnitten [Torsional buckling of thin-walled I-bars with variable, doubly symmetric cross-sections]." *Institut für Bauwissenschaftliche Forschung, Zürich.*

Dahlquist, G., and Björck, Å. (2003). *Numerical methods*. Dover publications.

Danielson, D. A. (1997). *Vectors and tensors in engineering and physics*. Addison-Wesley.

Dennis, S. T., and Jones, K. W. (2017). "Flexural-torsional vibration of a tapered C-section beam." *Journal of Sound and Vibration*, 393, 401–414.

Dow, J. A. (1998). *A unified approach to the finite element method and error analysis procedures*. Academic Press.

El Naschie, M. S. (1990). *Stress stability and chaos in the structural engineering and energy approach*. McGraw-Hill.

Fraser, D. J. (1983). "Design of tapered member portal frames." *Journal of Constructional Steel Research*, 3(3), 20–26.

Gantmakher, F. R. (2000). *The theory of matrices*. American Mathematical Society.

Gjelsvik, A. (1981). *The theory of thin walled bars*. Wiley.

Goldstein, H., Poole, C. P., and Safko, J. L. (2014). *Classical Mechanics*. Pearson Higher Edition.

Green, A. E., and Zerna, W. (1968). "Theoretical elasticity." Oxford University Press.

Greenwood, D. T. (1977). *Classical dynamics*. Prentice Hall.

Grinfeld, P. (2016). *Introduction to tensor analysis and the calculus of moving surfaces*. Springer.

Gurtin, M. E. (1981). *An introduction to continuum mechanics*. Academic press.

Jeevanjee, N. (2016). *An introduction to tensors and group theory for physicists*. Springer.

Joshi, A. W. (2005). *Matrices and tensors in physics*. New Age International.

Kim, N.-H. (2014). *Introduction to nonlinear finite element analysis*. Springer Science & Business Media.

Kitipornchai, S., and Trahair, N. S. (1972). "Elastic stability of tapered I-beams." *Journal of the Structural Division*, 98(3), 713–728.

Kitipornchai, S., and Trahair, N. S. (1975). "Elastic behavior of tapered monosymmetric I-beams." *Journal of the Structural Division*, 101(8), 1661–1678.

Kitipornchai, S., and Trahair, N. S. (1980). "Buckling properties of monosymmetric I-beams." *Journal of the Structural Division*, 106(5), 941–957.

Lebedev, L. P. (2010). *Tensor analysis with applications in mechanics*. World Scientific.

Lee, G. C., and Szabo, B. A. (1967). "Torsional response of tapered I-girders." *Journal of the Structural Division*, 93(5), 233–252.

Lee, L. H. N. (1956). "Non-uniform torsion of tapered I-beams." *Journal of the Franklin Institute*, 262(1), 37–44.

Mansfield, E., and Young, D. (1973). "Stephen Prokofievitch Timoshenko 1878-1972." *Biographical Memoirs of Fellows of the Royal Society*, 19, 679–694.

Marques, L. R. S. (2012). “Tapered steel members: flexural and lateral-torsional buckling.” *PhD thesis, Universidade de Coimbra*.

Mathematica. (2006). “Wolfram Mathematica.” *Modern technical computing*.

Miller, S. J., and Takloo-Bighash, R. (2006). *An invitation to modern number theory*. Princeton University Press.

Neutsch, W. (1996). *Coordinates*. Walter de Gruyter.

Pandrea, N., and Stănescu, N.-D. (2016). *Dynamics of the rigid solid with general constraints by a multibody approach*. Wiley.

Pars, L. A. (1964). *A treatise on analytical dynamics*. Heinemann.

Pignataro, M., Rizzi, N., and Luongo, A. (1991). *Stability, bifurcation and postcritical behaviour of elastic structures*. (Elsevier Science, ed.).

Pipkin, A. (1976). “Constraints in linearly elastic materials.” *Journal of Elasticity*, Springer, 6(2), 179–193.

Podio-Guidugli, P. (1989). “An exact derivation of the thin plate equation.” *Journal of Elasticity*, 22(2–3), 121–133.

Podio-Guidugli, P., and Vianello, M. (1992). “The representation problem of constrained linear elasticity.” *Journal of elasticity*, 28(3), 271–276.

Rajasekaran, S. (1994). “Equations for tapered thin-walled beams of generic open section.” *Journal of engineering mechanics*, 120(8), 1607–1629.

Rand, O., and Rovenski, V. (2004). *Analytical methods in anisotropic elasticity: with symbolic computational tools*. Birkhäuser.

Ray, S., and Shamanna, J. (2006). "On virtual displacement and virtual work in Lagrangian dynamics." *European journal of physics*, 27(2), 311.

Reddy, J. N. (2006). *Theory and analysis of elastic plates and shells*. CRC press.

Renteln, P. (2014). *Manifolds, tensors, and forms: An introduction for mathematicians and physicists*. Cambridge University Press.

Ronagh, H. R., Bradford, M. A., and Attard, M. M. (2000a). "Nonlinear analysis of thin-walled members of variable cross-section. Part I: Theory." *Computers & Structures*, 77(3), 285–299.

Ronagh, H. R., Bradford, M. A., and Attard, M. M. (2000b). "Nonlinear analysis of thin-walled members of variable cross-section. Part II: Application." *Computers & Structures*, 77(3), 301–313.

Rossmann, W. (2003). "Lectures on differential geometry." Lund University, Mathematical Faculty of Science, Lectures notes on the net.

Sadd, M. H. (2009). *Elasticity: theory, applications, and numerics*. Academic Press.

Simo, J. C., and Vu-Quoc, L. (1991). "A geometrically-exact rod model incorporating shear and torsion-warping deformation." *International Journal of Solids and Structures*, 27(3), 371–393.

Strang, G., and Borre, K. (1997). *Linear algebra, geodesy, and GPS*. Siam.

Stumpf, H. (1981). “On the linear and nonlinear stability analysis in the theory of thin elastic shells.” *Ingenieur-Archiv*, 51(3–4), 195–213.

Tarasov, V. E. (2010). *Fractional dynamics: applications of fractional calculus to dynamics of particles, fields and media*. Higher Education Press.

Timoshenko, S. P. (1910). “Einige Stabilitätsprobleme der Elastizitätstheorie [Some stability problems in the theory of elasticity].” *Zeitschrift für Mathematik und Physik*, 58(4), 337–385.

Tonti, E. (1975). *On the formal structure of physical theories*. Istituto di matematica del Politecnico di Milano.

Tonti, E. (1976). “The reason for analogies between physical theories.” *Applied Mathematical Modelling*, 1(1), 37–50.

Trahair, N., and Bradford, M. A. (1998). *Behaviour and design of steel structures to AS4100: Australian*. Taylor & Francis.

Trahair, N. S. (2014). “Bending and buckling of tapered steel beam structures.” *Engineering Structures*, 59, 229–237.

Ventsel, E., and Krauthammer, T. (2001). *Thin plates and shells: theory: analysis, and applications*. CRC press.

Vlasov, V. Z. (1961). *Thin-walled elastic beams*, [English translation of the 2nd Russian edition of 1959]. Jerusalem: Israel Program for Scientific Translation.

Wang, C., and Truesdell, C. (1973). *Introduction to rational elasticity*. Noordhoff .

Weber, C. (1926). "Übertragung des drehmomentes in balken mit doppelflanschigem querschnitt [Transmission of torque in bars with double-flanged cross-section]." *Zeitschrift für angewandte Mathematik und Mechanik*, 6(2), 85–97.

Wekezer, J. W. (1984). "Elastic torsion of thin walled bars of variable cross sections." *Computers & Structures*, 19(3), 401–407.

Wekezer, J. W. (1985). "Instability of thin walled bars." *Journal of Engineering Mechanics, ASCE*, 111(7), 923–935.

Wilde, P. (1968). "The torsion of thin-walled bars with variable cross-section [Torsion of variable cross sectional thin walled bars using shell theory equations]." *Archiwum Mechaniki Stosowanej*, 20(4), 431–443.

Yang, Y.-B., and McGuire, W. (1984). "A procedure for analysing space frames with partial warping restraint." *International Journal for Numerical Methods in Engineering*, 20(8), 1377–1398.

Yang, Y.-B., and Yau, J.-D. (1987). "Stability of beams with tapered I-sections." *Journal of Engineering Mechanics, ASCE*, 113(9), 1337–1357.

Part II.

DISCRETE ONE-DIMENSIONAL MODEL

Chapter 3

A DISCRETE ONE-DIMENSIONAL MODEL FOR THE STRETCHING, BENDING AND TWISTING OF TAPERED SINGLY SYMMETRIC I-SECTION BARS

THE STATIC CASE

The difference between discrete and continuous mathematics
is basically the difference between a bag of apples and a piece of wire.
In the former, the apples sit apart discretely from each other while in the latter,
the points on a wire spread themselves continuously from one end to the other.
Hence, in discrete mathematics we "count" the number of apples,
while in continuous mathematics we "measure" the length of the wire.

K. D. JOSHI, *FOUNDATIONS OF DISCRETE MATHEMATICS*

Philosophy (nature) is written in that great book whichever is before
our eyes – I mean the universe – but we cannot understand it if we do not first learn
the language and grasp the symbols in which it is written.
The book is written in mathematical language,
and the symbols are triangles, circles and other geometrical figures,
without whose help it is impossible to comprehend a single word of it;
without which one wanders in vain through a dark labyrinth.

GALILEO GALILEI, *THE ASSAYER*

Equations are just the boring part of mathematics.
I attempt to see things in terms of geometry.

STEPHEN HAWKING, *NATIONAL RESEARCH COUNCIL, 1989, P. 35*

3.1 INTRODUCTION

The key point behind the use of a fictitious discrete model of a structure, i.e., a finite set of structural members, as a numerical method to solve the continuum model is to establish an analogy, i.e., a relation of equivalency,[1] between the properties of the continuum and the properties of the discrete system, which may not necessarily correspond to exactly the same physical phenomenon.

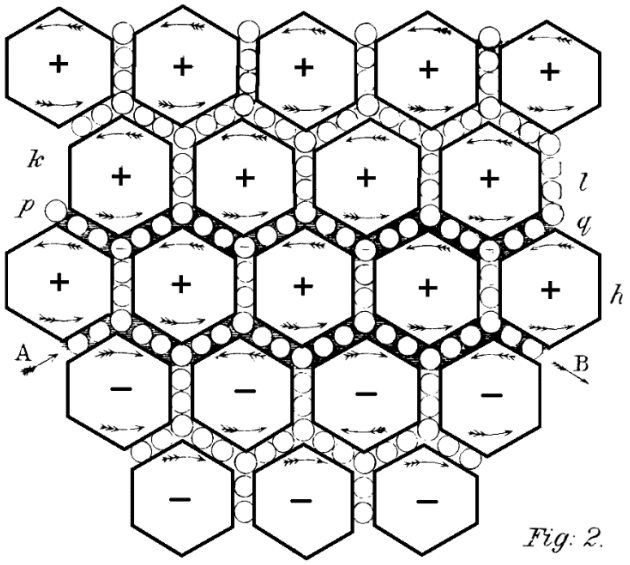

Figure 3.1.1: The elasticity of vacuum, modelled as discrete rotating vortices (Maxwell 1861) [p. 489]

For example, in order to study the nature of magnetic flux, Maxwell (1861, 1862) developed a discrete mechanical model for the vacuum, see Figure 3.1.1.[2] The model was based upon the analogy between a rotating vortex tube and a tube of magnetic flux, i.e., the relation of equivalency is that magnetic field lines expand apart, exactly as the particles moving across the vortex tube. In this chapter, a discrete one-dimensional model for stretching, bending and twisting of tapered singly symmetric I-section bars – limiting our interest to the case of the first-order response – is developed, by using an analogy with discrete structures.

[1] Analogies play a fundamental role in scientific research as well as in scientific education, e.g., Achinstein (1964) and Tonti (1975, 1976). Furthermore, an analogy between two phenomena permits one to make one phenomenon a model of the other, i.e., it allows to transfer without difficulty many concepts that are already known in one phenomenon to the other (Minati et al. 2006) [§ 49].

[2] Remarkably, this (physical) discrete approach for the vacuum can account for all known phenomena of electromagnetism, e.g., Longair (1984) [§ 3.2].

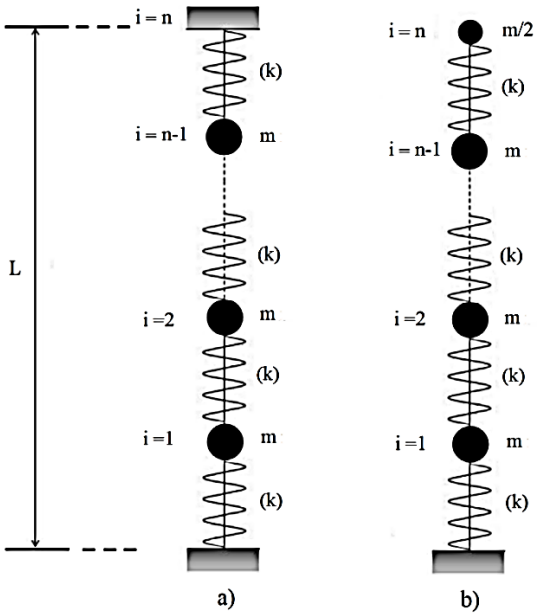

Figure 3.1.2: Axial bar-chain in vibration with discrete masses: a) fixed-fixed boundary condition, b) fixed-free boundary condition (Challamel et al. 2016)

As Challamel et al. (2016) pointed out that Lagrange (1759) [p. 367] was apparently the first one to show the analogy between the discrete one-dimensional model for axial bar-chains in vibration, with the fixed-fixed boundary condition, and its associated continuous structure (Figure 3.1.2.a), which is asymptotically obtained from the former for an infinite number of discrete elements. Another important example regarding continuous structures was the contribution of Winkler (1867), who modelled the soil medium as discrete independent (linear elastic) springs, e.g., see Figure 3.1.3.

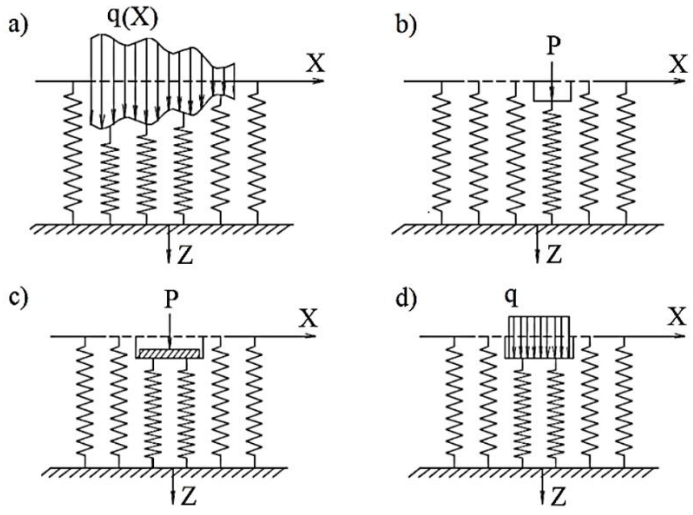

Figure 3.1.3: Winkler model due to a) a non-uniform “flexible load,” b) a concentrated load, c) a “rigid load,” d) a uniform “flexible load” (Selvadurai 1979) [p. 15]

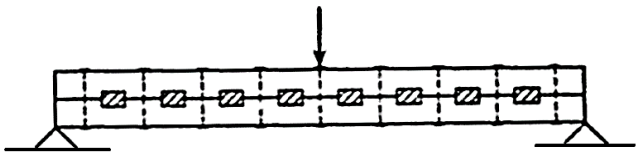

Figure 3.1.4: Jourawski mechanical discrete structure, made by discrete wooden segments, linked by elastic (axial) springs at the interfaces (Timoshenko 1953) [p. 143]

In order to measure the shear forces on continuous prismatic beams, Jourawski (1856) built-up a discrete structure (a composite beam) made of wooden segments linked by elastic (axial) springs as shown in Figure 3.1.4. The intuitive interpretation of Jourawski was that: *Mechanical discrete structures (i.e., the physical representation of discrete models) simulate the behaviour of continuous structures, if and only if, they share the same geometry (symmetry), satisfying the equivalent mechanical properties concerning the mechanical analogy: kinematic, stiffness, loading and boundary conditions*. However, the analytical development of physical discrete models had to wait for the work of Hencky (1920)[3] during his habilitation thesis on structural mechanics at the Technical University of Darmstadt, Germany (Kurrer 2008) [p. 736].

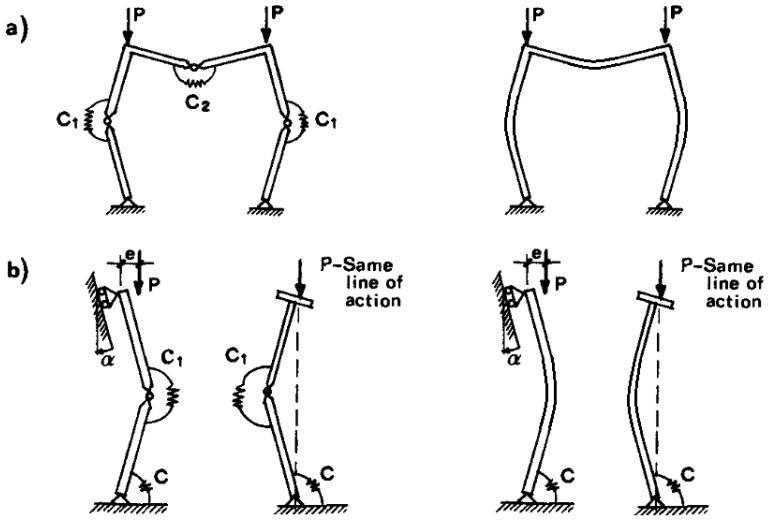

Figure 3.1.5: Hencky bar-chain model & continuous counterpart, adapted from Bažant and Cedolin (2003) [p. 259]

[3] The literature on continuum mechanics and rheology often mentions the name of Heinrich Hencky, e.g., he introduced the logarithmic strain tensor in 1928 (Tanner and Tanner 2003), yet there is no coherent appraisal of his contributions to discrete mechanics.

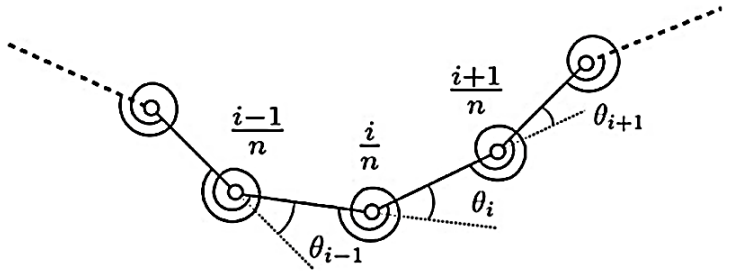

Figure 3.1.6: Graphical representation of Hencky bar-chain model, consisting of rigid bars and rotational springs (Alibert et al. 2017) [p. 4]

Basically, Hencky discretizes the continuum structure by using finite rigid segments which are connected by frictionless hinges with elastic rotational springs, see Figures 3.1.5-3.1.7. These structural models have since been referred to as Hencky bar-chain models (Zhang et al. 2016b, 2017b).[4] Other types of bar-chain models have been devised by other authors, e.g., see Figures 3.1.8-3.1.9.

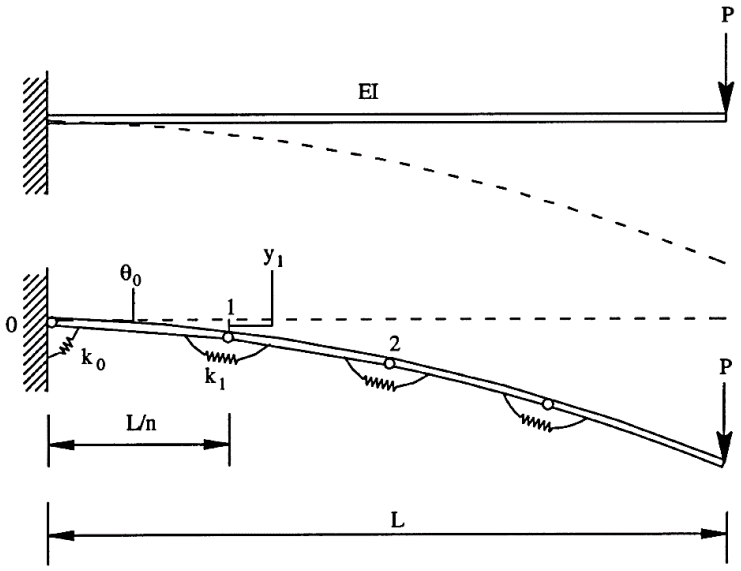

Figure 3.1.7: Schematic representation of an Hencky bar-chain model of a cantilever, defined by n discrete segments (Gambhir 2004) [p. 109]

[4] The Hencky bar-chain model has been called by different names in the literature, e.g., Prager and Prager (1979) referred to it as the discrete model, El Naschie et al. (1988), Sun et al. (1995) and Gambhir (2004) [§ 3.5] described it as the discrete element method (but this designation is more usually associated with another numerical method used in the analysis of discontinua), Wang (2001) named it as the segmented rod-column, Wang (2004) called it as the linked rod, Krishna and Ram (2007) referred to it as the discrete link-spring model, Challamel et al. (2013, 2014b), Wang et al. (2013, 2015a) and Duan et al. (2013) described it as the microstructured beam model, Dell'Isola et al. (2016) named it as the micro-model and Kawai (1977) distinguished it as the rigid body-spring model.

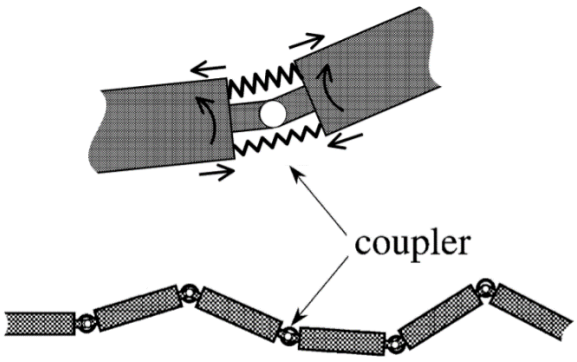

Figure 3.1.8: Discrete bar-chain model, where the discrete elements are interlinked by rotational couplers (Watanabe and Sugimoto 2005)

Although Hencky developed a systematic discrete approach for establishing a mechanical analogy between bending beams and discrete structural elements, the way in which the spring constants were defined was not very clear, since their values were assumed as *a priori postulates*, e.g., Challamel et al. (2015a) and Wang et al. (2017a). Later on, Salvadori (1951) published a paper about the application of a central finite difference scheme to the buckling problems of beams, plates and shells. In the same journal Silverman (1951), in a discussion note, pointed out that the algebraic equations developed by Salvadori for beams in bending were in fact the same linear equations of the Hencky bar-chain model. Leckie and Lindberg (1963) confirmed this mathematical equivalency for the vibration problem of beams.

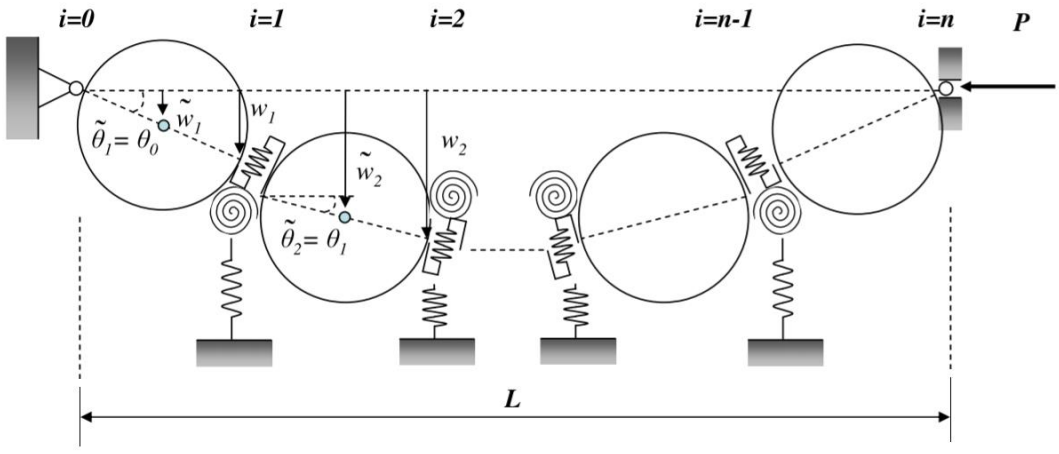

Figure 3.1.9: Granular bar-chain model (Challamel et al. 2014a)

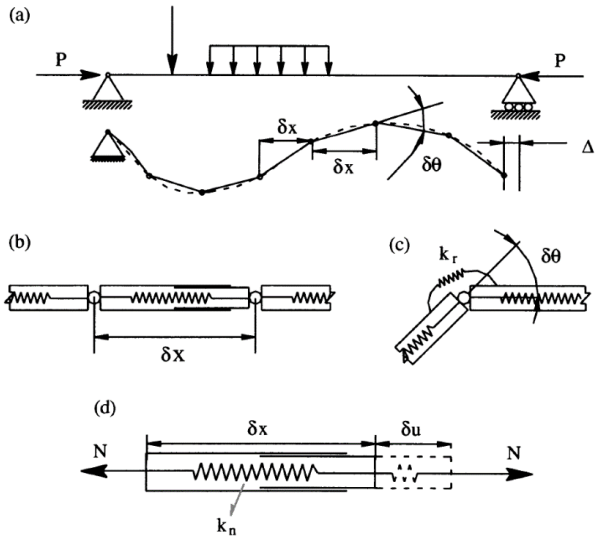

Figure 3.1.10: Hencky bar-chain model, defined by rigid hollow segments: a) discrete segments in the deformed configuration, b) internal elastic axial spring, c) elastic rotational hinge, d) distortion of the axial spring (Gambhir 2004) [p. 26]

A systematic calibration of the rotational spring constants may be established, e.g., Ruocco et al. (2016, 2017) and Zhang et al. (2013, 2016a, 2017a), with the mathematical equivalency between the physical Hencky bar-chain model and the numerical central finite difference scheme (applied to the differential equation of the problem). Furthermore, by using this technique of calibration, it is possible to define the equivalent axial and torsional springs of the discrete bar-chain model, e.g., Gambhir (2004) [§ 2.6] and Challamel et al. (2015a) see Figures 3.1.10 and 3.1.11 respectively. With respect to the shear behaviour, a shear spring is also easily defined, by adding a conventional elastic axial spring, transverse to the beam axis, e.g., Andrianov et al. (2010), see Figure 3.1.12.

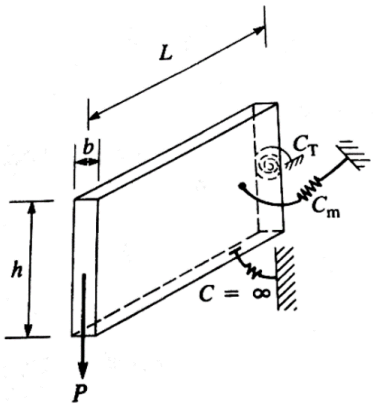

Figure 3.1.11: Torsional spring C_T (El Naschie 1990) [p. 220]

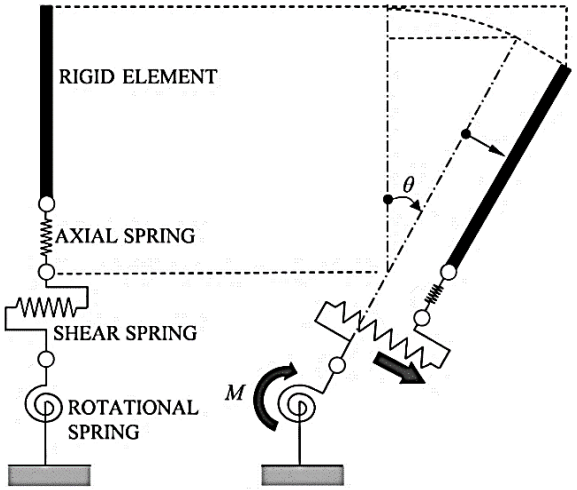

Figure 3.1.12: Characterization of a shear spring in the Hencky bar-chain model (Fukasawa et al. 2018)

Despite the simple assumptions adopted in the Hencky bar-chain model, it is still an open field of theoretical investigation, with a large variety of topics, including: nonlocal effects, e.g., Challamel et al. (2014c, 2015b, 2016) and Wang et al. (2016, 2017b), elastic stability (Wang et al. 2015b), circular shapes (Zhang and Wang 2018), chaotic behaviour, e.g., Gáspár and Domokos (1989) or Hunt et al. (1997), elastoplastic behaviour (Picandet and Challamel 2018), plates (Ruocco et al. 2018), etc.

In this chapter Hencky's original idea will be extended, to incorporate the mechanical calibration of spring constants, by using conservation laws concerning the physical nature of the discrete model, thus circumventing the need for an a priori knowledge of the differential equations and boundary conditions governing the mechanical problem. Furthermore, we used the label "Hencky bar-chain model," that in this chapter corresponds to singly symmetric I-section bars either prismatic or tapered, developing the discrete equations for the stretching, bending, and twisting, whose results are new in this kind. To verify the proposed discrete model and to assess its convergence rates, several illustrative examples, concerning different support and loading conditions, as well as different severities of taper, are discussed.

3.2 THE HENCKY BAR-CHAIN MODEL

This section aims to build a convenient link between linear difference equations and applied structural mechanics. The only prerequisites are elemental algebra and a spark of imagination.

3.2.1 Notation and characterization of springs

The case studies and their corresponding models are set up in a right-handed Cartesian coordinate system, where the *x*-axis coincides with the long axis of the bar, while the *y*- and *z*- axes define the directions of the cross-section. As a result, a continuum bar of length L measured along the *x*-axis, is represented by $\mathrm{n} \geq \mathrm{n}_{\min}$ weightless mobile segments with equal lengths $\Delta = L/\mathrm{n}$, where $\mathrm{n}_{\min}$ is a minimum number of segments (which will be defined later), connected by $\mathrm{n}-1$ frictionless hinges, whose abscissae are respectively $x = k\Delta$ with $k = 1,2,...,\mathrm{n}-1$. As a rule, when it comes to concepts of finite differences along the direction-χ (not necessarily parallel to the *x*-axis), we adopt the notation convention of LeVeque (2007) [pp. 3-4], where the first order differences, forwards (+), backwards (-), and central (o) are respectively

$$\Delta_\chi D_+(\bullet)_k = (\bullet)_{k+1} - (\bullet)_k \tag{3.2.1}$$

$$\Delta_\chi D_-(\bullet)_k = (\bullet)_k - (\bullet)_{k-1} \tag{3.2.2}$$

$$\Delta_\chi D_o(\bullet)_k = \frac{(\bullet)_{k+1} - (\bullet)_{k-1}}{2} \ , \tag{3.2.3}$$

with the reference of the segment length defined as

$$\Delta_\chi = \frac{\ell}{\mathrm{n}} \ , \tag{3.2.4}$$

where L is the projection of ℓ on x. For higher order differences

$$\left(\Delta_\chi\right)^2 D_o^2(\bullet)_k = \Delta_\chi D_+(\bullet)_k - \Delta_\chi D_+(\bullet)_{k-1} = \Delta_\chi D_-(\bullet)_{k+1} - \Delta_\chi D_-(\bullet)_k \tag{3.2.5}$$

$$\left(\Delta_\chi\right)^2 D_+^3(\bullet)_k = \Delta_\chi D_o^2(\bullet)_{k+1} - \Delta_\chi D_o^2(\bullet)_k \tag{3.2.6}$$

$$\left(\Delta_\chi\right)^2 D_-^3(\bullet)_k = \Delta_\chi D_o^2(\bullet)_k - \Delta_\chi D_o^2(\bullet)_{k-1} \ . \tag{3.2.7}$$

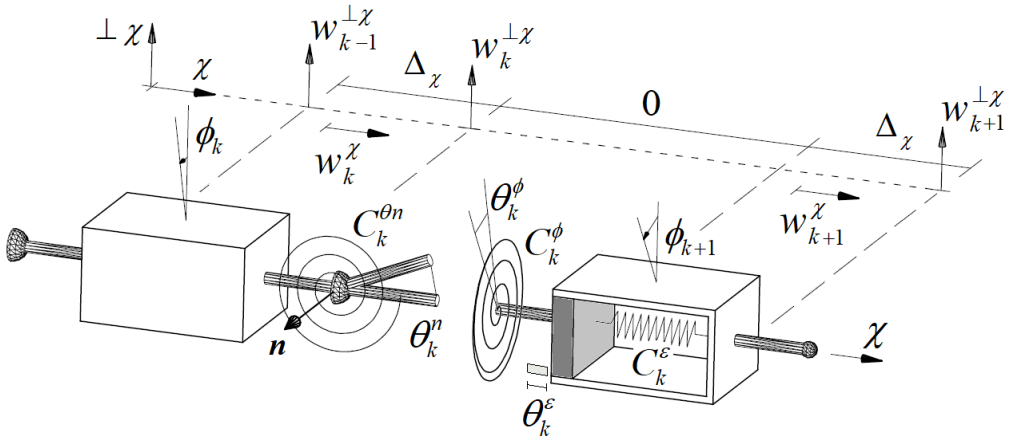

Figure 3.2.1: General springs characterization

The difference operator subscript is omitted when the reference segment has the direction of the *x*-axis, and the total derivatives up to fourth-order of a function $f(x)$ at x_o are denoted by $f'(x_o)$, $f''(x_o)$, $f'''(x_o)$ and $f^{IV}(x_o)$ respectively. For continuous variables with discrete counterparts, we adopt the subscript i or k for their discrete representation and the conventional function notation for their continuous values, e.g., ϕ_k, M_{yk}, h_k and $I_{z\omega k}$ versus $\phi(x)$, $M_y(x)$, $h(x)$ and $I_{z\omega}(x)$. All springs of the bar-chain are linear elastic and can be classified within one of the following three types: (i) axial-ε, (ii) flexural-θn, or (iii) torsional-ϕ, see Figure 3.2.1. Thus, each spring constant C_k^ξ with $\xi=\varepsilon,\theta n,\phi$ relates its generalized force to the corresponding spring deformation θ_k^ξ (i.e., θ_k^ε, $\theta_k^{\theta n}\equiv\theta_k^n$ and θ_k^ϕ), so that the stored elastic energy is given by

$$U_k^\xi=\frac{1}{2}C_k^\xi\left(\theta_k^\xi\right)^2 \text{ , with } \xi=\varepsilon,\theta n,\phi \text{ .} \tag{3.2.8}$$

Each flexural spring is defined by a vector $\boldsymbol{n}$ in three dimensional space, where the angular deformation θ_k^n is produced by the bending moment associated to that vector. Furthermore, the flexural deformation is related to the displacements $w_k^{\perp\chi}$ via

$$\theta_k^n\equiv\Delta_\chi D_o^2 w_k^{\perp\chi} \text{ .} \tag{3.2.9}$$

In the same way, the torsional deformation θ_k^ϕ (resp. axial deformation θ_k^ε) is associated to the twist rotations of the segments ϕ_k (resp. displacements of the segments w_k^χ), by

$$\theta_k^\phi\equiv\Delta_\chi D_+\phi_k \tag{3.2.10}$$

$$\theta_k^\varepsilon\equiv\Delta_\chi D_+ w_k^\chi \text{ .} \tag{3.2.11}$$

The displacements $w_k^{\chi}, w_k^{\perp\chi}$ and twist rotation ϕ_k are defined in the direction-χ, where $w_k^{\perp\chi}$ refers to the displacement of the right most end of the segment, while w_k^{χ}, ϕ_k refer to any point on the χ axis in the segment, i.e., its longitudinal displacement and rotation respectively.

3.2.2 The principle of conservation of stiffness distribution

Notice first that the bar-chain model is a physically discrete bar, so that the spring constants can have any value. However, since we want to use this fictitious structure to simulate the mechanical behaviour of its continuous counterpart, the spring constants of that discrete bar must be directly related to the resistance to deform offered by the continuous structure. First, let us consider the case of prismatic segments, linked by springs $\xi = \varepsilon, \theta n, \phi$. Because of the common origin of the bar-chain model and of the continuum bar, it is clear that the spring constants $C^{\xi}(\mathrm{n})$ of the former and the cross-sectional stiffness of the latter S^{ξ} are proportional,

$$S^{\varepsilon} = EA \tag{3.2.12}$$

$$S^{\theta n} = EI_n \tag{3.2.13}$$

$$S^{\phi} = GJ \ .^{5} \tag{3.2.14}$$

Hence

$$C^{\xi}(\mathrm{n}) \propto S^{\xi} \text{ , with } \xi = \varepsilon, \theta n, \phi \ . \tag{3.2.15}$$

Therefore, there must exist a scale factor $\Gamma^{\xi}(\mathrm{n})$ such that

$$C^{\xi}(\mathrm{n})\Gamma^{\xi}(\mathrm{n}) = S^{\xi} \text{ , with } \xi = \varepsilon, \theta n, \phi \ . \tag{3.2.16}$$

Moreover, since the dimensional formula[6] of the spring constant ξ is

$$\left[C^{\xi}(\mathrm{n})\right] = \left[\frac{S^{\xi}}{L}\right] \text{ , with } \xi = \varepsilon, \theta n, \phi \ , \tag{3.2.17}$$

the scale factor $\Gamma^{\xi}(\mathrm{n})$ must satisfy

$$\left[\Gamma^{\xi}(\mathrm{n})\right] = \left[L\right] . \tag{3.2.18}$$

---

[5] The elastic constants E and G are the Young's modulus and the shear modulus, respectively, while A, I_n and J are the well-known geometrical properties of the cross-section, i.e., the area, the second moment of area with respect to $\boldsymbol{n}$ and the torsional constant.

[6] The dimensional formula of a physical quantity shows how its magnitude is defined in terms of fundamental magnitudes (Palmer and Rogalski 2005) [§ 1.2].

As a matter of fact, this scale factor is defined as

$$\Gamma^{\xi}(\mathrm{n}) = \Delta_{\chi}(\mathrm{n}) \text{ , with } \xi = \varepsilon, \theta n, \phi \text{ .} \tag{3.2.19}$$

Hence, the elastic constant of each spring depends only on the corresponding stiffness of the continuous beam and the total number of mobile segments (or the discrete length of each segment), which is nothing more than a finite version of the well-known relation between generalized stresses and deformations (Timoshenko 1940) [pp. 3, 134 and 264],

$$C^{\xi}(\mathrm{n}) = \frac{\mathrm{n}\, S^{\xi}}{\ell} = \frac{S^{\xi}}{\Delta_{\chi}} \text{ , with } \xi = \varepsilon, \theta n, \phi \text{ .} \tag{3.2.20}$$

The principle of conservation of the stiffness distribution can now be stated: *the discrete spatial distribution of each type of spring constant is conserved for all possible bar-chain models*, in the sense that, the discrete stiffness distribution of the springs ξ along $\ell = \mathrm{n}\,\Delta_{\chi}$ is an invariant, i.e., there is a constant Λ^{ξ} with $\xi = \varepsilon, \theta n, \phi$ such that

$$\frac{C^{\xi}(\mathrm{n})}{\mathrm{n}} = \Lambda^{\xi} \text{ , } \forall\, \mathrm{n} \in \mathbb{N} \geq \mathrm{n}_{\min} \text{ , with } \Lambda^{\xi} = \frac{S^{\xi}}{\ell} \text{ .} \tag{3.2.21}$$

This global equivalence between the continuum and the discrete stiffnesses is interpreted as a relationship between the micro- and macro- media (Wang et al. 2017b). Let us now consider the more general case of non-prismatic bars. First the non-prismatic stiffness functions $S^{\xi}(\chi)$ with $\xi = \varepsilon, \theta n, \phi$ should be defined

$$S^{\varepsilon}(\chi) = EA(\chi) \text{ , } \qquad S^{\theta n}(\chi) = EI_{n}(\chi) \text{ , } \qquad S^{\phi}(\chi) = GJ(\chi) \text{ .} \tag{3.2.22}$$

One traditionally starts with a bounded real-valued function $S^{\xi}(\chi) : I \to \mathbb{R}$, where $I \in (0, \ell)$, and using the discrete sums corresponding to regular partitions of I, we establish again the finite set of n intervals of equal length Δ_{χ}, i.e., $\ell = \mathrm{n}\,\Delta_{\chi}$. In this way, it is always possible to define a one-to-one correspondence between the continuous stiffness functions $S^{\xi}(\chi)$ and the discrete values S_k^{ξ},

$$S_k^{\xi} = S^{\xi}(k\Delta_{\chi}) \text{ , } \xi = \varepsilon, \theta n, \phi \text{ with } k = 1, 2, ..., \mathrm{n}-1 \text{ .} \tag{3.2.23}$$

Thus, for a spring with constant $C_k^{\xi}(\mathrm{n})$, an extension of equation (3.2.16) can be written as

$$C_k^{\xi}(\mathrm{n})\Gamma_k^{\xi}(\mathrm{n}) = S_k^{\xi} \text{ , with } k = 1, 2, ..., \mathrm{n}-1 \text{ .} \tag{3.2.24}$$

The conservation law presented for the prismatic beam can still be applied, if we admit that the principle of conservation of stiffness distribution is valid locally,

$$\frac{C_k^{\xi}(\mathrm{n})}{\mathrm{n}} = \Lambda_k^{\xi} \text{ , } \xi = \varepsilon, \theta n, \phi \text{ with } k = 1, 2, ..., \mathrm{n}-1 \text{ ,} \tag{3.2.25}$$

with equation (3.2.19) given by

$$\Gamma_k^{\xi}(\mathrm{n}) = \Delta_{\chi}(\mathrm{n}) \text{ , with } k = 1, 2, ..., \mathrm{n}-1 \text{ .} \tag{3.2.26}$$

Consequently, for a finite set of springs, the above equations will be consistent if the set of finite constant terms Λ_k^{ξ} are evaluated at the same spatial points, giving, similarly to expression (3.2.20)

$$C_k^{\xi}(\mathrm{n}) = \frac{\mathrm{n}\, S_k^{\xi}}{\ell} = \frac{S_k^{\xi}}{\Delta_{\chi}} \text{ , } \xi = \varepsilon, \theta n, \phi \text{ with } k = 1, 2, ..., \mathrm{n}-1 \text{ .} \tag{3.2.27}$$

When this general expression is applied to the particular case of non-prismatic bar-chain columns, the results presented in Iremonger (1980) and Zhang et al. (2016b), where the finite difference method was used for calibration, are obtained.

3.2.3 The principle of conservation of elastic energy

Let us consider the stored elastic energy of a generic Hencky bar-chain model, with springs $\xi = \varepsilon, \theta n, \phi$ and n mobile segments

$$U^{\xi}(\mathrm{n}) = \frac{1}{2}\sum_{k=1}^{\mathrm{n}-1}\left\{C_k^{\xi}(\mathrm{n})\left(\theta_k^{\xi}\right)^2\right\} \text{ , } \xi = \varepsilon, \theta n, \phi \text{ .} \tag{3.2.28}$$

If the previous definition of the spring stiffness (3.2.27) is employed, the stored elastic energy of the bar-chain decreases with n, i.e., when n increases, and tends in the limit to the elastic energy of the continuum model. Conversely, the above expression allows us to establish a nonconventional definition of the stiffness of the springs, distinct of (3.2.21), if the principle of conservation of elastic energy was to be adopted as an alternative manner of calibration. This principle could be stated as: *the elastic energy is conserved for each type of spring for all possible bar-chain models.* For this alternative approach, the total elastic energy would not depend on the number of mobile segments of the bar chain, i.e., for any integer $\eta > -\mathrm{n}$

$$U^{\xi}(\mathrm{n}) = U^{\xi}(\mathrm{n}+\eta) = U^{\xi} \text{ , } \xi = \varepsilon, \theta n, \phi \text{ .} \tag{3.2.29}$$

In this case the stiffness of the springs would not be proportional to n.

3.2.4 Work of the loading for the general static case

For a bar of length L, the loading can be characterized by the corresponding applied forces q_{xk}, q_{yk}, q_{zk}, moments m_{xk}, m_{yk}, m_{zk}, and bimoment b_k per unit length of the discrete segment Δ (i.e., $\Delta = L/\mathrm{n}$) with $k = 1,2,..,\mathrm{n}-1$,[7] and the applied concentrated forces $Q_{0.x}$, $Q_{0.y}$, $Q_{0.z}$ and $Q_{L.x}$, $Q_{L.y}$, $Q_{L.z}$, moments $M_{0.x}$, $M_{0.y}$, $M_{0.z}$ and $M_{L.x}$, $M_{L.y}$, $M_{L.z}$ and bimoments B_0, B_L placed at the end segments respectively.[8] This loading of the bar-chain (see Figure 3.2.2) is such that the work done by the displacements W_{xk}, W_{yk}, W_{zk} and rotations $\phi_k, \Phi_{yk}, \Phi_{zk}$ (see Figure 3.2.3), defines the work it produces.[9] Hence

$$\begin{aligned}\mathcal{W}_e = \sum_k^{\mathrm{n}} \Big[& q_{xk} W_{xk} + q_{yk} W_{yk\text{-}1} + q_{zk} W_{zk\text{-}1} + m_{xk} \phi_k + m_{yk} \Phi_{yk\text{-}1} + m_{zk} \Phi_{zk\text{-}1} - b_k \, D_{-} \phi_k \Big] \Delta \\ & + Q_{0.x} W_{x0} + Q_{0.y} W_{y0} + Q_{0.z} W_{z0} + Q_{L.x} W_{xn} + Q_{L.y} W_{yn} + Q_{L.z} W_{zn} \\ & + M_{0.x} \phi_0 + M_{0.y} \Phi_{y0} + M_{0.z} \Phi_{z0} - B_0 \, D_{-} \phi_k \big|_{k=1} \\ & + M_{L.x} \phi_{\mathrm{n}} + M_{L.y} \Phi_{yn\text{-}1} + M_{L.z} \Phi_{zn\text{-}1} - B_L \, D_{-} \phi_k \big|_{k=\mathrm{n}} \, . \end{aligned} \tag{3.2.30}$$

In this geometrical representation, the bimoment is described by self-equilibrated quasi-tangential moments, whose effect is compatible with the twist rotations shown in Figure 3.2.3. Thus, when the rigid *k* segment twists, each moment follows opposite directions, so that, the work per unit discrete length Δ is equal to

$$-2 \, y_k^b \left(\frac{b_k}{h_k^b \, y_k^b} \right) \left(\frac{h_k^b D_{-} \phi_k}{2} \right) = -b_k \, D_{-} \phi_k \, . \tag{3.2.31}$$

---

[7] It should be noticed that the conservative moments per unit length can be applied in a variety of ways – e.g., quasi-tangential moments, semi-tangential moments and moments applied through Hooke joints, e.g., Simitses and Hodges (2006) [§ 8.3] or Ziegler (2013) [§ 5.4]. In this work, we restricted ourselves to quasi-tangential moments, as indicated in Figure 3.2.2.

[8] The boundary conditions at the ends of the bar-chain can be classified as either essential (Dirichlet boundary conditions) or natural (Neumann and/or Robin boundary conditions). Dirichlet conditions assign fixed values to the nodal displacements and/or rotations of the end segments of the bar-chain. Neumann conditions specify applied end forces and/or moments; regarding the latter, it is important to stress that conservative moments can be defined in a variety of ways, in this characterization, we restricted ourselves to quasi-tangential moments, as it is shown in Figure 3.2.2. Finally, Robin boundary conditions are a weighted combination of Dirichlet and Neumann boundary conditions and apply to elastic end restraints, e.g., Wang et al. (2015b).

[9] *Vide supra*, note 26 p. 51.

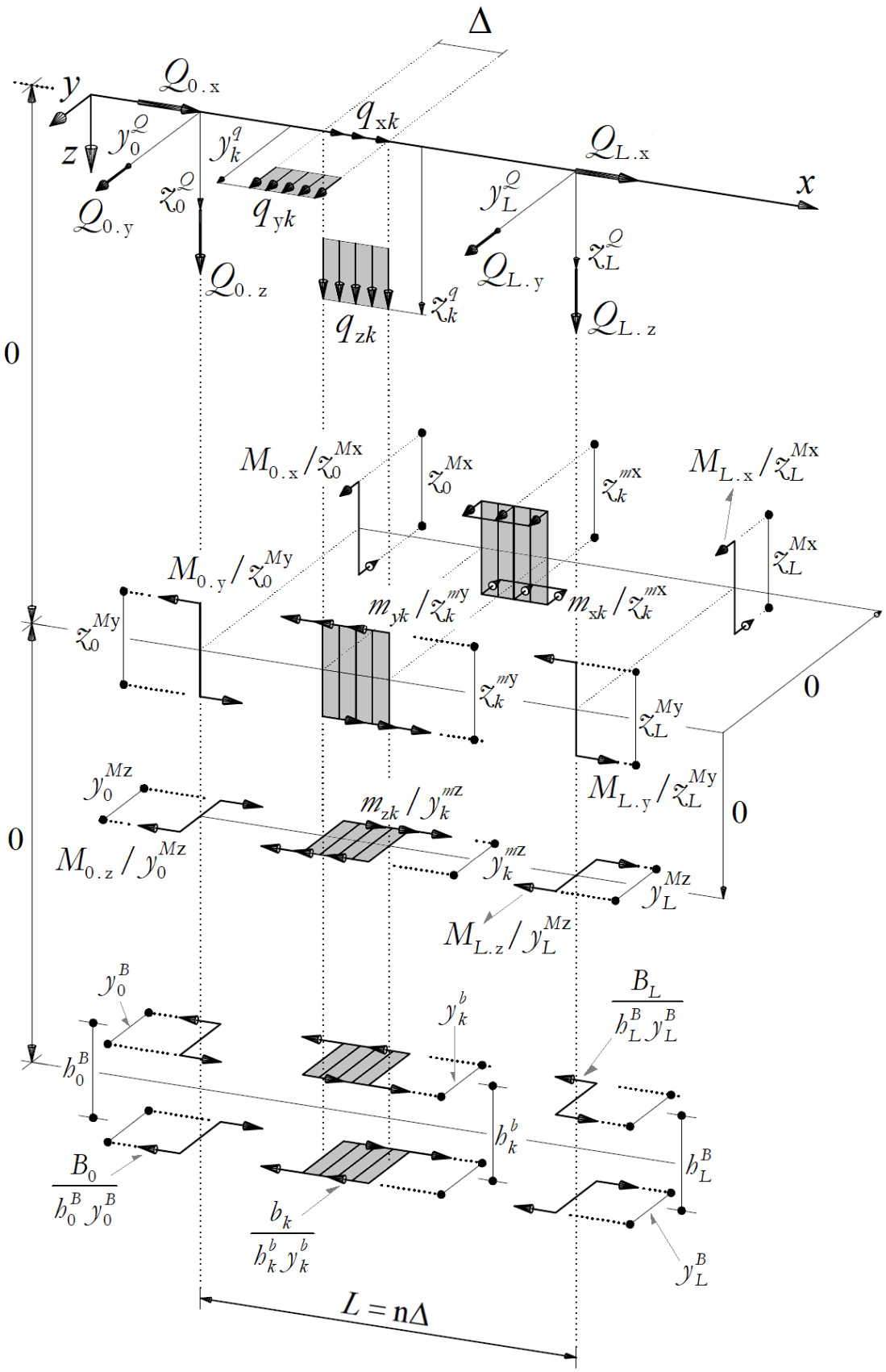

Figure 3.2.2: Applied loading – General static case

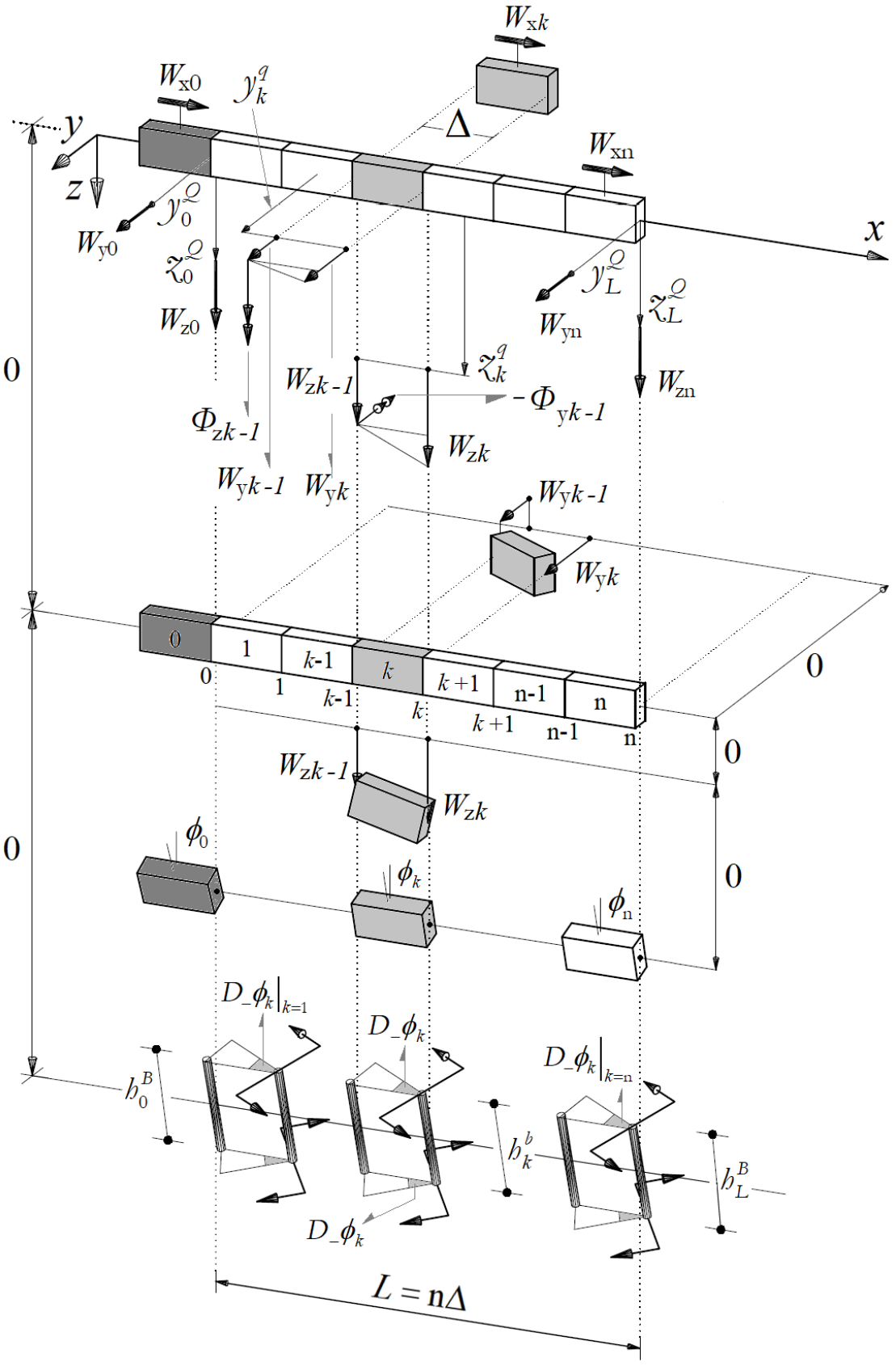

Figure 3.2.3: Work of the loading – General static case

Since displacements W_{yk}, W_{zk} are compatible with rotations Φ_{yk}, Φ_{zk}, we have

$$-\Phi_{yk} = D_{+} W_{zk} \tag{3.2.32}$$

$$\Phi_{zk} = D_{+} W_{yk} \ . \tag{3.2.33}$$

Hence, equation (3.2.30) is written as

$$\begin{aligned} \mathcal{W}_e = \sum_{k}^{n} \Big[& q_{xk} W_{xk} + q_{yk} W_{yk\text{-}1} + q_{zk} W_{zk\text{-}1} + m_{xk} \phi_k + m_{yk} \Phi_{yk\text{-}1} + m_{zk} \Phi_{zk\text{-}1} - b_k \, D_{-} \phi_k \Big] \Delta \\ & + Q_{0.x} W_{x0} + Q_{0.y} W_{y0} + Q_{0.z} W_{z0} + Q_{L.x} W_{xn} + Q_{L.y} W_{yn} + Q_{L.z} W_{zn} \\ & + M_{0.x} \phi_0 - M_{0.y} \, D_{+} W_{zk} \big|_{k=0} + M_{0.z} \, D_{+} W_{yk} \big|_{k=0} - B_0 \, D_{-} \phi_k \big|_{k=1} \\ & + M_{L.x} \phi_n - M_{L.y} \, D_{+} W_{zk} \big|_{k=n-1} + M_{L.z} \, D_{+} W_{yk} \big|_{k=n-1} - B_L \, D_{-} \phi_k \big|_{k=n} \ . \end{aligned} \tag{3.2.34}$$

As we discussed in § 2.2, a loading configuration cannot merely be replaced by a statically equivalent system of discrete loads, since the condition of static equivalence is not sufficient to fully characterize the system of bar loads, e.g., Vlasov (1961) [pp. 10-11] or Oden and Ripperger (1981) [§ 7.1]. Therefore, the discrete loading system must also be complete, in the sense that the equality between the work performed by the springs and the work performed by the bar-chain loads, is required to hold for every admissible configuration of the rigid segments.

3.2.5 The equations of the bar-chain model – General static case

In the characterization of more complex bar-chains (either prismatic or tapered), the geometry of the isolated segments should be defined first in order to retain the shape of its continuous counterpart.

A system of reference (embedded in the right-handed Cartesian coordinate system) should be selected to define the displacements W_{xk}, W_{yk}, W_{zk} and rotations ϕ_k that we are calling *the generalized coordinates* (Goldstein et al. 2014) [§ 1.3].[10] The problem reduces to finding a consistent relation between spring distortions and the generalized coordinates of the bar-chain, whose boundary conditions must also be mechanically characterized. Thus, the total potential energy of the bar-chain is equal to the contribution of the stored elastic energy in the springs $\mathcal{U}$ and the negative of the work of the loading,[11] i.e.,

$$\Pi = \mathcal{U} - \mathcal{W}_e \ . \tag{3.2.35}$$

We have already $4(\mathrm{n}-1)$ generalized coordinates. If the essential boundary conditions are expressed in n^{BC} known generalized coordinates, then the problem is left with a set of

$$\mathrm{q}_i \in \mathbf{q} \text{ with } i = 1, 2, ..., 4(\mathrm{n}-1) - \mathrm{n}^{\mathrm{BC}} \ , \tag{3.2.36}$$

where

$$\mathbf{q} = \{.., W_{xk}, W_{yk}, W_{zk}, \phi_k, ..\} \tag{3.2.37}$$

is the collection of unknown discrete variables, that define the degrees of freedom of the bar-chain. Hence, the configuration that satisfies the equilibrium equations, are given by the stationarity condition of equation (3.2.35),

$$\frac{\partial \Pi(\mathrm{q}_i)}{\partial \mathrm{q}_j} = 0 \ , \ j = 1, 2, ..., 4(\mathrm{n}-1) - \mathrm{n}^{\mathrm{BC}} \ , \tag{3.2.38}$$

e.g., Kim et al. (2018) [eq. 2.93]. The above equation represents a system of $4(\mathrm{n}-1) - \mathrm{n}^{\mathrm{BC}}$ linear equations, whose unknown degrees of freedom (resp. known loading coefficients) can be grouped into a column vector $\{\mathrm{q}\}$ (resp. $\{\mathrm{f}\}$) defined by four sub-column-vectors $\{W_{\mathrm{x}}\}$, $\{W_{\mathrm{y}}\}$, $\{W_{\mathrm{z}}\}$, and $\{\phi\}$ (resp. $\{\mathrm{f}_{\mathrm{x}}\}$, $\{\mathrm{f}_{\mathrm{y}}\}$, $\{\mathrm{f}_{\mathrm{z}}\}$ and $\{\mathrm{f}_{\phi}\}$) with dimensions $\mathrm{n}^x \times 1$, $\mathrm{n}^y \times 1$, $\mathrm{n}^z \times 1$ and $\mathrm{n}^\phi \times 1$ respectively, satisfying the following equality

$$\mathrm{n}^x + \mathrm{n}^y + \mathrm{n}^z + \mathrm{n}^\phi = 4(\mathrm{n}-1) - \mathrm{n}^{\mathrm{BC}} \ . \tag{3.2.39}$$

[10] Different coordinate systems will assign different values for the generalized coordinates, however, all of them, are invariant with respect to the springs distortions or the work done by the loading.

[11] See equation (3.2.34).

Hence,

$$\{\mathrm{q}\} = \begin{Bmatrix} \{W_{\mathrm{x}}\} \\ \{W_{\mathrm{y}}\} \\ \{W_{\mathrm{z}}\} \\ \{\phi\} \end{Bmatrix}, \qquad \{\mathrm{f}\} = \begin{Bmatrix} \{\mathrm{f}_{\mathrm{x}}\} \\ \{\mathrm{f}_{\mathrm{y}}\} \\ \{\mathrm{f}_{\mathrm{z}}\} \\ \{\mathrm{f}_{\phi}\} \end{Bmatrix} \tag{3.2.40}$$

so the system (3.2.38) can be written more compactly as

$$[K]\{\mathrm{q}\} = \{\mathrm{f}\}\ , \tag{3.2.41}$$

where the matrix $[K]$ is a block matrix, equal to

$$[K] = \begin{bmatrix} [K_{xx}] & [K_{xy}] & [K_{xz}] & [K_{x\phi}] \\ [K_{yx}] & [K_{yy}] & [K_{yz}] & [K_{y\phi}] \\ [K_{zx}] & [K_{zy}] & [K_{zz}] & [K_{z\phi}] \\ [K_{\phi x}] & [K_{\phi y}] & [K_{\phi z}] & [K_{\phi\phi}] \end{bmatrix}, \tag{3.2.42}$$

whose submatrices are defined as

$$[K_{\psi\zeta}] \in \mathbb{R}^{\mathrm{n}^{\psi}\times \mathrm{n}^{\zeta}}\ \text{, with } \psi,\zeta = x,y,z,\phi\ , \tag{3.2.43}$$

i.e., the original matrix $[K]$ is then a square $4(\mathrm{n}-1)-\mathrm{n}^{\mathrm{BC}}$ invertible matrix, so that equation (3.2.41) has exactly one solution for any loading configuration $\{\mathrm{f}\}$. The above statement is equivalent to say that

$$\{\mathrm{q}\} = \{0\}\ \text{ if and only if }\ \{\mathrm{f}\} = \{0\}\ . \tag{3.2.44}$$

Developing expression (3.2.41), we get four matrix equations of the form

$$[K_{xx}]\{W_{\mathrm{x}}\} + [K_{xy}]\{W_{\mathrm{y}}\} + [K_{xz}]\{W_{\mathrm{z}}\} + [K_{x\phi}]\{\phi\} = \{\mathrm{f}_{\mathrm{x}}\} \tag{3.2.45}$$

$$[K_{yx}]\{W_{\mathrm{x}}\} + [K_{yy}]\{W_{\mathrm{y}}\} + [K_{yz}]\{W_{\mathrm{z}}\} + [K_{y\phi}]\{\phi\} = \{\mathrm{f}_{\mathrm{y}}\} \tag{3.2.46}$$

$$[K_{zx}]\{W_{\mathrm{x}}\} + [K_{zy}]\{W_{\mathrm{y}}\} + [K_{zz}]\{W_{\mathrm{z}}\} + [K_{z\phi}]\{\phi\} = \{\mathrm{f}_{\mathrm{z}}\} \tag{3.2.47}$$

$$[K_{\phi x}]\{W_{\mathrm{x}}\} + [K_{\phi y}]\{W_{\mathrm{y}}\} + [K_{\phi z}]\{W_{\mathrm{z}}\} + [K_{\phi\phi}]\{\phi\} = \{\mathrm{f}_{\phi}\}\ . \tag{3.2.48}$$

Consider the particular case in which

$$[K_{\psi\zeta}] = [0]\ \text{ if }\ \psi \neq \zeta\ , \tag{3.2.49}$$

this means that, for the adopted system of reference, the springs deformations are uncoupled, so that equations (3.2.45)-(3.2.48) can be studied as independent effects, i.e.,

$$\left[K_{\zeta\zeta}\right]\left\{W_{\zeta}\right\}=\left\{\mathrm{f}_{\zeta}\right\} \text{ with } \zeta=x,y,z,\phi \ , \tag{3.2.50}$$

it follows that if matrices $\left[K_{\zeta\zeta}\right]$ are non-singular, the system of equations has a unique solution for any given right-hand side $\left\{\mathrm{f}_{\zeta}\right\}$, regardless of n^{ζ}.

3.2.6 The bar-chain conjecture for the general static case

Equations (3.2.45)-(3.2.48) are in fact the discrete version of the equilibrium equations (2.6.15)-(2.6.18) developed in chapter 2. This statement requires a formal proof. For the work of the loading the validation is almost trivial, i.e., compare equation (2.5.31) with (3.2.34). In the case of the elastic energy, the holonomic-scleronomic constraints (2.3.15)-(2.3.18) are compatible with the kinematics of a set of rigid segments. This fact, allows to establish a physical connection between both kinematics approaches, by using the following conjecture: *"there is at least one discrete bar-chain model*[12] *that satisfies the mechanical analogy: kinematic, stiffness, loading and boundary conditions of a specific thin-walled bar with open cross-section,"* where the problem statement consists in defining the springs connections and the mechanics of motion between segments.

3.3 PRISMATIC SINGLY SYMMETRIC I-SECTION BAR-CHAIN

The development of prismatic or tapered singly symmetric I-section bar-chains is not covered in the existing references about the Hencky bar-chain model. Hence, a convenient approach is performed considering the effect of mono-symmetry and other mechanical properties that arise naturally in the discrete model due to springs connectivity.

[12] Two or more bar-chain models can store equivalent amounts of elastic energy as shown by the prismatic example in §3.3.9.

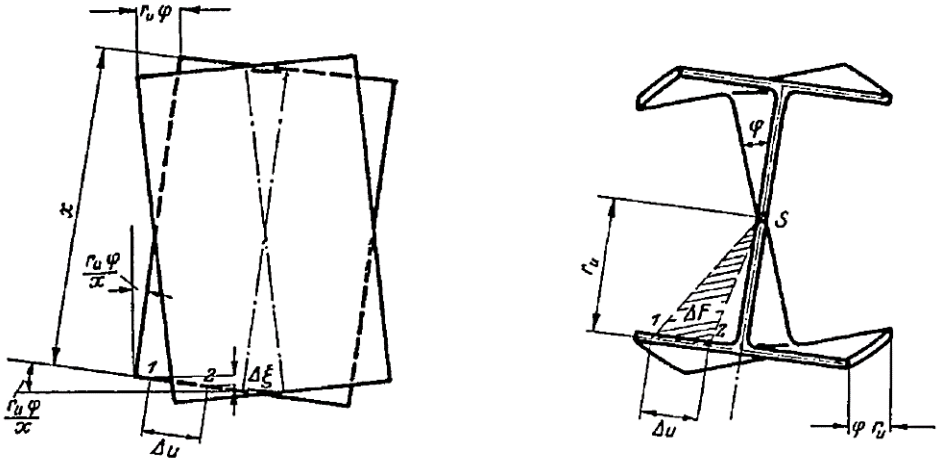

Figure 3.3.1: Distorted doubly symmetric I-section bar due to uniform torsion by Wagner and Pretschner (1936)

As a brief introduction, the main mechanical problems concerning the discrete model are described. Figure 3.3.1 depicts the uniform torsion characterization of a doubly symmetric I-section bar, that shows the rigid body motion of the flanges in agreement with the bar-chain model.[13] Concerning the behaviour of the bimoment, Yang and McGuire (1984) developed the warping spring in Figure 3.3.2. In our bar-chain the same flexural springs yield the bending and warping effect, as described below.

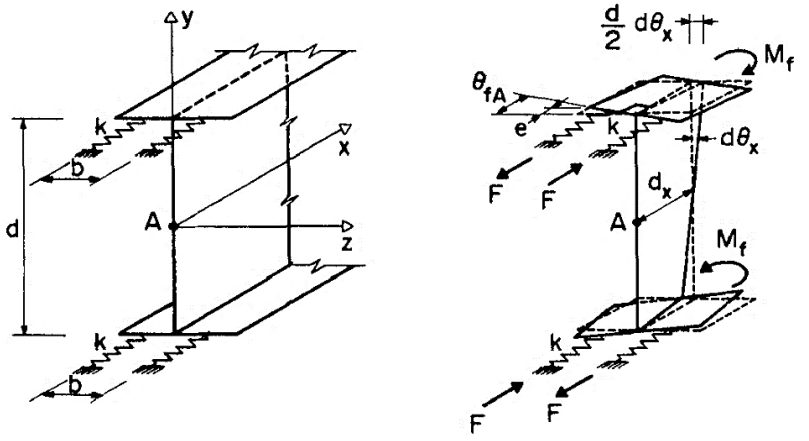

Figure 3.3.2: Physical model for a warping and lateral bending spring by Yang and McGuire (1984)

[13]In the bar-chain model, the connection along the flange-web junction is partially disconnected to keep flanges and webs as rigid bodies.

3.3.1 The kinematic of a generic segment

In the undeformed configuration, the prismatic singly symmetric I-section bar-chain is defined such that, its longitudinal centroidal axis (*c*) coincides with the *x*-axis, and the cross-section major and minor central axes correspond to the *y*- and *z*- directions. The degrees of freedom are associated to a second longitudinal axis χ -, corresponding to the shear centre axis (*sc*) as the system of reference.

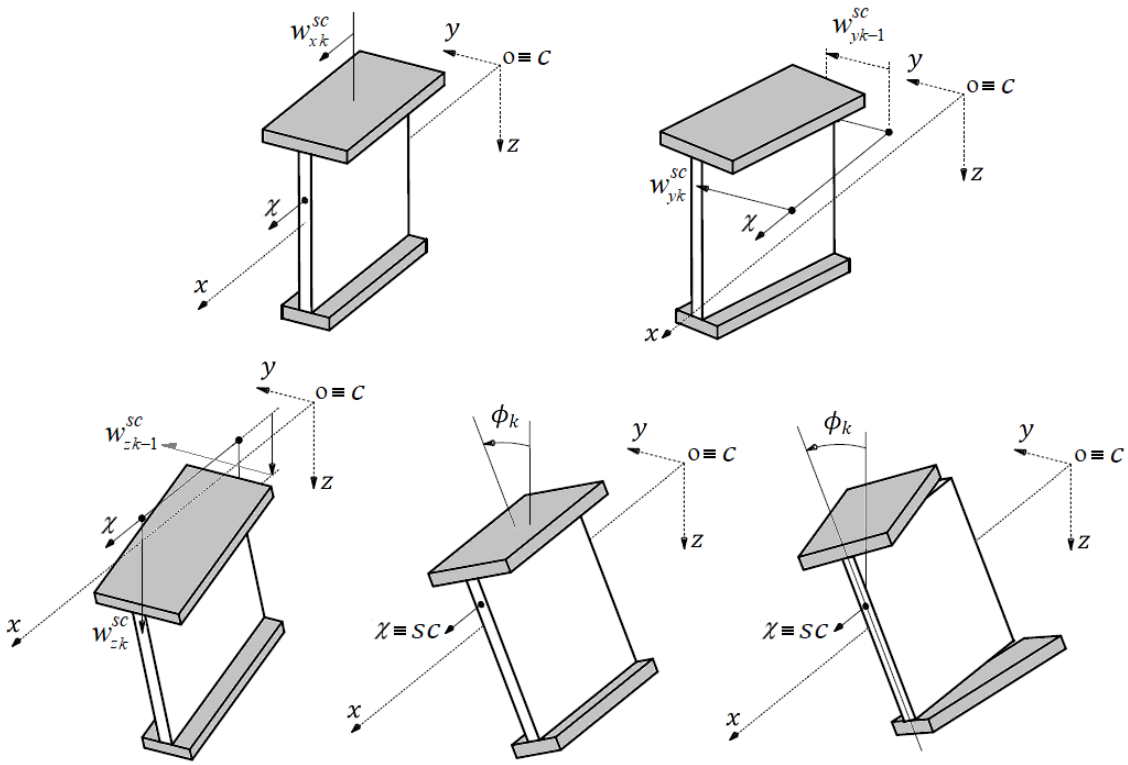

Figure 3.3.3: The degrees of freedom in the prismatic bar-chain

The kinematics of a generic segment *k*, delimited by positions $\chi = \Delta(k-1)$ and $\chi = \Delta k$ is described by the lateral displacements w_{yk-1}^{sc}, w_{zk-1}^{sc} and w_{yk}^{sc}, w_{zk}^{sc}, respectively, and the longitudinal displacement w_{xk}^{sc} with its corresponding twist rotation ϕ_k (of the web), where the warping effect corresponds to the motion of the flanges, which are connected to the web only at the front end, where they can rotate. Hence, the kinematics of the segment of the bar-chain can be represented by the scheme shown in Figure 3.3.3.

3.3.2 Springs characterization

The springs are installed between segments (see Figure 3.3.4). There are three (internal) axial springs located at each flange $C^{T\varepsilon}$, $C^{B\varepsilon}$ and the web mid-height $C^{(h/2)\varepsilon}$, one torsional spring C^{ϕ} at the χ axis, and three flexural springs $C^{T\theta z}$, $C^{B\theta z}$, $C^{(h/2)\theta y}$ connected at each flange and the web mid-high respectively.

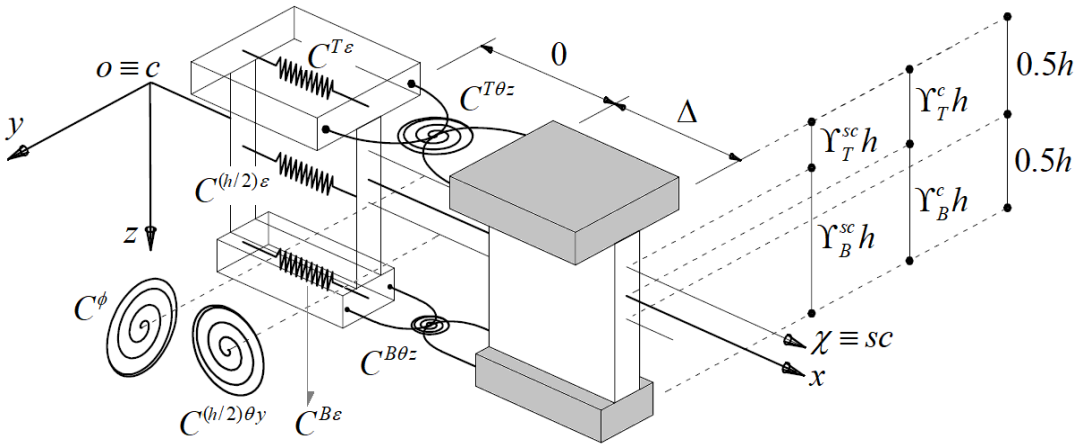

Figure 3.3.4: Type of springs for the prismatic singly symmetric I-section bar-chain

The springs deformations, with the labels *T*: top, *B*: bottom and *h*/2: web mid-height, correspond to: (i) bending $\theta_k^{Tz}, \theta_k^{Bz}, \theta_k^{(h/2)y}$ and torsional warping $\theta_k^{T\omega}, \theta_k^{B\omega}$, equal to

$$\theta_k^{Tz} = \theta_k^{Bz} = \Delta D_o^2 w_{yk}^{sc} \tag{3.3.1}$$

$$\theta_k^{(h/2)y} = -\Delta D_o^2 w_{zk}^{sc} \tag{3.3.2}$$

$$\theta_k^{T\omega} = \Upsilon_T^{sc} h \Delta D_o^2 \phi_k \tag{3.3.3}$$

$$\theta_k^{B\omega} = -\Upsilon_B^{sc} h \Delta D_o^2 \phi_k\,, \tag{3.3.4}$$

see Figures 3.3.6-3.3.8, (ii) the pure axial deformation $\theta_k^{T\varepsilon}, \theta_k^{B\varepsilon}, \theta_k^{(h/2)\varepsilon}$ (see Figure 3.3.5) and due to bending $\theta_k^{T\varepsilon y}, \theta_k^{B\varepsilon y}, \theta_k^{(h/2)\varepsilon y}$, given by

$$\theta_k^{T\varepsilon} = \theta_k^{B\varepsilon} = \theta_k^{(h/2)\varepsilon} = \Delta D_+ w_{xk}^{sc} \tag{3.3.5}$$

$$\theta_k^{T\varepsilon y} = \Upsilon_T^{c} h \Delta D_o^2 w_{zk}^{sc} \tag{3.3.6}$$

$$\theta_k^{B\varepsilon y} = -\Upsilon_B^{c} h \Delta D_o^2 w_{zk}^{sc} \tag{3.3.7}$$

$$\theta_k^{(h/2)\varepsilon y} = -\left(\Upsilon_B^{c} - 0.5\right) h \Delta D_o^2 w_{zk}^{sc}\,, \tag{3.3.8}$$

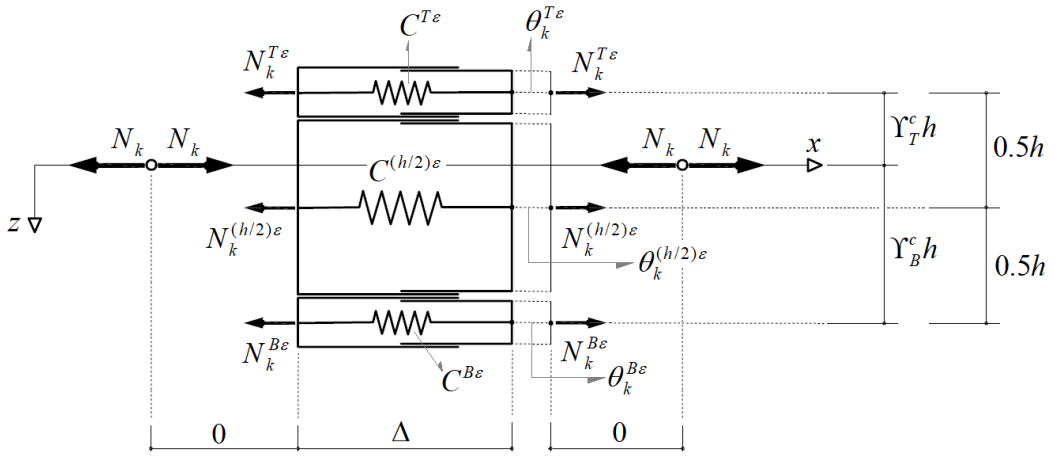

Figure 3.3.5: Deformation of the springs due to axial effects

and the (iii) torsional spring deformation θ_k^{ϕ}, see Figure 3.3.11

$$\theta_k^{\phi} = \Delta D_{+}\phi_k \ , \tag{3.3.9}$$

are consistent with the kinematics of the prismatic bar-chain corresponding to the definitions (3.2.9)-(3.2.11).

3.3.3 Internal forces and moments in the springs

When the bar-chain is subjected to an external loading, the deformations (3.3.1)-(3.3.9) are associated with pairs of internal forces via a linear relation, where the constant of proportionality is the spring constant itself. They are respectively (i) the discrete bending moments due to bending and torsional warping (see Figures 3.3.9-3.3.11)

$$M_k^{Tz} = C^{T\theta z}\theta_k^{Tz} \tag{3.3.10}$$

$$M_k^{Bz} = C^{B\theta z}\theta_k^{Bz} \tag{3.3.11}$$

$$M_k^{(h/2)y} = C^{(h/2)\theta y}\theta_k^{(h/2)y} \tag{3.3.12}$$

$$M_k^{T\omega} = C^{T\theta z}\theta_k^{T\omega} \tag{3.3.13}$$

$$M_k^{B\omega} = C^{B\theta z}\theta_k^{B\omega} \ , \tag{3.3.14}$$

(ii) the discrete axial forces caused by the axial and bending effects (Figures 3.3.5-3.3.6)

$$N_k^{T\varepsilon} = C^{T\varepsilon}\theta_k^{T\varepsilon} \tag{3.3.15}$$

$$N_k^{B\varepsilon} = C^{B\varepsilon}\theta_k^{B\varepsilon} \tag{3.3.16}$$

$$N_k^{(h/2)\varepsilon} = C^{(h/2)\varepsilon}\theta_k^{(h/2)\varepsilon} \tag{3.3.17}$$

$$N_k^{T\varepsilon y} = C^{T\varepsilon}\theta_k^{T\varepsilon y} \tag{3.3.18}$$

$$N_k^{B\varepsilon y} = C^{B\varepsilon}\theta_k^{B\varepsilon y} \tag{3.3.19}$$

$$N_k^{(h/2)\varepsilon y} = C^{(h/2)\varepsilon}\theta_k^{(h/2)\varepsilon y}\ , \tag{3.3.20}$$

and the (iii) discrete torsion due to the twist of the torsional spring (Figure 3.3.11)

$$T_k^{\phi} = C^{\phi}\theta_k^{\phi}\ . \tag{3.3.21}$$

In the following, we will be concerned with the application of the above equations, which are associated with the geometrical and mechanical properties of the singly symmetric I-section bars.

3.3.4 The centroidal axis of the cross-section

If the stiffnesses of the axial springs are $C^{T\varepsilon}, C^{(h/2)\varepsilon}, C^{B\varepsilon}$ respectively, their barycentre is such that it corresponds to a null first moment of area, i.e.,

$$\Upsilon_T^c = \frac{C^{B\varepsilon} + 0.5C^{(h/2)\varepsilon}}{C^{T\varepsilon} + C^{(h/2)\varepsilon} + C^{B\varepsilon}} \tag{3.3.22}$$

$$\Upsilon_B^c = \frac{C^{T\varepsilon} + 0.5C^{(h/2)\varepsilon}}{C^{T\varepsilon} + C^{(h/2)\varepsilon} + C^{B\varepsilon}}\ , \tag{3.3.23}$$

that define the position of the centroidal axis of the cross-section.

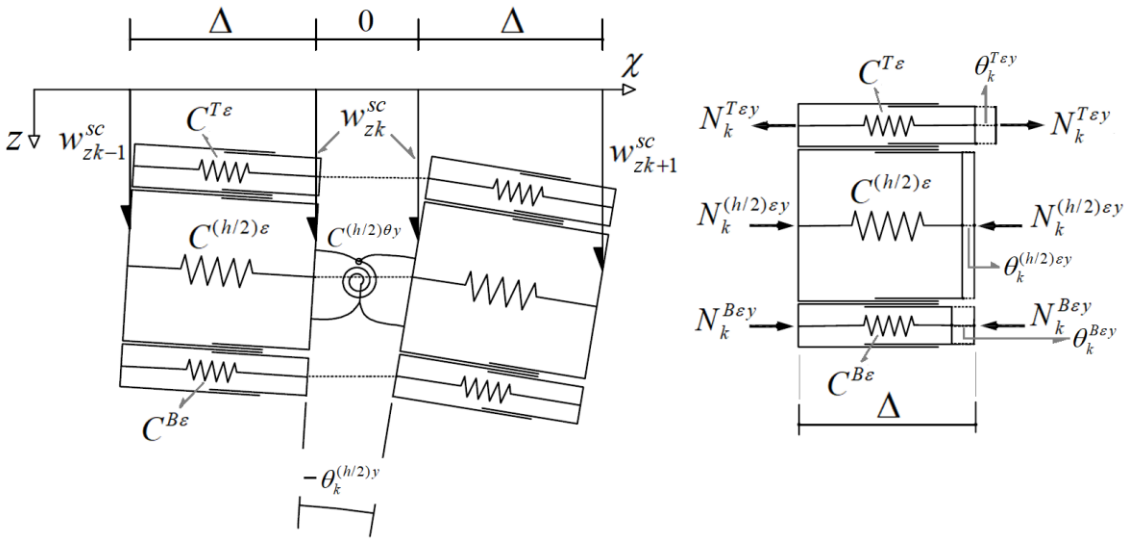

Figure 3.3.6: Springs deformations due to bending effects about the *y*-direction

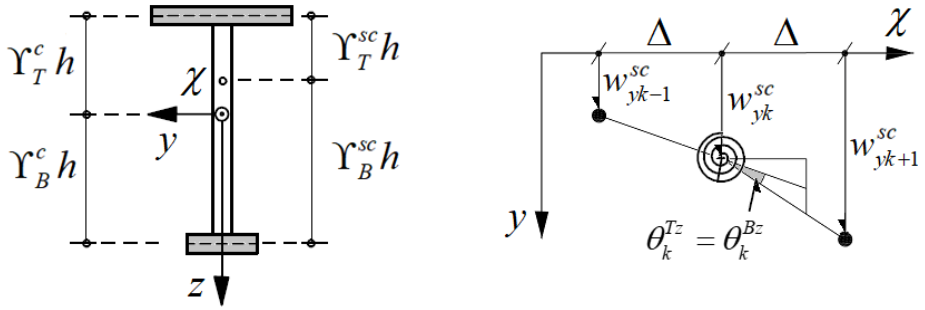

Figure 3.3.7: Springs deformations due to bending effects about the *z*-direction

And since the stiffness of each spring is proportional to the area of the corresponding wall,

$$\Upsilon_T^c = \frac{A^B + 0.5A^W}{A}\ , \qquad \Upsilon_B^c = \frac{A^T + 0.5A^W}{A} \tag{3.3.24}$$

where A^T, A^B and A^W are the area of the flanges and web, respectively, and

$$A = A^T + A^W + A^B\ , \tag{3.3.25}$$

represents the area of the cross-section.

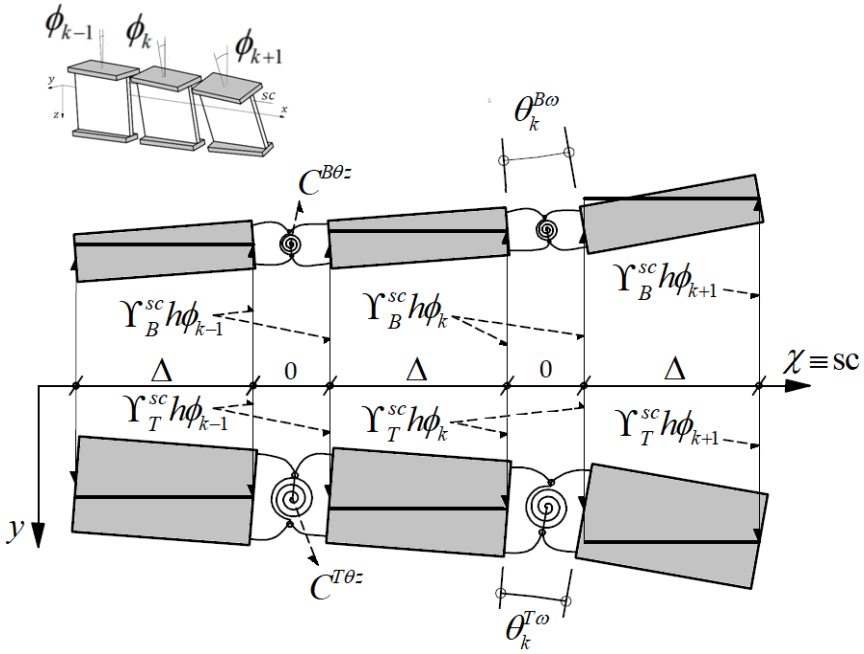

Figure 3.3.8: Springs deformations due to torsional warping effects, $\theta_k^{T\omega} \le \theta_k^{B\omega}$ (note that even though the web twist rotation is discontinuous, the lateral displacement of the flanges is continuous)

3.3.5 The shear centre axis of the cross-section

Similarly, the position of the shear centre is centroidal with respect to the shear forces $V_{yk}^{T\theta z}, V_{yk}^{B\theta z}$ in the flanges, i.e,

$$\Upsilon_T^{sc} V_{yk}^{T\theta z} = \Upsilon_B^{sc} V_{yk}^{B\theta z} \ . \tag{3.3.26}$$

Since these shear forces are given by the discrete derivative of the bending moment in the flanges, they are proportional to the corresponding bending stiffness $C^{T\theta z}$, $C^{B\theta z}$. Hence

$$\Upsilon_T^{sc} = \frac{C^{B\theta z}}{C^{T\theta z} + C^{B\theta z}} = \frac{I_z^B}{I_z} \tag{3.3.27}$$

$$\Upsilon_B^{sc} = \frac{C^{T\theta z}}{C^{T\theta z} + C^{B\theta z}} = \frac{I_z^T}{I_z} \ , \tag{3.3.28}$$

with the approximation for the second moment of area with respect to the z-direction of the cross-section given by

$$I_z = I_z^T + I_z^B \ , \tag{3.3.29}$$

where I_z^T and I_z^B are the second moment of area with respect to the *z*-direction of the top and bottom flange respectively.

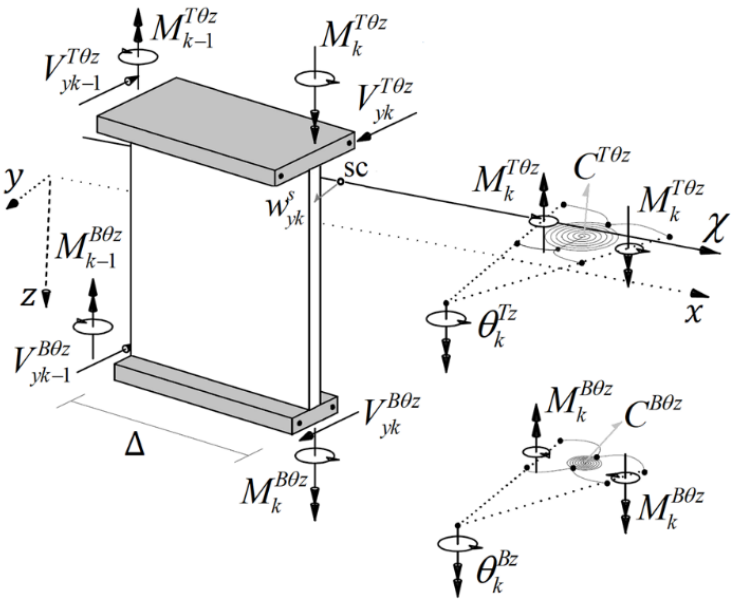

Figure 3.3.9: Internal forces in the springs, for bending about *z*-direction

3.3.6 Stored elastic energy and discrete stiffness coefficients

The adopted system of reference, allows to define the stored elastic energy as

$$\mathcal{U} = \mathcal{U}(\theta_i^{\mu}),\ i = 1,2,...,\mathrm{n}-1\ , \tag{3.3.30}$$

where the subscript μ is defined by the following spring deformations

$$\mu = \{Tz, Bz, (h/2)y, T\omega, B\omega, T\varepsilon, B\varepsilon, (h/2)\varepsilon, T\varepsilon y, B\varepsilon y, (h/2)\varepsilon y, \phi\}\ . \tag{3.3.31}$$

Hence

$$\begin{aligned}\mathcal{U}(\theta_i^{\mu}) = \frac{1}{2}\sum_{k}^{\mathrm{n}-1}\Big(& C^{T\theta z}\left[\left(\theta_k^{Tz}\right)^2 + \left(\theta_k^{T\omega}\right)^2\right] + C^{B\theta z}\left[\left(\theta_k^{Bz}\right)^2 + \left(\theta_k^{B\omega}\right)^2\right] + C^{(h/2)\theta y}\left(\theta_k^{(h/2)y}\right)^2 \\ & + C^{T\varepsilon}\left[\left(\theta_k^{T\varepsilon}\right)^2 + \left(\theta_k^{T\varepsilon y}\right)^2\right] + C^{B\varepsilon}\left[\left(\theta_k^{B\varepsilon}\right)^2 + \left(\theta_k^{B\varepsilon y}\right)^2\right] \\ & + C^{(h/2)\varepsilon}\left[\left(\theta_k^{(h/2)\varepsilon}\right)^2 + \left(\theta_k^{(h/2)\varepsilon y}\right)^2\right] + C^{\phi}\left(\theta_k^{\phi}\right)^2\Big)\ .\end{aligned} \tag{3.3.32}$$

Rewriting the spring deformations in function of the displacements w_{xi}^{sc}, w_{yi}^{sc}, w_{zi}^{sc} and the twist rotations ϕ_i, we get the classical equation for the prismatic bar-chain

$$\begin{aligned}\mathcal{U}(w_{xi}^{sc}, w_{yi}^{sc}, w_{zi}^{sc}, \phi_i) = \frac{1}{2}\sum_{k}^{\mathrm{n}-1}\Big[& C_x\left(\Delta D_{+} w_{xk}^{sc}\right)^2 + C_y\left(\Delta D_o^2 w_{zk}^{sc}\right)^2 + C_z\left(\Delta D_o^2 w_{yk}^{sc}\right)^2 \\ & + C_{\omega}\left(\Delta D_o^2 \phi_k\right)^2 + C_{\psi}\left(\Delta D_{+}\phi_k\right)^2\Big]\end{aligned} \tag{3.3.33}$$

where the discrete stiffness coefficients are reduced to

$$C_x = C^{T\varepsilon} + C^{B\varepsilon} + C^{(h/2)\varepsilon} = \frac{EA}{\Delta} \tag{3.3.34}$$

$$C_y = C^{(h/2)\theta y} + C^{T\varepsilon}\left(\Upsilon_T^c h\right)^2 + C^{B\varepsilon}\left(\Upsilon_B^c h\right)^2 + C^{(h/2)\varepsilon}\left[\left(\Upsilon_B^c - 0.5\right)h\right]^2 = \frac{EI_y}{\Delta} \tag{3.3.35}$$

$$C_z = C^{T\theta z} + C^{B\theta z} = \frac{EI_z}{\Delta} \tag{3.3.36}$$

$$C_{\omega} = h^2\left(\left(\Upsilon_T^{sc}\right)^2\ C^{T\theta z} + \left(\Upsilon_B^{sc}\right)^2\ C^{B\theta z}\right) = \frac{EI_{\omega}}{\Delta} \tag{3.3.37}$$

$$C_{\psi} = C^{\phi} = \frac{GJ}{\Delta}\ . \tag{3.3.38}$$

The above stiffness coefficients satisfy the relation

$$C_{\psi\zeta} = \delta_{\zeta}^{\psi} C_{\psi} \text{ with } \psi, \zeta = x, y, z, \psi, \omega\ , \tag{3.3.39}$$

i.e., in the adopted system of reference, the springs deformations are uncoupled.

3.3.7 Cross-sectional stress resultants, active and reactive

If we now characterize the equilibrium of the segments, we get the classical results of the thin-walled beam theory, e.g., Lonkar (1968) [pp. 20-21].

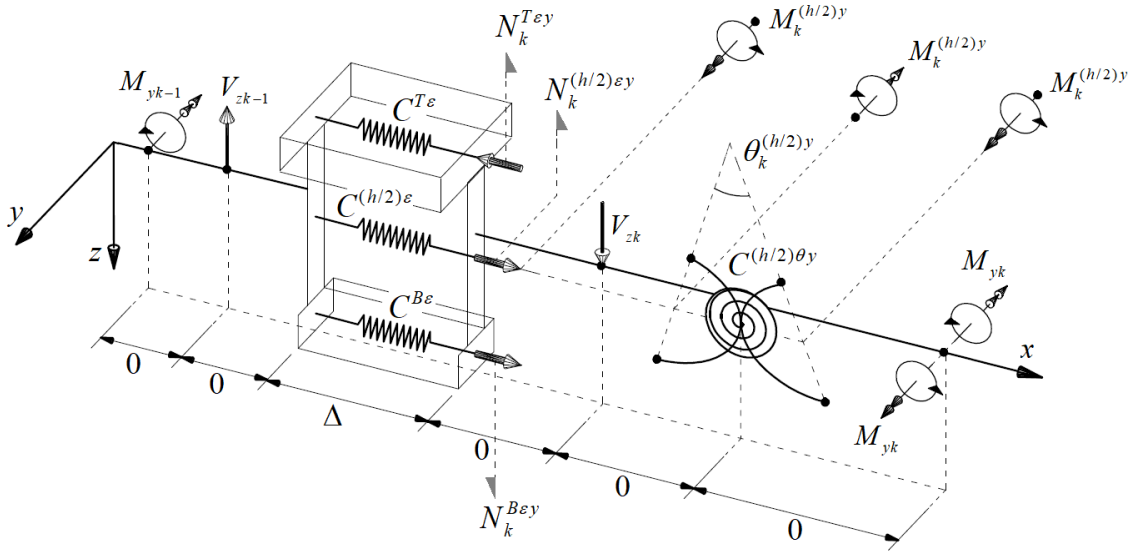

Figure 3.3.10: Equilibrium in the springs for bending about the *y*-direction

For the axial effect (see Figure 3.3.5)

$$N_k = N_k^{T\varepsilon} + N_k^{(h/2)\varepsilon} + N_k^{B\varepsilon} = EAD_+ w_{xk}^{sc} \ . \tag{3.3.40}$$

The discrete bending moment about the *z*-direction (see Figure 3.3.9) is given by

$$M_{zk} = M_k^{T\theta z} + M_k^{B\theta z} = EI_z D_o^2 w_{yk}^{sc} \ , \tag{3.3.41}$$

and is related to the discrete reactive shear force

$$V_{yk} = V_{yk}^{T\theta z} + V_{yk}^{B\theta z} \ , \tag{3.3.42}$$

via

$$V_{yk} = -D_- M_{zk} = -EI_z D_-^3 w_{yk}^{sc} \ . \tag{3.3.43}$$

In the same way, the discrete moment about the *y*-direction is defined by

$$M_{yk} = \left(N_k^{T\varepsilon y} \Upsilon_T^c + N_k^{(h/2)\varepsilon y} \left(\Upsilon_B^c - 0.5 \right) + N_k^{B\varepsilon y} \Upsilon_B^c \right) h + M_k^{(h/2)y} = -EI_y D_o^2 w_{zk}^{sc} \tag{3.3.44}$$

see Figure 3.3.10, and is associated to the discrete shear force V_{zk} by

$$V_{zk} = D_- M_{yk} = -EI_y D_-^3 w_{zk}^{sc} \ . \tag{3.3.45}$$

Concerning the torsional effect, the discrete warping torsion is equal to

$$T_k^{\omega} = \Upsilon_T^{sc} h V_{yk}^{T\omega} - \Upsilon_B^{sc} h V_{yk}^{B\omega} = -EI_{\omega} D_-^3 \phi_k = D_- B_k \ , \tag{3.3.46}$$

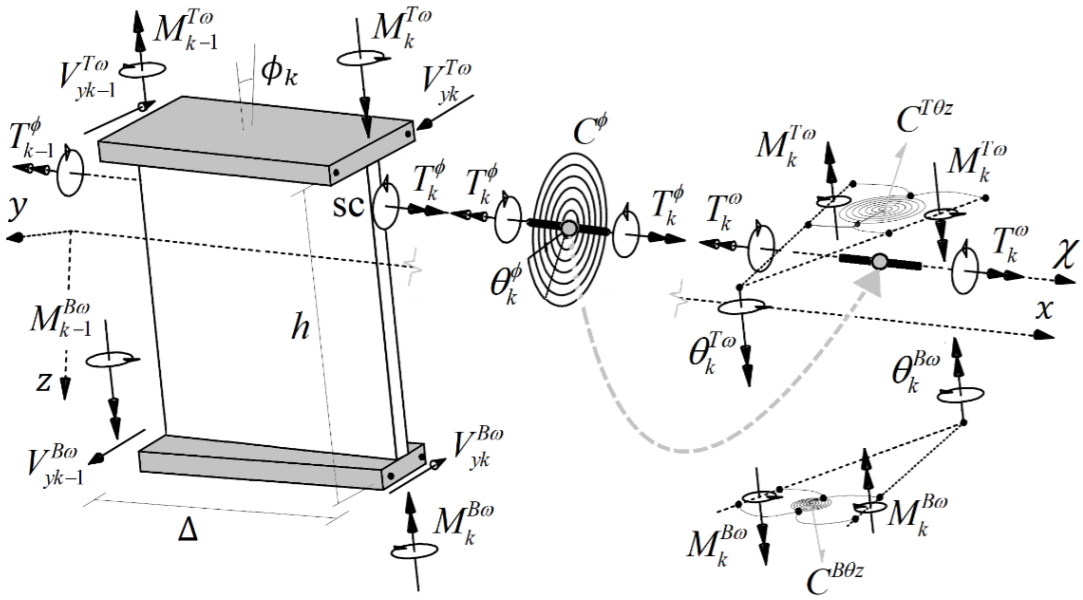

Figure 3.3.11: Internal forces in the springs due to torsional effects

where the discrete bimoment B_k is defined as

$$B_k = \left(-\Upsilon_T^{sc} M_k^{T\omega} + \Upsilon_B^{sc} M_k^{B\omega}\right) h = -EI_\omega D_o^2 \phi_k \ . \tag{3.3.47}$$

Hence, the total twist moment T_k is given by the superposition of two torsional effects,

$$T_k = T_k^{\omega} + T_k^{\phi} \ , \tag{3.3.48}$$

a reactive one associated to warping, i.e., equation (3.3.46) and the other, active, from the torsional spring

$$T_k^{\phi} = GJD_+ \phi_k \ . \tag{3.3.49}$$

3.3.8 Consistency between the discrete and continuous 1D model

If the finite twists and displacements are replaced by the exact values, i.e.,

$$w_{x\,i}^{sc} \coloneqq w_x^{sc}(\chi_i) \tag{3.3.50}$$

$$w_{y\,i}^{sc} \coloneqq w_y^{sc}(\chi_i) \tag{3.3.51}$$

$$w_{z\,i}^{sc} \coloneqq w_z^{sc}(\chi_i) \tag{3.3.52}$$

$$\phi_i \coloneqq \phi(\chi_i) \tag{3.3.53}$$

with

$$\chi_i = i\Delta \ , i = 1, 2, ..., \mathrm{n}-1 \ , \tag{3.3.54}$$

equation (3.3.33) is rewritten as

$$\mathcal{U}[w_x^{sc}(\chi_i), w_y^{sc}(\chi_i), w_z^{sc}(\chi_i), \phi(\chi_i)] = \frac{1}{2}\sum_{k}^{n-1}\Big[C_x\left(\Delta D_+ w_x^{sc}(\chi_k)\right)^2 + C_y\left(\Delta D_o^2 w_z^{sc}(\chi_k)\right)^2 + C_z\left(\Delta D_o^2 w_y^{sc}(\chi_k)\right)^2 + C_\omega\left(\Delta D_o^2 \phi(\chi_k)\right)^2 + C_\psi\left(\Delta D_+ \phi(\chi_k)\right)^2\Big] . \quad (3.3.55)$$

Expanding each value in a Taylor series around the position χ_k, i.e.,

$$w_\mu^{sc}(\chi_i) = w_\mu^{sc}(\chi_k) + \sum_{j=1}^{\infty}\left((i-k)^j \left.\frac{d^j w_\mu^{sc}(\chi)}{d\chi^j}\right|_{\chi=\chi_k} \Delta^j \right), \text{ with } \mu = \{x, y, z\}, \quad (3.3.56)$$

$$\phi(\chi_i) = \phi(\chi_k) + \sum_{j=1}^{\infty}\left((i-k)^j \left.\frac{d^j \phi(\chi)}{d\chi^j}\right|_{\chi=\chi_k} \Delta^j \right), \quad (3.3.57)$$

equation (3.3.55) is written as

$$\mathcal{U}[w_x^{sc}(\chi_i), w_y^{sc}(\chi_i), w_z^{sc}(\chi_i), \phi(\chi_i)] = \frac{1}{2}\sum_{k}^{n-1}\Big[C_x\Delta\left(w_x^{sc\prime}(\chi_k)\right)^2 + C_y\Delta\left(w_z^{sc\prime\prime}(\chi_k)\right)^2 + C_z\Delta\left(w_y^{sc\prime\prime}(\chi_k)\right)^2 + C_\omega\Delta\left(\phi''(\chi_k)\right)^2 + C_\psi\Delta\left(\phi'(\chi_k)\right)^2\Big]\Delta + O(\Delta^2) . \quad (3.3.58)$$

As a result, the error in the residual of the energy is proportional to Δ^2, so that at the limit when n approaches infinity

$$\lim_{n\to\infty}\mathcal{U}[w_x^{sc}(\chi_i), w_y^{sc}(\chi_i), w_z^{sc}(\chi_i), \phi(\chi_i)] = \lim_{\Delta\to 0}\frac{1}{2}\sum_{k}^{\infty}\Big[EA\left(w_x^{sc\prime}(\chi_k)\right)^2 + EI_y\left(w_z^{sc\prime\prime}(\chi_k)\right)^2 + EI_z\left(w_y^{sc\prime\prime}(\chi_k)\right)^2 + EI_\omega\left(\phi''(\chi_k)\right)^2 + GJ\left(\phi'(\chi_k)\right)^2\Big]\Delta + \lim_{\Delta\to 0} O(\Delta^2) = \mathcal{U}[w_x^{sc}(\chi), w_y^{sc}(\chi), w_z^{sc}(\chi), \phi(\chi)] , \quad (3.3.59)$$

the discrete positions χ_k converge to its continuous counterpart $\chi \in \mathbb{R} \cap [0, L]$. A more familiar form of equation (3.3.59) is given by

$$\mathcal{U}[w_x^{sc}(\chi), w_y^{sc}(\chi), w_z^{sc}(\chi), \phi(\chi)] = \frac{1}{2}\int_{\chi=0}^{\chi=L}\Big[EA\left(w_x^{sc\prime}(\chi)\right)^2 + EI_y\left(w_z^{sc\prime\prime}(\chi)\right)^2 + EI_z\left(w_y^{sc\prime\prime}(\chi)\right)^2 + EI_\omega\left(\phi''(\chi)\right)^2 + GJ\left(\phi'(\chi)\right)^2\Big] d\chi . \quad (3.3.60)$$

3.3.9 Unicity in the bar-chain model

At this stage, it is easy to conceive a univocal reciprocity between the continuous one-dimensional model and its physical model, i.e., a unique bar-chain configuration which however may have equivalent decompositions. For example, consider the above prismatic singly symmetric bar-chain model.

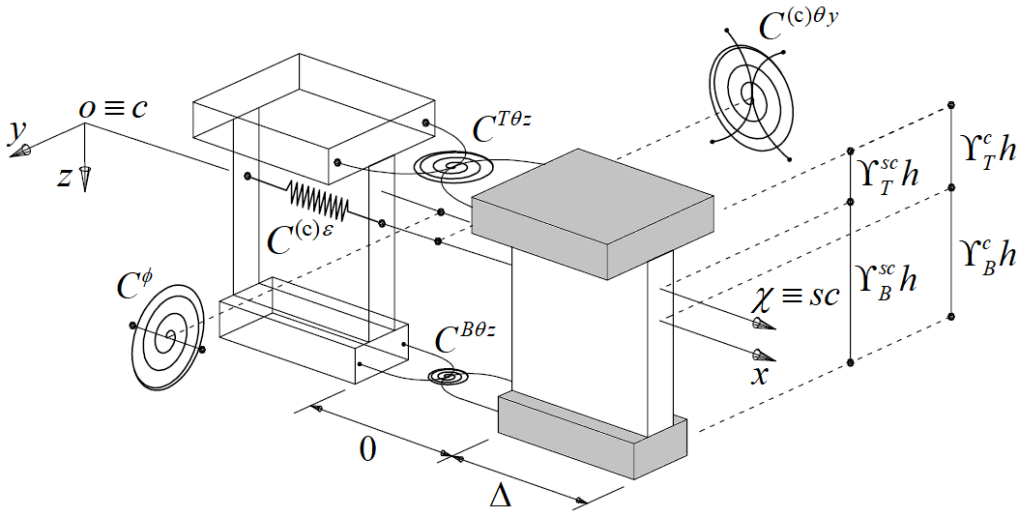

Figure 3.3.12: Alternative bar-chain model for the prismatic singly symmetric I-beam

By keeping the torsional spring C^{ϕ} (at the χ axis) and the flexural springs at the flanges $C^{T\theta z}$, $C^{B\theta z}$, the axial springs and the flexural spring at the middle of the web height can be replaced by only one axial and one flexural spring $C^{(c)\varepsilon}$ and $C^{(c)\theta y}$ respectively, located at the centroid (c) of the cross-section, see Figure 3.3.12, so that

$$C^{(c)\varepsilon} = \frac{EA}{\Delta} \tag{3.3.61}$$

$$C^{(c)\theta y} = \frac{EI_y}{\Delta} \ . \tag{3.3.62}$$

Therefore, the elastic energy of the bar-chain is rewritten as

$$\mathcal{U} = \mathcal{U}(\theta_i^{\beta}) \ , \ i = 1,2,...,n-1 \ , \tag{3.3.63}$$

with

$$\beta = \{Tz, Bz, T\omega, B\omega, (c)\varepsilon, (c)y, \phi\} \ . \tag{3.3.64}$$

Hence, the stored elastic energy has the following form

$$\mathcal{U}(\theta_i^\beta) = \frac{1}{2}\sum_k^{n-1}\Big(C^{T\theta z}\Big[\Big(\theta_k^{Tz}\Big)^2+\Big(\theta_k^{T\omega}\Big)^2\Big]+C^{B\theta z}\Big[\Big(\theta_k^{Bz}\Big)^2+\Big(\theta_k^{B\omega}\Big)^2\Big]$$
$$+C^{(c)\theta y}\Big(\theta_k^{(c)y}\Big)^2+\ C^{(c)\varepsilon}\Big(\theta_k^{(c)\varepsilon}\Big)^2+C^{\phi}\Big(\theta_k^{\phi}\Big)^2\Big)\ , \tag{3.3.65}$$

where

$$\theta_k^{(c)y} = -\Delta D_o^2 w_{zk}^{sc} \tag{3.3.66}$$

$$\theta_k^{(c)\varepsilon} = \Delta D_+ w_{xk}^{sc}\ . \tag{3.3.67}$$

Hence

$$\mathcal{U}(w_{xi}^{sc}, w_{yi}^{sc}, w_{zi}^{sc}, \phi_i) = \frac{1}{2}\sum_k^{n-1}\Big[C_x\Big(\Delta D_+ w_{xk}^{sc}\Big)^2+C_y\Big(\Delta D_o^2 w_{zk}^{sc}\Big)^2+C_z\Big(\Delta D_o^2 w_{yk}^{sc}\Big)^2$$
$$+\ C_\omega\Big(\Delta D_o^2\phi_k\Big)^2+C_\psi\Big(\Delta D_+\phi_k\Big)^2\Big] \tag{3.3.68}$$

where the discrete stiffness coefficients are reduced to

$$C_x = C^{(c)\varepsilon} = \frac{EA}{\Delta} \tag{3.3.69}$$

$$C_y = C^{(c)\theta y} = \frac{EI_y}{\Delta} \tag{3.3.70}$$

$$C_\psi = C^{\phi} = \frac{GJ}{\Delta} \tag{3.3.71}$$

$$C_z = C^{T\theta z} + C^{B\theta z} = \frac{EI_z}{\Delta} \tag{3.3.72}$$

$$C_\omega = h^2\Big(\Big(\Upsilon_T^{sc}\Big)^2\ C^{T\theta z}+\Big(\Upsilon_B^{sc}\Big)^2\ C^{B\theta z}\Big) = \frac{EI_\omega}{\Delta}\ , \tag{3.3.73}$$

we get equation (3.3.33), i.e., the bar-chain models are equivalent.

3.4 TAPERED SINGLY SYMMETRIC I-SECTION BAR-CHAIN

Figure 3.4.1 shows the reference shape of a tapered I-section bar-chain, which is formed by segments with linearly varying web depth and/or flanges width, with constant thicknesses t_T, t_B and t_W respectively. Taking as reference the Cartesian coordinate system (x, y, z) the width of the flanges and the depth of the web (measured between flange middle lines) are described by the following discrete maps

$$b_k^T = b_o^T + \frac{\gamma_T^f L}{\cos\varphi_T}\left(\frac{k}{\mathrm{n}}\right) \tag{3.4.1}$$

$$b_k^B = b_o^B + \frac{\gamma_B^f L}{\cos\varphi_B}\left(\frac{k}{\mathrm{n}}\right) \tag{3.4.2}$$

$$h_k = h_o + \gamma L\left(\frac{k}{\mathrm{n}}\right) \tag{3.4.3}$$

with $k = 0,1,2,..,\mathrm{n}$, where the corresponding slopes of the flanges γ_T^f and γ_B^f correspond to the angles with the web, via

$$\gamma_T^f = -2\tan\varphi_T^f \ , \qquad \gamma_B^f = -2\tan\varphi_B^f \tag{3.4.4}$$

while, the slope of the web is related to the inclined angles (relative the plane *x*-*z*) as

$$\gamma = -(\tan\varphi_T + \tan\varphi_B) \ . \tag{3.4.5}$$

Moreover, the position (z_k - coordinate) of the top and bottom flange middle planes are geometrically defined as

$$z_k^T = z_o^T + \left(z_{\mathrm{n}}^T - z_o^T\right)\left(\frac{k}{\mathrm{n}}\right) \tag{3.4.6}$$

$$z_k^B = z_k^T + h_k = (z_o^T + h_o) + \left[(z_{\mathrm{n}}^T + h_{\mathrm{n}}) - (z_o^T + h_o)\right]\left(\frac{k}{\mathrm{n}}\right) \tag{3.4.7}$$

with $k = 0,1,2,..,\mathrm{n}$.

3.4.1 Kinematics of the bar-chain model

Since in this case there is not a strictly defined shear centre axis (Trahair 2014), the solution adopted is to take the Cartesian coordinate system as the system of reference. Thus the degrees of freedom for a generic segment are defined by the lateral displacements W_{yk-1}, W_{zk-1} and W_{yk}, W_{zk}, the longitudinal displacement W_{xk} and the twist rotation ϕ_k. Likewise, we assumed that the flanges are connected to the web at their front end only by means of a frictionless axis parallel to *z*, see Figure 3.4.2.

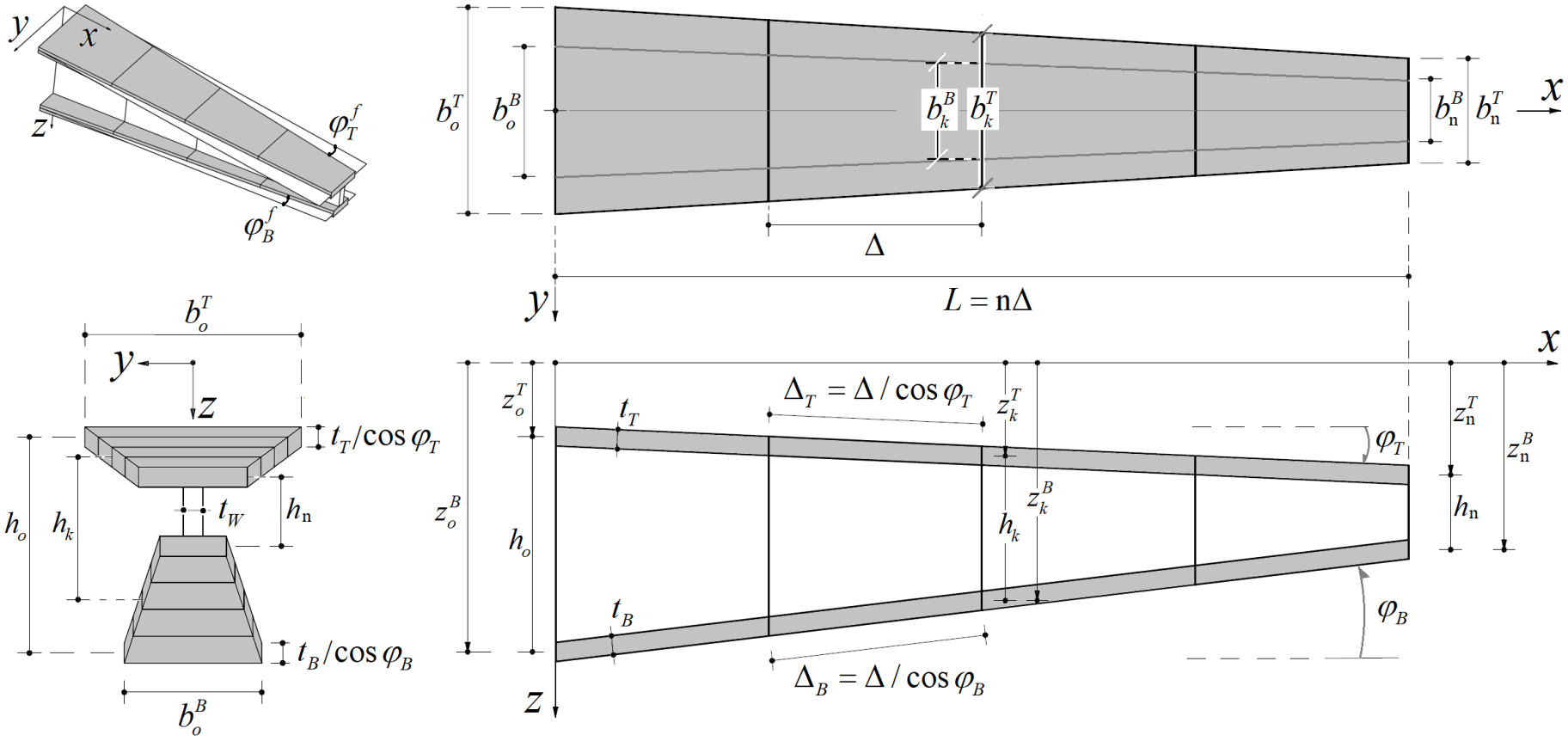

Figure 3.4.1: Reference shape, generic tapered I-section bar-chain

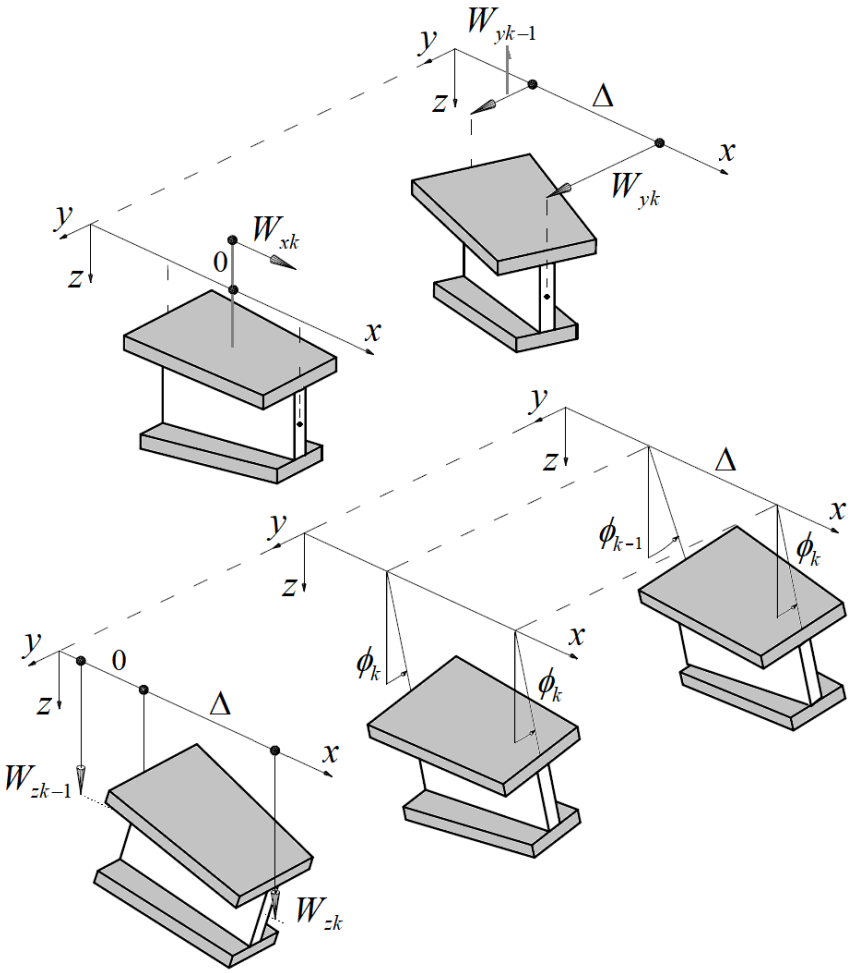

Figure 3.4.2: The degrees of freedom in the tapered I-section bar-chain model

This means that the lateral displacement of the top and bottom flange at the front section of the segment end are respectively

$$W_{yk}^{T} = W_{yk} - z_k^{T}\phi_k \ , \qquad W_{yk}^{B} = W_{yk} - z_k^{B}\phi_k \ , \tag{3.4.8}$$

while at the back end section, they are

$$W_{yk-1}^{T} = W_{yk-1} - z_{k-1}^{T}\phi_{k-1} \ , \qquad W_{yk-1}^{B} = W_{yk-1} - z_{k-1}^{B}\phi_{k-1} \ . \tag{3.4.9}$$

These displacements describe the kinematics of the combined bending (z-direction) and torsional effect. Note that both W_{yk} and ϕ_k maintain the continuity of the lateral displacements of the flanges ─ however this is not true for the web, because of the twist rotation ϕ_k, see Figure 3.4.6.

3.4.2 Springs characterization

We select three types of springs, one torsional, an internal axial and a flexural spring, all of them located at each flange (respective $C_k^{T\phi}$, $C_k^{T\varepsilon}$, $C_k^{T\theta n}$ and $C_k^{B\phi}$, $C_k^{B\varepsilon}$, $C_k^{B\theta n}$) and the web mid-high $C_k^{(h/2)\phi}$, $C_k^{(h/2)\varepsilon}$, $C_k^{(h/2)\theta y}$ as it shown in Figure 3.4.3.

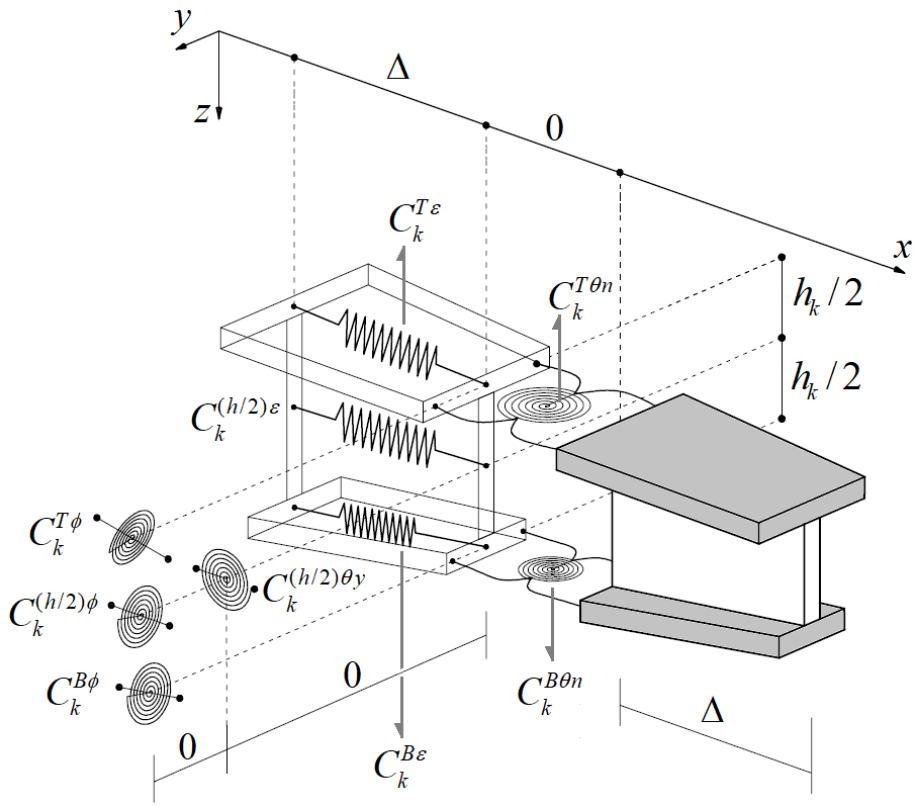

Figure 3.4.3: Type of springs for the tapered I-section bar-chain

By using the general definition (3.2.27), the above springs constants are defined as: (i) for the torsional type

$$C_k^{T\phi}=\frac{GJ_k^T}{\Delta_T}\,,\qquad C_k^{(h/2)\phi}=\frac{GJ_k^W}{\Delta}\,,\qquad C_k^{B\phi}=\frac{GJ_k^B}{\Delta_B}\,, \tag{3.4.10}$$

(ii) the axial springs

$$C_k^{T\varepsilon}=\frac{EA_k^T}{\Delta_T}\,,\qquad C_k^{(h/2)\varepsilon}=\frac{EA_k^W}{\Delta}\,,\qquad C_k^{B\varepsilon}=\frac{EA_k^B}{\Delta_B} \tag{3.4.11}$$

and (iii) the flexural springs, as

$$C_k^{T\theta n}=\frac{EI_{nk}^T}{\Delta_T}\,,\qquad C_k^{(h/2)\theta y}=\frac{EI_{yk}^{(h/2)}}{\Delta}\,,\qquad C_k^{B\theta n}=\frac{EI_{nk}^B}{\Delta_B} \tag{3.4.12}$$

with

$$\Delta_T = \frac{\Delta}{\cos\varphi_T} \ , \qquad \Delta_B = \frac{\Delta}{\cos\varphi_B} \ , \tag{3.4.13}$$

where the discrete properties of the flanges and web are: (i) the torsional constants

$$J_k^T = \frac{1}{3}\left(t_T\right)^3 b_k^T \ , \qquad J_k^W = \frac{1}{3}(t_W)^3 h_k \ , \qquad J_k^B = \frac{1}{3}\left(t_B\right)^3 b_k^B \ , \tag{3.4.14}$$

(ii) the area elements

$$A_k^T = t_T b_k^T \ , \qquad A_k^W = t_W h_k \ , \qquad A_k^B = t_B b_k^B \tag{3.4.15}$$

and (iii) the second moment of area of each flange and the web respectively

$$I_{nk}^T = \frac{(b_k^T)^3 t_T}{12} \ , \qquad I_{yk}^{(h/2)} = \frac{(h_k)^3 t_W}{12} \ , \qquad I_{nk}^B = \frac{(b_k^B)^3 t_B}{12} \ . \tag{3.4.16}$$

3.4.3 The equivalent torsional spring

The complete torsional spring characterization of the tapered segments requires three independent torsional springs, see Figure 3.4.4.

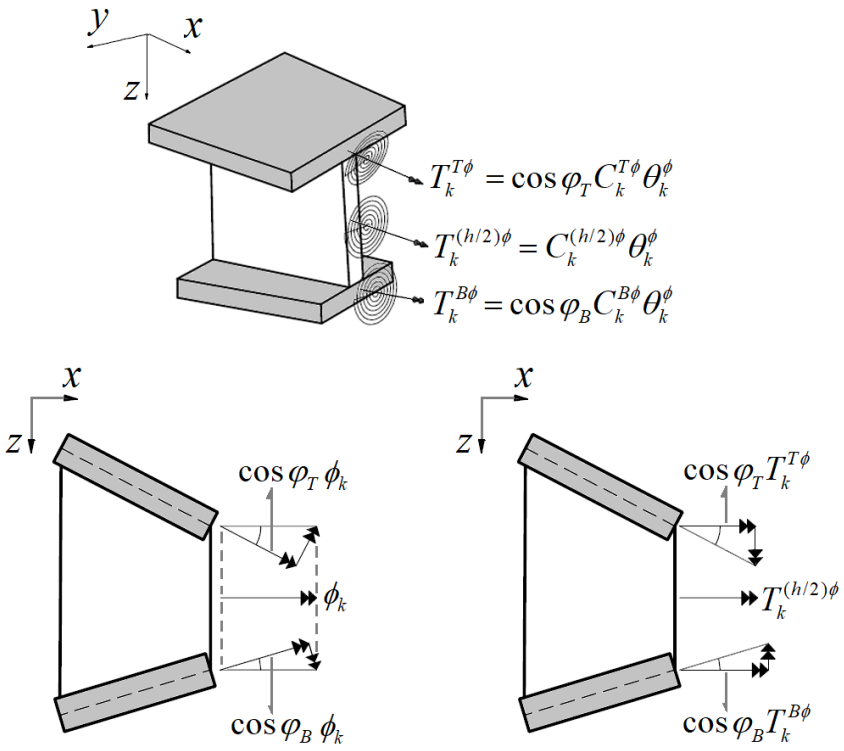

Figure 3.4.4: Effective twist rotations in the tapered I-section bar-chain

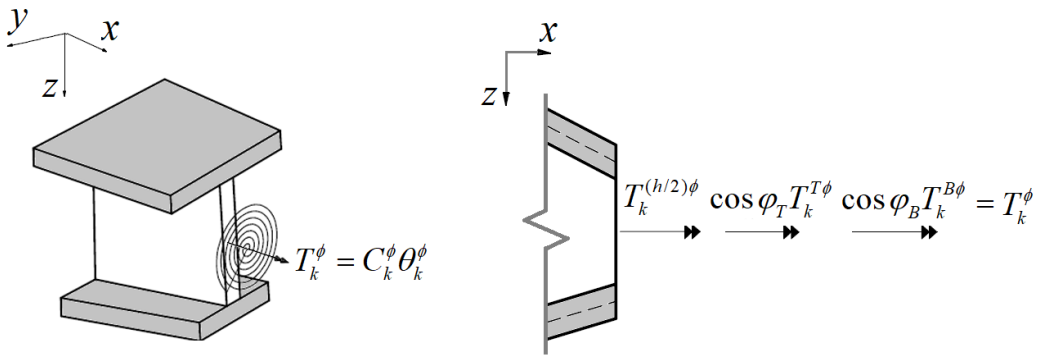

Figure 3.4.5: Equivalent torsional spring in the tapered I-section bar-chain

However, due to the slope of the flanges, the effective twist rotations of the flanges springs is generally smaller than the element twist rotation. Moreover, once the internal forces are established, we are only interested in the torsional moments parallel to the *x*-axis. Their transversal components (parallel to the *z*-axis) are neglected, since they have an order of magnitude $(\approx t^3)$ considerable smaller than the bimoment $(\approx t)$. This allows to define an equivalent torsional spring (see Figure 3.4.5) defined by

$$T_k^\phi = C_k^\phi \theta_k^\phi \ , \tag{3.4.17}$$

where the torsional spring deformation is simply

$$\theta_k^\phi = \Delta D_+ \phi_k \tag{3.4.18}$$

with the spring constant equal to

$$C_k^\phi = C_k^{(h/2)\phi} + \cos^2\varphi_T C_k^{T\phi} + \cos^2\varphi_B C_k^{B\phi} = \frac{GJ_k^*}{\Delta} \ . \tag{3.4.19}$$

Equation (3.4.19) defines the discrete torsion constant J_k^*, whose continuous counterpart is consistent with the generalized torsion formula by Cabrera et al. (2017) concerning tapered thin-walled bars with open cross-sections.

3.4.4 Springs deformations

The deformation (3.4.18) can be enhanced taking the average of the contiguous end deformations

$$\theta_k^{*\phi} = \frac{\theta_k^\phi + \theta_{k-1}^\phi}{2} = \Delta D_o \phi_k \ , \tag{3.4.20}$$

this torsional deformation gives a second order accurate approximation.[14]

[14] It is also possible to improve the axial deformation with a second order accurate approximation, but such improvement is omitted in this dissertation.

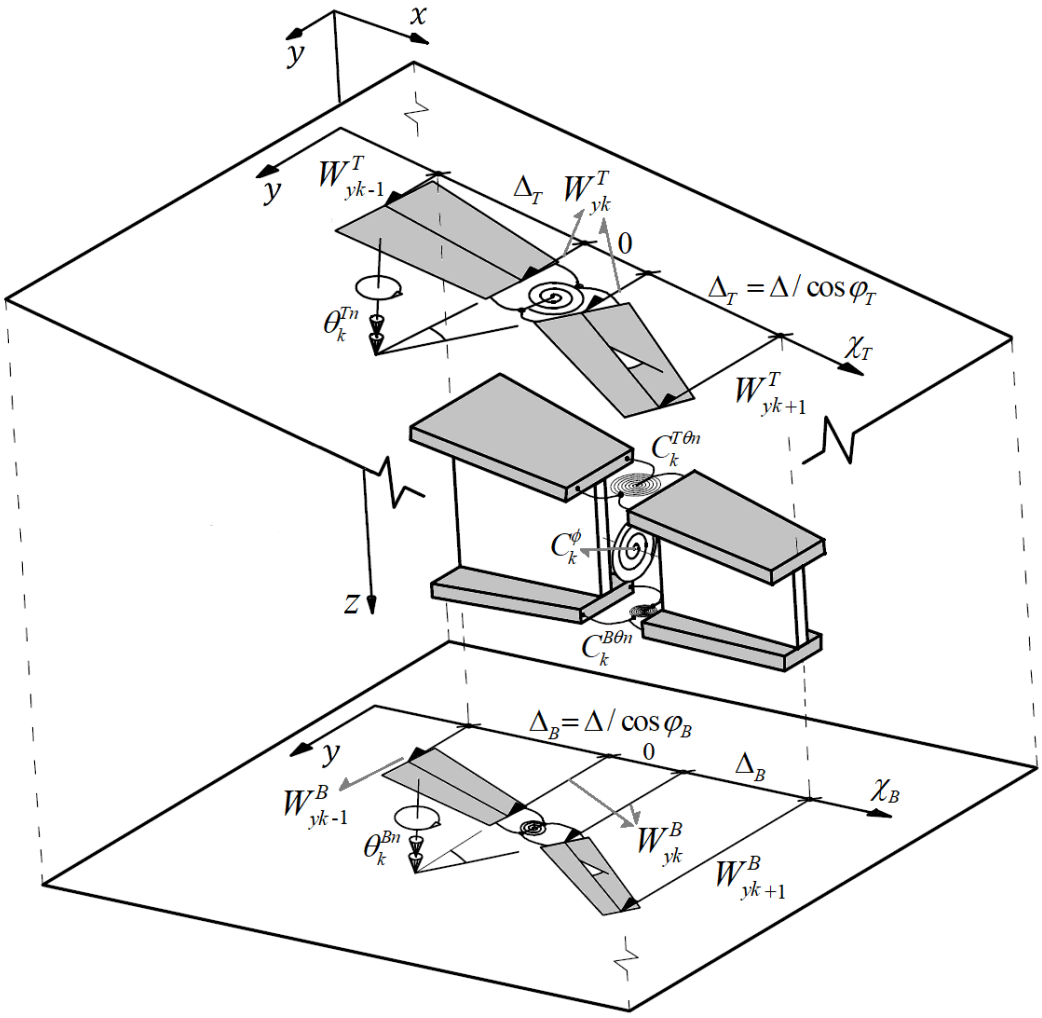

Figure 3.4.6: Tapered I-section bar-chain kinematics in a combination of bending (z-direction) and torsional warping

The assumptions adopted in the tapered bar-chain (reference shape and degrees of freedom), provide all the features required to compute the rotational deformations θ_k^{Tn} and θ_k^{Bn} (see Figure 3.4.6),

$$\theta_k^{Tn} = \cos\varphi_T \left(\Delta D_o^2 W_{yk} - z_k^T \Delta D_o^2 \phi_k \right) - 2\sin\varphi_T \Delta D_o \phi_k \tag{3.4.21}$$

$$\theta_k^{Bn} = \cos\varphi_B \left(\Delta D_o^2 W_{yk} - z_k^B \Delta D_o^2 \phi_k \right) + 2\sin\varphi_B \Delta D_o \phi_k \ . \tag{3.4.22}$$

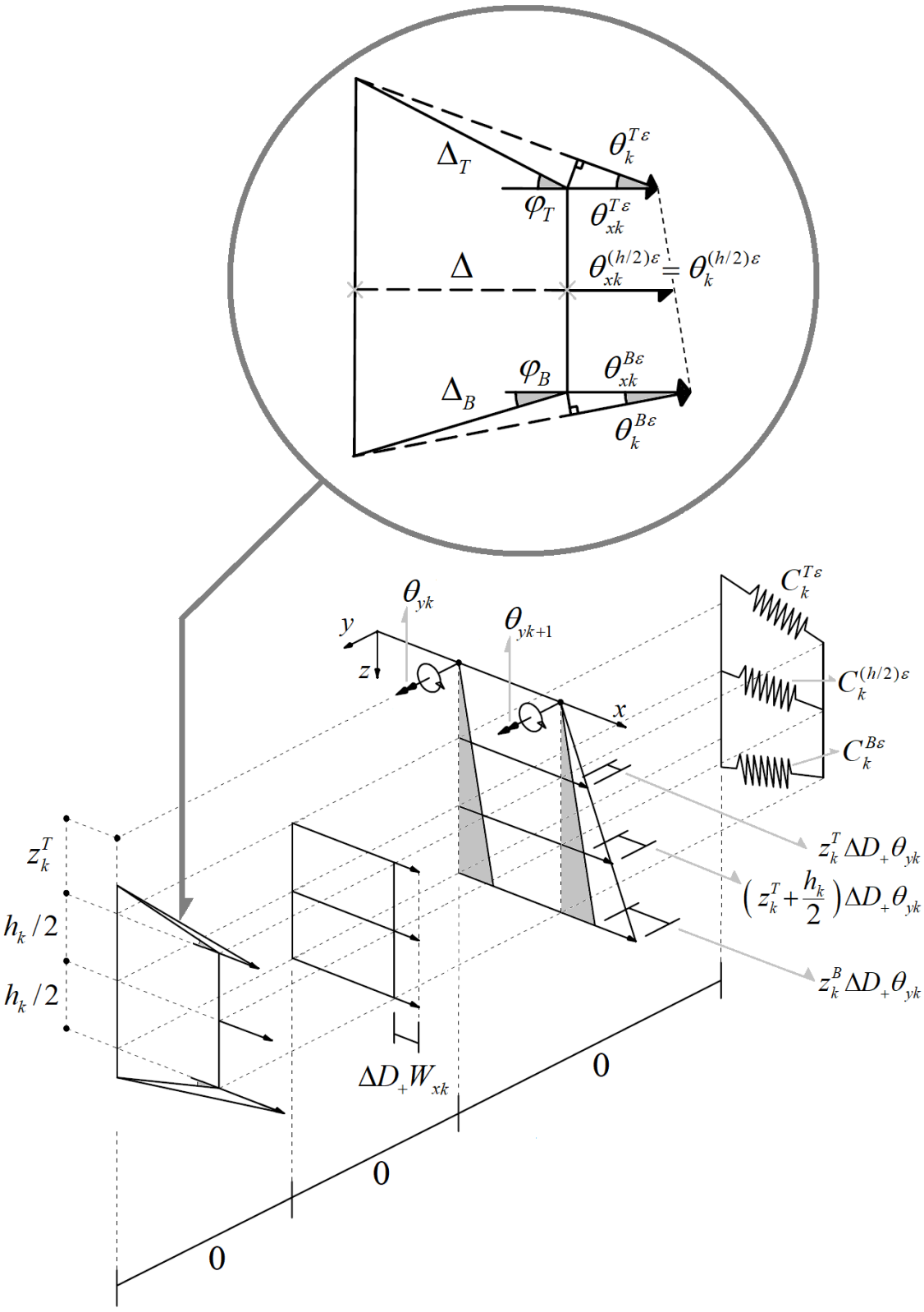

Figure 3.4.7: Axial deformation of the tapered bar-chain, due to the combined effect of axial and bending in the *y*-direction

The rotation about the *y*-direction and the axial deformation induces a longitudinal deformation at each flange and the web mid-high, equal to

$$\theta_{xk}^{T\varepsilon} = z_k^T \Delta D_+ \theta_{yk} + \Delta D_+ W_{xk} \tag{3.4.23}$$

$$\theta_{xk}^{(h/2)\varepsilon} = \left(z_k^T + \frac{h_k}{2} \right) \Delta D_+ \theta_{yk} + \Delta D_+ W_{xk} \tag{3.4.24}$$

$$\theta_{xk}^{B\varepsilon} = z_k^B \Delta D_+ \theta_{yk} + \Delta D_+ W_{xk} \ , \tag{3.4.25}$$

see Figure 3.4.7, where

$$\Delta D_+ \theta_{yk} = -\Delta D_o^2 W_{zk} \ , \tag{3.4.26}$$

like equation (3.4.30). Thus, the deformation at each axial spring is given by the following values

$$\theta_k^{T\varepsilon} = \theta_{xk}^{T\varepsilon} \cos\varphi_T \tag{3.4.27}$$

$$\theta_k^{(h/2)\varepsilon} = \theta_{xk}^{(h/2)\varepsilon} \tag{3.4.28}$$

$$\theta_k^{B\varepsilon} = \theta_{xk}^{B\varepsilon} \cos\varphi_B \ , \tag{3.4.29}$$

where the flexural deformation at the web mid-high is given by

$$\theta_k^{(h/2)y} = -\Delta D_o^2 W_{zk} \ . \tag{3.4.30}$$

3.4.5 Store elastic energy and discrete stiffness coefficients

Hence, the elastic energy stored in the tapered bar-chain can be easily established as the contribution of all springs

$$\mathcal{U} = \mathcal{U}(\theta_i^\mu), \ i = 1, 2, ..., \mathrm{n}-1 \ , \tag{3.4.31}$$

with the label μ defined by

$$\mu = \{Tn, Bn, *\phi, (h/2)y, T\varepsilon, (h/2)\varepsilon, B\varepsilon\} \ , \tag{3.4.32}$$

i.e., equations (3.4.20)-(3.4.22) and (3.4.27)-(3.4.30). Therefore, the elastic energy of the bar-chain is equal to

$$\mathcal{U}(\theta_i^\mu) = \frac{1}{2} \sum_k^{\mathrm{n}-1} \Big(C_k^{T\theta n} \left(\theta_k^{Tn} \right)^2 + C_k^{B\theta n} \left(\theta_k^{Bn} \right)^2 + C_k^{\phi} \left(\theta_k^{*\phi} \right)^2 + C_k^{(h/2)\theta y} \left(\theta_k^{(h/2)y} \right)^2 + C_k^{T\varepsilon} \left(\theta_k^{T\varepsilon} \right)^2 + C_k^{(h/2)\varepsilon} \left(\theta_k^{(h/2)\varepsilon} \right)^2 + C_k^{B\varepsilon} \left(\theta_k^{B\varepsilon} \right)^2 \Big) \ . \tag{3.4.33}$$

Rewriting the spring deformations in function of the degrees of freedom and the corresponding spring constants (3.4.11)-(3.4.12) and (3.4.19), one obtains

$$\mathcal{U}(W_{xi},W_{yi},W_{zi},\phi_i)=\frac{1}{2}\sum_{k}^{n-1}\Big(C_{xk}\left(\Delta D_{+}W_{xk}\right)^2-2C_{xyk}\left(\Delta D_{+}W_{xk}\right)\left(\Delta D_o^2W_{zk}\right)$$
$$+2C_{z\omega k}\left(\Delta D_o^2W_{yk}\right)\left(\Delta D_o^2\phi_k\right)-2C_{z\psi k}\left(\Delta D_o^2W_{yk}\right)\left(\Delta D_o\phi_k\right)$$
$$+C_{yk}\left(\Delta D_o^2W_{zk}\right)^2+C_{\omega k}\left(\Delta D_o^2\phi_k\right)^2+C_{zk}\left(\Delta D_o^2W_{yk}\right)^2$$
$$-2C_{\omega\psi k}\left(\Delta D_o^2\phi_k\right)\left(\Delta D_o\phi_k\right)+C_{\psi k}\left(\Delta D_o\phi_k\right)^2\Big) \tag{3.4.34}$$

where the discrete stiffness coefficients are reduced to

$$C_{xk}=\frac{EA_k^*}{\Delta}=\frac{E}{\Delta}\left(h_k\,t_W+b_k^T\,t_T\cos^3\varphi_T+b_k^B(\theta^1)t_B\cos^3\varphi_B\right) \tag{3.4.35}$$

$$C_{xyk}=\frac{ES_{yk}^*}{\Delta}=\frac{E}{\Delta}\left(\left(\frac{h_k}{2}+z_k^T\right)h_k\,t_W+z_k^T\,b_k^T t_T\cos^3\varphi_T+z_k^B\,b_k^B\,t_B\cos^3\varphi_B\right) \tag{3.4.36}$$

$$C_{z\omega k}=\frac{EI_{z\omega k}^*}{\Delta}=-\frac{E}{12\Delta}\left(t_T\cos^3\varphi_T(b_k^T)^3z_k^T+t_B\cos^3\varphi_B(b_k^B)^3z_k^B\right) \tag{3.4.37}$$

$$C_{z\psi k}=\frac{EI_{z\psi k}^*}{\Delta}=\frac{E}{6\Delta}\left(t_T\cos^3\varphi_T\tan\varphi_T(b_k^T)^3-t_B\cos^3\varphi_B\tan\varphi_B(b_k^B)^3\right) \tag{3.4.38}$$

$$C_{yk}=\frac{EI_{yk}^*}{\Delta}=\frac{E}{\Delta}\left(\frac{h_k{}^3t_W}{12}+\left(\frac{h_k}{2}+z_k^T\right)^2h_k\,t_W\right.$$
$$\left.+\left(z_k^T\right)^2b_k^T\,t_T\,\cos^3\varphi_T+\left(z_k^B\right)^2b_k^B\,t_B\cos^3\varphi_B\right) \tag{3.4.39}$$

$$C_{\omega k}=\frac{EI_{\omega k}^*}{\Delta}=\frac{E}{12\Delta}\left(t_T\cos^3\varphi_T(b_k^T)^3(z_k^T)^2+t_B\cos^3\varphi_B(b_k^B)^3(z_k^B)^2\right) \tag{3.4.40}$$

$$C_{zk}=\frac{EI_{zk}^*}{\Delta}=\frac{E}{12\Delta}\left(t_T\cos^3\varphi_T(b_k^T)^3+t_B\cos^3\varphi_B(b_k^B)^3\right) \tag{3.4.41}$$

$$C_{\omega\psi k}=\frac{EI_{\omega\psi k}^*}{\Delta}=\frac{E}{6\Delta}\left(-t_T\cos^3\varphi_T\tan\varphi_T(b_k^T)^3z_k^T+t_B\cos^3\varphi_B\tan\varphi_B(b_k^B)^3z_k^B\right) \tag{3.4.42}$$

$$C_{\psi k}=\frac{EI_{\psi k}^*+GJ_k^*}{\Delta}=\frac{E}{3\Delta}\left(t_T\cos^3\varphi_T\tan^2\varphi_T(b_k^T)^3+t_B\cos^3\varphi_B\tan^2\varphi_B(b_k^B)^3\right)$$
$$+\frac{G}{3\Delta}\left((t_T\cos\varphi_T)^3b_k^T+(t_B\cos\varphi_B)^3b_k^B+(t_W)^3h_k\right) \tag{3.4.43}$$

where the discrete cross-sectional properties of the bar-chain, i.e., the (i) area A_k^*, (ii) first moment of area S_{yk}^*, (iii) second moments of area I_{yk}^*, I_{zk}^*, (iv) second sectorial moments $I_{z\omega k}^*, I_{\omega k}^*$, (v) geometrical properties associated with cross-sectional tapering $I_{\psi k}^*, I_{z\psi k}^*, I_{\omega\psi k}^*$, and the (vi) torsional property J_k^*, emerge in a natural way as

$$A_k^* = h_k\, t_W + b_k^T\, t_T \cos^3\varphi_T + b_k^B\, t_B \cos^3\varphi_B \tag{3.4.44}$$

$$S_{yk}^* = \left(\frac{h_k}{2} + z_k^T\right) h_k\, t_W + z_k^T\, b_k^T t_T \cos^3\varphi_T + z_k^B\, b_k^B\, t_B \cos^3\varphi_B \tag{3.4.45}$$

$$I_{yk}^* = \frac{{h_k}^3\, t_W}{12} + \left(\frac{h_k}{2} + z_k^T\right)^2 h_k\, t_W + \left(z_k^T\right)^2 b_k^T\, t_T\, \cos^3\varphi_T + \left(z_k^B\right)^2 b_k^B\, t_B \cos^3\varphi_B \tag{3.4.46}$$

$$I_{zk}^* = \frac{1}{12}(b_k^T)^3 t_T \cos^3\varphi_T + \frac{1}{12}(b_k^B)^3 t_B \cos^3\varphi_B \tag{3.4.47}$$

$$I_{z\omega k}^* = -\frac{1}{12} z_k^T (b_k^T)^3 t_T \cos^3\varphi_T - \frac{1}{12} z_k^B (b_k^B)^3 t_B \cos^3\varphi_B \tag{3.4.48}$$

$$I_{\omega k}^* = \frac{1}{12}(z_k^T)^2 (b_k^T)^3 t_T \cos^3\varphi_T + \frac{1}{12}(z_k^B)^2 (b_k^B)^3 t_B \cos^3\varphi_B \tag{3.4.49}$$

$$I_{\psi k}^* = \frac{1}{3}(b_k^T)^3 t_T \tan^2\varphi_T \cos^3\varphi_T + \frac{1}{3}(b_k^B)^3 t_B \tan^2\varphi_B \cos^3\varphi_B \tag{3.4.50}$$

$$I_{z\psi k}^* = \frac{1}{6}(b_k^T)^3 t_T \tan\varphi_T \cos^3\varphi_T - \frac{1}{6}(b_k^B)^3 t_B \tan\varphi_B \cos^3\varphi_B \tag{3.4.51}$$

$$I_{\omega\psi k}^* = -\frac{1}{6} z_k^T (b_k^T)^3 t_T \tan\varphi_T \cos^3\varphi_T + \frac{1}{6} z_k^B (b_k^B)^3 t_B \tan\varphi_B \cos^3\varphi_B \tag{3.4.52}$$

$$J_k^* = \frac{1}{3}\left[h_k (t_W)^3 + b_k^T (t_T \cos\varphi_T)^3 + b_k^B (t_B \cos\varphi_B)^3 \right]. \tag{3.4.53}$$

They are equivalent with their corresponding continuous counterpart (2.9.30)-(2.9.39) developed in chapter 2.

3.4.6 Consistency between the discrete and continuous 1D model

Like the prismatic case, the continuous functional can be found by replacing the discrete values by the continuous functions evaluated at the discrete positions, i.e., for the case of the discrete displacements and rotations

$$W_{\mu i} \coloneqq W_\mu(x_i) \text{ with } \mu = \{x, y, z\} \ , \qquad \phi_i \coloneqq \phi(x_i) \ , \tag{3.4.54}$$

and for each discrete stiffness coefficient

$$C_{\beta\xi i} \coloneqq C_{\beta\xi}(x_i) \text{ with } C_{\beta\beta i} = C_{\beta i} \ , \ \beta, \xi = \{x, y, z, \psi, \omega\}^{15} \tag{3.4.55}$$

where the set of discrete positions are defined by

$$x_i = i\Delta \ , \ i = 1, 2, ..., \mathrm{n}-1 \ . \tag{3.4.56}$$

Expanding above functions in a Taylor series around the position x_k,

$$W_\mu(x_i) = W_\mu(x_k) + \sum_{j=1}^{\infty} \left((i-k)^j \left. \frac{d^j W_\mu(x)}{dx^j} \right|_{x=x_k} \Delta^j \right) \text{, with } \mu = \{x, y, z\} \ , \tag{3.4.57}$$

$$\phi(x_i) = \phi(x_k) + \sum_{j=1}^{\infty} \left((i-k)^j \left. \frac{d^j \phi(x)}{dx^j} \right|_{x=x_k} \Delta^j \right) \tag{3.4.58}$$

and

$$C_{\beta\xi}(x_i) = C_{\beta\xi}(x_k) + \sum_{j=1}^{\infty} \left((i-k)^j \left. \frac{d^j C_{\beta\xi}(x)}{dx^j} \right|_{x=x_k} \Delta^j \right) \text{, with } \beta, \xi = \{x, y, z, \psi, \omega\} \ . \tag{3.4.59}$$

[15] For tapered singly symmetric I-section bar-chains $C_{\beta\xi i} = 0$ with $\beta = \{x, y\}$ and $\xi = \{z, \psi, \omega\}$.

The Taylor series expansion of equation (3.4.34) gives

$$\mathcal{U}\left[W_x(x_i),W_y(x_i),W_z(x_i),\phi(x_i)\right]=\frac{1}{2}\sum_{k}^{\mathrm{n}-1}\Big(\Big(C_x(x_k)\Delta\Big)\Big(W_x'(x_k)\Big)^2$$
$$-2\Big(C_{xy}(x_k)\Delta\Big)W_x'(x_k)W_z''(x_k)+\Big(C_y(x_k)\Delta\Big)\Big(W_z''(x_k)\Big)^2$$
$$-2\Big(C_{z\psi}(x_k)\Delta\Big)W_y''(x_k)\phi'(x_k)+\Big(C_z(x_k)\Delta\Big)\Big(W_y''(x_k)\Big)^2$$
$$+2\Big(C_{z\omega}(x_k)\Delta\Big)W_y''(x_k)\phi''(x_k)+\Big(C_\omega(x_k)\Delta\Big)\Big(\phi''(x_k)\Big)^2$$
$$-2\Big(C_{\omega\psi}(x_k)\Delta\Big)\phi''(x_k)\phi'(x_k)+\Big(C_\psi(x_k)\Delta\Big)\big(\phi'(x_k)\big)^2\Big)\Delta+O(\Delta^2)\ . \qquad (3.4.60)$$

At the limit $\mathrm{n}\to\infty$, the residual converges to zero and the finite set $\{x_k\}$ tends to the continuous value $x\in\mathbb{R}\cap[0,L]$,

$$\mathcal{U}\left[W_x(x),W_y(x),W_z(x),\phi(x)\right]=\frac{1}{2}\int_0^L\Big(\Big(EA^*(x)W_x'(x)\Big)^2$$
$$-2ES_y^*(x)W_x'(x)W_z''(x)+EI_y^*(x)\Big(W_z''(x)\Big)^2$$
$$-2EI_{z\psi}^*(x)W_y''(x)\phi'(x)+EI_z^*(x)\Big(W_y''(x)\Big)^2$$
$$+2EI_{z\omega}^*(x)W_y''(x)\phi''(x)+EI_\omega^*(x)\Big(\phi''(x)\Big)^2$$
$$-2EI_{\omega\psi}^*(x)\phi''(x)\phi'(x)+\Big(EI_\psi^*(x)+GJ^*(x)\Big)\big(\phi'(x)\big)^2\Big)dx\ . \qquad (3.4.61)$$

In a close manner a complete agreement between the discrete bar-chain model and the continuous one-dimensional model (2.5.23) is achieved if

$$\tilde{E}=E\ ,^{16} \qquad \tilde{G}=G\ . \qquad (3.4.62)$$

This fact, not only proves the consistency of the discrete approach but it also shows that the bar-chain model incorporates the same constrain characterizations concerning the kinematics and the stiffness properties of the continuous one-dimensional model.

[16] Vlasov (1961) [p. 29] and Gjelsvik (1981) [p. 17] did this simplification for the prismatic case, arguing that the square of the Poisson ratio can be neglected in comparison with the unity.

3.4.7 Cross-sectional stress resultants, active and reactive

In what concerns the internal forces and moments in the springs, they are generated in response to the applied loading. If the springs are isolated, a pair of internal forces and moments are defined, related to each corresponding deformation. They are:

(i) The axial forces

$$N_k^{T\varepsilon} = C_k^{T\varepsilon}\theta_k^{T\varepsilon} \tag{3.4.63}$$

$$N_k^{(h/2)\varepsilon} = C_k^{(h/2)\varepsilon}\theta_k^{(h/2)\varepsilon} \tag{3.4.64}$$

$$N_k^{B\varepsilon} = C_k^{B\varepsilon}\theta_k^{B\varepsilon} \ , \tag{3.4.65}$$

(ii) the bending moments

$$M_k^{Tn} = C_k^{T\theta n}\theta_k^{Tn} \tag{3.4.66}$$

$$M_k^{(h/2)y} = C_k^{\theta y}\theta_k^{(h/2)y} \tag{3.4.67}$$

$$M_k^{Bn} = C_k^{B\theta n}\theta_k^{Bn} \ , \tag{3.4.68}$$

and (iii) the torsional moments

$$T_k^{\phi} = C_k^{\phi}\theta_k^{*\phi} \ . \tag{3.4.69}$$

Like in the pioneer work of Andrade (2013), the discrete cross-section forces and moments resultants are split into active and reactive categories, leading to a dual one-dimensional description, with the constitutive dependence of the active part on the springs deformations, and the reactive components due to equilibrium conditions.

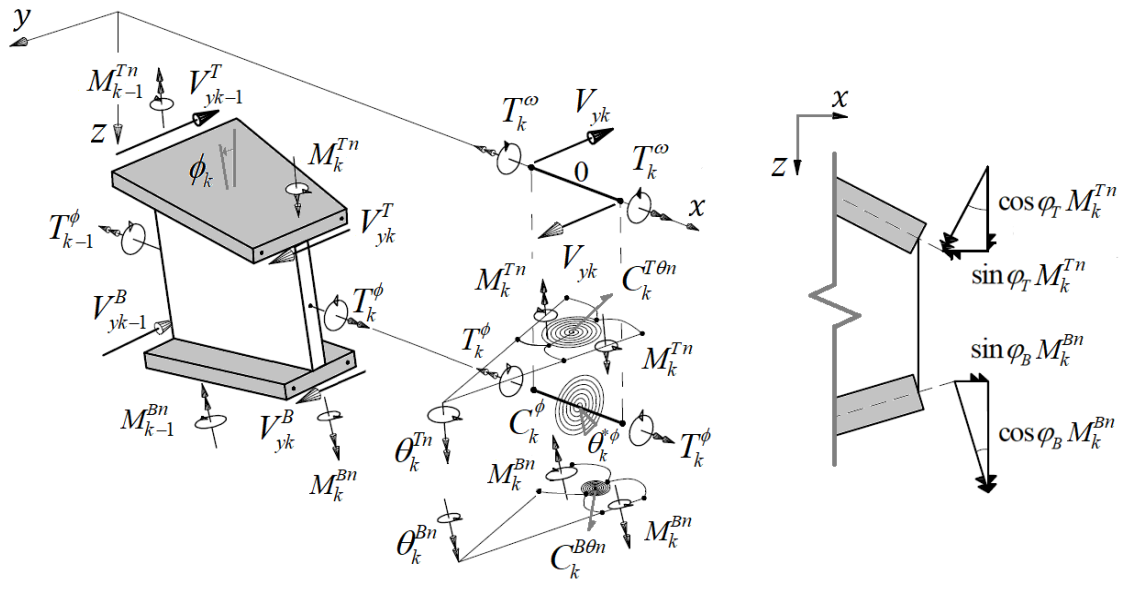

Figure 3.4.8: Equilibrium in the tapered bar-chain about the bending *z*-direction

Hence, the discrete bending moment M_{zk} (active) corresponds to the contribution of each transversal component of the flexural springs at the flanges (see Figure 3.4.8),

$$M_{zk} = \cos\varphi_T M_k^{Tn} + \cos\varphi_B M_k^{Bn} = EI_{zk}^* D_o^2 W_{yk} + EI_{z\omega k}^* D_o^2 \phi_k - EI_{z\psi k}^* D_o \phi_k \qquad (3.4.70)$$

while the equilibrium condition

$$V_{yk} = V_{yk}^T + V_{yk}^B = -D_- M_{zk} \qquad (3.4.71)$$

shows that the shear force is reactive. The discrete torque T_k is more subtle, since there is the contribution of the torsional springs

$$T_k^\phi = GJ_k^* D_o \phi_k \ , \qquad (3.4.72)$$

the x-components of the rotational springs (see Figure 3.4.8)

$$-\sin\varphi_T M_k^{Tn} + \sin\varphi_B M_k^{Bn} = \tfrac{1}{2} T_k^{\omega(a)} \qquad (3.4.73)$$

(active), and the torsion T_k^ω which combines reactive and active components

$$T_k^\omega = -z_k^T V_{yk}^T - z_k^B V_{yk}^B = D_- B_k + \tfrac{1}{2} T_k^{\omega(a)} \qquad (3.4.74)$$

where the discrete (active) bimoment B_k is defined as

$$B_k = -EI_{z\omega k}^* D_o^2 W_{yk} - EI_{\omega k}^* D_o^2 \phi_k + EI_{\omega\psi k}^* D_o \phi_k \ . \qquad (3.4.75)$$

Hence, the active $T_k^{(a)}$ and reactive part $T_k^{(r)}$ of the discrete torque T_k are established as

$$T_k = T_k^\phi + \tfrac{1}{2} T_k^{\omega(a)} + T_k^\omega = T_k^{(a)} + T_k^{(r)} \qquad (3.4.76)$$

with

$$T_k^{(a)} = T_k^\phi + T_k^{\omega(a)} = -EI_{z\psi k}^* D_o^2 W_{yk} - EI_{\omega\psi k}^* D_o^2 \phi_k + (EI_{\psi k}^* + GJ_k^*) D_o \phi_k \qquad (3.4.77)$$

and

$$T_k^{(r)} = T_k^\omega - \tfrac{1}{2} T_k^{\omega(a)} = D_- B_k \ . \qquad (3.4.78)$$

The above equations show the mechanical link between the torsional effect and the lateral bending behaviour. A similar connection is found concerning the axial effect and the bending on the plane of great stiffness, see Figure 3.4.9. Thus, the discrete bending moment M_{yk} (active) corresponds to the contribution of each moment due to the longitudinal component of the axial forces at the springs, plus the input of the internal bending moment (3.4.67). Hence

$$M_{yk} = z_k^T \cos\varphi_T N_k^{T\varepsilon} + \left(z_k^T + \frac{h_k}{2} \right) N_k^{(h/2)\varepsilon} + z_k^B \cos\varphi_B N_k^{B\varepsilon} + M_k^{(h/2)y} \ , \qquad (3.4.79)$$

replacing equations (3.4.63)-(3.4.65) and (3.4.27)-(3.4.29), we get

$$M_{yk} = ES^*_{yk} D_+ W_{xk} - EI^*_{yk} D_o^2 W_{zk} \ , \tag{3.4.80}$$

while the equilibrium condition shows that the corresponding shear force is reactive, i.e.,

$$V_{zk} = D_- M_{yk} \ . \tag{3.4.81}$$

The shear force V_{zk} also has an active component proportional to $\sin\varphi_T N_k^{T\varepsilon} - \sin\varphi_B N_k^{B\varepsilon}$ (see Figure 3.4.9), but the above quantity is neglected in comparison with the first difference of the moment $D_- M_{yk}$. The normal force (active) is given by the longitudinal components of the axial forces, equal to

$$N_k = \cos\varphi_T N_k^{T\varepsilon} + N_k^{(h/2)\varepsilon} + \cos\varphi_B N_k^{B\varepsilon} = EA^*_k D_+ W_{xk} - ES^*_{yk} D_o^2 W_{zk} \ , \tag{3.4.82}$$

in accordance with the general equation (2.7.1) for tapered thin-walled bars with open cross-sections.

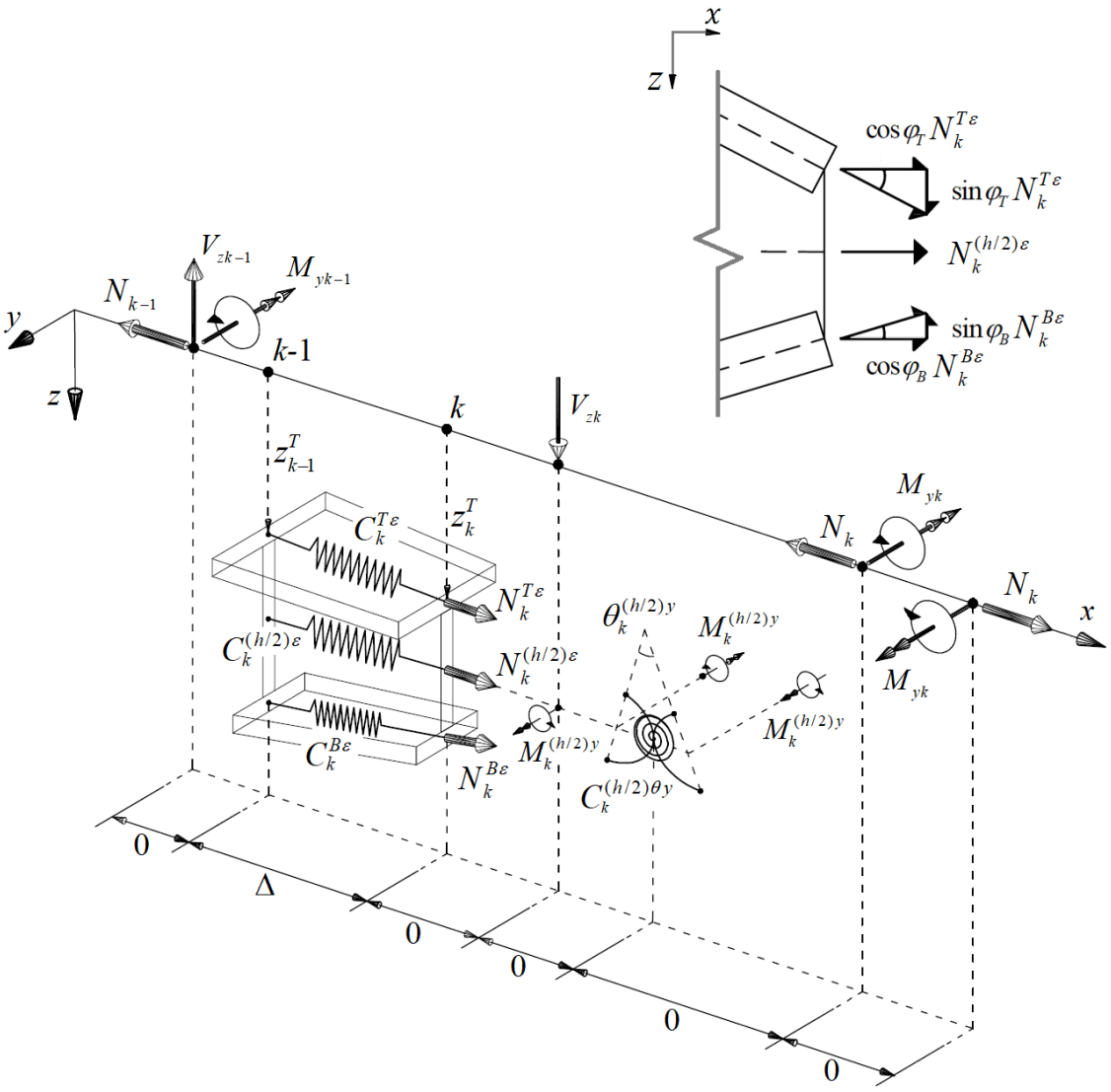

Figure 3.4.9: Equilibrium in the tapered bar-chain for bending about the *y*-direction

3.5 ILLUSTRATIVE EXAMPLES

There is no such a thing as a general-discretization solution in the bar-chain model, each bar-chain having its own peculiarities, depending on the characterization of the boundary conditions, type of loading or additional assumptions, e.g., Cajić and Lazarević (2016) or Turco et al. (2016). Thus, the aim of this section is to present two specific examples, concerning the torsional behaviour of I-section cantilevers, for the (i) prismatic doubly symmetric and the (ii) doubly symmetric web-tapered case respectively.[17] The last one, will help us to show the difference between the bar-chain model and the continuous one-dimensional approach developed in chapter 2.

Illustrative example 1: Torsional behaviour of prismatic doubly symmetric I-section cantilevers

As an example of the torsional behaviour of prismatic doubly symmetric I-beams, consider the bar-chain model of the cantilever whose reference shape and loading configuration is shown in Figure 3.5.1. The bar-chain model only has a concentrated twist moment at its tip, and therefore the displacements of its axis are null ─ Its total potential energy is then given by

$$\Pi(\phi_i) = \frac{1}{2}\sum_{k=1}^{\mathrm{n}-1}\left(C_\omega \left(\Delta D_o^2 \phi_k\right)^2 + C_\psi \left(\Delta D_+ \phi_k\right)^2 \right) - T\phi_{\mathrm{n}} \ , \tag{3.5.1}$$

depending only of the twist rotations of the segments ϕ_i, with $i = 0,1,...,\mathrm{n}$ where $\mathrm{n} \geq \mathrm{n}_{\min} = 2$. The discrete essential boundary conditions of the problem are defined as

$$\phi_o = 0 \tag{3.5.2}$$

$$\phi_1 = 0 \ , \tag{3.5.3}$$

their physical implementation being done by the supports shown in Figure 3.5.1, meanwhile the discrete natural conditions are described by the last two equilibrium equations,

$$\frac{\partial \Pi}{\partial \phi_{\mathrm{n}-1}} = 0 \tag{3.5.4}$$

$$\frac{\partial \Pi}{\partial \phi_{\mathrm{n}}} = 0 \ . \tag{3.5.5}$$

[17] Although both examples are isostatic, the developed bar-chain model can be applied to hyperstatic bars.

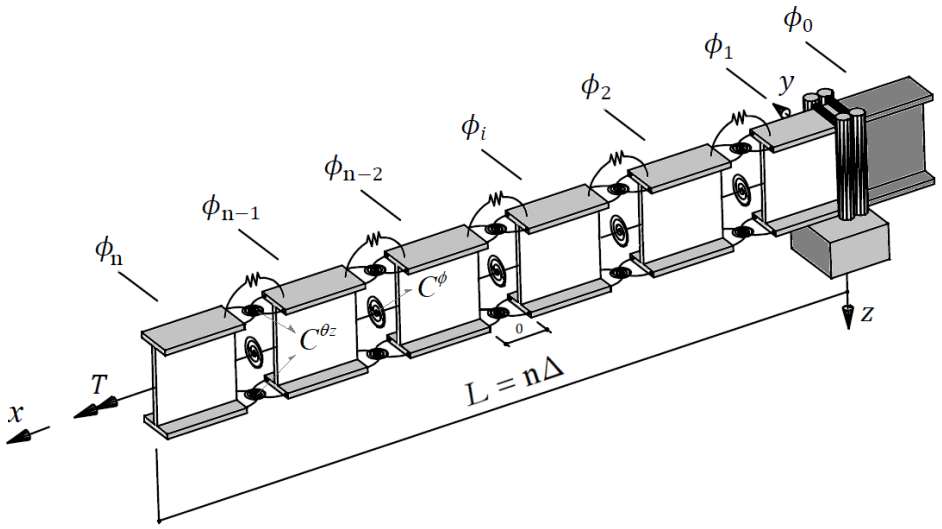

Figure 3.5.1: Illustrative example 1 – Bar-chain model of a cantilever I-beam under a concentrated torque

Thus, one obtains a system of linear algebraic equations, minimizing the total potential energy (3.5.1)

$$\frac{\partial \Pi}{\partial \phi_i} = 0\,,\ i = 2,..,n-2\ . \tag{3.5.6}$$

By using the non-dimensional warping rigidity

$$\kappa_\omega = \frac{\pi}{L}\sqrt{\frac{EI_\omega}{GJ}}\ , \tag{3.5.7}$$

equation (3.5.6) can be written independent of the cantilever length L,

$$\kappa_\omega^2 n^2\left(\phi_{i-2} - 4\phi_{i-1} + 6\phi_i - 4\phi_{i+1} + \phi_{i+2}\right) + \pi^2\left(-\phi_{i-1} + 2\phi_i - \phi_{i+1}\right) = 0\,,\ i = 2,..,n-2 \tag{3.5.8}$$

with the four boundary conditions (3.5.2)-(3.5.5) written as

$$\phi_o = 0 \tag{3.5.9}$$

$$\phi_1 = 0 \tag{3.5.10}$$

$$\kappa_\omega^2 n^2\left(\phi_{n-3} - 4\phi_{n-2} + 5\phi_{n-1} - 2\phi_n\right) + \left(-\phi_{n-2} + 2\phi_{n-1} - \phi_n\right)\pi^2 = 0 \tag{3.5.11}$$

$$\kappa_\omega^2 n^3\left(\phi_{n-2} - 2\phi_{n-1} + \phi_n\right) + \pi^2 n\left(\phi_n - \phi_{n-1}\right) = \pi^2\mu \tag{3.5.12}$$

where the last term, is the non-dimensional twist moment, defined as

$$\mu = \frac{TL}{GJ}\ . \tag{3.5.13}$$

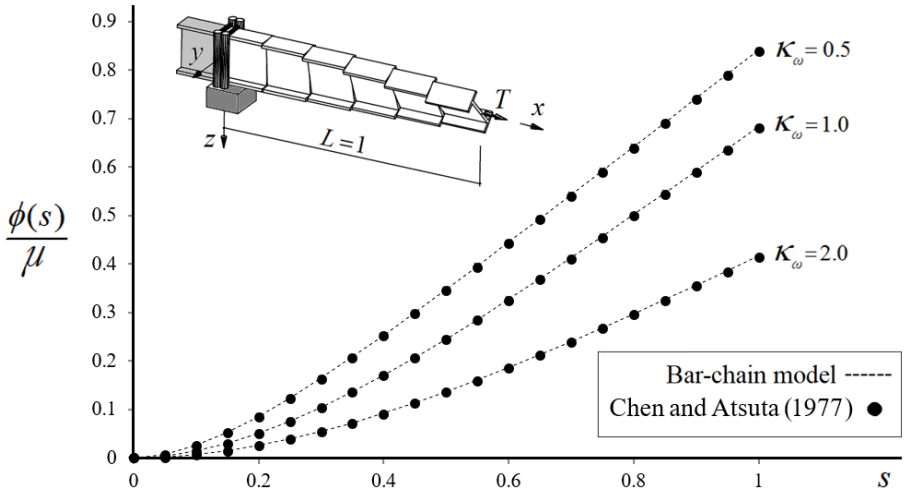

Figure 3.5.2: Illustrative example 1 – The solutions for the cantilever I-beam under a concentrated torque, $\mathrm{n} = 300$

The solutions to the non-dimensional version of the discrete equation per unit non-dimensional torque μ are plotted in Figure 3.5.2. Moreover, to assess the above approximate solutions, Figure 3.5.3 shows the relative error of the twist rotation measured at the tip of the bar.[18] Alternatively, the discrete equation (3.5.8) can be solved, computing a recurrence relation, where its associated characteristic polynomial $P(\lambda)$ is given by

$$P(\lambda) = \lambda^4 + \left(-4 - \left(\frac{\pi}{\mathrm{n}\kappa_\omega}\right)^2\right)\lambda^3 + \left(6 + 2\left(\frac{\pi}{\mathrm{n}\kappa_\omega}\right)^2\right)\lambda^2 + \left(-4 - \left(\frac{\pi}{\mathrm{n}\kappa_\omega}\right)^2\right)\lambda + 1 \ . \quad (3.5.14)$$

The roots of $P(\lambda)$ are all real, equal to

$$\lambda_{1,2} = 1 \ , \quad (3.5.15)$$

$$\lambda_{3,4} = 1 + \frac{1}{2}\left(\frac{\pi}{\mathrm{n}\kappa_\omega}\right)^2 \left(1 \pm \sqrt{1 + \left(\frac{2\mathrm{n}\kappa_\omega}{\pi}\right)^2}\right) . \quad (3.5.16)$$

Hence, by taking the solutions (3.5.15)-(3.5.16), the i-twist rotation ϕ_i $(i = 2,..,\mathrm{n}-2)$, can be expressed as

$$\phi_i = A + Bi + C\left(1 + \frac{\pi^2 + \sqrt{\pi^4 + 4\pi^2\kappa_\omega^2\mathrm{n}^2}}{2\kappa_\omega^2\mathrm{n}^2}\right)^i + D\left(1 + \frac{\pi^2 - \sqrt{\pi^4 + 4\pi^2\kappa_\omega^2\mathrm{n}^2}}{2\kappa_\omega^2\mathrm{n}^2}\right)^i \quad (3.5.17)$$

[18]The exact solution of the boundary value problem (Chen and Atsuta 1977) [p. 48], is given by

$$\phi(s) = \frac{\kappa_\omega \mu}{\pi}\left[\frac{\pi}{\kappa_\omega}s - \sinh\left(\frac{\pi}{\kappa_\omega}s\right) + \tanh\left(\frac{\pi}{\kappa_\omega}\right)\left(\cosh\left(\frac{\pi}{\kappa_\omega}s\right) - 1\right)\right] \text{ with } s \in \mathbb{R} \cap [0,1] \ .$$

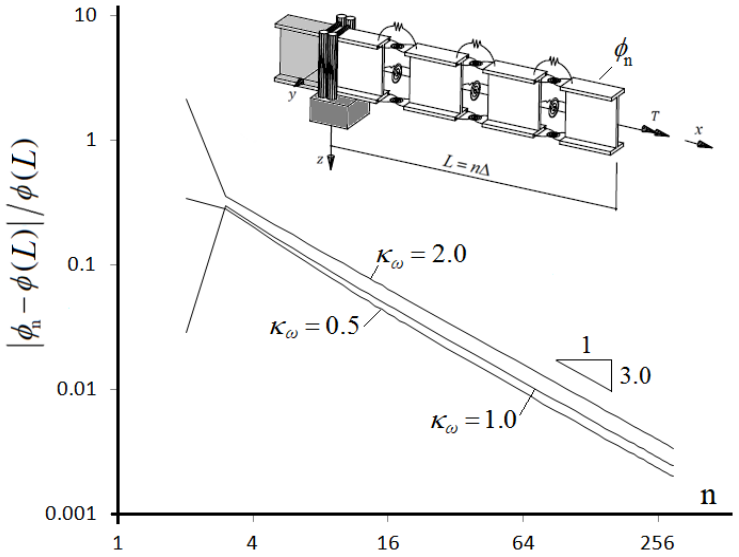

Figure 3.5.3: Illustrative example 1 – Convergence of the twist rotation measure at the tip of the bar-chain model

where the constants *A*, *B*, *C* and *D* can be found with the four boundary conditions (3.5.9)-(3.5.12). In order to analyse the consistency of the solution, the residuals are evaluated by replacing the exact twist rotations $\phi(x_i)$ with $x_i = i\Delta$ and $i = 2,..,n-2$ in the discrete equation (3.5.6)

$$\frac{C_\omega}{\Delta^2}\left(\phi(x_{i-2}) - 4\phi(x_{i-1}) + 6\phi(x_i) - 4\phi(x_{i+1}) + \phi(x_{i+2})\right) + C_\psi\left(-\phi(x_{i-1}) + 2\phi(x_i) - \phi(x_{i+1})\right) = r_i \ , \qquad (3.5.18)$$

the discrete values are expanded in a Taylor series around the position x_i, so that

$$\begin{aligned}
&\frac{C_\omega}{\Delta^2}\Bigg(\phi(x_i) - 2\Delta\phi'(x_i) + \frac{(2\Delta)^2}{2!}\phi''(x_i) - \frac{(2\Delta)^3}{3!}\phi'''(x_i) + \frac{(2\Delta)^4}{4!}\phi^{IV}(x_i) \\
&\quad -4\phi(x_i) + 4\Delta\phi'(x_i) - 4\frac{\Delta^2}{2!}\phi''(x_i) + 4\frac{\Delta^3}{3!}\phi'''(x_i) - 4\frac{\Delta^4}{4!}\phi^{IV}(x_i) \\
&\quad +6\phi(x_i) - 4\phi(x_i) - 4\Delta\phi'(x_i) - 4\frac{\Delta^2}{2!}\phi''(x_i) - 4\frac{\Delta^3}{3!}\phi'''(x_i) \\
&\quad -4\frac{\Delta^4}{4!}\phi^{IV}(x_i) + \phi(x_i) + 2\Delta\phi'(x_i) + \frac{(2\Delta)^2}{2!}\phi''(x_i) + \frac{(2\Delta)^3}{3!}\phi'''(x_i) \\
&\quad +\frac{(2\Delta)^4}{4!}\phi^{IV}(x_i) + O(\Delta^6)\Bigg) + C_\psi\Bigg(-\phi(x_i) + \Delta\phi'(x_i) - \frac{\Delta^2\phi''(x_i)}{2!} \\
&\quad +2\phi(x_i) - \phi(x_i) - \Delta\phi'(x_i) - \frac{\Delta^2\phi''(x_i)}{2!} + O(\Delta^4)\Bigg) = r_i
\end{aligned} \qquad (3.5.19)$$

reducing terms and factorising the discrete length Δ

$$\left[C_\omega \Delta\phi^{IV}(x_i) - C_\psi \Delta\phi''(x_i)\right]\Delta + O(\Delta^3) = r_i \text{ with } i = 2,..,\mathrm{n}-2 \ . \tag{3.5.20}$$

It follows that in the limit when $\Delta \to 0$,

$$C_\omega \Delta \to EI_\omega \ , \qquad C_\psi \Delta \to GJ \ , \tag{3.5.21}$$

and the finite set $\{x_i\}$ tends to the continuous value $x \in \mathbb{R} \cap [0, L]$, so the discrete equation converges to its corresponding continuous differential equation

$$EI_\omega \phi^{IV}(x) - GJ\phi''(x) = 0 \ . \tag{3.5.22}$$

In the case of the natural boundary conditions (3.5.4)-(3.5.5), their respective residuals are equal to

$$\frac{C_\omega}{\Delta^2}\left(\phi(x_{\mathrm{n}-3}) - 4\phi(x_{\mathrm{n}-2}) + 5\phi(x_{\mathrm{n}-1}) - 2\phi(x_{\mathrm{n}})\right) + C_\psi\left(-\phi(x_{\mathrm{n}-2}) + 2\phi(x_{\mathrm{n}-1}) - \phi(x_{\mathrm{n}})\right) = r_{\mathrm{n}-1} \tag{3.5.23}$$

$$\frac{C_\omega}{\Delta^2}\left(\phi(x_{\mathrm{n}-2}) - 2\phi(x_{\mathrm{n}-1}) + \phi(x_{\mathrm{n}})\right) + C_\psi\left(\phi(x_{\mathrm{n}}) - \phi(x_{\mathrm{n}-1})\right) - T = r_{\mathrm{n}} \ , \tag{3.5.24}$$

doing the same routing procedure around the last block $\phi(x_{\mathrm{n}})$

$$C_\omega\left(-\phi''(x_{\mathrm{n}})\right) + O(\Delta) = r_{\mathrm{n}-1} \tag{3.5.25}$$

$$-C_\omega \Delta\phi'''(x_{\mathrm{n}}) + C_\psi \Delta\phi'(x_{\mathrm{n}}) - T + O(\Delta) = r_{\mathrm{n}} \ , \tag{3.5.26}$$

once more, taking the limit, we get the bimoment and the torque at the tip of the bar

$$EI_\omega \phi''(L) = 0 \ , \qquad -EI_\omega \phi'''(L) + GJ\phi'(L) = T \ . \tag{3.5.27}$$

Doing the same routine to equations (3.5.2)-(3.5.3), we get respectively

$$\phi(0) = 0 \ , \qquad \phi'(0) = 0 \ , \tag{3.5.28}$$

which are, the essential boundary conditions of the continuous problem.

Illustrative example 2: Torsional behaviour of doubly symmetric web-tapered I-section cantilevers

Consider the bar-chain model of a doubly symmetric web-tapered I-section cantilever, whose reference shape, support conditions and applied torque are shown in Figure 3.5.4.

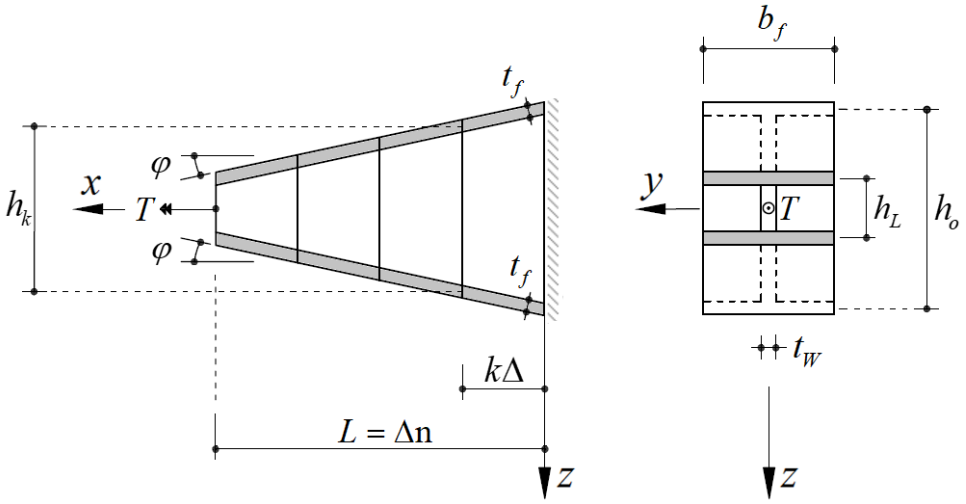

Figure 3.5.4: Illustrative example 2 – Reference shape for the bar-chain model of a doubly symmetric web-tapered I-section cantilever under a concentrated torque

with $k = 0,1,...,n$ where γ represents a measure of the slope of the tapered bar, defined as the first order difference of the depth,

$$\gamma = \frac{h_L - h_o}{L} \ . \tag{3.5.29}$$

Because of the symmetry of the flanges slopes φ, they can be related with γ, via

$$\tan\varphi = -\frac{\gamma}{2} \ . \tag{3.5.30}$$

Concerning the springs characterization, only the torsional and rotational-lateral springs are needed in order to model the torsional behaviour of the tapered bar-chain under a concentrated torque.[19] Hence, (i) for the torsional springs

$$C_k^{\phi} = \frac{GJ_k^*}{\Delta} = \frac{G}{3\Delta}\left[h_k (t_W)^3 + 2b_f (t_f \cos\varphi)^3\right] \tag{3.5.31}$$

with $k = 2,...,n$, while (ii) the flexural springs on the flanges are characterized by

$$C^{T\theta} = C^{B\theta} = \frac{EI_f}{\Delta_f} \ , \tag{3.5.32}$$

[19]The axial and the flexural springs (at the web) are entirely uncoupled with respect to the torsional mode of the problem.

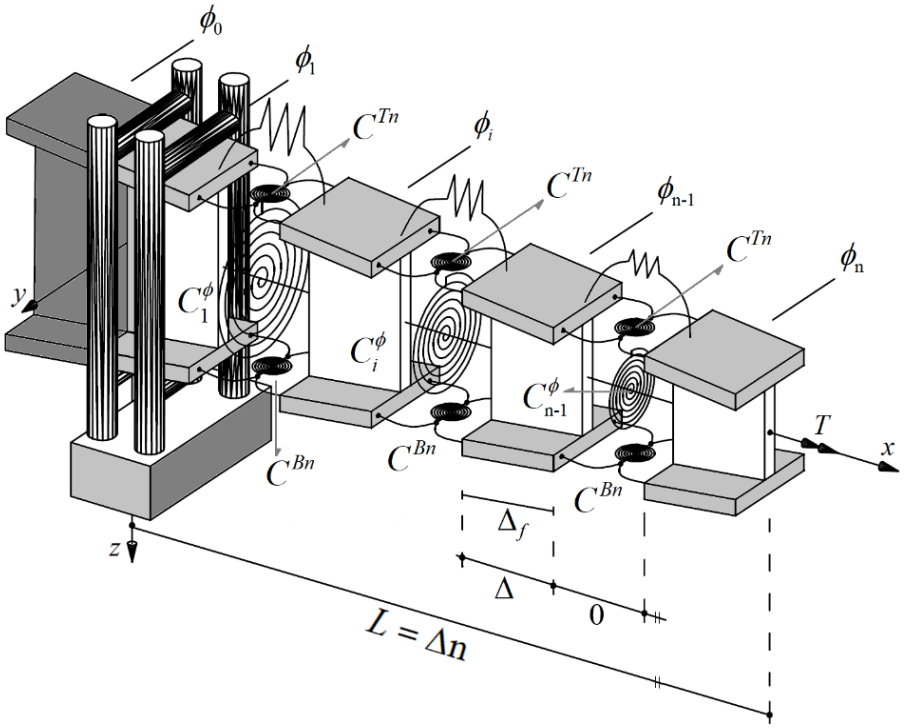

Figure 3.5.5: Illustrative example 2 – Springs characterization for the torsional behaviour of the cantilever I-beam under a concentrated torque

where the discrete length of each flange along its plane is defined as

$$\Delta_f = \frac{\Delta}{\cos\varphi} \tag{3.5.33}$$

and the second moment of area of each flange is equal to

$$I_f = \frac{(b_f)^3 t_f}{12} \ . \tag{3.5.34}$$

Due to the symmetry of the bar-chain model, its kinematics is reduced to the motion shown in Figure 3.5.6. As a result, the deformations of the rotational springs are equal to

$$\theta_k^{Tn} = +\left(\frac{h_k}{2}\Delta D_o^2 \phi_k \cos\varphi - 2\Delta D_o \phi_k \sin\varphi\right) \tag{3.5.35}$$

$$\theta_k^{Bn} = -\left(\frac{h_k}{2}\Delta D_o^2 \phi_k \cos\varphi - 2\Delta D_o \phi_k \sin\varphi\right) \tag{3.5.36}$$

with $k = 2,...,\mathrm{n}$, where the signs show that both springs always have opposite rotations.

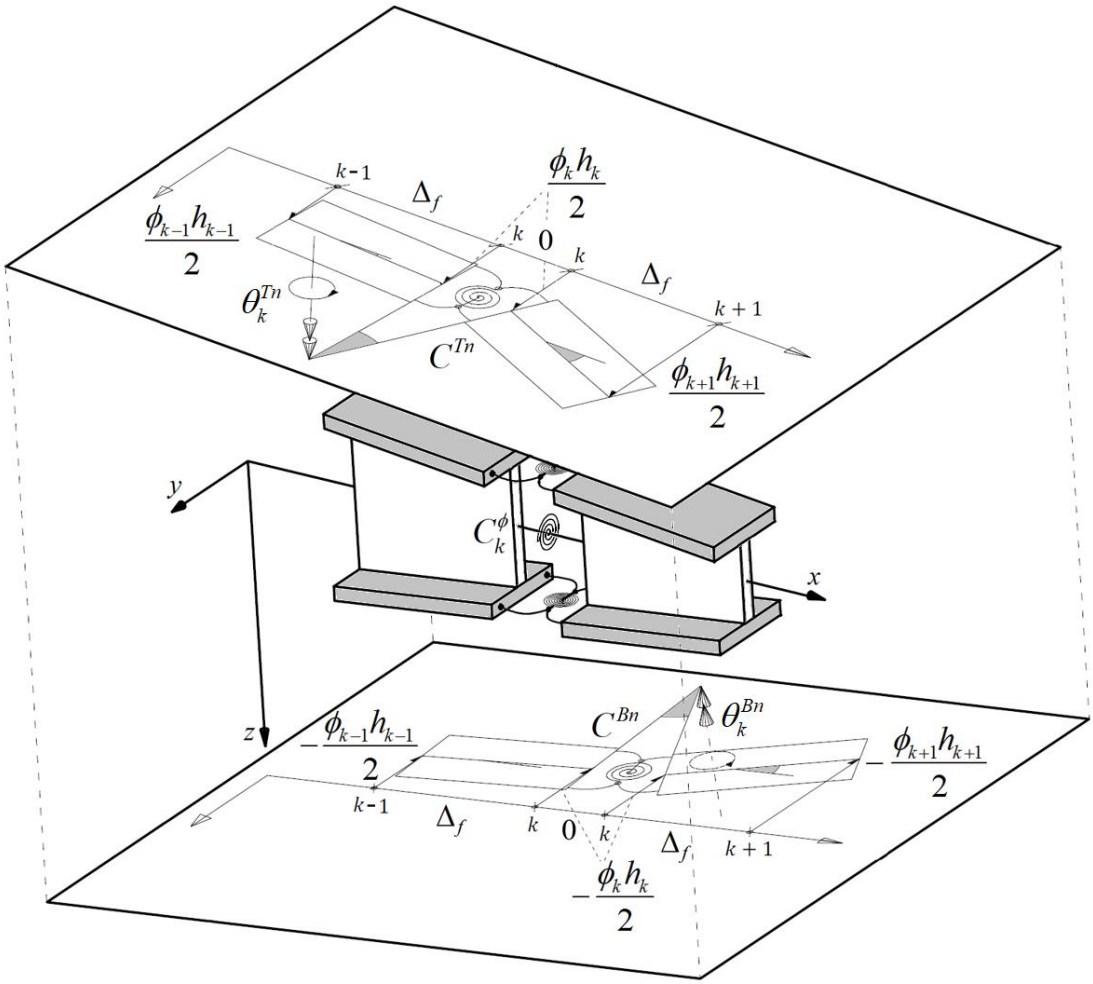

Figure 3.5.6: Illustrative example 2 – Warping kinematics of a doubly symmetric web-tapered I-section bar-chain model

The tapered bar-chain has a concentrated twist moment at its free end, so that the total potential energy is defined as

$$\Pi = \frac{1}{2}\sum_{k=1}^{n-1}\left(C_k^{Tn}\left(\theta_k^{Tn}\right)^2 + C_k^{Bn}\left(\theta_k^{Bn}\right)^2 + C_k^{\phi}\left(\theta_k^{*\phi}\right)^2\right) - T\phi_n \ . \tag{3.5.37}$$

Replacing equations (3.4.20) and (3.5.35)-(3.5.36), for the stored elastic energy term, the same results as in expression (3.4.34) are obtained

$$\Pi(\phi_i) = \frac{1}{2}\sum_{k=1}^{n-1}\left(C_{\omega k}\left(\Delta D_o^2\phi_k\right)^2 - 2C_{\omega\psi k}\left(\Delta D_o^2\phi_k\right)\left(\Delta D_o\phi_k\right) + C_{\psi k}\left(\Delta D_o\phi_k\right)^2\right) - T\phi_n \tag{3.5.38}$$

with $n \geq n_{min} = 2$, where the discrete stiffness coefficients are defined as

$$C_{\omega k} = \frac{EI_{\omega k}^*}{\Delta} = \frac{E}{\Delta}\left(\frac{(b_f)^3 (h_k)^2 t_f \cos^3\varphi}{24}\right) \tag{3.5.39}$$

$$C_{\omega\psi k} = \frac{EI^*_{\omega\psi k}}{\Delta} = \frac{E}{\Delta}\left(\frac{(b_f)^3 h_k t_f \cos^3\varphi \tan\varphi}{6}\right) \tag{3.5.40}$$

$$C_{\psi k} = \frac{EI^*_{\psi k} + GJ^*_k}{\Delta} = \frac{E}{\Delta}\left(\frac{2(b_f)^3 t_f \cos^3\varphi \tan^2\varphi}{3}\right) + \frac{G}{\Delta}\left(\frac{h_k (t_W)^3 + 2b_f (t_f \cos\varphi)^3}{3}\right) . \tag{3.5.41}$$

Finding the discrete stationary values

$$\frac{\partial\Pi}{\partial\phi_i} = \frac{C_{\psi i}}{4}\left(\phi_i - \phi_{i-2}\right) + \frac{C_{\psi i+2}}{4}\left(\phi_i - \phi_{i+2}\right) + \frac{C_{\omega i}}{\Delta^2}\left(\phi_{i-2} - 2\phi_{i-1} + \phi_i\right)$$

$$+ \frac{2C_{\omega i+1}}{\Delta^2}\left(-\phi_{i-1} + 2\phi_i - \phi_{i+1}\right) + \frac{C_{\omega i+2}}{\Delta^2}\left(\phi_i - 2\phi_{i+1} + \phi_{i+2}\right)$$

$$+ \frac{C_{\omega\psi i}}{\Delta}\left(\phi_{i-1} - \phi_i\right) + \frac{C_{\omega\psi i+1}}{\Delta}\left(\phi_{i+1} - \phi_{i-1}\right) + \frac{C_{\omega\psi i+2}}{\Delta}\left(\phi_i - \phi_{i+1}\right) = 0 \tag{3.5.42}$$

with $i = 2,..,\mathrm{n}-2$, the essential boundary conditions are specified as

$$\phi_o = 0 \ , \qquad \phi_1 = 0 \ . \tag{3.5.43}$$

The discrete natural boundary conditions are characterized by the last two twist segments, corresponding to the derivatives of Π with respect to the twits rotations $\phi_{\mathrm{n}-1}$ and ϕ_{n},

$$\frac{\partial\Pi}{\partial\phi_{\mathrm{n}-1}} = \frac{2C_{\omega\mathrm{n}-1}}{\Delta^2}\left(-\phi_{\mathrm{n}-2} + 2\phi_{\mathrm{n}-1} - \phi_{\mathrm{n}}\right) + \frac{C_{\omega\mathrm{n}-2}}{\Delta^2}\left(\phi_{\mathrm{n}-3} - 2\phi_{\mathrm{n}-2} + \phi_{\mathrm{n}-1}\right) + \frac{C_{\omega\psi\mathrm{n}-1}}{\Delta}\left(\phi_{\mathrm{n}} - \phi_{\mathrm{n}-2}\right)$$

$$+ \frac{C_{\omega\psi\mathrm{n}-2}}{\Delta}\left(\phi_{\mathrm{n}-2} - \phi_{\mathrm{n}-1}\right) + \frac{C_{\psi\mathrm{n}-2}}{4}\left(\phi_{\mathrm{n}-1} - \phi_{\mathrm{n}-3}\right) = 0 \tag{3.5.44}$$

$$\frac{\partial\Pi}{\partial\phi_{\mathrm{n}}} = \frac{C_{\omega\mathrm{n}-1}}{\Delta^2}\left(\phi_{\mathrm{n}-2} - 2\phi_{\mathrm{n}-1} + \phi_{\mathrm{n}}\right) + \frac{C_{\omega\psi\mathrm{n}-1}}{\Delta}\left(\phi_{\mathrm{n}-1} - \phi_{\mathrm{n}}\right) + \frac{C_{\psi\mathrm{n}-1}}{4}\left(\phi_{\mathrm{n}} - \phi_{\mathrm{n}-2}\right) - T = 0 \ . \tag{3.5.45}$$

The discrete problem can be non-dimensionalized by defining the following non-dimensional ratios

$$\kappa_{\omega 0} = \frac{\pi}{L}\sqrt{\frac{EI^*_{\omega}(0)}{GJ^*(0)}} \ , \qquad \kappa_{J0} = \frac{h_o t_w{}^3}{3J^*(0)} \ , \qquad \mu_0 = \frac{TL}{GJ^*(0)} \ , \tag{3.5.46}$$

where the geometrical properties at the origin, according to expressions (3.5.39) and (3.5.41), are respectively

$$I_{\omega}^{*}(0)=\frac{(b_f)^3(h_o)^2 t_f \cos^3\varphi}{24} \tag{3.5.47}$$

$$J^{*}(0)=\frac{h_o(t_W)^3+2b_f(t_f\cos\varphi)^3}{3}\ . \tag{3.5.48}$$

As an example, we determine a numerical solution for the following parameter values

$$\kappa_{\omega 0}=2.0\ , \qquad \kappa_{J0}=0.1\ , \tag{3.5.49}$$

for different values of the web slopes, which are plotted in Figure 3.5.7 for the bar-chain model with $\mathrm{n}=600$. The figure also represents the solution of the non-dimensional version of the differential equation developed in chapter 2, as expected, both lines match almost perfectly. Since the exact solution is known, it is possible to measure the convergence of the bar-chain model, computing the relative error between the twist rotation of the free end segment ϕ_{n} and the exact value $\phi(L)$ in function of the number of segments, see Figure 3.5.8.

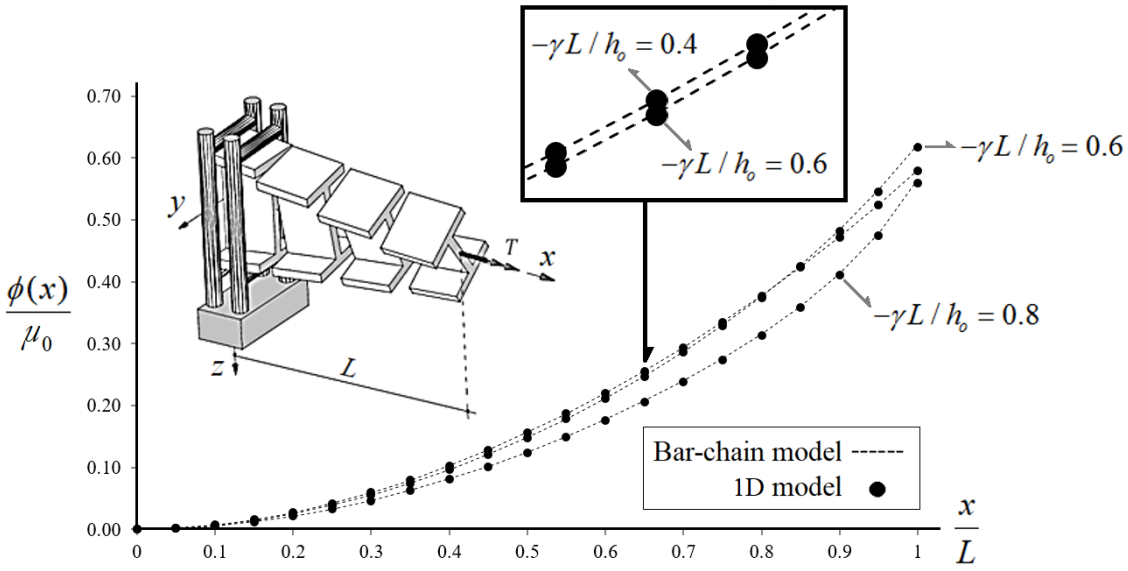

Figure 3.5.7: Illustrative example 2 ($\kappa_{\omega 0}=2.0$, $\kappa_{J0}=0.1$, $\mathrm{n}=600$) – Solutions of the twist rotations per unit non-dimensional torque μ_0, for the bar-chain model and the continuous one-dimensional

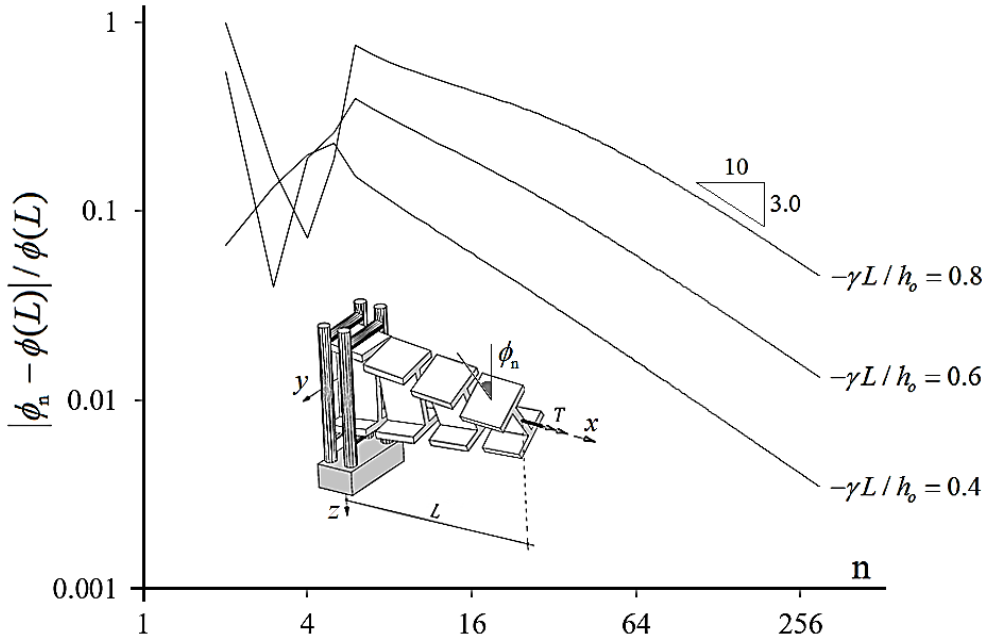

Figure 3.5.8: Illustrative example 2 ($\kappa_{\omega 0} = 2.0$, $\kappa_{J0} = 0.1$) – Convergence analysis of the twist rotation of the free end segment of the bar-chain model

The results reveal that the convergence rate is the same for every web slope. Moreover, if we compare the convergence rate with the prismatic case (see Figure 3.5.2), it gets slower as the slope increases. To analyse the consistency of solution (3.5.42), the residuals are determined by replacing the exact central twist rotations $\phi(x_i)$ and stiffness coefficients $C_\omega(x_i)$, $C_{\omega\psi}(x_i), C_\psi(x_i)$ with $x_i = i\Delta$, $i = 2,..,\mathrm{n}-2$. So that if the discrete values are expanded in a Taylor series around the central position, we get

$$\Delta\left(-C_\psi(x_i)\Delta\phi''(x_i)+O(\Delta^3)\right)-\Delta\left(C'_\psi(x_i)+O(\Delta)\right)\left(\Delta\phi'(x_i)+O(\Delta^2)\right)$$

$$+\Delta\left(C_\omega(x_i)\Delta\phi^{IV}(x_i)+O(\Delta^3)\right)+\left(C''_\omega(x_i)+O(\Delta)\right)\left(\phi''(x_i)\Delta^2+O(\Delta^3)\right)$$

$$+2\left(C'_\omega(x_i)\Delta+O(\Delta^2)\right)\left(\phi'''(x_i)\Delta+O(\Delta^2)\right)-\left(C'_{\omega\psi}(x_i)+O(\Delta)\right)\left(\phi'(x_i)\Delta+O(\Delta^2)\right)$$

$$+\left(C'_{\omega\psi}(x_i)+O(\Delta)\right)\left(\phi'(x_{i-1})\Delta+O(\Delta^2)\right)=r_i \text{ , with } i=2,..,\mathrm{n}-2 \text{ .} \qquad (3.5.50)$$

Reducing terms and factorising by grouping

$$\Delta\left(C_\omega(x_i)\Delta\phi^{IV}(x_i)+2C'_\omega(x_i)\Delta\phi'''(x_i)-C_\psi(x_i)\Delta\phi''(x_i)-C'_\psi(x_i)\Delta\phi'(x_i)\right)$$

$$+\Delta\left(C''_\omega(x_i)\Delta\phi''(x_i)-C'_{\omega\psi}(x_i)\left(\phi'(x_i)-\phi'(x_{i-1})\right)\right)+O(\Delta^2)=r_i \qquad (3.5.51)$$

by using the following identity

$$C_{\omega}''(x_i) = -C_{\omega\psi}'(x_i) = \frac{1}{2}\left(C_{\psi}(x_i) - \frac{GJ^*(x_i)}{\Delta} \right)' \tag{3.5.52}$$

and

$$\phi'(x_i) - \phi'(x_{i-1}) \approx \Delta\phi''(x_i) \ , \tag{3.5.53}$$

equation (3.5.51) is reduced to

$$\Delta\Big(C_{\omega}(x_i)\Delta\phi^{IV}(x_i) + 2C_{\omega}'(x_i)\Delta\phi'''(x_i) - GJ^*(x_i)\phi''(x_i) - \left(GJ^*(x_i)\right)'\phi'(x_i) \Big) + O(\Delta^2) = r_i \ . \tag{3.5.54}$$

In the limit, the residuals converge to zero, with

$$C_{\omega}(x_i)\Delta \to EI_{\omega}^*(x) \ , \qquad C_{\omega}'(x_i)\Delta \to \left(EI_{\omega}^*(x)\right)' \ , \qquad GJ^*(x_i) \to GJ^*(x) \tag{3.5.55}$$

and the differential equation of the one-dimensional model arises

$$EI_{\omega}^*(x)\phi^{IV}(x) + 2\left(EI_{\omega}^*(x)\right)'\phi'''(x) - GJ^*(x)\phi''(x) - \left(GJ^*(x)\right)'\phi'(x) = 0 \ , \tag{3.5.56}$$

which is equivalent to equation (2.10.4) developed in chapter 2. In the case of the natural boundary conditions (3.5.44)-(3.5.45), their respective residuals are equal to

$$-C_{\omega}(x_{\mathrm{n}})\phi''(x_{\mathrm{n}}) + C_{\omega\psi}(x_{\mathrm{n}})\phi'(x_{\mathrm{n}}) + O(\Delta) = r_{\mathrm{n}-1} \tag{3.5.57}$$

$$-\Big(C_{\omega}'(x_{\mathrm{n}})\Delta\phi''(x_{\mathrm{n}}) + C_{\omega}(x_{\mathrm{n}})\Delta\phi'''(x_{\mathrm{n}}) \Big) + \Big(C_{\omega\psi}'(x_{\mathrm{n}})\Delta + C_{\psi}(x_{\mathrm{n}})\Delta \Big)\phi'(x_{\mathrm{n}}) - T + O(\Delta) = r_{\mathrm{n}} \ . \tag{3.5.58}$$

At the limit, the above discrete natural boundary conditions become respectively the bimoment and the torque at the tip of the continuous tapered bar, i.e.,

$$-EI_{\omega}^*(L)\phi''(L) + EI_{\omega\psi}^*(L)\phi'(L) = 0 \ , \tag{3.5.59}$$

$$-\left(EI_{\omega}^*\phi''\right)'(L) + \left(GJ^*(L) + EI_{\psi}^*(L) + EI_{\omega\psi}^{*\,\prime}(L)\right)\phi'(L) = T \ . \tag{3.5.60}$$

Applying the same routine to equations (3.5.43), the essential boundary conditions of the continuous problem arise

$$\phi(0) = 0 \ , \qquad \phi'(0) = 0 \ . \tag{3.5.61}$$

REFERENCES

Achinstein, P. (1964). "Models, analogies, and theories." *Philosophy of Science*, 31(4), 328–350.

Alibert, J.-J., Della Corte, A., and Seppecher, P. (2017). "Convergence of Hencky-type discrete beam model to Euler inextensible elastica in large deformation: Rigorous proof." *Mathematical Modelling in Solid Mechanics*, 1–12.

Andrade, A. (2013). "One-dimensional models for the spacial behaviour of tapered thin-walled bars with open cross sections: static, dynamic and buckling analyses." *Ph.D. thesis, Universidade de Coimbra*.

Andrianov, I. V., Awrejcewicz, J., and Weichert, D. (2010). "Improved continuous models for discrete media." *Mathematical Problems in Engineering*, Hindawi, 2010.

Bažant, Z., and Cedolin, L. (2003). *Stability of structures: elastic, inelastic, fracture and damage theories*. Dover publications.

Cabrera, F., Andrade, A., Providência, P., and Camotim, D. (2017). "On the space behaviour of tapered thin-walled bars with open cross-sections." *Congress on Numerical Methods in Engineering, Valencia-Spain*, (606–626).

Cajić, M. S., and Lazarević, M. P. (2016). "Determination of joint reactions in a rigid multibody system, two different approaches." *FME Transactions*, 44(2), 165–173.

Challamel, N., Camotim, D., Wang, C. M., and Zhang, Z. (2015a). "On lateral-torsional buckling of discrete elastic systems: A nonlocal approach." *European Journal of Mechanics A/Solids*, 49, 106–113.

Challamel, N., Kocsis, A., and Wang, C. (2015b). “Discrete and non-local elastica.” *International Journal of Non-Linear Mechanics,* 77, 128–140.

Challamel, N., Lerbet, J., and Wang, C. M. (2014a). “On buckling of granular columns with shear interaction: Discrete versus nonlocal approaches.” *Journal of Applied Physics*, 115(23).

Challamel, N., Lerbet, J., Wang, C. M., and Zhang, Z. (2014b). “Analytical length scale calibration of nonlocal continuum from a microstructured buckling model.” *Zeitschrift für Angewandte Mathematik und Mechanik [Journal of Applied Mathematics and Mechanics]*, 94(5), 402–413.

Challamel, N., Wang, C., and Elishakoff, I. (2016). “Nonlocal or gradient elasticity macroscopic models: a question of concentrated or distributed microstructure.” *Mechanics Research Communications*, 71, 25–31.

Challamel, N., Wang, C. M., and Elishakoff, I. (2014c). “Discrete systems behave as nonlocal structural elements: bending, buckling and vibration analysis.” *European Journal of Mechanics-A/Solids*, 44, 125–135.

Challamel, N., Zhang, Z., and Wang, C. M. (2013). “Nonlocal equivalent continua for buckling and vibration analyses of microstructured beams.” *Journal of Nanomechanics and Micromechanics*, 5(1).

Chen, W. F., and Atsuta, T. (1977). *Theory of beam-columns, volume 2: space behaviour and design*. McGraw-Hill.

Dell’Isola, F., Giorgio, I., Pawlikowski, M., and Rizzi, N. L. (2016). “Large deformations of planar extensible beams and pantographic lattices: heuristic homogenization, experimental and numerical examples of equilibrium.” *Proc. Royal Society A*, The Royal Society, A472(2185).

Duan, W. H., Challamel, N., Wang, C. M., and Ding, Z. (2013). “Development of analytical vibration solutions for microstructured beam model to calibrate length scale coefficient in nonlocal Timoshenko beams.” *Journal of Applied Physics*, 114(10).

El Naschie, M. S. (1990). *Stress stability and chaos in the structural engineering and energy approach*. McGraw-Hill.

El Naschie, M. S., Wu, C. W., and Wifi, A. S. (1988). “A simple discrete element method for the initial postbuckling of elastic structures.” *International Journal for Numerical Methods in Engineering*, 26(9), 2049–2060.

Fukasawa, T., Okamura, S., Yamamoto, T., Kawasaki, N., Hirotani, T., Moriizumi, E., Sakurai, Y., and Masaki, N. (2018). “Research and development of rubber bearings for sodium-cooled fast reactor: Ultimate properties of half scale thick rubber bearings based on breaking tests.” *Journal of Pressure Vessel Technology*, 140(1), 011401.

Gambhir, M. L. (2004). *Stability analysis and design of structures*. Springer Science & Business Media.

Gáspár, Z., and Domokos, G. (1989). “Global investigation of discrete models of the Euler buckling problem.” *Acta Technica Acad. Sci. Hung*, 102, 227–238.

Gjelsvik, A. (1981). *The theory of thin walled bars*. Wiley.

Goldstein, H., Poole, C. P., and Safko, J. L. (2014). *Classical Mechanics*. Pearson Higher Edition.

Hencky, H. (1920). “Über die angenäherte Lösung von Stabilitätsproblemen im Raum mittels der elastischen Gelenkkette [The approximate solution of problems of stability in space by elastic joint chain].” *Der Eisenbau*, (11), 437–452.

Hunt, G. W., Lawther, R., and Providência, P. (1997). “Finite element modelling of spatially chaotic structures.” *International Journal for Numerical Methods in Engineering*, 40(12), 2237–2256.

Iremonger, M. J. (1980). “Finite difference buckling analysis of non-uniform columns.” *Computers & Structures*, 12(5), 741–748.

Jourawski, D. (1856). “Remarques sur la résistance d’un corps prismatique et d’une pièce composée en bois ou en tôle de fer a une force perpendiculaire à leur longueur [Notes on the resistance of a prismatic body and a composite part of wood or sheet iron to a force perpendicular to their length].” *Annales des Ponts et Chaussées*, 12, 328–351.

Kawai, T. (1977). “New element models in discrete structural analysis.” *Journal of the Society of Naval Architects of Japan*, (141), 174–180.

Kim, N. H., Sankar, B. V., and Kumar, A. V. (2018). *Introduction to finite element analysis and design*. John Wiley & Sons.

Krishna, S. G., and Ram, Y. M. (2007). “Discrete model analysis of optimal columns.” *International Journal of Solids and Structures*, 44(22–23), 7307–7322.

Kurrer, K.-E. (2008). *The history of the theory of structures: from arch analysis to computational mechanics*. Ernst & Sohn.

Lagrange, J. L. (1759). “Recherches sur la nature et la propagation du son [Research on the nature and propagation of sound].” *Miscellanea Philosophico-Mathematica Societatis Privatae Taurinensis I, 2rd Pagination*, 1(112), 39–148.

Leckie, F., and Lindberg, G. (1963). “The effect of lumped parameters on beam frequencies.” *The Aeronautical Quarterly*, 14(3), 224–240.

LeVeque, R. J. (2007). *Finite difference methods for ordinary and partial differential equations — steady state and time-dependent problems*. SIAM.

Longair, M. S. (1984). *Theoretical concepts in physics: An alternative view of theoretical reasoning in physics for final-year undergraduates*. Cambridge University Press.

Lonkar, S. (1968). *Bending and torsion of thin walled beams with variable, open cross sections*. Institut für Baustatik (Eidgenössische Technische Hochschule Zürich).

Maxwell, J. C. (1861). *On physical lines of force: Part I. The theory of molecular vortices applied to magnetic phenomena, 21, 161–175, Part II. The theory of molecular vortices applied to electric currents, 21, 338–348.* The London, Edinburgh, and Dublin Philosophical Magazine and Journal of Science, Reprint in the scientific papers of James Clerk Maxwell, 1965, Dover Publications, Edited by W. D. Niven, M. A., F. R. S., 451–488.

Maxwell, J. C. (1862). *On physical lines of force: Part III. The theory of molecular vortices applied to statical electricity, 23, 12–24, Part IV. The theory of molecular vortices applied to the action of magnetism on polarised light, 23, 85–95*. The London, Edinburgh, and Dublin Philosophical Magazine and Journal of Science, Reprint in the scientific papers of James Clerk Maxwell, 1965, Dover Publications, Edited by W. D. Niven, M. A., F. R. S., 489–525.

Minati, G., Pessa, E., and Abram, M. (2006). *Systemics of emergence: research and development*. Springer Science.

Oden, J. T., and Ripperger, E. A. (1981). *Mechanics of elastic structures*. Hemisphere Publishing Corporation.

Palmer, S. B., and Rogalski, M. S. (2005). *Advanced university physics*. CRC Press.

Picandet, V., and Challamel, N. (2018). “Bending of an elastoplastic Hencky bar-chain: from discrete to nonlocal continuous beam models.” *Meccanica*, 1–22.

Prager, S., and Prager, W. (1979). “A note on optimal design of columns.” *International Journal of Mechanical Sciences*, 21(4), 249–251.

Ruocco, E., Wang, C. M., Zhang, H., and Challamel, N. (2017). “An approximate model for optimizing Bernoulli columns against buckling.” *Engineering Structures*, 141, 316–327.

Ruocco, E., Zhang, H., and Wang, C. M. (2016). “Hencky bar-chain model for buckling analysis of non-uniform columns.” *Engineering Structures*, 6, 73–84.

Ruocco, E., Zhang, H., and Wang, C. M. (2018). “Hencky bar-net model for buckling and vibration analyses of rectangular plates with non-uniform thickness.” *Engineering Structures*, 168, 653–668.

Salvadori, M. G. (1951). “Numerical computation of buckling loads by finite differences.” *Trans. ASCE*, 116, 590–636.

Selvadurai, A. P. S. (1979). *Elastic analysis of soil-foundation interaction*. Elsevier.

Silverman, I. K. (1951). “Discussion on the paper of ‘Salvadori M.G., Numerical computation of buckling loads by finite differences, Transactions of the ASCE, 116, 590–636, 1951.” *Trans. the ASCE*, 116 (1), 625–626.

Simitses, G. J., and Hodges, D. H. (2006). *Fundamentals of structural stability*. Butterworth-Heinemann.

Sun, C., Shaw, W. J. D., and Vinogradov, A. M. (1995). “Discrete-element model for buckling analysis of thin ring confined within rigid boundary.” *Journal of Engineering Mechanics, ASCE*, 121(1), 71–79.

Tanner, R. I., and Tanner, E. (2003). “Heinrich Hencky: a rheological pioneer.” *Rheologica acta*, Springer, 42(1–2), 93–101.

Timoshenko, S. P. (1940). *Strength of materials. Part I, Elementary theory and problems*, 2nd ed. D. Van Nostrand Company.

Timoshenko, S. P. (1953). *History of strength of materials: with a brief account of the history of theory of elasticity and theory of structures*. Dover Publications.

Tonti, E. (1975). *On the formal structure of physical theories*. Istituto di matematica del Politecnico di Milano.

Tonti, E. (1976). “The reason for analogies between physical theories.” *Applied Mathematical Modelling*, 1(1), 37–50.

Trahair, N. S. (2014). “Bending and buckling of tapered steel beam structures.” *Engineering Structures*, 59, 229–237.

Turco, E., Dell’Isola, F., Cazzani, A., and Rizzi, N. L. (2016). “Hencky-type discrete model for pantographic structures: numerical comparison with second gradient continuum models.” *Zeitschrift für angewandte Mathematik und Physik*, Springer, 67(4), 85.

Vlasov, V. Z. (1961). *Thin-walled elastic beams*, [English translation of the 2nd Russian edition of 1959]. Jerusalem: Israel Program for Scientific Translation.

Wagner, H., and Pretschner, W. (1936). "Torsion and buckling of open sections." *National Advisory Committee for Aeronautics, Technical Memorandum No 784*, XI(6).

Wang, C. M., Gao, R. P., Zhang, H., and Challamel, N. (2015a). "Treatment of elastically restrained ends for beam buckling in finite difference, microstructured and nonlocal beam models." *Acta Mechanica*, 226(2), 419–436.

Wang, C. M., Zhang, H., Challamel, N., and Duan, W. H. (2017a). "On boundary conditions for buckling and vibration of nonlocal beams." *European Journal of Mechanics A/Solids*, 61, 73–81.

Wang, C. M., Zhang, H., Challamel, N., and Duan, W. H. (2017b). "Eringen's small length scale coefficient for vibration of axially loaded nonlocal Euler beams with elastic end restraints." *Journal of Modeling in Mechanics and Materials*, 1(2).

Wang, C. M., Zhang, H., Challamel, N., and Xiang, Y. (2016). "Buckling of nonlocal columns with allowance for selfweight." *Journal of Engineering Mechanics, ASCE*, 142(7).

Wang, C. M., Zhang, H., Gao, R. P., Duan, W. H., and Challamel, N. (2015b). "Hencky bar-chain model for buckling and vibration of beams with elastic end restraints." *International Journal of Structural Stability and Dynamics*, 15(7).

Wang, C. M., Zhang, Z., Challamel, N., and Duan, W. H. (2013). "Calibration of Eringen's small length scale coefficient for initially stressed vibrating nonlocal Euler beams based on microstructured beam model." *Journal of Physics D: Applied Physics*, 46(34).

Wang, C. Y. (2001). "Stability of a heavy segmented column." *Mechanics Research Communications*, 28(5), 493–497.

Wang, C. Y. (2004). “Free vibration of a linked rod.” *Journal of Sound and Vibration*, 274(1–2), 455–459.

Watanabe, Y., and Sugimoto, N. (2005). “Flexural wave propagation in a spatially periodic structure of articulated beams.” *Wave Motion*, 42(2), 155–167.

Winkler, E. (1867). *Die lehre von der elasticität und festigkeit [Theory of elasticity and strength]*. Prague: Dominicus.

Yang, Y.-B., and McGuire, W. (1984). “A procedure for analysing space frames with partial warping restraint.” *International Journal for Numerical Methods in Engineering*, 20(8), 1377–1398.

Zhang, H., and Wang, C. M. (2018). “Hencky bar-chain model for optimal circular arches against buckling.” *Mechanics Research Communications*, 88(7–11).

Zhang, H., Wang, C. M., and Challamel, N. (2016a). “Buckling and vibration of Hencky bar-chain with internal elastic springs.” *International Journal of Mechanical Sciences*, 119, 383–395.

Zhang, H., Wang, C. M., and Challamel, N. (2017a). “Small length scale coefficient for Eringen’s and lattice-based continualized nonlocal circular arches in buckling and vibration.” *Composite Structures*, 165, 148–159.

Zhang, H., Wang, C. M., Challamel, N., and Ruocco, E. (2017b). “Semi-analytical solutions for optimal design of columns based on Hencky bar-chain model.” *Engineering Structures*, 136, 87–99.

Zhang, H., Wang, C. M., Ruocco, E., and Challamel, N. (2016b). “Hencky bar-chain model for buckling and vibration analyses of non-uniform beams on variable elastic foundation.” *Engineering Structures*, 126, 252–263.

Zhang, Z., Challamel, N., and Wang, C. (2013). "Eringen's small length scale coefficient for buckling of nonlocal Timoshenko beam based on microstructured beam model." *Journal of Applied Physics*, 114(11).

Ziegler, H. (2013). *Principles of structural stability*. Birkhäuser.

Chapter 4

A DISCRETE ONE-DIMENSIONAL MODEL FOR THE FLEXURAL-TORSIONAL STABILITY OF TAPERED SINGLY SYMMETRIC I-SECTION BEAM-COLUMNS

THE LATERAL-TORSIONAL BUCKLING PROBLEM

A slender column shortens when compressed by a weight applied to its top, and, in so doing, lowers the weight's position. The tendency of all weights to lower their position is a basic law of nature. It is another basic law of nature that, whenever there is a choice between different paths, a physical phenomenon will follow the easiest path. Confronted with the choice of bending out or shortening, the column finds it easier to shorten for relatively small loads and to bend out for relatively large loads. In other words, when the load reaches its buckling value the column finds it easier to lower the load by bending than by shortening.

SALVADORI AND HELLER, *STRUCTURE IN ARCHITECTURE*

In condensed matter physics, the idea of *spontaneous symmetry breaking*, means that the lowest energy state of a system can have a lower symmetry than the forces acting among its constituents and on the system as a whole. As an analogy, consider a long elastic column on top of which we apply a concentric compression force directed along its axis. Clearly there is rotational symmetry around the bar which is maintained as long as the force is not too strong, there is simply a shortening according to Hooke's law. However, when the force reaches its critical value the column bends and we have an infinite number of equivalent lowest energy states which differ by the rotation.

G. JONA-LASINIO, *SCHOLARPEDIA*

4.1 INTRODUCTION

The phenomenon of lateral-torsional buckling has been a subject of interest since the last decades of the 19th century (Singer et al. 1998) [pp. 320-321], but the first rigorous analyses of the phenomenon were those published independently and almost simultaneously by Prandtl (1899) and Michell (1899) concerning prismatic strip beams more than a century after Euler (1744) derived his critical buckling load,[1] yielding the maximum axial load a perfect column can support without bending.

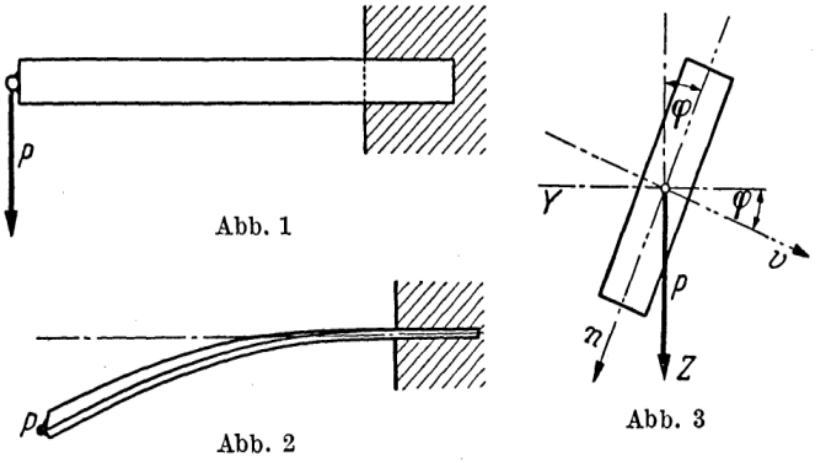

Figure 4.1.1: The lateral-torsional buckling of a cantilever strip beam under a centre loading at the tip (Prandtl 1899) [pp. 13-33]

Michell as well as Prandt used geometrical hypotheses to arrive at the correct differential equations. Moreover, for the case of cantilever strip beams, see Figure 4.1.1, they solved the buckling problem by using the Bessel functions of fractional order, e.g., Hodges and Peters (2001) [eq. 22].[2] Later on, Reissner (1904) showed that the Michell-Prandtl results could in fact be considered as an appropriate specialization of Kirchhoff's general theory of space-curved beams, with the analysis of the secondary order effects being automatically included in the analysis of the problem, e.g., Reissner (1979, 1989). Concerning the physics behind the mechanical phenomenon, the above studies showed that the instability of the bar is due to its lack of torsional rather than of flexural rigidity,

[1] Euler presented his results in the first part of the appendix "*De curvis elasticis*" to his 1744 treatise on the calculus of variations, assuming an integral equation suggested by Daniel Bernoulli, corresponding in modern terminology as the strain energy of the elastica (Fraser 1991), so that, the functional of the stability problem can be minimized, getting the equilibrium equation of the buckling problem.

[2] The use of convergence series was the classical analytical solutions until the advent of discrete methods.

so that the same kind of instability that occurs in a thin blade may affect beams of others types of open cross-sections. This led in 1905 a young Timoshenko began to work on the problem of lateral-torsional buckling of doubly symmetric I-beams under Prandtl's suggestion at the University of Göttingen (Soderberg 1982) [pp. 326-327].

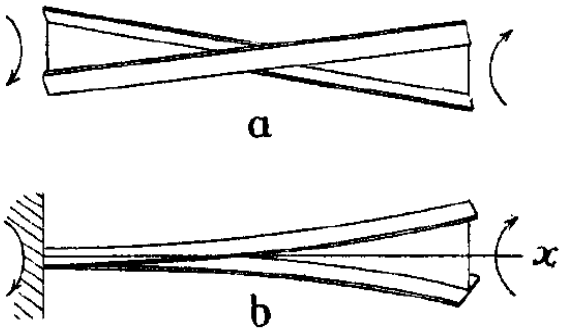

Figure 4.1.2: Saint-Venant and warping torsion of a doubly symmetric I-beam by Timoshenko (1913)

In order to solve the problem, Timoshenko realizes that instead of the usual Saint-Venant torsion equation, he has to introduce another term corresponding to the warping torsion response due to the moment of a couple defined by the balanced shear forces (with respect to the lateral curvatures of the flanges) and the distance between middle lines of the flanges as the arm of the couple,[3] see Figure 4.1.2. Having solved the torsion problem, he studied the lateral-torsional buckling of I-beams, computing the critical loads for various special cases, e.g., Timoshenko and Gere (1961) [pp. 251-272].[4] More memorable was his three consecutive papers (Timoshenko 1945) in which he described his own ideas and others researcher's contributions, e.g., Weber (1926), Wagner (1929), Kappus (1937),

[3] Timoshenko narrated this exciting discovery in his autobiography (Timoshenko 1968):

> He [Ludwing Prandtl] had been investigating the lateral buckling in flexure of a beam of narrow rectangular section, though for practical purposes, of course, it was more important to study the lateral stability of an I-beam. In that case one had to start with the torsion of an I-beam … It took me about two weeks to figure out how to allow for this bending, to realize that the torque is counterbalanced by the same stresses as in ordinary torsion, added to the moment produced by the shear forces resulting from the buckling of the I-beam's flanges. Once this was understood, writing an equation for the torsion was no longer difficult.

[4] Other relevant references concerning the flexural-torsional buckling of prismatic I-beams were reported by Lyse and Johnston (1936), Dumont and Hill (1940), Johnston and Bethlehem (1941), Dohrenwend (1941), Goodier (1942) and Ingerslev (1948), restricted to an elastic material.

Goodier (1941) and Vlasov (1961), establishing the standard theory of flexural-torsional buckling of thin-walled members of open cross-section.[5] The next step into the lateral stability analysis was the insertion of monosymmetric I-beams into the one-dimensional equations, e.g., see Figure 4.1.3, that in virtue of its monosymmetry, induces an imbalanced torque due to normal stresses.[6] [7]

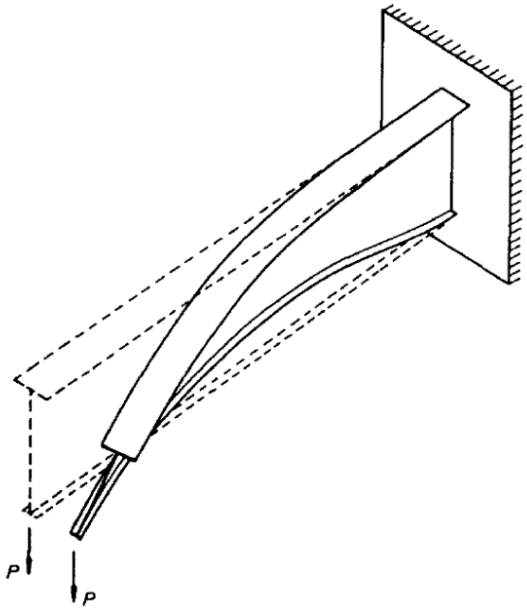

Figure 4.1.3: Buckled monosymmetric cantilevered I-beam by Wang and Kitipornchai (1986)

The earlier reports were given by Hill (1942) and Winter (1943), who developed a set of tests concerning the lateral buckling of unsymmetrical I-beams under pure bending. Since that, some theoretically solutions have been proposed, with the inclusion of a new cross-sectional property related to the asymmetry of the flanges, e.g., Petterson (1951), Kerensky et al. (1956) and O'Connor (1964), being the work of Anderson and Trahair (1972) the most relevant, deducing and verifying through experimental work, the appropriate expression form for this new geometric characteristic.[8]

[5] A historical sketch concerning the combined flexural-torsional instability of one-dimensional members of constant cross-section are discussed in some detail by Lee (1960) [pp. B2-B6], in his memorable Appendix B: known solutions to elastic cases.

[6] This is known as the Wagner effect (Chen and Atsuta 1977) [p. 55], (Gambhir 2013) [p. 48].

[7] In fact Vlasov (1961) [p. 267] developed a general expression to introduce the second-order effect of the normal stresses that produce a torsional moment due to the warping deformation in the cross-section.

[8] For further reading on the buckling properties of (prismatic) monosymmetric I-beams, the reports given by Kitipornchai and Trahair (1980) & Wang and Kitipornchai (1986) are highly recommended.

Despite the above efforts to study the lateral-torsional buckling of beams by using one-dimensional models, the work was limited to prismatic bars with either doubly or singly symmetric I-sections, respectively. The first attempts to derive one-dimensional models for the spatial behaviour of tapered I-section bars were done by Lee (1956) and Lee and Szabo (1967): the problem was tackled by regarding each plated component as an Euler-Bernoulli member, i.e., the same approach done by Timoshenko. The same approach was used later by Kitipornchai and Trahair (1972, 1975), who also dealt with the problem of elastic lateral-torsional buckling of tapered monosymmetric I-beams, reporting numerical results by using the finite integral method.[9]

Later on, Wekezer (1984, 1985, 1990), by using the membrane shell characterization of Wilde (1968), developed a finite element formulation to study the stability of simply supported I-beams with variable flanges and tapered I-beams cantilevers. Other relevant examples are the finite element formulations to perform the linear stability analyses for tapered I-beams by Yang and Yau (1987) for doubly symmetric bars, Bradford (1988) & Bradford and Cuk (1988) for tapered singly symmetric bars, Boissonnade and Muzeau (2001) & Boissonnade and Braham (2002) for doubly and singly symmetric web-tapered bars. For the more general equations, Rajasekaran (1994) based on the membrane theory of shells, developed nonlinear equations for tapered thin-walled beams of generic open cross-section, and Ronagh et al. (2000a; b) developed a theory for the nonlinear axial strain and Kirchhoff stress resultants for a thin-walled beam-column whose cross-section is tapered. It was showed in chapter 3, that the Hencky bar-chain model can be extended to more complex symmetries, e.g., the prismatic and tapered singly symmetric I-section bar-chains. Thus, in this chapter, we extend the above static case to the elastic flexural-torsional buckling of tapered singly symmetric I-section beam-columns. Flangeless members – i.e., members with narrow rectangular cross-section – and prismatic members are treated as special cases.

[9] Since then, several contributions considering other numerical approaches have appeared, including convergence series solutions by trigonometric series, e.g., Burt (1984), Roberts and Burt (1985) or power series, e.g., Asgarian et al. (2013), variational methods such as the Galerkin's method, e.g., Braham and Hanikenne (1993), Braham (1997) and Valicourt (2000), or the Rayleigh-Ritz energy approach, e.g., Wang and Kitipornchai (1986), Kováč (2012) and Abdelrahmane et al. (2013), leading to the framework for the matrix analysis, with both the finite difference method and the finite element method good options to be applied, with the latter being unquestionably the most commonly used.

The discrete equations are obtained via energy methods and it is shown that they are consistent with the Vlasov-type one-dimensional model developed by Andrade and Camotim (2005) in the sense that the local truncation errors approach zero as the length of the segments tends to zero. To verify the proposed discrete one-dimensional models and to assess its convergence rates, several illustrative examples, i.e., analytical (when feasible) and numerical results, concerning different support and loading conditions as well as different severities of taper are discussed.

4.2 THE STABILITY OF EQUILIBRIUM

This section begins with a summary of the fundamental concepts regarding the elastic buckling analysis of ideal discrete conservative systems. The equations presented will help us to solve the particular examples of the following sections, that at the end, are reduced to simple routine calculations. However, it seems best to treat them separately in order to discuss some implications of the general theory relative the stability of discrete conservative systems.

4.2.1 The bar-chain model as a discrete conservative system

A mechanical discrete system is a system with a finite number of degrees of freedom, characterized by n generalized coordinates $\mathbf{q} \equiv \{q_i\}$ with $i = 1, ..., n$.[10] They are described by the single-valued total potential energy function Π, which is defined by the stored elastic energy $\mathcal{U}$ minus the work done by the loading $\mathcal{W}$ (at the deformed configuration), assumed to be continuous and well-behaved[11] by a single control parameter λ (which may represent a single load or the parameter of a system of loads). It is denoted by

$$\Pi(\mathbf{q};\lambda) = \mathcal{U}(\mathbf{q}) - \mathcal{W}(\mathbf{q};\lambda) \ . \tag{4.2.1}$$

[10] Usually chosen to be the displacements or rotations at certain discrete points of the system or the parameters of some deformation modes.

[11] The term "well-behaved" function, defined in the interval $(\mathbf{q}, \mathbf{q}+d\mathbf{q})$ is given in terms of the following Dirichlet conditions (Yarlagadda 2010) [p. 71]:

(i) The function must be single valued within the given interval $d\mathbf{q}$.

(ii) The function can have at most a finite number of discontinuities and a finite number of maxima and minima in the interval $d\mathbf{q}$.

(iii) The function must be absolutely integrable on the interval $d\mathbf{q}$, i.e., $\int_{\mathbf{q}}^{\mathbf{q}+d\mathbf{q}} |\Pi(\mathbf{q};\lambda)| \, d\mathbf{q} = \text{finite}$.

In the case of conservative systems,[12] the variation of $\prod$ with $\mathbf{q}$ should be path-independent, that is, reversible (Bažant and Cedolin 2003) [p. 207].

4.2.2 Stability criterion in terms of the second variation of the total potential energy

In a practical sense, an equilibrium configuration[13] of a discrete mechanical system is said to be stable if accidental forces, shocks, vibrations, eccentricities, imperfections, residual stresses, inhomogeneities, or other probable irregularities do not cause the system to depart excessively or disastrously from that configuration (Langhaar 1962) [p. 29]. According to the principle of stationary potential energy, the generalized coordinates

$$\mathbf{q}^F \equiv \left\{ \mathrm{q}_i^F \right\} \text{ with } i = 1,...,\mathrm{n} \ , \tag{4.2.2}$$

specify an equilibrium configuration at load level λ if and only if the n independent equations

$$\frac{\partial \prod\left(\mathbf{q}^F;\lambda\right)}{\partial \mathbf{q}^F} = \mathbf{0} \tag{4.2.3}$$

are satisfied. Let the following variables be defined

$$\mathbf{h} \equiv \left\{ \mathrm{h}_i \right\} \text{ with } i = 1,...,\mathrm{n} \tag{4.2.4}$$

as small variations (not all simultaneously zero) of the generalized coordinates from the equilibrium configuration (4.2.2), assumed to occur at constant λ. Expanding $\prod\left(\mathbf{q}^F + \mathbf{h};\lambda\right)$ into a Taylor series,

$$\prod\left(\mathbf{q}^F + \mathbf{h};\lambda\right) - \prod\left(\mathbf{q}^F;\lambda\right) =$$

$$\sum_{i=1}^{\mathrm{n}} \left(\frac{\partial \prod\left(\mathbf{q}^F;\lambda\right)}{\partial \mathrm{q}_i^F} \mathrm{h}_i \right) + \frac{1}{2!} \sum_{i=1}^{\mathrm{n}} \sum_{j=1}^{\mathrm{n}} \left(\frac{\partial^2 \prod\left(\mathbf{q}^F;\lambda\right)}{\partial \mathrm{q}_i^F \partial \mathrm{q}_j^F} \mathrm{h}_i \mathrm{h}_j \right) + ... \ , \tag{4.2.5}$$

[12] A mechanical system is said to be "conservative" if the virtual work vanishes for a virtual displacement that carries the system completely around any closed path (Langhaar 1962) [p. 18].

[13] An equilibrium configuration of a structure under load may be stable, neutral or unstable; One method of determining the type of equilibrium is to consider the behaviour of the structure and its loads when an infinitesimally small disturbance is first applied to displace the structure while its loads remain constant and is then removed (Trahair 1993) [§ 2.5]. Hence, if the structure returns to its original position the equilibrium is stable, if it remains in the displaced position it is neutral and if it moved further from the original position it is unstable.

where

$$\delta \prod \equiv \sum_{i=1}^{n} \left(\frac{\partial \prod \left(\mathbf{q}^F ; \lambda \right)}{\partial \mathrm{q}_i^F} \mathrm{h}_i \right) \tag{4.2.6}$$

and

$$\delta^2 \prod \equiv \frac{1}{2!} \sum_{i=1}^{n} \sum_{j=1}^{n} \left(\frac{\partial^2 \prod \left(\mathbf{q}^F ; \lambda \right)}{\partial \mathrm{q}_i^F \partial \mathrm{q}_j^F} \mathrm{h}_i \mathrm{h}_j \right) \tag{4.2.7}$$

define the first and second variations of the total potential energy respectively. By virtue of expression (4.2.3), since $\mathbf{q}^F$ is an equilibrium state, we get

$$\delta \prod = 0 \ , \tag{4.2.8}$$

and the second variation behaves as the relevant term, reducing equation (4.2.5) to the classical Lagrange-Dirichlet theorem, e.g., Slivker (2006) [p. 608], in which the equilibrium state is stable if and only if

$$\delta^2 \prod > 0 \text{ for any } \mathrm{h}_i , \mathrm{h}_j \text{ with } i, j = 1, ..., \mathrm{n} \ , \tag{4.2.9}$$

that is, if the quadratic form $\delta^2 \prod$ is positive definite.[14]

4.2.3 Stability criterion in terms of the Hessian operator associated to the quadratic form

The partial derivatives of equation (4.2.7) enable to define the Hessian operator

$$\mathbf{H} = \nabla \otimes \nabla \ .^{[15]} \tag{4.2.10}$$

Hence, the Hessian operator applied to the total potential energy Π, defines the coefficients $\mathbf{S}_{ij}$ of a symmetric matrix $\mathbf{S}$[16] given by

$$\mathbf{S}_{ij} = \mathbf{e}_i \circ \mathbf{H} \left(\Pi \right) \mathbf{e}_j \text{ with } i, j = 1, ..., \mathrm{n} \ ,^{[17]} \tag{4.2.11}$$

---

[14] Notice that equation (4.2.9) is valid only in a small neighborhood of the equilibrium state.

[15] The gradient vector field denotes the vector differential operator in the configuration space, i.e.,

$$\nabla \equiv \frac{\partial}{\partial \mathrm{q}_i} \mathbf{e}_i \text{ with } i = 1, ..., \mathrm{n} \ .$$

Where the unit vectors $\mathbf{e}_i$ represent the Cartesian coordinate system in the configuration space.

[16] The condition of symmetry imply that the total potential energy must be continuous, i.e.,

$$\frac{\partial^2 \Pi}{\partial \mathrm{q}_i \partial \mathrm{q}_j} = \frac{\partial^2 \Pi}{\partial \mathrm{q}_j \partial \mathrm{q}_i} \text{ with } i, j = 1, ..., \mathrm{n} \ .$$

[17] In general $\mathbf{S}_{ij}$ does not have a diagonal form, i.e., some $\mathbf{S}_{ij} \neq 0$ for $i \neq j$ (Godoy 1999) [p. 78].

establishing a relation between the quadratic form and the coefficients of the matrix (4.2.11), so that, *a necessary and sufficient condition for stability of an equilibrium state is that the symmetric matrix* $\mathbf{S}$ *should be positive definite*.[18]

4.2.4 Stability criterion in terms of the determinant of the quadratic form

By using the Sylvester criterion,[19] concerning the property of positive definite matrices, *a necessary and sufficient condition for stability of a state of equilibrium is that the determinant of the matrix* $\mathbf{S}$ *and all its minors should be positive*. If the determinant or one of its minors is negative, the equilibrium state is unstable, while a null determinant specifies a critical state.[20]

4.2.5 The Trefftz criterion

The critical equilibrium state[21] requires that the first variation of $\delta^2 \prod$ must turn to zero (Trefftz 1931, 1933), thus

$$\delta\left(\delta^2 \prod\right) = 0 \ .^{22} \tag{4.2.12}$$

This is called the Trefftz criterion. So the critical state, can be written as

$$\sum_{i=1}^{n}\left(\frac{\partial\left(\delta^2 \prod\right)}{\partial \mathrm{h}_i}\mathrm{h}_i\right) = 0 \text{ for all } \mathrm{h}_i \ . \tag{4.2.13}$$

---

[18] The matrix $\mathbf{S}$ is defined positive definite, when the associated quadratic form has a strict minimum, that is, when $\mathbf{q}^T\mathbf{S}\mathbf{q} > 0$ for all q_i with $i = 1,...,\mathrm{n}$ (except $\mathrm{q}_i = 0$). If the matrix $\mathbf{S}$ is defined negative definite (when $-\mathbf{q}^T\mathbf{S}\mathbf{q} > 0$ for all q_i) or indefinite (when $\mathbf{q}^T\mathbf{S}\mathbf{q} > 0$ for some q_i and $\mathbf{q}^T\mathbf{S}\mathbf{q} < 0$ for some other q_i), then the equilibrium state is unstable; and when the matrix $\mathbf{S}$ is defined positive semidefinite or negative semidefinite (when $\mathbf{q}^T\mathbf{S}\mathbf{q} \geq 0$ or $\mathbf{q}^T\mathbf{S}\mathbf{q} \leq 0$ for all q_i, while $\mathbf{q}^T\mathbf{S}\mathbf{q} = 0$ for some nonzero q_i respectively), the equilibrium state is associated with the critical state.

[19] A real symmetric $\mathrm{n}\times\mathrm{n}$ matrix $[\mathrm{A}]$ is positive definite, if and only if $\det[\mathrm{A}_k] > 0$ with $k = 1,2,...,\mathrm{n}$ where $[\mathrm{A}_k]$ is the $k \times k$ matrix formed by the intersection of the first k rows and columns of $[\mathrm{A}]$, e.g., Dahlquist and Björck (2003) [p. 163].

[20] Different types of stability criterion can be establish, in function of other properties of the positive definite matrices, e.g., considering the positive values of the coefficients in the diagonal form of the matrix $\mathbf{S}$, or that every eigenvalue of $\mathbf{S}$ must be positive, etc.

[21] The critical equilibrium state can be defined in terms of the "bifurcation phenomenon" in which the (primary or fundamental) equilibrium path (i.e., load-displacement plot) is intersected by a secondary path, defining a bifurcation point, e.g., Seydel (1988) [§ 2.4].

[22] Note that $\delta\left(\delta^2 \prod\right) = 0$ is not the third variation of $\prod$.

Since the small variations are linearly independent, the above equation is reduced to

$$\frac{\partial\left(\delta^2 \Pi\right)}{\partial \mathrm{h}_i} = 0 \text{ for all } i \ . \tag{4.2.14}$$

For this system to have non-trivial solutions, its determinant must vanish. This condition yields the buckling values of the control parameter, i.e., the buckling loads, where the non-trivial solutions define the corresponding buckling modes. In practice, we are mainly interested in the critical mode, or first buckling mode, associated to the minimum buckling load level. Although equation (4.2.14) looks abstruse, it can be proven that if the total potential energy is a quadratic form, and if $\mathrm{q}_i = 0$ for all $i = 1,...,\mathrm{n}$ is the equilibrium state, then, it is reduced to the classical method of adjacent equilibrium, e.g., Bažant and Cedolin (2003) [eq. 4.2.7] or Brush and Almroth (1975) [§ A.5].[23]

4.2.6 Illustrative example

Consider now a simple example: a strip bar-chain cantilever of length L, made of two segments, i.e., $\Delta = L/2$, and loading with a point load at the free tip, see Figure 4.2.1.

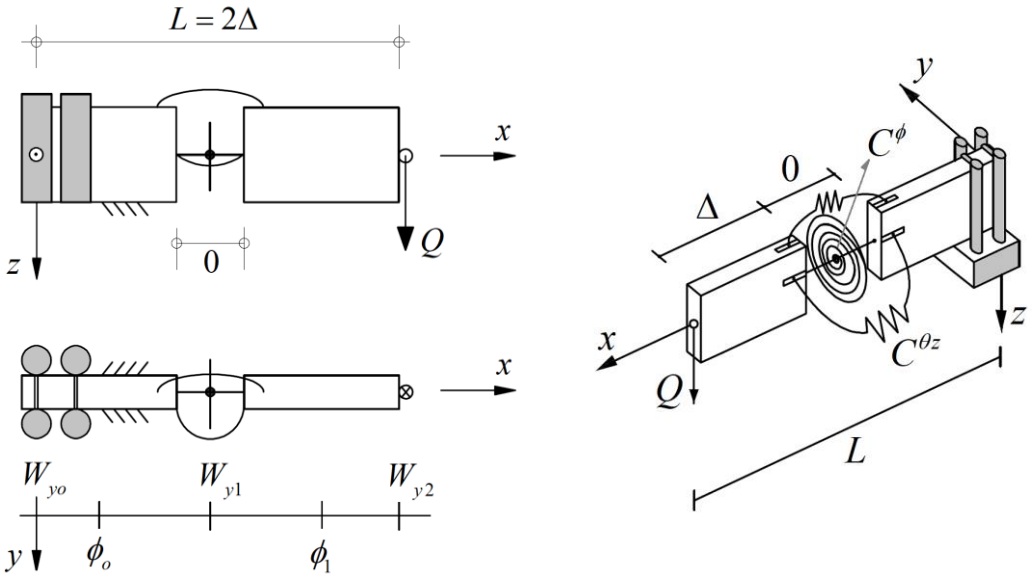

Figure 4.2.1: Illustrative example – A strip bar-chain cantilever

[23] An interesting discussion concerning the adjacent equilibrium method and its relation to the regular perturbation method and the energy method for neutral equilibrium can be found in a paper of Kerr (1977).

The total potential energy equation for the buckled position has the following form[24]

$$\prod(\theta^z,\theta^\phi;Q)=\frac{1}{2}C^{\theta z}\left(\theta^z\right)^2+\frac{1}{2}C^{\phi}\left(\theta^\phi\right)^2-Q\theta^\phi\theta^z\Delta\ , \tag{4.2.15}$$

where the springs deformations are equal to

$$\theta^z=\frac{W_{yo}-2W_{y1}+W_{y2}}{\Delta}\ , \qquad \theta^\phi=\phi_1-\phi_o\ , \tag{4.2.16}$$

and the springs constants are characterized by

$$C^{\theta z}=\frac{EI_z}{\Delta}\ , \qquad C^{\phi}=\frac{GJ}{\Delta}\ . \tag{4.2.17}$$

Due to the support condition, the first twist rotation is equal to

$$\phi_o=0\ , \tag{4.2.18}$$

and the value of the initial lateral displacements in the *y*-direction are respectively

$$W_{yo}=0\ , \qquad W_{y1}=0\ . \tag{4.2.19}$$

By defining the following generalized coordinates and the single load parameter

$$q_1=\sqrt{\frac{EI_z}{L^3}}\ W_{y1}\ , \qquad q_2=\sqrt{\frac{GJ}{L}}\ \phi_1\ , \qquad \lambda=\frac{QL^2}{\sqrt{EI_zGJ}}\ , \tag{4.2.20}$$

the total potential energy (4.2.15) is rewritten as

$$\tilde{\prod}(q_1,q_2;\lambda)=4\left(q_1\right)^2+\left(q_2\right)^2-q_1q_2\lambda\ . \tag{4.2.21}$$

In matrix notation

$$\tilde{\prod}(q_1,q_2;\lambda)=\frac{1}{2}\mathbf{q}^T\tilde{\mathbf{S}}\mathbf{q}=\frac{1}{2}\begin{pmatrix}q_1 & q_2\end{pmatrix}\begin{bmatrix}8 & -\lambda\\ -\lambda & 2\end{bmatrix}\begin{pmatrix}q_1\\ q_2\end{pmatrix}\ . \tag{4.2.22}$$

Hence, applying the general equations of sections § 4.2.2-4.2.5, the different types of criterion concerning the equilibrium states are established.

Equilibrium state	Type of Geometry	Classical criterion	The Hessian operator	The determinant criterion	The Trefftz criterion
Stable	Elliptic	$\delta^2\tilde{\prod}>0$	$\mathbf{q}^T\tilde{\mathbf{S}}\mathbf{q}>0$	$\det\left(\tilde{\mathbf{S}}\right)>0$	$\delta\left(\delta^2\tilde{\prod}\right)<0$
Critical	Parabolic	$\delta^2\tilde{\prod}=0$	$\mathbf{q}^T\tilde{\mathbf{S}}\mathbf{q}=0$	$\det\left(\tilde{\mathbf{S}}\right)=0$	$\delta\left(\delta^2\tilde{\prod}\right)=0$
Unstable	Hyperbolic	$\delta^2\tilde{\prod}<0$	$\mathbf{q}^T\tilde{\mathbf{S}}\mathbf{q}<0$	$\det\left(\tilde{\mathbf{S}}\right)<0$	$\delta\left(\delta^2\tilde{\prod}\right)>0$

Table 4.2.1: Illustrative example – Types of criterion concerning the equilibrium state

[24]The deduction of the total potential energy will be clarified in the following sections.

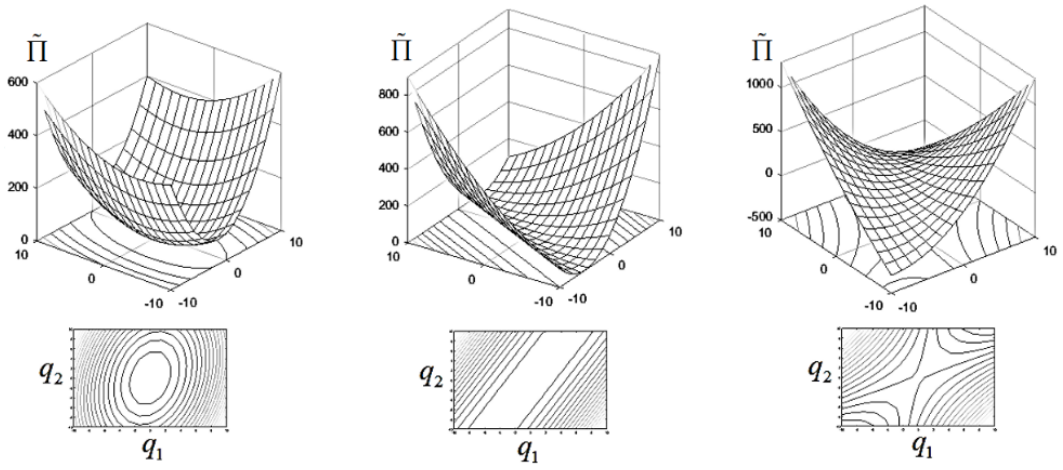

a) Stable equilibrium b) Critical equilibrium c) Unstable equilibrium

Figure 4.2.2: Illustrative example – Nature of the equilibrium states

The results are summarized in Table 4.2.1, with their graphically representation in Figure 4.2.2. Other fundamental matrix representation of equation (4.2.22) has the form

$$\tilde{\Pi}(q_1, q_2; \lambda) = \frac{1}{2}\mathbf{q}^T\left(\tilde{\mathbf{K}} - \lambda\tilde{\mathbf{G}}\right)\mathbf{q} = \frac{1}{2}\begin{pmatrix} q_1 & q_2 \end{pmatrix}\left[\begin{pmatrix} 8 & 0 \\ 0 & 2 \end{pmatrix} - \lambda\begin{pmatrix} 0 & 1 \\ 1 & 0 \end{pmatrix}\right]\begin{pmatrix} q_1 \\ q_2 \end{pmatrix}, \qquad (4.2.23)$$

where $\tilde{\mathbf{G}}$ and $\tilde{\mathbf{K}}$ are the (global) geometric and elastic stiffness matrices of the discrete mechanical system, so that the critical equilibrium state is written as

$$\tilde{\mathbf{K}}\mathbf{q}_{cr} = \lambda_{cr}\tilde{\mathbf{G}}\mathbf{q}_{cr}\ , \qquad (4.2.24)$$

or

$$\left[\tilde{\mathbf{K}} - \lambda_{cr}\tilde{\mathbf{G}}\right]\mathbf{q}_{cr} = \mathbf{0}\ . \qquad (4.2.25)$$

The system of linear equations has a nontrivial solution if and only if the determinant equals zero, i.e.,

$$\det\left(\tilde{\mathbf{K}} - \lambda_{cr}\tilde{\mathbf{G}}\right) = 0\ . \qquad (4.2.26)$$

By solving the above characteristic equation, the buckled shape is found, see Figure 4.2.3, expressed in function of the components of the eigenvector $\mathbf{q}_{cr}$

$$W_{y1}^{cr} = \sqrt{\frac{L^3}{EI_z}}\ q_{cr1}\ , \qquad \phi_1^{cr} = \sqrt{\frac{L}{GJ}}\ q_{cr2}\ . \qquad (4.2.27)$$

In the buckled position, the components of the eigenvector can be scaled arbitrary, satisfying equation (4.2.25). For our illustrative example, we can adopt any value $q_{cr1},\ q_{cr2} \in \mathbb{R} \neq 0$ as long as they fulfil the following relation $q_{cr2}/q_{cr1} = 2$.

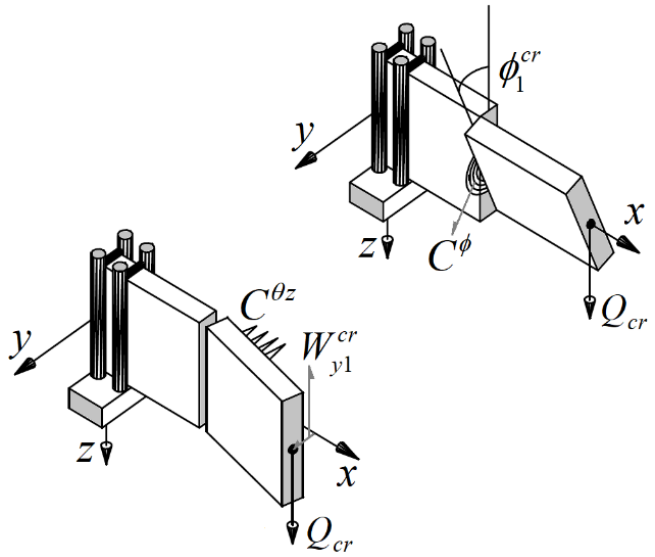

Figure 4.2.3: Illustrative example – Buckling mode components for the critical state

In order to have a complete picture of the stability behaviour, we need the information about the natural (or fundamental or primary) equilibrium path, corresponding to the equilibrium path passing through the origin, i.e.,

$$\mathbf{q} = \mathbf{0} \text{ with } \lambda < \lambda_{cr} \ . \tag{4.2.28}$$

Since the second variation of the total potential energy excludes most of the terms which define the post-buckling behaviour, the secondary paths cannot be fully defined. Therefore, the only information that we can infer is their direction near the bifurcation points, e.g., see Figure 4.2.4.

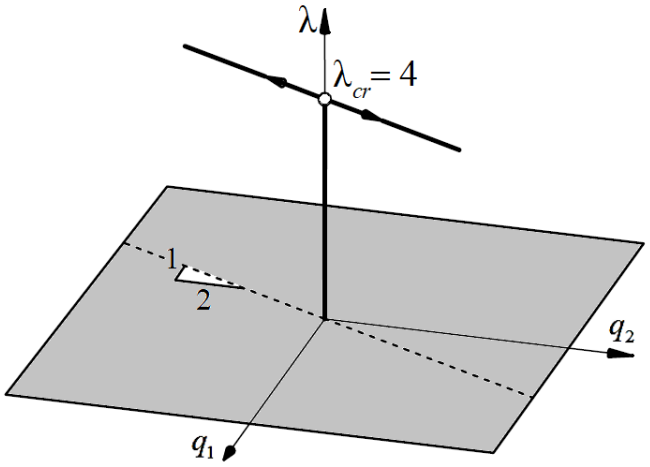

Figure 4.2.4: Illustrative example – Fundamental and linearized bifurcated equilibrium paths

4.3 THE PROBLEM AND ITS PHYSICAL FORMULATION

It is known from the general approach presented in the previous section, that the critical equilibrium state arises from the solution of the variational problem, which expresses the stationarity condition of the total potential energy (4.2.1). In the case of singly symmetric bar-chains (either prismatic or tapered, including the case of flangeless segments, i.e., segments with narrow rectangular cross-sections), their symmetry with respect to the plane defined by their web and the manner in which they are loaded, enable us to assume some simplifications in the (elastic) flexural-torsional buckling phenomenon. Hence, in this section, we define the main assumptions and all the second-order terms that are in common in the expression for the total potential energy, whose complete expression will be defined (separately) in sections below for each type of bar-chain.

4.3.1 The basic assumptions of the flexural-torsional buckling problem

All the bar-chains are defined in a right-handed Cartesian frame of reference *x-y-z*, with undeformed configurations in agreement with the definitions given in chapter 3. Therefore, the following equations are valid for a generic bar-chain, and can obviously still be applied for the particular case of prismatic singly symmetric segments, where the χ-axis should be used instead of the x-axis.

The main hypothesis of the bar-chain model is that the motion of thin-walled open cross-section bars can be described according to the laws of the kinematics of rigid segments (i.e., local buckling is not considered), linked by elastic springs, whose deformations are described by the degrees of freedom corresponding to the displacements (two transverse, and one axial) and the twist rotations around the longitudinal axis. In the following, our main interest is the critical state of bar-chains which, in the fundamental equilibrium configurations, are subjected to compression and/or bending. We also assume that *the pre-buckling (springs') deformations are negligible*.[25] [26]

[25] The effect of in-plane springs' deformations is ignored.

[26] This assumption implies that the segments are assumed to be inextensional, that means, during buckling, axial springs do not deform, and in the case of the lateral-torsional buckling only the transverse loading will be considered in the functional equation.

The first-order discrete equations that govern the axial extension and bending in the plane of loading are uncoupled from the twist rotations ϕ_k and lateral displacements of the segments W_{yk} with $k=1,2,...,\mathrm{n}-1$ (or w_{yk}^{sc} for the case of prismatic singly symmetric bar-chains). Therefore, *at the buckling configuration, the stored elastic energy of the bar-chain model is characterized only by the torsional and lateral bending springs*.

4.3.2 Second-order effects due to the applied loading

The generic bar-chain is subjected to the general system of applied loads and moments caused by the discrete loading distribution q_{zk} and the concentrated forces Q_{zo}, Q_{zL} and quasi-tangential moments M_{yo}, M_{yL}, located at the ends of the bar-chain, as indicated in Figure 4.3.1 (including their points of application z_k^q, z_o, z_L respectively, corresponding to the major plane of stiffness). Recall that ϕ_k, W_{yk} (or w_{yk}^{sc}) with $k=1,2,...,\mathrm{n}-1$ are identically zero in the fundamental equilibrium state, to which corresponds the bending moment diagram M_{yk}^F. All the applied loads are conservative, and the work during buckling can be defined as

$$\mathcal{W}_e^{II} = -\frac{1}{2}\left(\sum_k^{\mathrm{n}-1} \left\{ z_k^q q_{zk} \phi_k^{\,2} \right\} \Delta + z_o Q_{zo} \phi_o^{\,2} + z_L Q_{zL} \phi_L^{\,2} \right.$$
$$\left. -2M_{yo}\phi_o D\_W_{y1} - 2M_{yL}\phi_L D\_W_{y\mathrm{n}} \right). \qquad (4.3.1)$$

Finally, it is mentioned that essential boundary conditions should have a mechanical (i.e., physical) representation in the sense that they are in fact real constraints of the generalized displacements.

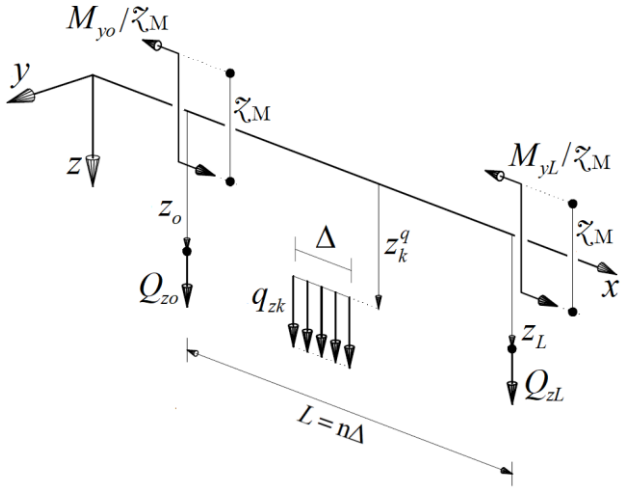

Figure 4.3.1: Applied transverse forces and end moments

4.3.3 Work due to the curvature of the buckled bar-chain

In the deformed configuration, the term

$$\theta_k^{II-y} = \phi_k \theta_k^z \text{ with } k = 1,...,\mathrm{n}-1 \,, \tag{4.3.2}$$

represents the second-order curvature in the loading plane xz, resulting from the (first-order) minor axis curvature

$$\theta_k^z = \Delta D_o^2 W_{yk} \,, \tag{4.3.3}$$

and the discrete rotation ϕ_k. Hence, the bending moment in the fundamental equilibrium state M_{yk}^F with $k = 1,...,\mathrm{n}-1$, induces a work, equal to

$$\mathcal{W}_c^{II} = -\sum_k^{\mathrm{n}-1} \left\{ M_{yk}^F \theta_k^{II-y} \right\} \,.^{27} \tag{4.3.4}$$

The above equation couples the effects of twist and lateral displacement, considering the bending moment about the y-axis.

4.3.4 Elastic stability of bar-chains under axial compression

Concerning the critical load for buckling of (continuous) non-prismatic columns, there are many specialized publications on the subject, e.g., Gere and Carter (1962), Williams and Aston (1989), Siginer (1992), Darbandi et al. (2010), etc. We must emphasize the contributions of Arbabi and Li (1991) & Nikolić and Šalinić (2017), who approximated the continuously varying cross-section by a set of step changes of the profile, proving that the jump discontinuity of the stepped approach converges to the local smoothness of the continuous cross-section. In the case of beam-columns with thin-walled open-cross sections, the flexural-torsional buckling induces a torque due to the second-order effects of the axial loading, often described as the Wagner's torque, e.g., Megson (1975), Chan and Kitipornchai (1987), Alwis and Wang (1996), Xiong and Li (2007) & Trahair (2014).

[27] An alternative interpretation of the decrease in the potential energy of the loading system given in equation (4.3.4) is reported by Trahair (1993) [§ 2.8.4.1], concerning the internal transverse forces (undergoing transverse displacements) and internal torques (undergoing twist rotations).

In the Hencky bar-chain model (either prismatic or tapered), by using the assumption of rigid segments kinematics, the classical Euler buckling results are obtained,[28] i.e., *the effects of pre-buckling shortening and shear deformation are ignored*.[29] In the case of out-of-plane bending (see Figure 4.3.2), the second-order axial shortening is given by the difference between the segment length and its *x*-projection,

$$w_k^{II(\theta z)} \approx \frac{1}{2}\left(D_+ W_{yk}\right)^2 \Delta, \text{ with } k = 1,...,\mathrm{n}-1 \ . \tag{4.3.5}$$

Hence, the total work of the compressive loading is given by

$$\mathcal{W}_{P\theta z}^{II} = \sum_{k}^{\mathrm{n}-1} \left\{ P \ w_k^{II(\theta z)} \right\} \ . \tag{4.3.6}$$

In the case of the effect of the compressive load under twisting, consider the deformed configuration of the x-axis fiber shown in Figure 4.3.2, where the cross-section planes in the undeformed and buckled configurations[30] are defined by ψ_k and Ψ_k respectively (with $k = 1,...,\mathrm{n}-1$). Since the lateral stiffness of the bar-chain is lower than its in-plane stiffness, the displacements W_{yk}^{dAk} and W_{zk}^{dAk} of the differential area of the cross-section, can be approximated by

$$W_{yk}^{dAk} = W_{yk} - z_k^{dAk}\phi_k \ , \qquad W_{zk}^{dAk} = y_k^{dAk}\phi_k \ ,^{31} \tag{4.3.7}$$

where the differential axial load is defined by

$$dP_k = \left(\frac{dA_k}{A_k} \right) P \ , \ k = 1,...,\mathrm{n}-1 \ . \tag{4.3.8}$$

Therefore, in the deformed configuration Ψ_k, transverse forces $d\mathrm{f}_{yk}^{dAk}$ and $d\mathrm{f}_{zk}^{dAk}$ arise,

$$d\mathrm{f}_{yk}^{dAk} = dP_k \left(D_+ W_{yk}^{dAk} \right)\Big|_{z_k^{dAk}} \ , \qquad d\mathrm{f}_{zk}^{dAk} = dP_k \left(D_+ W_{zk}^{dAk} \right)\Big|_{y_k^{dAk}} \ . \tag{4.3.9}$$

Hence, they induce a twist moment equal to

$$dT_k^{P\phi} = -z_k^{dAk} d\mathrm{f}_{yk}^{dAk} + y_k^{dAk} d\mathrm{f}_{zk}^{dAk} \ , \ k = 1,...,\mathrm{n}-1 \ . \tag{4.3.10}$$

---

[28] See for example: Challamel et al. (2013), Challamel et al. (2014a), Challamel et al. (2014b), Zhang et al. (2016a), Zhang et al. (2016b), Zhang et al. (2017) and Ruocco et al. (2017).

[29] These assumptions are valid when the (lateral) inverse slenderness ratio of any cross-section, i.e., $\sqrt{I_{zk} / (A_k L^2)}$ with $k = 0,1,...,\mathrm{n},$ is less or equal than 0,01 for clamped-hinged and clamped-clamped columns, and, less or equal than 0,005 for clamped-free and hinged-hinged columns (Xiang et al. 1992).

[30] The so-called flexural plane (Gjelsvik 1981) [p. 171].

[31] $z_k^{dAk} = Z_k^{dAk}$ and $y_k^{dAk} = Y_k^{dAk}$ with $k = 1,...,\mathrm{n}-1$.

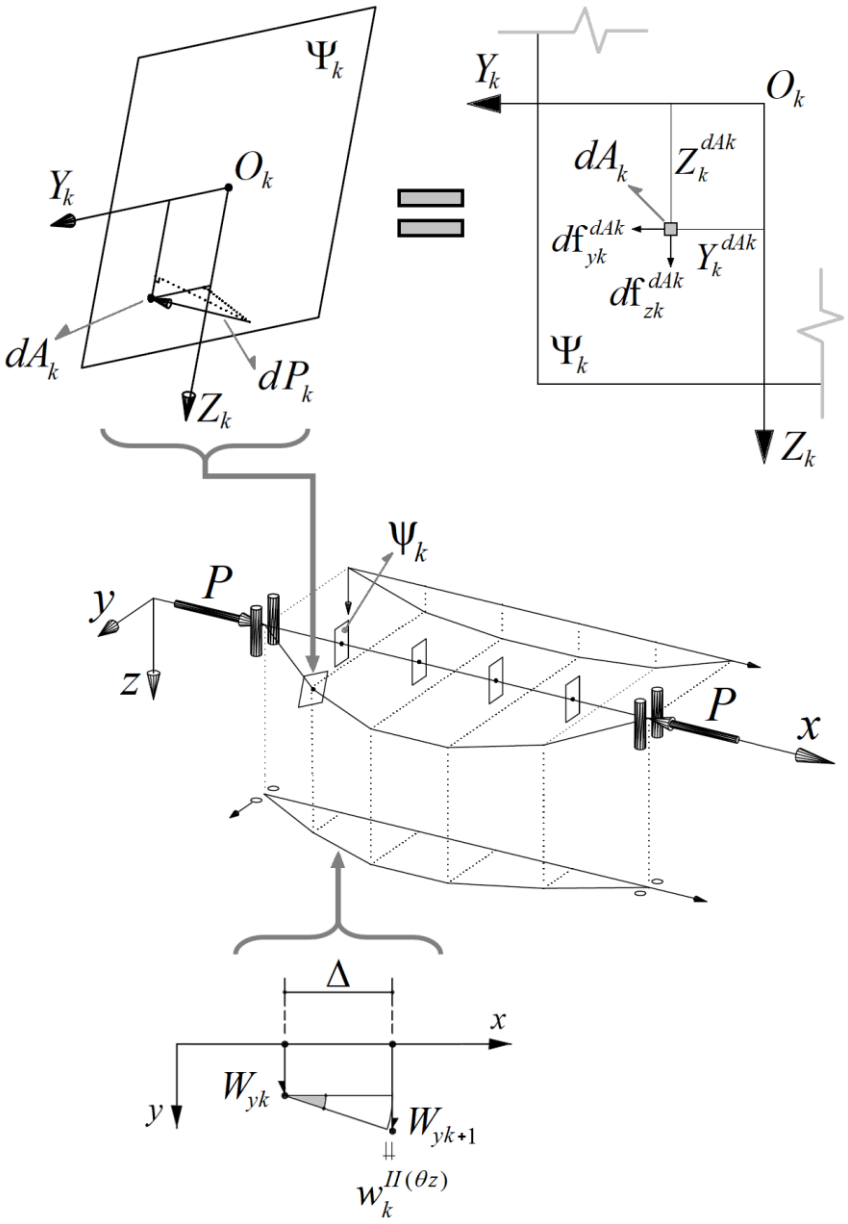

Figure 4.3.2: Cross-section planes before and after flexural-torsional buckling

Integrating over the cross-section

$$T_k^{P\phi} = P\left(-\frac{S_{yk}}{A_k} D_+ W_{yk} + r_{ok}^2 D_+ \phi_k \right),\ k = 1,...,\mathrm{n}-1 \tag{4.3.11}$$

where S_{yk} and r_{ok} are the cross-sectional properties of the bar, i.e., the (i) first moment of area, and the (ii) polar radius of gyration. So, the total work of the twist moment (4.3.11) is given by

$$\mathcal{W}_{P\phi}^{II} = \frac{P}{2} \sum_k^{\mathrm{n}-1} \left\{ -\frac{2S_{yk}}{A_k} D_+ W_{yk} D_+ \phi_k + r_{ok}^2 \left(D_+ \phi_k \right)^2 \right\}. \tag{4.3.12}$$

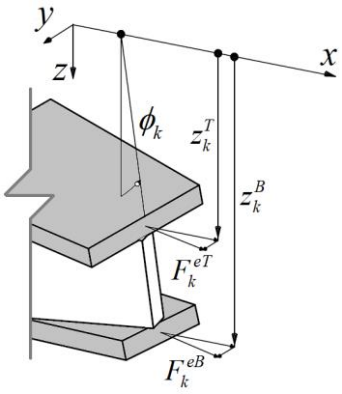

Figure 4.3.3: The out-of-balance forces due to the twist of the flanges

Once expressions (4.3.6) and (4.3.12) have been determined, the second-order effect of the axial compressive load has the following form

$$\mathcal{W}_P^{II} = \mathcal{W}_{P\theta z}^{II} + \mathcal{W}_{P\phi}^{II} \ . \tag{4.3.13}$$

To incorporate the out-of-balance forces due to the twist of the flanges (see Figure 4.3.3), we can simplify the problem by assuming that only the effective forces on the flanges (i.e., the component- x of the axial forces), produce the internal bending moment

$$M_{yk}^F = z_k^T F_k^{eT} + z_k^B F_k^{eB} \ . \tag{4.3.14}$$

Therefore, the disturbing torque T_k^d is easily determined as

$$T_k^d = F_k^{eB}(z_k^B)^2 D_+\phi_k + F_k^{eT}(z_k^T)^2 D_+\phi_k = M_{yk}^F \beta_{yk} D_+\phi_k \ , \tag{4.3.15}$$

where the additional term β_{yk}, is defined as

$$\beta_{yk} = \frac{\left(z_k^B\right)^2 - \left(z_k^T\right)^2}{h_k} \ , \tag{4.3.16}$$

representing a geometric property of the monosymmetric cross-section,[32] related to the asymmetry of the flanges. Hence, its internal work over all the bar-chain is given by

$$\mathcal{W}_d^{II} = -\frac{1}{2}\sum_k^{n-1}\left\{M_{yk}^F \beta_{yk}\left(D_+\phi_k\right)^2\right\}\Delta \ . \tag{4.3.17}$$

For the particular case of prismatic bar-chains,[33] equation (4.3.16) is reduced to

$$\frac{\beta_{yk}}{h_k} \coloneqq \frac{\beta_y}{h} = \left(\Upsilon_B^{sc}\right)^2 - \left(\Upsilon_T^{sc}\right)^2 = 2\Upsilon_B^{sc} - 1 \ .^{34\ 35} \tag{4.3.18}$$

---

[32] Chen and Atsuta (1977) [p. 55] called it "the Wagner coefficient."

[33] For prismatic bar-chains the position vector refers to the χ -axis, i.e., $z_k^T / h_k \coloneqq -\Upsilon_T^{sc}$ and $z_k^B / h_k \coloneqq \Upsilon_B^{sc}$.

[34] The non-dimensional ratio Υ_B^{sc} is better known as the degree of monosymmetry (Mohammadi et al. 2016).

[35] Kitipornchai and Trahair (1980) studied empirical expressions to compute the coefficient β_y, having proposed one: $\beta_y \approx (9/10)\left(2\Upsilon_B^{sc} - 1\right)\left(1 - \left(I_z / I_y\right)^2\right)h$. Since $I_y \gg I_z$, equation (4.3.18) represents a reasonable approximation.

4.4 FORMULATION OF THE DISCRETE PROBLEM OF STABILITY

Mathematics is the cheapest science. Unlike physics or chemistry,
it does not require any expensive equipment. All one needs is a pencil and paper.
POLYA GEORGE, *SPEAKING OF SCIENCE*

It is known from the general approach presented in the previous sections, that the critical equilibrium state arises from the stationarity of the total potential energy (4.2.1). Therefore, we are going to formulate the general discrete equations for the flexural-torsional buckling of tapered singly symmetric I-section beam-columns, beginning with the flangeless members – i.e., members with narrow rectangular cross-section – and prismatic members that can be treated as special cases of the tapered bar-chain. The procedure is similar for all types of bar-chain models, since the spring characterization is given by the torsional and the (lateral) flexural springs. Additionally, the only difference between singly symmetric and doubly symmetric segments, will be the definition of an unbalance torque due to the asymmetry of the flanges.

4.4.1 Prismatic and (linearly) tapered strip bar-chain model

Prismatic or tapered strip bar-chains of length L, are composed of n rigid segments with length $\Delta = L/\mathrm{n}$ (see Figures 4.4.1-4.4.2).

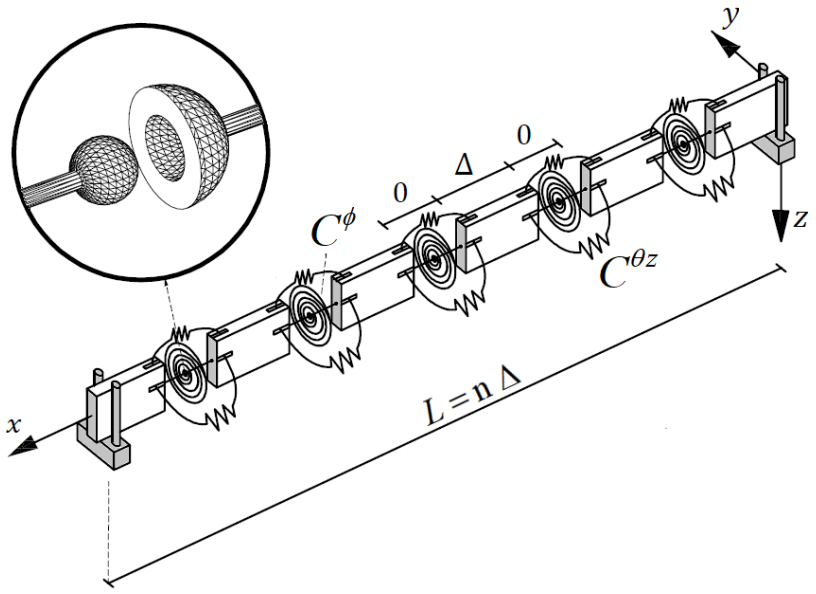

Figure 4.4.1: Bar-chain model of a simply supported (with forks) prismatic strip bar

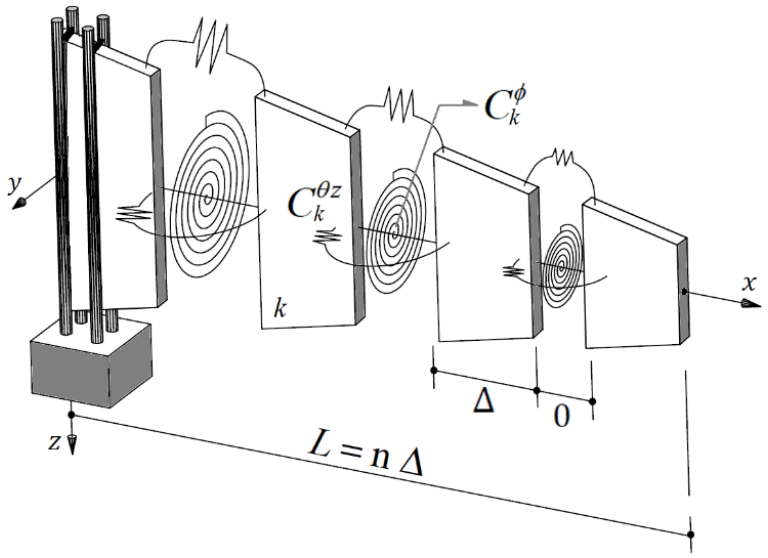

Figure 4.4.2: Tapered bar-chain model of a cantilever strip bar

These segments are defined similarly, such that, the initial configuration is described by the longitudinal centroidal axis, that coincides with the *x*-axis, and the cross-section major and minor central axes correspond to the *y*- and *z*- directions respectively. Hence, the kinematics for a generic segment (either prismatic or tapered) is defined by the lateral displacements W_{yk-1}, W_{yk} and the twist rotation ϕ_k, see Figure 4.4.3.

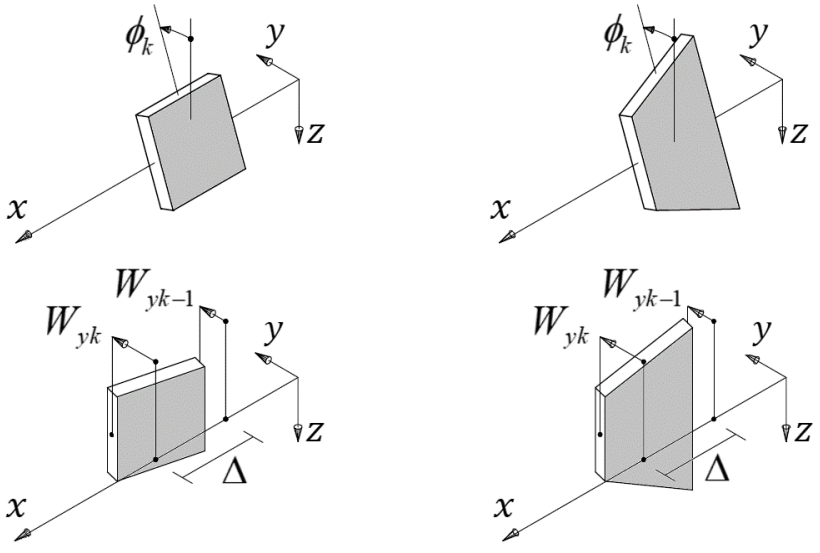

a) Prismatic segment b) Tapered segment

Figure 4.4.3: The degrees of freedom in the strip bar-chain model

Two types of springs are considered, the torsional C_k^{ϕ} and the (lateral) flexural spring $C_k^{\theta z}$, with $k=1,2,...,\mathrm{n}-1$, which are defined by

$$C_k^{\phi}=\frac{GJ_k}{\Delta}\ , \tag{4.4.1}$$

$$C_k^{\theta z}=\frac{EI_{zk}}{\Delta}\ , \tag{4.4.2}$$

where I_{zk} and J_k with $k=1,2,...,\mathrm{n}-1$, are the well-known geometrical properties of the strip-section evaluated at the discrete position k. For the case of prismatic segments, equations (4.4.1)-(4.4.2) get reduced to

$$C^{\phi}=\frac{GJ}{\Delta}\ , \tag{4.4.3}$$

$$C^{\theta z}=\frac{EI_z}{\Delta}\ , \tag{4.4.4}$$

The system of reference adopted allows to describe the springs deformations (either for prismatic or tapered strip segments), due to torsion θ_k^{ϕ} and lateral bending θ_k^{z}, by

$$\theta_k^{z}=\Delta D_o^2 W_{yk}\ , \tag{4.4.5}$$

$$\theta_k^{\phi}=\Delta D_{+}\phi_k\ , \tag{4.4.6}$$

with $k=1,2,...,\mathrm{n}-1$. Hence, the stored elastic energy has the following forms, (i) for the tapered strip bar-chain

$$\mathcal{U}=\frac{1}{2}\sum_{k=1}^{\mathrm{n}-1}\left[C_k^{\theta z}\left(\theta_k^{z}\right)^2+C_k^{\phi}\left(\theta_k^{\phi}\right)^2\right], \tag{4.4.7}$$

and the (ii) prismatic strip bar-chain (as a particular case)

$$\mathcal{U}=\frac{1}{2}\sum_{k=1}^{\mathrm{n}-1}\left[C^{\theta z}\left(\theta_k^{z}\right)^2+C^{\phi}\left(\theta_k^{\phi}\right)^2\right]. \tag{4.4.8}$$

Thus, according to the energy formulation of equations (4.3.1), (4.3.4) and (4.3.13), the total potential energy is reduced to

$$\Pi=\mathcal{U}-\left(\mathcal{W}_e^{II}+\mathcal{W}_c^{II}+\mathcal{W}_P^{II}\right). \tag{4.4.9}$$

Illustrative bar-chain model examples

Now the application of the strip bar-chain model to several illustrative examples is presented. The proposed examples reveal the more important aspects of the discrete process to derive the governing algebraic equations and compute the corresponding critical loads, showing convergence to the values found in the literature.

Illustrative example 1: Prismatic simply supported strip beam-column

As a first illustrative example, consider the prismatic bar-chain model of a simply supported strip beam-column shown in Figure 4.4.4.

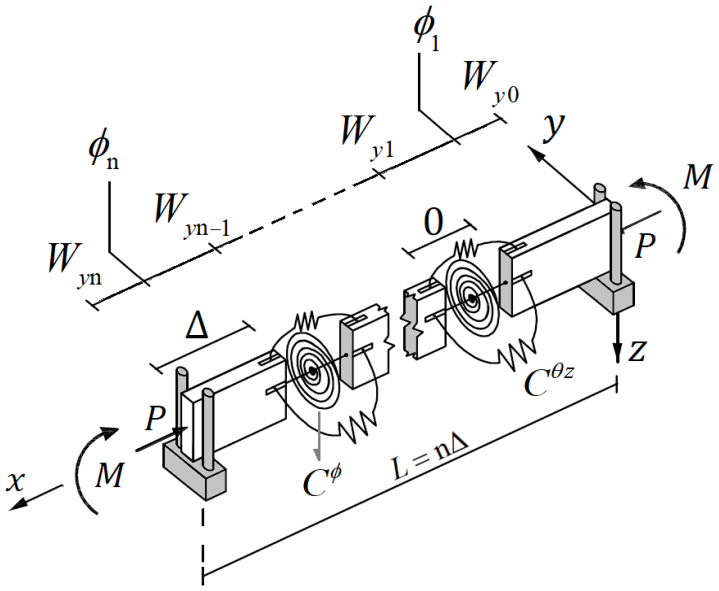

Figure 4.4.4: Prismatic bar-chain model of a simply supported strip beam-column

Using the general equation (4.4.9), the total potential energy is written as

$$\Pi = \frac{1}{2}\sum_{i=1}^{n-1}\left(C^{\theta z}\left(\frac{W_{yi+1}-2W_{yi}+W_{yi-1}}{\Delta}\right)^2 + C^{\phi}\left(\phi_{i+1}-\phi_i\right)^2 \right.$$

$$\left. +2M\,\phi_i\left(\frac{W_{yi+1}-2W_{yi}+W_{yi-1}}{\Delta}\right) - P\,r_o^2\frac{\left(\phi_{i+1}-\phi_i\right)^2}{\Delta}\right) - \frac{P}{2\Delta}\sum_{i=1}^{n}\left(W_{yi}-W_{yi-1}\right)^2 , \quad (4.4.10)$$

with the essential boundary conditions given by

$$W_{y0} = 0 , \qquad W_{yn} = 0 , \quad (4.4.11)$$

$$\phi_1 = 0 , \qquad \phi_n = 0 . \quad (4.4.12)$$

Hence, the stationary values of the adjacent equilibrium equations are respectively

$$\frac{\partial \prod}{\partial W_{yj}} = \frac{C^{\theta z}}{\Delta^2}\left(W_{yj+2} - 4W_{yj+1} + 6W_{yj} - 4W_{yj-1} + W_{yj-2}\right) + \frac{P}{\Delta}\left(W_{yj+1} - 2W_{yj} + W_{yj-1}\right)$$

$$+ \frac{M}{\Delta}\left(\phi_{j+1} - 2\phi_j + \phi_{j-1}\right) = 0 \ , \ j = 2,\ldots,\mathrm{n}-2 \ , \tag{4.4.13}$$

and

$$\frac{\partial \prod}{\partial \phi_j} = \left(\frac{P}{\Delta} r_o^2 - C^{\phi}\right)\left(\phi_{j+1} - 2\phi_j + \phi_{j-1}\right)$$

$$+ \frac{M}{\Delta}\left(W_{yj+1} - 2W_{yj} + W_{yj-1}\right) = 0 \ , \ j = 2,\ldots,\mathrm{n}-1 \ , \tag{4.4.14}$$

where the partial derivatives of the initial and final non null lateral displacements are respectively

$$\frac{\partial \prod}{\partial W_{y1}} = \frac{C^{\theta z}}{\Delta^2}\left(W_{y3} - 4W_{y2} + 5W_{y1}\right) + \frac{P}{\Delta}\left(W_{y2} - 2W_{y1}\right) + \frac{M}{\Delta}\phi_2 = 0 \ , \tag{4.4.15}$$

$$\frac{\partial \prod}{\partial W_{yn-1}} = \frac{C^{\theta z}}{\Delta^2}\left(-5W_{yn-1} + 4W_{yn-2} - W_{yn-3}\right) + \frac{P}{\Delta}\left(2W_{yn-1} - W_{yn-2}\right)$$

$$+ \frac{M}{\Delta}\left(2\phi_{n-1} - \phi_{n-2}\right) = 0 \ . \tag{4.4.16}$$

By defining the following mathematical relations

$$W_{y(-1)} = -W_{y1} \ , \tag{4.4.17}$$

$$W_{yn+1} = -W_{yn-1} \ , \tag{4.4.18}$$

$$\phi_o = \phi_{n+1} = 0 \ , \tag{4.4.19}$$

the adjacent equilibrium equations (4.4.13)-(4.4.16) can be written uniformly as

$$\frac{C^{\theta z}}{\Delta^2}\left(W_{yj+2} - 4W_{yj+1} + 6W_{yj} - 4W_{yj-1} + W_{yj-2}\right)$$

$$+ \frac{P}{\Delta}\left(W_{yj+1} - 2W_{yj} + W_{yj-1}\right) + \frac{M}{\Delta}\left(\phi_{j+1} - 2\phi_j + \phi_{j-1}\right) = 0 \ , \tag{4.4.20}$$

and

$$\left(\frac{P}{\Delta}r_o^2 - C^{\phi}\right)\left(\phi_{j+1} - 2\phi_j + \phi_{j-1}\right) + \frac{M}{\Delta}\left(W_{yj+1} - 2W_{yj} + W_{yj-1}\right) = 0 \ , \tag{4.4.21}$$

with $j = 1,\ldots,\mathrm{n}-1$. Integrating equations (4.4.20) and (4.4.21) twice in the sense of finite increments, we obtain

$$C^{\theta z}\left(W_{yj+1} - 2W_{yj} + W_{yj-1}\right) + PW_{yj}\Delta + M\phi_j\Delta = C_1\, j\,\Delta + C_2 \tag{4.4.22}$$

$$\left(P\, r_o^2 - C^{\phi}\,\Delta\right)\phi_j\Delta + MW_{yj}\Delta = D_1\, j\,\Delta + D_2 \ . \tag{4.4.23}$$

At the ends of the beam-column ($j = 0$ and $j = \mathrm{n}$), we find[36]

$$C_1 = C_2 = 0 \ , \qquad\qquad D_1 = D_2 = 0 \ , \tag{4.4.24}$$

and consequently equation (4.4.23) gets reduced to

$$\phi_j = \frac{M}{GJ - P\, r_o^2}\, W_{yj} \ \text{ with } \ j = 1,\ldots,\mathrm{n}-1 \ . \tag{4.4.25}$$

Introducing this relation in equation (4.4.22), we are left with the problem of solving the following homogeneous second-order difference equation

$$\frac{EI_z}{\Delta^2}\left(W_{yj+1} - 2W_{yj} + W_{yj-1}\right) + \left(P + \frac{M^2}{GJ - P\, r_o^2}\right)W_{yj} = 0 \ , \tag{4.4.26}$$

with $j = 1,\ldots,\mathrm{n}-1$ and $W_{y0} = W_{y\mathrm{n}} = 0$. This difference equation and boundary conditions are consistent with the boundary value problem

$$EI_z\, W_y''(x) + \left(P + \frac{M^2}{GJ - P\, r_o^2}\right)W_y(x) = 0 \ , \tag{4.4.27}$$

with $0 < x < L$ and $W_y(0) = W_y(L) = 0$, in the sense that the local truncation errors tend to zero as $\Delta \to 0$. The discrete equation (4.4.26) can be rewritten in the form

$$W_{yj+1} + \left[\frac{\pi^2}{\mathrm{n}^2}\left(\frac{P}{P_z} + \left(\frac{M}{M_{z\phi}}\right)^2\left(1 - \frac{P}{P_{\phi}}\right)^{-1}\right) - 2\right]W_{yj} + W_{yj-1} = 0 \ \text{ with } \ j = 1,\ldots,\mathrm{n}-1 \ , \tag{4.4.28}$$

[36] Using equations (4.4.11)-(4.4.12).

where

$$P_z = \frac{\pi^2 EI_z}{L^2} \ , \tag{4.4.29}$$

$$P_\phi = \frac{GJ}{r_o^2} \ , \tag{4.4.30}$$

$$M_{z\phi} = \frac{\pi}{L}\sqrt{EI_z GJ} \ . \tag{4.4.31}$$

The characteristic polynomial associated with equation (4.4.28) is

$$p(r) = r^2 + \left[\frac{\pi^2}{\mathrm{n}^2}\left(\frac{P}{P_z} + \left(\frac{M}{M_{z\phi}}\right)^2\left(1-\frac{P}{P_\phi}\right)^{-1}\right) - 2\right] r + 1 \ , \tag{4.4.32}$$

with roots

$$r_{1,2} = \left[1 - \frac{\pi^2}{2\mathrm{n}^2}\left(\frac{P}{P_z} + \left(\frac{M}{M_{z\phi}}\right)^2\left(1-\frac{P}{P_\phi}\right)^{-1}\right)\right] \pm \sqrt{-1 + \left[\frac{\pi^2}{2\mathrm{n}^2}\left(\frac{P}{P_z} + \left(\frac{M}{M_{z\phi}}\right)^2\left(1-\frac{P}{P_\phi}\right)^{-1}\right)\right]^2 - 1} \ . \tag{4.4.33}$$

Three cases can be distinguished: (i) Case 1- $p(r)$ has two distinct real roots, i.e.,

$$\frac{\pi^2}{2\mathrm{n}^2}\left(\frac{P}{P_z} + \left(\frac{M}{M_{z\phi}}\right)^2\left(1-\frac{P}{P_\phi}\right)^{-1}\right) > 2 \tag{4.4.34}$$

or

$$\frac{\pi^2}{2\mathrm{n}^2}\left(\frac{P}{P_z} + \left(\frac{M}{M_{z\phi}}\right)^2\left(1-\frac{P}{P_\phi}\right)^{-1}\right) < 0 \ . \tag{4.4.35}$$

Therefore, the general solution of (i) is

$$W_{yj} = A r_1^j + B r_2^j \ , \tag{4.4.36}$$

and $W_{y0} = W_{y\mathrm{n}} = 0$ if and only if $A = B = 0$ (the trivial solution).

(ii) Case 2- $p(r)$ has a single real root (with multiplicity 2), i.e.,

$$\frac{\pi^2}{2\mathrm{n}^2}\left(\frac{P}{P_z}+\left(\frac{M}{M_{z\phi}}\right)^2\left(1-\frac{P}{P_\phi}\right)^{-1}\right)=2\ , \tag{4.4.37}$$

or

$$\frac{\pi^2}{2\mathrm{n}^2}\left(\frac{P}{P_z}+\left(\frac{M}{M_{z\phi}}\right)^2\left(1-\frac{P}{P_\phi}\right)^{-1}\right)=0\ . \tag{4.4.38}$$

The general solution of (ii) is then

$$W_{yj}=\left(A+B\,j\right)r_1^j \tag{4.4.39}$$

and, once again $W_{y0}=W_{y\mathrm{n}}=0$ if and only if $A=B=0$ (the trivial solution).

(iii) Case 3- $p(r)$ has two conjugate complex roots, i.e.,

$$0<\frac{\pi^2}{2\mathrm{n}^2}\left(\frac{P}{P_z}+\left(\frac{M}{M_{z\phi}}\right)^2\left(1-\frac{P}{P_\phi}\right)^{-1}\right)<2\ , \tag{4.4.40}$$

we can write

$$r_{1,2}=\cos\vartheta\pm\sqrt{-1}\sin\vartheta\ , \tag{4.4.41}$$

where

$$\cos\vartheta=1-\frac{\pi^2}{2\mathrm{n}^2}\left(\frac{P}{P_z}+\left(\frac{M}{M_{z\phi}}\right)^2\left(1-\frac{P}{P_\phi}\right)^{-1}\right)\qquad(0<\vartheta<\pi)\ , \tag{4.4.42}$$

and the general solution of (iii) is then

$$W_{yj}=A\sin(j\,\vartheta)+B\cos(j\,\vartheta)\ , \tag{4.4.43}$$

the boundary conditions yield

$$B=0\ ,\qquad\qquad A\sin(\mathrm{n}\,\vartheta)=0\ . \tag{4.4.44}$$

As a result, the necessary and sufficient condition for non-trivial solutions is given by

$$\sin(\mathrm{n}\,\vartheta)=0\rightarrow\vartheta=\frac{k\,\pi}{\mathrm{n}}\ ,\qquad k=1,\ldots,\mathrm{n}-1\ . \tag{4.4.45}$$

In other words, for non-trivial solutions to exist, M and P must satisfy

$$\left(\frac{M}{M_{z\phi}}\right)^2=\left[\frac{4\mathrm{n}^2}{\pi^2}\sin^2\frac{k\,\pi}{2\mathrm{n}}-\frac{P}{P_z}\right]\left(1-\frac{P}{P_\phi}\right)\ \text{, with } k=1,\ldots,\mathrm{n}-1\ . \tag{4.4.46}$$

Notice that since

$$\lim_{\mathrm{n}\rightarrow+\infty}\left(\frac{4\mathrm{n}^2}{\pi^2}\sin^2\frac{k\,\pi}{2\mathrm{n}}\right)=k^2\ , \tag{4.4.47}$$

for $k=1$ and an infinite number of segments, the first interaction curve of the continuum case,

$$\left(\frac{M}{M_{z\phi}}\right)^2=\left(1-\frac{P}{P_z}\right)\left(1-\frac{P}{P_\phi}\right) \tag{4.4.48}$$

is recovered, e.g., Challamel et al. (2009), see Figure 4.4.5.

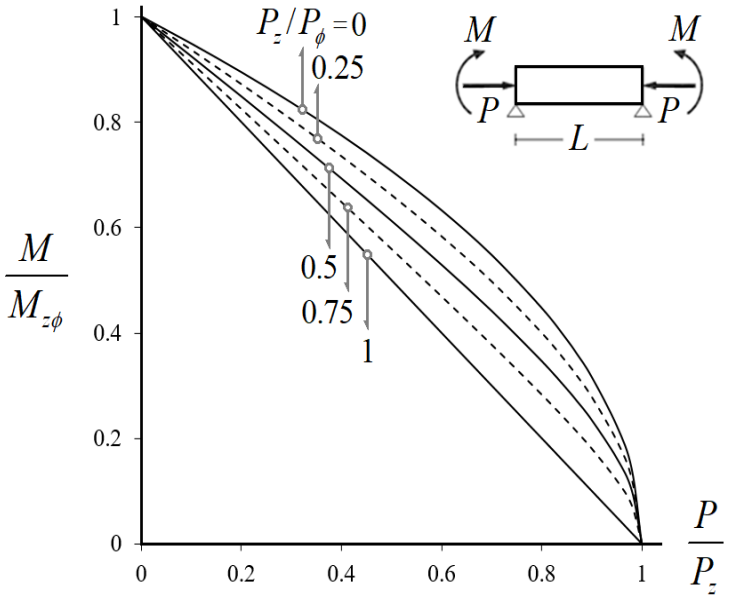

Figure 4.4.5: Interaction buckling diagram of the strip bar-chain model of Figure 4.4.4 when $n\to+\infty$

Illustrative example 2: Prismatic strip bar subjected to concentric loading

Figure 4.4.6 shows the examples with the in-plane loading applied on the axis of shear centres, and the corresponding values of the critical loads computed with the general equation (4.4.9) with n=300. Moreover, Figure 4.4.7 represents the difference between the exact solutions, e.g., Pignataro et al. (1991) [p. 258] and the bar-chain model in function of the number of segments, showing the same rate of convergence in all cases.

Case 1

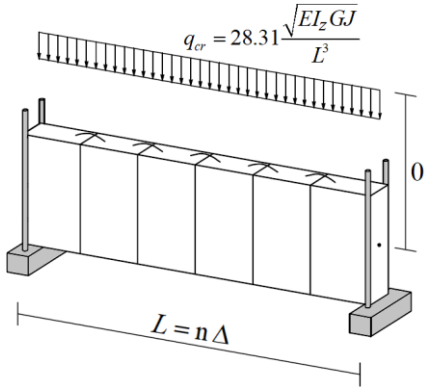

$$M_{cr} = \frac{q_{cr} L^2}{8} = 3.54\frac{\sqrt{EI_z GJ}}{L}$$

a) Simply supported bar-chain under uniformly distributed load

Case 2

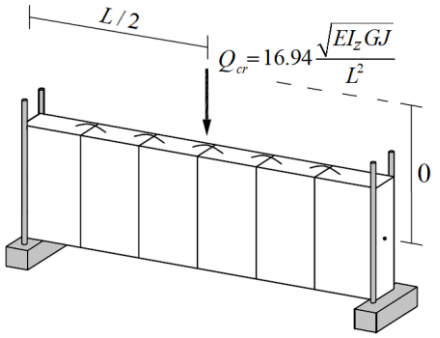

$$M_{cr} = \frac{Q_{cr} L}{4} = 4.24\frac{\sqrt{EI_z GJ}}{L}$$

b) Simply supported bar-chain subjected to a mid-span concentric load

Case 3

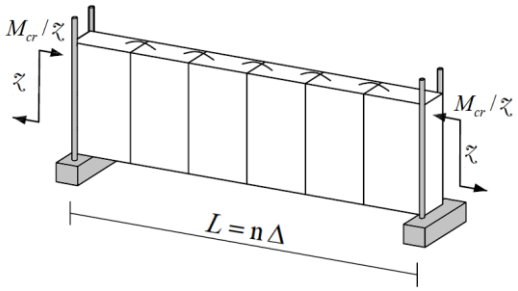

$$M_{cr} = 3.14\frac{\sqrt{EI_z GJ}}{L}$$

c) Simply supported bar-chain subjected to symmetric end moments

Case 4

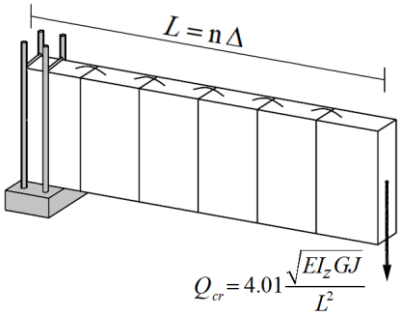

$$M_{cr} = Q_{cr} L = 4.01\frac{\sqrt{EI_z GJ}}{L}$$

d) Bar-chain cantilever supporting a concentric load at the free tip

Figure 4.4.6: Load cases for the strip bar-chain subjected to concentric loading and critical buckling loads, with n=300

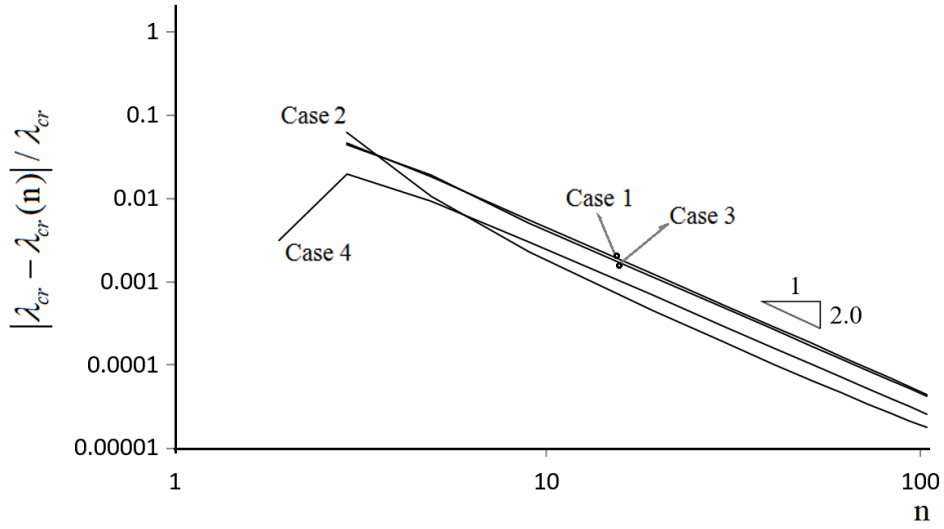

Figure 4.4.7: Strip bar-chain subjected to concentric loading: Convergence rate of the critical buckling loads

As an example let us consider the simply supported bar-chain of case 1, see Figure 4.4.6-a. Its bar-chain model is defined in Figure 4.4.8,[37] where we have chosen to have a rigid segment on the symmetry plane (the other alternative being to have a node on that plane)

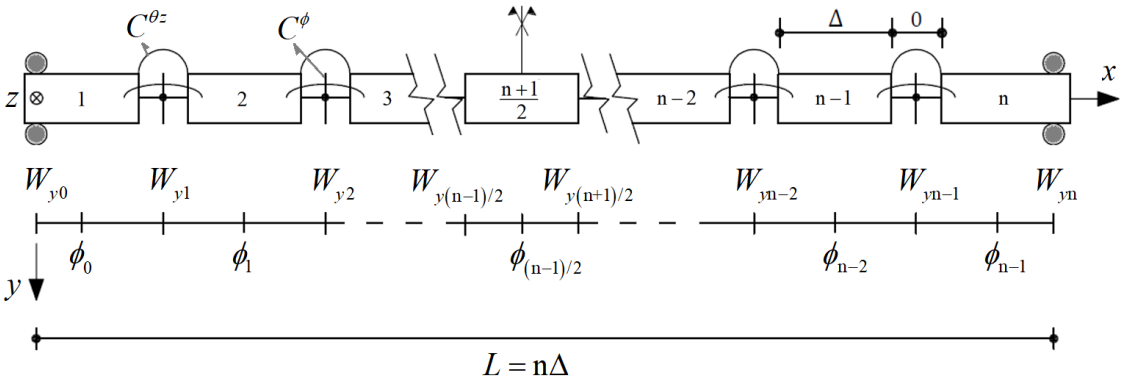

Figure 4.4.8: Bar-chain model of a symmetric simply supported (with forks) strip bar

By using the general equation (4.4.9) and the symmetric configuration of the bar-chain model, the total potential energy is written as

$$\frac{\Pi}{2} = \sum_{k=1}^{(n-1)/2} \left(\frac{1}{2} C^{\theta z} \left(\frac{W_{yk-1} - 2W_{yk} + W_{yk+1}}{\Delta} \right)^2 + \frac{1}{2} C^{\phi} \left(\phi_k - \phi_{k-1} \right)^2 + \frac{q\Delta}{2} k(n-k) \left(W_{yk-1} - 2W_{yk} + W_{yk+1} \right) \phi_k \right), \tag{4.4.49}$$

[37] ϕ_k is defined in more than one section.

where n is an odd number, with the symmetric property given by

$$W_{yi} = W_{yn-i} \text{ for } i = 0,1,...,(n-1)/2 \ , \tag{4.4.50}$$

and

$$\phi_i = \phi_{n-1-i} \text{ for } i = 0,1,...,(n-3)/2 \ .^{38} \tag{4.4.51}$$

The essential boundary conditions are defined as

$$W_{y0} = 0 \ , \qquad W_{yn} = 0 \ , \tag{4.4.52}$$

$$\phi_0 = 0 \ , \qquad \phi_{n-1} = 0 \ . \tag{4.4.53}$$

Therefore, the discrete stationary values W_{yi}, ϕ_i are respectively

$$\frac{1}{2}\frac{\partial \prod}{\partial W_{yi}} = \frac{C^{\theta z}}{\Delta^2}\left(W_{yi+2} - 4W_{yi+1} + 6W_{yi} - 4W_{yi-1} + W_{yi-2}\right)$$

$$+\frac{q\Delta}{2}\left[(i-1)(n-i-1)\phi_{i-1} - 2i(n-i)\phi_i + (i+1)n\phi_{i+1}\right] = 0 \ , \tag{4.4.54}$$

and

$$\frac{1}{2}\frac{\partial \prod}{\partial \phi_i} = C^{\phi}\left(-\phi_{i-1} + 2\phi_i - \phi_{i+1}\right) + \frac{q\Delta}{2} i(n-i)\left(W_{yi-1} - 2W_{yi} + W_{yi+1}\right) = 0 \tag{4.4.55}$$

with

$$i = 1,..,(n-3)/2 \ , \qquad W_{y(-1)} = -W_{y1} \ .^{39} \tag{4.4.56}$$

In addition, the displacement and the twist rotation at the central segment is equal to

$$\frac{1}{2}\frac{\partial \prod}{\partial W_{y(n-1)/2}} = \frac{C^{\theta z}}{\Delta^2}\left(W_{y(n-5)/2} - 3W_{y(n-3)/2} + 2W_{y(n-1)/2}\right)$$

$$+\frac{q\Delta}{8}\left(2(n-1)n\phi_{(n-3)/2} - (n-1)(n+1)\phi_{(n-1)/2}\right) = 0 \ , \tag{4.4.57}$$

and

$$\frac{1}{2}\frac{\partial \prod}{\partial \phi_{(n-1)/2}} = C^{\phi}\left(-\phi_{(n-3)/2} + \phi_{(n-1)/2}\right)$$

$$+\frac{q\Delta}{8}(n-1)(n+1)\left(W_{y(n-3)/2} - W_{y(n-1)/2}\right) = 0 \ . \tag{4.4.58}$$

---

[38] In particular $W_{y(n-1)/2} = W_{y(n+1)/2}$ and $\phi_{(n+1)/2} = \phi_{(n-3)/2}$ at mid span.

[39] This is not an additional condition, it is only the correct arithmetic equivalency in order that equation (4.4.54) gets the same result as $\partial \prod / 2\partial W_{y1} = 0$ (with $W_{y0} = 0$).

The algebraic equations (4.4.54)-(4.4.58) can be written in a matrix (block) equation as

$$\boldsymbol{K}\boldsymbol{q} = \lambda \boldsymbol{G}\boldsymbol{q} \ , \tag{4.4.59}$$

where the symmetric block matrices are defined as follow

$$\underset{2\times 2}{\boldsymbol{K}} = \left[\begin{array}{c|c} \boldsymbol{K}_{zz} & \boldsymbol{0} \\ \hline \boldsymbol{0} & \boldsymbol{K}_{\phi\phi} \end{array}\right], \qquad \underset{2\times 2}{\boldsymbol{G}} = \left[\begin{array}{c|c} \boldsymbol{0} & \boldsymbol{G}_{z\phi} \\ \hline \boldsymbol{G}_{\phi z} & \boldsymbol{0} \end{array}\right] \tag{4.4.60}$$

with

$$\underset{\frac{(n-1)}{2}\times\frac{(n-1)}{2}}{\boldsymbol{K}_{zz}} = \frac{C^{\theta z}}{\Delta^2}\begin{bmatrix} 5 & -4 & 1 & 0 & \cdots & \cdots & \cdots & 0 \\ -4 & 6 & -4 & 1 & 0 & \cdots & \cdots & 0 \\ 1 & -4 & 6 & -4 & 1 & 0 & \cdots & 0 \\ \vdots & \ddots & \ddots & \ddots & \ddots & \ddots & \ddots & \vdots \\ 0 & \cdots & \cdots & 0 & 1 & -4 & 6 & -3 \\ 0 & \cdots & \cdots & \cdots & 0 & 1 & -3 & 2 \end{bmatrix} \tag{4.4.61}$$

$$\underset{\frac{(n-1)}{2}\times\frac{(n-1)}{2}}{\boldsymbol{K}_{\phi\phi}} = C^{\phi}\begin{bmatrix} 2 & -1 & 0 & \cdots & \cdots & \cdots & 0 \\ -1 & 2 & -1 & 0 & \cdots & \cdots & 0 \\ 0 & -1 & 2 & -1 & 0 & \cdots & 0 \\ \vdots & \ddots & \ddots & \ddots & \ddots & \ddots & \vdots \\ 0 & \cdots & \cdots & 0 & -1 & 2 & -1 \\ 0 & \cdots & \cdots & \cdots & 0 & -1 & 1 \end{bmatrix} \tag{4.4.62}$$

$$\underset{\frac{(n-1)}{2}\times\frac{(n-1)}{2}}{\boldsymbol{G}_{z\phi}} = \frac{\sqrt{EI_z GJ}}{2nL^2}\begin{bmatrix} 2(n-1) & -2(n-2) & 0 & \cdots & \cdots & \cdots & 0 \\ -(n-1) & 4(n-2) & -3(n-3) & 0 & \cdots & \cdots & 0 \\ 0 & -2(n-2) & 6(n-3) & -4(n-4) & 0 & \cdots & 0 \\ \vdots & \ddots & \ddots & \ddots & \ddots & \ddots & \vdots \\ 0 & \cdots & \cdots & \cdots & 0 & -\frac{(n-1)}{2} & \frac{(n-1)(n+1)}{4} \end{bmatrix} \tag{4.4.63}$$

$$\underset{\frac{(n-1)}{2}\times\frac{(n-1)}{2}}{\boldsymbol{G}_{\phi z}} = \frac{\sqrt{EI_z GJ}}{2nL^2}\begin{bmatrix} 2(n-1) & -(n-1) & 0 & \cdots & \cdots & \cdots & 0 \\ -2(n-2) & 4(n-2) & -2(n-2) & 0 & \cdots & \cdots & 0 \\ 0 & -3(n-3) & 6(n-3) & -3(n-3) & 0 & \cdots & 0 \\ \vdots & \ddots & \ddots & \ddots & \ddots & \ddots & \vdots \\ 0 & \cdots & \cdots & \cdots & 0 & -\frac{(n-1)(n+1)}{4} & \frac{(n-1)(n+1)}{4} \end{bmatrix} \tag{4.4.64}$$

i.e., $\boldsymbol{G}_{z\phi} = \left(\boldsymbol{G}_{\phi z}\right)^T$ and

$$\boldsymbol{q} = \begin{bmatrix} \boldsymbol{u} \\ \boldsymbol{\varphi} \end{bmatrix}, \qquad \lambda = \frac{qL^3}{\sqrt{EI_z GJ}} \ , \tag{4.4.65}$$

where

$$\underset{(\mathrm{n}-1)/2}{\boldsymbol{u}} = \begin{bmatrix} W_{y1} \\ \vdots \\ W_{y(\mathrm{n}-1)/2} \end{bmatrix}, \qquad \underset{(\mathrm{n}-1)/2}{\boldsymbol{\varphi}} = \begin{bmatrix} \phi_1 \\ \vdots \\ \phi_{(\mathrm{n}-1)/2} \end{bmatrix}. \tag{4.4.66}$$

Hence, the nontrivial solutions are found by solving the following characteristic equation

$$\det\left(\boldsymbol{K} - \lambda \boldsymbol{G}\right) = 0 \ , \tag{4.4.67}$$

and the critical load factor is defined as the minimum value of the set of above solutions

$$\lambda_{cr} = \min\left\{\lambda\right\} \ . \tag{4.4.68}$$

Thus, the critical buckling load is given by

$$q_{cr} = \lambda_{cr} \frac{\sqrt{EI_z GJ}}{L^3} \ . \tag{4.4.69}$$

Illustrative example 3: Tapered cantilever strip bar

As a simple example of a linearly tapered bar-chain, we will compute the critical buckling load of a family of cantilevers whose reference shape is shown in Figure 4.4.9, loaded by an eccentric load at the free tip.

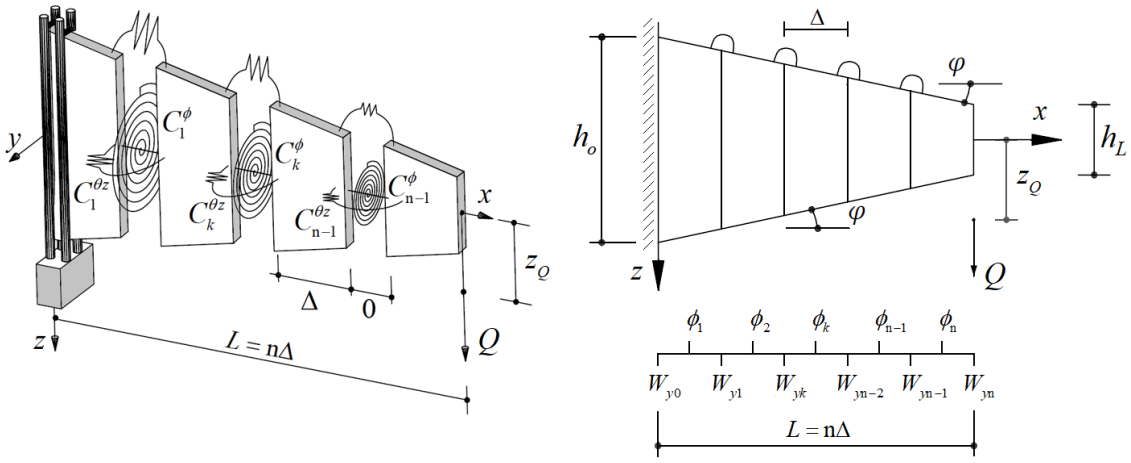

Figure 4.4.9: Linearly tapered bar-chain model of a strip cantilever, loaded by an eccentric load at the free tip

The discrete functional (4.4.9) is defined by

$$\Pi\left(W_{yk},\phi_k;Q\right)=\frac{1}{2}\sum_{k=1}^{\mathrm{n}-1}\left(C_k^{\theta z}\left(\frac{W_{yk-1}-2W_{yk}+W_{yk+1}}{\Delta}\right)^2+C_k^{\phi}\left(\phi_{k+1}-\phi_k\right)^2\right.$$

$$\left.-2Q\left(\mathrm{n}-k\right)\left(W_{yk-1}-2W_{yk}+W_{yk+1}\right)\phi_{k+1}\right)+\frac{1}{2}Q\ \mathrm{z}_Q\left(\phi_{\mathrm{n}}\right)^2\ , \tag{4.4.70}$$

where the springs constants are equal to

$$C_k^{\theta z}=\frac{EI_z(x_k)}{\Delta}\ , \qquad C_k^{\phi}=\frac{GJ(x_k)}{\Delta}\ , \tag{4.4.71}$$

with

$$x_k=k\Delta\ ,\ k=1,2,...,\mathrm{n}-1\ , \tag{4.4.72}$$

and the cross-sectional properties are given by

$$I_z(x)=\left(1-\left(1-\alpha\right)\frac{x}{L}\right)I_z(0)\ , \qquad J(x)=\left(1-\left(1-\alpha\right)\frac{x}{L}\right)J(0)\ , \tag{4.4.73}$$

with $x\in\mathbb{R}\cap\left(0,L\right)$, where the taper ratio α is defined by

$$\alpha=\frac{h_L}{h_o}\ ,\ \left(0<\alpha\le 1\right)\ , \tag{4.4.74}$$

while, due to the support conditions, the first twist rotation is given by

$$\phi_1=0\ , \tag{4.4.75}$$

and the value of the first lateral displacements in the *y*-direction are respectively

$$W_{y0}=0\ , \qquad W_{y1}=0\ . \tag{4.4.76}$$

Therefore, the stationarity condition of equation (4.4.70) requires that

$$\frac{\partial\Pi}{\partial\phi_i}=-C_{i-1}^{\phi}\phi_{i-1}+\left(C_{i-1}^{\phi}+C_i^{\phi}\right)\phi_i-C_i^{\phi}\phi_{i+1}$$

$$-Q\ \left(W_{yi-2}-2W_{yi-1}+W_{yi}\right)\left(\mathrm{n}-i+1\right)\ ,\ i=2,...,\mathrm{n}-1\ , \tag{4.4.77}$$

and

$$\frac{\partial\Pi}{\partial W_{yi}}=\frac{C_{i-1}^{\theta z}}{\Delta^2}\left(W_{yi-2}-2W_{yi-1}+W_{yi}\right)+\frac{2C_i^{\theta z}}{\Delta^2}\left(-W_{yi-1}+2W_{yi}-W_{yi+1}\right)$$

$$+\frac{C_{i+1}^{\theta z}}{\Delta^2}\left(W_{yi}-2W_{yi+1}+W_{yi+2}\right)-Q\left[\left(\mathrm{n}-i+1\right)\phi_i-2\left(\mathrm{n}-i\right)\phi_{i+1}\right.$$

$$\left.+\left(\mathrm{n}-i-1\right)\phi_{i+2}\right]=0\ ,\ i=2,...,\mathrm{n}-2\ , \tag{4.4.78}$$

with the following three natural conditions at the last segment

$$\frac{\partial \Pi}{\partial \phi_{\mathrm{n}}} = C^{\phi}_{\mathrm{n}-1}\left(\phi_{\mathrm{n}} - \phi_{\mathrm{n}-1}\right) - Q\left(W_{y\mathrm{n}-2} - 2W_{y\mathrm{n}-1} + W_{y\mathrm{n}}\right) + Q\, z_Q \phi_{\mathrm{n}} = 0 \ , \tag{4.4.79}$$

$$\frac{\partial \Pi}{\partial W_{y\mathrm{n}-1}} = \frac{C^{\theta z}_{\mathrm{n}-2}}{\Delta^2}\left(W_{y\mathrm{n}-3} - 2W_{y\mathrm{n}-2} + W_{y\mathrm{n}-1}\right) + \frac{2C^{\theta z}_{\mathrm{n}-1}}{\Delta^2}\left(-W_{y\mathrm{n}-2} + 2W_{y\mathrm{n}-1} - W_{y\mathrm{n}}\right)$$
$$+2Q\left(\phi_{\mathrm{n}} - \phi_{\mathrm{n}-1}\right) = 0 \ , \tag{4.4.80}$$

$$\frac{\partial \Pi}{\partial W_{y\mathrm{n}}} = \frac{C^{\theta z}_{\mathrm{n}-1}}{\Delta^2}\left(W_{y\mathrm{n}-2} - 2W_{y\mathrm{n}-1} + W_{y\mathrm{n}}\right) - Q\phi_{\mathrm{n}} = 0 \ . \tag{4.4.81}$$

If we define the following non-dimensional eccentricity ε_o

$$\varepsilon_o = \frac{z_Q}{\alpha L}\sqrt{\frac{EI_z(0)}{GJ(0)}} \ , \tag{4.4.82}$$

the discrete equations (4.4.77)-(4.4.81) are easily written in a programming language. Figure 4.4.10 plots the critical loads in function of the taper ratio α and the non-dimensional eccentricity ε_o, for $\mathrm{n} = 500$, as well the numerical solution of the corresponding continuum model determined by Andrade (2013) [p. 260].

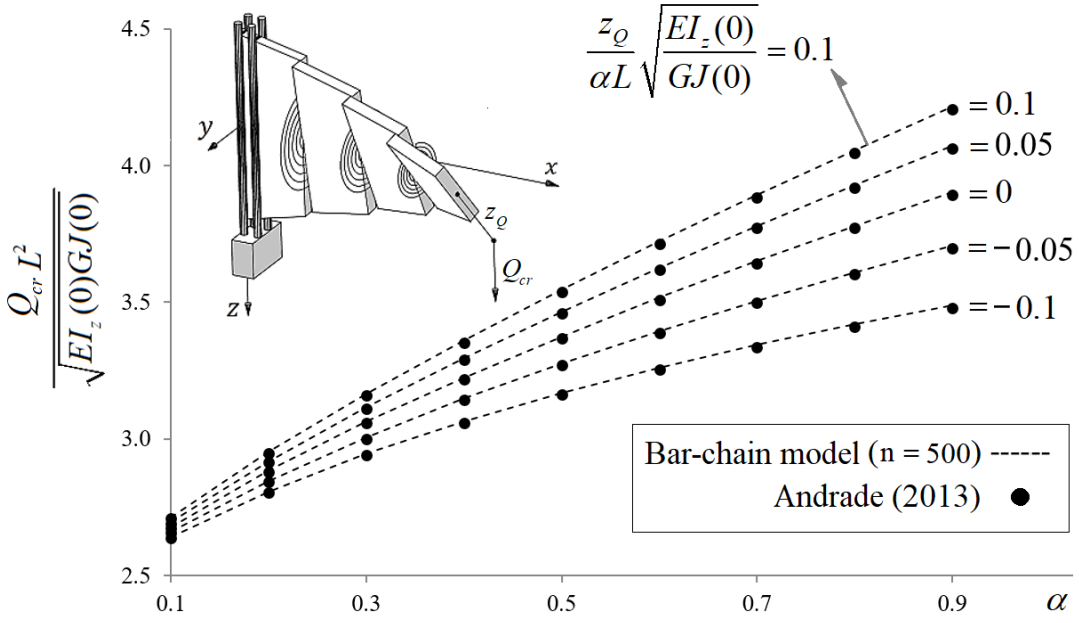

Figure 4.4.10: Linearly tapered strip cantilevers — Non-dimensional critical loads

By computing the residuals of the discrete one-dimensional equations (4.4.77)-(4.4.78)

$$\Delta\left[C^{\theta z}(0)\left(1-\left(1-\alpha\right)\frac{k}{\mathrm{n}}\right)W_y''(x)-Q\mathrm{n}\left(1-\frac{k}{\mathrm{n}}\right)\phi(x)\right]''+O(\Delta^2)=r_{kw}\ , \tag{4.4.83}$$

$$\Delta\left[C^{\phi}(0)\left(1-\left(1-\alpha\right)\frac{k}{\mathrm{n}}\right)\phi'(x)\right]'+Q\mathrm{n}\Delta\left(1-\frac{k}{\mathrm{n}}\right)W_y''(x)+O(\Delta^2)=r_{k\phi}\ , \tag{4.4.84}$$

the essential boundary conditions (4.4.75)-(4.4.76)

$$\left(W_y(0)-W_{yo}\right)+O(\Delta)=r_{1w}\ , \tag{4.4.85}$$

$$\left(\frac{W_{y1}-W_{yo}}{\Delta}-W_y'(0)\right)+O(\Delta)=r_{2w}\ , \tag{4.4.86}$$

$$\left(\phi(0)-\phi_1\right)+O(\Delta)=r_{\phi}\ , \tag{4.4.87}$$

and the natural boundary conditions (4.4.79)-(4.4.81)

$$GJ(L)\phi'(L)+Q\ z_Q\phi(L)+O(\Delta^2)=r_T\ , \tag{4.4.88}$$

$$EI_z(L)W_y'''(L)+\left(\frac{EI_z(L)-EI_z(0)}{L}\right)W_y''(L)+Q\phi(L)+O(\Delta^2)=r_V\ , \tag{4.4.89}$$

$$EI_z(L)W_y''(L)+O(\Delta^2)=r_M\ , \tag{4.4.90}$$

at the limit, i.e., $\Delta\to 0$, the bar-chain model converges to its corresponding 1D continuum model (Andrade 2013) [eq. 5.2.14-5.2.21], i.e.,

$$\left[EI_z(x)W_y''(x)-QL\left(1-\frac{x}{L}\right)\phi(x)\right]''=0\ , \tag{4.4.91}$$

and

$$\left[GJ(x)\phi'(x)\right]'+QL\left(1-\frac{x}{L}\right)W_y''(x)=0\ , \tag{4.4.92}$$

on the open interval $(0,L)$ together with the following boundary conditions

$$W_y(0)=0\ , \tag{4.4.93}$$

$$W_y'(0)=0\ , \tag{4.4.94}$$

$$\phi(0)=0\ , \tag{4.4.95}$$

$$GJ(L)\phi'(L)+Q\ z_Q\phi(L)=0\ , \tag{4.4.96}$$

$$EI_z(L)W_y'''(L)+\left(\frac{EI_z(L)-EI_z(0)}{L}\right)W_y''(L)+Q\phi(L)=0\ , \tag{4.4.97}$$

$$EI_z(L)W_y''(L)=0\ . \tag{4.4.98}$$

Illustrative example 4: Tapered strip beam-column

As a simple example of a bar-chain model for tapered beam-columns, we will compute the critical buckling loads of the family of cantilevers whose reference shape is shown in Figure 4.4.11. The bar-chain is loaded by two conservative point loads: a transverse load Q and an axial compressive load P.

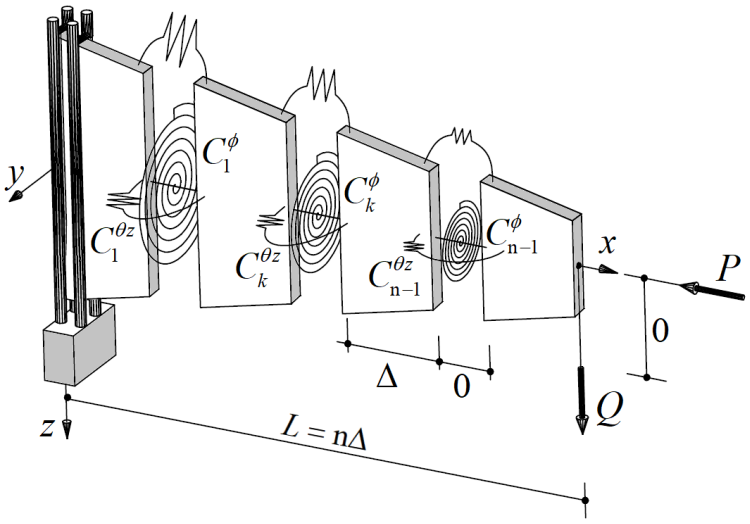

a) Bar-chain model for the strip cantilevered beam-column

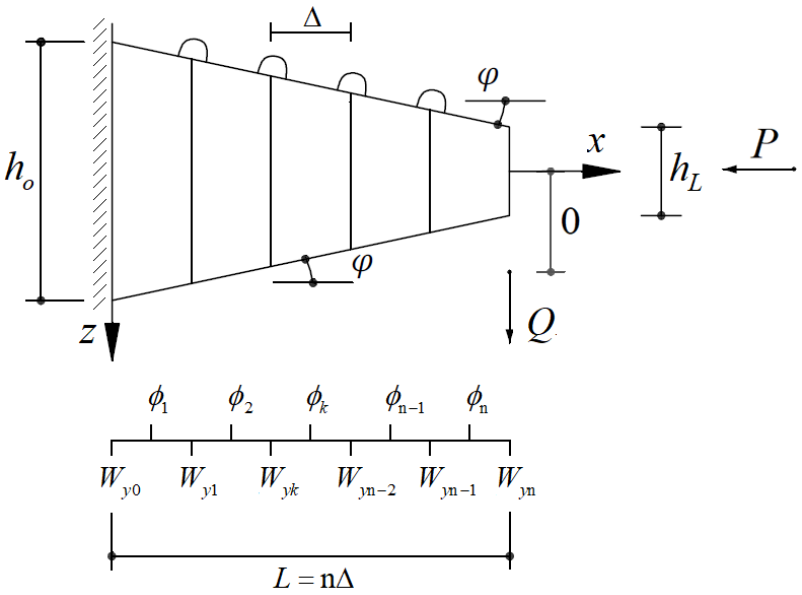

b) Degrees of freedom for the bar-chain model

Figure 4.4.11: Tapered bar-chain model of a cantilevered beam-column, loaded by concentric loads at the free tip

The discrete functional (4.4.9) is defined by

$$\Pi\left(W_{yk},\phi_k;P,Q\right)=\frac{1}{2}\sum_{k=1}^{\mathrm{n}-1}\left(C_k^{\theta z}\left(\frac{W_{yk-1}-2W_{yk}+W_{yk+1}}{\Delta}\right)^2+C_k^{\phi}\left(\phi_{k+1}-\phi_k\right)^2\right.$$

$$\left.-2\phi_{k+1}\left(W_{yk-1}-2W_{yk}+W_{yk+1}\right)\left(\mathrm{n}-k\right)Q-\frac{P}{\Delta}\left(W_{yk+1}-W_{yk}\right)^2\right)\ , \tag{4.4.99}$$

where the springs constants are equal to

$$C_k^{\theta z}=\frac{EI_z(x_k)}{\Delta}\ , \qquad C_k^{\phi}=\frac{GJ(x_k)}{\Delta}\ , \tag{4.4.100}$$

with

$$x_k=k\Delta\ ,\ k=1,2,...,\mathrm{n}-1\ , \tag{4.4.101}$$

and the cross-sectional properties are given by

$$I_z(x)=\left(1-\left(1-\alpha\right)\frac{x}{L}\right)I_z(0)\ , \qquad J(x)=\left(1-\left(1-\alpha\right)\frac{x}{L}\right)J(0)\ , \tag{4.4.102}$$

with $x\in\mathbb{R}\cap\left(0,L\right)$, where the taper ratio α is defined by

$$\alpha=\frac{h_L}{h_o}\ ,\ \left(0<\alpha\le 1\right)\ . \tag{4.4.103}$$

By using the stationarity condition of the total potential energy (4.4.99), i.e., the fundamental lemma of the calculus of variations in its discrete version, we have

$$\frac{\partial\Pi}{\partial\phi_i}=-C_{i-1}^{\phi}\phi_{i-1}+\left(C_{i-1}^{\phi}+C_i^{\phi}\right)\phi_i-C_i^{\phi}\phi_{i+1}$$

$$-Q\ \left(W_{yi-2}-2W_{yi-1}+W_{yi}\right)\left(\mathrm{n}-i+1\right)\ ,\ i=2,...,\mathrm{n}-1\ , \tag{4.4.104}$$

$$\frac{\partial\Pi}{\partial W_{yi}}=\frac{C_{i-1}^{\theta z}}{\Delta^2}\left(W_{yi-2}-2W_{yi-1}+W_{yi}\right)+\frac{2C_i^{\theta z}}{\Delta^2}\left(-W_{yi-1}+2W_{yi}-W_{yi+1}\right)$$

$$+\frac{C_{i+1}^{\theta z}}{\Delta^2}\left(W_{yi}-2W_{yi+1}+W_{yi+2}\right)-Q\left[\left(\mathrm{n}-i+1\right)\phi_i-2\left(\mathrm{n}-i\right)\phi_{i+1}+\left(\mathrm{n}-i-1\right)\phi_{i+2}\right]$$

$$+\frac{P}{\Delta}\left(W_{yi-1}-2W_{yi}+W_{yi+1}\right)=0\ ,\ i=2,...,\mathrm{n}-2\ . \tag{4.4.105}$$

The boundary conditions of the buckling problem are defined by three essential conditions

$$W_{y0}=W_{y1}=\phi_1=0\ , \tag{4.4.106}$$

and the following three natural conditions at the last segment

$$\frac{\partial \Pi}{\partial \phi_{\mathrm{n}}} = C^{\phi}_{\mathrm{n}-1}\left(\phi_{\mathrm{n}} - \phi_{\mathrm{n}-1}\right) - Q\left(W_{y\mathrm{n}-2} - 2W_{y\mathrm{n}-1} + W_{y\mathrm{n}}\right) = 0 \ , \tag{4.4.107}$$

$$\frac{\partial \Pi}{\partial W_{y\mathrm{n}-1}} = \frac{C^{\theta z}_{\mathrm{n}-2}}{\Delta^2}\left(W_{y\mathrm{n}-3} - 2W_{y\mathrm{n}-2} + W_{y\mathrm{n}-1}\right) + \frac{2C^{\theta z}_{\mathrm{n}-1}}{\Delta^2}\left(-W_{y\mathrm{n}-2} + 2W_{y\mathrm{n}-1} - W_{y\mathrm{n}}\right) + 2Q\left(\phi_{\mathrm{n}} - \phi_{\mathrm{n}-1}\right)$$

$$-\frac{P}{\Delta}\left(-W_{y\mathrm{n}} + 2W_{y\mathrm{n}-1} - W_{y\mathrm{n}-2}\right) = 0 \ , \tag{4.4.108}$$

$$\frac{\partial \Pi}{\partial W_{y\mathrm{n}}} = \frac{C^{\theta z}_{\mathrm{n}-1}}{\Delta^2}\left(W_{y\mathrm{n}-2} - 2W_{y\mathrm{n}-1} + W_{y\mathrm{n}}\right) - Q\phi_{\mathrm{n}} - \frac{P}{\Delta}\left(W_{y\mathrm{n}} - W_{y\mathrm{n}-1}\right) = 0 \ . \tag{4.4.109}$$

By solving the above discrete equations, the stability boundaries defined by pairs of P and Q can be determined for several values of the taper parameter α. Figure 4.4.12 represents these interaction buckling diagrams, determined with $\mathrm{n} = 500$ and contrast with the numerical solution of the corresponding 1D continuum model determined by Andrade (2013) [p. 295].

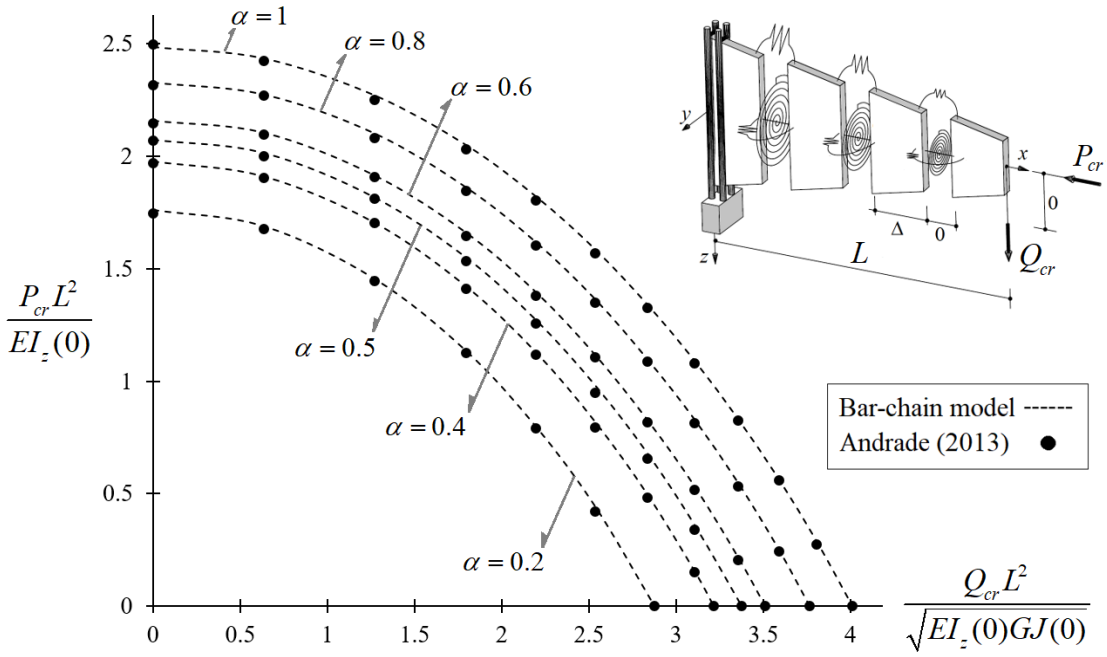

Figure 4.4.12: Tapered strip beam-column ─ Interaction buckling diagram with $\mathrm{n} = 500$

Interestingly, by computing the residuals of the discrete equations (4.4.104)-(4.4.105) and the corresponding essential and natural boundary conditions, i.e., equations (4.4.106) and (4.4.107)-(4.4.109) respectively, we have: (i) for the discrete equations

$$\Delta\left[C^{\theta z}(0)\left(1-(1-\alpha)\frac{k}{\mathrm{n}}\right)W_y''(x)+\frac{P}{\Delta}W_y(x)-Q\mathrm{n}\left(1-\frac{k}{\mathrm{n}}\right)\phi(x)\right]''+O(\Delta^2)=r_{kw}\ , \quad (4.4.110)$$

$$\Delta\left[C^{\phi}(0)\left(1-(1-\alpha)\frac{k}{\mathrm{n}}\right)\phi'(x)\right]'+Q\mathrm{n}\Delta\left(1-\frac{k}{\mathrm{n}}\right)W_y''(x)+O(\Delta^2)=r_{k\phi}\ , \quad (4.4.111)$$

(ii) the essential boundary conditions

$$\left(W_y(0)-W_{yo}\right)+O(\Delta)=r_{1w}\ , \quad (4.4.112)$$

$$\left(\frac{W_{y1}-W_{yo}}{\Delta}-W_y'(0)\right)+O(\Delta)=r_{2w}\ , \quad (4.4.113)$$

$$\left(\phi(0)-\phi_1\right)+O(\Delta)=r_{\phi}\ , \quad (4.4.114)$$

and (ii) the natural boundary conditions

$$GJ(L)\phi'(L)+O(\Delta^2)=r_T\ , \quad (4.4.115)$$

$$EI_z(L)W_y'''(L)+\left(\frac{EI_z(L)-EI_z(0)}{L}\right)W_y''(L)+PW_y'(L)+Q\phi(L)+O(\Delta^2)=r_V\ , \quad (4.4.116)$$

$$EI_z(L)W_y''(L)+O(\Delta^2)=r_M\ . \quad (4.4.117)$$

so that at the limit, the bar-chain model converges to its corresponding 1D continuum model (Andrade 2013) [eq. 5.7.4-5.7.11], i.e.,

$$\left[EI_z(x)W_y''(x)+PW_y(x)-QL\left(1-\frac{x}{L}\right)\phi(x)\right]''=0\ , \quad (4.4.118)$$

and

$$\left[GJ(x)\phi'(x)\right]'+QL\left(1-\frac{x}{L}\right)W_y''(x)=0\ , \quad (4.4.119)$$

on the open interval $(0,L)$ together with the following boundary conditions

$$W_y(0)=0\ , \quad (4.4.120)$$

$$W_y'(0)=0\ , \quad (4.4.121)$$

$$\phi(0) = 0 \ , \tag{4.4.122}$$

$$GJ(L)\phi'(L) = 0 \ , \tag{4.4.123}$$

$$EI_z(L)W_y'''(L) + \left(\frac{EI_z(L) - EI_z(0)}{L}\right)W_y''(L) + PW_y'(L) + Q\phi(L) = 0 \ , \tag{4.4.124}$$

$$EI_z(L)W_y''(L) = 0 \ . \tag{4.4.125}$$

4.4.2 Prismatic I-section bar-chain model

Elastic lateral-torsional buckling analyses of prismatic members have been proposed in several papers, e.g., Flint (1952), Horne (1954), Clark and Hill (1960) & Helwig et al. (1997). Later on, the basic theory of (elastic) torsional-flexural buckling was treated, e.g., Renton (1960), Hone (1967), Pekoz and Winter (1969) & Attard (1992). In the case of discrete bar-chain models, Challamel et al. (2015) developed the Hencky bar-chain model of double symmetric prismatic I-beams (subjected to symmetric end moments) to characterize the lateral-torsional buckling.

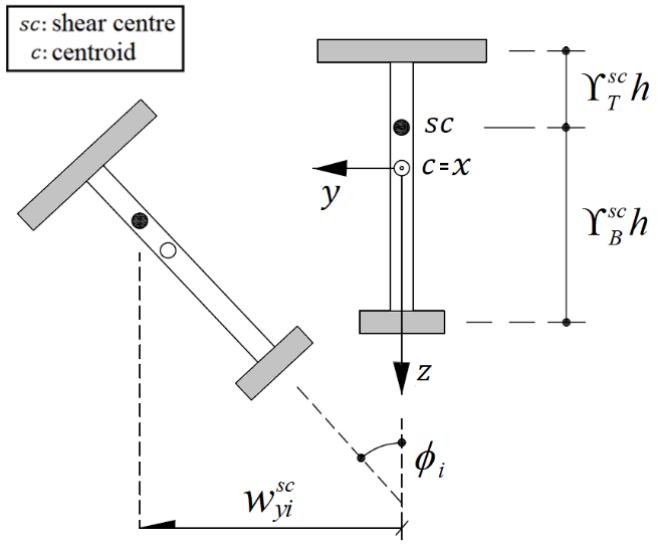

Figure 4.4.13: Degrees of freedom in the lateral-torsional buckling of prismatic bar-chain models

The system of reference adopted in chapter 3 allows to define the degrees of freedom w_{yi}^{sc} and ϕ_i with $k = 1, 2, ..., \mathrm{n}-1$ (see Figure 4.4.13).

Hence the stored elastic energy is defined by

$$\mathcal{U} = \mathcal{U}\left(\theta_i^{\mu}\right),\ i = 1,2,...,\mathrm{n}-1\ , \tag{4.4.126}$$

where the subscript μ defines the type of spring deformations

$$\mu = \left\{Tz, Bz, T\omega, B\omega, \phi\right\}\ . \tag{4.4.127}$$

The labels *T* (top) and *B* (bottom), correspond to the flanges (lateral) rotational springs associated to bending ($\theta_k^{Tz} = \theta_k^{Bz}$) and torsional warping ($\theta_k^{T\omega}$, $\theta_k^{B\omega}$), while the label ϕ corresponds to the torsional spring deformation θ_k^{ϕ}. These deformations are defined by

$$\theta_k^{Tz} = \theta_k^{Bz} = \Delta D_o^2 w_{yk}^{sc} \tag{4.4.128}$$

$$\theta_k^{T\omega} = \Upsilon_T^{sc} h \Delta D_o^2 \phi_k \tag{4.4.129}$$

$$\theta_k^{B\omega} = -\Upsilon_B^{sc} h \Delta D_o^2 \phi_k\ , \tag{4.4.130}$$

$$\theta_k^{\phi} = \Delta D_+ \phi_k\ . \tag{4.4.131}$$

Thus

$$\mathcal{U}\left(\theta_i^{\mu}\right) = \frac{1}{2}\sum_k^{\mathrm{n}-1}\left(C^{T\theta z}\left[\left(\theta_k^{Tz}\right)^2 + \left(\theta_k^{T\omega}\right)^2\right] + C^{B\theta z}\left[\left(\theta_k^{Bz}\right)^2 + \left(\theta_k^{B\omega}\right)^2\right] + C^{\phi}\left(\theta_k^{\phi}\right)^2\right)\ , \tag{4.4.132}$$

rewriting the spring deformations in function of the degrees of freedom w_{yi}^{sc} and ϕ_i, we get the stored elastic energy for the prismatic bar-chain model

$$\mathcal{U}\left(w_{yi}^{sc}, \phi_i\right) = \frac{1}{2}\sum_k^{\mathrm{n}-1}\left[C_z\left(\Delta D_o^2 w_{yk}^{sc}\right)^2 + C_{\omega}\left(\Delta D_o^2 \phi_k\right)^2 + C_{\psi}\left(\Delta D_+ \phi_k\right)^2\right] \tag{4.4.133}$$

where the discrete stiffness coefficients are reduced to

$$C_z = C^{T\theta z} + C^{B\theta z} = \frac{EI_z}{\Delta} \tag{4.4.134}$$

$$C_{\omega} = h^2\left(\left(\Upsilon_T^{sc}\right)^2\ C^{T\theta z} + \left(\Upsilon_B^{sc}\right)^2\ C^{B\theta z}\right) = \frac{EI_{\omega}}{\Delta} \tag{4.4.135}$$

$$C_{\psi} = C^{\phi} = \frac{GJ}{\Delta}\ . \tag{4.4.136}$$

Hence, according to the energy formulation of equations (4.4.133), (4.3.1), (4.3.4), (4.3.13) and (4.3.17)-(4.3.18), the total potential energy is defined by

$$\Pi = \mathcal{U} - \left(\mathcal{W}_e^{II} + \mathcal{W}_c^{II} + \mathcal{W}_P^{II} + \mathcal{W}_d^{II}\right)\ . \tag{4.4.137}$$

Illustrative bar-chain model examples

In the following, the application of the prismatic bar-chain model to several illustrative examples is presented. The proposed examples will offer different types of boundary conditions, and represent several types of analytical procedures, showing convergence to the solutions found in the literature.

Illustrative example 1: Symmetric bars subjected to concentric loading

Figure 4.4.14 shows the bar-chain models of the doubly symmetric bars subjected to concentric loading, whose critical loads are shown in Table 4.4.1, computed using the critical load factor $\lambda_{cr}\left(\kappa_{\omega}\right)$ in function of the the non-dimensional warping rigidity

$$\kappa_{\omega} = \frac{\pi}{L}\sqrt{\frac{EI_{\omega}}{GJ}} \ . \tag{4.4.138}$$

Case 1

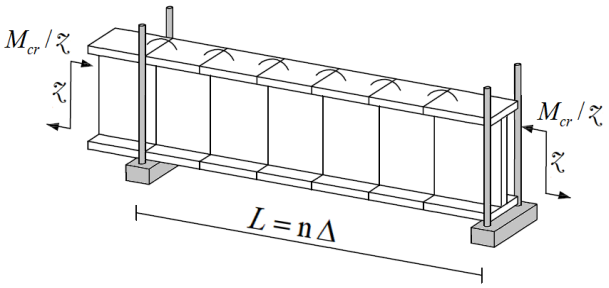

$$M_{cr} = \lambda_{cr} \frac{\sqrt{EI_z GJ}}{L}$$

a) Simply supported bar-chain subjected to symmetric end moments

Case 2

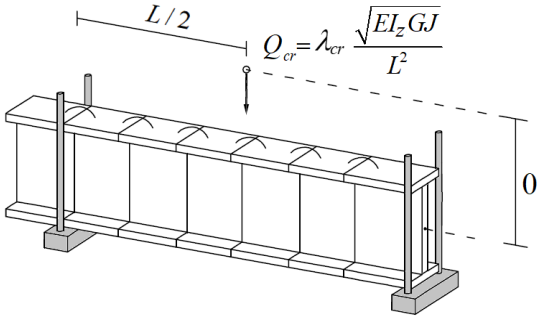

$$M_{cr} = \frac{Q_{cr} L}{4} = \frac{\lambda_{cr}}{4} \frac{\sqrt{EI_z GJ}}{L}$$

b) Simply supported bar-chain subjected to a mid-span concentric load

Case 3

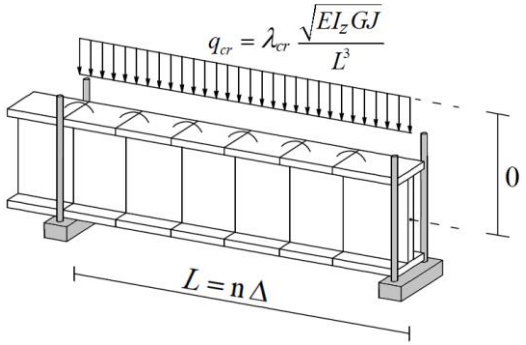

$$M_{cr} = \frac{q_{cr} L^2}{8} = \frac{\lambda_{cr}}{8} \frac{\sqrt{EI_z GJ}}{L}$$

c) Simply supported bar-chain under uniformly distributed load

Case 4

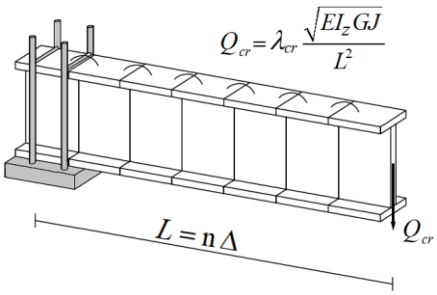

$$M_{cr} = Q_{cr} L = \lambda_{cr} \frac{\sqrt{EI_z GJ}}{L}$$

d) Bar-chain cantilever supporting a concentric load at the free tip

Figure 4.4.14: Load cases for the prismatic bar-chain subjected to concentric loading and critical buckling loads

	$\kappa_\omega = (\pi / L)\sqrt{(EI_\omega / GJ)}$								
Case 1	4.97	1.57	1.11	0.79	0.56	0.39	0.28	0.20	0.14
λ_{cr} (1)	15.78	5.79	4.65	3.96	3.56	3.33	3.23	3.17	3.13
λ_{cr} (2)	15.78	5.85	4.69	4.00	3.60	3.37	3.26	3.20	3.17

Case 2	4.97	1.57	1.11	0.79	0.64	0.56	0.45	0.39	0.35	0.32	0.25	0.20	0.18	0.16
λ_{cr} (1)	86.8	31.9	25.6	21.8	20.3	19.5	18.7	18.3	18.1	17.9	17.5	17.3	17.2	17.2
λ_{cr} (3)	86.4	31.9	25.6	21.8	20.3	19.6	18.8	18.3	18.1	17.9	17.5	17.4	17.2	17.2
λ_{cr} (4)	86.8	31.9	25.6	21.8	---	19.5	---	18.3	---	---	---	---	---	---

Case 3	4.97	1.57	1.11	0.79	0.56	0.39	0.28	0.20	0.14
λ_{cr} (1)	144.1	52.9	42.5	36.1	32.5	30.5	29.4	28.9	28.6
λ_{cr} (4)	144.2	52.9	42.5	36.1	32.5	30.5	29.4	28.9	28.6

Case 4	9.93	2.22	1.57	1.28	1.11	0.79	0.64	0.56	0.50
λ_{cr} (1)	44.33	12.15	9.75	8.69	8.05	6.81	6.25	5.91	5.69
λ_{cr} (3)	44.30	12.20	9.76	8.69	8.03	6.73	6.19	5.87	5.64

(1) Bar-chain model, i.e., equation (4.4.137), with n=300.

(2) Exact solution $\lambda_{cr} = \pi\sqrt{1+(\kappa_\omega)^2}$, e.g., Coates et al. (1988) [eq. 9.6-12].

(3) Timoshenko and Gere (1961) [pp. 251-267] by using the Bessel equation (Gray et al. 1895).

(4) Yoo and Lee (2011) [pp. 339-340], using convergence series.

Table 4.4.1: Critical load coefficients for the prismatic bar-chains of Figure 4.4.14, in function of the non-dimensional warping rigidity κ_ω

As an example, let us consider the simply supported bar-chain of case 1, see Figure 4.4.14-a, whose model is defined in Figure 4.4.15. This model appears not to be fully symmetric, because of the extra segment outside the beam left end, but its advantages will become clear in the following.[40] Its distribution of elasticity is however clearly symmetric. By using equation (4.4.137) the total potential energy is written as

$$\prod = \frac{1}{2}\sum_{k=1}^{n-1}\left(C_z\left(\Delta D_o^2 W_{yk}\right)^2 + C_\omega\left(\Delta D_o^2 \phi_k\right)^2 + C_\psi\left(\Delta D_+ \phi_k\right)^2 + 2M\left(\Delta D_o^2 W_{yk}\right)\phi_k \right), \quad (4.4.139)$$

[40] Certainly the additional segment defined in the simply supported bar-chain needs an important clarification. It represents the physical mechanics in which is possible impost a constraint displacement or twist rotation under the general definition of the kinematic of prismatic (resp. tapered) segments shown in §3.3.1 (resp. §3.4.1).

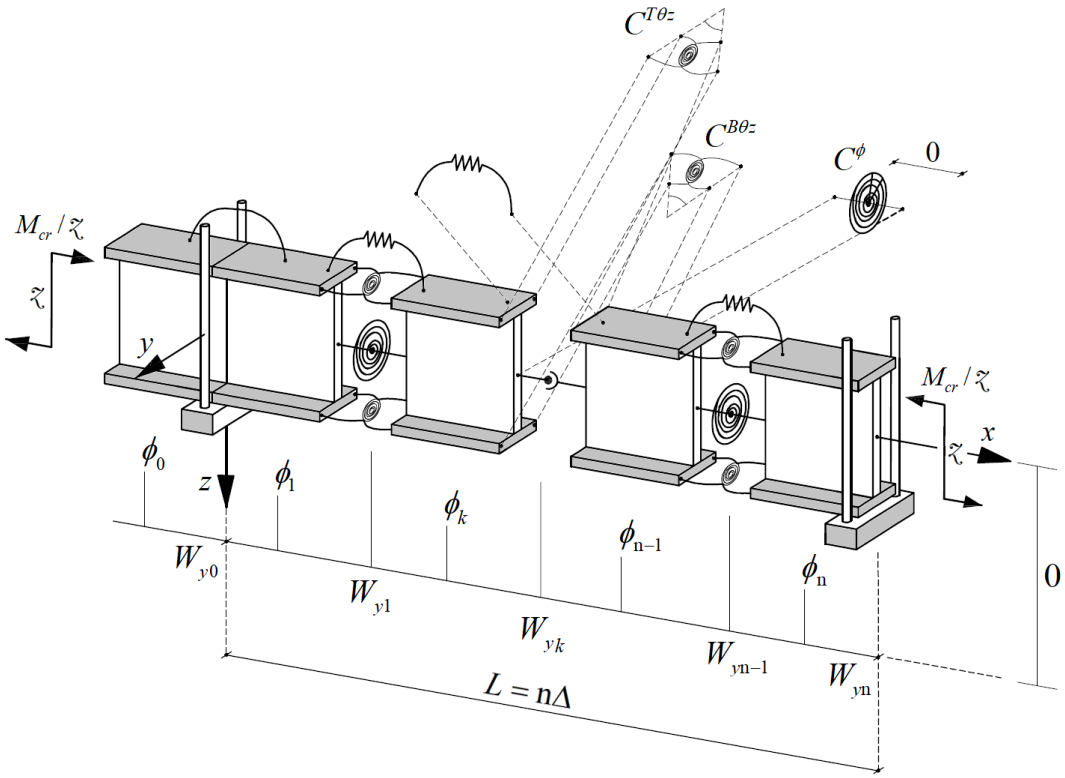

Figure 4.4.15: Bar-chain model of a simply supported (double) symmetric I-beam subjected to symmetric end moments

where the discrete stiffness coefficients are equal to

$$C_z = \frac{EI_z}{\Delta} \ , \qquad C_\omega = \frac{EI_\omega}{\Delta} \ , \qquad C_\psi = \frac{GJ}{\Delta} \ . \tag{4.4.140}$$

The essential boundary conditions are defined by

$$W_{y0} = 0 \ , \qquad W_{yn} = 0 \ , \tag{4.4.141}$$

and

$$\phi_0 = 0 \ , \qquad \phi_n = 0 \ . \tag{4.4.142}$$

Therefore, the stationarity condition of the total potential energy leads to

$$\frac{C_z}{\Delta^2}\left(W_{yi+2} - 4W_{yi+1} + 6W_{yi} - 4W_{yi-1} + W_{yi-2}\right) + \frac{M}{\Delta}\left(\phi_{i-1} - 2\phi_i + \phi_{i+1}\right) = 0 \ , \tag{4.4.143}$$

and

$$C_\psi\left(\phi_{i-1} - 2\phi_i + \phi_{i+1}\right) - \frac{M}{\Delta}\left(W_{yi-1} - 2W_{yi} + W_{yi+1}\right) - \frac{C_\omega}{\Delta^2}\left(\phi_{i+2} - 4\phi_{i+1} + 6\phi_i - 4\phi_{i-1} + \phi_{i-2}\right) = 0 \ , \tag{4.4.144}$$

with $i=1,..,\mathrm{n}$. In order to incorporate all the admissible displacements and rotations into the above discrete equations, the following relations should be defined[41]

$$W_{y(-1)}=-W_{y1}\ , \qquad W_{y\mathrm{n}+1}=-W_{y\mathrm{n}-1}, \tag{4.4.145}$$

$$\phi_{-1}=-\phi_{1}\ , \qquad \phi_{\mathrm{n}+1}=-\phi_{\mathrm{n}-1}\ . \tag{4.4.146}$$

integrating equation (4.4.143) twice in the sense of the difference equations, one gets

$$C_z\left(W_{yi-1}-2W_{yi}+W_{yi+1}\right)+M\phi_i\Delta+c_1 i+c_2=0\ . \tag{4.4.147}$$

Considering $i=0$ since $W_{y-1}=-W_{y1}$, the last equation is reduced to

$$C_z\left(W_{yi-1}-2W_{yi}+W_{yi+1}\right)+M\phi_i\Delta=0\ \text{, with}\ i=1,..,\mathrm{n}\ . \tag{4.4.148}$$

Moreover, by replacing equation (4.4.148) in (4.4.144), the following homogeneous fourth-order difference equation is obtained, which is the discrete equation of the buckling problem

$$\left(\frac{\kappa_\omega \mathrm{n}^2}{\pi}\right)^2\left(\phi_{i+2}-4\phi_{i+1}+6\phi_i-4\phi_{i-1}+\phi_{i-2}\right)-\mathrm{n}^2\left(\phi_{i-1}-2\phi_i+\phi_{i+1}\right)-\lambda^2\phi_i=0 \tag{4.4.149}$$

with $i=1,..,\mathrm{n}$, where the load coefficient λ is defined by

$$\lambda=\frac{ML}{\sqrt{EI_zGJ}}\ . \tag{4.4.150}$$

Then, the characteristic polynomial associated with equation (4.4.149) is given by

$$r^4-\alpha_{11}r^3+\alpha_{12}r^2-\alpha_{11}r+1=0\ , \tag{4.4.151}$$

with

$$\alpha_{11}=4+\left(\frac{\pi}{\kappa_\omega \mathrm{n}}\right)^2\ , \qquad \alpha_{12}=6+2\left(\frac{\pi}{\kappa_\omega \mathrm{n}}\right)^2-\left(\frac{\pi\lambda}{\kappa_\omega \mathrm{n}^2}\right)^2\ . \tag{4.4.152}$$

[41] Equations (4.4.145)-(4.4.146) are not additional conditions, they are the arithmetic equivalency, so that equations (4.4.143)-(4.4.144) can get the same result for $i=1,\mathrm{n}$; when we solve $\partial\prod/\partial W_{yi}=0$ and $\partial\prod/\partial\phi_i=0$ with the boundary conditions (4.4.141)-(4.4.142).

Its roots are equal to

$$r_{1,2} = \cos\vartheta \pm \sqrt{-1}\sin\vartheta \ , \tag{4.4.153}$$

$$r_{3,4} = 0.5\alpha_{11} - \cos\vartheta \pm \sqrt{\left(0.5\alpha_{11} - \cos\vartheta\right)^2 - 1} \ , \tag{4.4.154}$$

where

$$\cos\vartheta = \frac{\alpha_{11}}{4} - \sqrt{\left(\frac{\alpha_{11}}{4} - 1\right)^2 + \left(\frac{\pi\lambda}{2\kappa_\omega \mathrm{n}^2}\right)^2} \ , \tag{4.4.155}$$

Thus, the general discrete solution has the following form

$$\phi_k = c_1\cos(k\vartheta) + c_2\sin(k\vartheta) + c_3(r_3)^k + c_4(r_4)^k \ . \tag{4.4.156}$$

The discrete values (4.4.142)-(4.4.146) yield the non-trivial solution, i.e., $c_1 = c_3 = c_4 = 0$. Thus, the critical mode is obtained as

$$c_2\sin(\mathrm{n}\vartheta) = 0 \rightarrow \vartheta = \frac{\pi}{\mathrm{n}} \ . \tag{4.4.157}$$

In the limit[42]

$$\lim_{\mathrm{n}\to\infty}\left\{\left(1-\cos\left(\frac{\pi}{\mathrm{n}}\right)\right)\mathrm{n}^2\right\} = \lim_{\mathrm{n}\to\infty}\left\{\left(1-\frac{\alpha_{11}}{4}+\sqrt{\left(\frac{\alpha_{11}}{4}-1\right)^2+\left(\frac{\pi\lambda}{2\kappa_\omega \mathrm{n}^2}\right)^2}\right)\mathrm{n}^2\right\} = \frac{\pi^2}{2} \ . \tag{4.4.158}$$

Hence, the critical load factor is given by

$$\lambda_{cr} = \pi\sqrt{1+\left(\kappa_\omega\right)^2} \ , \tag{4.4.159}$$

i.e., the critical buckling moment is equal to

$$M_{cr} = \lambda_{cr}\frac{\sqrt{EI_z GJ}}{L} = \frac{\pi}{L}\sqrt{EI_z GJ\left(1+\frac{\pi^2}{L^2}\frac{EI_\omega}{GJ}\right)} \ , \tag{4.4.160}$$

which is the exact solution, e.g., Coates et al. (1988) [eq. 9.6-12] or Bažant and Cedolin (2003) [eq. 6.3.6]. Figure 4.4.16 represents the error in the critical moment, as function of the number of rigid segments, revealing that it converges linearly.

[42] We know that

$$\lim_{\mathrm{n}\to\infty}\left\{2\mathrm{n}^2\left(1-\cos\left(\frac{\pi}{\mathrm{n}}\right)\right)\right\} = \pi^2 \ .$$

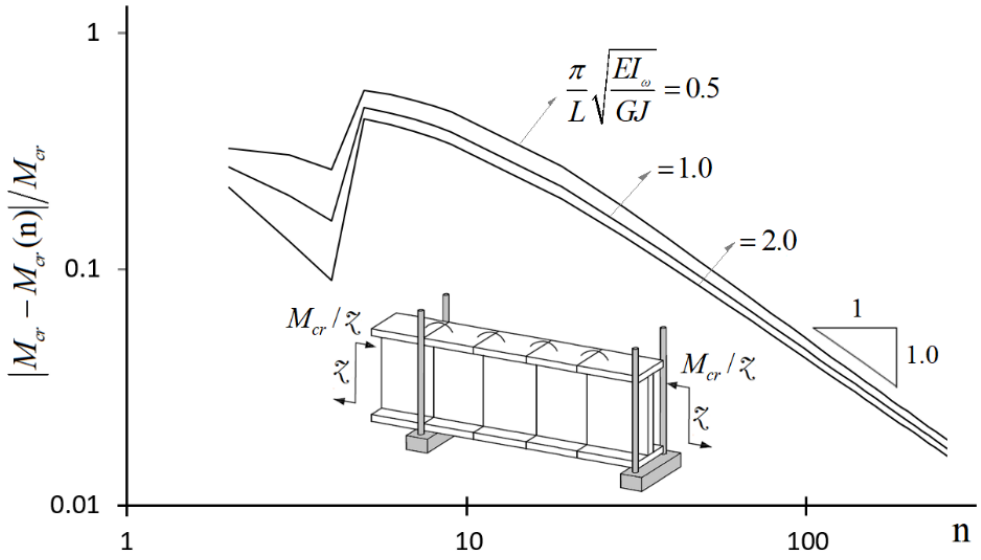

Figure 4.4.16: Simply supported bar-chain subjected to symmetric end moments: Convergence rate of the critical buckling load

Illustrative example 2: Prismatic bars subjected to eccentric loading

Figure 4.4.17 shows the bar-chain models for prismatic bars subjected to eccentric loading. By using equation (4.4.137) is possible get their corresponding critical loads in function of the following non-dimensional eccentricities

$$\frac{z_Q}{L}\sqrt{\frac{EI_z}{GJ}} \quad \text{or} \quad \frac{z_q}{L}\sqrt{\frac{EI_z}{GJ}} \tag{4.4.161}$$

as shown in Figure 4.4.18 for cases 1 to 4. As an example let us consider the cantilever bar-chain of case 1, whose model is defined in Figure 4.4.19. Its essential boundary conditions are given by

$$W_{y0} = W_{y1} = \phi_0 = \phi_1 = 0 \ , \tag{4.4.162}$$

while the discrete first order bending moment is equal to

$$M_{yk}^F = -(\mathrm{n}-k)Q\Delta \ , \ k = 1,...,\mathrm{n}-1 \ . \tag{4.4.163}$$

Thus the potential energy is written as

$$\Pi(W_{yk},\phi_k;Q) = \frac{1}{2}\sum_{k=1}^{\mathrm{n}-1}\left(C_\omega\left(\frac{\phi_{k-1}-2\phi_k+\phi_{k+1}}{\Delta}\right)^2 + C_\psi\left(\phi_{k+1}-\phi_k\right)^2 + C_z\left(\frac{W_{yk-1}-2W_{yk}+W_{yk+1}}{\Delta}\right)^2 \right.$$
$$\left. +2\phi_{k+1}\left(\frac{W_{yk-1}-2W_{yk}+W_{yk+1}}{\Delta}\right)M_{yk}^f \right) + \frac{1}{2}Q\, z_Q\left(\phi_{\mathrm{n}}\right)^2 \ . \tag{4.4.164}$$

Case 1

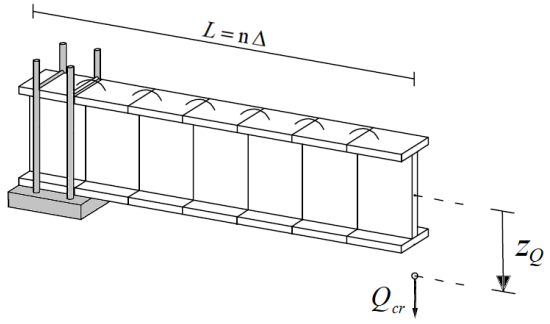

a) Bar-chain cantilever supporting an eccentric load at the free tip

Case 2

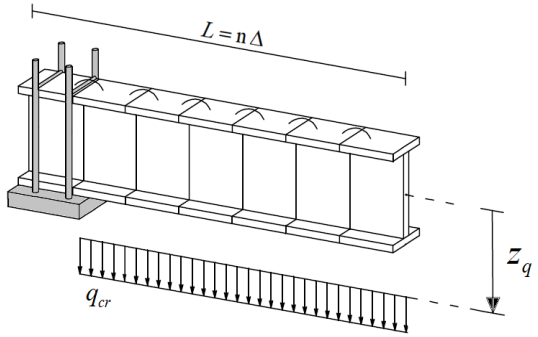

b) Bar-chain cantilever with an eccentric uniformly distributed load

Case 3

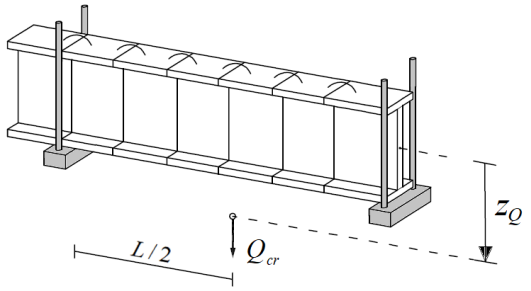

c) Simply supported bar-chain subjected to a mid-span eccentric load

Case 4

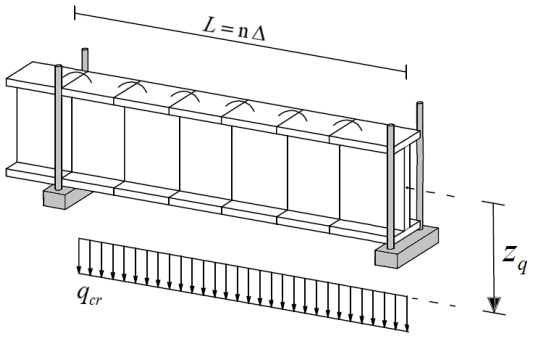

d) Simply supported bar-chain under uniformly distributed load

Figure 4.4.17: Load cases for the prismatic bar-chain subjected to eccentric loading and critical buckling loads

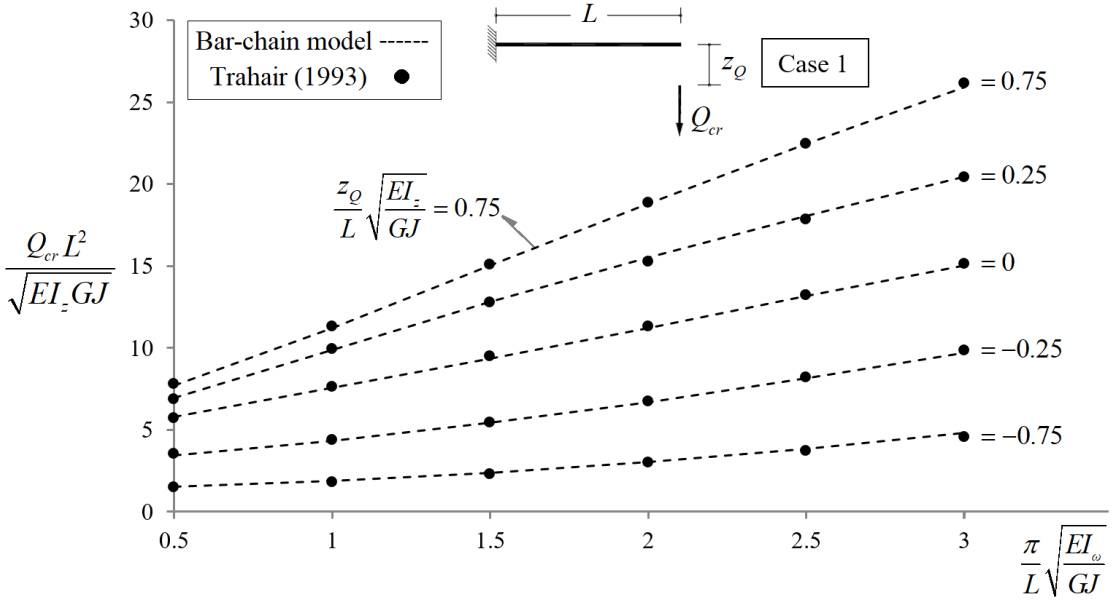

a) Bar-chain cantilever supporting an eccentric load at the free tip (n=300)

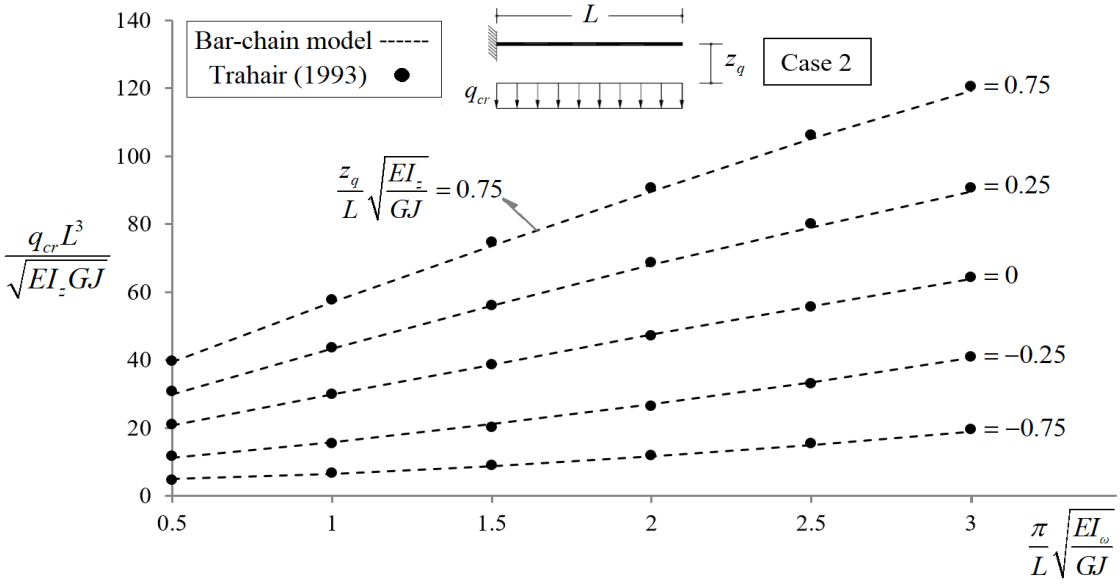

b) Bar-chain cantilever with an eccentric uniformly distributed load (n=300)

Figure 4.4.18: Critical loads of eccentrically loaded prismatic I-beams

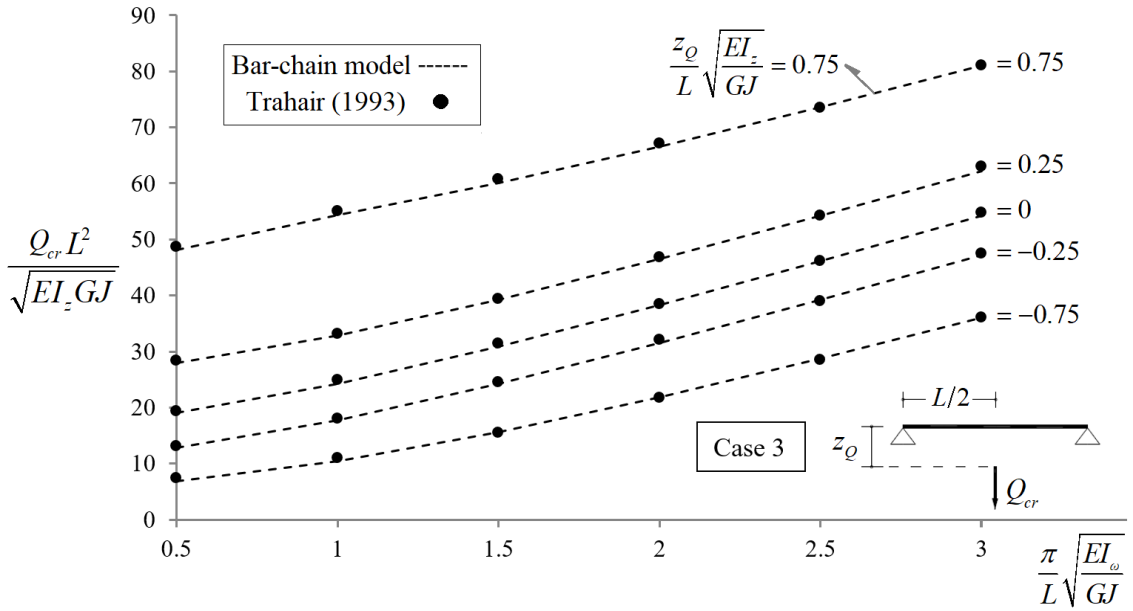

c) Simply supported bar-chain subjected to a mid-span eccentric load (n=300)

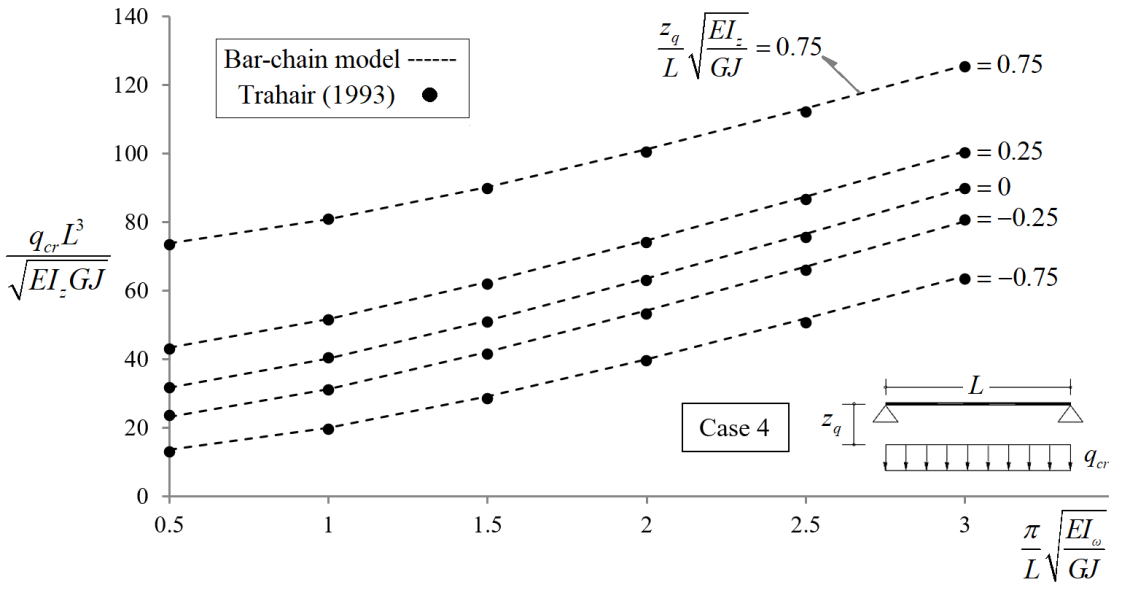

d) Simply supported bar-chain under uniformly distributed load (n=300)

Figure 4.4.18 (continued): Critical loads of eccentrically loaded prismatic I-beams

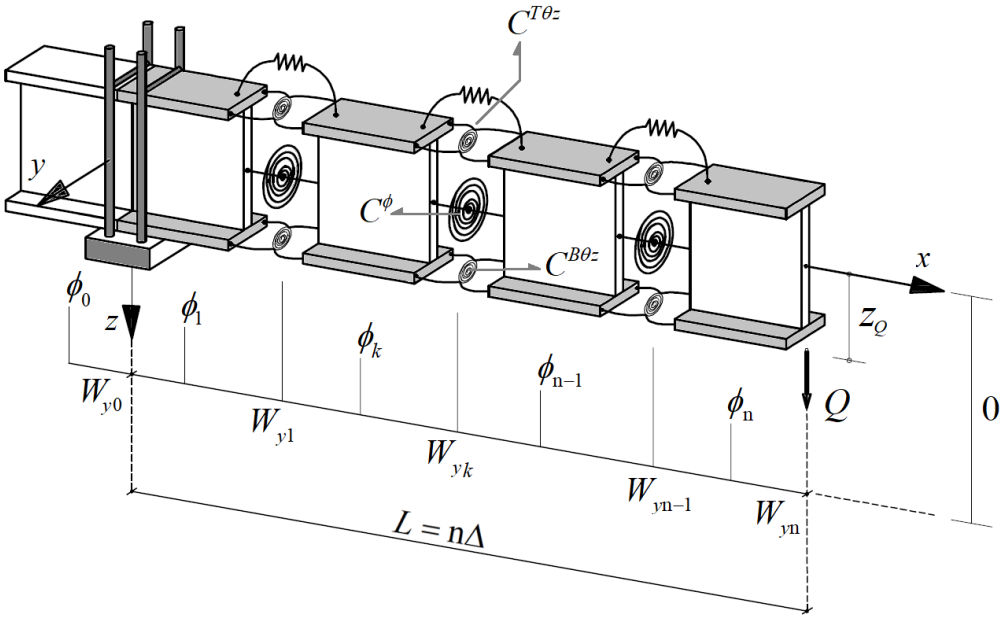

Figure 4.4.19: Bar-chain model of a cantilever I-beam, supporting an eccentric load at its free tip

Now, the vanishing of the first variation of the total potential energy (4.4.164), leads to

$$\frac{\partial \Pi}{\partial \phi_i} = -C_\psi\left(\phi_{i-1} - 2\phi_i + \phi_{i+1}\right) + \frac{C_\omega}{\Delta^2}\left(\phi_{i-2} - 4\phi_{i-1} + 6\phi_i - 4\phi_{i+1} + \phi_{i+2}\right)$$
$$-Q\left(W_{yi-2} - 2W_{yi-1} + W_{yi}\right)\left(\mathrm{n} - i + 1\right) = 0 \ , \ i = 2,...,\mathrm{n}-2 \ . \qquad (4.4.165)$$

and

$$\frac{\partial \Pi}{\partial W_{yi}} = \frac{C_z}{\Delta^2}\left(W_{yi-2} - 4W_{yi-1} + 6W_{yi} - 4W_{yi+1} + W_{yi+2}\right) - Q\left[\left(\mathrm{n} - i + 1\right)\phi_i\right.$$
$$\left. -2\left(\mathrm{n} - i\right)\phi_{i+1} + \left(\mathrm{n} - i - 1\right)\phi_{i+2}\right] = 0 \ , \ i = 2,...,\mathrm{n}-2 \ . \qquad (4.4.166)$$

The application of the natural boundary conditions is given by

$$\frac{\partial \Pi}{\partial \phi_{\mathrm{n}-1}} = -C_\psi\left(\phi_{\mathrm{n}-2} - 2\phi_{\mathrm{n}-1} + \phi_{\mathrm{n}}\right) + \frac{C_\omega}{\Delta^2}\left(\phi_{\mathrm{n}-3} - 4\phi_{\mathrm{n}-2} + 5\phi_{\mathrm{n}-1} - 2\phi_{\mathrm{n}}\right)$$
$$-2Q\left(W_{y\mathrm{n}-3} - 2W_{y\mathrm{n}-2} + W_{y\mathrm{n}-1}\right) = 0 \ , \qquad (4.4.167)$$

$$\frac{\partial \Pi}{\partial \phi_{\mathrm{n}}} = C_\psi\left(\phi_{\mathrm{n}} - \phi_{\mathrm{n}-1}\right) + \frac{C_\omega}{\Delta^2}\left(\phi_{\mathrm{n}-2} - 2\phi_{\mathrm{n}-1} + \phi_{\mathrm{n}}\right)$$
$$-Q\left(W_{y\mathrm{n}-2} - 2W_{y\mathrm{n}-1} + W_{y\mathrm{n}} - z_Q\phi_{\mathrm{n}}\right) = 0 \ , \qquad (4.4.168)$$

$$\frac{\partial \Pi}{\partial W_{y\mathrm{n}-1}} = \frac{C_z}{\Delta^2}\left(W_{y\mathrm{n}-3} - 4W_{y\mathrm{n}-2} + 5W_{y\mathrm{n}-1} - 2W_{y\mathrm{n}}\right) + 2Q\left(\phi_{\mathrm{n}} - \phi_{\mathrm{n}-1}\right) = 0 \ , \qquad (4.4.169)$$

$$\frac{\partial \Pi}{\partial W_{y\mathrm{n}}} = \frac{C_z}{\Delta^2}\left(W_{y\mathrm{n}-2} - 2W_{y\mathrm{n}-1} + W_{y\mathrm{n}}\right) - Q\phi_{\mathrm{n}} = 0 \ . \qquad (4.4.170)$$

If we replace the central discrete values by their exact solutions,

$$\phi_i \coloneqq \phi(x_i) \ , \qquad W_{yi} \coloneqq W_y(x_i) \ , \qquad (4.4.171)$$

with $i = 2,...,\mathrm{n}-2$, in equations (4.4.165)-(4.4.166), the following residuals for each discrete one-dimensional equation are obtained

$$\Delta\left(C_\omega \Delta\phi^{IV}(x_i) - C_\psi \Delta\phi''(x_i) - Q\left(\mathrm{n} - (i-1)\right)\Delta W_y''(x_i)\right) + O(\Delta^3) = r_{\phi i} \qquad (4.4.172)$$

and

$$\left[C_z \Delta W_y^{\ IV}(x_i) - Q\left(\mathrm{n} - \left(i-1\right)\right)\Delta\phi''(x_i) + 2Q\phi'(x_i)\right]\Delta + O(\Delta^3) = r_{ui} \ . \qquad (4.4.173)$$

At the limit $\Delta \to 0$,

$$C_\omega \Delta \to EI_\omega \ , \qquad C_\psi \Delta \to GJ \ , \qquad C_z \Delta \to EI_z \ , \qquad (4.4.174)$$

the residuals converge to zero, and the discrete positions x_i tend to $x \in \mathbb{R} \cap (0, L)$, i.e.,

$$EI_\omega \phi^{IV}(x) - GJ\phi''(x) - Q\left(L - x\right)W_y''(x) = 0 \ , \qquad (4.4.175)$$

and

$$EI_z W_y^{\ IV}(x) - Q\left(L - x\right)\phi''(x) + 2Q\phi'(x) = 0 \ . \qquad (4.4.176)$$

By applying the same methodology to the discrete equations (4.4.167)-(4.4.170), we get the continuous natural boundary conditions at the free tip of the bar

$$EI_\omega \phi''(L) = 0 \ , \qquad (4.4.177)$$

$$-EI_\omega \phi'''(L) + GJ\phi'(L) + Qz_Q\phi(L) = 0 \ , \qquad (4.4.178)$$

$$EI_z W_y''(L) = 0 \ , \qquad (4.4.179)$$

$$EI_z W_y'''(L) + Q\phi(L) = 0 \ , \qquad (4.4.180)$$

while the essential boundary conditions are

$$W_y(0) = \phi(0) = W_y'(0) = \phi'(0) = 0 \ . \qquad (4.4.181)$$

Illustrative example 3: Singly symmetric bar under uniform bending

Let us consider the simply supported bar-chain with length L loaded by a pair of symmetric end moments M. From the several options available for the corresponding bar-chain model, the one represented in Figure 4.4.20 will be employed, which has n segments between the supports connected by $\mathrm{n}-1$ elastic sections.[43]

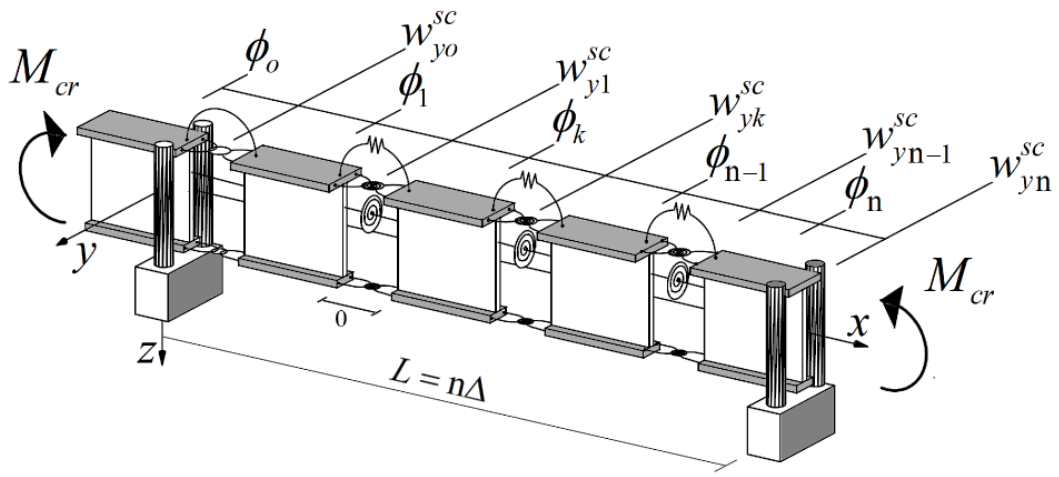

Figure 4.4.20: Prismatic bar-chain under uniform bending

For an arbitrary number of segments between supports $\mathrm{n} > \mathrm{n}_{\min}=2$, the total potential energy (4.4.137) is given by

$$\Pi\left(w_{yk}^{sc},\phi_k;M\right)=\frac{1}{2}\sum_{k=1}^{\mathrm{n}-1}\left(C_z\left(\Delta D_o^2 w_{yk}^{sc}\right)^2+C_\omega\left(\Delta D_o^2\phi_k\right)^2+C_\psi\left(\Delta D_+\phi_k\right)^2\right.$$

$$\left.+\left(\frac{\beta_y}{\Delta}\left(\Delta D_+\phi_k\right)^2+2\phi_k\Delta D_o^2 w_{yk}^{sc}\right)M\right). \qquad (4.4.182)$$

The essential boundary conditions are given by

$$w_{yo}^{sc}=w_{y\mathrm{n}}^{sc}=\phi_o=\phi_{\mathrm{n}}=0\ . \qquad (4.4.183)$$

If we define[44]

$$w_{y(-1)}^{sc}=-w_{y1}^{sc}\ , \qquad w_{y\mathrm{n}+1}^{sc}=-w_{y\mathrm{n}-1}^{sc}\ , \qquad (4.4.184)$$

$$\phi_{-1}=-\phi_1\ , \qquad \phi_{\mathrm{n}+1}=-\phi_{\mathrm{n}-1}\ . \qquad (4.4.185)$$

[43] *Vide supra*, note 40 p. 227.

[44] *Vide supra*, note 41 p. 229.

The stationary condition of the above functional can be written uniformly as

$$\frac{\partial \Pi}{\partial w_{yi}^{sc}} = \frac{C_z}{\Delta^2}\left(w_{yi-2}^{sc} - 4w_{yi-1}^{sc} + 6w_{yi}^{sc} - 4w_{yi+1}^{sc} + w_{yi+2}^{sc} \right) + \frac{M}{\Delta}\left(\phi_{i-1} - 2\phi_i + \phi_{i+1} \right) = 0 \ , \quad (4.4.186)$$

$$\frac{\partial \Pi}{\partial \phi_i} = \frac{C_\omega}{\Delta^2}\left(\phi_{i-2} - 4\phi_{i-1} + 6\phi_i - 4\phi_{i+1} + \phi_{i+2} \right) - \left(C_\psi + \frac{\beta_y M}{\Delta} \right)\left(\phi_{i-1} - 2\phi_i + \phi_{i+1} \right)$$

$$+ \frac{M}{\Delta}\left(w_{yi-1}^{sc} - 2w_{yi}^{sc} + w_{yi+1}^{sc} \right) = 0 \ , \text{ with } i = 1,..,\mathrm{n}-1 \ . \quad (4.4.187)$$

At this stage, it is easy to solve the problem numerically. However, we are also interested in finding an exact solution to the buckling problem. Thus, integrating expression (4.4.186) twice in the sense of finite increments, we obtain

$$C_z \Delta^2 D_o^2 w_{yi}^{sc} + M\Delta\phi_i + c_1 i + c_2 = 0 \ . \quad (4.4.188)$$

The constants c_1, c_2 vanish due to equations (4.4.183)-(4.4.185). Replacing this into expression (4.4.187), with

$$C_z = \frac{EI_z}{\Delta} \ , \qquad C_\omega = \frac{EI_\omega}{\Delta} \ , \qquad C_\psi = \frac{GJ}{\Delta} \ , \quad (4.4.189)$$

we get the non-dimensional homogeneous fourth-order discrete equation

$$\left(\phi_{i-2} - 4\phi_{i-1} + 6\phi_i - 4\phi_{i+1} + \phi_{i+2} \right) - 4\alpha_{11}\left(\phi_{i-1} - 2\phi_i + \phi_{i+1} \right) - 4\alpha_{12}\phi_i = 0 \ , \quad (4.4.190)$$

where

$$\alpha_{11} = \frac{(GJ + \beta_y M)L^2}{4\mathrm{n}^2 EI_\omega} \ , \qquad \alpha_{12} = \frac{M^2 L^4}{4\mathrm{n}^4 EI_\omega EI_z} \ , \quad (4.4.191)$$

The corresponding characteristic equation is obtained by introducing $\phi_i = r^k$,

$$r^4 + 4(1-\alpha_{11})r^3 + 2(3 + 4\alpha_{11} - 2\alpha_{12})r^2 + 4(1-\alpha_{11})r + 1 = 0 \ . \quad (4.4.192)$$

This polynomial can be factorized into a more convenient algebraic expression,

$$\left(\frac{r^2+1}{r} \right)^2 - 4(1+\alpha_{11})\left(\frac{r^2+1}{r} \right) + 4(1 + 2\alpha_{11} - \alpha_{12}) = 0 \ . \quad (4.4.193)$$

whose roots are

$$r_{1,2} = \cos\vartheta \pm \sqrt{-1}\sin\vartheta \ , \quad (4.4.194)$$

$$r_{3,4} = 2 - \cos\vartheta + 2\alpha_{11} \pm \sqrt{\left(2 - \cos\vartheta + 2\alpha_{11} \right)^2 - 1} \ , \quad (4.4.195)$$

with

$$\cos\vartheta = 1 + \alpha_{11} - \sqrt{(\alpha_{11})^2 + \alpha_{12}} \ . \quad (4.4.196)$$

Thus, the general discrete solution has the form

$$\phi_k = c_1 \cos(k\vartheta) + c_2 \sin(k\vartheta) + c_3 (r_3)^k + c_4 (r_4)^k \ . \tag{4.4.197}$$

By replacing the condition $\phi_o = \phi_{\mathrm{n}} = 0$ and (4.4.185), the non-trivial solution corresponds to $c_1 = c_3 = c_4 = 0$ and $c_2 \neq 0$. Hence, the critical mode is obtained as

$$c_2 \sin(\mathrm{n}\vartheta) = 0 \rightarrow \vartheta = \frac{\pi}{\mathrm{n}} \ . \tag{4.4.198}$$

For an infinite number of segments

$$\lim_{\mathrm{n}\to\infty}\left\{\left[1-\cos\left(\frac{\pi}{\mathrm{n}}\right)\right]\mathrm{n}^2\right\} = \lim_{\mathrm{n}\to\infty}\left\{\left[-\alpha_{11}+\sqrt{(\alpha_{11})^2+\alpha_{12}}\right]\mathrm{n}^2\right\} = \frac{\pi^2}{2} \ . \tag{4.4.199}$$

Thus the well-known exact solution for the critical uniform moment can now be obtained

$$M_{cr} = \frac{\pi^2 E I_z \beta_y}{2L^2}\left(1 \pm \sqrt{1+\frac{4}{\beta_y^2}\left(\frac{L^2 GJ}{\pi^2 E I_z}+\frac{E I_\omega}{E I_z}\right)}\right) \ . \tag{4.4.200}$$

The positive solutions correspond to positive moments, causing compression in the top flange and tension in the bottom. Since we know the exact solution, it is possible to assess the convergence of the discrete solutions with the number of segments, see Figure 4.4.21.

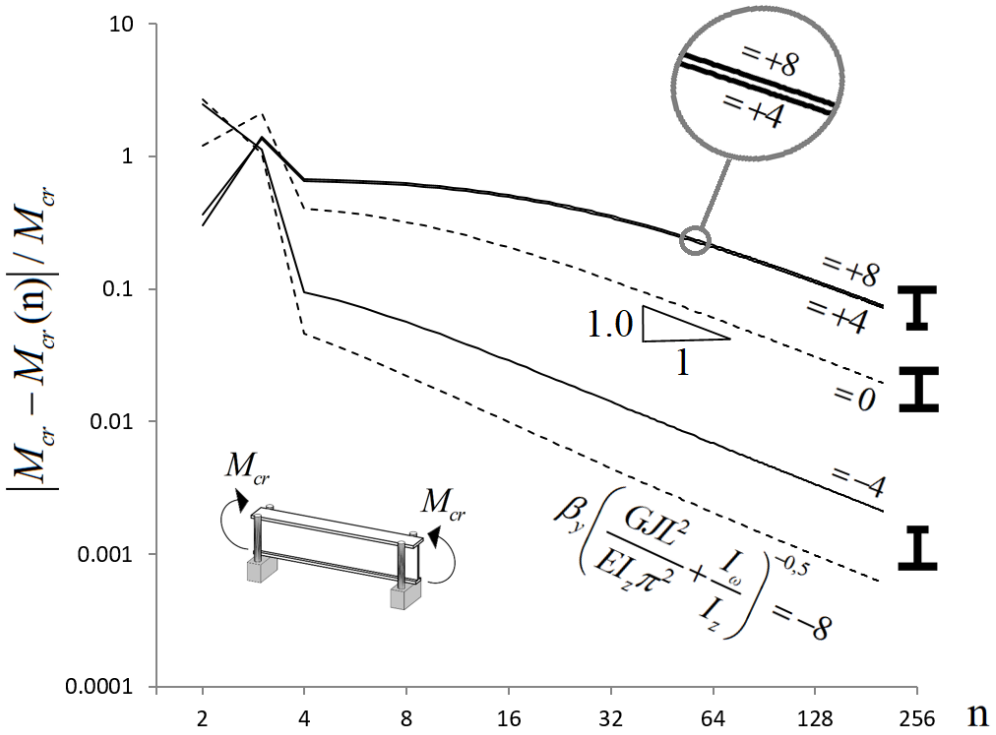

Figure 4.4.21: Simply supported mono symmetric bar-chain subjected to symmetric end moments: Convergence rate of the critical buckling load

Illustrative example 4: Doubly symmetric beam-columns

Figure 4.4.22 shows some examples of bar-chain models of doubly symmetric beam-columns subjected to concentric loading.

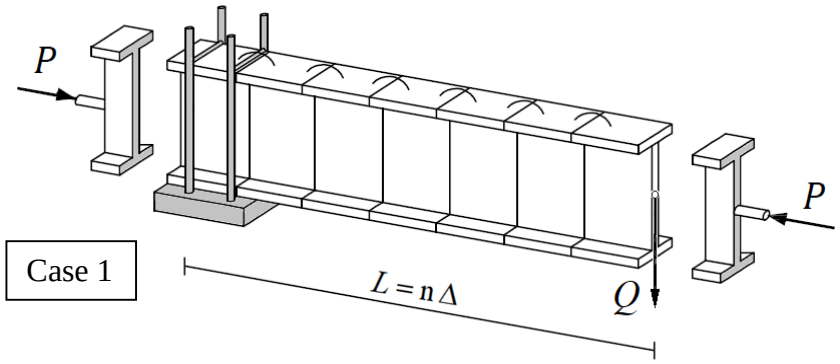

a) Bar-chain cantilever supporting a concentric load at the free tip

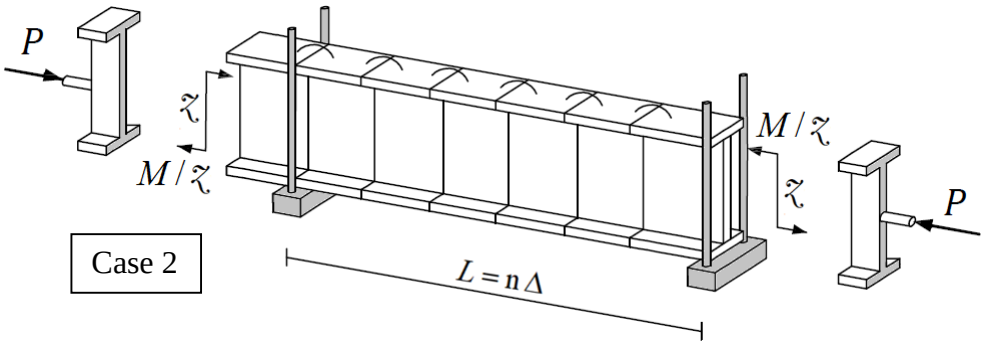

b) Simply supported bar-chain subjected to symmetric end moments

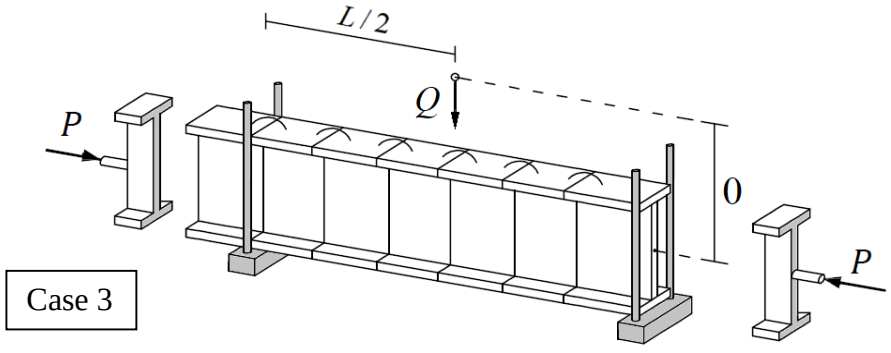

c) Simply supported bar-chain subjected to a mid-span load

Figure 4.4.22: Illustrative examples of bar-chain models for prismatic beam-columns subjected to concentric loading

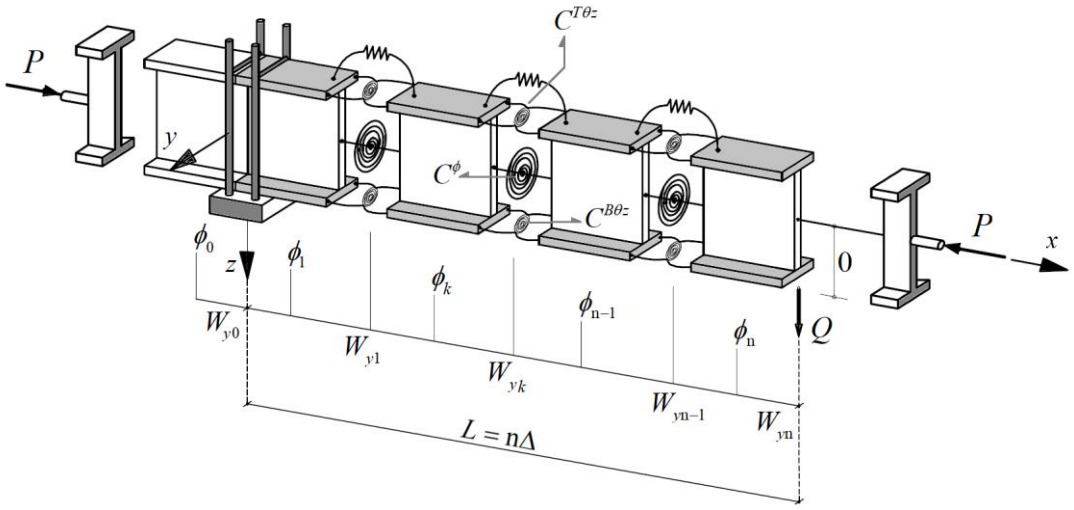

Figure 4.4.23: Illustrative example: Bar-chain model for a prismatic beam-column cantilever with a vertical load at its free end

As an illustrative example, consider the first case of Figure 4.4.23, i.e., a bar-chain loaded under combined axial and bending effects due to the compressive load P and a vertical load Q at its free end. Thus, the total potential energy is given by

$$\Pi\left(W_{yk},\phi_k;P,Q\right)=\frac{1}{2}\sum_{k=1}^{n-1}\left(C_{\omega}\left(\frac{\phi_{k-1}-2\phi_k+\phi_{k+1}}{\Delta}\right)^2+C_{\psi}\left(\phi_{k+1}-\phi_k\right)^2\right.$$

$$+C_z\left(\frac{W_{yk-1}-2W_{yk}+W_{yk+1}}{\Delta}\right)^2-2\phi_{k+1}\left(W_{yk-1}-2W_{yk}+W_{yk+1}\right)(n-k)Q$$

$$\left.-\frac{P}{\Delta}\left(\left(W_{yk+1}-W_{yk}\right)^2+r_o^2\left(\phi_{k+1}-\phi_k\right)^2\right)\right). \qquad (4.4.201)$$

The essential boundary conditions are given by

$$W_{yo}=W_{yn}=\phi_o=\phi_1=0\ , \qquad (4.4.202)$$

and four natural boundary conditions equal to

$$\frac{\partial\Pi}{\partial\phi_{n-1}}=-C_{\psi}\left(\phi_{n-2}-2\phi_{n-1}+\phi_n\right)+\frac{C_{\omega}}{\Delta^2}\left(\phi_{n-3}-4\phi_{n-2}+5\phi_{n-1}-2\phi_n\right)$$

$$-2Q\left(W_{yn-3}-2W_{yn-2}+W_{yn-1}\right)+\frac{Pr_o^2}{\Delta}\left(\phi_{n-2}-2\phi_{n-1}+\phi_n\right)=0\ , \qquad (4.4.203)$$

$$\frac{\partial\Pi}{\partial\phi_n}=C_{\psi}\left(\phi_n-\phi_{n-1}\right)+\frac{C_{\omega}}{\Delta^2}\left(\phi_{n-2}-2\phi_{n-1}+\phi_n\right)$$

$$-Q\left(W_{yn-2}-2W_{yn-1}+W_{yn}\right)-\frac{P}{\Delta}r_o^2\left(\phi_n-\phi_{n-1}\right)=0\ , \qquad (4.4.204)$$

$$\frac{\partial \Pi}{\partial W_{yn-1}} = \frac{C_z}{\Delta^2}\left(W_{yn-3} - 4W_{yn-2} + 5W_{yn-1} - 2W_{yn}\right)$$

$$+2Q\left(\phi_n - \phi_{n-1}\right) + \frac{P}{\Delta}\left(W_{yn} - 2W_{yn-1} + W_{yn-2}\right) = 0 \ , \qquad (4.4.205)$$

$$\frac{\partial \Pi}{\partial W_{yn}} = \frac{C_z}{\Delta^2}\left(W_{yn-2} - 2W_{yn-1} + W_{yn}\right) - Q\phi_n - \frac{P}{\Delta}\left(W_{yn} - W_{yn-1}\right) = 0 \ . \qquad (4.4.206)$$

The stationary condition of the total potential energy, requires that the set W_{yk}, ϕ_k minimized above functional by doing

$$\frac{\partial \Pi}{\partial \phi_i} = -C_\psi\left(\phi_{i-1} - 2\phi_i + \phi_{i+1}\right) + \frac{C_\omega}{\Delta^2}\left(\phi_{i-2} - 4\phi_{i-1} + 6\phi_i - 4\phi_{i+1} + \phi_{i+2}\right)$$

$$-Q\left(W_{yi-2} - 2W_{yi-1} + W_{yi}\right)\left(n - i + 1\right) + \frac{Pr_o^2}{\Delta}\left(\phi_{i-1} - 2\phi_i + \phi_{i+1}\right) = 0 \ , \qquad (4.4.207)$$

and

$$\frac{\partial \Pi}{\partial W_{yi}} = \frac{C_z}{\Delta^2}\left(W_{yi-2} - 4W_{yi-1} + 6W_{yi} - 4W_{yi+1} + W_{yi+2}\right) - Q\left[\left(n - i + 1\right)\phi_i - 2\left(n - i\right)\phi_{i+1}\right.$$

$$\left. + \left(n - i - 1\right)\phi_{i+2}\right] + \frac{P}{\Delta}\left(W_{yi-1} - 2W_{yi} + W_{yi+1}\right) = 0 \ , \qquad (4.4.208)$$

with $i = 2,...,n-2$. As an example, consider the geometry and material properties of the prismatic thin-walled bar shown in Figure 4.4.24.

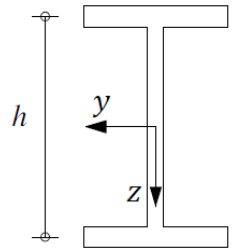

$A =$	$5884\ \text{mm}^2$	$E = 206.8$	kN/mm^2
$h =$	$192\ \text{mm}$	$G = 82.7$	kN/mm^2
$I_y = 45.7\times10^6\ \text{mm}^4$		$I_\omega = 220.0\times10^6\ \text{mm}^6$	
$I_z = 23.9\times10^3\ \text{mm}^4$		$J = 222.3\times10^3\ \text{mm}^4$	

Figure 4.4.24: Double symmetric prismatic bar: Geometry and material data (Pi and Trahair 1992 & Vacharajittiphan et al. 1974)

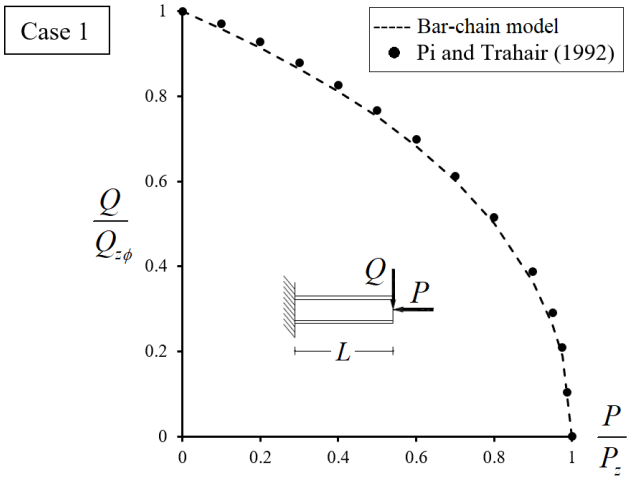

a) Cantilever supporting a concentric load at the free tip ($L = 4.2\text{m}$, $Q_z = 4.0\text{kN}$ and $P_z = 0.7\text{kN}$)

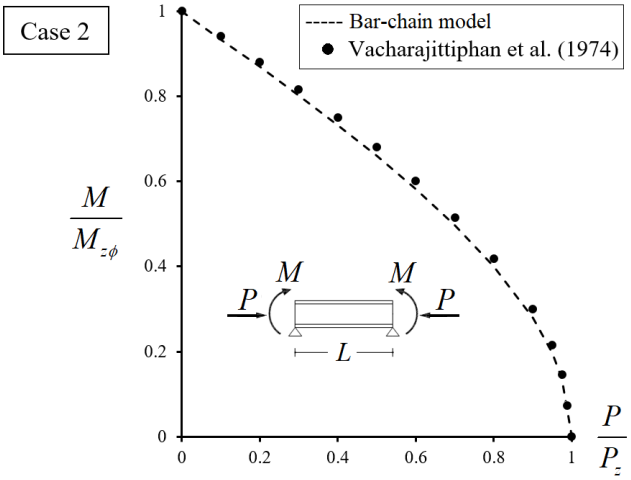

b) Simply supported bar subjected to symmetric end moments ($L = 7.6\text{m}$, $M_{z\phi} = 4.4\text{kNm}$ and $P_z = 0.8\text{kN}$)

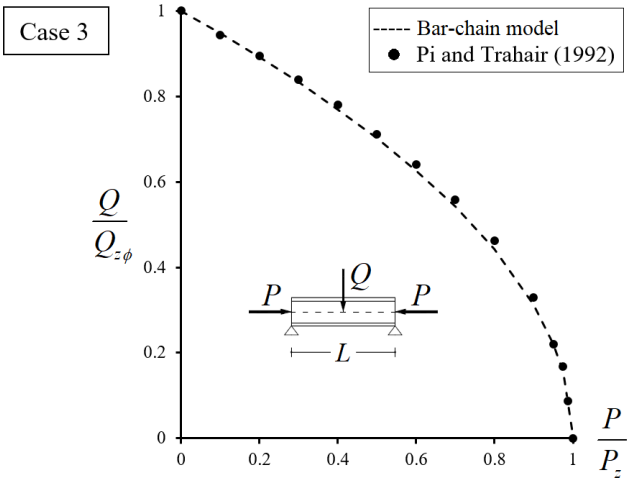

c) Simply supported bar subjected to a mid-span load ($L = 12.0\text{m}$, $Q_z = 1.2\text{kN}$ and $P_z = 0.3\text{kN}$)

Figure 4.4.25: Illustrative examples ─ Interaction buckling diagrams for prismatic beam-columns, for the bar-chain model with n=500

Figure 4.4.25 shows the determined interaction buckling diagram, for the above example and the remaining cases of Figure 4.4.22, as well as the results of Pi and Trahair (1992) and Vacharajittiphan et al. (1974).[45] Again, in order to get the continuous version of the one-dimensional model, we begin by determining the residuals

$$\Delta\Big(C_{\omega}\Delta\phi^{IV}(x_i)-C_{\psi}\Delta\phi''(x_i) \\ -Q\big(\mathrm{n}-(i-1)\big)W_y''(x_i)\Delta+r_o^2P\phi''(x_i)\Big)+O(\Delta^3)=r_{\phi i} \tag{4.4.209}$$

and

$$\Big[C_z\Delta W_y{}^{IV}(x_i)-Q\big(\mathrm{n}-(i-1)\big)\phi''(x_i)\Delta \\ +2Q\phi'(x_i)+PW_y''(x_i)\Big]\Delta+O(\Delta^3)=r_{ui}\ . \tag{4.4.210}$$

At the limit, we get the continuous functions

$$W_y(x_i)\to W_y(x)\ , \qquad \phi(x_i)\to\phi(x)\ , \tag{4.4.211}$$

where $x\in\mathbb{R}\cap(0,L)$, and the discrete coefficients became the cross-sectional stiffnesses

$$C_{\omega}\Delta\to EI_{\omega}\ , \qquad C_{\psi}\Delta\to GJ\ , \qquad C_z\Delta\to EI_z\ . \tag{4.4.212}$$

Thus, the continuous one-dimensional models are equal to

$$\Big[EI_{\omega}\phi''(x)-GJ\phi(x)\Big]''-\big(L-x\big)QW_y''(x)+Pr_o^2\phi''(x)=0\ , \tag{4.4.213}$$

and

$$EI_zW_y{}^{IV}(x)-\Big[\big(L-x\big)Q\phi(x)\Big]''+PW_y''(x)=0\ . \tag{4.4.214}$$

In the same manner, the residuals for the natural boundary conditions are given by

$$C_{\omega}\Delta\phi''(x_{\mathrm{n}})+O(\Delta^2)=r_{B,\mathrm{n}}\ , \tag{4.4.215}$$

$$C_{\psi}\Delta\phi'(x_{\mathrm{n}})-C_{\omega}\Delta\phi'''(x_{\mathrm{n}})-r_o^2P\big(\phi'(x_{\mathrm{n}})\big)+O(\Delta^2)=r_{T,\mathrm{n}}\ , \tag{4.4.216}$$

$$C_z\Delta W_y''(x_{\mathrm{n}})+O(\Delta^2)=r_{M,\mathrm{n}}\ , \tag{4.4.217}$$

$$-C_z\Delta W_y'''(x_{\mathrm{n}})-PW_y'(x_{\mathrm{n}})-Q\phi(x_{\mathrm{n}})+O(\Delta^2)=r_{V,\mathrm{n}}\ . \tag{4.4.218}$$

[45] The last authors used the method of finite integrals to replace the governing differential equations by a set of linear combinations of highest derivatives of the unknown buckling resultants.

At the limit, i.e., when $\Delta \to 0$, the natural boundaries conditions of the corresponding continuum model are found (Murray 1984) [eq. 2.5.14]

$$EI_{\omega}\phi''(L) = 0 \ , \tag{4.4.219}$$

$$-EI_{\omega}\phi'''(L) + GJ\phi'(L) - Pr_o^2\phi'(L) = 0 \ , \tag{4.4.220}$$

$$EI_z W_y''(L) = 0 \ , \tag{4.4.221}$$

$$EI_z W_y'''(L) + PW_y'(L) + Q\phi(L) = 0 \ . \tag{4.4.222}$$

4.4.3 Tapered I-section bar-chain model

The assumptions adopted (reference shape and notations) in the last chapter, with respect to the bar-chain model of tapered singly symmetric bars, provide all the discrete features that are required to compute the respective rotational deformations when the flexural-torsional buckling takes place, see Figure 4.4.26.

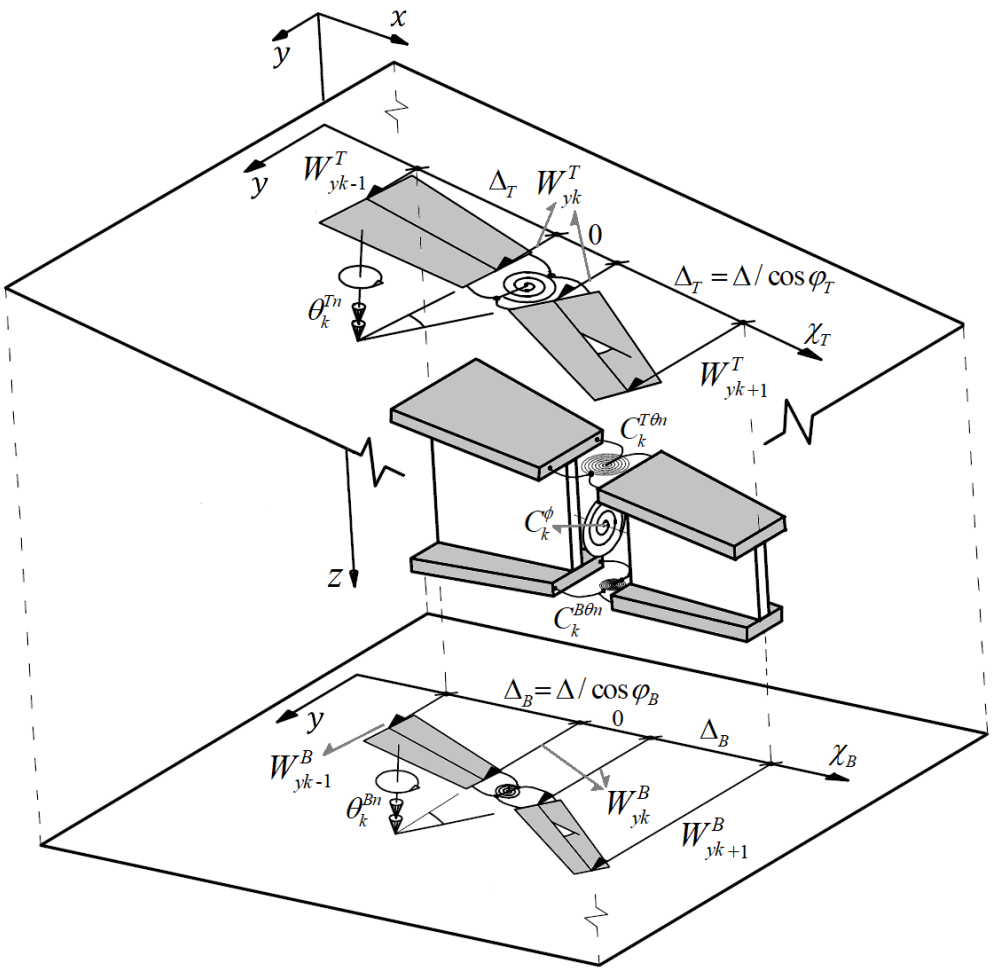

Figure 4.4.26: Tapered bar-chain kinematics in lateral bending and torsional warping

Hence, the rotational deformations at each rotational spring are given by

$$\theta_k^{Tn} = \cos\varphi_T \left(\Delta D_o^2 W_{yk} - z_k^T \Delta D_o^2 \phi_k \right) - 2\sin\varphi_T \Delta D_o \phi_k \ , \tag{4.4.223}$$

$$\theta_k^{Bn} = \cos\varphi_B \left(\Delta D_o^2 W_{yk} - z_k^B \Delta D_o^2 \phi_k \right) + 2\sin\varphi_B \Delta D_o \phi_k \ . \tag{4.4.224}$$

Moreover, considering a torsional deformation of second-order in the equivalent torsional spring, the total elastic energy stored in the bar-chain can be easily established as

$$\mathcal{U}(\theta_i^{Tn}, \theta_i^{Bn}, \theta_i^{*\phi}) = \frac{1}{2} \sum_k^{\mathrm{n-1}} \left\{ C_k^{T\theta n} \left(\theta_k^{Tn} \right)^2 + C_k^{B\theta n} \left(\theta_k^{Bn} \right)^2 + C_k^{\phi} \left(\theta_k^{*\phi} \right)^2 \right\} \ , \tag{4.4.225}$$

where the spring deformation $\theta_k^{*\phi}$ is equal to

$$\theta_k^{*\phi} = \Delta D_o \phi_k \ , \tag{4.4.226}$$

and the spring constants are defined by

$$C_k^{T\theta n} = \frac{EI_{nk}^T}{\Delta_T} \ , \qquad C_k^{B\theta n} = \frac{EI_{nk}^B}{\Delta_B} \ , \qquad C_k^{\phi} = \frac{GJ_k^*}{\Delta} \ . \tag{4.4.227}$$

Rewriting the springs deformations in function of the degrees of freedom, i.e., equations (4.4.223)-(4.4.224) & (4.4.226), and replacing the values of the spring constants in terms of the stiffness properties of the cross-section, i.e., equations (4.4.227), one obtains

$$\begin{aligned} \mathcal{U}(W_{yi}, \phi_i) = \frac{1}{2} \sum_k^{\mathrm{n-1}} \Big\{ & C_{zk} \left(\Delta D_o^2 W_{yk} \right)^2 + C_{\omega k} \left(\Delta D_o^2 \phi_k \right)^2 + C_{\psi k} \left(\Delta D_o \phi_k \right)^2 \\ & - 2C_{z\psi k} \left(\Delta D_o^2 W_{yk} \right) \left(\Delta D_o \phi_k \right) \\ & + 2C_{z\omega k} \left(\Delta D_o^2 W_{yk} \right) \left(\Delta D_o^2 \phi_k \right) - 2C_{\omega\psi k} \left(\Delta D_o^2 \phi_k \right) \left(\Delta D_o \phi_k \right) \Big\} \ , \end{aligned} \tag{4.4.228}$$

where the discrete stiffness coefficients are reduced to

$$C_{zk} = \frac{EI_{zk}^*}{\Delta} = \frac{E\left\{ t_T \cos^3\varphi_T (b_k^T)^3 + t_B \cos^3\varphi_B (b_k^B)^3 \right\}}{12\Delta} \ , \tag{4.4.229}$$

$$C_{\omega k} = \frac{EI_{\omega k}^*}{\Delta} = \frac{E\left\{ t_T \cos^3\varphi_T (b_k^T)^3 (z_k^T)^2 + t_B \cos^3\varphi_B (b_k^B)^3 (z_k^B)^2 \right\}}{12\Delta} \ , \tag{4.4.230}$$

$$\begin{aligned} C_{\psi k} &= \frac{EI_{\psi k}^* + GJ_k^*}{\Delta} \\ &= \frac{E\left\{ t_T \cos^3\varphi_T \tan^2\varphi_T (b_k^T)^3 + t_B \cos^3\varphi_B \tan^2\varphi_B (b_k^B)^3 \right\} + 3GJ_k^*}{3\Delta} \ , \end{aligned} \tag{4.4.231}$$

$$C_{z\psi k} = \frac{EI_{z\psi k}^*}{\Delta} = \frac{E\left\{ t_T \cos^3\varphi_T \tan\varphi_T (b_k^T)^3 - t_B \cos^3\varphi_B \tan\varphi_B (b_k^B)^3 \right\}}{6\Delta} \ , \tag{4.4.232}$$

$$C_{z\omega k} = \frac{EI^*_{z\omega k}}{\Delta} = \frac{-E\left\{t_T \cos^3\varphi_T (b_k^T)^3 z_k^T + t_B \cos^3\varphi_B (b_k^B)^3 z_k^B\right\}}{12\Delta} \ , \qquad (4.4.233)$$

$$C_{\omega\psi k} = \frac{EI^*_{\omega\psi k}}{\Delta} = \frac{E\left\{-t_T \cos^3\varphi_T \tan\varphi_T (b_k^T)^3 z_k^T + t_B \cos^3\varphi_B \tan\varphi_B (b_k^B)^3 z_k^B\right\}}{6\Delta} \ . \qquad (4.4.234)$$

Therefore, according to the energy formulation of equations (4.3.1), (4.3.4), (4.3.13) and (4.3.17), the work done by the loading including second-order effects is given by

$$\mathcal{W}^{II} = \mathcal{W}_e^{II} + \mathcal{W}_c^{II} + \mathcal{W}_P^{II} + \mathcal{W}_d^{II} \ . \qquad (4.4.235)$$

Thus, the total potential energy of the bar-chain model is defined by the elastic energy (4.4.228) minus the contribution of the work done by the loading (4.4.235), i.e.,

$$\Pi = \mathcal{U} - \mathcal{W}^{II} \ . \qquad (4.4.236)$$

Illustrative bar-chain model examples

In order to verify the proposed tapered bar-chain model, several illustrative examples, i.e., numerical results, concerning different support and loading conditions as well as different severities of taper are discussed.

Illustrative example 1: Bar cantilever with eccentric point load

Consider the lateral-torsional buckling of a bar-chain cantilever of length $L = \mathrm{n}\Delta$, with perfectly straight doubly symmetric web-tapered segments, acted by a point load applied at its free tip with eccentricity z_Q. The origin and the direction of the *y* and *z* axis coincide with the centroid and that of the principal axis, see Figure 4.4.27.

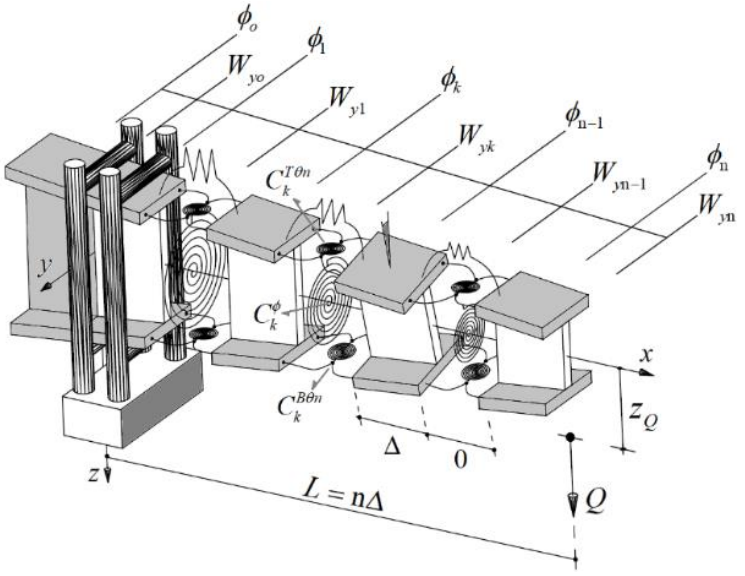

Figure 4.4.27: Web-tapered bar-chain cantilever with eccentric pointing load

Thus the potential energy (4.4.236) can be written as

$$\Pi\left(W_{yk},\phi_k;Q\right)=\frac{1}{2}\sum_{k=1}^{\mathrm{n}-1}\Bigg(C_{\omega k+1}\left(\frac{\phi_{k-1}-2\phi_k+\phi_{k+1}}{\Delta}\right)^2-C_{\omega\psi k+1}\left(\frac{\phi_{k-1}-2\phi_k+\phi_{k+1}}{\Delta}\right)\left(\phi_{k+1}-\phi_{k-1}\right)$$
$$+C_{\psi k+1}\left(\frac{\phi_{k+1}-\phi_{k-1}}{2}\right)^2+C_z\left(\frac{W_{yk-1}-2W_{yk}+W_{yk+1}}{\Delta}\right)^2$$
$$+2\phi_{k+1}\left(\frac{W_{yk-1}-2W_{yk}+W_{yk+1}}{\Delta}\right)M_{yk}^F\Bigg)+\frac{1}{2}Q\,z_Q\left(\phi_{\mathrm{n}}\right)^2\ , \qquad (4.4.237)$$

where the discrete first order bending moment is equal to

$$M_{yk}^F=-\left(\mathrm{n}-k\right)Q\Delta\ ,\ k=1,...,\mathrm{n}-1\ . \qquad (4.4.238)$$

The essential boundary conditions are given by

$$W_{yo}=W_{y1}=\phi_o=\phi_1=0\ , \qquad (4.4.239)$$

and the four natural boundary conditions at the last two segments give

$$\frac{\partial\Pi}{\partial\phi_{\mathrm{n}-1}}=\frac{C_{\psi\mathrm{n}-1}}{4}\left(\phi_{\mathrm{n}-1}-\phi_{\mathrm{n}-3}\right)+\frac{C_{\omega\mathrm{n}-1}}{\Delta^2}\left(\phi_{\mathrm{n}-3}-2\phi_{\mathrm{n}-2}+\phi_{\mathrm{n}-1}\right)+\frac{2C_{\omega\mathrm{n}}}{\Delta^2}\left(-\phi_{\mathrm{n}-2}+2\phi_{\mathrm{n}-1}-\phi_{\mathrm{n}}\right)$$
$$+\frac{C_{\omega\psi\mathrm{n}-1}}{\Delta}\left(\phi_{\mathrm{n}-2}-\phi_{\mathrm{n}-1}\right)+\frac{C_{\omega\psi\mathrm{n}}}{\Delta}\left(\phi_{\mathrm{n}}-\phi_{\mathrm{n}-2}\right)-2Q\left(W_{y\mathrm{n}-3}-2W_{y\mathrm{n}-2}+W_{y\mathrm{n}-1}\right)=0\ , \qquad (4.4.240)$$

$$\frac{\partial\Pi}{\partial\phi_{\mathrm{n}}}=\frac{C_{\psi\mathrm{n}}}{4}\left(\phi_{\mathrm{n}}-\phi_{\mathrm{n}-2}\right)+\frac{C_{\omega\mathrm{n}}}{\Delta^2}\left(\phi_{\mathrm{n}-2}-2\phi_{\mathrm{n}-1}+\phi_{\mathrm{n}}\right)+\frac{C_{\omega\psi\mathrm{n}}}{\Delta}\left(\phi_{\mathrm{n}-1}-\phi_{\mathrm{n}}\right)$$
$$-Q\left(W_{y\mathrm{n}-2}-2W_{y\mathrm{n}-1}+W_{y\mathrm{n}}-z_Q\phi_{\mathrm{n}}\right)=0 \qquad (4.4.241)$$

$$\frac{\partial\Pi}{\partial W_{y\mathrm{n}-1}}=\frac{C_z}{\Delta^2}\left(W_{y\mathrm{n}-3}-4W_{y\mathrm{n}-2}+5W_{y\mathrm{n}-1}-2W_{y\mathrm{n}}\right)+2Q\left(\phi_{\mathrm{n}}-\phi_{\mathrm{n}-1}\right)=0 \qquad (4.4.242)$$

$$\frac{\partial\Pi}{\partial W_{y\mathrm{n}}}=\frac{C_z}{\Delta^2}\left(W_{y\mathrm{n}-2}-2W_{y\mathrm{n}-1}+W_{y\mathrm{n}}\right)-Q\phi_{\mathrm{n}}=0\ . \qquad (4.4.243)$$

Now, by virtue of the fundamental lemma of the calculus of variations, the vanishing of the first variation of the total potential energy (4.4.237), leads to

$$\frac{\partial \Pi}{\partial \phi_i}=\frac{C_{\psi i}}{4}\left(\phi_i-\phi_{i-2}\right)+\frac{C_{\psi i+2}}{4}\left(\phi_i-\phi_{i+2}\right)+\frac{C_{\omega i}}{\Delta^2}\left(\phi_{i-2}-2\phi_{i-1}+\phi_i\right)+\frac{2C_{\omega i+1}}{\Delta^2}\left(-\phi_{i-1}+2\phi_i-\phi_{i+1}\right)$$
$$+\frac{C_{\omega i+2}}{\Delta^2}\left(\phi_i-2\phi_{i+1}+\phi_{i+2}\right)-\frac{C_{\omega\psi i}}{\Delta}\left(\phi_i-\phi_{i-1}\right)+\frac{C_{\omega\psi i+1}}{\Delta}\left(\phi_{i+1}-\phi_{i-1}\right)-\frac{C_{\omega\psi i+2}}{\Delta}\left(\phi_{i+1}-\phi_i\right)$$
$$-Q\left(W_{yi-2}-2W_{yi-1}+W_{yi}\right)\left(\mathrm{n}-i+1\right)=0 \tag{4.4.244}$$

and

$$\frac{\partial \Pi}{\partial W_{yi}}=\frac{C_z}{\Delta^2}\left(W_{yi-2}-4W_{yi-1}+6W_{yi}-4W_{yi+1}+W_{yi+2}\right)-Q\left[\left(\mathrm{n}-i+1\right)\phi_i\right.$$
$$\left.-2\left(\mathrm{n}-i\right)\phi_{i+1}+\left(\mathrm{n}-i-1\right)\phi_{i+2}\right]=0\ , \tag{4.4.245}$$

with $i=2,...,\mathrm{n}-2$. In equations (4.4.244)-(4.4.245), when the central discrete values are replaced by their exact solutions

$$\phi_i:=\phi(x_i)\ , \qquad W_{yi}:=W_y(x_i)\ , \tag{4.4.246}$$

and their corresponding continuous stiffnesses

$$C_{\omega i}:=C_\omega(x_i)\ , \qquad C_{\psi i}:=C_\psi(x_i)\ , \qquad C_{\omega\psi i}:=C_{\omega\psi}(x_i)\ , \tag{4.4.247}$$

with

$$C_\omega''(x_i)=-C_{\omega\psi}'(x_i)=\frac{1}{2}\left(C_\psi(x_i)-\frac{GJ^*(x_i)}{\Delta}\right)'\ ,\ i=2,...,\mathrm{n}-2\ , \tag{4.4.248}$$

the residuals for each discrete one-dimensional equation are easily gotten as

$$\Delta\left(C_\omega(x_i)\Delta\phi^{IV}(x_i)+2C_\omega'(x_i)\Delta\phi'''(x_i)-GJ^*(x_i)\phi''(x_i)\right.$$
$$\left.-\left(GJ^*(x_i)\right)'\phi'(x_i)-Q\left(\mathrm{n}-(i-1)\right)\Delta W_y''(x_i)\right)+O(\Delta^2)=r_{\phi i} \tag{4.4.249}$$

and

$$\left[C_z\Delta W_y^{\ IV}(x_i)-Q\left(\mathrm{n}-\left(i-1\right)\right)\Delta\phi''(x_i)+2Q\phi'(x_i)\right]\Delta+O(\Delta^3)=r_{ui}\ . \tag{4.4.250}$$

At the limit $\Delta\to 0$,

$$W_y(x_i)\to W_y(x)\ , \qquad \phi(x_i)\to\phi(x)\ , \tag{4.4.251}$$

$$C_\omega(x_i)\Delta\to EI_\omega^*(x)\ , \qquad C_z\Delta\to EI_z^*\ , \tag{4.4.252}$$

the residuals converge to zero, and the discrete positions x_i tend to $x\in\mathbb{R}\cap\left(0,L\right)$, i.e.,

$$EI_\omega^*(x)\phi^{IV}(x)+2\left(EI_\omega^*(x)\right)'\phi'''(x)-\left(GJ^*(x)\phi'(x)\right)'-Q\left(L-x\right)W_y''(x)=0\ , \tag{4.4.253}$$

$$EI_z^*W_y^{\ IV}(x)-Q\left(L-x\right)\phi''(x)+2Q\phi'(x)=0\ . \tag{4.4.254}$$

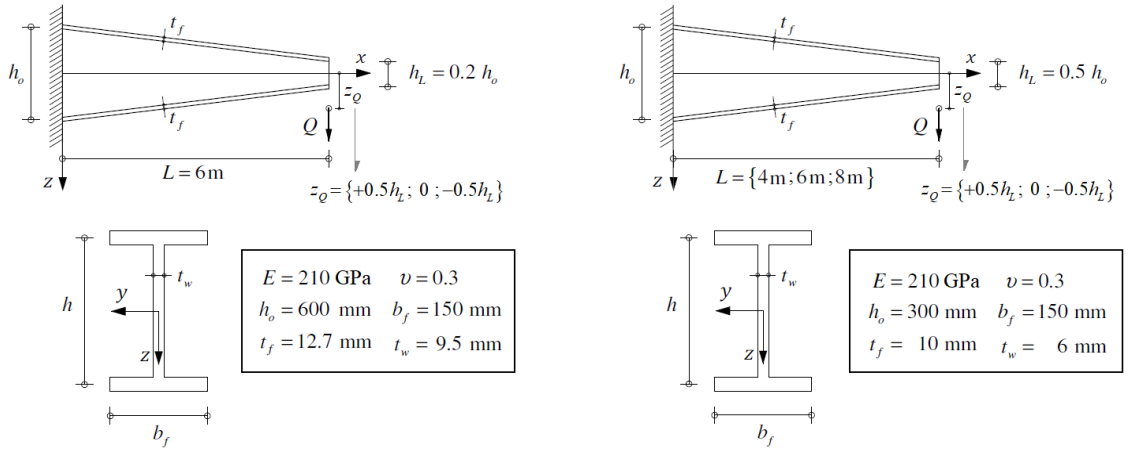

a) Load case A b) Load case B

Figure 4.4.28: Web-tapered cantilevers: Geometry, loading and material data

Using the same methodology for the expressions derived from the natural boundary conditions (4.4.240)-(4.4.243)

$$-\left(C_\omega(x_{\text{n}})\Delta\phi''(x_{\text{n}}) - C_{\omega\psi}(x_{\text{n}})\Delta\phi'(x_{\text{n}})\right) + O(\Delta) = r_{\phi,\text{n}-1}\ , \tag{4.4.255}$$

$$\begin{aligned}&\frac{1}{2}\left(\Delta C_\psi(x_{\text{n}+1}) - GJ^*(x_{\text{n}+1})\right)\phi'(x_{\text{n}+1}) + C_\omega(x_{\text{n}+1})\left(-\Delta\phi'''(x_{\text{n}+1})\right)\\ &\quad -C_{\omega\psi}(x_{\text{n}})\left(-\Delta\phi''(x_{\text{n}})\right) + GJ^*(x_{\text{n}+1})\phi'(x_{\text{n}+1})\\ &\quad +O(\Delta) - Q\left(O(\Delta^2) - z_Q\phi_{\text{n}}\right) = r_{\phi,\text{n}}\ ,\end{aligned} \tag{4.4.256}$$

$$-C_z\Delta W_y''(x_{\text{n}}) + O(\Delta^2) = r_{u,\text{n}-1}\ , \tag{4.4.257}$$

$$-C_z\Delta W_y'''(x_{\text{n}}) - Q\phi_{\text{n}} + O(\Delta) = r_{u,\text{n}}\ . \tag{4.4.258}$$

Again, at the limit $\Delta \to 0$, the residuals converge to zero, and the discrete equations become the continuous natural boundary conditions at the free tip of the bar

$$\left(EI_\omega^*\phi'\right)'(L) = 0\ , \tag{4.4.259}$$

$$-\left(EI_\omega^*\phi''\right)'(L) + \left(\left(EI_\omega^*\right)'' + GJ^*\right)(L)\phi'(L) + z_Q\phi(L)Q = 0\ , \tag{4.4.260}$$

$$EI_z^*W_y''(L) = 0\ , \tag{4.4.261}$$

$$\left(EI_z^*W_y''' + \phi Q\right)(L) = 0\ . \tag{4.4.262}$$

On the other side, the essential boundary conditions give

$$W_y(0) = \phi(0) = W_y'(0) = \phi'(0) = 0\ . \tag{4.4.263}$$

Load application	P_{cr} [kN]		
	(1)	(2)	(3)
Top flange	38.31	38.70	38.34
Centroid	44.36	44.40	44.27
Bottom flange	48.40	48.50	48.42

(1) Shell finite element model (Andrade et al. 2007).

(2) One-dimensional model (Andrade et al. 2007).

(3) Bar-chain model with n=600.

Table 4.4.2: Illustrative example 1: Critical loads for the load case A

As numerical examples, consider the lateral-torsional buckling behaviour of singly symmetric web-tapered cantilevers under a top flange, centre and bottom flange loading respectively. Figure 4.4.28 summarises the geometry and material properties of two particular examples, taken from Andrade et al. (2007), who developed a comparative study involving the critical loads and buckling modes by using 1D models and 2D shell finite element analyses, using the commercial code ABAQUS, the latter taken as reference. The critical loads concerning the load case A are shown in Table 4.4.2. We also assess the accuracy of the buckling shapes yielded by the bar-chain model, which are expressed in terms of the normalised torsional rotation field ϕ_{cr}, subject to a tip point load applied at the top flange, centroid and bottom flange respectively, see Figure 4.4.29. The first mode of stability, i.e., the critical mode expressed in terms of the torsional rotation, provided by the one-dimensional model and the shell finite element coincide with the bar-chain model results.

L [m]	Top flange [kN]			Centroid [kN]			Bottom flange [kN]		
	(1)	(2)	(3)	(1)	(2)	(3)	(1)	(2)	(3)
4	34.0	31.6	33.7	56.6	53.5	56.4	70.4	70.0	70.2
6	15.5	15.2	15.4	20.5	20.3	20.4	23.8	23.7	23.7
8	8.5	8.4	8.5	10.2	10.2	10.2	11.4	11.4	11.4

(1) One-dimensional model (Andrade et al. 2007).

(2) Shell finite element model (Andrade et al. 2007).

(3) Bar-chain model, by using n=600.

Table 4.4.3: Illustrative example 1: Critical loads for the load case B

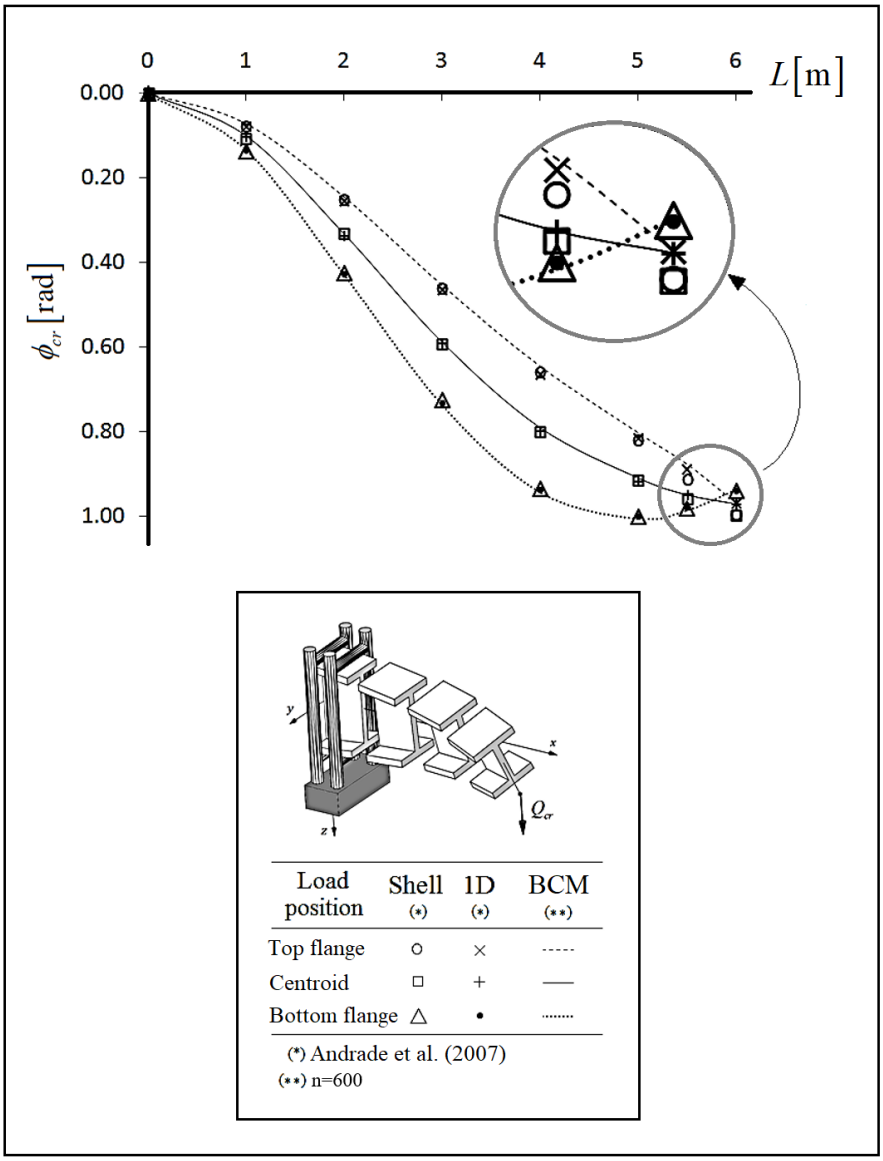

Figure 4.4.29: Normalise critical mode for the load case A

Indeed, the one-dimensional continuum model and the bar-chain model have similar results since they share equivalent kinematics constraints. The difference between the shell finite element and the 1D models appears near the free end section, when the load acts either at the top flange or at the centroid of the cross-section. This small discrepancy is caused by the shell finite element model capability to represent the local effect of the point load.

The results of the critical loads for the load case B, see Table 4.4.3, indicate that the discrete model is in good agreement with the results obtained by the one-dimensional continuum and the shell finite element models. Again the little difference between the bar-chain model and the shell finite element occurs when the tip load is applied at the top flange, most likely because local effects in the concentration of stresses induced by the tip load cannot be captured by the 1D approaches. On the other hand, the results of the three methods are almost the same for longer bars, their critical loads being practically equal.

Illustrative example 2: Simply supported bar under a moment gradient

A simply supported depth-tapered singly symmetric bar-chain, see Figure 4.4.30, is under a moment gradient when its bending moment diagram varies linearly; the case where the end moments are respectively M and $\beta_M M$ with

$$-1 \le \beta_M \le 1 \,, \tag{4.4.264}$$

will be considered.

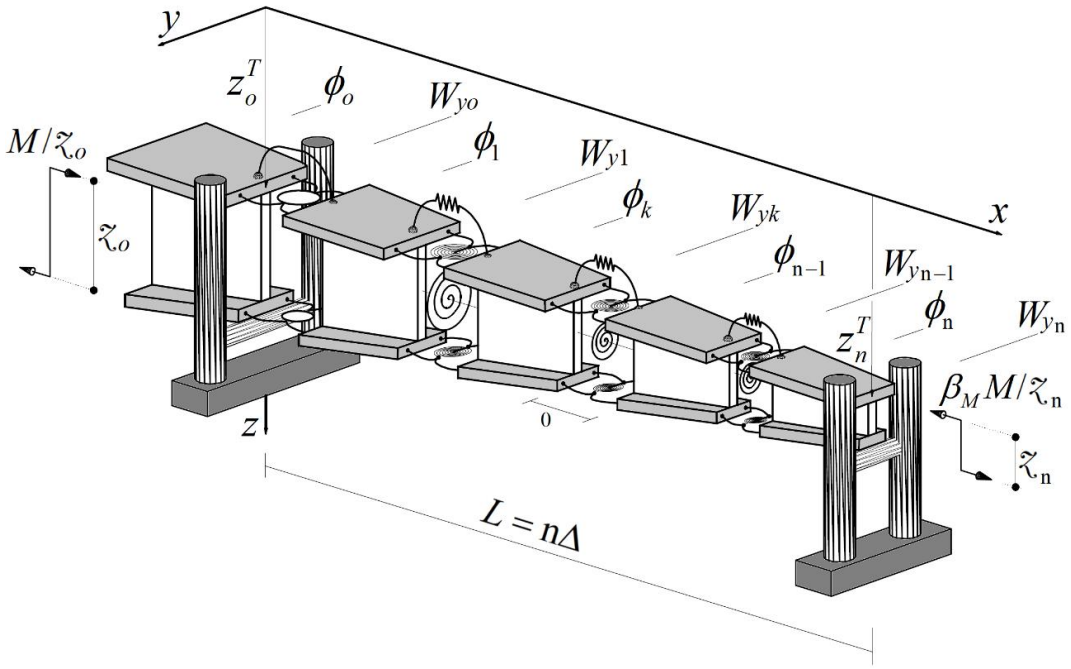

Figure 4.4.30: Simply supported depth-tapered singly symmetric bar-chain under a moment gradient

Hence, by using the definitions given in the previous section, the total potential energy is written as

$$\Pi\left(W_{yk},\phi_k;M\right)=\frac{1}{2}\sum_{k=1}^{\mathrm{n}-1}\Big\{C_{zk}\left(\Delta D_o^2 W_{yk}\right)^2+C_{\omega k}\left(\Delta D_o^2\phi_k\right)^2+C_{\psi k}\left(\Delta D_o\phi_k\right)^2$$
$$-2C_{z\psi k}\left(\Delta D_o^2 W_{yk}\right)\left(\Delta D_o\phi_k\right)+2C_{z\omega k}\left(\Delta D_o^2 W_{yk}\right)\left(\Delta D_o^2\phi_k\right)$$
$$-2C_{\omega\psi k}\left(\Delta D_o^2\phi_k\right)\left(\Delta D_o\phi_k\right)+M_{yk}^{F}\Delta\left(2\phi_k D_o^2 W_{yk}+\beta_{yk}\left(D_+\phi_k\right)^2\right)\Big\} \qquad (4.4.265)$$

with

$$M_{yk}^{F}=\left\{1+(\beta_M-1)\frac{k}{\mathrm{n}}\right\}M \text{ , and } k=1,2,...,\mathrm{n}-1 \text{ .} \qquad (4.4.266)$$

Like in the prismatic case, the essential boundary conditions are defined as

$$W_{yo}=W_{y\mathrm{n}}=\phi_o=\phi_{\mathrm{n}}=0 \text{ .} \qquad (4.4.267)$$

If we define again the external displacements and rotations by[46]

$$W_{y-1}=-W_{y1} \text{ ,} \qquad \phi_{-1}=-\phi_1 \text{ ,} \qquad (4.4.268)$$

$$W_{y\mathrm{n}+1}=-W_{y\mathrm{n}-1} \text{ ,} \qquad \phi_{\mathrm{n}+1}=-\phi_{\mathrm{n}-1} \text{ .} \qquad (4.4.269)$$

and by using the definition of the Kronecker delta

$$\delta_j^i=\begin{cases}1 \text{ if } i=j\\ 0 \text{ if } i\neq j\end{cases} \qquad (4.4.270)$$

the minimum potential energy can be rewritten as

$$4\Delta^2\frac{\partial\Pi}{\partial\phi_i}=\sum_{j=1}^{3}\Big[(\aleph 6)\Big\{C_{\omega(\aleph 2)}\left(4\phi_{(\aleph 3)}-8\phi_{(\aleph 2)}+4\phi_{(\aleph 1)}\right)+C_{z\omega(\aleph 2)}\left(4W_{y\,(\aleph 3)}-8W_{y\,(\aleph 2)}+4W_{y\,(\aleph 1)}\right)\Big\}$$
$$+(\aleph 5)\Big\{C_{\psi(\aleph 7)}\left(\phi_i-\phi_{(\aleph 8)}\right)\left(1-\delta_i^{\mathrm{n}-1}\delta_{(\aleph 7)}^{\mathrm{n}-1}\right)\left(1-\delta_i^1\delta_{(\aleph 7)}^{o}\right)\Delta^2-4M_{y\,(\aleph 2)}^{f}\beta_{y(\aleph 2)}\left(\phi_{(\aleph 1)}-\phi_{(\aleph 2)}\right)\Delta$$
$$+4M_{yi}^{f}\left(W_{y\,(\aleph 7)}-W_{yi}\right)\Delta\Big\}+(\aleph 4)C_{z\psi(\aleph 2)}\left(-2W_{y\,(\aleph 3)}+4W_{y\,(\aleph 2)}-2W_{y\,(\aleph 1)}\right)\Delta$$
$$+4C_{\omega\psi(\aleph 2)}\left\{\phi_{(\aleph 10)}-\phi_{(\aleph 9)}\right\}\left(1-\delta_i^{\mathrm{n}-1}\delta_{(\aleph 10)}^{\mathrm{n}-1}\right)\left(1-\delta_i^1\delta_{(\aleph 2)}^{o}\right)\Delta\Big]=0 \text{ ,} \qquad (4.4.271)$$

[46] *Vide supra*, note 41 p. 229.

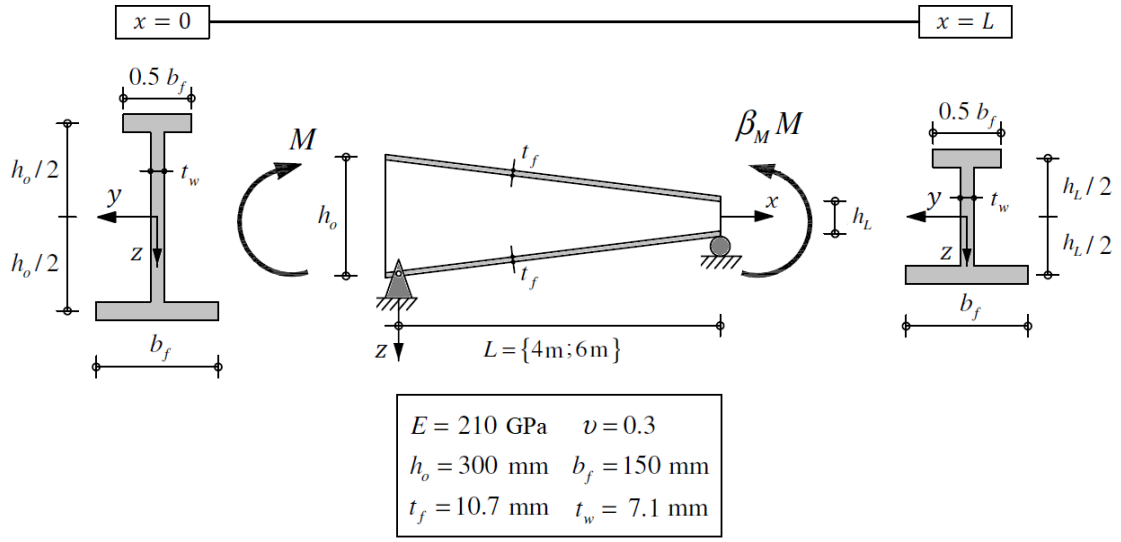

Figure 4.4.31: Singly symmetric tapered bar: Geometry, loading and material data

and

$$2\Delta^2\frac{\partial\Pi}{\partial W_{yi}}=\sum_{j=1}^{3}\Big[(\aleph 6)\Big\{C_{z(\aleph 2)}\left(2W_{y\,(\aleph 3)}-4W_{y\,(\aleph 2)}+2W_{y\,(\aleph 1)}\right)+2M^{\,f}_{y\,(\aleph 2)}\phi_{(\aleph 2)}\Delta$$
$$+C_{z\psi(\aleph 2)}\left(\phi_{(\aleph 3)}-\phi_{(\aleph 1)}\right)\left(1-\delta_i^{\text{n-1}}\delta_{(\aleph 3)}^{\text{n-1}}\right)\left(1-\delta_i^{1}\delta_{(\aleph 2)}^{o}\right)\Delta$$
$$+C_{z\omega(\aleph 2)}\left(2\phi_{(\aleph 3)}-4\phi_{(\aleph 2)}+2\phi_{(\aleph 1)}\right)\Big\}\Big]=0\ , \qquad (4.4.272)$$

with $i=1,2,...,\text{n}-1$, where the discrete coefficients

$$(\aleph k)\ \text{, with}\ k=1,2,...,10\ , \qquad (4.4.273)$$

are defined as

$$(\aleph 1)=i+j-1\ , \qquad (\aleph 2)=i+j-2\ , \qquad (4.4.274)$$

$$(\aleph 3)=i+j-3\ , \qquad (\aleph 4)=2-j\ , \qquad (4.4.275)$$

$$(\aleph 5)=(3-j)^{j-1}\ , \qquad (\aleph 6)=(-2)^{(j-1)(3-j)}\ , \qquad (4.4.276)$$

$$(\aleph 7)=i+(-1)^{j}\ , \qquad (\aleph 8)=i+2(-1)^{j}\ , \qquad (4.4.277)$$

$$(\aleph 9)=i+(1-j)^{3-j}\ , \qquad (\aleph 10)=i+(-1)^{j}(3-j)^{j-1}\ . \qquad (4.4.278)$$

For the above illustrative example, the discrete coefficients are variable, so that a closed solution cannot be obtained. Figure 4.4.31 summarises the geometry and material properties for the particular simply supported continuous bars investigated by Asgarian et al. (2013), corresponding to three variants where the following parameters are varied: i) the length of the bar, ii) the longitudinal slope, defined by the relation h_L/h_o and iii)

#	L [m]	$\frac{h_L}{h_o}$	$\beta_M = 0.25$			$\beta_M = 0.50$			$\beta_M = 0.75$			$\beta_M = 1.00$		
			(1)	(2)	(3)	(1)	(2)	(3)	(1)	(2)	(3)	(1)	(2)	(3)
A	4	0.6	65.7	66.5	1.2	56.8	57.5	1.2	49.4	50.0	1.2	43.3	43.9	1.4
B	4	0.8	65.1	65.8	1.1	56.2	57.0	1.4	48.8	49.5	1.4	42.8	43.4	1.4
C	6	0.6	46.7	47.6	1.9	40.8	41.5	1.7	35.7	36.4	1.9	31.4	32.0	1.9
D	6	0.8	46.3	47.0	1.5	40.3	41.0	1.7	35.2	35.8	1.7	30.9	31.5	1.9

(1) Bar-chain model, with n=500.

(2) ANSYS-Academic, with SOLID187 and 7500 elements.

(3) The relative error value, given by $|(1)-(2)|\times 100/(2)$.

Table 4.4.4: Critical buckling moments [kNm] for the tapered bars of Figure 4.4.31

the gradient moment β_M, while the flanges width and the thicknesses of flanges and web are fixed. The critical moments determined with the bar-chain model (with n=500) are presented in Table 4.4.4. This table includes the values determined by a finite element analysis with solid elements [47] in ANSYS-Academic (Ansys 2018). In the finite element analysis, the loading is modelled at the web mid-height by concentrated moments at both ends; moreover, the displacement is not allowed at web mid-height along directions -x and -z at the left end and z at the right end and the lateral displacement -y is not allowed through the web height at both ends. The relative error values in Table 4.4.4, always below 2%, are given by $|\text{BCM}-\text{ANSYS}|\times 100/\text{ANSYS}$.

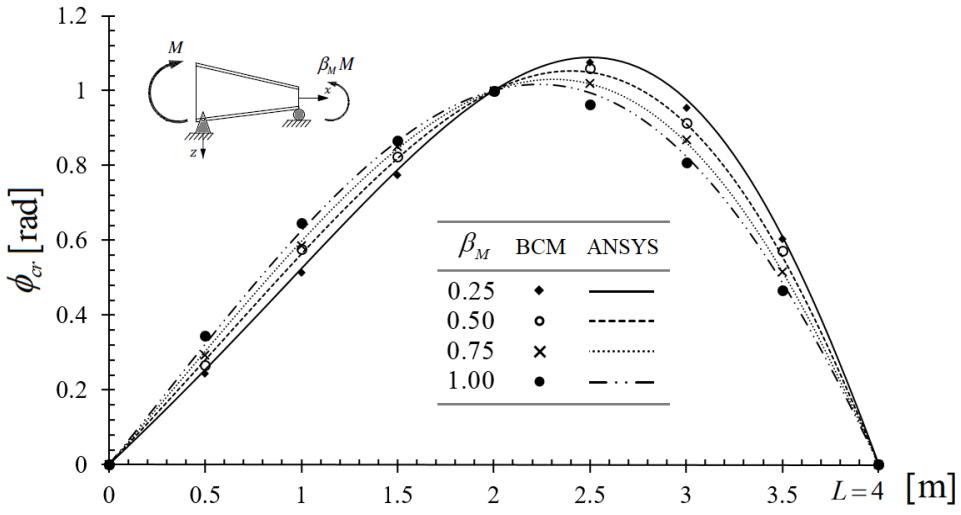

Figure 4.4.32: Normalized critical model shape of case #A in Table 4.4.4, with n=500

[47] SOLID187 element is a higher order 3D tetrahedral solid. It is defined by 10 nodes having three degrees of freedom at each node: translations in the nodal x, y, and z directions.

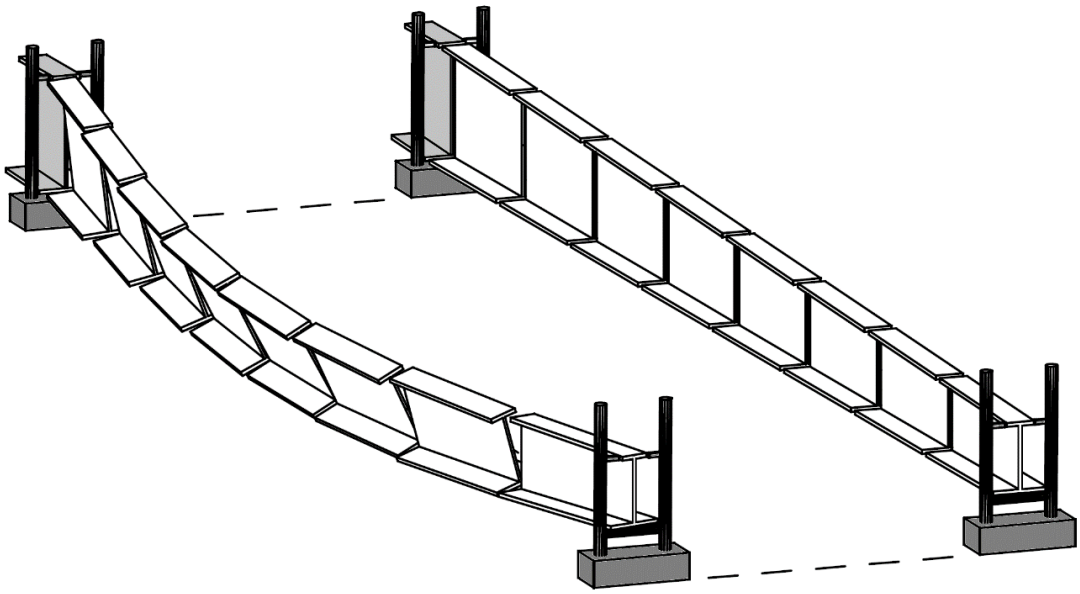

a) Bar-chain model with 8 segments

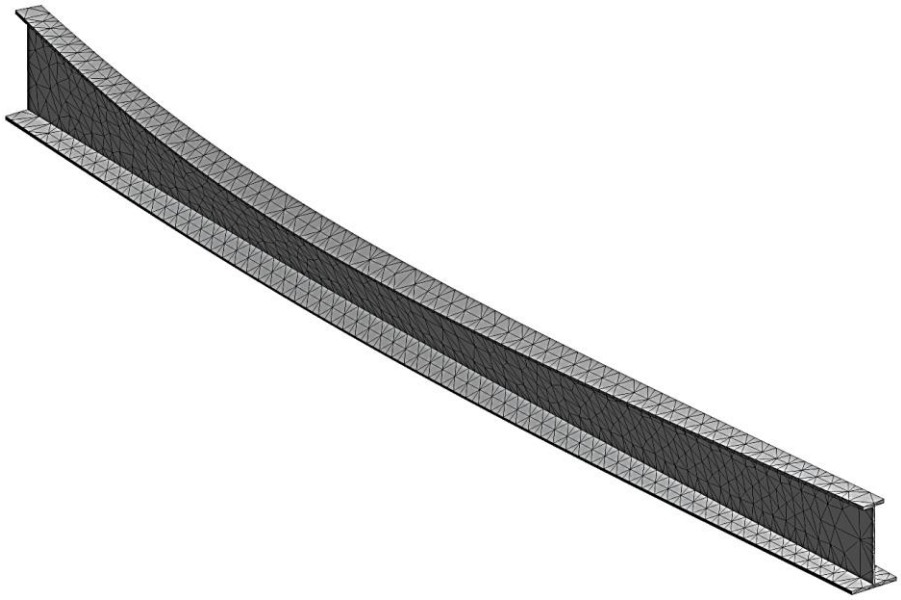

b) ANSYS-Academic

Figure 4.4.33: Critical mode shape for Case #A in Table 4.4.4 with $\beta_M = 0.25$

Figure 4.4.33 represents the critical mode determined with the finite element analysis (FEA) and the bar-chain model (BCM) with n=8, and Figure 4.4.32 represents, for the BCM (with n=500) and FEA solutions, the normalized twist rotations of the critical mode for Case #A.

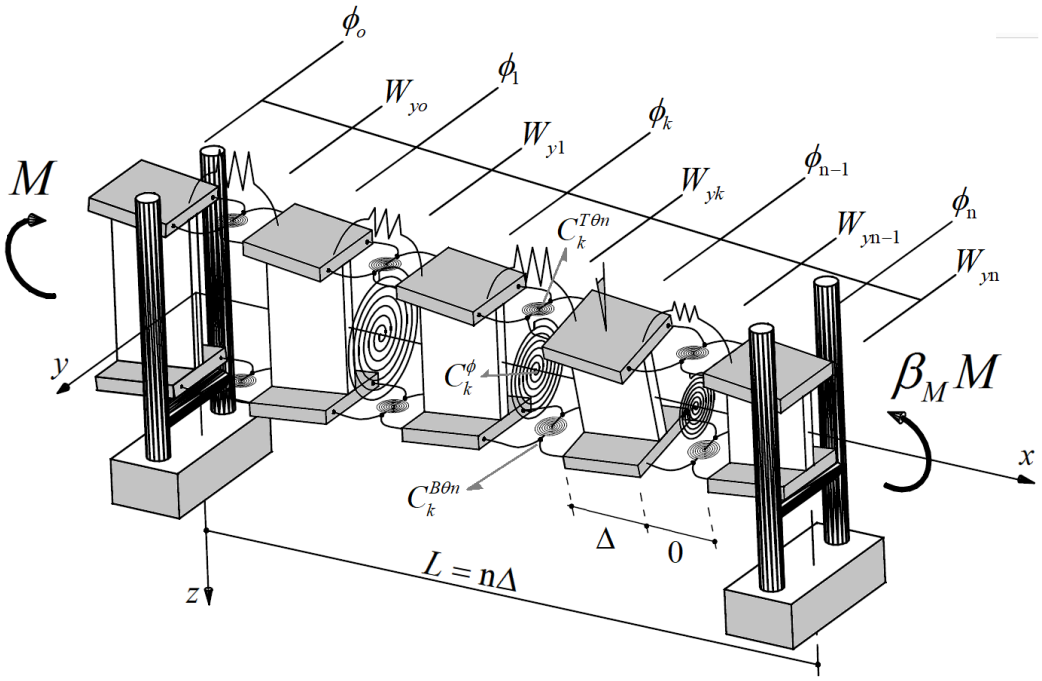

Figure 4.4.34: Simply supported depth-tapered double symmetric bar-chain under a moment gradient

A relevant case of study, is the doubly symmetric web-tapered bar-chain, whose reference shape is shown in Figure 4.4.34. Hence, equations (4.4.271)-(4.4.278) are reduced to

$$\begin{aligned}\frac{\partial \Pi}{\partial \phi_i} = & \frac{C_{\psi i-1}}{4}\left(\phi_i - \phi_{i-2}\right) + \frac{C_{\psi i+1}}{4}\left(\phi_i - \phi_{i+2}\right) + \frac{C_{\omega i-1}}{\Delta^2}\left(\phi_{i-2} - 2\phi_{i-1} + \phi_i\right) \\ & + \frac{2C_{\omega i}}{\Delta^2}\left(-\phi_{i-1} + 2\phi_i - \phi_{i+1}\right) + \frac{C_{\omega i+1}}{\Delta^2}\left(\phi_i - 2\phi_{i+1} + \phi_{i+2}\right) \\ & - \frac{C_{\omega\psi i-1}}{\Delta}\left(\phi_i - \phi_{i-1}\right) - \frac{C_{\omega\psi i}}{\Delta}\left(\phi_{i-1} - \phi_{i+1}\right) - \frac{C_{\omega\psi i+1}}{\Delta}\left(\phi_{i+1} - \phi_i\right) \\ & + \frac{M}{\Delta}\left(W_{yi-1} - 2W_{yi} + W_{yi+1}\right)\left(1 + (\beta_M - 1)\frac{i}{\mathrm{n}}\right) = 0 \ , \ i = 2,..,\mathrm{n}-2 \ , \end{aligned} \quad (4.4.279)$$

and

$$\begin{aligned}\frac{\partial \Pi}{\partial W_{yi}} = & \frac{C_z}{\Delta^2}\left(W_{yi-2} - 4W_{yi-1} + 6W_{yi} - 4W_{yi+1} + W_{yi+2}\right) \\ & + \frac{M}{\Delta}\left(1 + (\beta_M - 1)\frac{i-1}{\mathrm{n}}\right)\phi_{i-1} - \frac{2M}{\Delta}\left(1 + (\beta_M - 1)\frac{i}{\mathrm{n}}\right)\phi_i \\ & + \frac{M}{\Delta}\left(1 + (\beta_M - 1)\frac{i+1}{\mathrm{n}}\right)\phi_{i+1} = 0 \ , \ i = 2,..,\mathrm{n}-2 \ . \end{aligned} \quad (4.4.280)$$

With the following essential boundary conditions

$$W_{yo} = W_{y\mathrm{n}} = \phi_o = \phi_{\mathrm{n}} = 0 \ , \tag{4.4.281}$$

and the corresponding natural boundary conditions at the free ends

$$\frac{\partial \Pi}{\partial \phi_1} = \frac{C_{\psi 2}}{4}\left(\phi_1 - \phi_3\right) + \frac{C_{\omega 1}}{\Delta^2}\left(4\phi_1 - 2\phi_2\right) + \frac{C_{\omega 2}}{\Delta^2}\left(\phi_1 - 2\phi_2 + \phi_3\right) + \frac{C_{\omega\psi 1}}{\Delta}\phi_2$$
$$-\frac{C_{\omega\psi 2}}{\Delta}\left(\phi_2 - \phi_1\right) + \frac{M}{\Delta}\left(-2W_{y1} + W_{y3}\right)\left(1 + \frac{\beta_M - 1}{\mathrm{n}}\right) = 0 \ , \tag{4.4.282}$$

$$\frac{\partial \Pi}{\partial \phi_{\mathrm{n}-1}} = \frac{C_{\psi \mathrm{n}-2}}{4}\left(\phi_{\mathrm{n}-1} - \phi_{\mathrm{n}-3}\right) + \frac{C_{\omega \mathrm{n}-2}}{\Delta^2}\left(\phi_{\mathrm{n}-3} - 2\phi_{\mathrm{n}-2} + \phi_{\mathrm{n}-1}\right)$$
$$+\frac{2C_{\omega \mathrm{n}-1}}{\Delta^2}\left(2\phi_{\mathrm{n}-1} - \phi_{\mathrm{n}-2}\right) - \frac{C_{\omega\psi \mathrm{n}-2}}{\Delta}\left(\phi_{\mathrm{n}-1} - \phi_{\mathrm{n}-2}\right) - \frac{C_{\omega\psi \mathrm{n}-1}}{\Delta}\phi_{\mathrm{n}-2}$$
$$+\frac{M}{\Delta}\left(W_{y\mathrm{n}-2} - 2W_{y\mathrm{n}-1}\right)\left(1 + (\beta_M - 1)\frac{\mathrm{n}-1}{\mathrm{n}}\right) = 0 \ , \tag{4.4.283}$$

$$\frac{\partial \Pi}{\partial W_{y1}} = \frac{C_z}{\Delta^2}\left(5W_{y1} - 4W_{y2} + W_{y3}\right) - \frac{2M}{\Delta}\left(1 + \frac{\beta_M - 1}{\mathrm{n}}\right)\phi_1$$
$$+\frac{M}{\Delta}\left(1 + \frac{2(\beta_M - 1)}{\mathrm{n}}\right)\phi_2 = 0 \ , \tag{4.4.284}$$

$$\frac{\partial \Pi}{\partial W_{y\mathrm{n}-1}} = \frac{C_z}{\Delta^2}\left(W_{y\mathrm{n}-3} - 4W_{y\mathrm{n}-2} + 5W_{y\mathrm{n}-1}\right) + \frac{M}{\Delta}\left(1 + (\beta_M - 1)\frac{\mathrm{n}-2}{\mathrm{n}}\right)\phi_{\mathrm{n}-2}$$
$$-\frac{2M}{\Delta}\left(1 + (\beta_M - 1)\frac{\mathrm{n}-1}{\mathrm{n}}\right)\phi_{\mathrm{n}-1} = 0 \ . \tag{4.4.285}$$

Again, by replacing the discrete central values of the degrees of freedom and the stiffness coefficients, the residuals of equations (4.4.279)-(4.4.280) are computed

$$\Delta\left(C_\omega(x_i)\Delta\phi^{IV}(x_i) + 2C'_\omega(x_i)\Delta\phi'''(x_i) - GJ^*(x_i)\phi''(x_i) - \left(GJ^*\right)'(x_i)\phi'(x_i)\right.$$
$$\left.+M\left(1 + (\beta_M - 1)\frac{i\Delta}{L}\right)W_y''(x_i)\right) + O(\Delta^2) = r_{\phi i} \ , \ i = 2,..,\mathrm{n}-2 \ , \tag{4.4.286}$$

and

$$\left[C_z \Delta W_y{}^{IV}(x_i) + M \left(1+(\beta_M -1)\frac{i\Delta}{L}\right)\phi''(x_i) \right.$$
$$\left. + \frac{2M(\beta_M -1)}{L}\phi'(x_i) \right] \Delta + O(\Delta^3) = r_{ui} \ , \ i = 2,..,\mathrm{n}-2 \ . \qquad (4.4.287)$$

At the limit

$$W_y(x_i) \to W_y(x) \ , \qquad \phi(x_i) \to \phi(x) \ , \qquad (4.4.288)$$

the continuous one-dimensional equations arise, i.e., $x \in \mathbb{R} \cap (0, L)$ so that

$$EI_\omega^*(x)\phi^{IV}(x) + 2\left(EI_\omega^*(x)\right)'\phi'''(x) - \left(GJ^*(x)\phi'(x)\right)'$$
$$+M \left(1+(\beta_M -1)\frac{x}{L}\right) W_y{}''(x) = 0 \ , \qquad (4.4.289)$$

and

$$EI_z^* W_y{}^{IV}(x) + M \left(1+(\beta_M -1)\frac{x}{L}\right)\phi''(x) + \frac{2M(\beta_M -1)}{L}\phi'(x) = 0 \ . \qquad (4.4.290)$$

Using the same methodology for our natural boundary conditions (4.4.282)-(4.4.285)

$$C_\omega(x_o)\Delta\phi''(x_o) - C_{\omega\psi}(x_o)\Delta\phi'(x_o) + O(\Delta) = r_{\phi,o} \ , \qquad (4.4.291)$$

$$C_\omega(x_\mathrm{n})\Delta\phi''(x_\mathrm{n}) - C_{\omega\psi}(x_\mathrm{n})\Delta\phi'(x_\mathrm{n}) + O(\Delta) = r_{\phi,\mathrm{n}} \ , \qquad (4.4.292)$$

$$-C_z \Delta W_y{}''(x_o) + O(\Delta^2) = r_{u,o} \ , \qquad (4.4.293)$$

$$-C_z \Delta W_y{}''(x_\mathrm{n}) + O(\Delta^2) = r_{u,\mathrm{n}} \ . \qquad (4.4.294)$$

At the limit (i.e., $\Delta \to 0$) the residuals converge to zero, and the continuous natural boundary conditions emerge

$$EI_\omega^*(0)\phi''(0) + \left(EI_\omega^*\right)'(0)\phi'(0) = 0 \ , \qquad (4.4.295)$$

$$EI_\omega^*(L)\phi''(L) + \left(EI_\omega^*\right)'(L)\phi'(L) = 0 \ , \qquad (4.4.296)$$

$$EI_z^* W_y{}''(0) = 0 \ , \qquad (4.4.297)$$

$$EI_z^* W_y{}''(L) = 0 \ , \qquad (4.4.298)$$

while the essential boundary conditions are

$$W_y(0) = W_y(L) = \phi(0) = \phi(L) = 0 \ . \qquad (4.4.299)$$

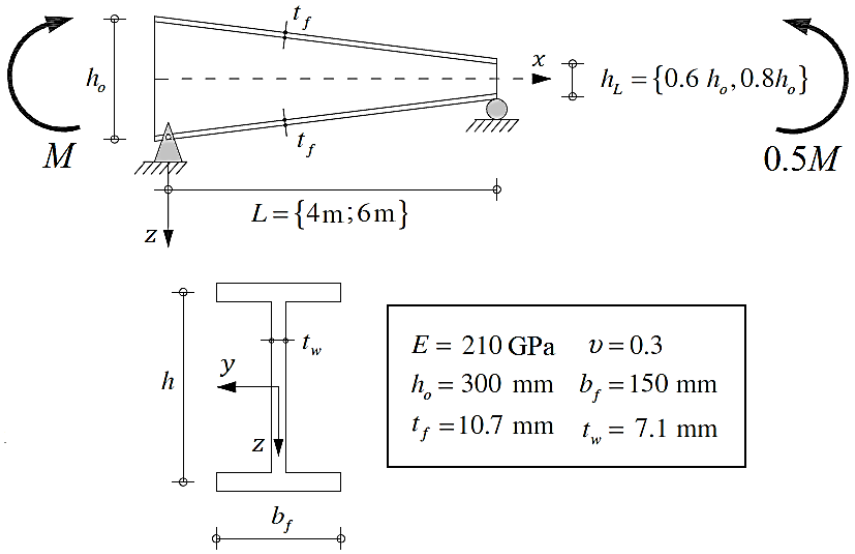

Figure 4.4.35: Double symmetric tapered bar: Geometry, loading and material data

As a numerical example, Figure 4.4.35 summarises the general geometry and material properties for a particular problem taken from Asgarian et al. (2013), who developed a numerical method based on the power series expansion of 1D models, to evaluate the stability of tapered thin-walled beams subjected to lateral loads. Table 4.4.5 shows the critical moment for the bar-chain model, i.e., the discrete equations (4.4.279)-(4.4.285) with n=600, as well as other solutions reported in the literature. Moreover, by using the property that the bar-chain model is a mechanical structure by itself, it is possible to grasp the first two buckling modes as it is shown in Figure 4.4.36.

#	L [m]	h_L	M_{cr} [kNm]			
			(1)	(2)	(3)	(4)
A	4	$0.6h_o$	175.6	182.8	175.5	182.3
B	4	$0.8h_o$	187.0	189.6	186.9	192.5
C	6	$0.6h_o$	100.8	103.5	100.8	103.9
D	6	$0.8h_o$	105.1	106.4	105.0	107.5

(1) One-dimensional model (Soltani et al. 2013).

(2) Timoshenko's approach (Zhang and Tong 2008).

(3) One-dimensional model ─ Power series solution (Asgarian et al. 2013).

(4) Bar-chain model, with n=600.

Table 4.4.5: Critical buckling moments for the tapered bars shown in Figure 4.4.35

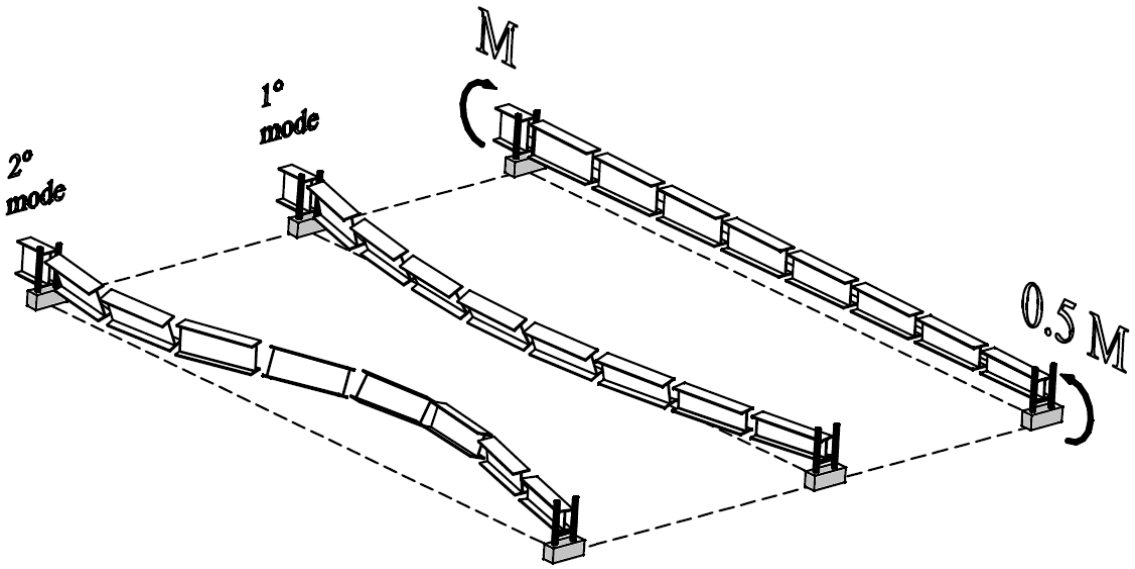

Figure 4.4.36: Bar-chain first two modes of stability, for Case #C in Table 4.4.5, n=8

Illustrative example 3: Simply supported beam-column

In this example, the bar-chain model for the elastic lateral-torsional buckling of a tapered beam-column, with depth varying linearly in the longitudinal direction is developed, see Figure 4.4.37.

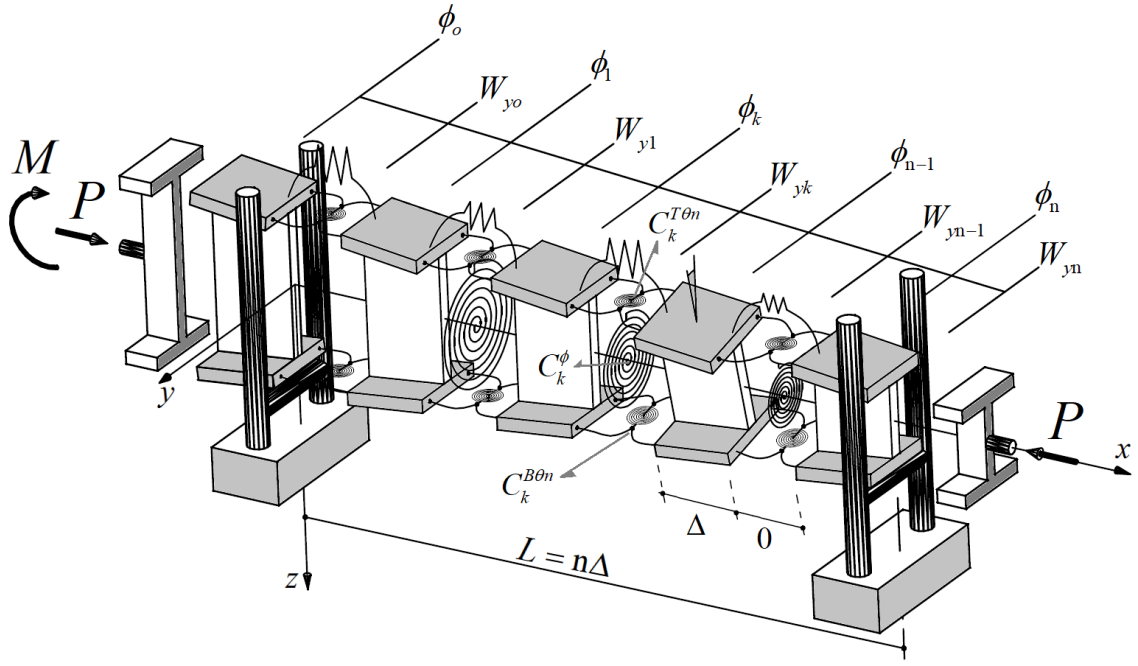

Figure 4.4.37: Illustrative example 3: Bar-chain model for a tapered simply supported beam-column with a bending moment located at one end

The bar-chain is simply supported at both ends, i.e., the essential boundary conditions are defined by[48]

$$W_{yo} = W_{y\mathrm{n}} = \phi_o = \phi_{\mathrm{n}} = 0 \ , \tag{4.4.300}$$

and loaded under the combined effect of an axial compressive load P and a bending moment M at its left end with respect to the strong stiffness plane, i.e.,

$$M_{yk}^{F} = \left(1 - \frac{k}{\mathrm{n}}\right) M \ , \tag{4.4.301}$$

with $k = 1, 2, ..., \mathrm{n}-1$. Hence, the total potential energy is given by

$$\begin{aligned}\Pi\left(W_{yk}, \phi_k; P, M\right) = \frac{1}{2}\sum_{k=1}^{\mathrm{n}-1}\Bigg(& C_{\omega k}\left(\frac{\phi_{k-1} - 2\phi_k + \phi_{k+1}}{\Delta}\right)^2 + C_{\psi k}\left(\frac{\phi_{k+1} - \phi_{k-1}}{2}\right)^2 \\ & - C_{\omega\psi k}\left(\frac{\phi_{k-1} - 2\phi_k + \phi_{k+1}}{\Delta}\right)\left(\phi_{k+1} - \phi_{k-1}\right) + C_z\left(\frac{W_{yk-1} - 2W_{yk} + W_{yk+1}}{\Delta}\right)^2 \\ & + 2\phi_k\left(\frac{W_{yk-1} - 2W_{yk} + W_{yk+1}}{\Delta}\right)\left(1 - \frac{k}{\mathrm{n}}\right)M \\ & - \frac{P}{\Delta}\left(\left(W_{yk} - W_{yk-1}\right)^2 + r_{ok}^2\left(\phi_k - \phi_{k-1}\right)^2\right)\Bigg) \ , \ k = 1, 2, ..., \mathrm{n}-2 \ . \end{aligned} \tag{4.4.302}$$

The stationary condition of the total potential energy requires that the first variation of each independent degree of freedom W_{yk} , ϕ_k must vanish. Thus

$$\begin{aligned}\frac{\partial\Pi}{\partial\phi_i} = & \frac{C_{\psi i-1}}{4}\left(\phi_i - \phi_{i-2}\right) + \frac{C_{\psi i+1}}{4}\left(\phi_i - \phi_{i+2}\right) + \frac{C_{\omega i-1}}{\Delta^2}\left(\phi_{i-2} - 2\phi_{i-1} + \phi_i\right) \\ & + \frac{2C_{\omega i}}{\Delta^2}\left(-\phi_{i-1} + 2\phi_i - \phi_{i+1}\right) + \frac{C_{\omega i+1}}{\Delta^2}\left(\phi_i - 2\phi_{i+1} + \phi_{i+2}\right) - \frac{C_{\omega\psi i-1}}{\Delta}\left(\phi_i - \phi_{i-1}\right) \\ & - \frac{C_{\omega\psi i}}{\Delta}\left(\phi_{i-1} - \phi_{i+1}\right) - \frac{C_{\omega\psi i+1}}{\Delta}\left(\phi_{i+1} - \phi_i\right) + \frac{M}{\Delta}\left(W_{yi-1} - 2W_{yi} + W_{yi+1}\right)\left(1 - \frac{i}{\mathrm{n}}\right) \\ & + \frac{P}{\Delta}\left(r_{oi}^2\phi_{i-1} - \left(r_{oi}^2 + r_{oi+1}^2\right)\phi_i + r_{oi+1}^2\phi_{i+1}\right) = 0 \ . \end{aligned} \tag{4.4.303}$$

[48]The natural boundary conditions are defined in equations (4.4.305)-(4.4.308).

and

$$\frac{\partial \Pi}{\partial W_{yi}} = \frac{C_z}{\Delta^2}\left(W_{yi-2} - 4W_{yi-1} + 6W_{yi} - 4W_{yi+1} + W_{yi+2}\right) + \frac{M}{\Delta}\left(1 - \frac{i-1}{\mathrm{n}}\right)\phi_{i-1}$$

$$-\frac{2M}{\Delta}\left(1 - \frac{i}{\mathrm{n}}\right)\phi_i + \frac{M}{\Delta}\left(1 - \frac{i+1}{\mathrm{n}}\right)\phi_{i+1} + \frac{P}{\Delta}\left(W_{yi-1} - 2W_{yi} + W_{yi+1}\right) = 0 \ . \qquad (4.4.304)$$

with $k = 2, ..., \mathrm{n}-2$. While the natural boundary conditions are given by

$$\frac{\partial \Pi}{\partial \phi_1} = \frac{C_{\psi 2}}{4}\left(\phi_1 - \phi_3\right) + \frac{C_{\omega 1}}{\Delta^2}\left(4\phi_1 - 2\phi_2\right) + \frac{C_{\omega 2}}{\Delta^2}\left(\phi_1 - 2\phi_2 + \phi_3\right)$$

$$+\frac{C_{\omega\psi 1}}{\Delta}\phi_2 - \frac{C_{\omega\psi 2}}{\Delta}\left(\phi_2 - \phi_1\right) + \frac{M}{\Delta}\left(-2W_{y1} + W_{y3}\right)\left(1 - \frac{1}{\mathrm{n}}\right)$$

$$-\frac{P}{\Delta}\left[\left(r_{o1}^2 + r_{o2}^2\right)\phi_1 - r_{o2}^2\phi_2\right] = 0 \ , \qquad (4.4.305)$$

$$\frac{\partial \Pi}{\partial \phi_{\mathrm{n}-1}} = \frac{C_{\psi \mathrm{n}-2}}{4}\left(\phi_{\mathrm{n}-1} - \phi_{\mathrm{n}-3}\right) + \frac{C_{\omega \mathrm{n}-2}}{\Delta^2}\left(\phi_{\mathrm{n}-3} - 2\phi_{\mathrm{n}-2} + \phi_{\mathrm{n}-1}\right) + \frac{2C_{\omega \mathrm{n}-1}}{\Delta^2}\left(2\phi_{\mathrm{n}-1} - \phi_{\mathrm{n}-2}\right)$$

$$-\frac{C_{\omega\psi \mathrm{n}-2}}{\Delta}\left(\phi_{\mathrm{n}-1} - \phi_{\mathrm{n}-2}\right) - \frac{C_{\omega\psi \mathrm{n}-1}}{\Delta}\phi_{\mathrm{n}-2}$$

$$+\frac{M}{\Delta}\left(W_{y\mathrm{n}-2} - 2W_{y\mathrm{n}-1}\right)\left(1 - \frac{\mathrm{n}-1}{\mathrm{n}}\right) + \frac{P}{\Delta}r_{o\mathrm{n}-1}^2\left(\phi_{\mathrm{n}-2} - \phi_{\mathrm{n}-1}\right) = 0 \ , \qquad (4.4.306)$$

$$\frac{\partial \Pi}{\partial W_{y1}} = \frac{C_z}{\Delta^2}\left(5W_{y1} - 4W_{y2} + W_{y3}\right) - \frac{2M}{\Delta}\left(1 - \frac{1}{\mathrm{n}}\right)\phi_1$$

$$+\frac{M}{\Delta}\left(1 - \frac{2}{\mathrm{n}}\right)\phi_2 + \frac{P}{\Delta}\left(-2W_{y1} + W_{y2}\right) = 0 \ , \qquad (4.4.307)$$

$$\frac{\partial \Pi}{\partial W_{y\mathrm{n}-1}} = \frac{C_z}{\Delta^2}\left(W_{y\mathrm{n}-3} - 4W_{y\mathrm{n}-2} + 5W_{y\mathrm{n}-1}\right) + \frac{M}{\Delta}\left(1 - \frac{\mathrm{n}-2}{\mathrm{n}}\right)\phi_{\mathrm{n}-2}$$

$$-\frac{2M}{\Delta}\left(1 - \frac{\mathrm{n}-1}{\mathrm{n}}\right)\phi_{\mathrm{n}-1} - \frac{P}{\Delta}\left(W_{y\mathrm{n}-1} - W_{y\mathrm{n}-2}\right) = 0 \ . \qquad (4.4.308)$$

In order to get the continuous one-dimensional equations of the buckling problem, we get the residual for each discrete equation (4.4.303) and (4.4.304), i.e.,

$$\Delta\left(C_\omega(x_i)\Delta\phi^{IV}(x_i) + 2C_\omega'(x_i)\Delta\phi'''(x_i) - GJ^*(x_i)\phi''(x_i) - \left(GJ^*\right)'(x_i)\phi'(x_i)\right.$$

$$\left. +M\left(1 - \frac{i\Delta}{L}\right)W_y''(x_i) + P\phi''(x_i)r_o^2(x_i) + P\phi'(x_i)\left(r_o^2(x_i)\right)'\right) + O(\Delta^2) = r_{\phi i} \ . \qquad (4.4.309)$$

and

$$\left[C_z \Delta W_y^{IV}(x_i) + M \left(1-\frac{i\Delta}{L}\right)\phi''(x_i) - \frac{2M}{L}\phi'(x_i) + PW_y''(x_i) \right]\Delta + O(\Delta^3) = r_{ui} \ . \qquad (4.4.310)$$

with $k = 1,2,...,\mathrm{n}-2$. Again, at the limit

$$x_i \in \mathbb{N} \cap (1,\mathrm{n}-2) \to x \in \mathbb{R} \cap (0,L) \ , \qquad (4.4.311)$$

the residuals converge to zero, and the following continuous equations arise

$$EI_\omega^*(x)\phi^{IV}(x) + 2\left(EI_\omega^*(x)\right)'\phi'''(x) - \left(GJ^*(x)\phi'(x)\right)' + M\left(1-\frac{x}{L}\right)W_y''(x) + P\phi''(x)r_o^2(x) + P\phi'(x)\left(r_o^2(x)\right)' = 0 \ , \qquad (4.4.312)$$

$$EI_z^* W_y^{IV}(x) + M\left(1-\frac{x}{L}\right)\phi''(x) - \frac{2M}{L}\phi'(x) + PW_y''(x) = 0 \ . \qquad (4.4.313)$$

Using the same methodology for the natural boundary conditions (4.4.305)-(4.4.308)

$$C_\omega(x_o)\Delta\phi''(x_o) - C_{\omega\psi}(x_o)\Delta\phi'(x_o) + O(\Delta) = r_{\phi,o} \ , \qquad (4.4.314)$$

$$C_\omega(x_\mathrm{n})\Delta\phi''(x_\mathrm{n}) - C_{\omega\psi}(x_\mathrm{n})\Delta\phi'(x_\mathrm{n}) + O(\Delta) = r_{\phi,\mathrm{n}} \ , \qquad (4.4.315)$$

$$-C_z\Delta W_y''(x_o) + O(\Delta^2) = r_{u,o} \ , \qquad (4.4.316)$$

$$-C_z\Delta W_y''(x_n) + O(\Delta^2) = r_{u,n} \ . \qquad (4.4.317)$$

At the limit, i.e., $\Delta \to 0$, we get

$$\left(EI_\omega^*\phi'\right)'(0) = 0 \ , \qquad (4.4.318)$$

$$\left(EI_\omega^*\phi'\right)'(L) = 0 \ , \qquad (4.4.319)$$

$$EI_z^* W_y''(0) = 0 \ , \qquad (4.4.320)$$

$$EI_z^* W_y''(L) = 0 \ , \qquad (4.4.321)$$

while the essential boundary conditions are

$$W_y(0) = W_y(L) = \phi(0) = \phi(L) = 0 \ . \qquad (4.4.322)$$

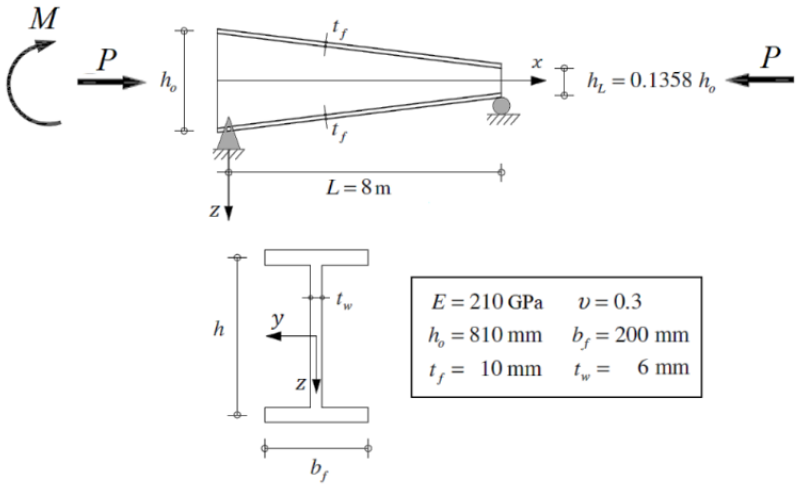

Figure 4.4.38: Tapered beam-column: Geometry, loading and material data

As an example, consider the geometry and material properties of the tapered thin-walled beam-column shown in Figure 4.4.38.[49] To solve the buckling problem, we fix the value of P and determine the corresponding critical bending moment M_{cr}. By repeating this procedure for several (fixed) values of P the interaction buckling diagram (or stability boundary) is determined. This curve is represented in Figure 4.4.39.

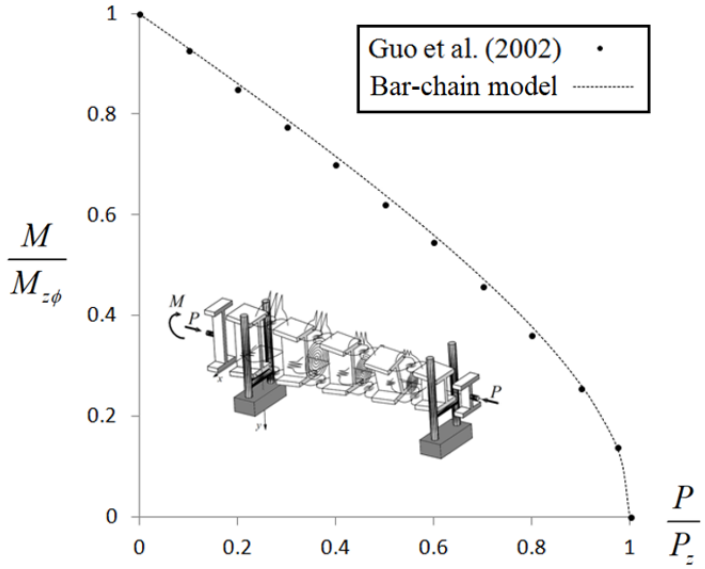

Figure 4.4.39: Illustrative example — Interaction buckling diagram of the tapered bar-chain with $n = 600$, $P_z = 432.2\text{kN}$ and $M_{z\phi} = 280.0\text{kNm}$

[49] This example is taken from Guo et al. (2002), who solved the (elastic) flexural-torsional buckling problem with a conventional finite element analysis.

Illustrative example 4: Tapered beam-column cantilever

The load-carrying capacity corresponding to the elastic lateral-torsional buckling of a tapered beam-column cantilever is now investigated. As Figure 4.4.40 shows, its bar-chain model is loaded under the combined axial and bending effects due to the compressive load P and a vertical load Q at its free end.

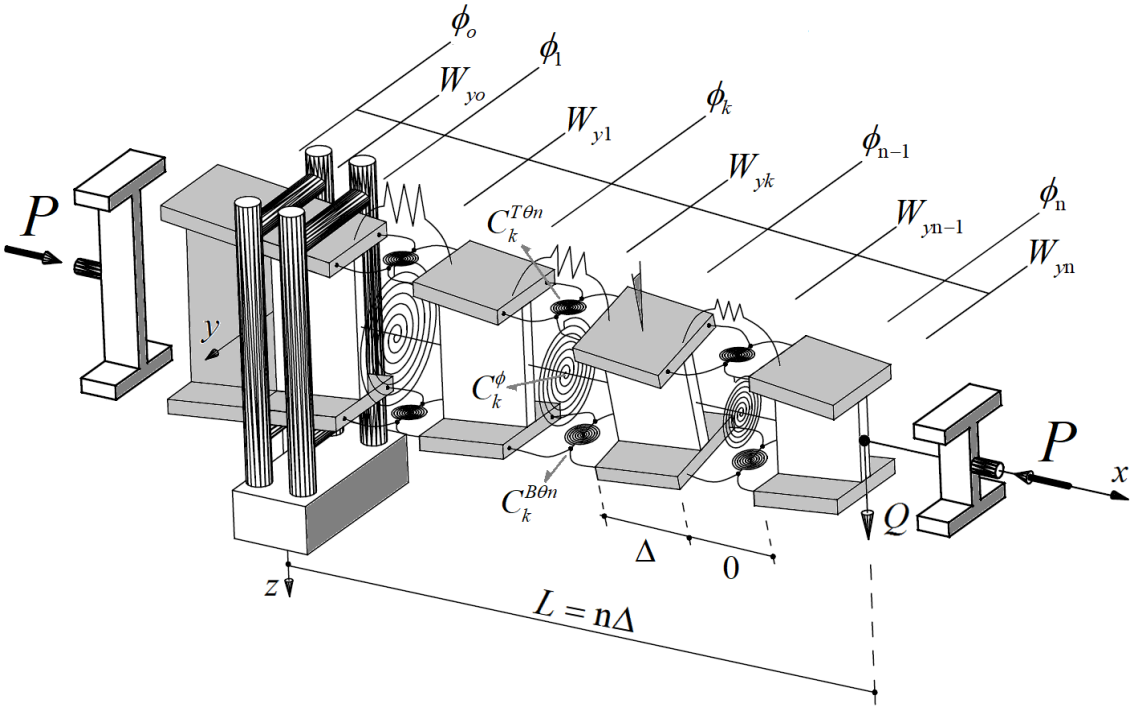

Figure 4.4.40: Illustrative example 4: Bar-chain model for a tapered beam-column cantilever with a vertical load at its free end

The total potential energy is given by

$$\Pi\left(W_{yk},\phi_k;P,Q\right)=\frac{1}{2}\sum_{k=1}^{n-1}\left(C_{\omega k}\left(\frac{\phi_{k-1}-2\phi_k+\phi_{k+1}}{\Delta}\right)^2+C_{\psi k}\left(\frac{\phi_{k+1}-\phi_{k-1}}{2}\right)^2\right.$$

$$-C_{\omega\psi k}\left(\frac{\phi_{k-1}-2\phi_k+\phi_{k+1}}{\Delta}\right)\left(\phi_{k+1}-\phi_{k-1}\right)+C_z\left(\frac{W_{yk-1}-2W_{yk}+W_{yk+1}}{\Delta}\right)^2$$

$$-2\phi_{k+1}\left(W_{yk-1}-2W_{yk}+W_{yk+1}\right)\left(n-k\right)Q$$

$$\left.-\frac{P}{\Delta}\left(\left(W_{yk+1}-W_{yk}\right)^2+r_{ok+1}^2\left(\phi_{k+1}-\phi_k\right)^2\right)\right). \qquad (4.4.323)$$

The boundary conditions of the buckling problem are defined by four essential boundary conditions

$$W_{yo} = W_{y\mathrm{n}} = \phi_o = \phi_1 = 0 \ , \tag{4.4.324}$$

and four natural boundary conditions equal to

$$\frac{\partial \Pi}{\partial \phi_{\mathrm{n}-1}} = \frac{\partial \Pi}{\partial \phi_{\mathrm{n}}} = \frac{\partial \Pi}{\partial W_{y\mathrm{n}-1}} = \frac{\partial \Pi}{\partial W_{y\mathrm{n}}} = 0 \ . \tag{4.4.325}$$

That means,

$$\begin{aligned}\frac{\partial \Pi}{\partial \phi_{\mathrm{n}-1}} &= \frac{C_{\psi \mathrm{n}-1}}{4}\left(\phi_{\mathrm{n}-1} - \phi_{\mathrm{n}-3}\right) + \frac{C_{\omega \mathrm{n}-1}}{\Delta^2}\left(\phi_{\mathrm{n}-3} - 2\phi_{\mathrm{n}-2} + \phi_{\mathrm{n}-1}\right) + \frac{2C_{\omega \mathrm{n}}}{\Delta^2}\left(-\phi_{\mathrm{n}-2} + 2\phi_{\mathrm{n}-1} - \phi_{\mathrm{n}}\right) \\ &- \frac{C_{\omega\psi \mathrm{n}-1}}{\Delta}\left(\phi_{\mathrm{n}-1} - \phi_{\mathrm{n}-2}\right) - \frac{C_{\omega\psi \mathrm{n}}}{\Delta}\left(\phi_{\mathrm{n}-2} - \phi_{\mathrm{n}}\right) - 2Q\left(W_{y\mathrm{n}-3} - 2W_{y\mathrm{n}-2} + W_{y\mathrm{n}-1}\right) \\ &+ \frac{P}{\Delta}\left(r_{o\mathrm{n}-1}^2\phi_{\mathrm{n}-2} - \left(r_{o\mathrm{n}}^2 + r_{o\mathrm{n}-1}^2\right)\phi_{\mathrm{n}-1} + r_{o\mathrm{n}}^2\phi_{\mathrm{n}}\right) = 0 \ ,\end{aligned} \tag{4.4.326}$$

$$\begin{aligned}\frac{\partial \Pi}{\partial \phi_{\mathrm{n}}} &= \frac{C_{\psi \mathrm{n}}}{4}\left(\phi_{\mathrm{n}} - \phi_{\mathrm{n}-2}\right) + \frac{C_{\omega \mathrm{n}}}{\Delta^2}\left(\phi_{\mathrm{n}-2} - 2\phi_{\mathrm{n}-1} + \phi_{\mathrm{n}}\right) - \frac{C_{\omega\psi \mathrm{n}}}{\Delta}\left(\phi_{\mathrm{n}} - \phi_{\mathrm{n}-1}\right) \\ &- Q\left(W_{y\mathrm{n}-2} - 2W_{y\mathrm{n}-1} + W_{y\mathrm{n}}\right) - \frac{P}{\Delta}r_{o\mathrm{n}}^2\left(\phi_{\mathrm{n}} - \phi_{\mathrm{n}-1}\right) = 0 \ ,\end{aligned} \tag{4.4.327}$$

$$\begin{aligned}\frac{\partial \Pi}{\partial W_{y\mathrm{n}-1}} &= \frac{C_z}{\Delta^2}\left(W_{y\mathrm{n}-3} - 4W_{y\mathrm{n}-2} + 5W_{y\mathrm{n}-1} - 2W_{y\mathrm{n}}\right) \\ &+ 2Q\left(\phi_{\mathrm{n}} - \phi_{\mathrm{n}-1}\right) - \frac{P}{\Delta}\left(-W_{y\mathrm{n}} + 2W_{y\mathrm{n}-1} - W_{y\mathrm{n}-2}\right) = 0 \ ,\end{aligned} \tag{4.4.328}$$

$$\frac{\partial \Pi}{\partial W_{y\mathrm{n}}} = \frac{C_z}{\Delta^2}\left(W_{y\mathrm{n}-2} - 2W_{y\mathrm{n}-1} + W_{y\mathrm{n}}\right) - Q\phi_{\mathrm{n}} - \frac{P}{\Delta}\left(W_{y\mathrm{n}} - W_{y\mathrm{n}-1}\right) = 0 \ . \tag{4.4.329}$$

Thus the minimum potential energy (4.4.323) can be written as

$$\begin{aligned}\frac{\partial \Pi}{\partial \phi_i} &= \frac{C_{\psi i}}{4}\left(\phi_i - \phi_{i-2}\right) + \frac{C_{\psi i+2}}{4}\left(\phi_i - \phi_{i+2}\right) + \frac{C_{\omega i}}{\Delta^2}\left(\phi_{i-2} - 2\phi_{i-1} + \phi_i\right) + \frac{2C_{\omega i+1}}{\Delta^2}\left(-\phi_{i-1} + 2\phi_i - \phi_{i+1}\right) \\ &+ \frac{C_{\omega i+2}}{\Delta^2}\left(\phi_i - 2\phi_{i+1} + \phi_{i+2}\right) - \frac{C_{\omega\psi i}}{\Delta}\left(\phi_i - \phi_{i-1}\right) - \frac{C_{\omega\psi i+1}}{\Delta}\left(\phi_{i-1} - \phi_{i+1}\right) - \frac{C_{\omega\psi i+2}}{\Delta}\left(\phi_{i+1} - \phi_i\right) \\ &- Q\left(W_{yi-2} - 2W_{yi-1} + W_{yi}\right)\left(\mathrm{n} - i + 1\right) + \frac{P}{\Delta}\left(r_{oi}^2\phi_{i-1} - \left(r_{oi}^2 + r_{oi+1}^2\right)\phi_i + r_{oi+1}^2\phi_{i+1}\right) = 0 \ ,\end{aligned} \tag{4.4.330}$$

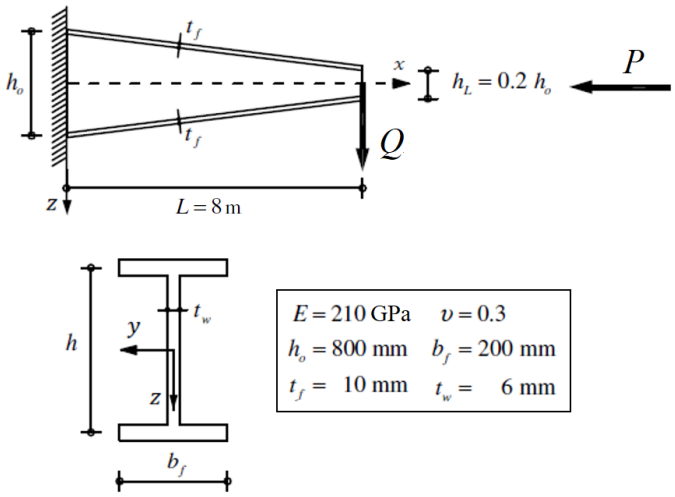

Figure 4.4.41: Tapered beam-column (cantilever): Geometry, loading and material data

and

$$\frac{\partial \Pi}{\partial W_{yi}} = \frac{C_z}{\Delta^2}\left(W_{yi-2} - 4W_{yi-1} + 6W_{yi} - 4W_{yi+1} + W_{yi+2}\right) - Q\left[\left(\mathrm{n}-i+1\right)\phi_i - 2\left(\mathrm{n}-i\right)\phi_{i+1}\right.$$

$$\left. + \left(\mathrm{n}-i-1\right)\phi_{i+2}\right] + \frac{P}{\Delta}\left(W_{yi-1} - 2W_{yi} + W_{yi+1}\right) = 0\ , \qquad (4.4.331)$$

with $k = 2,...,\mathrm{n}-2$. As an example, consider the geometry and material properties of the tapered thin-walled cantilever shown in Figure 4.4.41. Like in previous example, its interaction buckling diagram is determined by computing the critical load of Q under a fixed value of the axial load P.

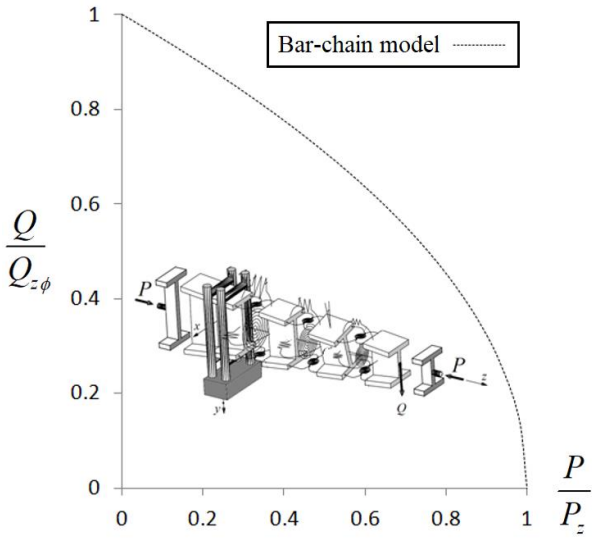

Figure 4.4.42: Illustrative example — Interaction buckling diagram for the tapered bar-chain, with $\mathrm{n} = 600$, $P_z = 108.0$kN and $Q_{z\phi} = 37.2$kN

By repeating this procedure for several (fixed) values of P the interaction buckling diagram is determined. This curve is represented in Figure 4.4.42. Again, in order to get the one-dimensional models in their continuous version, we get the residual for each discrete equation (4.4.330) and (4.4.331)

$$\Delta\Big(C_{\omega}(x_i)\Delta\phi^{IV}(x_i)+2C_{\omega}'(x_i)\Delta\phi'''(x_i)-GJ^{*}(x_i)\phi''(x_i)-\left(GJ^{*}\right)'(x_i)\phi'(x_i)$$

$$-Q\left(\mathrm{n}-(i-1)\right)W_y''(x_i)\Delta+P\phi''(x_i)r_o^2(x_i)+P\phi'(x_i)\left(r_o^2(x_i)\right)'\Big)+O(\Delta^2)=r_{\phi i} \quad (4.4.332)$$

and

$$\Big[C_z\Delta W_y{}^{IV}(x_i)-Q\left(\mathrm{n}-\left(i-1\right)\right)\phi''(x_i)\Delta$$

$$+2Q\phi'(x_i)+PW_y''(x_i)\Big]\Delta+O(\Delta^3)=r_{ui}\ . \quad (4.4.333)$$

with $k=1,2,...,\mathrm{n}-2$. At the limit $\Delta\to 0$

$$x_i\in\mathbb{N}\cap\left(1,\mathrm{n}-2\right)\to x\in\mathbb{R}\cap\left(0,L\right)\ , \quad (4.4.334)$$

the continuous one-dimensional equations are found, i.e.,

$$\Big[EI_{\omega}^{*}(x)\phi''(x)\Big]''-\Big[\left(EI_{\omega}^{*''}+GJ^{*}\right)(x)\phi'(x)\Big]'$$

$$-\left(L-x\right)QW_y''(x)+P\Big[r_o^2(x)\phi'(x)\Big]'=0\ , \quad (4.4.335)$$

and

$$EI_z^{*}W_y{}^{IV}(x)-\Big[\left(L-x\right)Q\phi(x)\Big]''+PW_y''(x)=0\ . \quad (4.4.336)$$

In the same manner, the residuals for the natural boundary conditions (4.4.326)-(4.4.329) are obtained

$$C_{\omega}(x_{\mathrm{n}})\Delta\phi''(x_{\mathrm{n}})-C_{\omega\psi}(x_{\mathrm{n}})\Delta\phi'(x_{\mathrm{n}})+O(\Delta)=r_{B,\mathrm{n}}\ , \quad (4.4.337)$$

$$C_{\psi}\Delta\phi'(x_{\mathrm{n}})+C_{\omega}(x_{\mathrm{n}})\left(-\Delta\phi'''(x_{\mathrm{n}})\right)+C_{\omega\psi}(x_{\mathrm{n}})\left(-\Delta\phi''(x_{\mathrm{n}})\right)$$

$$-P\Big[r_o^2(x_{\mathrm{n}})\phi'(x_{\mathrm{n}})\Big]+O(\Delta)=r_{T,\mathrm{n}}\ , \quad (4.4.338)$$

$$C_z\Delta W_y''(x_{\mathrm{n}})+O(\Delta^2)=r_{M,\mathrm{n}}\ , \quad (4.4.339)$$

$$-C_z\Delta W_y'''(x_{\mathrm{n}})-PW_y'(x_{\mathrm{n}})-Q\phi(x_{\mathrm{n}})+O(\Delta^2)=r_{V,\mathrm{n}}\ . \quad (4.4.340)$$

At the limit, i.e., when $\Delta \to 0$, the continuous natural boundaries conditions are found

$$\left(EI_{\omega}^{*}\phi'\right)'(L) = 0 \ , \tag{4.4.341}$$

$$\begin{aligned} &-EI_{\omega}^{*}(L)\phi'''(L) - \left(EI_{\omega}^{*}\right)'(L)\phi''(L) + \left(EI_{\omega}^{*}\right)''(L)\phi'(L) \\ &+GJ^{*}(L)\phi'(L) - P\left(r_{o}^{2}\phi'\right)(L) = 0 \ , \end{aligned} \tag{4.4.342}$$

$$EI_{z}^{*}W_{y}''(L) = 0 \ , \tag{4.4.343}$$

$$\left(EI_{z}^{*}W_{y}''' + PW_{y}' + Q\phi\right)(L) = 0 \ , \tag{4.4.344}$$

with the essential boundary conditions defined as

$$W_{y}(0) = W_{y}'(0) = \phi(0) = \phi'(0) = 0 \ . \tag{4.4.345}$$

REFERENCES

Abdelrahmane, B. B., Sid Ahmed, M., Foudil, M., and El Mostafa, D. (2013). "Analytical solutions attempt for lateral torsional buckling of doubly symmetric web-tapered I-beams." *Engineering Structures*, 56, 1207–1219.

Alwis, W. A. M., and Wang, C. M. (1996). "Wagner term in flexural-torsional buckling of thin-walled open-profile columns." *Engineering Structures*, 18(2), 125–132.

Anderson, J. M., and Trahair, N. S. (1972). "Stability of monosymmetric beams and cantilevers." *Journal of the Structural Division, ASCE*, 98(ST1), 269–286.

Andrade, A. (2013). "One-dimensional models for the spacial behaviour of tapered thin-walled bars with open cross sections: static, dynamic and buckling analyses." *Ph.D. thesis, Universidade de Coimbra*.

Andrade, A., and Camotim, D. (2005). "Lateral-torsional buckling of singly symmetric tapered beams: theory and applications." *Journal of Engineering Mechanics, ASCE*, 131(6), 586–597.

Andrade, A., Camotim, D., and Dinis, P. B. (2007). "Lateral-torsional buckling of singly symmetric web-tapered thin-walled I-beams: 1D model vs. shell FEA." *Computers & Structures*, 85(17-18), 1343–1359.

Ansys. (2018). "https://www.ansys.com/academic/free-student-products." *Release v19.0*.

Arbabi, F., and Li, F. (1991). "Buckling of variable cross-section columns: integral-equation approach." *Journal of Structural Engineering*, 117(8), 2426–2441.

Asgarian, B., Soltani, M., and Mohri, F. (2013). "Lateral-torsional buckling of tapered thin-walled beams with arbitrary cross-sections." *Thin-walled Structures*, 62, 96–108.

Attard, M. M. (1992). "Flexural-torsional buckling of monosymmetric columns." *Journal of Constructional Steel Research*, 23(1–3), 117–126.

Bažant, Z., and Cedolin, L. (2003). *Stability of structures: elastic, inelastic, fracture and damage theories*. Dover publications.

Boissonnade, N., and Braham, M. (2002). "Elastic lateral-torsional buckling of tapered members with monosymmetric cross-sections: new approaches and correct? solutions." *Proc., 3rd European Conf. on Steel Structures, Coimbra, A. Lamas and L. S. Silva, eds.*, 311–320.

Boissonnade, N., and Muzeau, J. P. (2001). "A new beam finite element for tapered members." *Proceedings of the eighth international conference on The application of artificial intelligence to Civil and Structural engineering Computing, Vienna, B. Topping, ed., Civil-Comp Press*, 73–74.

Bradford, M. A. (1988). "Stability of tapered I-beams." *Journal of Constructional Steel Research*, 9(3), 195–216.

Bradford, M. A., and Cuk, P. E. (1988). "Elastic buckling of tapered monosymmetric I-beams." *Journal of Structural Engineering*, 114(5), 977–996.

Braham, M. (1997). "Elastic lateral-torsional buckling of web tapered I-beams subjected to end moments." *Proc. 18th Czech-Slovak International Conf. on Steel Structures and Bridges*, 37–42.

Braham, M., and Hanikenne, D. (1993). “Lateral buckling of web tapered beams: An original design method confronted with a computer simulation.” *Journal of Constructional Steel Research*, 27(1-3), 23–36.

Brush, D. O., and Almroth, B. O. (1975). *Buckling of bars, plates, and shells*. (McGraw-Hill, Inc., ed.), McGraw-Hill Inc.

Burt, C. A. (1984). *Instability of monosymmetric I-beams and cantilevers*. M. Sc. Dissertation, Department of Civil and Structural Enginnering.

Challamel, N., Andrade, A., Camotim, D., and Milisavlevich, B. M. (2009). “Flexural-torsional buckling of cantilever strip beam-columns with linearly varying depth.” *Journal of Engineering Mechanics*, 136(6), 787–800.

Challamel, N., Camotim, D., Wang, C. M., and Zhang, Z. (2015). “On lateral-torsional buckling of discrete elastic systems: A nonlocal approach.” *European Journal of Mechanics A/Solids*, 49, 106–113.

Challamel, N., Lerbet, J., Wang, C. M., and Zhang, Z. (2014a). “Analytical length scale calibration of nonlocal continuum from a microstructured buckling model.” *Zeitschrift für Angewandte Mathematik und Mechanik [Journal of Applied Mathematics and Mechanics]*, 94(5), 402–413.

Challamel, N., Wang, C. M., and Elishakoff, I. (2014b). “Discrete systems behave as nonlocal structural elements: bending, buckling and vibration analysis.” *European Journal of Mechanics-A/Solids*, 44, 125–135.

Challamel, N., Zhang, Z., and Wang, C. M. (2013). “Nonlocal equivalent continua for buckling and vibration analyses of microstructured beams.” *Journal of Nanomechanics and Micromechanics*, 5(1), A4014004.

Chan, S. L., and Kitipornchai, S. (1987). “Geometric nonlinear analysis of asymmetric thin-walled beam-columns.” *Engineering Structures*, 9(4), 243–254.

Chen, W. F., and Atsuta, T. (1977). *Theory of beam-columns, volume 2: space behaviour and design*. McGraw-Hill.

Clark, J. W., and Hill, H. N. (1960). “Lateral buckling of beams.” *Transactions of the American Society of Civil Engineers*, 86, Issue 7, 175–196.

Coates, R. C., Coutie, M. G., and Kong, F. K. (1988). *Structural analysis*. Chapman & Hall, Third edition.

Dahlquist, G., and Björck, Å. (2003). *Numerical methods*. Dover publications.

Darbandi, S. M., Firouz-Abadi, R. D., and Haddadpour, H. (2010). “Buckling of variable section columns under axial loading.” *Journal of Engineering Mechanics*, 136(4), 472–476.

Dohrenwend, C. O. (1941). “Action of deep beams under combined vertical, lateral and torsional loads.” *Journal of Applied Mechanics*, A–130.

Dumont, C., and Hill, H. N. (1940). “The lateral stability of equal-flanged aluminium alloy I-beams subjected to pure bending.” *National Advisory Committee for Aeronautics*, Technical note 270.

Euler, L. (1744). “Additamentum I. De curvis elasticis. Methodus inveniendi lineas curvas maximi minimive proprietate gaudentes, sive solutio problematis isoperimetrici lattissimo sensu accepti.” [A method of finding curved lines enjoying properties of maximum or minimum, or solution of isoperimetric problems in the broadest accepted sense]. Lausanne & Geneva: Marcum–Michaelem Bousquet & Socios, 245–310. Reprinted in Leonhardi Euleri opera omnia, Series Prima (Opera Mathematica), Volume 24, C. Carathéodory (Ed.), 1952. Zurich: Orell Füssli, 231–297. Annotated English translation by W.A. Oldfather, C.A. Ellis and D.M. Brown (1933), Leonhard Euler’s elastic curves, Isis, 20(1), 72–160.

Flint, A. R. (1952). “The lateral stability of unrestrained beams.” *Engineering*, 170(12), 65–67.

Fraser, C. G. (1991). “Mathematical technique and physical conception in Euler’s investigation of the elastica.” *Centaurus*, 34(3), 211–246.

Gambhir, M. L. (2013). *Fundamentals of structural steel design*. McGraw-Hill Education (India) Private Limited.

Gere, J. M., and Carter, W. O. (1962). “Critical buckling loads for tapered columns.” *Journal of the Structural Division*, 88(1), 1–12.

Gjelsvik, A. (1981). *The theory of thin walled bars*. John Wiley & Sons.

Godoy, L. A. (1999). *Theory of elastic stability: Analysis and sensitivity*. CRC Press.

Goodier, J. N. (1941). *The buckling of compressed bars by torsion and flexure*. Bulletin n. 27, Cornell University Engineering Experiment Station.

Goodier, J. N. (1942). “Torsional and flexural buckling of bars of thin-walled open section under compressive and bending loads.” *Journal of Applied Mechanics*, 9(3), 103–107.

Gray, A., Gray, E., Mathews, G. B., and Meissel, E. (1895). *A treatise on Bessel functions and their applications to physics*. Macmillan and Company.

Guo, Y. L., Han, Y., Hao, W. Q., and Liu, T. (2002). “Elastic torsional-flexural buckling of tapered I beam-columns.” *Advances in Steel Structures (Proceedings of the third international conference on advances in steel structures)*, 155–162.

Helwig, T. A., Frank, K. H., and Yura, J. A. (1997). “Lateral-torsional buckling of singly symmetric I-beams.” *Journal of Structural Engineering*, 123(9), 1172–1179.

Hill, N. S. (1942). “The lateral instability of unsymmetrical I-sections.” *Journal of the Aeronautical Sciences*, 9(5), 175–180.

Hodges, D. H., and Peters, D. A. (2001). “Lateral-torsional buckling of cantilevered elastically coupled composite strip-and I-beams.” *International Journal of Solids and Structures*, 38(9), 1585–1603.

Hone, C. P. (1967). “Torsional-flexural buckling of axially-loaded, thin-walled, elastic struts of open cross-section.” *Thin-Walled Structures, ed. A. H. Chilver. Chatton and Windus, London*, 103–35.

Horne, M. R. (1954). “The flexural-torsional buckling of members of symmetrical I-section under combined thrust and unequal terminal moments.” *The Quarterly Journal of Mechanics and Applied Mathematics*, 7(4), 410–426.

Ingerslev, E. (1948). “Lateral stability of I-beams (Method of super-position).” IABSE congress report, 309–313.

Johnston, B. G., and Bethlehem, P. (1941). “Lateral buckling of I-section column with eccentric end loads in plane of the web.” *Journal of Applied Mechanics*, A76–A180.

Kappus, R. (1937). “Drillknicken zentrisch gedrückter stäbe mit offenen profil im elastischen bereich.” *Luftfahrtforschung*, 14(9), 444–457. English translation by J. Vanier (1938), Twisting failure of centrally loaded open–section columns in the elastic range, National Advisory Committee for Aeronautics (NACA), Technical Memorandum n. 851.

Kerensky, O. A., Flint, A. R., and Brown, W. C. (1956). “The basis for design of beams and plate girders in the revised British Standard 153.” *Proceedings of the Institution of Civil Engineers*, 5(4), 396–461.

Kerr, A. D. (1977). “On the adjacent equilibrium method in the stability theory of conservative elastic continua.” *International Journal of Non-Linear Mechanics*, 12(5), 269–283.

Kitipornchai, S., and Trahair, N. S. (1972). “Elastic stability of tapered I-beams.” *Journal of the Structural Division*, 98(3), 713–728.

Kitipornchai, S., and Trahair, N. S. (1975). “Elastic behavior of tapered monosymmetric I-beams.” *Journal of the Structural Division*, 101(8), 1661–1678.

Kitipornchai, S., and Trahair, N. S. (1980). “Buckling properties of monosymmetric I-beams.” *Journal of the Structural Division*, 106(5), 941–957.

Kováč, M. (2012). “Lateral-torsional buckling of web-tapered I-beams. 1D and 3D FEM approach.” *Procedia Engineering*, 40, 217–222.

Langhaar, H. L. (1962). *Energy methods in applied mechanics*. John Wiley and Sons.

Lee, G. C. (1960). “A survey of literature on the lateral instability of beams.” *Welding Research Council Bulletin,* No. 63, (August 1960), Reprint No. 163 (60–3).

Lee, G. C., and Szabo, B. A. (1967). “Torsional response of tapered I-girders.” *Journal of the Structural Division,* 93(5), 233–252.

Lee, L. H. N. (1956). “Non-uniform torsion of tapered I-beams.” *Journal of the Franklin Institute,* 262(1), 37–44.

Lyse, I., and Johnston, B. G. (1936). “Structural beams in torsion.” *Trans. ASCE,* Vol. 101 p. 857, Reprint No. 8 (36-1).

Megson, T. H. G. (1975). “Extension of the Wagner torsion bending theory to allow for general systems of loading.” *The Aeronautical Quarterly,* Cambridge University Press, 26(3), 155–164.

Michell, A. M. (1899). “XXXII. Elastic stability of long beams under transverse forces.” *The London, Edinburgh, and Dublin Philosophical Magazine and Journal of Science,* 48(292), 298–309.

Mohammadi, E., Hosseini, S. S., and Rohanimanesh, M. S. (2016). “Elastic lateral-torsional buckling strength and torsional bracing stiffness requirement for monosymmetric I-beams.” *Thin-Walled Structures,* 104, 116–125.

Murray, N. W. (1984). “Introduction to the theory of thin-walled structures.” *Oxford University Press, New York (Sec. 6.0)*.

Nikolić, A., and Šalinić, S. (2017). “Buckling analysis of non-prismatic columns: A rigid multibody approach.” *Engineering Structures,* 143, 511–521.

O'Connor, C. (1964). "The buckling of a monosymmetric beam loaded in the plane of symmetry." *Australian Journal of Applied Science*, 15, 191–203.

Pekoz, T. B., and Winter, G. (1969). "Torsional-flexural buckling of thin-walled sections under eccentric load." *Journal of the Structural Division*, 95(5), 941–964.

Petterson, O. (1951). "Combined bending and torsion of I-beams of monosymmetric cross-section." *Division of Building Statics and Structural Engineering, Royal Institute of Technology*, Bulletin No. 10.

Pi, Y. L., and Trahair, N. S. (1992). "Prebuckling deflections and lateral buckling. II: applications." *Journal of Structural Engineering*, 118(11), 2967–2985.

Pignataro, M., Rizzi, N., and Luongo, A. (1991). *Stability, bifurcation and postcritical behaviour of elastic structures*. (Elsevier Science, ed.).

Prandtl, L. (1899). "Kipp-erscheinungen − Ein fall von instabilem elastischem gleichgewicht." [Lateral-torsional buckling phenomena − A case of unstable elastic equilibrium], Dissertation, Ludwing-Maximilians-Universität München. Reprinted in Ludwing Prandtl gesammelte abhandlungen zur angewandten mechanik, hydro- und aerodynamik [Ludwing Prandtl collected works on applied mechanics, hydro- and aerodynamics], Volume 1, W. Tollmien, H. Schlichting and H. Görtler (Eds.), 1961, Berlin: Springer, 10−74.

Rajasekaran, S. (1994). "Equations for tapered thin-walled beams of generic open section." *Journal of Engineering Mechanics*, 120(8), 1607–1629.

Reissner, E. (1979). "On lateral buckling of end-loaded cantilever beams." *Journal of Applied Mathematics and Physics*, 30(1), 31–40.

Reissner, E. (1989). “Lateral buckling of beam.” *Computers & structures*, 33(5), 1289–1306.

Reissner, H. (1904). “Über die stabilität der biegung.” *[On the stability of beams], Sitzungsberichte der Berliner Mathematischen Gesellschaft*, 3, 53–56.

Renton, J. D. (1960). “A direct solution of the torsional-flexural buckling of axially loaded thin-walled bars.” *The Structural Engineer*, 38(9), 273–276.

Roberts, T. M., and Burt, C. A. (1985). “Instability of monosymmetric I-beams and cantilevers.” *International Journal of Mechanical Sciences*, 27(5), 313–324.

Ronagh, H. R., Bradford, M. A., and Attard, M. M. (2000a). “Nonlinear analysis of thin-walled members of variable cross-section. Part I: Theory.” *Computers & Structures*, 77(3), 285–299.

Ronagh, H. R., Bradford, M. A., and Attard, M. M. (2000b). “Nonlinear analysis of thin-walled members of variable cross-section. Part II: Application.” *Computers & Structures*, 77(3), 301–313.

Ruocco, E., Wang, C. M., Zhang, H., and Challamel, N. (2017). “An approximate model for optimizing Bernoulli columns against buckling.” *Engineering Structures*, 141, 316–327.

Seydel, R. (1988). *From equilibrium to chaos: Practical bifurcation and stability analysis*. (New York, Elsevier, ed.).

Siginer, A. (1992). “Buckling of columns of variable flexural rigidity.” *Journal of engineering mechanics*, 118(3), 640–643.

Singer, J., Arboz, J., and Weller, T. (1998). *Buckling experiments: Experimental methods in buckling of thin-walled structures. Basic concepts, columns, beams and plates – Volume 1*. John Wiley & Sons, Inc.

Slivker, V. (2006). *Mechanics of structural elements: Theory and applications*. Springer Science & Business Media.

Soderberg, C. R. (1982). *Stephen P. Timoshenko 1878-1972*. (Biographical Memoir, ed.), National Academy of Sciences.

Soltani, M., Asgarian, B., and Mohri, F. (2013). "Finite element method for stability analysis of tapered thin-walled beams under lateral loads." *Proceedings, Congress on Advances in Structural Engineering and Mechanics, Jeju, Korea*, 1358–1372.

Timoshenko, S. P. (1913). "Sur la stabilité des systems élastiques." [On the stability of elastic systems], Annales des Ponts et Chaussées, 9 Série, Tome XV, Volume 3, 496−566; Tome XVI, Volume 4, 73−132; Tome XVII, Volume 5, 372−412. Reprinted in The Collected Papers of Stephen P. Timoshenko, 1953. New York: McGraw-Hill, 92−224.

Timoshenko, S. P. (1945). "Theory of bending, torsion and buckling of thin-walled members of open cross section." *Journal of the Franklin Institute*, 239(3, 4, 5), 201–219, 249–268, 343–361.

Timoshenko, S. P. (1968). *As I remember: The autobiography*. Princeton, Van Nostrand.

Timoshenko, S. P., and Gere, J. M. (1961). *Theory of elastic stability*. McGrawHill, New York.

Trahair, N. S. (1993). *Flexural-torsional buckling of structures*. CRC Press.

Trahair, N. S. (2014). “Bending and buckling of tapered steel beam structures.” *Engineering Structures*, 59, 229–237.

Trefftz, E. (1931). “Über die ableitung der stabilitätskriterien des elastischen gleichgewichtes aus der elastizitätstheorie endlicher deformationen.” *[On the derivation of the stability criteria of elastic equilibrium from the elasticity theory of finite deformations], Verh. 3. Internat. Kongr. Techn. Mech*, 3, 44–50.

Trefftz, E. (1933). “Zur theorie der stabilität des elastischen gleichgewichts.” *[On the stability of elastic equilibrium], Zeitschrift für Angewandte Mathematik und Mechanik [Journal of Applied Mathematics and Mechanics]*, 13(2), 160–165.

Vacharajittiphan, P., Woolcock, S. T., and Trahair, N. S. (1974). “Effect of in-plane deformation on lateral buckling.” *Journal of Structural Mechanics*, 3(1), 29–60.

Valicourt, B. (2000). “Lateral-torsional buckling of web-tapered I-beams acted by a non uniform bending moment diagram.” *Graduation Rep.*, No. 16, Civil & Urban Engineering Dept., INSA, Rennes, France.

Vlasov, V. Z. (1961). *Thin-walled elastic beams*, [English translation of the 2nd Russian edition of 1959]. Jerusalem: Israel Program for Scientific Translation.

Wagner, H. (1929). “Verdrehung und knickung von offenen profilen.” *Veröffentlichung zum 25 jährigen Jubiläum, Technische Hochschule Danzing, 1904-1929*, Danzig: Verlag A. W. Kaffemann, 329-343. English translation by S. Reiss (1936), Torsion and buckling of open sections, Technical Memorandum n. 807, National Advisory Committee for Aeronautics (NACA).

Wang, C. M., and Kitipornchai, S. (1986). “On stability of monosymmetric cantilevers.” *Engineering Structures*, 8(3), 169–180.

Weber, C. (1926). “Übertragung des drehmomentes in balken mit doppelflanschigem querschnitt [Transmission of torque in bars with double-flanged cross-section].” *Zeitschrift für angewandte Mathematik und Mechanik*, 6(2), 85–97.

Wekezer, J. W. (1984). “Elastic torsion of thin walled bars of variable cross sections.” *Computers & structures*, 19(3), 401–407.

Wekezer, J. W. (1985). “Instability of thin walled bars.” *Journal of engineering mechanics*, 111(7), 923–935.

Wekezer, J. W. (1990). “A thin-walled bar element as a special case of a shell with internal constraints.” *Finite Element Applications to Thin-Walled Structures*, 41–62.

Wilde, P. (1968). “The torsion of thin-walled bars with variable cross-section [Torsion of variable cross sectional thin walled bars using shell theory equations].” *Archiwum Mechaniki Stosowanej*, 20(4), 431–443.

Williams, F. W., and Aston, G. (1989). “Exact or lower bound tapered column buckling loads.” *Journal of Structural Engineering*, 115(5), 1088–1100.

Winter, G. (1943). “Lateral stability of unsymmetrical I-beams and trusses in bending.” *Transactions of the American Society of Civil Engineers*, 108(1), 247–260.

Xiang, Y., Wang, C. M., and Kitipornchai, S. (1992). “Column buckling under general loads with allowances for pre-buckling shortening and shear deformation.” *Archive of Applied Mechanics*, 62(8), 544–556.

Xiong, X.-L., and Li, K.-X. (2007). “Wagner effect in flexural-torsional buckling of open-profile thin-walled columns.” *Journal of Xi’an University of Architecture & Technology*, 3, 18.

Yang, Y.-B., and Yau, J.-D. (1987). “Stability of beams with tapered I-sections.” *Journal of engineering mechanics*, 113(9), 1337–1357.

Yarlagadda, R. K. R. (2010). *Analog and digital signals and systems*. Springer.

Yoo, C. H., and Lee, S. (2011). *Stability of structures: principles and applications*. Elsevier.

Zhang, H., Wang, C. M., and Challamel, N. (2016a). “Buckling and vibration of Hencky bar-chain with internal elastic springs.” *International Journal of Mechanical Sciences*, 119, 383–395.

Zhang, H., Wang, C. M., Challamel, N., and Ruocco, E. (2017). “Semi-analytical solutions for optimal design of columns based on Hencky bar-chain model.” *Engineering Structures*, 136, 87–99.

Zhang, H., Wang, C. M., Ruocco, E., and Challamel, N. (2016b). “Hencky bar-chain model for buckling and vibration analyses of non-uniform beams on variable elastic foundation.” *Engineering Structures*, 126, 252–263.

Zhang, L., and Tong, G. S. (2008). “Lateral buckling of web-tapered I-beams: A new theory.” *Journal of Constructional Steel Research*, 64(12), 1379–1393.

Chapter 5

SUMMARY AND CONCLUSIONS. RECOMMENDATIONS FOR FUTURE RESEARCH

> You know that I write slowly. This is chiefly because I am never satisfied until I have said as much as possible in a few words, and writing briefly takes far more time than writing at length.
>
> CARL FRIEDRICH GAUSS

5.1 SUMMARY AND CONCLUSIONS

The main task of the present dissertation was to prove that one-dimensional models, in both continuous and discrete versions, are powerful enough to characterize the space behaviour of tapered thin-walled bars with open and continuously varying cross-section. Bearing this in mind, an outline of the contents of the dissertation is now presented, emphasizing the main conclusions and original contributions, which contribute to the state-of-the-art knowledge.

In chapter 2, a linear one-dimensional model for the stretching, bending and twisting of tapered thin-walled bars with open cross-sections under general static loading conditions was presented. Its main features may be summarized as follows:

(i) Thin-walled bars are treated as two-dimensional Kirchhoff-Love shells, exhibiting both membrane and flexural behaviours independent of the choice of parametrisation.

(ii) The necessary dimensional reduction is achieved by systematically regarding the classical assumptions of Vlasov (prismatic bar theory) and Kirchhoff-Love (plate bending theory) as internal constraints, that is, *a priori restrictions*, of a constitutive nature, on the possible deformations of the bars.

(iii) The above internal constraints can alternatively be viewed as *holonomic-scleronomic constraints*, whose physical representation is given by the kinematics of a rigid body.

(iv) The shell actions are decomposed additively into the active and reactive parts, with the constitutive dependence of the active forces and moments on the membrane strains and change of curvatures, respectively, reflecting the maximal symmetry compatible with the assumed internal constraints. Stress resultants are likewise split into active and reactive categories: the normal force, bending moments and bimoment are strictly active, while the shear forces are strictly reactive. The torque, having two components, one active and other reactive, is the only stress resultant having a mixt nature.

(v) The geometrical properties associated with the cross-section tapering, fully investigated by Andrade, were now complemented with the contribution of the through-the-thickness warping effect.

(vi) The most relevant consequence of the last additional contribution is the inclusion of the shear moduli into the constitutive equations, improving on previous approximations to the torsion constant.

(vii) The fundamental inequalities of the cross-sectional properties of tapered thin-walled bars with open cross-sections are established.

In chapter 3, we developed the discrete one-dimensional model, or Hencky bar-chain model, for the stretching, bending and twisting under general static loading of depth-tapered singly symmetric I-section bars. Basically, the Hencky bar-chain model consists in replacing the continuous bar by a set of finite rigid segments, connected by elastic rotational springs, whose kinematics are characterized by elementary geometrical relations. The existing Hencky bar-chain model for prismatic beams and tapered doubly symmetric columns, without taking the torsional warping effect under consideration, was the point of departure of the present research.

In the Hencky bar-chain model the spring constants are usually calibrated by imposing the mathematical equivalency between the discrete model and the application of the central finite difference scheme to the continuous model. A novel approach was developed herein, which is based on the postulation of *the principle of conservation of stiffness distribution.*

According to this principle "*the discrete spatial distribution of each type of spring constant is conserved for all possible bar-chain models,*" which is a mere implementation of the common definition of the stiffness of individual springs as the ratio between a cross-sectional stiffness and the length of each discrete rigid segment.

This directly determines the spring constants for (the prismatic or tapered) bar-chain model, circumventing the need for an *a priori* knowledge of the differential equations governing the continuous model. This result allowed for the statement of the fundamental *bar-chain conjecture*: "*There is at least one discrete bar-chain model that satisfies the mechanical analogy – comprising kinematic, stiffness, loading and boundary conditions – of a specific thin-walled bar with open cross-section.*"

This allows to establish a physical connection between the continuous one-dimensional model and its discrete counterpart, since the holonomic-scleronomic constraints defined in chapter 2 are compatible with a rigid body motion.

In addition, the most distinctive features of the bar-chain model are the following:

(i) The rigid segments *per se* have no intrinsic meaning, apart from affecting the deformation modes. Indeed, the irreducible element of the mechanical description is the link between segments set up by the (linearly) elastic springs.

(ii) In order to achieve a correct characterization of the boundary conditions – an essential ingredient in the setting up of the structural problem, the bar-chain model does not need to be artificially lengthened at the ends by means of fictitious segments, in contrast with the so-called "ghost point method" used to handle boundary conditions involving derivatives in central finite difference schemes.

(iii) The bar-chain model is consistent with (but not subordinate to or in any away dependent on) the Vlasov-type continuum model developed in chapter 2, in the sense that the local truncation errors tend to zero as the length of the segments approaches zero. Furthermore, the geometrical properties associated with the cross-sectional tapering and torsion (*i.e.*, the non-standard terms absent in the conventional but flawed stepped approach) arise as a natural consequence of the kinematics of the segments.

(iv) More than an idealization of a (continuous) member, the bar-chain model can be thought of as an actual mechanical structure in its own right, the inherent simplicity and transparency of which makes its qualitative behaviour most easily grasped.

In chapter 4, by using the discrete kinematical characterization established in chapter 3, the bar-chain model for the flexural-torsional stability of tapered singly symmetric I-section beam-columns is derived. Flangeless members – *i.e.*, members with narrow rectangular cross-section – and prismatic members are treated as special cases. Since the associated kinematics is based on the motion of rigid segments, this precludes the discrete model from capturing any local instability phenomena.

The chapter begins with a discussion of the well-known fundamental concepts regarding the stability analysis of ideal discrete conservative systems and the different types of criteria for characterizing the equilibrium states. The elastic flexural-torsional buckling problem (*i.e.*, the combined-interdependent lateral bending and axial torsion under an orthogonal symmetric loading), consists in determining the load levels and corresponding buckling modes, that stationaries the total potential energy of the bar-chain.

To verify the proposed discrete one-dimensional models and to assess their convergence rates, several illustrative examples, including analytical (when feasible) and numerical results, concerning different support and loading conditions as well as different severities of taper were discussed.

5.2 RECOMMENDATIONS FOR FUTURE RESEARCH

Based on the work carried out in the scope of this dissertation, some recommendations for future research are given below.

The topic which would require a more intensive study, is that of the fundamental principles and conjecture established in the thesis. Even though this requires a more formal and theoretical type of investigation, the impact of their possible conclusions may deserve that investment.

To extend the scope of the present investigation, allowing for local instability phenomena, and, therefore for their interaction with global instability phenomena. This will require the generalization of the kinematic description of the constraint shell developed in chapter 2. One approach is to define *ad hoc* vector functions, or assumed local buckling modes, that characterize the distortion of the cross-section. For example, the displacement field $\bar{\boldsymbol{U}}:\bar{\Omega}\to\mathbb{R}^3$ of $\bar{\boldsymbol{\chi}}(\theta^1,\theta^2)\in S$, may be written as

$$\bar{\boldsymbol{U}}(\theta^1,\theta^2)=\boldsymbol{W}(\theta^1)+\boldsymbol{\Phi}(\theta^1)\times\left(\bar{x}_2(\theta^1,\theta^2)\,\boldsymbol{e}_2+\bar{x}_3(\theta^1,\theta^2)\,\boldsymbol{e}_3+\Im\,(\theta^1,\theta^2)\right)+\zeta(\theta^1,\theta^2)\,\boldsymbol{e}_1\ ,$$

where the distortional vector $\Im\,(\theta^1,\theta^2)$ is defined only for the material points of the middle surface.

Another possible direction in which the one-dimensional models developed in chapter 2 can be expanded, is to consider the case of tapered thin-walled bars with closed cross-section, which will require a special attention to the characterization of their torsional behaviour and the corresponding flexural-torsional buckling problem.

It was concluded in chapter 3 that discrete one-dimensional models of tapered singly symmetric I-section bars are equivalent to (but not subordinate to or in any away dependent on) the corresponding continuous one-dimensional models of chapter 2. A significant contribution would be to investigate the case of singly symmetric web-tapered C-segments, whose corresponding bar-chain models may be developed using an approach similar to that employed for the tapered I-segments.

Although the discrete and continuous one-dimensional models are equivalent, in the sense that the solutions to the latter converge to those of the former as the length of the discrete elements tends to zero, the discrete model has a rather general applicability with a range variety of open topics:

(i) The mechanical vibration of the bar-chain model, i.e. the additional elements that should be incorporated in the discrete model include the mass of the segments, the dampers (linked in the springs) and the excitation.

(ii) The developed principles of conservation (of stiffness and elastic energy distribution) can be extended to the case of discrete two-dimensional models e.g. *the bar-net model*, which combines two interconnected bar-chains, in order to establish a discrete model for plates.

(iii) The spring constants were defined as perfectly elastic. The next step is the consideration of nonlinear elastic springs, as well as the incorporation of plasticity and collapse.

(iv) The application of the chain-models to the exploration of the post-buckling behaviour is still an open problem, which may be prone to interesting developments.